



5-1997

Cessation of Grand Cycle Deposition in the Framework of Passive Margin Evolution: Controlling Mechanisms and Effects on Carbonate Deposition and Diagenesis, Cambrian Maynardville Formation, Southern Appalachians

Bosiljka Glumac

University of Tennessee - Knoxville

Follow this and additional works at: https://trace.tennessee.edu/utk_graddiss

 Part of the [Geology Commons](#)

Recommended Citation

Glumac, Bosiljka, "Cessation of Grand Cycle Deposition in the Framework of Passive Margin Evolution: Controlling Mechanisms and Effects on Carbonate Deposition and Diagenesis, Cambrian Maynardville Formation, Southern Appalachians. " PhD diss., University of Tennessee, 1997.
https://trace.tennessee.edu/utk_graddiss/2644

This Dissertation is brought to you for free and open access by the Graduate School at TRACE: Tennessee Research and Creative Exchange. It has been accepted for inclusion in Doctoral Dissertations by an authorized administrator of TRACE: Tennessee Research and Creative Exchange. For more information, please contact trace@utk.edu.

To the Graduate Council:

I am submitting herewith a dissertation written by Bosiljka Glumac entitled "Cessation of Grand Cycle Deposition in the Framework of Passive Margin Evolution: Controlling Mechanisms and Effects on Carbonate Deposition and Diagenesis, Cambrian Maynardville Formation, Southern Appalachians." I have examined the final electronic copy of this dissertation for form and content and recommend that it be accepted in partial fulfillment of the requirements for the degree of Doctor of Philosophy, with a major in Geology.

Kenneth R. Walker, Major Professor

We have read this dissertation and recommend its acceptance:

Steve Driese, Claudia Mora, George K. Schweitzer

Accepted for the Council:


Carolyn R. Hodges

Vice Provost and Dean of the Graduate School

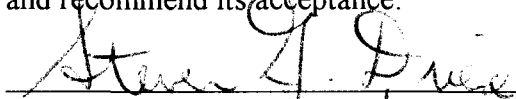
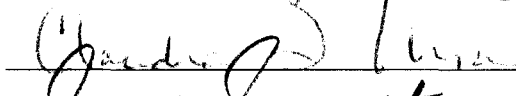
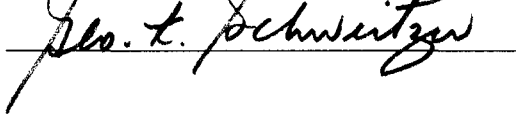
(Original signatures are on file with official student records.)

To the Graduate Council:


I am submitting herewith a dissertation written by Bosiljka Glumac entitled "Cessation of Grand Cycle Deposition in the Framework of Passive Margin Evolution: Controlling Mechanisms and Effects on Carbonate Deposition and Diagenesis, Cambrian Maynardville Formation, Southern Appalachians." I have examined the final copy of this dissertation for form and content and recommend that it be accepted in partial fulfillment of the requirements for the degree of Doctor of Philosophy, with a major in Geology.


Kenneth R. Walker, Major Professor

We have read this dissertation
and recommend its acceptance:

Accepted for the Council:


Associate Vice Chancellor
and Dean of The Graduate School

**CESSATION OF GRAND CYCLE DEPOSITION IN THE FRAMEWORK OF
PASSIVE MARGIN EVOLUTION: CONTROLLING MECHANISMS AND
EFFECTS ON CARBONATE DEPOSITION AND DIAGENESIS, CAMBRIAN
MAYNARDVILLE FORMATION, SOUTHERN APPALACHIANS**

A Dissertation
Presented for the
Doctor of Philosophy
Degree
The University of Tennessee, Knoxville

Bosiljka Glumac

May 1997

DEDICATION

This dissertation is dedicated to my grandparents

nona Albina (1913 - 1988) & **nono Pepo Josip Radović** (1903 - 1976),

and

baka Koka Sofija (1914 - 1992) & **djed Milan Glumac** (1911 - 1995),

and to my parents

Aurelija & Nikola Glumac

who provided me and my brothers with valuable examples,
and an inexhaustible source of encouragement.

ACKNOWLEDGMENTS

First of all, I would like to thank my academic advisor, Dr. Kenneth R. Walker, for being my teacher and mentor, and for his moral and financial support during my graduate studies at the University of Tennessee. Dr. Steven G. Driese and Dr. Claudia I. Mora from the Department of Geological Sciences are thanked for serving on my committee. I am also thankful to Dr. Driese for offering courses in various aspects of sedimentology from which I learned a great deal. Dr. Mora's expertise in stable isotope geochemistry and access to laboratory facilities contributed towards some of the most exciting findings of this study. I would also like to thank my committee members from the Chemistry Department, Dr. Craig E. Barnes and Dr. George K. Schweitzer.

I am grateful to the Department of Geological Sciences for providing me with financial support. My research was partially funded by a NSF grant to Dr. Walker, a Geological Society of America student research grant, the Faculty Senate Research Council Summer Graduate Research Assistantship, and the Mobil Carbonate Research Fund at the University of Tennessee. Assistance with the analytical aspects of this research was provided by Ken Tobin, Krishnan Srinivasan, Kevin Howard, Ian Richards, Andrew Stefaniak, Amy Halleran, and Allan Patchen. Strontium isotope analyses were performed by Dr. Steven Goldberg at the University of North Carolina, Chapel Hill. Field assistance was provided by Tony Caldanaro, Brian Freshour, Andrew Stefaniak, and Krishnan Srinivasan. I would also like to thank Mike Green for his help with statistical analysis, Bob Sepanski for developing photographs, and the departmental secretaries, Melody, Cindy and Denise for numerous favors.

Inspiring discussions with members of the Carbonate Research Group, Krishnan Srinivasan, Ken Tobin, Andrew Stefaniak, Stan Dunagan, Gary Ottinger, Chris Foster, Mark Steinhauß, and Gene Rankey were an invaluable part of my experience at UT. Numerous other people are responsible for making my stay in Knoxville very enjoyable:

Mike and Barb Green, Kevin and Kathy Smart, Chris Olson and Kelly Gardener, Brent Couzens, Michael Neton, Greg Yanagihara, Marta and Joe Corbin, RaNaye Dreier and Kim Kasten, Ian and Maria Richards, Landon and Alison Davidson, Jeff and Kelly Connelly, Tim and Sally Davis, Ellen Williams, Marvin Bennett, Mike Caudill, Jim Heller, Janee Ansley; my “international friends” Ronnie Minniti and Leticia Pibida + Melissa, Abir and Ehab Abourashed, Daniela and Kole Kovač; and many others. Thank you all!

I am truly grateful to my parents, Aurelija and Nikola Glumac, for their love, support and encouragement. Thank you for understanding the unusual requests of your only daughter, for your unlimited confidence in me, for letting me believe that dreams can come true, and for teaching me, by your examples, the importance of hard work, honesty, tolerance, and sacrifice. I would like to thank my parents simply, in the language they understand, with verses of a song that I used to sing to them as a child: “Hvala mama, hvala tata, hvala vam za sve.” My brothers also deserve special recognition. My older brother Miodrag for his expertise in solving computer and math problems, ski trips, and for just talking to me. It is so nice to have someone like you around! My younger brother Ranko for the summers we spent together in the States, for his sincere sense of humor, and for reminding us what being a teenager is all about. Thanks to all other relatives and friends for their thoughts and words of support.

At the end, my most sincere gratitude goes to my very best friend, Anthony J. Caldanaro, Jr., for his love, patience, and reassurance. Words cannot express my feelings and deep appreciation for Tony’s help with countless “little” things without which it would have been difficult (if not impossible) to accomplish so much. Thank you Tony for joining me in my journey, and for sharing very special moments with me.

Reflections on the landscapes and beaches of the Istrian peninsula, the pristine mountains and meadows of Lika, and thoughts and memories of people I love provided me with unending inspiration.

ABSTRACT

The Middle and Upper Cambrian deposits of the southern Appalachians reveal the existence of a broad carbonate platform that was facing the Iapetus Ocean to the east and was separated from the exposed craton to the west by the Conasauga intrashelf basin. This study focuses on the Maynardville Formation, which was deposited during the early Late Cambrian along the western carbonate platform margin. As the uppermost carbonate unit of the alternating shale and carbonate units or Grand Cycles of the Conasauga Group (Middle to Upper Cambrian), the Maynardville marks a change in style of passive-margin deposition reflected in the cessation of Grand Cycle deposition.

The Maynardville is a transitional interval between the largely subtidal carbonate and siliciclastic deposits of the Conasauga Group, and the peritidal carbonate deposits of the overlying Knox Group (Upper Cambrian to Lower Ordovician). The Maynardville consists of a lower subtidal package, underlain by the Nolichucky Shale, and an upper peritidal package, overlain by the Copper Ridge Dolomite. Mixed carbonate/siliciclastic deposition took place in a deep ramp (upper Nolichucky) to shallow-ramp and lagoonal (subtidal Maynardville) setting. To the east was a broad, semi-arid carbonate tidal flat with a variety of peritidal environments (upper Maynardville/Copper Ridge). The Nolichucky represents a retrogradational depositional package that formed in response to an increase in the rate of relative sea-level rise. Deposition of a shallowing-upward succession of the Maynardville reflects carbonate platform aggradation and progradation favored by a subsequent decrease in the rate of relative sea-level rise. Stacking patterns of the Maynardville are a result of the interplay between intrinsic factors of carbonate depositional systems, the mechanisms related to the history of the adjacent siliciclastic basin, and possible eustatic sea-level changes.

The cessation of Grand Cycle deposition is a consequence of passive-margin

evolution. The abrupt change from carbonate to shale deposition in the Grand Cycles may have been caused by short-term, episodic, non-thermal tectonic subsidence related to active extension and vertical readjustments, enhanced by sediment and water loading, during the immature stage of passive-margin development. These processes were superimposed on eustatic sea-level changes and thermal post-rift subsidence. The transition from an immature to a mature passive-margin setting occurred during deposition of the Maynardville Formation. The mature margin was characterized by the cessation of tectonic activity in the area. Decreased rates of thermal subsidence and the complete infilling of the Conasauga basin favored shallow-water deposition and carbonate platform progradation. The Maynardville grades conformably into the Copper Ridge Dolomite. This conformable interval is interpreted as a sequence boundary zone correlative to the Dresbachian/Franconian (Sauk II/Sauk III) unconformity. This boundary separates a third-order sequence (terminal Grand Cycle), composed of the Upper Shale Member of the Nolichucky and the Maynardville, from the thick peritidal carbonate deposits of the Knox Group, which reflect the final passive-margin stabilization.

The transition from the Conasauga into the Knox Group is characterized by a shift in diagenetic patterns. The distribution of early diagenetic phases within the Maynardville was controlled by changes in the depositional setting from a subtidal to a semi-arid tidal flat. The infilling of the Conasauga basin and carbonate platform progradation at the end of Grand Cycle deposition influenced the regional facies distribution, which consequently affected the burial diagenesis of this transitional interval.

The subtidal deposits of the Maynardville contain a variety of calcite cements that represent marine, meteoric and burial diagenetic environments. Dolomite is not abundant within these deposits, and it primarily occurs associated with argillaceous layers. The subtidal deposits contain rare ferroan saddle dolomite cement associated with Mississippi Valley Type (MVT) minerals. Pressure dissolution, diagenetic alteration of clay minerals,

and pore fluids expelled from interbedded shale, provided a local source for the formation of ferroan dolomite during burial. The presence of MVT minerals suggests the involvement of externally derived diagenetic fluids.

The peritidal deposits have been extensively dolomitized. Fine-crystalline penecontemporaneous dolomite formed under sabkha-like conditions. Coarser-crystalline replacement dolomite formed from recrystallization of early dolomite and from dolomitization of limestone during burial. Fenestrae, desiccation and evaporite dissolution voids are occluded with dolomite cement, which is often complexly zoned. Zoned dolomite cement precipitated from modified marine, mixed meteoric/marine, and burial fluids. Saddle dolomite cement in pore-centers, tectonic fractures, and dissolutional voids formed during late burial from warm, basinal fluids associated with the migration of MVT mineralizing brines, and from fluids provided locally by pressure solution.

The formation and preservation of Upper Cambrian microbial deposits were controlled by the conditions within the environments of deposition, but were also biotically influenced. Digitate stromatolites and thrombolites formed by calcification of cyanobacteria in lower intertidal and upper subtidal environments, which were not primary sites for dolomitization. Early diagenetic calcification of cyanobacteria reduced the susceptibility of these deposits to dolomitization. Laterally linked hemispheroidal (LLH), vertically stacked hemispheroidal (SH), and columnar stromatolites, as well as most stratiform stromatolite laminae formed by the trapping of sediment in supratidal and intertidal environments on semi-arid tidal flats. Extensive dolomitization altered these peritidal carbonate deposits early in their diagenetic history.

The Maynardville Formation records an increase in the $^{13}\text{C}/^{12}\text{C}$ ratio of Late Cambrian sea water. Comparison with studies of time-equivalent deposits elsewhere suggests that this positive carbon-isotope excursion is secular in scope. Petrographic and geochemical analyses were used to evaluate the extent of variations related to the

depositional and diagenetic environments, which are superimposed on the secular marine carbon-isotope trend. This approach enables carbon-isotope variations to be used as a stratigraphic tool, and as an indicator of the global cycling of carbon. The excursion is related to changes in the rate of organic-carbon burial, which can be linked to changes in ocean stratification, climate, sea-level, and paleoproductivity rate.

The excursion started during deposition of the Nolichucky Shale, and ended during the deposition of the Copper Ridge Dolomite. The maximum $\delta^{13}\text{C}$ values (4 to 5‰ PDB) are associated with the sequence boundary zone at the Maynardville/Copper Ridge Dolomite transition. Elsewhere, the excursion started at the base of the Pterocephaliid Biomere (near the base of the *Aphelaspis* zone). The excursion ended prior to the end of the Pterocephaliid Biomere, with the maximum excursion at the Sauk II/Sauk III unconformity. This supports the correlation between the Late Steptoean (Dresbachian/Franconian) sea-level fall and the sequence boundary at the end of Grand Cycle deposition, and demonstrates the application of carbon-isotope stratigraphy to successions with poorly constrained biostratigraphy.

TABLE OF CONTENTS

Chapter	Page
1. INTRODUCTION	1
PURPOSE AND SIGNIFICANCE	6
GEOLOGIC SETTING	7
OVERVIEW OF PREVIOUS RESEARCH	11
INVESTIGATIVE METHODS	13
DISSERTATION ORGANIZATION	18
2. CARBONATE DEPOSITIONAL DYNAMICS AND SEQUENCE STRATIGRAPHY IN THE FRAMEWORK OF GRAND CYCLE CESSATION	20
INTRODUCTION	20
MAYNARDVILLE LITHOFACIES	22
Lithofacies Description	22
Environments of Deposition	30
CARBONATE PLATFORM DEPOSITIONAL DYNAMICS	38
SEQUENCE STRATIGRAPHY	44
Nolichucky/Maynardville Transition	44
Stacking Patterns of the Maynardville Lithofacies	45
Maynardville/Copper Ridge Transition: Termination of Grand Cycle Deposition	49
DISCUSSION: CONTROLS ON CARBONATE DEPOSITION	52
CONCLUSIONS	57
3. SEDIMENTOLOGIC CONSEQUENCES OF PASSIVE-MARGIN EVOLUTION: TRANSITION FROM CAMBRIAN GRAND CYCLES TO MATURE PASSIVE-MARGIN DEPOSITION, SOUTHERN APPALACHIANS	59
INTRODUCTION	59
PASSIVE-MARGIN SETTING	60
TRANSITIONAL NATURE OF THE MAYNARDVILLE FORMATION AND IMPLICATIONS FOR PASSIVE-MARGIN EVOLUTION	63
Eustasy and Grand Cycle Formation	63

	x
Middle Cambrian Immature Passive Margin: Role of Non-Thermal Subsidence	64
Late Cambrian Mature Passive Margin	69
CONCLUSIONS	74
4. DIAGENETIC HISTORY OF A TERMINAL CAMBRIAN GRAND CYCLE CARBONATE SUCCESSION, SOUTHERN APPALACHIANS	75
INTRODUCTION	75
METHODS	76
PETROGRAPHIC OBSERVATIONS	78
Subtidal Package	78
Peritidal Package	88
Fractures	92
Silicification	92
GEOCHEMISTRY	95
Stable Isotope Compositions	95
Major and Trace Element Compositions	104
Strontium Isotope Ratios	115
INTERPRETATION OF DIAGENETIC HISTORY	115
Limestone Deposits	120
<i>Dolomite</i>	128
Extensively Dolomitized Peritidal Deposits	133
<i>Replacement Dolomite</i>	133
<i>Dolomite Cement</i>	139
COMPARISON WITH THE UNDERLYING AND THE OVERLYING STRATA	144
Maryville Limestone	144
Nolichucky Shale	148
Knox Group	152
DIAGENETIC HISTORY IN THE CONTEXT OF GRAND CYCLE CESSATION	157
CONCLUSIONS	165

5.	A LATE CAMBRIAN CARBON-ISOTOPE EXCURSION: RELATION TO BIOSTRATIGRAPHY AND SEQUENCE STRATIGRAPHY, AND IMPLICATIONS FOR INTERPRETING DIAGENETIC HISTORY	167
	INTRODUCTION	167
	INVESTIGATIVE METHODS AND SAMPLING STRATEGY	171
	RESULTS OF STABLE ISOTOPE ANALYSIS	174
	RELATIONSHIP OF CARBON-ISOTOPE STRATIGRAPHY TO BIOSTRATIGRAPHY AND SEQUENCE STRATIGRAPHY	179
	RELATION TO ENVIRONMENTS OF DEPOSITION AND DIAGENESIS	191
	Environmental Influence	191
	Diagenetic Influence	198
	DISCUSSION	204
	CONCLUSIONS	214
6.	SELECTIVE DOLOMITIZATION OF CAMBRIAN MICROBIAL CARBONATE DEPOSITS: A KEY TO MECHANISMS AND ENVIRONMENTS OF ORIGIN	215
	INTRODUCTION	215
	UPPER CAMBRIAN MICROBIAL CARBONATE DEPOSITS	216
	FORMATION OF MICROBIAL DEPOSITS: AN OVERVIEW	216
	SELECTIVE DOLOMITIZATION OF MICROBIAL DEPOSITS	225
	Mechanisms of Microbial Deposit Origin	226
	Environments of Deposition and Early Diagenetic History	227
	DISCUSSION	231
	CONCLUSIONS	235
7.	CONCLUSIONS	236
	REFERENCES CITED	242
	APPENDICES	282
	APPENDIX A: DESCRIPTION OF STRATIGRAPHIC SECTIONS	283
	APPENDIX B: STABLE ISOTOPE DATA	354
	APPENDIX C: ELECTRON MICROPROBE DATA	363
	APPENDIX D: DATA FOR CARBON-ISOTOPE STRATIGRAPHY	375
	VITA	380

LIST OF TABLES

Table	Page
2.1. Lithofacies of the subtidal package.	25
2.2. Lithofacies of the peritidal package.	26
4.1. Description of calcitic diagenetic components of the subtidal depositional package.	79
4.2. Description of dolomitic diagenetic components of the subtidal depositional package.	80
4.3. Description of dolomitic diagenetic components of the peritidal depositional package.	91
4.4. Summary of geochemical data for the depositional and diagenetic components of the deposits that have not been extensively dolomitized.	96
4.5. Summary of geochemical data for the depositional and diagenetic components of extensively dolomitized peritidal deposits.	97
5.1. Phanerozoic positive carbon-isotope excursions with durations greater than the residence time of carbon in the modern ocean.	169
6.1. Description of microbial deposits.	217

LIST OF FIGURES

Figure	Page
1.1. Generalized, restored paleogeography of Tennessee during the Middle and early Late Cambrian.	2
1.2. Middle to Upper Cambrian stratigraphy of eastern Tennessee.	4
1.3. Generalized stratigraphy of the Upper Proterozoic and Lower Paleozoic strata in eastern Tennessee and adjacent southwestern Virginia.	9
1.4. A map showing location of outcrops studied.	15
1.5. Location of outcrops along western carbonate platform margin.	17
2.1. Stratigraphic columns of the Maynardville Formation and the lower Copper Ridge Dolomite.	23
2.2. Photographs illustrating the most common Maynardville lithofacies.	27
2.3. Generalized illustration of depositional environments for the most common lithofacies present within the succession examined.	32
2.4. Photographs illustrating details of Maynardville lithofacies.	34
2.5. A model for the deposition of the Maynardville in the study area.	39
2.6. Outcrop photograph, with accompanying explanation, for the exposure surface and drowning interval within the subtidal package at the Tazewell outcrop.	41
2.7. Occurrence of detrital quartz and feldspar sand grains marks the sequence boundary zone represented by a conformable interval correlative with the Dresbachian/Franconian unconformity.	43
2.8. Examples of a subdivision of depositional packages in meter-scale successions or parasequences.	48
2.9. Interpretation of sequence stratigraphy for the terminal southern Appalachian Grand Cycle.	50
3.1. Stratigraphy of the Lower Paleozoic passive-margin succession of the Southern Appalachian Valley and Ridge physiographic province in eastern Tennessee.	61

3.2.	Middle Cambrian immature passive-margin setting.	66
3.3.	Late Cambrian mature passive-margin setting.	71
4.1.	Photomicrographs illustrating characteristic features of the subtidal deposits.	82
4.2.	Paired plain light and CL photomicrographs of the most common cement types in the subtidal deposits.	84
4.3.	Paired plain light and CL photomicrographs of the equant calcite cement and saddle dolomite from the subtidal deposits.	86
4.4.	Photomicrographs illustrating replacement dolomite types from the peritidal deposits.	89
4.5.	Photomicrographs illustrating dolomite cements from the peritidal deposits.	93
4.6.	Stable isotope composition of various carbonate components from the subtidal deposits.	98
4.7.	Stable isotope composition of various carbonate components from the extensively dolomitized peritidal deposits.	101
4.8.	Elemental composition of various depositional and diagenetic components from the subtidal deposits, composed of calcite.	105
4.9.	Comparison between elemental compositions of subtidal and peritidal dolomite phases.	109
4.10.	Compositional transects for peritidal dolomite cement.	112
4.11.	Variations in Sr isotope composition.	116
4.12.	Paragenetic sequences for the Upper Cambrian deposits.	118
4.13.	Burial curve for the Maynardville Formation.	119
4.14.	Comparison of stable isotope compositions between carbonate components from the subtidal Maynardville deposits and the Middle Cambrian Maryville Limestone.	145

4.15.	Stable isotope compositions of the comparable carbonate components from the Maynardville Formation and the underlying Upper Cambrian Nolichucky Shale.	150
4.16.	Stable isotope compositions of the comparable carbonate components from the peritidal deposits of the upper Maynardville/lower Copper Ridge Dolomite and the Lower Ordovician Upper Knox Group from the Copper Creek thrust sheet in eastern Tennessee.	154
4.17.	Schematic illustration of the topography-driven fluid flow (arrows) through the sedimentary succession of southwestern Virginia during the late Paleozoic Alleghenian orogeny.	158
4.18.	Schematic illustration of the compaction-driven fluid flow from the Sevier shale basin into the adjacent carbonate platform successions in eastern Tennessee.	162
5.1.	Stratigraphic column of the Thorn Hill section.	172
5.2.	Variations in $\delta^{13}\text{C}$ and $\delta^{18}\text{O}$ values as a function of stratigraphic position of the micrite and dolomicrite samples.	175
5.3.	Crossplot illustrating poor correlation or covariation between $\delta^{13}\text{C}$ and $\delta^{18}\text{O}$ values for the micrite and dolomicrite samples.	177
5.4.	Comparison of carbon and oxygen isotope compositions of matrix samples and individual diagenetic phases.	180
5.5.	Positive carbon excursions documented for several time-equivalent Upper Cambrian sedimentary successions.	182
5.6.	The Upper Cambrian stratigraphy of the southern Appalachians of northeastern Tennessee in relation to established Cambrian stratigraphy and biostratigraphy.	186
5.7.	A range of $\delta^{13}\text{C}$ values for various lithofacies studied.	194
5.8.	Paleogeographic reconstruction for the: A) Late Cambrian; and B) the Latest Ordovician.	210
6.1.	Photographs and photomicrographs illustrating different microbial deposits.	218

6.2.	Photographs and photomicrographs illustrating different microbial deposits.	220
6.3.	Schematic illustration of mechanisms responsible for the formation of microbial deposits using filamentous cyanobacteria as an example.	222
6.4.	Interpretation of the environments of deposition.	228
A.1.	Stratigraphic column measured at the Thorn Hill outcrop.	285
A.2.	Stratigraphic column measured at the River Ridge outcrop.	301
A.3.	Stratigraphic column measured at the Tazewell outcrop.	313
A.4.	Stratigraphic column measured at the Flat Gap outcrop.	324
A.5.	Stratigraphic column measured at the Lee Valley outcrop.	337

CHAPTER 1

INTRODUCTION

The Upper Cambrian carbonate strata of the southern Appalachians are a part of a thick sedimentary succession deposited on the lower Paleozoic passive margin of eastern North America. This passive margin formed by rifting of a supercontinent in the Late Proterozoic and Early Cambrian (Bond et al. 1984). Following rifting, sedimentary basins characterized by the deposition of sediments derived from the craton formed along the margin. The Conasauga intrashelf basin was one such depocenter that was, during the Middle and early Late Cambrian, separated from the Iapetus Ocean to the east by a broad carbonate platform (Fig. 1.1). A complex interplay between siliciclastic deposition, characteristic of the deeper intrashelf basin, and carbonate-platform deposition resulted in the formation of alternating shale and carbonate units of the Middle and Upper Cambrian Conasauga Group (Fig. 1.2). This distinct pattern of deposition is commonly referred to as Grand Cycles. The Conasauga Grand Cycles are interpreted as third-order depositional sequences of Vail et al. (1977), reflecting shallowing-upward from the basinal shales into platform carbonates (Kozar et al. 1990; Srinivasan and Walker 1993). These sequences are bounded by subaerial exposure surfaces and/or drowning unconformities. Cessation of Grand Cycle deposition in the southern Appalachians is marked by the progradation of the carbonate platform in a cratonward direction over the Conasauga basin, which consequently ceased to exist. The thick peritidal carbonate succession of the Upper Cambrian to Lower Ordovician Knox Group overlies the Conasauga Group. The deposits of the Conasauga and the Knox Groups represent deposition within the two apparently different depositional regimes on the passive margin. The transition between these two distinct sedimentary successions is marked by the deposition of the uppermost carbonate

Figure 1.1. Generalized, restored paleogeography of Tennessee during the Middle and early Late Cambrian. Note the position of the carbonate platform bordered by the Conasauga intrashelf basin to the west and the Iapetus ocean to the east. Palinspastic reconstruction is based on Roeder and Whitherspoon (1978).

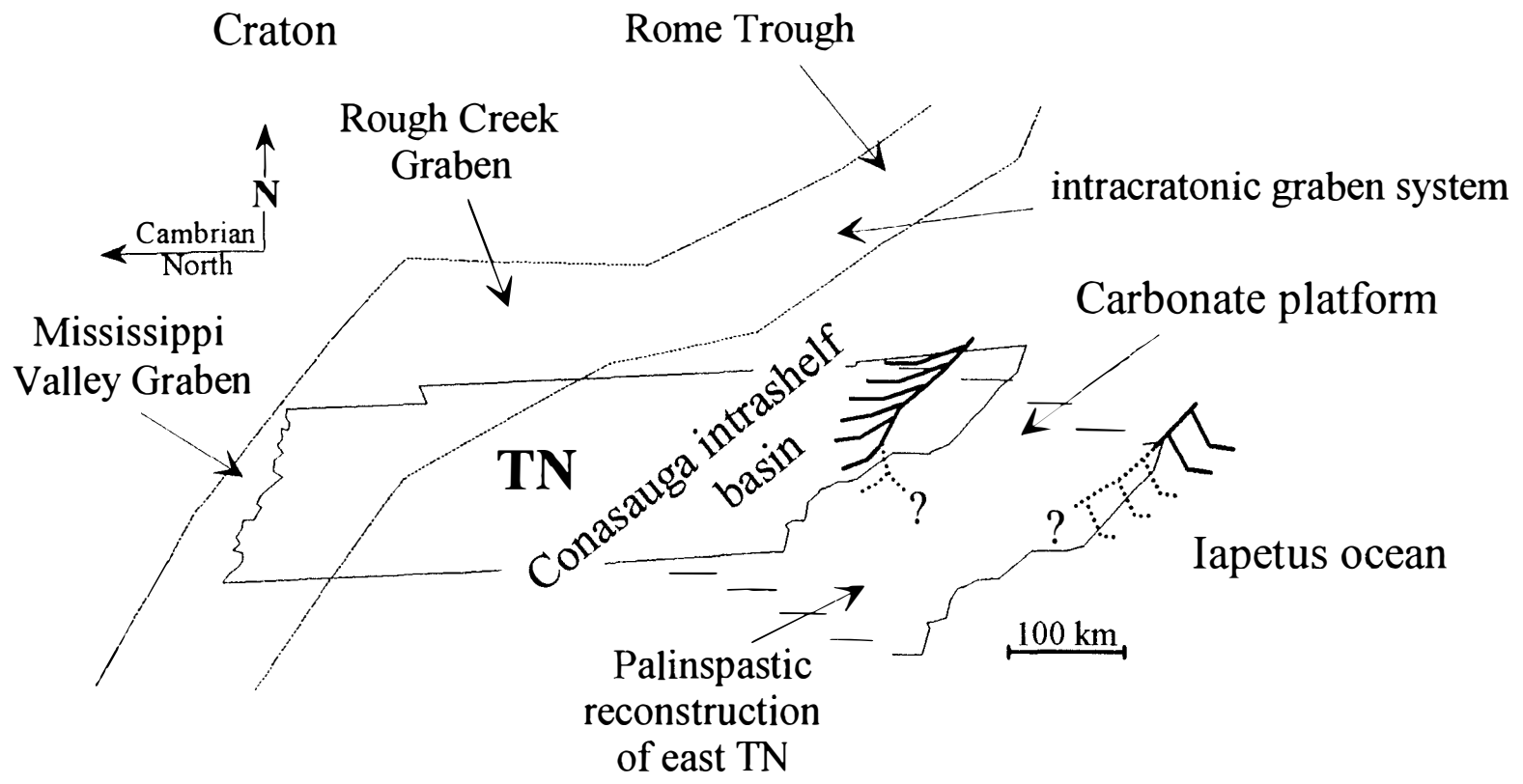
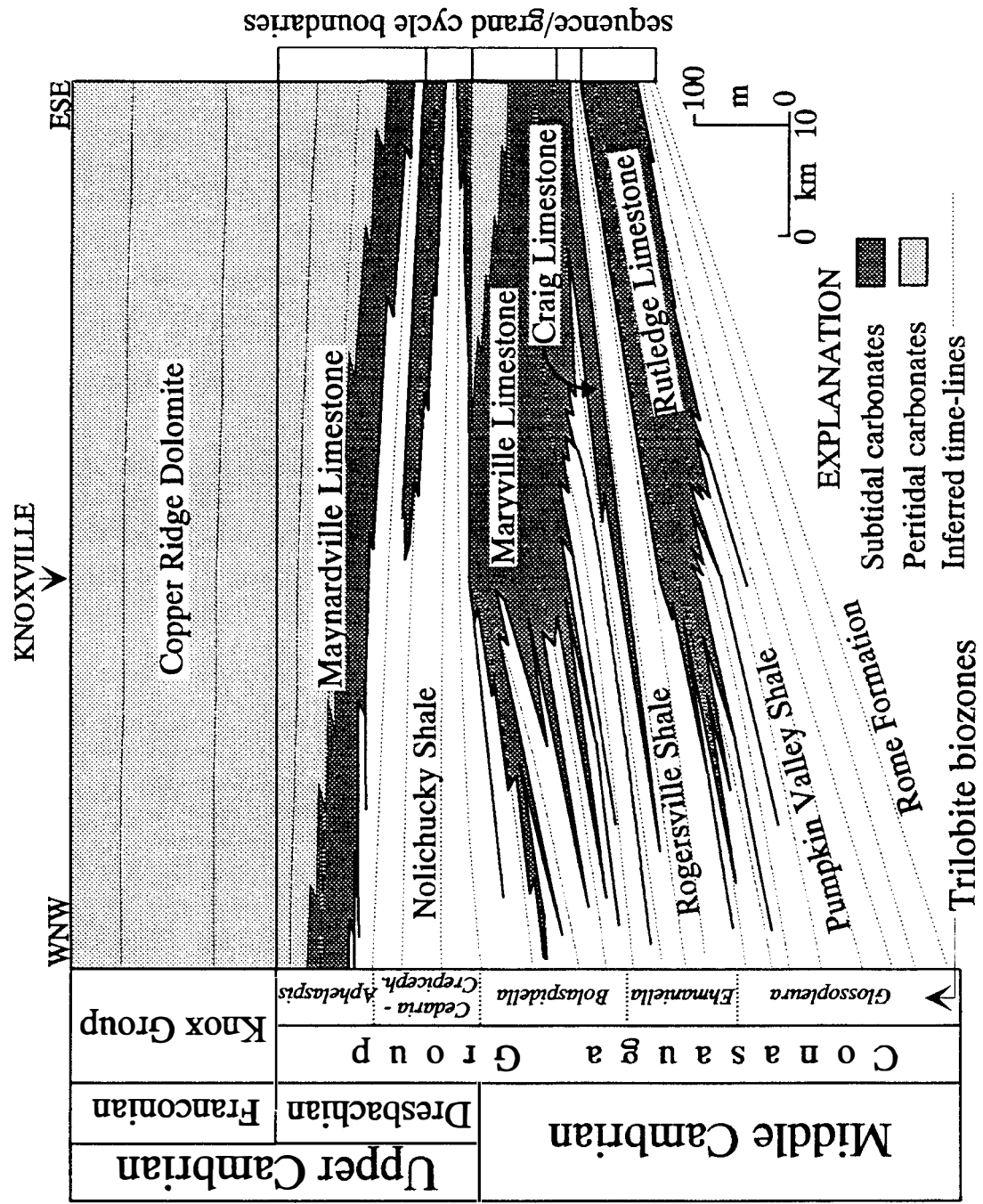


Figure 1.2. Middle to Upper Cambrian stratigraphy of eastern Tennessee. Modified from Walker et al. (1990).



unit of the Conasauga Group—the Maynardville Formation (Fig. 1.2). This transitional nature makes the Maynardville an important part of the lower Paleozoic sedimentary succession of the southern Appalachians with the potential of providing information for the interpretation of carbonate-platform depositional and diagenetic history in the framework of passive-margin evolution.

PURPOSE AND SIGNIFICANCE

In order to better understand the sedimentologic consequences of passive-margin evolution this study focuses on the Upper Cambrian Maynardville Formation (Conasauga Group), and its transition into the overlying Copper Ridge Dolomite of the Knox Group. The main objectives of this study are: 1) reconstruction of the depositional environments for the lithofacies present within the Maynardville Formation; 2) interpretation of the Upper Cambrian carbonate-platform depositional dynamics and sequence stratigraphy; 3) interpretation of passive-margin evolution based on the information inferred from the study of the sedimentary record; and 4) determination of the diagenetic history of the studied units.

The selected stratigraphic succession is of interest because a distinct change in the pattern of passive-margin sedimentation took place during deposition of this interval. This change is reflected in the termination of Grand Cycle deposition in the southern Appalachians. The rocks in the lower part of the Maynardville Formation resemble the predominately subtidal, mixed siliciclastic and carbonate (mostly limestone) deposition of the remainder of the Conasauga Group, whereas the rocks in the upper part of the Maynardville are similar to the substantially dolomitized peritidal carbonates found in the Knox Group. Unlike older carbonate formations of the Conasauga, deposition of the Maynardville was not terminated by a subaerial exposure and/or drowning event followed by the deposition of siliciclastics. The Maynardville is conformably overlain by the Copper

Ridge Dolomite of the Knox Group (Fig. 1.2). The study of sedimentary packaging, regional distribution, and the transitional nature of the Maynardville provides information for a better understanding of the processes which controlled the cessation of subtidal Grand Cycle deposition of the Conasauga Group and the transition into peritidal carbonate deposition of the Knox Group. Consequently, the results of this study aid in the interpretation of the southeastern North American continental-margin development during the Late Cambrian, and the consequences of passive-margin evolution upon the dynamics of carbonate deposition and the style of diagenetic alterations.

GEOLOGIC SETTING

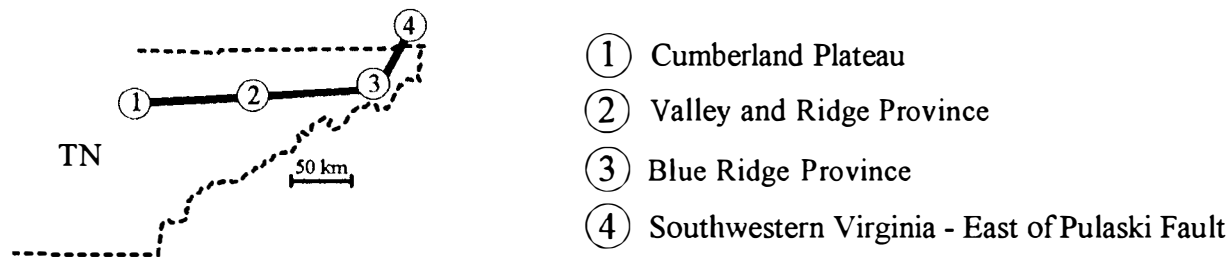
A thick lower Paleozoic sedimentary succession of the U.S. Appalachians was deposited on a passive continental margin (Rodgers 1968; Bird and Dewey 1970) that formed along eastern North American or the Laurentian continent by rifting and breakup of the supercontinent Rodinia in the Late Proterozoic to Early Cambrian (Bond et al. 1984; Hatcher 1989; Read 1989). Sediments derived from the craton were deposited in block-faulted basins along the subsiding continental margin (Thomas 1977, 1983; Hatcher 1987). The Conasauga Basin of southwestern Virginia, eastern Tennessee, and northwestern Georgia was a depocenter located between the exposed craton to the west and northwest (present-day orientation), and a broad shallow carbonate platform facing the Iapetus ocean to the east, during the Middle and early Late Cambrian (Fig. 1.1). During the Early to early Late Cambrian the Mississippi Valley-Rough Creek-Rome Trough intracratonic graben or rift system was located inland from the shelf edge (Fig. 1.1; Webb 1980; Thomas 1991, 1993). Siliciclastic material derived from the exposed craton was deposited in the Conasauga basin and the graben system possibly by large delta systems (Rankin et al. 1989). Deposition of siliciclastics during the Early and Middle Cambrian is represented by the Rome Formation and the overlying Conasauga Group

shale in the southern Appalachians (Fig. 1.3). Carbonate sedimentation was first initiated along the margin during the Early Cambrian as evidenced by the deposition of the Shady Dolomite (Fig. 1.3; Pfeil and Read 1980; Read 1989; Barnaby and Read 1990).

Sedimentation continued along this broad carbonate platform-bound passive margin during the Middle and early Late Cambrian (Rodgers 1968; Palmer 1971, Markello and Read 1981, 1982; Srinivasan 1993; Srinivasan and Walker 1993; among others). This period of sedimentation is represented by the deposits of the Conasauga Group (Figs. 1.2, 1.3). The Conasauga Group reveals three distinct phases of sedimentation: 1) dominantly dolostone in northeastern Tennessee and southwestern Virginia, represented by the Honaker and Elbrook Dolomite; 2) alternating carbonate and shale units in the central part of eastern Tennessee (the Knoxville area), where the Group is divided into six formations (in ascending stratigraphic order, see Fig. 1.2): the Pumpkin Valley Shale, the Rutledge Limestone, the Rogersville Shale, the Maryville Limestone, the Nolichucky Shale, and the Maynardville Formation; and 3) predominantly shale toward the west and southwest (Fig. 1.3; Rodgers 1953). These three phases represent deposition on a carbonate platform to the east, and in a deeper intrashelf basin, filled with siliciclastics to the west (Fig. 1.1).

The alternating shale and carbonate units of the Conasauga Group are interpreted as Grand Cycles (Aitken 1966, 1981; Palmer 1971; Koerschner and Read 1989; Srinivasan and Walker 1993; Rankey et al. 1994). Grand Cycles are recognized in the Paleozoic sedimentary successions of the southern Great Basin (Palmer and Halley 1976; Mount and Rowland 1981), the southern Canadian Rocky Mountains (Aitken 1966, 1978), and the northern Appalachians (Chow and James 1987; Cowan and James 1993). The thickness of these large-scale cycles varies from 100 to 650 m (Aitken 1981), and they can be related to the third-order sequences, which represent time periods of 1 to 10 my (Vail et al. 1977). The formation of Grand Cycles is the result of a complex interplay of different factors such as relative sea-level change (Aitken 1978; Bond et al. 1988), tectonism

Figure 1.3. Generalized stratigraphy of the Upper Proterozoic and Lower Paleozoic strata in eastern Tennessee and adjacent southwestern Virginia. Unit thickness is not to scale. Based on the COSUNA (Correlation of Stratigraphic Units of North America) chart for the southern Appalachian region (Patchen et al. 1985).



		①	②	③	④
		Knox unconformity			Beekmantown unconformity
Lower Ordovician	Knox Group	Mascot Dolomite			Beekmantown Fm.
		Kingsport Formation			
		Longview Dolomite			
		Chepultepec Dolomite			
Upper Cambrian	Knox Group	Copper Ridge Dolomite			Conococheague Fm.
		Maynardville Fm.	Maynardville Fm.		
Middle Cambrian	Conasauga Group	Nolichucky Shale			Elbrook Fm.
		Maryville Limestone			
		Conasauga Shale	Rogersville Shale	Honaker Dolomite	
		Rutledge Limestone			
		Pumpkin Valley Shale			
Lower Cambrian		Rome Formation			
	?	Shady Dolomite			
		?	Chilhowee Group		
Proterozoic				Ocoee Supergroup	?

(Rankey et al. 1994), and rate of sedimentation and sediment supply (Walker et al. 1990; Cowan and James 1993; Srinivasan and Walker 1993), superimposed on thermal post-rift subsidence.

The Conasauga Group is conformably overlain by the Cambro-Ordovician Knox Group. In eastern Tennessee the Knox Group is divided into five formations (in ascending stratigraphic order): the Copper Ridge Dolomite, the Chepultepec Dolomite, the Longview Dolomite, the Kingsport Formation, and the Mascot Dolomite (Fig. 1.3; Rodgers 1953; Bridge 1956). The Copper Ridge Dolomite represents the beginning of complete predominance of carbonate deposition over siliciclastics during the Late Cambrian and Early Ordovician that was established by progradation of shallow carbonate-shelf environments across the intrashelf basin (Read 1989; Walker et al. 1990). The shallow carbonate-platform deposition continued until the late Early Ordovician, when it was interrupted by subaerial exposure in response to the transition from passive-margin to convergent-margin setting (Benedict and Walker 1978; Shanmugam and Walker 1978, 1980; Read 1980). The regional Knox-Beekmantown unconformity, which is characterized by the development of paleokarst on top of the Lower Ordovician carbonate succession, marks the end of the first stratigraphic (Sauk) sequence in the Paleozoic history of the southern Appalachians (Fig. 1.3; Walker 1985; Read 1989).

OVERVIEW OF PREVIOUS RESEARCH

The name Maynardville Limestone for the Cambrian carbonate unit deposited on top of the Nolichucky Shale (the Conasauga Group), and overlain by the Knox Dolomite was first proposed by Oder in 1934. Prior to 1953, the Maynardville Limestone was considered a transitional unit between the Conasauga Group and the Knox Group. The "transitional" status of the Maynardville Limestone was a matter of controversy, with some authors considering the Maynardville part of the Nolichucky Shale (Rodgers and

Kent 1948; Bridge 1956), while others grouped it within the Knox Group (Ulrich 1911; Oder 1934). In 1953, Rodgers promoted the Maynardville Limestone to the uppermost formational unit of the Middle to Upper Cambrian Conasauga Group. The base of the Maynardville Formation is defined at the point in the stratigraphic section above which carbonate becomes the predominant lithologic type (Bridge 1956), or at the base of the first thick carbonate unit above the Nolichucky Shale (Tarkoy 1970; Simmons 1984; Weber 1988). The base of the Maynardville corresponds approximately with the boundary between *Crepicephalus* and *Aphelaspis* faunal zones (Derby 1965). Since only the *Aphelaspis* zone is represented in the Maynardville Formation (Derby 1965), its age is Late Dresbachian (Steptoean). The upper contact of the Maynardville is conformable and is usually recognized during field mapping by the first appearance of abundant chert within the Knox Group (Bridge 1956). Different criteria, however, have been suggested for the placement of the upper boundary of the Maynardville, such as: 1) "two feet of dark-gray, shaly dolomite" (Oder 1934); 2) "a thin shale parting" (Bridge 1956); 3) the base of the first massive, more coarsely crystalline dolomite of the Knox Group (Bridge 1956; Milici 1973); or 4) the appearance of a thin quartz sandstone (Finlayson et al. 1965; Oder and Milici 1965). The overall reported thickness of the Maynardville Formation ranges from 42 to 155 m (Hasson and Haase 1988). In the field mapping of some areas the division of the Maynardville into a lower Low Hollow Limestone Member, and an upper Chances Branch Dolomite Member (Miller and Fuller 1954) has been used (Harris 1965; Helton 1967; Harris and Mixon 1970).

Descriptions of the lithologies and fossil assemblages of the upper Conasauga Group in the southern Appalachians can be found in published geologic maps and investigative reports (Hall and Amick 1934; Rodgers and Kent 1948; King and Ferguson 1960; Oder and Bumgardner 1961; Harris 1964; Milici 1973; among others), as well as in unpublished Master's and Ph.D. theses (Raymond 1959; Helton 1967; McConnell 1967;

Tarkoy 1967; VanArsdall 1974; Weber 1988; among others). Based on the work of many authors, the generalized stratigraphy of the Conasauga Group in the Tennessee Appalachians has been established (Hasson and Haase 1988; Walker et al. 1990; Fig. 1.2).

Various depositional models have been proposed for the upper Conasauga Group in eastern Tennessee and southwestern Virginia. Milici and others (1973) interpreted the Nolichucky Shale and Maynardville Formation from central eastern Tennessee to represent deposition in a protected lagoonal environment, bounded to the east by a carbonate bank and to the west by a siliciclastic depocenter. Markello and Read (1981, 1982) recognized three depositional environments: 1) an intrashelf basin (for example, the Nolichucky Shale); 2) a gently westward-sloping carbonate ramp (Maynardville Formation); and 3) a peritidal carbonate platform (Elbrook and Honaker Formations), in the Virginia Appalachians. Weber (1988) interpreted the upper Conasauga of central eastern Tennessee as transitional between an intrashelf basin and a shallow-water carbonate platform. The Maynardville represents small tidal flats that accreted vertically and migrated laterally (Weber 1988). Koerschner and Read (1989) studied the cyclic peritidal carbonates of the Elbrook and Conococheague Formations in the Virginia Appalachians that formed on the aggraded, rimmed shelf of the passive continental margin. These formations are time-equivalents to the Conasauga Group and Copper Ridge Dolomite in Tennessee (Fig. 1.3). Osleger (1990), and Osleger and Read (1991) described the Late Cambrian peritidal cycles of Tennessee, Virginia and east Pennsylvania composed of basal ooid-intraclast grainstone lag deposits overlain by ribbon carbonates or thrombolites, and capped by mudcracked laminates. The authors interpreted these "cycles" to be a result of high-frequency eustatic sea-level oscillations.

INVESTIGATIVE METHODS

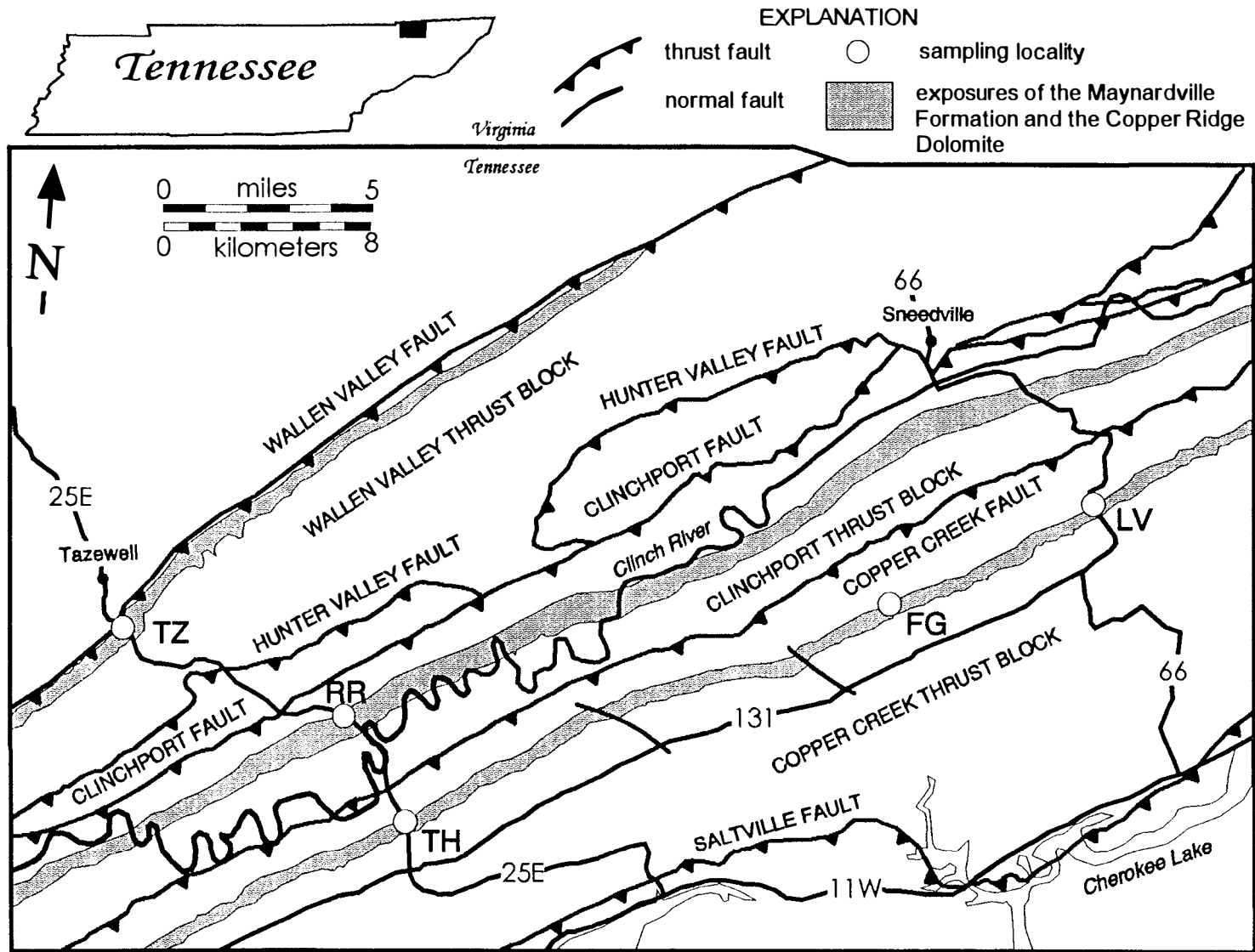
Despite the uniqueness of the Maynardville, the data on this formation from the

northeastern Tennessee Appalachians are rather scarce (Hall and Amick 1934; Rodgers and Kent 1948; Osleger and Read 1991). The present research represents the first comprehensive study of the Maynardville Formation from this part of the southern Appalachians. The investigative methods used to accomplish the research objectives include: 1) field work; 2) petrographic analysis; 3) paleoenvironmental reconstruction with interpretation of sequence stratigraphy; and 4) diagenetic study including petrographic and geochemical analyses.

Field work focused on the detailed measuring and sampling of five stratigraphic sections located within the Valley and Ridge physiographic province of northeastern Tennessee (Fig. 1.4). Detailed descriptions of measured sections are given in Appendix A. Palinspastic reconstruction of the position of the outcrops on the prograding Upper Cambrian carbonate platform reveals two distinct transects (Fig. 1.5). The transect outlined by the Tazewell-River Ridge-Thorn Hill outcrops trends northwest-southeast, and is approximately perpendicular to the reconstructed western margin of the carbonate platform facing the Conasauga intrashelf basin (Fig. 1.5). The palinspastic reconstruction by Roeder and Witherspoon (1978) was used to estimate the actual distance between the outcrops prior to thrusting. The second transect consists of the Thorn Hill-Flat Gap-Lee Valley outcrops, all of which are contained within the Copper Creek thrust sheet. This transect trends southwest-northeast and is approximately parallel to the reconstructed platform margin (Fig. 1.5).

Petrographic analysis included detailed conventional microscopy of 330 thin sections prepared from over 600 collected samples. Selected thin sections were also analyzed by using cathodoluminescence microscopy. As a result, the lithofacies present were determined and described. From the features observed, depositional environments were inferred. Stratigraphic stacking patterns were interpreted in terms of depositional sequences and sequence boundaries. In the diagenetic study, an integrated approach

Figure 1.4. A map showing location of outcrops studied. Outcrop key: TZ–Tazewell, RR–River Ridge, TH–Thorn Hill, FG–Flat Gap, and LV–Lee Valley.



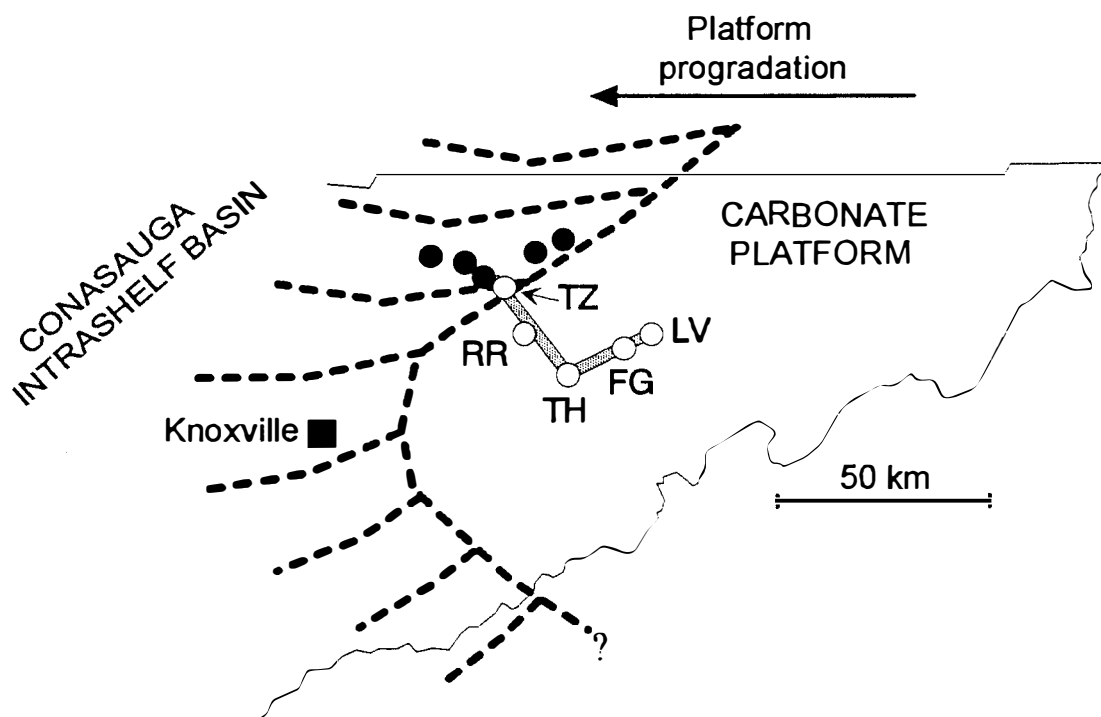


Figure 1.5. Location of outcrops along western carbonate platform-margin. Position of outcrops is palinspastically reconstructed (open circles), and shown relative to the carbonate platform-margin (dashed line), and present-day outcrop location (solid circles). Outcrop key: TZ–Tazewell, RR–River Ridge, TH–Thorn Hill, FG–Flat Gap, and LV–Lee Valley. Northwest-southeast trending transect, marked by the Tazewell–River Ridge–Thorn Hill outcrops, represents a basin-to-platform transition. The Thorn Hill–Flat Gap–Lee Valley outcrops are located more on-platform and they mark a southwest-northeast transect that runs approximately parallel to the prograding platform margin. Palinspastic reconstruction is based on Roeder and Whitherspoon (1978).

consisting of detailed petrographic analyses and geochemistry was utilized. Geochemistry involved the determination of major and trace elements, along with stable isotope (carbon and oxygen) and radiogenic strontium isotope analyses on individual depositional and diagenetic components. Details of the analytical procedures are presented in the chapters dealing with the diagenesis of the units studied. The collected data were integrated to interpret diagenetic history. Combined with the data from studies of time-equivalent units from throughout the southern Appalachians, this study broadens the regional perspective of Upper Cambrian passive-margin sedimentation along eastern North America.

DISSERTATION ORGANIZATION

Including the introductory chapter this dissertation contains seven chapters. Chapter 2 focuses on environmental interpretations for the various lithofacies present within the Maynardville Formation and the lower part of the overlying Copper Ridge Dolomite. Vertical stacking patterns and the regional distribution of lithofacies are described and interpreted in order to provide insights into carbonate-platform depositional dynamics and sequence stratigraphy. In Chapter 3, the findings from Chapter 2 are used to make interpretations for passive-margin evolution. The transition from the Conasauga into the Knox Group is related to passive-margin stabilization and a shift from an immature into a mature passive margin. The processes operating in these two different passive-margin stages and their sedimentologic consequences are discussed. Chapter 4 deals with interpretation of the diagenetic history of the deposits studied. In this Chapter the diagenesis of the subtidal deposits of the lower Maynardville is compared with that of the peritidal deposits from the upper Maynardville and the lower Copper Ridge Dolomite. A comparison is also made between the diagenetic history of the Maynardville and the older carbonate units of the Conasauga Group, as well as the upper Knox Group deposits, in order to evaluate the effect of the end of Grand Cycle deposition on the style of

diagenesis. In Chapter 5, unusual carbon isotope values of various components of the Maynardville Formation are interpreted as a large positive carbon-isotope excursion. The relationships between the excursion and Late Cambrian biostratigraphy and sequence stratigraphy are discussed, and implications are proposed for the interpretation of diagenesis. Chapter 6 explores the selective dolomitization of the microbial deposits present in the succession. The pattern of dolomitization is used as an indicator of mechanisms and environments of origin for the microbial deposits. The concluding Chapter 7 is a summary of the major findings of this study.

CHAPTER 2

CARBONATE DEPOSITIONAL DYNAMICS AND SEQUENCE STRATIGRAPHY IN THE FRAMEWORK OF GRAND CYCLE CESSATION

INTRODUCTION

Recognizing and distinguishing the influence of different mechanisms on carbonate deposition has been the matter of much debate among carbonate sedimentologists. The two main controlling mechanisms, allocyclic and autocyclic, are based upon the predominant influence of extrinsic and intrinsic factors, respectively. It is not yet certain that extrinsic controls, such as tectonic subsidence (Schlager 1981; Cloetingh et al. 1985), eustatic sea-level changes (Fischer 1964; Vail et al. 1977; Goodwin and Anderson 1985; Read et al. 1986; Goldhammer et al. 1987; among others), or clastic sediment input (Walker et al. 1983; Doyle and Roberts 1988; Budd and Harris 1990; Lomando and Harris 1991), can be distinguished from intrinsic factors, such as antecedent topography, biotic evolution, carbonate growth potential and lag time (Ginsburg 1971; Schlager 1981; Jones and Desrochers 1992), based upon signatures preserved in the rock record. The concept of an exclusive role of eustasy in controlling the succession and geometry of sequences in classical sequence stratigraphy (Vail et al. 1977; Haq et al. 1987; Van Wagoner et al. 1988) has been challenged by many authors (Watts 1982; Cloetingh et al. 1985; Miall 1986, 1992; Summerhayes 1986; Hubbard 1988; Sloss 1991; among others). It is now recognized that the development and anatomy of sequences are controlled by a complex interplay of eustasy, regional tectonics, and various sedimentologic processes, and that extrinsic and intrinsic factors act simultaneously, imposing a complex set of controlling mechanisms (Reynolds et al. 1991; Schlager 1991, 1992; Loucks and Sarg 1993; Posamentier et al. 1993; Christie-Blick and Driscoll 1995; Haq 1995).

The primary objective of this study is unraveling mechanisms that controlled the deposition of the Upper Cambrian Maynardville Formation (Conasauga Group) of the southern Appalachians. The Maynardville marks a distinct change in the pattern of lower Paleozoic passive-margin sedimentation, which is reflected in the cessation of Grand Cycle deposition. The termination of Grand Cycle deposition is recorded in the transition from the alternating shale and carbonate units or Grand Cycles of the Conasauga Group (Middle to Upper Cambrian) into the thick dolostone succession of the Knox Group (Upper Cambrian to Lower Ordovician). The advantages of studying this particular stratigraphic interval are: 1) the Maynardville Formation is a transitional unit between the Conasauga and the Knox passive-margin sedimentary successions; 2) a depositional setting, in which a carbonate platform was adjacent to a deeper-water siliciclastic basin, allows for the evaluation of the response of carbonate deposition to varying siliciclastic input; and 3) deposition in a passive-margin setting characterized by variable rates of thermal and non-thermal tectonic subsidence, and with relatively high sedimentation rates, promoting sediment loading and compaction, provides a means for examining the influence of actively changing accommodation space on sequence development.

In order to gain a better understanding of the response of a carbonate system to various mechanisms operating in the passive-margin setting, a detailed sedimentological and stratigraphic analysis of the Maynardville Formation is focused on the interpretation of carbonate depositional dynamics and sequence stratigraphy of this transitional interval. The relative importance of the controlling mechanisms is evaluated in the context of a regional tectono-sedimentary setting, sea-level fluctuations, and other paleoenvironmental changes. The main objectives of sequence stratigraphic analysis were to: 1) determine the character of transition between the underlying Nolichucky Shale and the Maynardville Formation; 2) interpret the stacking patterns of the Maynardville; and 3) characterize the transition between the Maynardville and the overlying Copper Ridge Dolomite. The lack

of widespread unconformities within the succession examined seems to preclude the first step in carbonate sequence stratigraphy, which is the division of a stratigraphic interval into unconformity-bounded sequences. The definition of sequence, however, allows for the recognition of conformable surfaces that may be laterally correlative to unconformities representing sequence boundaries. In addition, a process-oriented approach permits the recognition of a genetically related succession of strata deposited under similar environmental regimes, and separated by surfaces or intervals that represent changes in the pattern of sedimentation, including sediment input and distribution within the depositional system. The principles of "classic" sedimentologic analysis are very important in a sequence stratigraphic study of conformable successions with gradual transitions both within and between the sequences, and in the absence of abrupt breaks in the stratigraphic record (Schlager 1992).

MAYNARDVILLE LITHOFACIES

The sedimentary packaging of the Maynardville Formation lithofacies was studied at five outcrops in northeastern Tennessee (Fig. 1.4). These outcrops define two transects, one trending approximately perpendicular and the other parallel to the reconstructed western margin of the carbonate platform (Fig. 1.5). Generalized stratigraphic sections of the intervals measured are shown in Figure 2.1. A summary of lithofacies characteristics is given in Tables 2.1 and 2.2.

Lithofacies Description

The Maynardville Formation conformably overlies the Nolichucky Shale (Upper Cambrian; Figs. 1.2, 2.1). The base of the Maynardville is placed at the base of the first thick-bedded limestone unit above the Nolichucky (Fig. 2.2A). At the Tazewell outcrop the Maynardville is in thrust contact with the Middle Ordovician strata (Fig. 2.1). Due to

Figure 2.1. Stratigraphic columns of the Maynardville Formation and the lower Copper Ridge Dolomite. See Tables 2.1 and 2.2 for the explanation of the symbols. See text for interpretation of sequence stratigraphy. Key to distance between outcrops: present day/reconstructed distance. Outcrop key: TZ–Tazewell, RR–River Ridge, TH–Thorn Hill, FG–Flat Gap, and LV–Lee Valley.

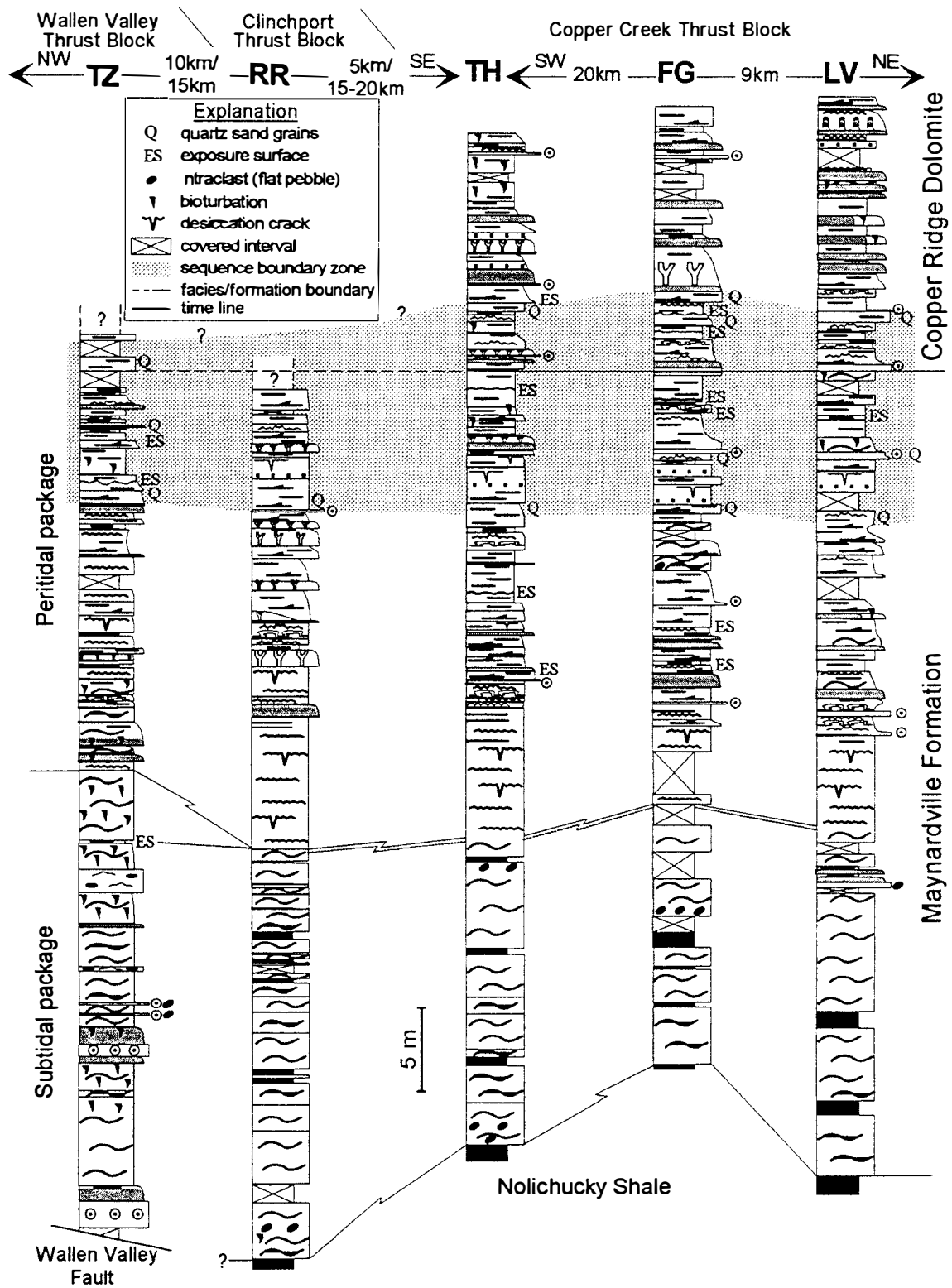


Table 2.1. Lithofacies of the subtidal package. Symbols correspond to those on Figure 2.1.





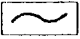

Lithofacies		Symbols and Descriptions	Environments
Thrombolites		bioherms with synoptic relief; <i>Renalcis-Epyphyton-Girvanella</i> boundstones; originate on coarse-grained intraclastic lithology (flat-pebble conglomerate); burrowed and preserved as patches of dark, dense micrite embedded in fossiliferous-peloidal wackestone/packstone; clay seams and quartz silt grains present.	Shallow subtidal patch reefs
Oolite		ooid- and/or intraclastic-ooid grainstone; cross-bedding present; rare echinoderm, trilobite and brachiopod fragments as ooid nuclei and in the matrix; micritized ooids and peloids common; intraclasts composed of burrow-mottled mudstone, peloidal packstone/grainstone, ooid grainstone, and thrombolite fragments.	Agitated shallow subtidal shoals
Fossiliferous-peloidal packstone/ grainstone		common echinoderm and trilobite fragments, intraclasts, pellets, and some ooids; horizontally and cross-laminated; intraclasts composed of mudstone, peloidal packstone, and fossiliferous wackestone; some burrows present.	Moderately agitated shallow subtidal
Ribbon rock		wavy-laminated and nodular appearance; alternating limestone and fine grained siliciclastic layers; carbonate interlayers commonly contain clay seams, quartz silt grains, and framboidal pyrite; occasional flat-pebble conglomerates; hardgrounds with pyrite crusts and coated grains present.	Protected to agitated subtidal:
		with shale carbonate interbeds alternating with siltstone and shale; carbonates commonly make fining upward sequences (skeletal grainstone→peloidal-fossil wackestone/packstone→horizontally laminated and burrowed mudstone); skeletal fragments: trilobites, articulate and inarticulate brachiopods, echinoderms.	Storm-dominated shallow ramp
		without shale carbonate interbeds alternating with argillaceous dolostone and calcareous siltstone; carbonate interbeds composed primarily of burrow-mottled mudstone or peloidal packstone.	Protected lagoon
Shale		silty shale and calcareous siltstone; with or without thin limestone interbeds compositionally similar to limestone interbeds from the ribbon rocks.	Shallow to deep ramp

Table 2.2. Lithofacies of the peritidal package. Symbols correspond to those on Figure 2.1. See Chapter 6 for more detailed description of microbial deposits.

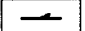
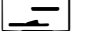
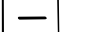
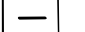




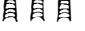
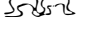



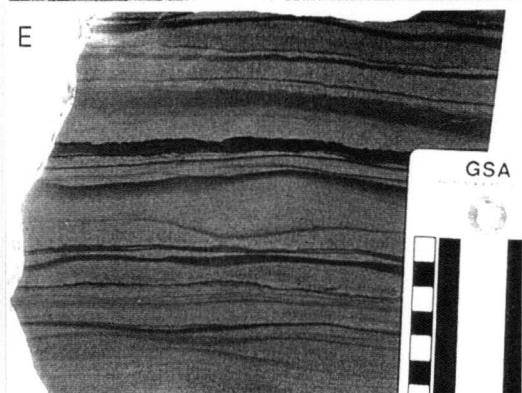
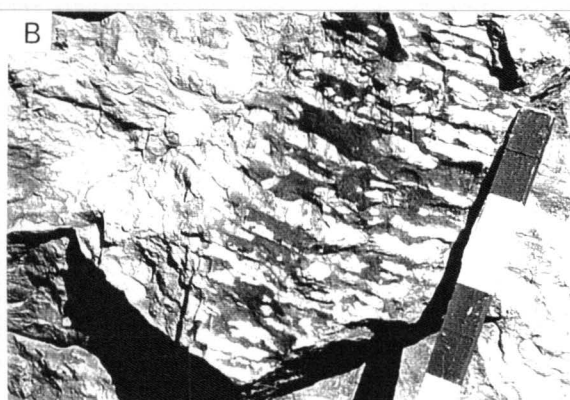
Lithofacies	Symbols and Descriptions		Environments
"Couplets"		Coarse-grained alternating "couplets" of basal coarse-grained deposit grading upward into laminated and sporadically burrowed finer-grained deposits; extensively dolomitized; common stylolites. intraclastic packstone/grainstone (+/- ooids, quartz sand and silt grains), grading upward into peloidal packstone and mudstone; "couplet" bases sharp and truncational.	Storm-, wave-, and tide-dominated semi-arid tidal flat:
		Medium-grained horizontally and cross-laminated peloidal packstone/grainstone (+/- small intraclasts, ooids, and quartz silt), grading upward into mudstone with occasional desiccation cracks; "couplet" bases wavy (truncational) to planar.	Agitated shallow subtidal to intertidal
		Fine-grained laminated dolomicrite with thin laminae or lenses of peloidal packstone at the base (starved ripple); desiccation cracks, evaporite molds, and cryptalgal laminae present in the upper part of some "couplets".	Less agitated upper intertidal to supratidal
Dolomitized mudstone		completely dolomitized micrite; some horizontal (microbial?) lamination and mottling (burrows?) present; evaporite molds common.	
Calcareous siltstone		thinly bedded; horizontally and cross-laminated micritic and peloidal deposits with abundant quartz silt; desiccation cracks common; microbial laminae and fenestrae present; interbedded with calcareous and silty shale.	Moderately agitated intertidal
Oolites		single layers of variable thickness or composite bodies made up of several ooid grainstone layers; completely dolomitized and commonly silicified; evidence for compaction and pressure solution common; ooid packstones sometimes present at bases of coarse-grained "couplets".	Small localized high energy ooid shoals
Microbial deposits		Thrombolites bioherms with clotted fabric; contain irregular to digitate and branching patches of dense micrite and scattered in fossiliferous-peloidal wackestone/packstone; some <i>Renalcis</i> (?) grains present; common burrows.	Agitated shallow subtidal
		Digitate stromatolites bioherms composed of branching columns of low relief; crudely laminated micritic pelleted fabric; columns composed of micrite with some scattered dolomite crystals; burrows present.	
		Columnar stromatolites laminated, non-linked, vertically stacked columns of cylindrical or clubbed shape; lamination is obscured by dolomitization and silicification; desiccation cracks and fenestrae present.	Agitated to protected intertidal
		SH stromatolites individual hemispheroids composed of wavy laminated micritic deposit which is entirely dolomitized and sometimes silicified; small desiccation cracks and fenestrae present.	
		LLH stromatolites low relief, linked hemispheroids containing wavy crinkly dolomicritic laminae, common desiccation cracks and fenestrae; some pellets/peloids, ooids, and burrows present.	Restricted upper intertidal and supratidal
		Microbial laminates (Stratiform stromatolites) flat, planar crinkly laminae composed of micrite, dolomicrite and dolomicrosparite; common desiccation cracks; large prism cracks; contain lenses of coarser-grained deposits containing pellets, peloids, ooids, and quartz silt grains; common fenestrae; evaporite molds and some burrows present.	
Shale		silty and calcareous shale; max. 10 cm thick; thin shale commonly occurs along prominent bedding planes.	Lag deposits

Figure 2.2. Photographs illustrating the most common Maynardville lithofacies. Intervals on Jacob's staff = 10 cm. **A)** Base of the Maynardville (arrow) is placed at the base of first thick limestone unit overlying shale of the Nolichucky Formation. **B)** Maynardville subtidal depositional package is dominated by ribbon rocks composed of light-colored limestone layers alternating with darker argillaceous layers. **C)** Gradual transition between ribbon rocks and microbial laminates marks a transition from subtidal into peritidal depositional package. **D)** Microbial laminates are characterized by crinkly, wavy lamination and prominent desiccation cracks. **E)** "Couplets" or mechanical laminates are a predominant lithofacies of the peritidal package. Note truncational bases, cross-laminated coarser-grained lower parts, and laminated mudstone tops of individual "couplets". Intervals on scale bar = 1 cm. **F)** Interbedded with "couplets" in the peritidal package are various microbial carbonate deposits such as digitate stromatolite bioherms. Photo scale is 16.5 cm long.



low resistance to weathering, thick soil cover and dense vegetation, the shale-rich deposits of the Conasauga are, in general, poorly exposed in the southern Appalachians. In the field area, poorly exposed parts of the Nolichucky are primarily composed of paper-laminated shale. The uppermost part of the Nolichucky Shale consists of calcareous and silty shale interbedded with carbonate layers, which are compositionally similar to carbonate deposits from the lower part of the overlying Maynardville.

The Maynardville Formation consists of a lower subtidal and an upper peritidal depositional package (Figs. 1.2, 2.1). The subtidal depositional package is dominated by ribbon rocks which consist of layers and lenses of limestone alternating with argillaceous dolostone, siltstone or thin shale layers (Fig. 2.2B; Table 2.1). Shale, thrombolitic bioherms, and flat-pebble conglomerate (coarse-grained intraclastic packstone/grainstone) layers occur interbedded within the ribbon rocks (Fig. 2.1). At the most basinward outcrop (Tazewell), the subtidal package also contains ooid grainstone, intraclastic-ooid grainstone and fossiliferous-peloidal packstone/grainstone deposits (Fig. 2.1; Table 2.1). Biohermal bodies characterized by thrombolitic microbial fabric are more common at Tazewell than in the subtidal packages at other outcrops (Fig. 2.1).

The transition from the subtidal to the peritidal package of the Maynardville is marked by a change from ribbon rocks into relatively thick, microbial laminates or stratiform stromatolites (Figs. 2.1, 2.2C, 2.2D). At the Tazewell outcrop, the subtidal to peritidal transition is denoted by the first occurrence of microbial laminates and by thrombolitic bodies overlain by ribbon rocks (Fig. 2.1). Overlying the transitional interval at Tazewell, and the microbial units at other localities, is a part of the peritidal package containing a variety of lithofacies, most of which are substantially dolomitized (Fig. 2.1; Table 2.2). Fining-upward centimeter-scale "couplets" or mechanical laminates make up the predominant lithofacies at this part of the peritidal package (Fig. 2.2E). A variety of "couplets" occur interbedded with dolomitized mudstone and several different types of

microbial carbonate deposits (Figs. 2.1, 2.2F; Table 2.2). The vertical stacking pattern of the peritidal lithofacies is very complex, revealing some meter-scale shallowing-upward successions composed of coarser-grained oolitic and/or intraclastic bases overlain by thrombolites, stromatolites, and/or "couplets", and capped by microbial laminates. Both prominent and more subtle subaerial exposure surfaces are present in the peritidal package (Fig. 2.1).

The peritidal package of the Maynardville grades conformably upward into the peritidal carbonate deposits of the Copper Ridge Dolomite. There is no uniform field criteria for determining the position of the upper boundary of the Maynardville (see Chapter 1). For the present study a combination of several criteria (bedding, quartz content, chert) was used for the placement of this boundary (Fig. 2.1).

Environments of Deposition

In central east Tennessee the most basinward lithofacies of the Nolichucky Shale represent deposition in slope and basinal environments reaching 250-300 m water depth (Foreman et al. 1991). The Nolichucky Shale exposed within the Copper Creek thrust sheet in east Tennessee was deposited in a moderate depth (30-50 m) to shallow-water (5-30 m) intrashelf basin setting (Weber 1988). Similarly, in southwestern Virginia the Lower and Upper Shale members of the Nolichucky represent deposition in an intrashelf basin, with the Middle Limestone member marking shoaling of the basin and the deposition of carbonates in a deeper-ramp setting (Markello and Read 1982). The upper part of the Nolichucky in the study area was deposited in a similar setting. The transition from the Nolichucky Shale to the carbonate-dominated Maynardville Formation reflects the shallowing of the Conasauga intrashelf basin, aggradation of the carbonate platform and its progradation in cratonward direction.

A generalized illustration of the depositional environments for the various

Maynardville lithofacies is shown in Figure 2.3. The occurrences of Upper Cambrian ribbon rocks are most commonly interpreted as a result of shallow subtidal deposition (Demicco 1983; Osleger and Read 1991; Chow and James 1992). The shaley, subtidal ribbon rocks of the lower part of the Maynardville Formation were deposited on a storm-dominated shallow ramp. Fining-upward carbonate layers that are interbedded with argillaceous layers were deposited as a result of storm wave and current action as evidenced by their truncational bases and skeletal lag deposits (Fig. 2.4A; see also Kriesa 1981; Markello and Read 1981). High-energy storm waves, such as those produced by hurricanes, were capable of breaking the semilithified carbonate layers into clasts, which were then redeposited forming storm-lag flat-pebble conglomerate layers interbedded within ribbon rocks (Fig. 2.4B; see Sepkoski 1982; Demicco 1985). Periods of prolonged residence of clasts on the sea floor are suggested by the presence of pyrite coatings, which are a common feature of submarine hardgrounds (Fig. 2.4B; e.g. Chow and James 1992).

The deposition of finer-grained, laminated carbonate and argillaceous layers of the ribbon rocks took place during quiet periods between major storms. Storm remobilization of the fine-grained siliciclastic sediment from the Conasauga intrashelf basin was also the important mechanism for the deposition of shale units of variable thickness present within the Maynardville Formation (Fig. 2.1). Others have reported that periods with an increased supply of siliciclastic material may be related to possible climatic changes (Read 1989; Cowan and James 1993). Some of the fine-grained siliciclastic particles within the subtidal deposits may have been transported by wind directly from the exposed craton to the west (Dalrymple et al. 1985).

The ribbon rocks containing bioturbated mudstones interbedded with calcareous siltstone and argillaceous dolostone represent deposition in a less agitated subtidal setting. This setting may have existed in the shallow subtidal lagoonal environment protected by locally developed microbial buildups and ooid shoals. This interpretation is supported by

Figure 2.3. Generalized illustration of depositional environments for the most common lithofacies present within the succession examined (not to scale). See Tables 2.1 and 2.2 for additional explanation of the symbols used.

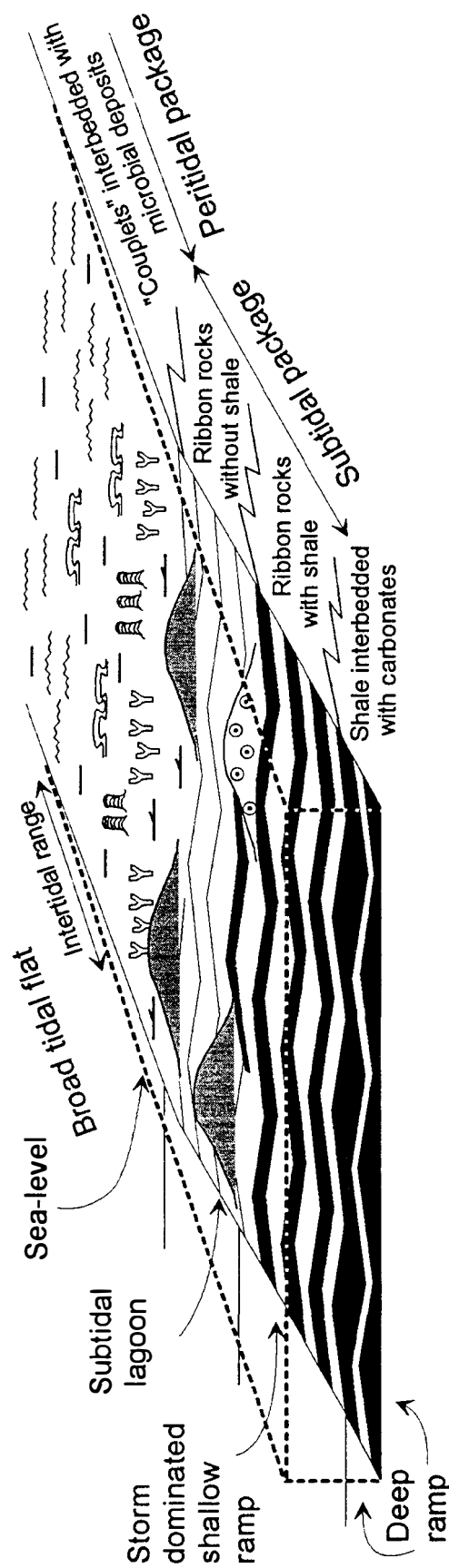
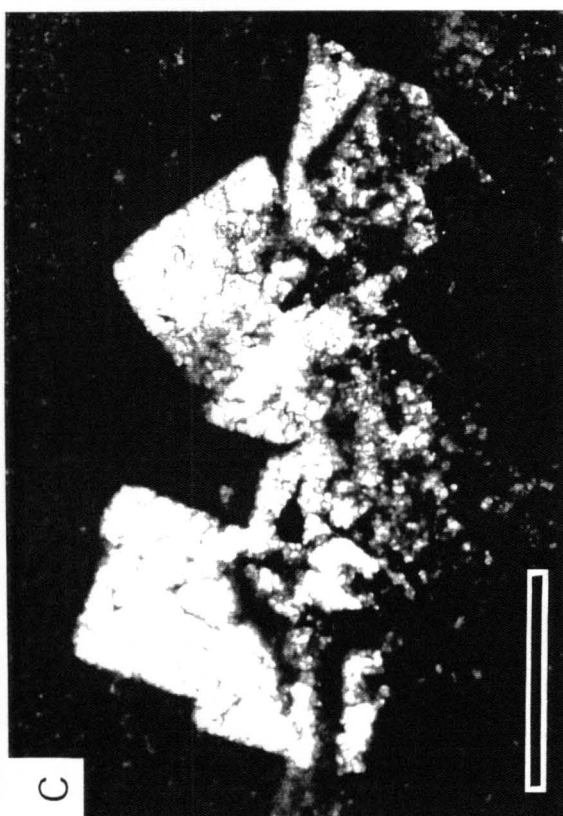
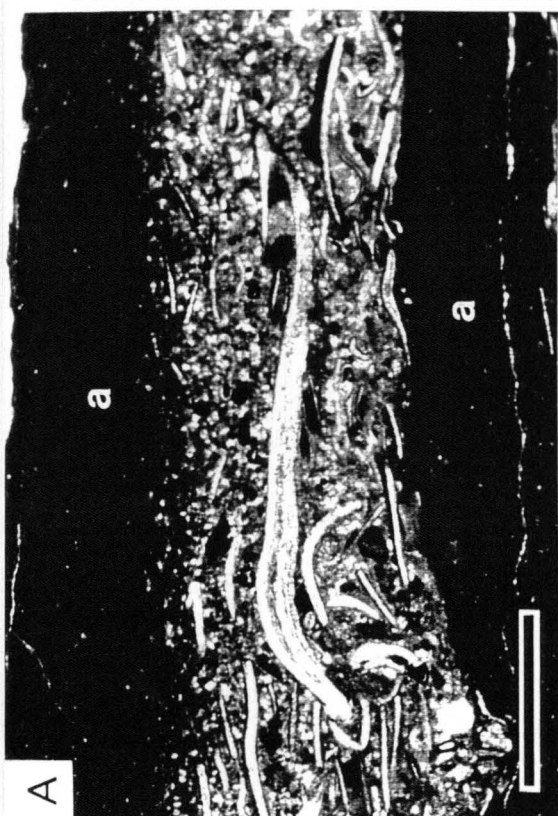
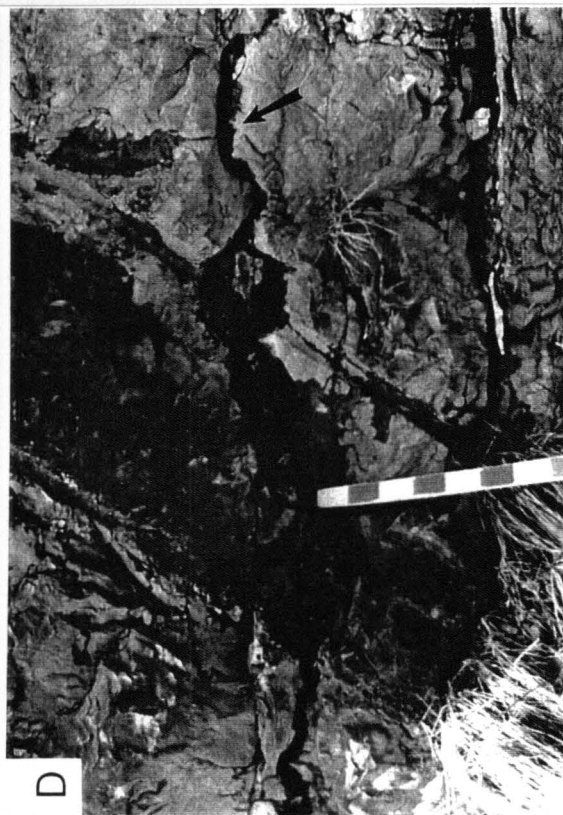
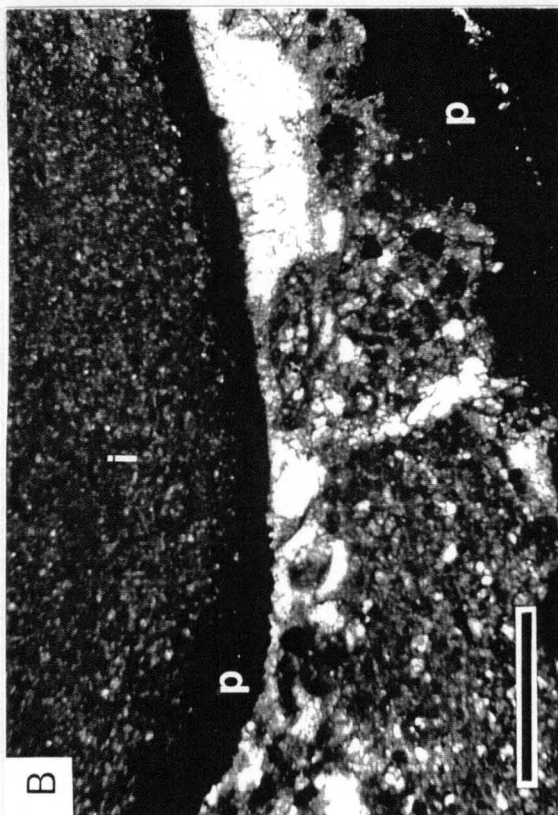


Figure 2.4. Photographs illustrating details of Maynardville lithofacies. **A)** Truncational bases and skeletal lag deposits characterize limestone layers alternating with argillaceous layers (a) within the ribbon rocks. Scale bar = 1 mm. **B)** Flat-pebble conglomerates composed of cm-scale micritic intraclasts (i) occur interbedded with the ribbon rocks in the subtidal package. Note common pyrite (p) as coatings on intraclasts and in the matrix. Scale bar = 1 mm. **C)** Evaporite molds (occluded by dolomite cement) in a completely dolomitized fine-crystalline matrix of peritidal lithofacies. Scale bar = 0.5 mm. **D)** Subaerial exposure surface (arrow) in the peritidal package characterized by erosional relief and a thin shaley condensed interval deposited prior to the reestablishment of peritidal carbonate deposition. Intervals on Jacob's scale = 10 cm.



the paucity of skeletal allochems and shale. In addition, the occurrence of thrombolites within the subtidal package reflects deposition within a shallow subtidal setting where the thrombolites were forming broad, low-relief patch reefs (Figs. 2.1, 2.3).

The transition from ribbon rocks into the microbially laminated carbonate deposits (Fig. 2.2C) represents a change from entirely subtidal into predominantly peritidal carbonate deposition in response to aggradation and shallowing of the carbonate platform. Peritidal environments encompass a variety of depositional settings on a broad tidal flat, ranging from supratidal to shallow subtidal. Evaporite molds and desiccation cracks, as evidence of increased salinity and periodic exposure, are common in some of the peritidal lithofacies (Figs. 2.2D, 2.4C). The lack of evidence for abundant evaporite deposits suggests semi-arid climatic conditions during the deposition of the Maynardville. Periods of more prolonged subaerial exposure are marked by prominent surfaces with up to 30 cm of erosional relief (Fig. 2.4D). Thin shaley layers were deposited on these surfaces as condensed intervals during the lag time following subsequent reflooding. Overlying the condensed intervals are dolomitized carbonate deposits that represent the reestablishment of peritidal sedimentation.

An array of environmental settings for the peritidal Maynardville is suggested by the diversity of lithofacies present, among which "couplets" predominate (Fig. 2.2E; Table 2.2). The coarse- to medium-grained "couplets" represent deposition in tide-, wave- and storm-dominated, shallow subtidal and intertidal settings. Truncational bases of coarser-grained "couplets", and their intraclastic lag deposits, are indicative of storm activity. Storms may have also been responsible for the reworking of ooids forming on small, locally developed, high-energy shoals (Fig. 2.3). The ooids were redeposited and incorporated in the bases of some of the "couplets" or scattered in the muddy matrix of other lithofacies. The effect of wave and tidal currents is reflected in the rounding of micritic clasts and in the trough-, hummocky-, and wave-ripple (including starved ripples)

cross-stratification of the peloidal sediment comprising coarse- and medium-grained "couplets" (Fig. 2.2E). Similar sedimentary structures are present within the calcareous siltstones from the peritidal Maynardville, suggesting deposition in a moderately agitated intertidal setting. This interpretation also accounts for the presence of desiccation cracks and microbial laminae. An intertidal setting is likewise proposed for the medium-grained "couplets" from the Maynardville based on their similarity with peloidal silt and carbonate mud deposited by storm and tidal currents in a modern intertidal setting in the Bahamas (Hardie and Ginsburg 1977). The fine-grained "couplets" and dolomitized mudstone were deposited on the upper intertidal to supratidal muddy flats of the Maynardville platform. This interpretation is substantiated by the presence of desiccation cracks, evaporite molds, and extensive early diagenetic (penecontemporaneous) dolomitization (Fig. 2.4C).

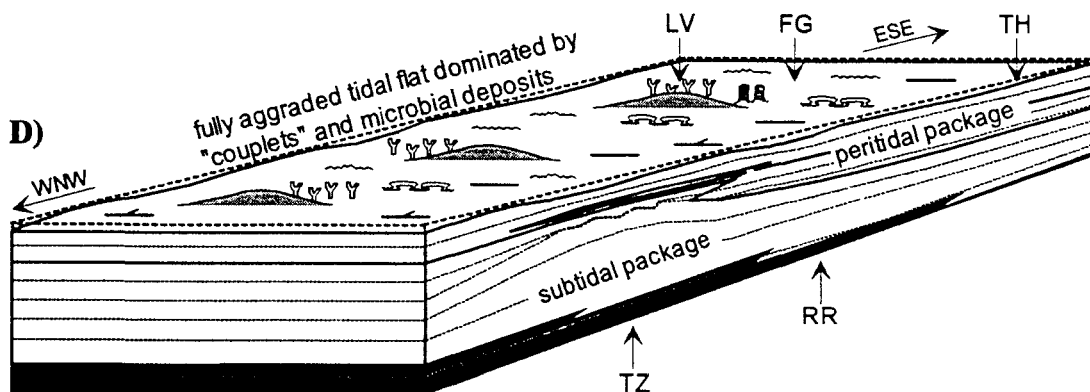
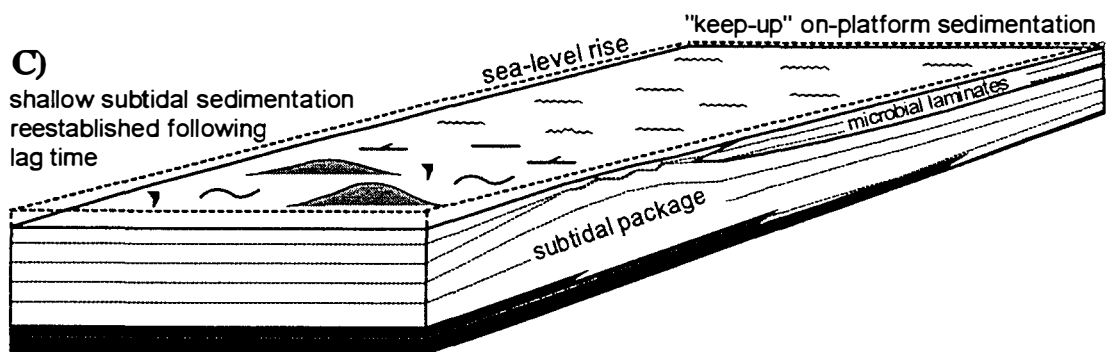
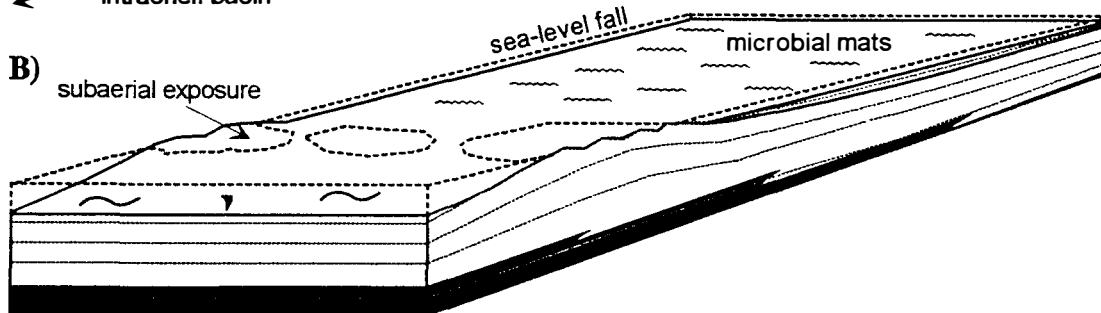
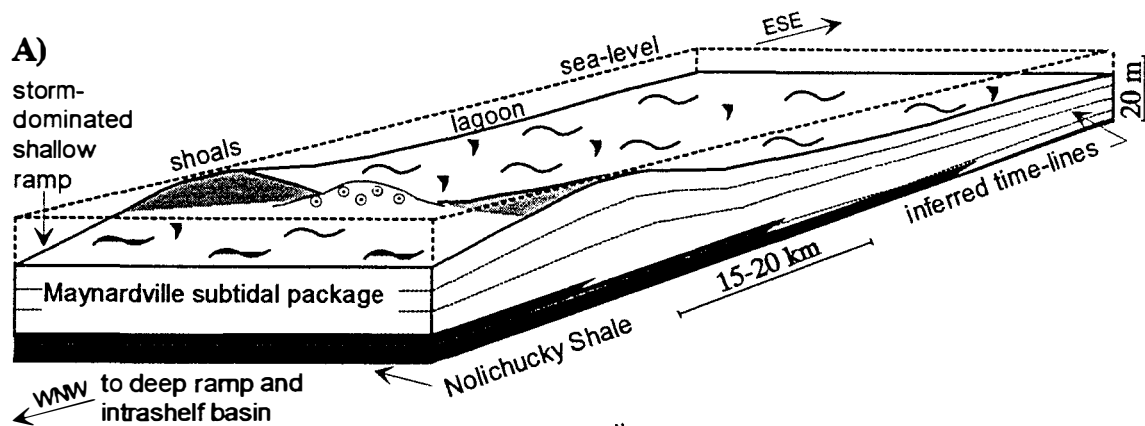
Thrombolites and digitate stromatolites are generally the only two lithofacies from the peritidal package that have not been completely dolomitized. The susceptibility of these deposits to early dolomitization may have been reduced by microbial calcification in a shallow subtidal to lower intertidal environment (see also Chapter 6). This environmental setting is supported by the presence of thrombolites within the subtidal package, and by the association with coarse- and medium-grained peritidal "couplets". The succession from thrombolites, digitate stromatolites, columnar stromatolites, stacked hemispheroidal (SH) stromatolites, and laterally linked hemispheroidal (LLH) stromatolites, to microbial laminates or stratiform stromatolites, represents decreasing water turbulence from a subtidal to a supratidal depositional environment (Logan et al. 1964; Aitken 1967; Chafetz 1973; see also Chapter 6). The entire succession was never observed in the field, and is inferred from the vertical stacking of two to as many as four different types of microbial deposits. Microbial laminates, LLH, SH, and columnar stromatolites formed primarily by sediment trapping in environments ranging from supratidal to lower intertidal. This interpretation is supported by the association with fine-

to medium-grained "couplets", and the presence of desiccation cracks, fenestrae, and evaporite pseudomorphs. These microbial deposits have experienced extensive penecontemporaneous dolomitization.

CARBONATE PLATFORM DEPOSITIONAL DYNAMICS

The vertical stacking pattern of the Maynardville lithofacies reveals the changing style of the carbonate deposition from subtidal into peritidal depositional regime, and implies shallowing upward of the carbonate platform (Fig. 2.1). The lateral lithofacies distribution reflects platform progradation in a westward direction across the Conasauga intrashelf basin (Figs. 1.2, 1.5). A model for the deposition of the Maynardville Formation in the study area is shown in Figure 2.5. The subtidal package of the Maynardville was deposited on a ramp to a lagoonal setting protected by locally developed shoals, as evidenced by the presence of oolites, microbial buildups and fossiliferous-peloidal grainstone deposits. These deposits produced a slightly elevated platform rim at the most basinally located Tazewell outcrop (Fig. 2.5A). The transition from subtidal into peritidal deposition was a result of platform aggradation, but was also triggered by a sea-level fall that caused the development of an irregular, erosional exposure surface on subtidal, burrow-mottled ribbon limestone at the Tazewell locality (Figs. 2.5B, 2.6). This event also caused the conversion of on-platform lagoonal areas into a wide, restricted tidal flat covered by extensive microbial mats, as evidenced by a transition from ribbon rocks into stratiform stromatolites or microbial laminates observed at other localities (Figs. 2.2C, 2.5B). Upon reflooding, on-platform deposition was able to "keep-up" with changing accommodation, as suggested by thick, uniform microbial carbonate deposits (Figs. 2.2D, 2.5C). Laminated dolomicrite, reaching a maximum thickness of 0.5 m, overlies the exposure surface at the Tazewell locality (Fig. 2.6). This unit was deposited in a very shallow intertidal to a supratidal environment established during initial reflooding. When

Figure 2.5. A model for the deposition of the Maynardville in the study area. See Tables 2.1 and 2.2 for the explanation of the lithofacies symbols. **A)** The subtidal depositional package was deposited on a shallow ramp and within a lagoonal setting protected by locally developed shoals. **B)** The transition from the subtidal into the peritidal depositional package was a result of a sea-level fall, which exposed an area along the elevated platform rim and converted on-platform lagoonal area into a tidal flat covered by extensive microbial mats. **C)** Following lag time, subtidal deposition was reestablished on the former platform rim during a sea-level rise. On-platform deposition kept pace with changing accommodation space and a resulting thick microbially laminated deposit formed. **D)** The upper part of the peritidal package was deposited on a broad, aggraded, semi-arid tidal flat dominated by "couplets" or mechanical laminates and diverse microbial deposits, which formed in a variety of environments, ranging from shallow subtidal to supratidal. Note the approximate position of the outcrops studied.



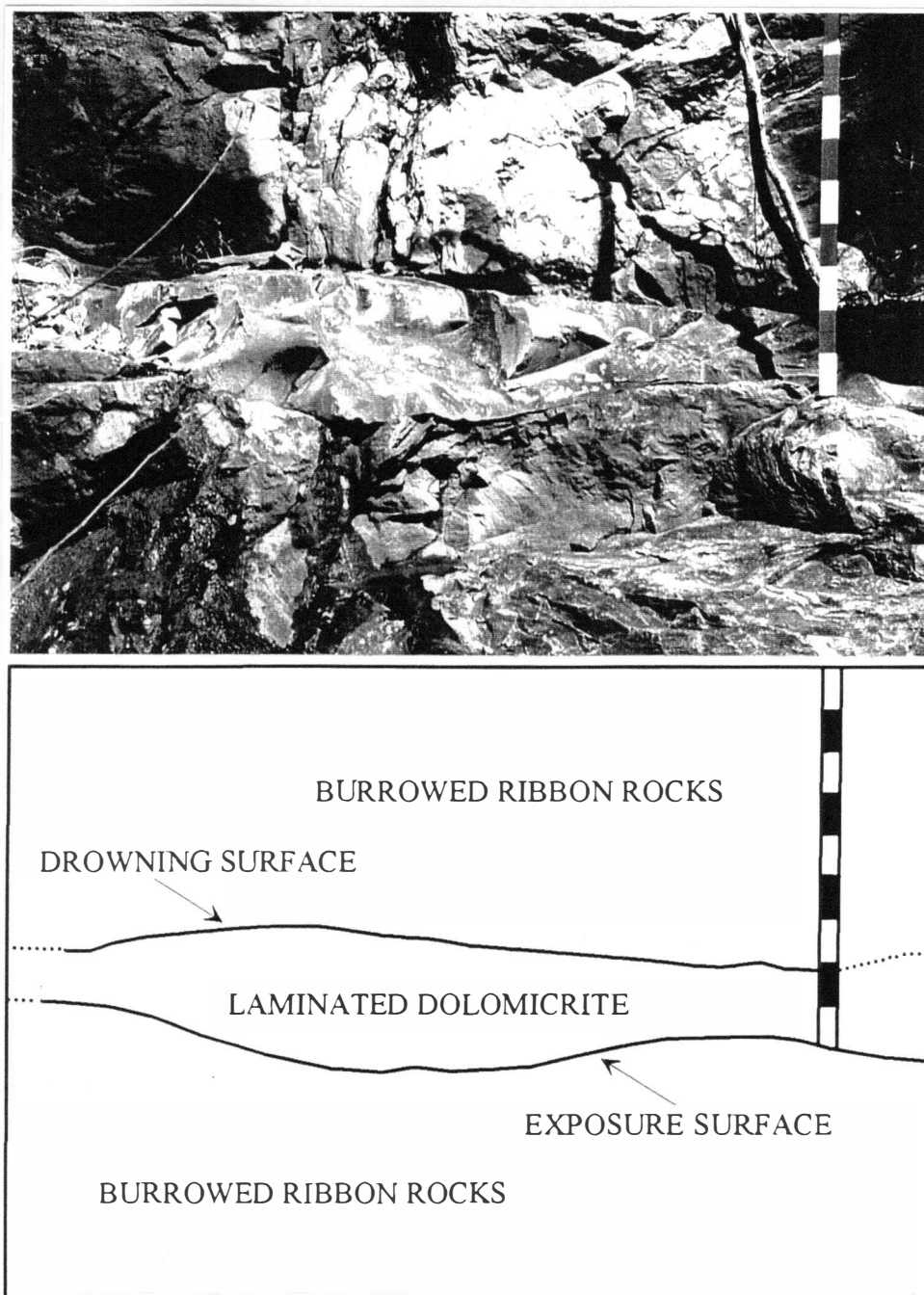


Figure 2.6. Outcrop photograph, with accompanying explanation, for the exposure surface and drowning interval within the subtidal package at the Tazewell outcrop. Intervals on Jacob's scale = 10 cm.

the rate of relative sea-level rise outpaced the rate of carbonate production, a sharp truncational drowning surface formed on top of the dolomicritic unit (Fig. 2.6). Following lag time, subtidal depositional regime was reestablished in this area as evidenced by the overlying subtidal, burrow-mottled ribbon limestone (Figs. 2.5C, 2.6). Thrombolitic bioherms and other shallow subtidal peritidal lithofacies overlie the subtidal package at the Tazewell locality, causing aggradation and allowing progradation of microbial deposits over the area (Fig. 2.1). Eventually, the entire area was converted into a fully aggraded tidal flat characterized by a variety of environments, ranging from shallow subtidal to supratidal islands (Fig. 2.5D). The conditions within these environments of deposition varied greatly, with respect to water agitation, circulation, and salinity levels, from agitated to protected, and from hypersaline and very restricted, to areas with normal or close to normal salinity. This is substantiated by a variety of deposited peritidal lithofacies (Table 2.2). A very complex vertical stacking pattern of peritidal lithofacies reflects an intricate pattern of tidal-flat facies migration, including vertical aggradation and lateral progradation.

The peritidal package of the Maynardville grades conformably into the overlying peritidal deposits of the Copper Ridge Dolomite. The lack of uniform criteria, such as a laterally extensive marker bed or other firm datum, as well as the paucity of skeletal fauna that can be used for successful biostratigraphic determination, all preclude the determination of the precise position of the Maynardville/Copper Ridge transition in the stratigraphic succession. The transition is contained within a relatively conformable interval that contains common detrital quartz and feldspar sand grains (Figs. 2.1, 2.7). The deposition of this interval was influenced by the shallowing of the intrashelf basin, in addition to an increasing input of cratonically-derived sediments. These conditions were established during the well-documented, craton-wide Dresbachian/Franconian unconformity (Lochman-Balk 1971; Palmer 1971, 1981b; Osleger and Read 1993). The

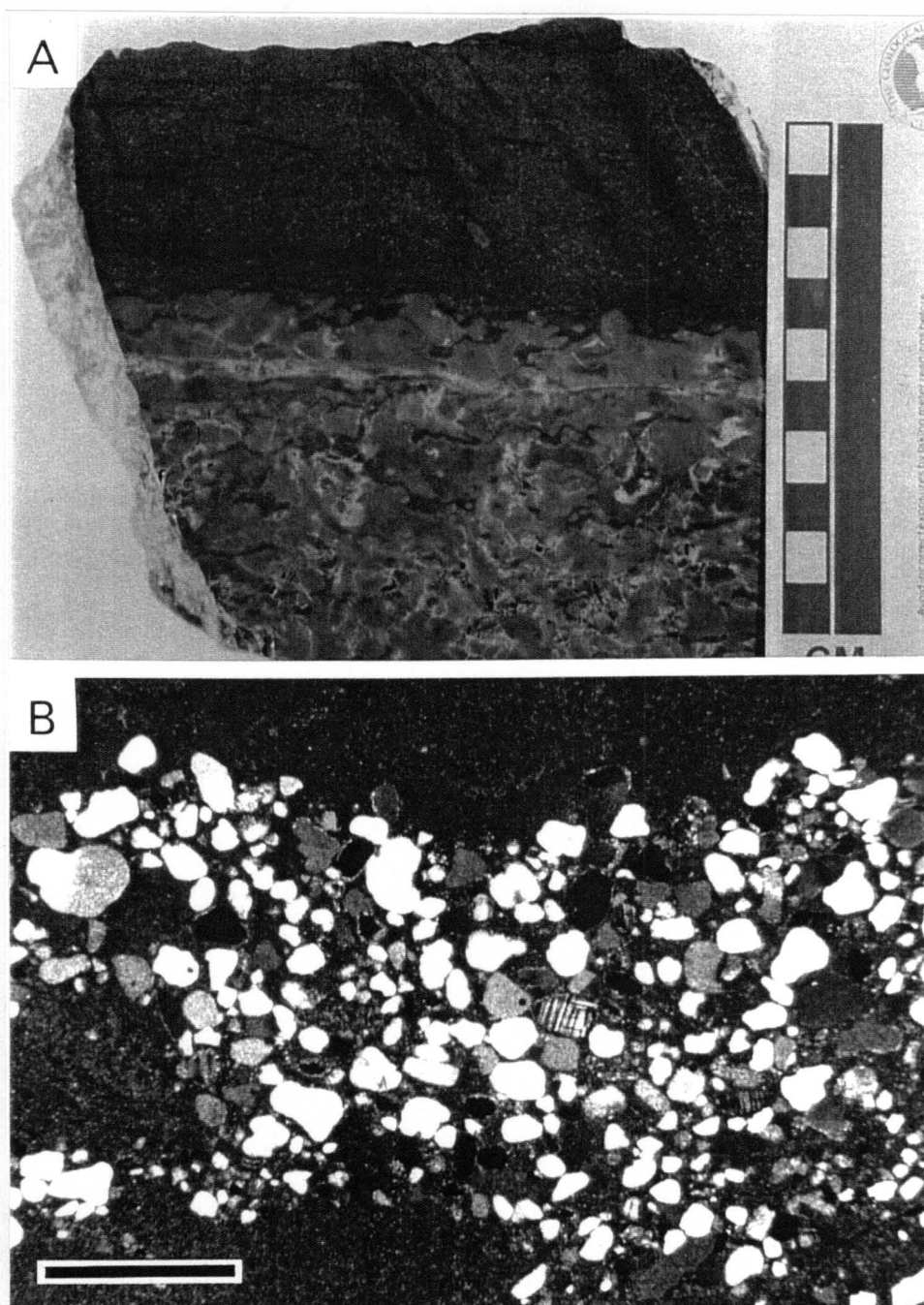


Figure 2.7. Occurrence of detrital quartz and feldspar sand grains marks the sequence boundary zone represented by a conformable interval correlative with the Dresbachian/Franconian unconformity. **A)** Hand sample showing a darker layer with abundant sand grains overlying mottled dolomicrite. Intervals on scale bar = 1 cm. **B)** Photomicrograph of a lens with common quartz and occasional microcline grains. Scale bar = 1 mm.

deposition of the Copper Ridge Dolomite of the Knox Group marks the predominance of peritidal carbonate deposition in the study area.

SEQUENCE STRATIGRAPHY

Nolichucky/Maynardville Transition

The Grand Cycles of the Conasauga Group have been interpreted as third-order depositional sequences composed of a lower shale half-cycle and an upper carbonate half-cycle (Fig. 1.2; Kozar et al. 1990; Srinivasan and Walker 1993). The termination of carbonate platform deposition by subaerial exposure and drowning, followed by an abrupt onlap of basinal shales, produced sequence boundaries at the end of each Grand Cycle (Srinivasan and Walker 1993). The deposition of shale half-cycles resulted from the migration of deep water siliciclastic depositional environments towards the carbonate platform as a consequence of an increased rate of sea-level rise (Srinivasan and Walker 1993).

The Nolichucky Shale consists of the Lower and Upper Shale Members and the Middle Limestone Member (Fig. 1.2). The Lower Shale Member onlaps on the Middle Cambrian Maryville Limestone, thus marking a sequence boundary on top of the upper Rogersville Shale/Maryville Limestone Grand Cycle (Fig. 1.2; see also Srinivasan and Walker 1993). In a similar way, the onlap of the Upper Shale Member of the Nolichucky Shale on the carbonate deposits of the Middle Limestone Member is interpreted as a sequence boundary on top of the sequence composed of the Lower Shale/Middle Limestone Members of the Nolichucky (Fig. 1.2). The deposition of the Upper Shale Member of the Nolichucky represents a retrogradational depositional package deposited in response to deepening that indicates an increase in the rate of sea-level rise. Retrogradational stacking patterns are a common characteristic of transgressive depositional conditions and are an important part of transgressive system tracts (e.g. Van

Wagoner et al. 1988).

A shift from shale- to carbonate-dominated deposition within Grand Cycles does not represent a sequence boundary. The transition between the Nolichucky Shale and the Maynardville subtidal depositional package is gradational, and it corresponds to the period of maximum flooding of the carbonate platform during the early Late Cambrian (see Bond et al. 1988). This is also substantiated by the presence of common hardground surfaces observed in the upper part of the Nolichucky and the lower Maynardville in the study area. The Nolichucky/Maynardville transition represents a change from retrogradational into aggradational-to-progradational stacking patterns as a result of a decrease in the rate of relative sea-level rise.

Stacking Patterns of the Maynardville Lithofacies

The Maynardville subtidal depositional package represents the establishment of predominantly carbonate deposition following the deposition of the Nolichucky Shale (Fig. 1.2, 2.1). Following the drowning of the carbonate platform and shale onlap in response to a rapid, relative rise of sea level, carbonate deposition can be reestablished through start-up, catch-up, and keep-up phases (Kendall and Schlager 1981). Deposition of the mixed siliciclastic/carbonate deposits of the upper part of the Nolichucky Shale and the lowermost part of the Maynardville subtidal depositional package represents the start-up of carbonate platform deposition, with the rate of relative sea-level rise still exceeding the rate of carbonate sediment accumulation. This is suggested by the relatively high shale/carbonate ratio, and common hardground surfaces observed in this part of the stratigraphic succession, which is composed primarily of shale interbedded with carbonate layers (Nolichucky) and ribbon rocks interbedded with shale (Maynardville; Figs. 2.1, 2.2A, 2.3). The remainder of the subtidal package is characteristic of catch-up phase during which the carbonate accumulation rate exceeds the rate of sea-level rise and the

platform builds or aggrades to sea level. The increasing rate of carbonate production is reflected in the decreasing shale/carbonate ratio in the upper part of the subtidal deposits, which consists predominantly of shale-free ribbon rocks (Fig. 2.1, 2.2B, 2.3).

The most prominent change in the pattern of deposition within the Maynardville is the transition from the subtidal into the peritidal depositional package (Fig. 2.1). This shift occurred in response to carbonate-platform aggradation, but was also facilitated by a sea-level fall (Fig. 2.5B). In an area along the slightly elevated platform rim (the Tazewell outcrop) this event is reflected in a subaerial exposure/drowning unconformity (Figs. 2.1, 2.6). Conformable intervals correlative to this unconformity mark the transition from ribbon rocks into microbial laminates in on-platform areas (Figs. 2.1, 2.2C, 2.5B). The reestablishment of subtidal deposition, following exposure and drowning, is the reason why the transition between the subtidal and peritidal depositional package, defined on the basis of lithofacies distribution, is younger at the Tazewell locality than at the other outcrops (Fig. 2.1).

The peritidal depositional package of the Maynardville is characteristic of keep-up phase of carbonate platform deposition, with the rate of carbonate accumulation matching or exceeding the rate of relative sea-level rise. This is evidenced by the succession of carbonate deposits that are representative of shallow water deposition, and carbonate-platform progradation in a cratonward direction (Figs. 2.1, 2.3). High rates of carbonate-sediment accumulation are favored during sea-level highstands which promote carbonate production by increasing the areas with active carbonate production (carbonate factory) because of the great extent of carbonate-platform flooding (Handford and Loucks 1993; Schlager et al. 1994). The vertical stacking pattern of the Maynardville, which consists of the subtidal depositional package overlain by the peritidal package, represents an aggradational-to-progradational stacking pattern (Fig. 2.1). Such stacking patterns are typical of highstand system tracts that are deposited during decreasing rates of relative

sea-level rise, a sea-level stillstand, and during an initial relative sea-level fall (e.g. Van Wagoner et al. 1988).

The stacking pattern within the two depositional packages of the Maynardville is complex (Fig. 2.1). Certain parts of the subtidal package can be divided into meter-scale successions based on the occurrence of shale intervals (Figs. 2.1, 2.8A). The amount of shale interbedded with ribbon rocks decreases upward within some of these subtidal successions, possibly indicating a shallowing-upward trend (Fig. 2.8A). Parts of the peritidal package can be similarly divided into meter-scale shallowing-upward successions based primarily on the presence of subaerial exposure surfaces (Figs. 2.1, 2.8B). These meter-scale successions can be regarded as parasequences, possibly representing short-term eustatic sea-level oscillations (e.g. Koerschner and Read 1989; Bond et al. 1991; Osleger and Read 1991, 1993; Montañez and Osleger 1993; McLean and Mountjoy 1994; Yang et al. 1995; among others). An alternative explanation for the deposition of subtidal parasequences is changes in the supply and dispersal of siliciclastic sediment that can be caused by climatic variations, or by physiographic changes within the source area, or the basin itself. Peritidal parasequences, on the other hand, may reflect the complex pattern of random tidal flat lithofacies migration independent of periodic extrinsic mechanisms (e.g. Kozar et al. 1990; Hardie et al. 1991; Drummond and Wilkinson 1993; Wilkinson et al. 1996). The meter-scale successions of the Maynardville Formation cannot be laterally correlated between outcrops with certainty. This poor lateral correlation can be attributed to the substantial distance between outcrops and to the fact that the observed successions may not be laterally extensive. Poorly exposed sections of the outcrops additionally preclude lateral correlation. Because of these reasons, in addition to the apparent non-cyclic nature of parts of the stratigraphic succession, and possible subjectivity in determining shallowing-upward peritidal successions (see Wilkinson et al. 1996), the subdivision of the measured stratigraphic intervals in meter-scale successions and their

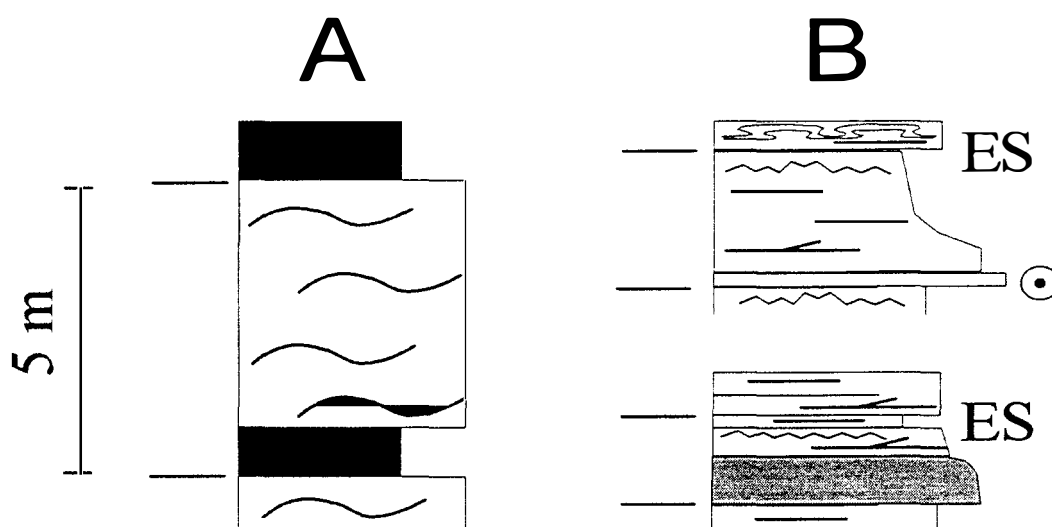


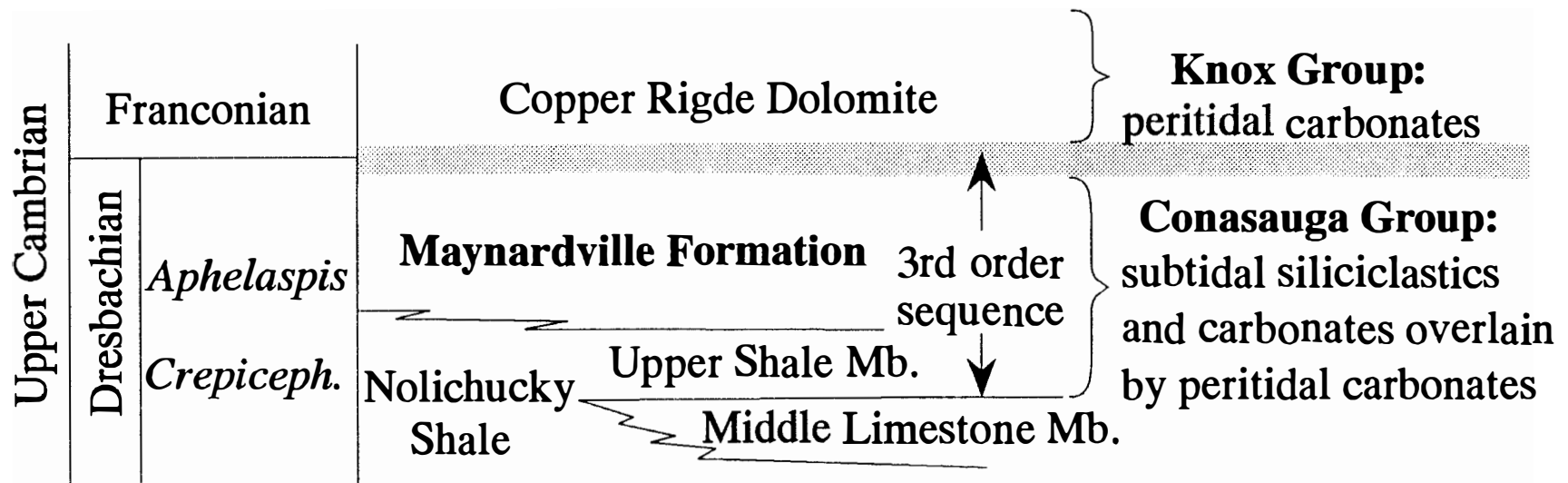
Figure 2.8. Examples of a subdivision of depositional packages in meter-scale successions or parasequences. See Figure 2.1, Tables 2.1 and 2.2 for the explanation of the symbols. **A)** Subtidal subpackages contain basal shale units overlain by shaley ribbon rocks. Upper parts of the subpackage are composed of shale-free ribbon rocks. Hardgrounds occasionally develop on top of subtidal subpackages. **B)** Peritidal subpackages have coarser-grained oolitic/intraclastic or thrombolitic bases overlain by "couplets" and microbial deposits, and capped by subaerial exposure surfaces.

lateral correlation was not attempted (Fig. 2.1).

Maynardville/Copper Ridge Transition: Termination of Grand Cycle Deposition

The transition between the peritidal package of the Maynardville and the overlying peritidal deposits of the Copper Ridge Dolomite is contained within a 10-20 m thick, relatively conformable interval characterized by the occurrence of layers with common quartz and feldspar sand grains (Figs. 2.1, 2.7). The Dresbachian/Franconian episode of sea-level lowering, subaerial exposure of the craton, and eastward migration of siliciclastic source areas affected deposition of this interval by allowing the transport of coarser-grained siliciclastic detritus onto the carbonate platform (Fig. 2.7). This sea-level fall also facilitated the complete infilling of the Conasauga intrashelf basin, which allowed carbonate-platform progradation across the former basin during a subsequent sea-level rise (Fig. 1.2). The recognition of these events, and their consequences upon the style of deposition, led to the interpretation of this conformable interval as a sequence boundary. In this study, this sequence boundary is referred to as a *sequence boundary zone* correlative to the Dresbachian/Franconian unconformity (Figs. 2.1, 2.9). The sequence boundary zone marks the end of Grand Cycle deposition in the southern Appalachians, thereby separating two distinct sedimentary successions deposited within different environmental settings: the Conasauga Group deposited on a carbonate platform laterally linked to a siliciclastic basin, and the Knox Group representing deposition on a broad carbonate platform that was established following westward progradation of the platform over the completely infilled siliciclastic basin (Fig. 2.9). The lower depositional sequence, composed of the Upper Shale Member of the Nolichucky Formation and the overlying Maynardville Formation, is interpreted as a third-order depositional sequence (Fig. 2.9). This sequence reflects a Conasauga Group style of deposition characterized by subtidal, mixed siliciclastic and carbonate deposits overlain by peritidal carbonates. The

Figure 2.9. Interpretation of sequence stratigraphy for the terminal southern Appalachian Grand Cycle. The Maynardville Formation and the underlying Upper Shale Member of the Nolichucky Shale comprise a third-order sequence. This sequence is bounded on top by a conformable interval (shaded pattern) that represents a sequence boundary zone correlative with the Dresbachian/Franconian unconformity. The sequence boundary zone separates the deposits typical of the Conasauga Group from the overlying peritidal carbonate deposits of the Knox Group.



depositional sequence overlying the sequence boundary zone is typical of Knox deposition and consists of peritidal carbonate deposits (Fig. 2.9).

DISCUSSION: CONTROLS ON CARBONATE DEPOSITION

The deposition of Cambrian Grand Cycles is most commonly attributed to eustatic sea-level changes (Aitken 1978, 1981; Palmer and Halley 1979; Palmer 1981b; Bond et al. 1988; James et al. 1989; Read 1989). Glacio-eustasy is a plausible mechanism for third-order sea-level fluctuations (Vail et al. 1977), but an unequivocal evidence for continental glaciation during the Cambrian is not present in the geological record (Hambrey and Harland 1981; Scotese and McKerrow 1990). Small-scale continental or alpine glaciations have been proposed as a possible cause for small amplitude (10-50 m) sea-level changes responsible for Grand Cycle formation (Read 1989; Osleger and Read 1993). The unsuccessful interbasinal correlation of all Cambrian Grand Cycles suggests factors beyond eustasy as controls for the formation of at least some Cycles (Palmer 1981b; Rankey et al. 1994). Kozar and others (1990) referred to mechanisms such as tectono-eustasy and geoidal eustasy, which can operate at the same time scale and may be important controlling mechanisms for Grand Cycle development. In a preliminary stratigraphic model for the Conasauga Group, developed by Walker and others (1990), the carbonates of the Rutledge, Maryville and the Maynardville were interpreted as the result of basinward progradation of a shallow-water platform, whereas the shale units of the Conasauga represent the encroachment of shale onto the platform in response to increased input of siliciclastic sediment from source regions to the west and northwest (Fig. 1.2). In this model the environmental factors, especially the suppression of carbonate production due to increased siliciclastic input, were invoked as controlling mechanisms for the deposition of the Conasauga Group depositional sequences. Rankey (1993) and Rankey and others (1994) examined the two Middle Cambrian third-order sequences of the

Conasauga: 1) the lower shale member and the Craig Limestone Member of the Rogersville Shale; 2) the upper shale member of the Rogersville and the overlying Maryville Limestone (Fig. 1.2). Their study demonstrated that carbonate-platform aggradation and progradation are the main controls on internal stratigraphic packaging within a sequence, whereas the development of sequence boundaries is controlled by the sedimentologic response to subaerial exposure and changing rates of subsidence caused by thermal cooling of the lithosphere, sediment loading, regional extension, and eustasy. Srinivasan (1993) and Srinivasan and Walker (1993) proposed the general model for the deposition of the Conasauga Grand Cycles based on a study of the Middle Cambrian Maryville Formation. The Conasauga Group reveals a cyclical pattern of development from a ramp to a carbonate platform. Gentle sloping ramps existed during the deposition of shale units, whereas the carbonate units represent the gradual establishment of a flat-topped rimmed carbonate platform as a result of aggradation and progradation in a basinward direction. Carbonate platform deposition ended by subaerial exposure and drowning events, producing surfaces recognized as sequence boundaries. Continuing subsidence, coupled with lag time on the platform, allowed basinal siliciclastic deposits to retrograde onto the platform again, thereby forming a ramp profile. The characteristic stacking patterns of the Conasauga are the result of a variable sedimentation rate, subsidence, and eustatic sea level change (Srinivasan and Walker 1993).

Comparison between the depositional models proposed for the older Conasauga sequences, especially the Maryville Formation (Srinivasan and Walker 1993; Rankey et al. 1994), and the Maynardville Formation (this study), provides important information for the changing style of passive-margin deposition from the Middle into the Late Cambrian. Even though the Maynardville at the Tazewell locality contains lithofacies indicative of platform-margin deposition, the Maynardville in the study area lacks well-developed shelf margin buildups comparable to those of the Maryville Formation (Srinivasan and Walker

1993). In addition, the Maryville contains abundant intraclastic packstone or flat-pebble conglomerate deposits interpreted as debris-flow deposits. These differences suggest that the platform-to-basin slope was gentler during deposition of the Maynardville Formation (Upper Cambrian) as opposed to the Maryville Limestone (Middle Cambrian). As a consequence, the development from a ramp to a high-relief, rimmed platform during deposition of the Maryville Formation (Middle Cambrian) was replaced in the Late Cambrian by the evolution from a gently sloping ramp, and a lagoonal subtidal environment, protected by locally developed shoals, into the broad, flat-topped tidal flat of the Maynardville platform (Fig. 2.5).

Another pronounced difference between the two Conasauga carbonate platforms is that carbonate deposition of the Maryville was terminated by subaerial exposure and a drowning unconformity, followed by deposition of a relatively thin, subtidal, backstepping package in on-platform areas, and by the Nolichucky Shale onlap (Fig. 1.2). The transition from the Maynardville into the overlying Copper Ridge Dolomite represents a conformable interval stratigraphically correlated with the Dresbachian/Franconian unconformity. The absence of a major unconformity in the southern Appalachians suggests that the rate of thermal passive-margin subsidence was higher than the rate of sea-level fall (Bond et al. 1989; Osleger and Read 1993; this study). Biostratigraphic control is insufficient to precisely determine the time interval represented by this conformable succession, which may represent a condensed interval (see also Chapter 5). The presence of *Aphelaspis* fauna verifies Dresbachian age for the Maynardville (Fig. 1.2; Resser 1938; Rasetti 1965; Derby 1965). Preserved skeletal fragments are very rare in the uppermost, highly dolomitized part of the Maynardville and in the overlying Copper Ridge Dolomite. The presence of a Franconian fauna has not yet been identified in the southern Appalachians (Fig. 1.2).

The Dresbachian/Franconian episode of sea-level lowering initiated a significant

paleogeographic change in the southern Appalachians. The complete infilling of the Conasauga intrashelf basin facilitated carbonate-platform progradation toward the craton upon subsequent reflooding (Fig. 1.5). Similar paleogeographic changes have been documented for the Great Basin area where a flood of terrigenous sediment (Warm Creek Quartzite), reflecting a brief sea-level lowering prior to *Elvinia* zone (lowermost Franconian), was followed by elimination of the Eureka-House Range embayment and establishment of carbonate sedimentation in the entire Great Basin region (Palmer 1971).

The Late Cambrian Grand Cycle cessation and establishment of peritidal carbonate deposition of the Knox Group can also be attributed to the mechanisms related to the evolution of the passive margin (see Chapter 3). The Middle Cambrian was a time interval characterized by prominent tectonic activity in southeastern North America, represented by extension and vertical readjustments along an intracratonic graben system to the west and northwest, a fault system to the south, and other basement faults to the southwest and west from the study area in eastern Tennessee (Thomas 1991). The Middle Cambrian Conasauga Group Grand Cycles were deposited under such an immature passive-margin depositional regime (Rankey et al. 1994). A shift from carbonate into shale deposition at the end of each Grand Cycle could have been related to episodic, short-term, tectonic (non-thermal) subsidence enhanced by loading and coupled with possible eustatic sea-level changes, all superimposed on thermal passive-margin subsidence. Deposition of the Maynardville Formation (Upper Cambrian) marks a transition into the mature passive-margin stage, which was characterized by the cessation of the tectonic activity along the intracratonic fault and graben systems (see Thomas 1991). This time interval is also characterized by significantly decreased rates of thermal passive-margin subsidence, coupled with a long-term eustatic sea-level fall during the Late Cambrian and Early Ordovician (Bond et al. 1988, 1989). A direct consequence of the changes in rate of passive-margin subsidence is changing accommodation space. A decrease in

accommodation space favored shallow-water carbonate deposition, which resulted in deposition of the thick (about 1000 m) peritidal succession of the upper Maynardville Formation and the overlying Knox Group.

This study demonstrates that deposition of the Maynardville Formation was influenced by numerous mechanisms, both intrinsic and extrinsic, and that these mechanisms were likely highly variable both temporally and spatially. Intrinsic properties of carbonate depositional systems that are reflected in the Maynardville packaging are, in particular, the effects of differing sedimentation rates related to the productivity of the carbonate "factory", and the effect of lag time (Fig. 2.5). The extrinsic factors affecting the Maynardville deposition were operational on various scales. The distribution of siliciclastic sediment can be attributed to local- to regional-scale mechanisms related to the depositional history of the adjacent Conasauga intrashelf basin. The history of the basin was, on the other hand, controlled by tectonic and thermal subsidence, eustatic sea-level changes, climate, and other changes (physiographic, structural) in the source area. The effects of possible local to regional tectonic events are not clearly discernible from the sedimentary record of the Maynardville. Some of the recorded events of sea-level fluctuation may be related to minor tectonic readjustments during the time period that represents cessation of tectonic activity in the area and transition into the mature or stable passive-margin depositional regime. Large-scale (passive-margin scale to global) factors substantially influenced the overall Maynardville sedimentary packaging, which represents shallowing-upward as a result of carbonate-platform aggradation and progradation facilitated by decreased rates of thermally controlled passive-margin subsidence, stabilization of the margin, infilling of the intrashelf basin, and long-term eustatic sea-level fall. The effects of short-term sea-level fluctuations are reflected in the nature of the transition between the subtidal and peritidal package and in the Maynardville/Copper Ridge transition. Meter-scale shallowing-upward peritidal successions similar to those in

the upper part of the Maynardville have been described as common in the overlying Knox Group, and are interpreted as a result of high-frequency eustatic sea-level fluctuations (Osleger 1990; Osleger and Read 1991, 1993). The formation of subaerial exposure surfaces and meter-scale Maynardville successions can be attributed to similar sea-level fluctuations coupled with mechanisms intrinsic to the carbonate depositional system, such as facies migration and lag time.

CONCLUSIONS

The termination of Grand Cycle deposition in the southern Appalachians represents a prominent change in the pattern of passive-margin sedimentation, which occurred during the deposition of the Maynardville Formation (Upper Cambrian). The Maynardville was deposited in a gently sloping, shallow subtidal ramp and lagoonal environment, protected by locally developed microbial patch reefs and ooid shoals, and laterally linked to a broad, semi-arid tidal flat characterized by an array of peritidal environments. The Maynardville represents an aggradational to progradational stacking pattern, overlying the retrogradational depositional package of the Nolichucky Shale. The transition from the Nolichucky into the Maynardville corresponds to a maximum flooding of the carbonate platform during the early Late Cambrian and a change from transgressive into highstand system tracts. The vertical stacking pattern of the Maynardville lithofacies reveals overall shallowing upward from entirely subtidal, mixed carbonate and siliciclastic deposits to predominantly peritidal dolostone deposits in response to numerous processes operating on various scales. The processes related to the evolution of the passive margin are stabilization of the margin, reflected in the cessation of tectonic activity by the early Late Cambrian, and the decreased rate of thermal subsidence, favoring both the infilling of the Conasauga siliciclastic basin and carbonate-platform progradation. The effects of eustatic sea-level changes are more easily discernible from a stabilized passive-margin

sedimentary succession, as evidenced by the transition from the Maynardville into the overlying Copper Ridge Dolomite, which is contained within a conformable interval interpreted as a sequence boundary zone correlative with the Dresbachian/Franconian unconformity. This sequence boundary separates the underlying third-order depositional sequence, which consists of the Upper Shale Member of the Nolichucky Shale and the Maynardville Formation, and represents the terminal Grand Cycle in the southern Appalachians, from the overlying Knox Group. The transition from the subtidal to peritidal depositional regime, minor subaerial exposure surfaces, as well as some of the meter-scale depositional successions within the Maynardville, may also reflect possible eustatic sea-level changes. Local- to regional-scale processes that controlled deposition of the Maynardville Formation are closely related to the intrinsic properties of the carbonate depositional system such as differing sedimentation rates, tidal flat migration, and the effect of lag time, as well as the extrinsic factors related to the history of the adjacent siliciclastic basin controlling the rate of sediment input, dispersal, and the infilling of the basin.

CHAPTER 3

SEDIMENTOLOGIC CONSEQUENCES OF PASSIVE-MARGIN EVOLUTION: TRANSITION FROM CAMBRIAN GRAND CYCLES TO MATURE PASSIVE- MARGIN DEPOSITION, SOUTHERN APPALACHIANS

INTRODUCTION

Early studies of the dynamics of passive margins focused primarily on the "crystalline crust and deeper rocks", whereas detailed studies of associated sedimentary successions played only a smaller role in deciphering the mechanisms of passive-margin evolution (Scruton 1982a). More recently, the processes operating in passive-margin depositional settings have been extensively studied and modeled based on outcrop studies of the ancient passive-margin sedimentary successions, and seismic studies of modern examples (Beaumont et al. 1982; Scruton 1982b; Bond and Kominz 1984; Bond et al. 1988, 1989; Manspeizer 1988; Sheridan and Grow 1988; Tankard and Balkwill 1989; Edwards and Santogross 1990; Meyer et al. 1991; Steckler et al. 1993; among others). Many of these studies identified carbonate platforms as a common component of a passive margin depositional setting (Read 1982). Deposition on a passive margin is strongly influenced by mechanisms such as thermal evolution of the margin, eustatic sea-level changes, and sediment supply. Therefore, the detailed study of carbonate successions may provide unique insights into these mechanisms because of the sensitivity of carbonate systems to small changes in accommodation space and other environmental conditions.

Deciphering the steps in the evolution of the Lower Paleozoic passive margin of southeastern North America has been of interest to numerous researchers (Hatcher 1989; Read 1989; Thomas 1991, 1993; Bond et al. 1984, 1988, 1989; among others). This study focuses on a part of the passive-margin sedimentary succession that contains a

record of a distinct change in the style of passive-margin sedimentation as reflected in: 1) the cessation of alternating shale and carbonate Grand Cycle deposition of the Conasauga Group (Middle to Upper Cambrian); and 2) the establishment of shallow-water, peritidal carbonate deposition of the overlying Knox Group (Upper Cambrian to Lower Ordovician) in the southern Appalachians. The primary objective of this study is to relate processes responsible for the formation of the observed sedimentary packaging to passive-margin evolution. This study is an example how a detailed sedimentologic study of a passive-margin succession, when considered in a regional context of passive-margin sedimentation, can provide insights into the relationship between sedimentologic processes and passive-margin evolution.

PASSIVE-MARGIN SETTING

The rifting and breakup of the supercontinent Rodinia in the Late Proterozoic to Early Cambrian produced a passive continental margin along eastern North American or the Laurentian continent (Bond et al. 1984; Hatcher 1989; Read 1989). The passive-margin sedimentary succession of the southern Appalachians contains rift-related volcanic rocks and clastic deposits (Upper Proterozoic Ocoee Supergroup, and the lower part of the Upper Proterozoic to Lower Cambrian Chilhowee Group), unconformably overlying the Grenville basement (Fig. 3.1; see also Rast and Kohles 1986; Hatcher 1989; Read 1989; Thomas 1991). The rift-to-drift transition occurred during the Early Cambrian as evidenced by more laterally extensive, deep to shallow marine shelf clastics in the upper part of the Chilhowee Group that were deposited in post-rift environments (Fig. 3.1; Williams and Hiscott 1987; Hatcher 1989; Simpson and Eriksson 1989). The Middle to Upper Cambrian passive-margin sedimentary record reveals the existence of a broad carbonate platform facing the Iapetus Ocean to the east, and the Conasauga intrashelf basin to the west (Fig. 1.1). The western margin of the carbonate platform was

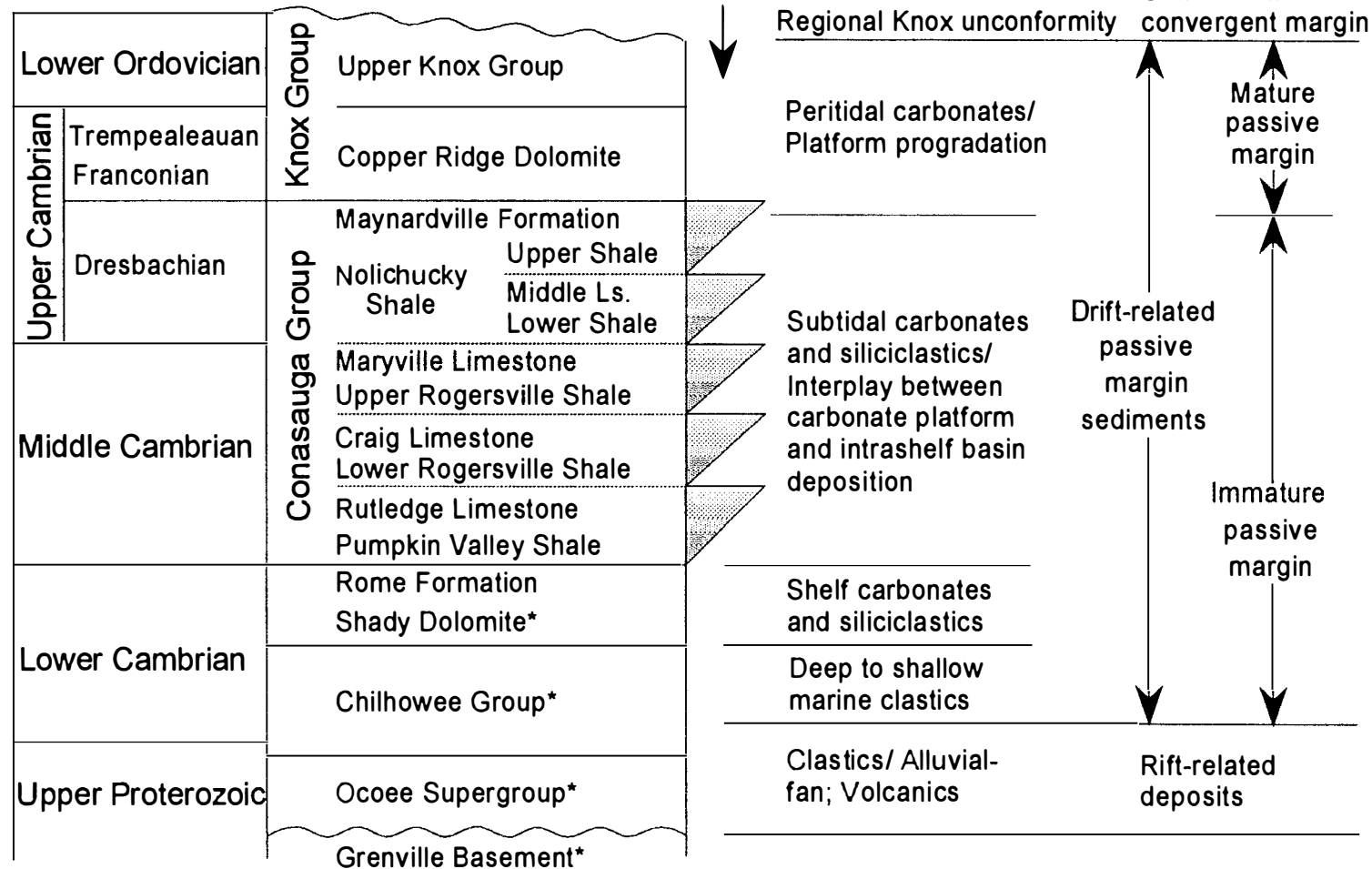
Figure 3.1. Stratigraphy of the Lower Paleozoic passive-margin succession of the Southern Appalachian Valley and Ridge physiographic province in eastern Tennessee.

**Southern Appalachian Stratigraphy,
Valley and Ridge, Eastern Tennessee:**

**Depositional
Sequences/
Grand Cycles:**

**Description/
Interpretation:**

**Passive-Margin
Evolution:**



* Not exposed in the study area

characterized by deposition of alternating shale and carbonate units, or Grand Cycles, of the Conasauga Group (Figs. 3.1, 1.1, 1.2). The Maynardville Formation is the uppermost carbonate unit of the Conasauga, and it grades conformably upward into the Copper Ridge Dolomite (Upper Cambrian) of the Knox Group (Figs. 3.1, 1.2). The Lower Paleozoic passive-margin sedimentation terminated in the early Middle Ordovician by a prolonged subaerial exposure that produced the Knox unconformity (Fig. 3.1). This event marks the transition into a convergent-margin setting (Benedict and Walker 1978; Shanmugam and Walker 1978, 1980; Mussman and Read 1986; Read 1989).

TRANSITIONAL NATURE OF THE MAYNARDVILLE FORMATION AND IMPLICATIONS FOR PASSIVE-MARGIN EVOLUTION

Unlike the older carbonate units of the Conasauga Group, deposition of the Maynardville was not terminated by subaerial exposure and/or drowning followed by siliciclastic deposition (Fig. 1.2). Instead, the transition from Conasauga-like, mixed carbonate and siliciclastic subtidal deposition of the lower Maynardville, to peritidal carbonate deposition of the upper Maynardville, and the conformable transition into the overlying Copper Ridge Dolomite (Knox Group) mark the rise to nearly complete dominance by carbonate deposition in the area (Fig. 3.1, 1.2). These differences in the sedimentation pattern can be related to the mechanisms that controlled the Middle to Late Cambrian subsidence of the southern Appalachian passive margin, and consequently influenced the sedimentary regime on the margin. The mechanisms given special attention here are eustasy, episodic non-thermal tectonic subsidence, and thermal post-rift subsidence.

Eustasy and Grand Cycle Formation

Eustatic sea-level fluctuations are commonly considered to be a primary cause for

the deposition of Grand Cycles based on their ubiquitous occurrence in the Cambrian sedimentary successions of the Appalachians, the southern Great Basin, and the southern Canadian Rocky Mountains (see Chapter 2). The cause for the third-order sea-level fluctuations, which could have been responsible for the formation of Grand Cycles, remains unclear (Read 1989). The glacio-eustatic explanations for the formation of Cambrian Grand Cycles face two major problems: 1) the Cambrian was a time interval without geological evidence for glaciation; and 2) the inability of glacio-eustasy to cause uniform sea-level changes because the magnitude and sign of the change depend on the distance from ice caps (Cloetingh 1991). Interbasinal correlation of Cambrian strata has been used to evaluate the extent of eustatic control on Grand Cycle development (Palmer 1981a; Bond et al. 1989; Osleger and Read 1993). The detailed correlation is hindered by poor biostratigraphic resolution. The correlation of depositional sequences additionally encounters the difficulties in the interpretation of stratigraphic patterns in terms of eustasy as discussed by Pitman (1978), Pitman and Golovchenko (1988), and Angevine (1989). These authors recognized that transgressive and regressive events recorded in passive-margin sedimentary successions may not be related to eustatic sea-level changes, but may instead be caused by changes in the rate of sea-level change. Additionally, the deposition of transgressive and regressive successions is commonly not synchronized with highstands and lowstands in the eustatic record (Angevine 1989). Because of these reasons, it has been recognized that, in addition to eustasy, other factors may have played an important role in the formation of the Grand Cycles (Palmer 1981a; James et al. 1989; Kozar et al. 1990; Rankey et al. 1994).

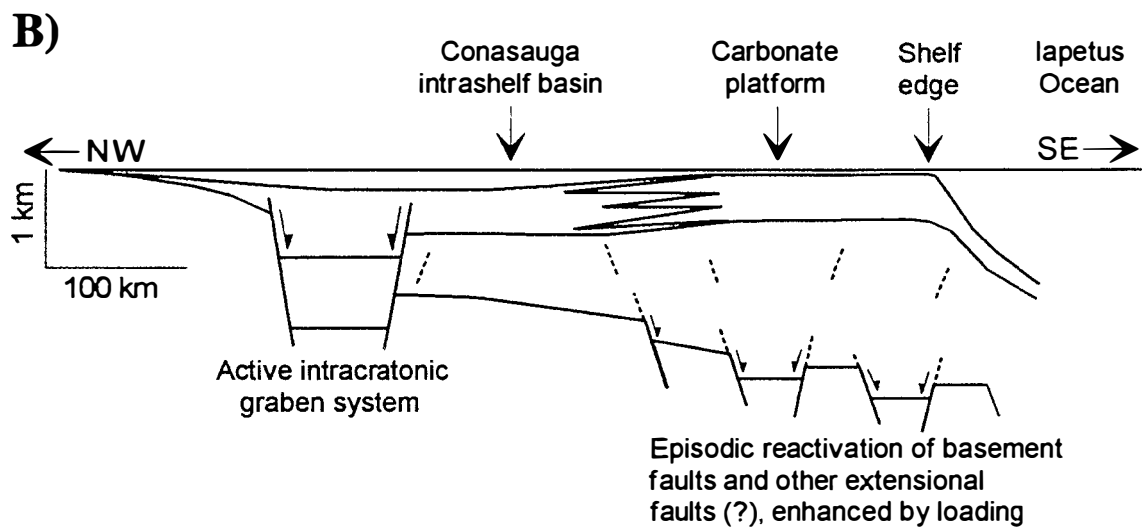
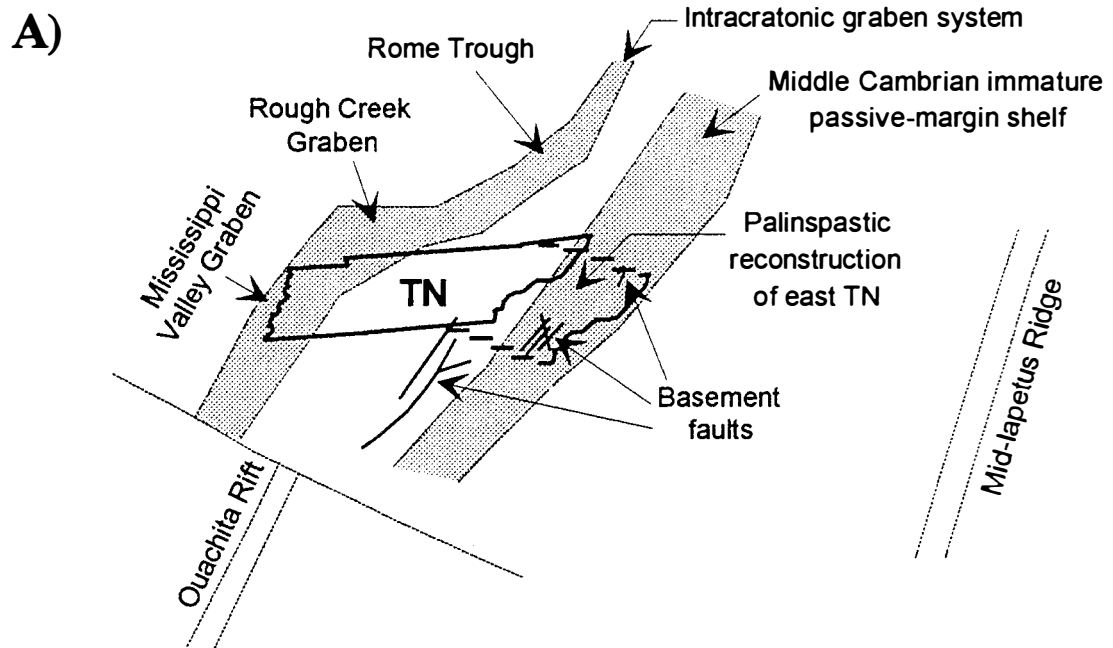
Middle Cambrian Immature Passive Margin: Role of Non-Thermal Subsidence

Detailed studies of the Conasauga Group in the southern Appalachians demonstrated that the formation of Grand Cycles was controlled by tectonism (Rankey et

al. 1994), and varying rate of sedimentation and sediment supply (Walker et al. 1990; Srinivasan and Walker 1993). Rankey and others (1994) linked the formation of Middle Cambrian Conasauga Grand Cycles to the complex evolution of the passive margin. During the Middle Cambrian, the margin was not completely stabilized and the development of depositional sequences was governed by sedimentological responses to subaerial exposure and non-thermal tectonic subsidence (Rankey et al. 1994). The Middle Cambrian was a period of pronounced tectonic activity along the Mississippi Valley-Rough Creek-Rome Trough intracratonic graben system to the west, the Birmingham fault system to the southwest, and other basement faults to the east of the study area in eastern Tennessee (Fig. 3.2A; see also Thomas 1991). The Mississippi Valley-Rough Creek-Rome Trough graben system was a site of active extension that developed about 300 km from the shelf edge (Fig. 3.2A; Webb 1980, Read 1989; Thomas 1991). Thomas (1991) documented synsedimentary fault movement during the Middle Cambrian, and infilling of the resulting grabens by the Late Cambrian, when the region around the graben became a part of a stable cratonic setting. Similarly, Early Cambrian initiation of the Birmingham basement fault system (Fig. 3.2A), and continued fault movement until the early Late Cambrian was suggested based on evidence of synsedimentary movement (Thomas 1986, 1991; Ferrill 1989). Ferrill (1989) observed that the thickness and distribution of the Conasauga Group facies in Alabama are related to separate Birmingham basement fault blocks.

Deposition of the Conasauga Group Grand Cycles took place during this immature stage of passive-margin development. Abrupt changes from carbonate- to siliciclastic-dominated deposition may represent a consequence of short-term, non-thermal, tectonic events related to episodic reactivation of extensional faults, enhanced by sediment and water loading (Fig. 3.2B). Reactivation of older faults is common during the post-rift stage of divergent plate-margin basin development (Frostick and Steel 1993a). For

Figure 3.2. Middle Cambrian immature passive-margin setting. **A)** Immature passive margin reconstruction (after Thomas 1991). Note the position of the intracratonic graben and basement fault systems. **B)** Schematic cross-section through the immature passive margin (modified after Read 1989), showing the Grand Cycles as a result of a complex interplay between Conasauga intrashelf basin deposition and carbonate platform deposition. Abrupt changes from carbonate- to siliciclastic-dominated deposition may be a consequence of short-term, episodic, non-thermal tectonic events related to vertical readjustments along extensional faults.



example, faulting in the continental basement and the overlying sedimentary succession of the Atlantic passive margin extended into the Late Cretaceous and the Eocene (Heller et al. 1982; Scruton 1982a). The disruption of planar horizons in the Atlantic passive-margin strata by faulting related exclusively to sedimentary processes was described by Pitman and Golovchenko (1988). Episodic post-rift subsidence of passive margins, caused by tectonism and amplified by loading, represents a relatively rapid subsidence superimposed on the slower thermal subsidence (Heller et al. 1982). Sediment and water loading creates passive-margin subsidence by causing lithospheric flexure, sediment compaction, and displacement along marginal faults (Watts 1981; Heller et al. 1982; Steckler and Watts 1982; Turcotte 1982; Pitman and Golovchenko 1988; Reynolds et al. 1991; Bott 1992). Consequently, tectonism and subsidence due to loading are recognized as important mechanisms controlling the development of depositional sequences (Bally 1982; Watts 1982; Watts and Thorne 1984; Cloetingh et al. 1985; Summerhayes 1986; Lambeck et al. 1987; Stephenson 1989; Embry 1989; Sloss 1991; Aubry 1991; Frostick and Steel 1993b). These mechanisms provide an alternative to primarily eustatic control on sequence development (Haq et al. 1987, 1988; Vail et al. 1977, 1987; Hallam 1984; Van Wagoner et al. 1988). "Jerky" subsidence produced by these mechanisms may have caused drowning and the "shut-down" of the Conasauga carbonate-platform production followed by basinal shale onlap (Figs. 3.2B, 1.2). In conjunction with possible eustatic sea-level fluctuations, these mechanisms created exposure surfaces/drowning unconformities on top of the Middle Cambrian Conasauga carbonate platform successions, thus producing surfaces identified as third-order sequence boundaries (Fig. 1.2; Kozar et al. 1990; Walker et al. 1990; Srinivasan and Walker 1993; Rankey et al. 1994). Thus, deposition on the Middle Cambrian immature margin was primarily controlled by episodic tectonic subsidence, sediment loading, and eustatic sea-level changes superimposed on thermal post-rift subsidence.

One criticism of these ideas was that researchers have not specifically located the extensional faults in the field and proved their synsedimentary activity. The southern Appalachian passive-margin sedimentary succession has, of course, been subjected to substantial post-depositional structural deformation. The most prominent deformation was folding and thrust faulting during the Late Paleozoic Alleghanian orogeny (Hatcher 1987, 1989). It is likely that Cambrian faults were obscured during these later tectonic events. Post-Cambrian, especially Late Paleozoic, reactivation of Cambrian faults has been documented in southeastern North America (Dever 1986; Thomas 1986, 1991; Ferrill 1989). Another argument against "jerky" subsidence, and in support of eustasy as a controlling factor for the formation of Appalachian Grand Cycles is based on the synchronicity of relative sea-level changes along the length of the passive margin, and on the restriction of major pulses of Middle Cambrian subsidence to the intracratonic graben system and the basement fault zone (Read 1989). Cloetingh (1986, 1988), however, proposed an explanation for a tectonic cause of third-order sea-level cycles deduced from passive-margin stratigraphic records. Apparent sea-level changes of up to 100 m can be caused by the interaction of intraplate-stress fluctuations and lithosphere deflection due to loading (Cloetingh 1988). Short-term sea-level variations of up to 50 m, such as those proposed for the Grand Cycles in the Appalachians (Read 1989), may be produced by intraplate-stress variations associated with local adjustments of stresses at passive margins (Cloetingh 1988). Because of the extensional regime, local fluctuations and adjustments of stresses likely occurred in southeastern North America during the Middle Cambrian, thereby providing a mechanism for tectonic sea-level change (Rankey et al. 1994).

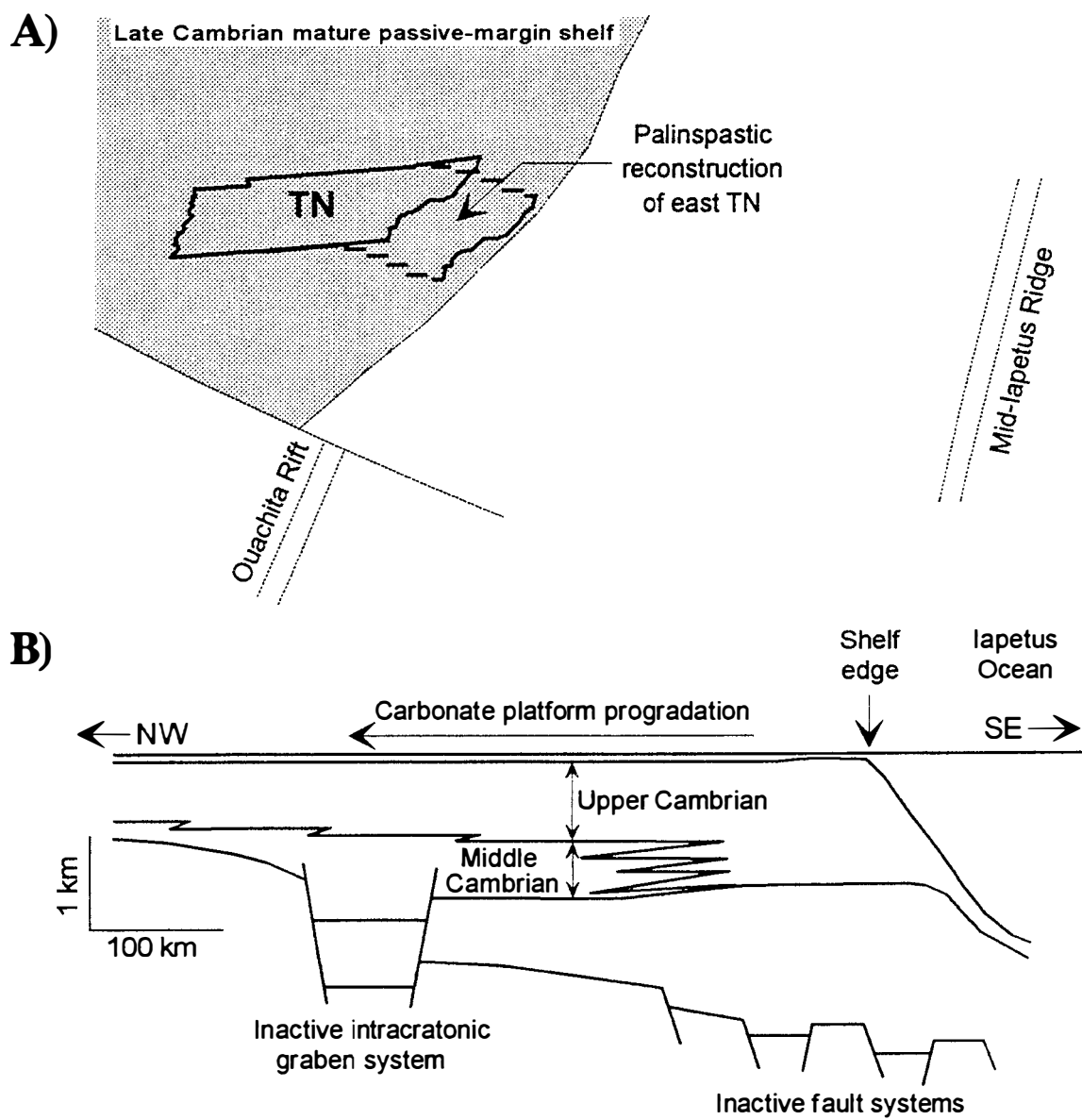
Late Cambrian Mature Passive Margin

Carbonate deposits of the Knox Group (Upper Cambrian to Lower Ordovician) extend across the intracratonic graben and basement fault systems without substantial

thickness variations indicative of synsedimentary tectonics, thus indicating that by Knox time, extension in the area had ended (Thomas 1991). Thus, the change from Conasauga Grand Cycle deposition to the thick peritidal carbonate sequence of the Knox Group is interpreted to correspond with the cessation of tectonic activity along extensional fault systems (Fig. 3.3). The stabilization of the margin and the transition from immature into mature passive margin occurred during the Late Cambrian, and is marked by the deposition of the Maynardville Formation.

The proposed cessation of tectonic activity was associated with a decrease in the rate of passive-margin subsidence. The rates of passive-margin net subsidence were determined to be high and rapidly decreasing (from 95 to 35 m/Ma) during the Middle Cambrian, and much lower and slowly decreasing (from 35 to <10 m/Ma) for the Late Cambrian and Early Ordovician based on one-dimensional modeling of early Paleozoic passive margins in the Cordillera and the Appalachians (Bond et al. 1989). The change in subsidence rate was a direct consequence of the exponential decline of thermally controlled subsidence caused by an increase in lithospheric rigidity due to crustal cooling and thickening (Watts 1982; Steckler and Watts 1982; Bond and Kominz 1984; Bond et al. 1988, 1989; Bott 1992). This change was probably coupled with long-term eustatic sea-level fall related to the subsidence of the mid-oceanic ridges with progressive cooling and consumption of ridges at subduction zones (Bond et al. 1988, 1989; Read 1989). An increase in flexural rigidity of the lithosphere can cause significant changes in passive margin stratigraphy because of the modification in the distribution of accommodation space produced by isostatic processes (Reynolds et al. 1991). Lower flexural rigidities cause vertical distribution of accommodation space favoring narrow shelves and the formation of Type 2 sequence boundaries (Reynolds et al. 1991). This was the case for the Middle Cambrian passive margin, which was characterized by an isolated carbonate platform and deposition of Conasauga Grand Cycles separated by Type 2 sequence

Figure 3.3. Late Cambrian mature passive-margin setting. **A)** Mature passive margin reconstruction (after Thomas 1991). Note the lateral expansion of the shelf, related to carbonate platform progradation. **B)** Schematic cross-section through the mature passive margin, illustrating cessation of tectonic activity and the carbonate-platform progradation.



boundaries (Kozar et al. 1990). Type 2 sequence boundaries are interpreted to form when the rate of sea-level fall is lower than the rate of basin subsidence (Van Wagoner et al. 1988). On the other hand, higher flexural rigidities promote horizontal distribution of accommodation space. This favors wide shelves and the formation of Type 1 sequence boundaries (Reynolds et al. 1991), which are interpreted to form when the rate of sea-level fall exceeds the rate of basin subsidence (Van Wagoner et al. 1988). The Maynardville Formation (Upper Cambrian) reflects shallowing-upward in response to platform aggradation, enhanced by decreased accommodation related to increased lithospheric rigidity, the absence of episodic non-thermal tectonic subsidence, and possible long-term sea-level fall. The combination of these factors resulted in a significantly lower and much more steady subsidence rate during the Late Cambrian, allowing carbonate production to keep pace more easily with changing accommodation. These conditions also favored lateral expansion of the upper Maynardville/Copper Ridge Dolomite peritidal carbonate platform by progradation towards the craton over the completely infilled intrashelf basin and inactive graben system (Fig. 3.3B). Within this peritidal carbonate succession, a Type 1 sequence boundary was recognized between the Maynardville and the Copper Ridge Dolomite, or within the basal Copper Ridge (Kozar et al. 1990; Osleger and Read 1993). The Maynardville/Copper Ridge transition is interpreted in the present study as a sequence boundary zone, contained within a relatively conformable succession, correlative to the Dresbachian/Franconian unconformity. In the absence of pronounced short-term tectonically induced subsidence, the sedimentologic consequences of this eustatic sea-level fluctuation are discernible from the sedimentary record of a stabilized or mature passive margin. The final establishment of a mature passive margin, with sedimentation controlled primarily by thermal subsidence and eustatic sea-level fluctuations, is reflected in the deposition of an approximately 1000 m thick, relatively uniform peritidal carbonate succession of the Knox Group.

Similar changes in the sedimentation patterns of other passive-margin depositional successions may represent the same sedimentologic consequences of continental-margin stabilization. Understanding the response by a sedimentary system to a set of conditions that exist during different stages in passive-margin development is a necessary step towards refinements in the reconstruction of passive-margin evolutionary histories.

CONCLUSIONS

The Middle Cambrian Grand Cycles of the Conasauga Group in the southern Appalachians were deposited during an immature passive-margin stage. This stage was characterized by episodic, non-thermal tectonic subsidence, sediment loading, and eustatic sea-level changes, superimposed on thermal post-rift passive margin subsidence. Deposition of the uppermost Conasauga carbonate unit, the Maynardville Formation (Upper Cambrian), reflects a transition from an immature into a mature stage in passive-margin evolution. Sedimentation on the mature passive margin was primarily controlled by thermal subsidence and eustatic sea-level changes. The final stabilization of the passive margin is reflected by deposition of the thick peritidal carbonates of the Knox Group (Upper Cambrian to Lower Ordovician). The presence of similar transitions in passive-margin successions elsewhere, can be the result of the same sedimentologic response to continental-margin stabilization.

CHAPTER 4

DIAGENETIC HISTORY OF A TERMINAL CAMBRIAN GRAND CYCLE CARBONATE SUCCESSION, SOUTHERN APPALACHIANS

INTRODUCTION

The termination of Grand Cycle deposition represents a prominent change in the Lower Paleozoic passive-margin sedimentation of the southern Appalachians. The deposition of the Maynardville Formation (Upper Cambrian) marks a transition between the alternating shale and carbonate units or Grand Cycles of the Conasauga Group (Middle to Upper Cambrian), and the overlying thick peritidal carbonate succession of the Knox Group (Upper Cambrian to Lower Ordovician). This Chapter presents the results of the first detailed diagenetic study of this transitional interval. The distribution and characteristics of various diagenetic and depositional components were examined in order to document the relationship between the shift in the sedimentation regime and the prominent change in the diagenetic patterns recorded within this terminal Grand Cycle carbonate succession.

The Maynardville consists of a lower subtidal depositional package and an upper peritidal depositional package (Fig. 2.1). The subtidal package contains mixed siliciclastic and carbonate deposits (predominantly limestone), and is lithologically similar to the rest of the underlying Conasauga Group deposits. Therefore, the diagenesis of the subtidal deposits of the Maynardville is compared to that of the Maryville Formation (Middle Cambrian; Srinivasan 1993; Srinivasan et al. 1994), and the Nolichucky Shale (Upper Cambrian; Foreman 1991) of the Conasauga Group. The peritidal package of the Maynardville consists primarily of extensively dolomitized carbonate deposits which are similar to the overlying Copper Ridge Dolomite and the rest of the Knox Group.

Consequently, diagenesis of the peritidal deposits of the Maynardville is compared with the results of diagenetic studies of the Upper Knox Group (Lower Ordovician; Montañez and Read 1992a, 1992b; Montañez 1994).

The transition from the subtidal to the peritidal depositional regime at the end of Grand Cycle deposition resulted in the formation of lithofacies which differ in type and distribution of porosity, and have accordingly undergone different early diagenesis. The late diagenesis of these deposits is examined in the context of changes in regional facies distribution, and the complex burial history controlled by the latest stages of passive-margin development and the transition into a convergent margin setting.

METHODS

Following field work and sample collection, detailed petrographic and geochemical analyses were performed on a selected set of samples from the Maynardville Formation and the lower part of the overlying Copper Ridge Dolomite. Petrographic analysis included examination of over 600 cut hand samples. Standard (transmitted light) petrographic microscopy was carried out on 330 thin sections (75x50 mm), that were stained following the procedure outlined in Dickson (1965, 1966). Selected thin sections were examined using a Citl Cold Cathode Luminescence 8200 mk3 microscope under the following operating conditions: voltage 10-12 kV, beam current 150-180 μ A, and chamber pressure 180-200 millitorr. Scanning electron microscopy (SEM) was performed using a low energy beam (10 keV) on a small subset of unetched, coated samples, that were broken off thin section billets. Crystal sizes were described using the terminology after Boggs (1987). Detailed microscopic analyses aided in the identification of components for geochemical analysis.

The samples for stable isotope (oxygen and carbon) analysis were collected by drilling 2-10 mg of individual carbonate depositional and diagenetic components from

polished thin-section billets using a microscope-mounted microdrill. Organic matter was removed by roasting the powdered samples at 380°C for one hour. Samples were reacted off-line with 100% H₃PO₄ at 25°C for 24 hours (calcite) and 48 hours (dolomite). For mixed calcite/dolomite samples, a time extraction procedure was used (Epstein et al. 1963; Walters et al. 1972; Wada and Suzuki 1983). The carbon dioxide evolved within one hour after the start of the reaction with phosphoric acid is primarily generated by the dissolution of calcite, whereas the gas produced during the following three hours of the reaction represents a mixture of calcite- and dolomite-derived CO₂. The gas evolved after 48 hours is considered representative of the dolomite present in the sample. Isotope values were obtained on a VG-903 isotope ratio mass spectrometer and are reported as $\delta^{13}\text{C}$ and $\delta^{18}\text{O}$ in permil (‰) relative to the PDB standard. External precision was ± 0.05 ‰ for both $\delta^{13}\text{C}$ and $\delta^{18}\text{O}$; sample reproducibility ($\pm 1\sigma$) was 0.2 ‰.

Major and trace element compositions of selected carbonate components were analyzed on a Cameca SX-50 Electron Microprobe equipped with four wavelength-dispersive spectrometers and one energy-dispersive spectrometer. Analyses were performed on polished thin sections using a defocused beam (10-20 μm in diameter), 25 kV accelerating voltage, and 10 nA beam current. Detection limits were 0.1 mole % MgCO₃ for Mg (count time = 20 sec), 100 ppm for Mn and Fe, and 200 ppm for Sr (count time = 60 sec). Well-characterized carbonate standards were analyzed to monitor the calibration error.

Radiogenic strontium isotope analyses were performed by Dr. Steven A. Goldberg at the University of North Carolina at Chapel Hill. Samples for Sr isotopic analysis were dissolved in 1.0 M Ultrex II acetic acid at room temperature. Prior to carbonate dissolution, samples were washed twice in 500 ml of 0.25 M Ultrex II acetic acid at room temperature for 5 minutes, followed by two rinses with ultraclean Milli-Q deionized water to remove exchangeable Sr from any clay minerals or other residue. Splits of powdered

samples were also washed with 0.25 M ammonium acetate and leached in the same manner as above. The $^{87}\text{Sr}/^{86}\text{Sr}$ of samples treated with ammonium acetate were compared with that of dilute acetic acid washed splits to ensure that Sr was not derived from clays or other impurities. Sr isotope data were collected on a VG sector54 thermal ionization mass spectrometer in quintuple collector dynamic mode.

A burial curve for the Maynardville Formation in northeastern Tennessee was constructed using the SUBSIDE computer program (Wilkerson and Hsui 1989). The information on the lithologic content, thickness, and age of the units for the construction of the burial curve was compiled from Walker (1985), Harland et al. (1989), and the COSUNA (Correlation of Stratigraphic Units of North America) chart for the southern Appalachian region (Patchen et al. 1985).

PETROGRAPHIC OBSERVATIONS

As a function of different environmental regimes, the subtidal and peritidal sedimentary packages of the Maynardville have different lithologic content (Fig. 2.1; Tables 2.1, 2.2). This is accompanied by difference in the diagenetic patterns observed. The two packages differ in the occurrence and distribution of pore types and the occluding cement phases, as well as in the mineral composition of the micritic matrix and allochems present.

Subtidal Package

The characteristics of the various diagenetic phases present within the subtidal depositional package of the Maynardville are summarized in Tables 4.1 and 4.2. The subtidal depositional package is dominated by centimeter-scale interbedded limestone and argillaceous layers, which comprise the ribbon rocks (Fig. 2.1; Table 2.1). The depositional micrite is composed of a mosaic of non-ferroan, aphanocrystalline to very

Table 4.1. Description of calcitic diagenetic components of the subtidal depositional package.

Diagenetic component	Occurrence	Description	CL pattern
Microsparite	Patchy distribution within mud-rich layers, associated with burrows with diffuse walls and framboidal pyrite. Comprises internal sediment at bottoms of burrows with sharp walls. In ribbon rocks occurs adjacent to and within argillaceous layers. In packstone layers present in interparticle space and as a replacement of skeletal fragments and micritic allochems.	Mosaic of very fine- to fine-crystalline (10-25 μm) calcite. Commonly stains ferroan.	Primarily non- to dark dull luminescent. Individual crystals are more brightly luminescent.
Fibrous/bladed calcite cement	First generation of cement. Fibrous morphology is occasionally replaced by bladed (prismatic) crystals with subsequent precipitation, widening and enlarging of crystals away from the substrate. Fibrous cement is common as isopachous rims on ooids and trilobite fragments. Fibrous/bladed calcite also originates on burrow walls and framework voids of microbial deposits.	Radial- and radial-fibrous crystals (length:width ratio > 6:1), and bladed (prismatic) crystals (length:width ratio < 6:1) reaching maximum width of 200 μm and length of 500 μm . Cloudy or turbid appearance (inclusion rich).	Uniform to patchy distribution of non- to dark dull luminescence. Some crystals have non-luminescent cores and dull to bright luminescent outlines and terminations which occasionally show complex CL banding.
Syntaxial calcite cement	Present in packstone/grainstone deposits as syntaxial overgrowth cement precipitated as individual crystals sharing crystallographic orientation with host echinoderm fragments. Rare coarse crystals poikilotopically engulf other allochems present.	Coarse crystals (up to 2.5 mm) share compromise growth boundaries with fibrous/bladed cement. Turbid appearance (inclusion-rich), with less turbid outer parts.	Dark dull luminescence. Occasional patches and thin outer crystal rims of more brightly luminescent calcite.
Equant calcite cement	Precipitated on fibrous/bladed cement, or as the first generation of cement in intergranular pores, some burrows and dissolutional voids. Fills in small fractures formed by mechanical compaction of allochems, which are in turn truncated by stylolites.	Drusy and non-drusy fabric of equidimensional fine- to medium-crystalline (up to 80 μm) turbid crystals, and coarse-crystalline (up to 0.5 mm) less turbid crystals.	Uniformly dark dull luminescent or zoned with dull luminescent cores and thicker, more brightly orange/yellow luminescent outer parts which commonly contain dull luminescent patches or subzones.
Ferroan equant calcite cement	Subsequently precipitated on non-ferroan calcite cements. Commonly forms the pore-central cement. Also occurs as the first generation of cement in some burrows and dissolutional voids.	Coarse- to very coarse-crystalline (0.5-3 mm) calcite. Also forms clear overgrowths on turbid non-ferroan equant calcite.	Complexly zoned with numerous non- to dark dull luminescent subzones. Some coarser crystals are uniformly non- to dark dull luminescent.
Ferroan calcite in fractures	Ferroan equant calcite occludes bed-oblique and bed-normal fractures. Bed-parallel fractures within ribbon rocks also contain ferroan fibrous calcite.	Equant and fibrous crystal morphologies comprise massive and "stretched" vein fills, respectively.	Non-luminescent (fibrous) and non- to dull orange luminescent (equant).

Table 4.2. Description of dolomitic diagenetic components of the subtidal depositional package.

Diagenetic component	Occurrence	Description	CL pattern
Ferroan fine-crystalline dolomite	Associated with clay seams within argillaceous layers of the ribbon rocks and with small amplitude stylolites in other less argillaceous deposits. Also occurs as scattered crystals replacing micritic matrix and allochems (peloids, intraclasts). Commonly associated with ferroan calcite and framboidal pyrite.	Ferroan, mostly very fine- to fine-crystalline (10 - 50 μm) anhedral to subhedral dolomite, associated with some medium-crystalline (up to 150 μm) rhombohedral (planar-e) dolomite.	Dark, non-luminescent. Rare rhombohedral crystals have uniform or zoned dull to bright luminescence.
Replacement saddle dolomite	Selectively replaces allochems (skeletal fragments, peloids). Also common in interparticle pores of skeletal packstone/grainstone as a possible replacement of preexisting cement phases. Associated with hardgrounds characterized by pyrite crusts and coatings on allochems.	Ferroan, coarse- to very coarse-crystalline (250 μm - 1.5 mm) saddle dolomite with characteristic undulatory extinction.	Non-luminescent. Less common dark dull luminescent crystals.
Saddle dolomite cement	Pore central cement phase, postdates ferroan calcite cement, and was preceded by a dissolutional event. Association with pyrite, rare galena and sphalerite observed in coarse-grained intraclastic layers, rare shaley layers of the ribbon rocks, and some dissolutional voids.	Ferroan, very coarse-crystalline (1-4 mm) saddle dolomite crystals with curved boundaries and undulatory extinction. Some crystals have brownish color in plane light.	Non-luminescent to very dark dull reddish/brown luminescent. Occasionally one thin brightly red/orange luminescent zone present.

fine-crystalline calcite (Fig. 4.1A), that shows patches of bright to dull luminescence, and contains many individual non-luminescent crystals. The subtidal micritic deposits are commonly burrow-mottled (Fig. 4.1A). Burrows with diffuse walls are represented by patches of fine-crystalline ferroan calcite or microsparite which is commonly associated with framboidal pyrite (Fig. 4.1A; Table 4.1).

Interparticle pores are common in subtidal ooid, skeletal (trilobite, brachiopod), and intraclastic packstone/grainstone deposits (Figs. 4.1C-E). These pores are occluded by various calcite cement types including fibrous/bladed, equant and syntaxial overgrowth cement (Figs. 4.1C-E, 4.2; Table 4.1). Subtidal microbial deposits (thrombolites and digitate stromatolites) also contain framework voids and burrows with sharp walls. These voids commonly show geopetal features, and have the upper parts occluded with calcite cement (Table 4.1; Fig. 4.1F). Dissolutional pores are not abundant within the subtidal deposits. Some of the burrow- and framework-related voids are dissolution enlarged (Fig. 4.1G). Dissolution voids have also been observed associated with an exposure surface developed on subtidal lithofacies at the Tazewell outcrop (Fig. 2.6). Such voids are primarily occluded with equant calcite cement and rare dolomite cement (Figs. 4.1G; 4.3A-B; Tables 4.1-2).

Dolomite is not an abundant diagenetic phase in the subtidal package and it occurs exclusively in a ferroan form. The most common dolomite type is fine-crystalline dolomite associated with argillaceous layers of the ribbon rocks (Figs. 2.2B, 2.4A, 4.1A-B, 4.1E; Table 4.2). The argillaceous layers contain numerous pressure dissolution surfaces that represent non-sutured dissolution seams, microstylolites, or clay seams (Fig. 4.1A; Wanless 1979; Simpson 1985; Bathurst 1987; Choquette and James 1987; Railsback 1993). Clay- to silt-size quartz grains, pyrite, ferroan calcite, and rare glauconite are also present within the argillaceous layers. Ferroan dolomite also occurs along small amplitude stylolites developed in less argillaceous subtidal deposits (Table 4.2). Coarser-crystalline,

Figure 4.1. Photomicrographs illustrating characteristic features of the subtidal deposits.

A) Photomicrograph of a ribbon rock showing the contact between a dark-colored argillaceous dolomicritic layer (a) above, and a limestone layer below. Partial dissolution of a trilobite skeletal fragment in the upper left corner of the photograph is indicative of the presence of pressure solution surfaces (arrow) within the argillaceous layer. The limestone layer is composed of burrow-mottled micrite (m). Burrows and areas adjacent to argillaceous layer are composed of ferroan microsparite (ms). Framboidal pyrite (p) is common within both limestone and argillaceous layers. Scale bar = 1 mm. **B)** SEM photomicrograph of dolomite (d) within clay matrix (a) of argillaceous layers from the ribbon rocks. Scale bar = 20 μm . **C)** Photomicrograph of an ooid grainstone deposit with intergranular space occluded primarily by turbid fibrous/bladed calcite cement (f). Ooids have a variable degree of preservation, from well preserved radial fabric (r), to altered (a). Scale bar = 1 mm. **D)** Photomicrograph showing a compromise boundary (arrow) between fibrous/bladed calcite cement (f) and syntaxial calcite cement (s) that precipitated as overgrowth on an echinoderm skeletal fragment (e). Scale bar = 100 μm . **E)** Photomicrograph of a ribbon rock showing a skeletal packstone/grainstone layer adjacent to an argillaceous layer (a) with scattered dolomite crystals (d). Intergranular space is occluded with: syntaxial calcite cement overgrowth (s) on an echinoderm fragment (e), fibrous/bladed calcite (f) that precipitated on trilobite fragments in shelter voids, and some equant calcite cement (q). Arrow points at the boundary between an initial turbid and later clear syntaxial overgrowth cement. Scale bar = 1 mm. **F)** Framework void in thrombolitic deposit occluded with pore-rim turbid fibrous/bladed calcite (f), and pore-central clear equant calcite cement (e). Scale bar = 1 mm. **G)** Dissolution-enlarged void within thrombolitic deposit occluded with ferroan equant calcite cement (e), and rare, pore-rim, rhombohedral dolomite (d). Scale bar = 1 mm.

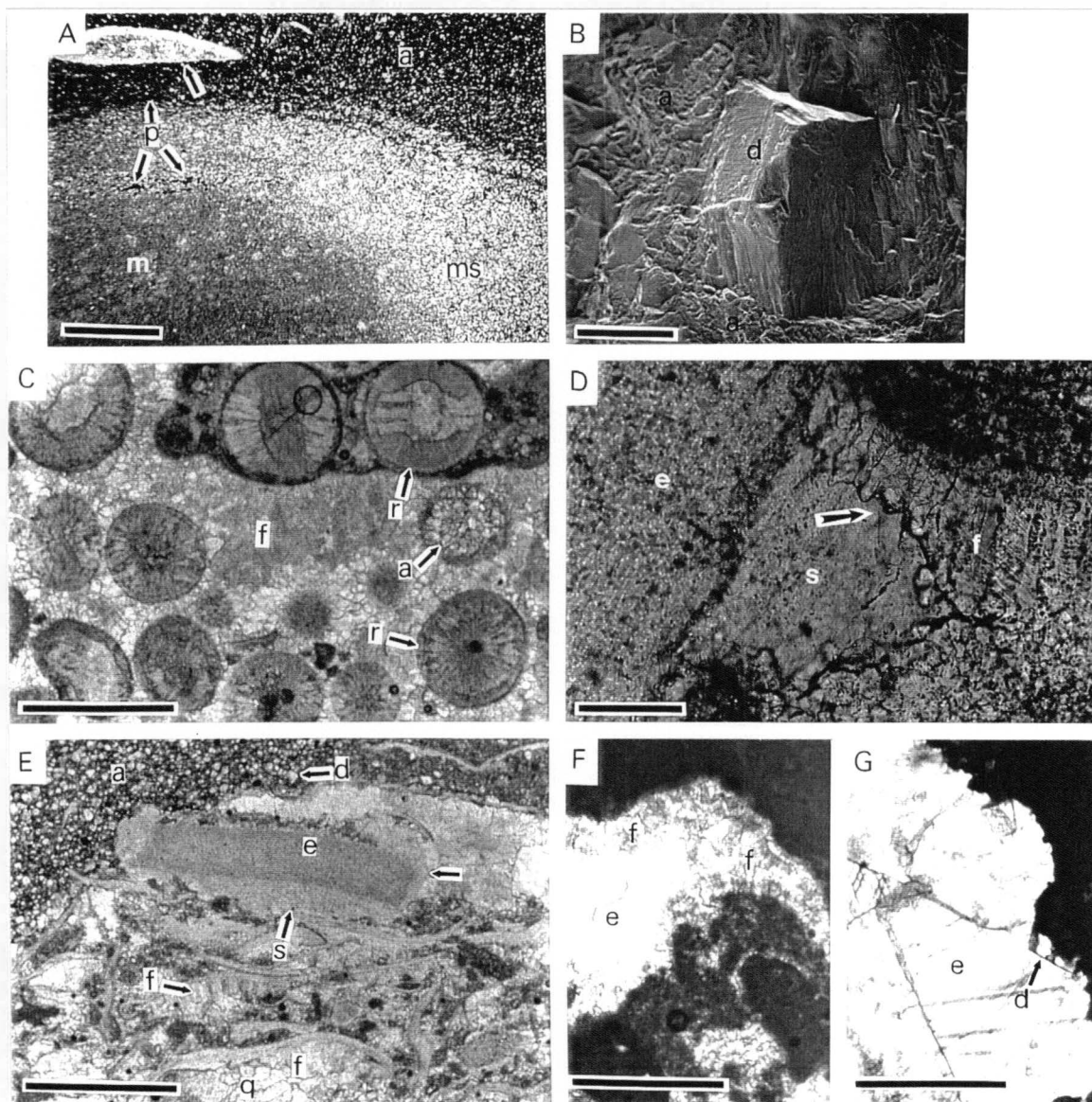


Figure 4.2. Paired plain-light and CL photomicrographs of the most common cement types in the subtidal deposits. **A)** Plain-light photomicrograph of a fibrous/bladed calcite cement (f) and pore-central equant calcite cement (e). The cements show patchy distribution of non- to dark dull luminescence on the paired CL photomicrograph **B**. Scale bar = 1 mm. **C)** Cross-polarized light photomicrograph of the fibrous/bladed calcite cement (f), postdated by turbid to clear equant calcite cement (e). On the paired CL photomicrograph **D**, fibrous/bladed calcite has non-luminescent cores (c) and more brightly luminescent crystal terminations (t). Equant calcite is non to dark dull luminescent and shows faint zonation. Scale bar = 250 μm . **E)** Shelter void underneath a trilobite fragment occluded with fibrous/bladed calcite (f), and equant calcite cement (e). Internal sediment on the bottom of the void is composed of microsparite (ms). On the paired CL photomicrograph **F**, the initial fibrous/bladed calcite shows a patchy distribution of luminescence. Crystal terminations show complex CL zonation with several non- and dull luminescent zones, and a more brightly luminescent outer part (arrow). Equant calcite cement is dull luminescent and does not show obvious zonation. Scale bar = 0.5 mm.

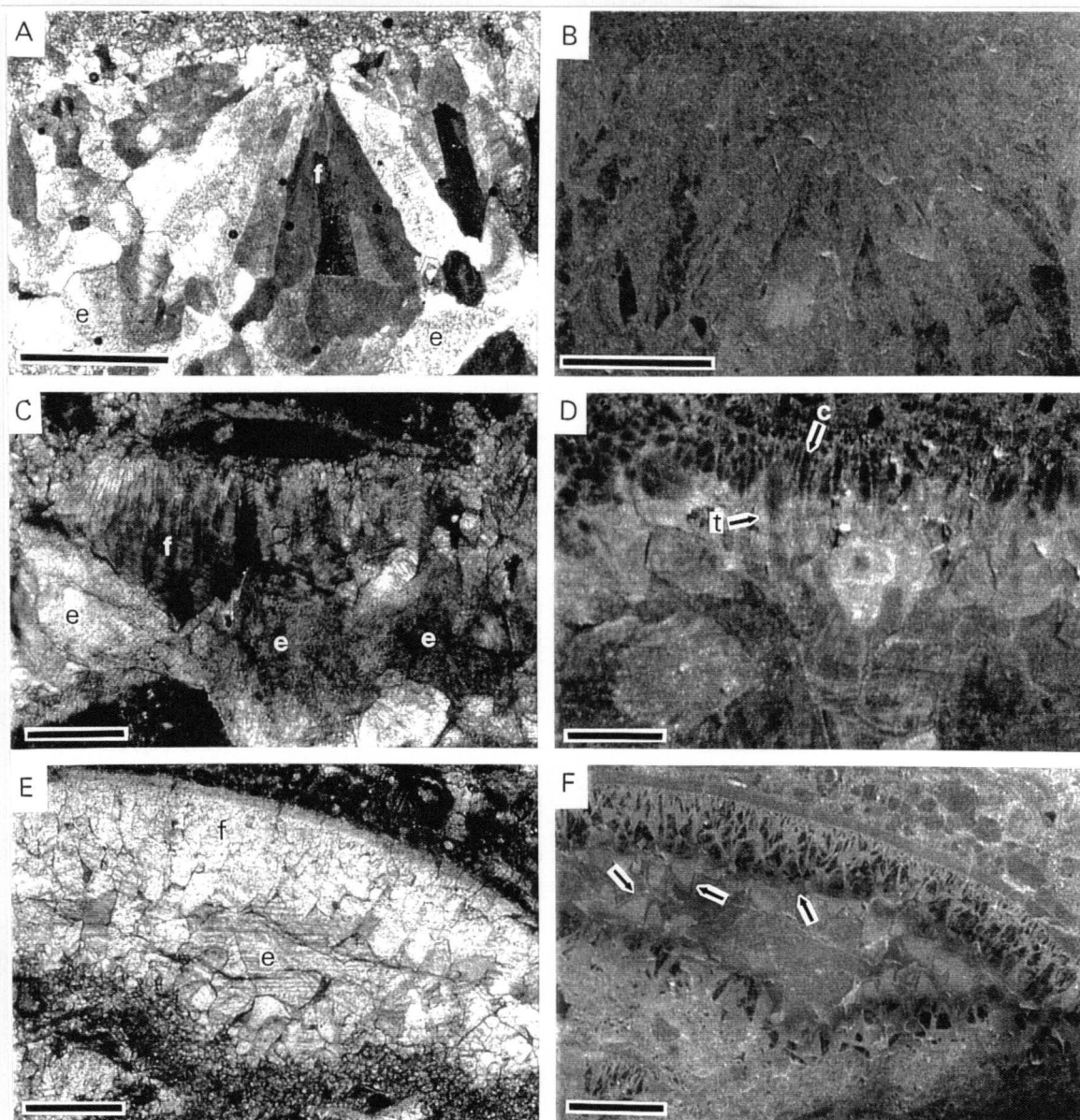
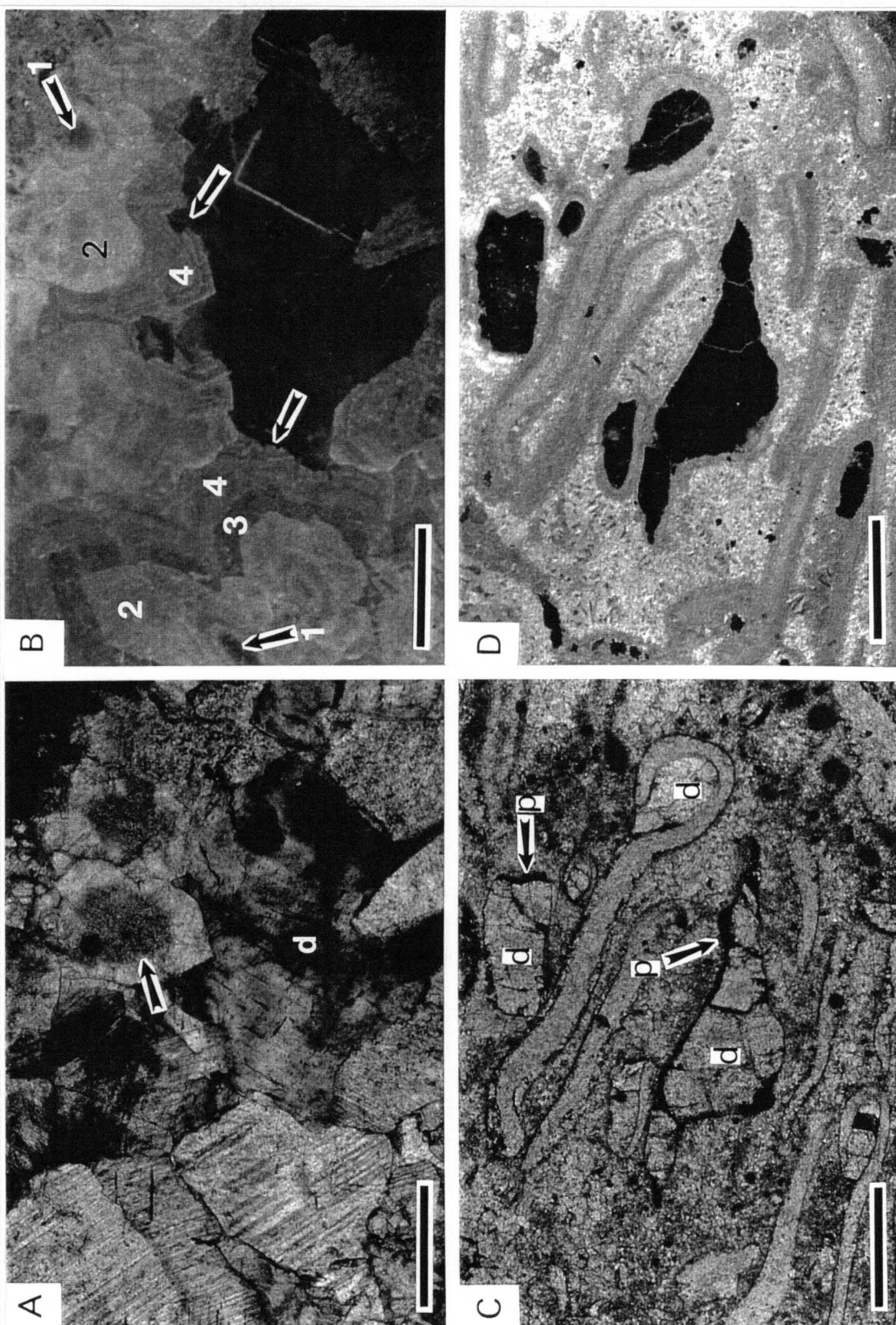


Figure 4.3. Paired plain-light and CL photomicrographs of the equant calcite cement and saddle dolomite from the subtidal deposits. **A)** Pore-central saddle dolomite cement (d), surrounded by equant to prismatic calcite cement. Arrow indicates a boundary between an initial turbid, and a later clear calcite cement. On the paired CL photomicrograph **B**, dolomite is non-luminescent with the exception of one thin brightly luminescent zone. Equant calcite cement shows complex CL zonation including: 1) non-luminescent core; 2) bright to light dull luminescent zone with minor subzones; 3) non-luminescent zone; and 4) dark dull luminescent zone with numerous subzones. The boundary between zones 2 and 3 represents a transition from nonferroan to ferroan calcite. Ferroan equant calcite was partially dissolved (arrows) prior to the deposition of the saddle dolomite. Scale bar = 0.5 mm. **C)** Replacement saddle dolomite (d) in a skeletal packstone layer, about 1 cm below a hardground surface. Note common pyrite (p). On the paired CL photomicrograph **D** saddle dolomite is non-luminescent. Scale bar = 0.5 mm.



ferroan saddle dolomite is present within the subtidal lithofacies as a replacement phase commonly associated with hardgrounds characterized by pyrite crusts and coatings (Fig. 4.3C-D; Table 4.2). Saddle dolomite also occurs as a pore central cement phase (Fig. 4.3A-B). The association of saddle dolomite cement with Mississippi Valley Type (MVT) minerals such as galena, sphalerite, and pyrite has also been observed.

Peritidal Package

The deposits of the peritidal package that have not been completely dolomitized include: 1) lower parts of microbial laminates or stratiform stromatolites which mark the transition from the subtidal into the peritidal depositional regime; and 2) shallow subtidal microbial deposits such as thrombolites and digitate stromatolites. These deposits are composed primarily of aphanocrystalline to fine-crystalline non-ferroan calcite. The most common type of voids within these deposits are burrows. In the stratiform stromatolite deposits, burrows contain framboidal pyrite and equant calcite cement which is commonly ferroan. The small burrows in the thrombolites and digitate stromatolites are also occluded by fibrous/bladed calcite. Dolomite is present within these deposits as a replacement of micritic laminae in the stratiform stromatolites, and as a selective replacement of non-microbial allochems within the thrombolites and digitate stromatolites. Details on the selective dolomitization of microbial deposits and its implications are presented later in Chapter 6.

The remaining peritidal lithofacies have been extensively dolomitized. Four dolomite replacement fabrics are recognized within the upper Maynardville Formation and the overlying Copper Ridge Dolomite: 1) dolomicrite; 2) dolomicrosparite; 3) coarser-crystalline dolomite; and 4) saddle dolomite (Fig. 4.4; Table 4.3). Dolomicrite and dolomicrosparite are the most abundant types of dolomite (Figs. 4.4A-C). They are finer-crystalline, have abundant planar crystal boundaries, and are fabric retentive in comparison

Figure 4.4. Photomicrographs illustrating replacement dolomite types from the peritidal deposits. **A)** Dolomicrite. Scale bar = 0.5 mm. **B)** SEM photomicrograph of dolomicrite. Scale bar = 5 μm . **C)** Photomicrograph of dolomicrosparite. Scale bar = 0.5 mm. **D)** Photomicrograph showing a typical xenotopic texture of coarser-crystalline replacement dolomite. Arrow points at an allochem ghost. Scale bar = 0.5 mm. **E)** Photomicrograph of saddle dolomite in a dark bituminous matrix. Scale bar = 0.5 mm.

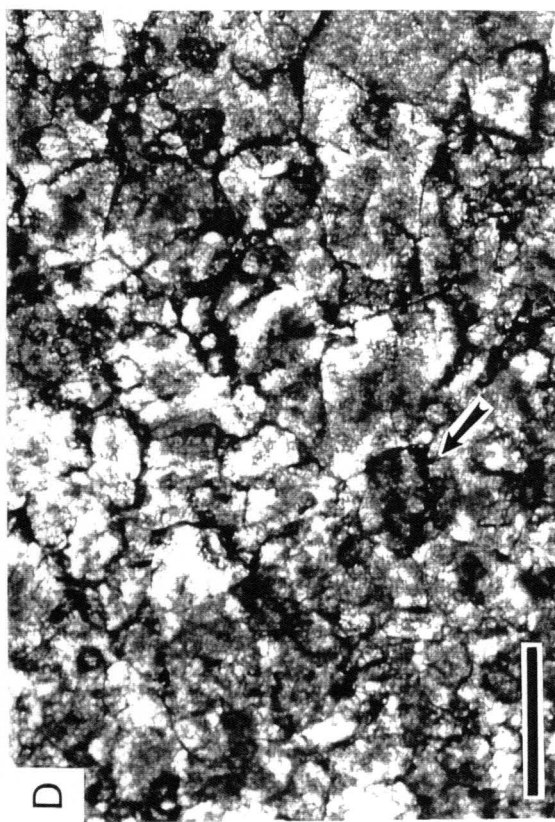
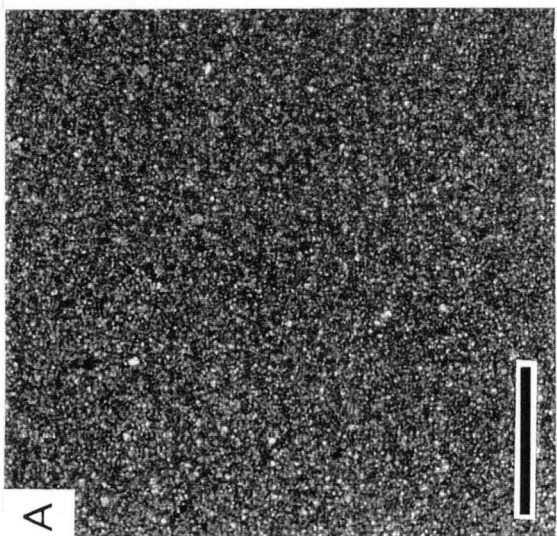
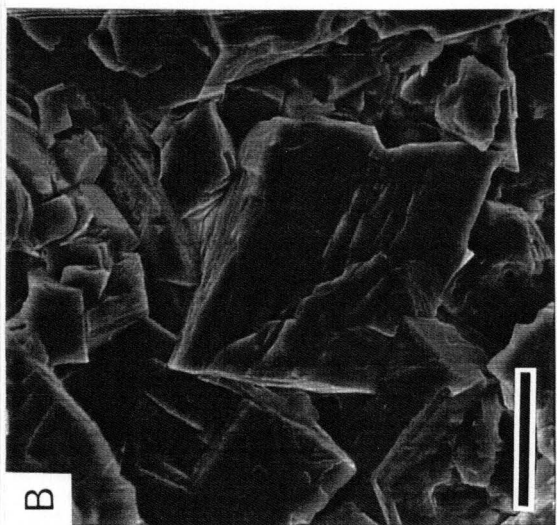
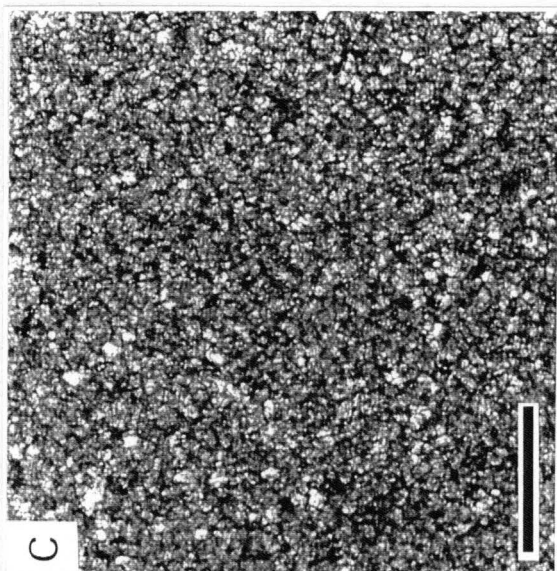


Table 4.3. Description of dolomitic diagenetic components of the peritidal depositional package.

Replacement dolomite	Occurrence	Description	CL pattern
Dolomicrite	The primary component of mud-rich deposits including: dolomitized mudstone, fine-grained mechanical laminates or "couplets", upper micritic parts of medium- to coarse-grained "couplets", and micritic laminae of stratiform, LLH and SH stromatolites.	Fabric retentive mosaic of aphanocrystalline to very fine-crystalline (<10-15 μm) anhedral to euhedral (planar-e) dolomite.	Uniform to patchy distribution of non- to dark dully orange luminescence.
Dolomicrosparite	Similar to dolomicrite. More abundant in lower, grainy portions of medium- to coarse-grained "couplets" and in laminated microbial deposits. Also occurs in irregular patches that cross-cut lithologic boundaries.	Fabric retentive mosaic of fine-crystalline (15-60 μm) subhedral (planar-s) to euhedral (planar-e) dolomite.	Patchy distribution of non- to bright orange luminescence.
Coarser-crystalline dolomite	Increases in abundance upsection. Comprises microbial (SH and columnar stromatolites), and coarser-grained oolitic, intraclastic and peloidal deposits with laminae and allochem ghosts preserved. In some cases fabric is completely obliterated. Patchy distribution within rare partially dolomitized microbial deposits.	Mosaic of medium- to coarse-crystalline (60-300 μm) dolomite with irregular and non-planar boundaries (xenotopic mosaic). Some crystals have turbid cores and less turbid to clear outer parts.	Non- to dark dull luminescent. Patchy distribution of dull luminescence is related to the presence of allochem ghosts.
Saddle dolomite	Volumetrically least abundant replacement phase restricted to the uppermost Maynardville and the Copper Ridge Dolomite. Fabric obliterate. Patchy, irregular distribution and rare remnant fibrous/bladed calcite may suggest preferential replacement of burrows. Embedded in brownish to black, argillaceous or bituminous matrix.	Coarse- to very coarse-crystalline (up to 1-2 mm) saddle dolomite. Well developed curved crystal faces. Some crystals have turbid centers and less turbid to clear outer parts.	Non-luminescent to dark dull brown luminescent. Surrounding bituminous matrix has dark blue luminescence.
Cement dolomite	Occurrence	Description	CL pattern
Zoned dolomite cement	Completely occludes smaller desiccation, evaporite dissolution, fenestral and rare intergranular voids. In larger voids forms pore rim cement. Individual rhombohedral crystals occur on burrow walls and rims of dissolution enlarged voids in rare non-dolomitized thrombolitic deposits. Also occludes rare oomoldic voids.	Medium- to coarse-crystalline (200 μm - 1 mm). Individual pore-rim rhombohedral crystals are < 300 μm . Commonly zoned with turbid centers and less turbid to clear outer parts. Uniform to undulatory extinction.	Complexly zoned. Number and thickness of zones vary. Turbid cores are dull luminescent, followed by several bright to dull luminescent zones and an outermost non to dark dull luminescent zone.
Saddle dolomite cement	Subsequently precipitated on pore rim zoned dolomite cement in larger desiccation and evaporite dissolution voids as the last, pore occluding cement phase. Completely occludes tectonic fractures, dissolution voids and some voids of uncertain origin in fabric-obliterated deposits.	Very coarse-crystalline (1-3 mm) saddle dolomite. Well developed curved crystal faces and undulatory extinction. Some crystals are uniformly turbid or have turbid cores and less turbid rims.	Similar to outermost zone of zoned dolomite cement: non-luminescent with some faint, dark dully luminescent zones. Turbid crystals are bright to dull luminescent and show no zonation.

to the coarser-crystalline and saddle dolomite (Fig. 4.4; Table 4.3). The amount of coarser-crystalline replacement dolomite and saddle dolomite increases upsection, with saddle dolomite being the least abundant dolomite replacement type (Figs. 4.4D-E).

The most common pore types in the peritidal package are desiccation voids, evaporite dissolution voids, and fenestral voids (Fig. 4.5A). These pores are occluded with zoned dolomite cement and a pore-central, coarse-crystalline saddle dolomite cement (Fig. 4.5; Table 4.3). The number and thickness of individual zones of dolomite cement, recognized using cathodoluminescence (CL), vary substantially between pores (Fig. 4.5D-E). Small fenestral and evaporite dissolution voids are occluded by non-luminescent dolomite which is petrographically similar to cores of complexly zoned dolomite crystals from larger pores (Fig. 4.5). In the rare, partially dolomitized, shallow subtidal microbial deposits, zoned rhombohedral dolomite crystals precipitated on pore walls (Figs. 4.5B-C). The centers of large pores are occluded with coarse-crystalline saddle dolomite cement (Table 4.3). This cement type also occludes dissolutional voids and tectonic fractures (Fig. 4.5F-G).

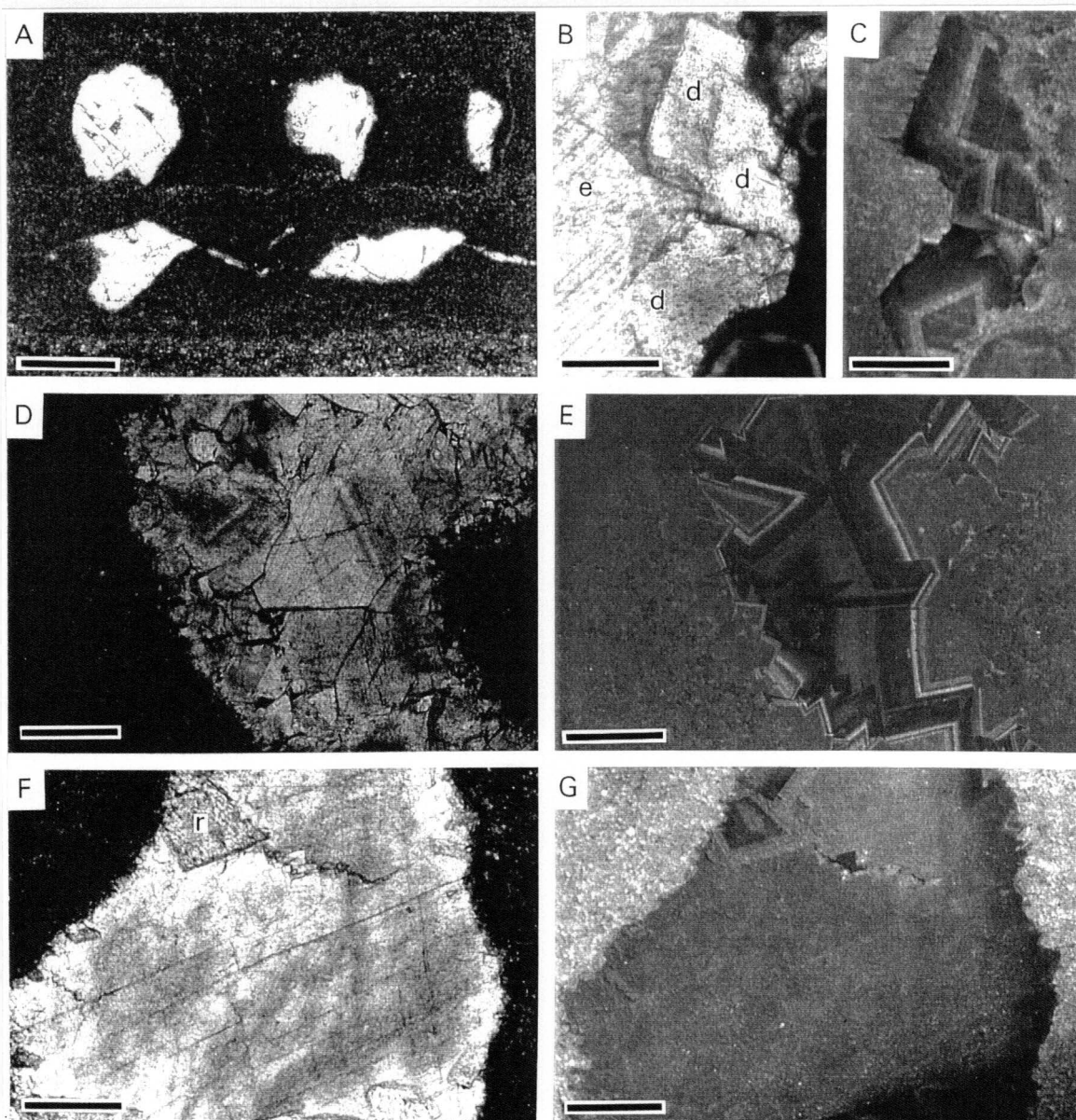
Fractures

Tectonic fractures are not abundant in the Maynardville Formation, except at the River Ridge outcrop where more prominent structural deformation features have been observed (see Appendix A). Bed-oblique and bed-perpendicular fractures are occluded by medium- to very coarsely-crystalline equant calcite cement, which is commonly ferroan (Table 4.1), and/or by saddle dolomite cement (Table 4.3). Rare bed-parallel fractures from subtidal ribbon rocks also contain ferroan fibrous calcite (Table 4.1).

Silicification

The first occurrence of chert in the peritidal succession is one of the criteria used

Figure 4.5. Photomicrographs illustrating dolomite cements from the peritidal deposits. **A)** Fenestral voids occluded with dolomite cement. Scale bar = 1 mm. **B)** Plain-light, and the paired CL photomicrograph **C**, of a pore-rim, zoned rhombohedral dolomite (d) postdated by ferroan equant calcite cement (e). See also Fig. 4.1G. Scale bar = 250 μm . **D)** Desiccation void occluded by zoned dolomite cement which on the paired CL photomicrograph **E**, shows a complex CL zonation pattern. Scale bar = 0.5 mm. **F)** A void occluded primarily by saddle dolomite cement and a rare pore-rim rhombohedral dolomite (r). On a paired CL photomicrograph **G**, rhombohedral dolomite shows zonation, whereas saddle dolomite is uniformly non to dark dull luminescent. Scale bar = 0.5 mm.



for the placement of the boundary between the Maynardville and the Copper Ridge Dolomite. Even though chert is more common in the overlying Copper Ridge Dolomite, silicification is also associated with rare ooid grainstone layers, intraclastic-ooid packstone/grainstone layers, and microbial deposits (stratiform, LLH, SH, and columnar stromatolites) of the upper part of the Maynardville. Chert replaces micritic allochems and matrix, whereas the pore space is infilled with two types of silica cement: 1) an earlier, often banded, chalcedony cement; and 2) a later, pore-central, coarser-crystalline, equant quartz cement. The later cement type also precipitated on pore rims in the absence of chalcedony. The silica cements are commonly associated with replaced evaporite nodules.

GEOCHEMISTRY

The geochemistry of various depositional and diagenetic components, including stable isotope (oxygen and carbon) values, major (Ca, Mg) and trace element (Fe, Mn, Sr) compositions, and Sr isotope ratios, are summarized in Tables 4.4 and 4.5. See Appendices B and C for a more detailed description of individual samples and results of geochemical analyses.

Stable Isotope Compositions

Lohmann and Walker (1989), estimated a $\delta^{18}\text{O}$ value of -5 ‰ PDB, and a $\delta^{13}\text{C}$ value of -0.5 ‰ PDB for Cambrian marine calcite. Gao and Land (1991b), proposed a range of stable isotope values for Late Cambrian/Early Ordovician marine carbonate deposits of -5 to -3 ‰ PDB for oxygen, and -1 to +2 ‰ PDB for carbon. In comparison to these values, all of the depositional and diagenetic components analyzed in this study are depleted in ^{18}O , and are generally enriched in ^{13}C (Figs. 4.6, 4.7). The significance of a large scatter in $\delta^{13}\text{C}$ values and the overall ^{13}C -enrichment for the samples analyzed is discussed later in Chapter 5.

Table 4.4. Summary of geochemical data for the depositional and diagenetic components of the deposits that have not been extensively dolomitized.

Component	$\delta^{18}\text{O} \text{ ‰ PDB}$		$\delta^{13}\text{C} \text{ ‰ PDB}$		$^{87}\text{Sr}/^{86}\text{Sr}$
	Range	Avg (n)	Range	Avg (n)	
Micritic matrix: non-microbial	-8.98 to -7.16	-7.82 (20)	0.49 to 4.09	2.40 (20)	—
Micritic matrix: microbial	-10.98 to -8.63	-9.54 (10)	1.53 to 3.68	2.89 (10)	0.70920
Fibrous/bladed calcite	-10.16 to -7.48	-8.92 (17)	2.31 to 4.89	3.48 (17)	0.70910
Equant calcite cement	-10.65 to -8.83	-9.53 (11)	1.24 to 4.72	2.76 (11)	—
Ferroan equant calcite	-11.00 to -9.07	-9.87 (8)	1.97 to 3.19	2.53 (8)	0.70889
Dolomite from argillaceous layers	-8.15 to -6.05	-7.07 (12)	2.83 to 4.99	3.71 (12)	—
Calcite from argillaceous layers	-8.92 and -8.23	-8.57 (2)	1.98 and 2.35	2.17 (2)	—
Equant calcite cement in fractures	-12.92 to -9.38	-11.22 (10)	0.70 to 3.29	2.28 (10)	—
Saddle dolomite replacement	—	-8.13 (1)	—	3.39 (1)	—
Saddle dolomite cement	-9.90 to -8.41	-8.94 (3)	3.44 to 3.97	3.65 (3)	0.70960

Component	CaCO_3 mole %		MgCO_3 mole %		Fe ppm		Mn ppm		Sr ppm	
	Range	Avg	Range	Avg	Range	Avg*	Range	Avg*	Range	Avg*
Micritic matrix: non-microbial	96.85 - 98.23	97.55	1.63 - 2.50	2.22	335 - 3181	847	< 100 - 169	57/154	200 - 673	463
Altered ooids	97.72 and 98.03	97.88	1.79 and 2.09	1.94	910 and 998	954	< 100	—	< 200	—
Fibrous/bladed calcite	97.38 - 99.54	98.24	0.16 - 2.52	1.58	< 100 - 1712	33/306	< 100 - 531	40/213	< 200 - 2695	11/1092
Syntaxial calcite cement	97.46 - 99.21	98.32	0.71 - 2.37	1.54	153 - 1039	698	< 100 - 264	69/154	< 200	—
Equant calcite cement	96.98 - 99.18	98.23	0.75 - 2.90	1.63	< 100 - 1337	43/633	< 100 - 403	43/233	< 200 - 1874	47/730
Ferroan equant calcite	97.31 - 99.31	98.63	0.62 - 2.53	1.25	345 - 727	512	< 100 - 275	43/174	< 200	—
Equant calcite cement in fractures	97.29 - 99.75	98.46	0.24 - 2.37	1.41	< 100 - 1748	54/1259	< 100 - 331	42/192	< 200 - 340	96/340
Saddle dolomite replacement	53.83 - 55.28	54.74	39.59 - 42.22	41.10	20752 - 32663	23995	429 - 1057	653	< 200	—
Saddle dolomite cement	53.23 - 55.57	54.53	40.95 - 43.91	42.36	12821 - 21962	17584	472 - 1100	847	< 200	—

* for the set of data containing values below detection limits (100 ppm for Fe and Mn, and 200 ppm for Sr), the first number represents the percentage of analyses below detection limit, and the second number represents the average value for the analyses above the detection limit

Table 4.5. Summary of geochemical data for the depositional and diagenetic components of extensively dolomitized peritidal deposits.

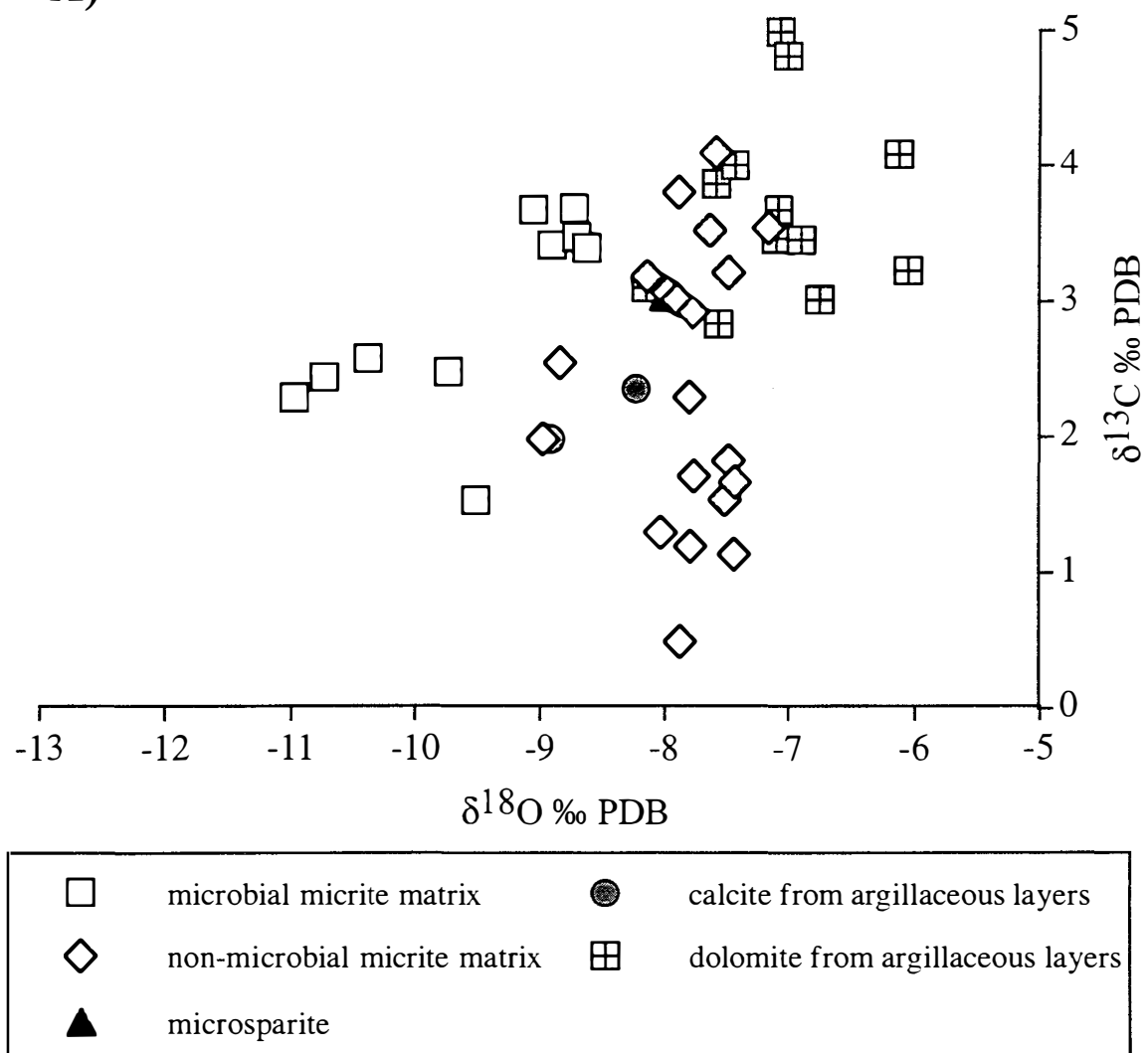
Component	$\delta^{18}\text{O}$ ‰PDB		$\delta^{13}\text{C}$ ‰PDB		$^{87}\text{Sr}/^{86}\text{Sr}$
	Range	Avg (n)	Range	Avg (n)	
Dolomicritic matrix: non-microbial	-7.88 to -5.86	-6.78 (41)	0.32 to 4.68	3.13 (41)	0.70970
Dolomicritic matrix: microbial	-7.77 to -6.21	-6.70 (11)	0.67 to 4.38	3.13 (11)	—
Dolomicrosparite	-8.07 to -6.14	-6.83 (15)	1.52 to 4.78	3.51 (15)	—
Coarser-crystalline replacement dolomite	-9.04 to -6.09	-7.42 (12)	0.62 to 3.52	2.34 (12)	—
Saddle dolomite (replacement)	-10.51 to -6.44	-7.75 (8)	2.64 to 4.32	3.22 (8)	—
Dolomite cement: zoned	-8.46 to -6.87	-7.70 (11)	1.27 to 3.37	2.46 (11)	0.70865; 0.70874
Dolomite cement: saddle	-9.80 to -6.88	-8.21 (18)	-0.61 to 4.39	2.81 (18)	0.70866; 0.70896

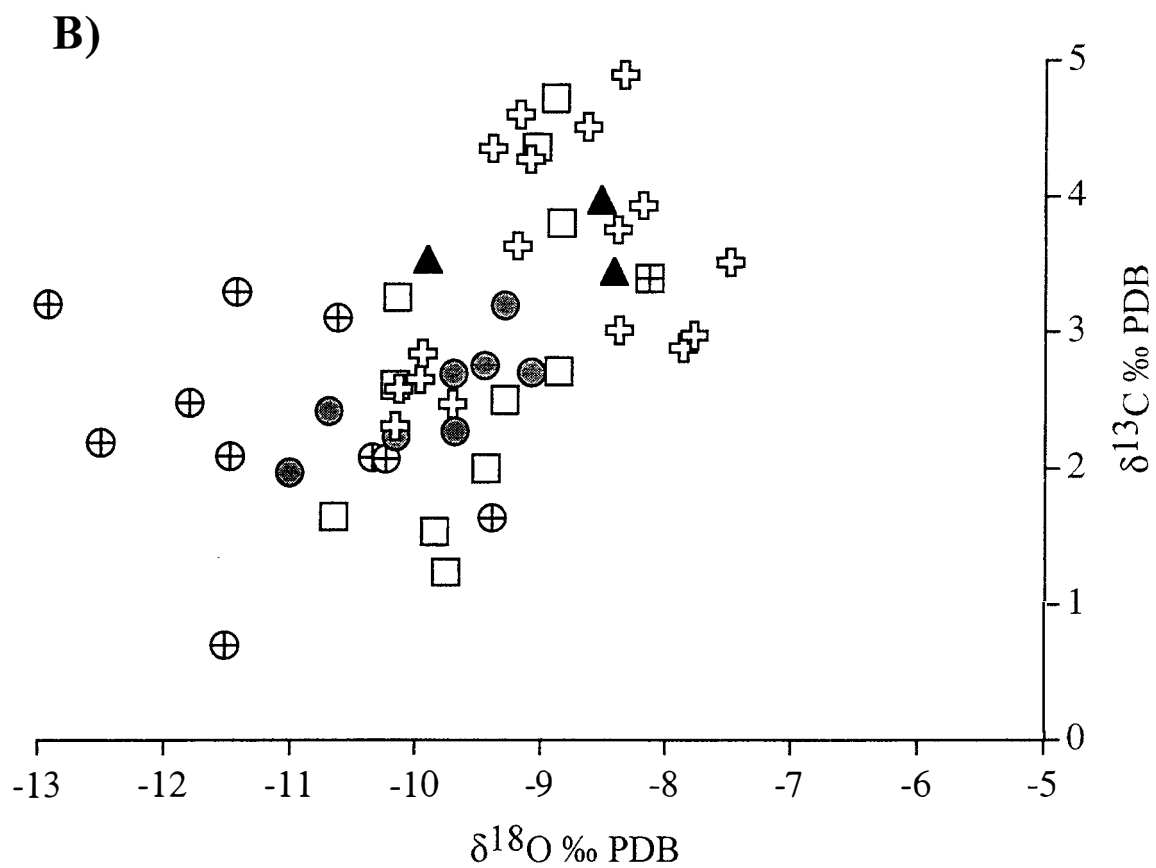
Component	CaCO_3 mole %		MgCO_3 mole %		Fe ppm		Mn ppm		Sr ppm	
	Range	Avg	Range	Avg	Range	Avg*	Range	Avg*	Range	Avg*
Dolomicritic matrix: non-microbial	52.77 - 55.92	54.16	43.92 - 47.10	45.70	281 - 1315	774	< 100 - 124	56/112	< 200 - 288	78/254
Dolomicritic matrix: microbial	50.61 - 51.50	51.04	48.38 - 49.30	48.84	349 - 892	623	< 100 - 157	78/154	< 200	—
Coarser-crystalline repl. dolomite	53.84 - 56.69	55.00	43.19 - 45.15	44.29	343 - 8214	4025	< 100 - 431	27/274	< 200	—
Saddle dolomite (replacement)	52.92 - 54.84	53.58	43.63 - 45.99	45.21	5426 - 9867	7025	< 100 - 488	11/246	< 200	—
Dolomite cement: zoned	50.26 - 54.10	52.28	45.51 - 49.64	47.30	< 100 - 4982	5/2471	< 100 - 408	16/222	< 200	—
Dolomite cement: saddle	51.47 - 56.59	53.70	43.30 - 47.60	45.21	458 - 10670	6264	< 100 - 618	11/339	< 200 - 261	99/261

* for the set of data containing values below detection limits (100 ppm for Fe and Mn, and 200 ppm for Sr), the first number represents the percentage of analyses below detection limit, and the second number represents the average value for the analyses above the detection limit

Figure 4.6. Stable isotope composition of various carbonate components from the subtidal deposits. **A)** Matrix calcite and dolomite samples. **B)** Calcite and dolomite cement and saddle dolomite replacement samples.

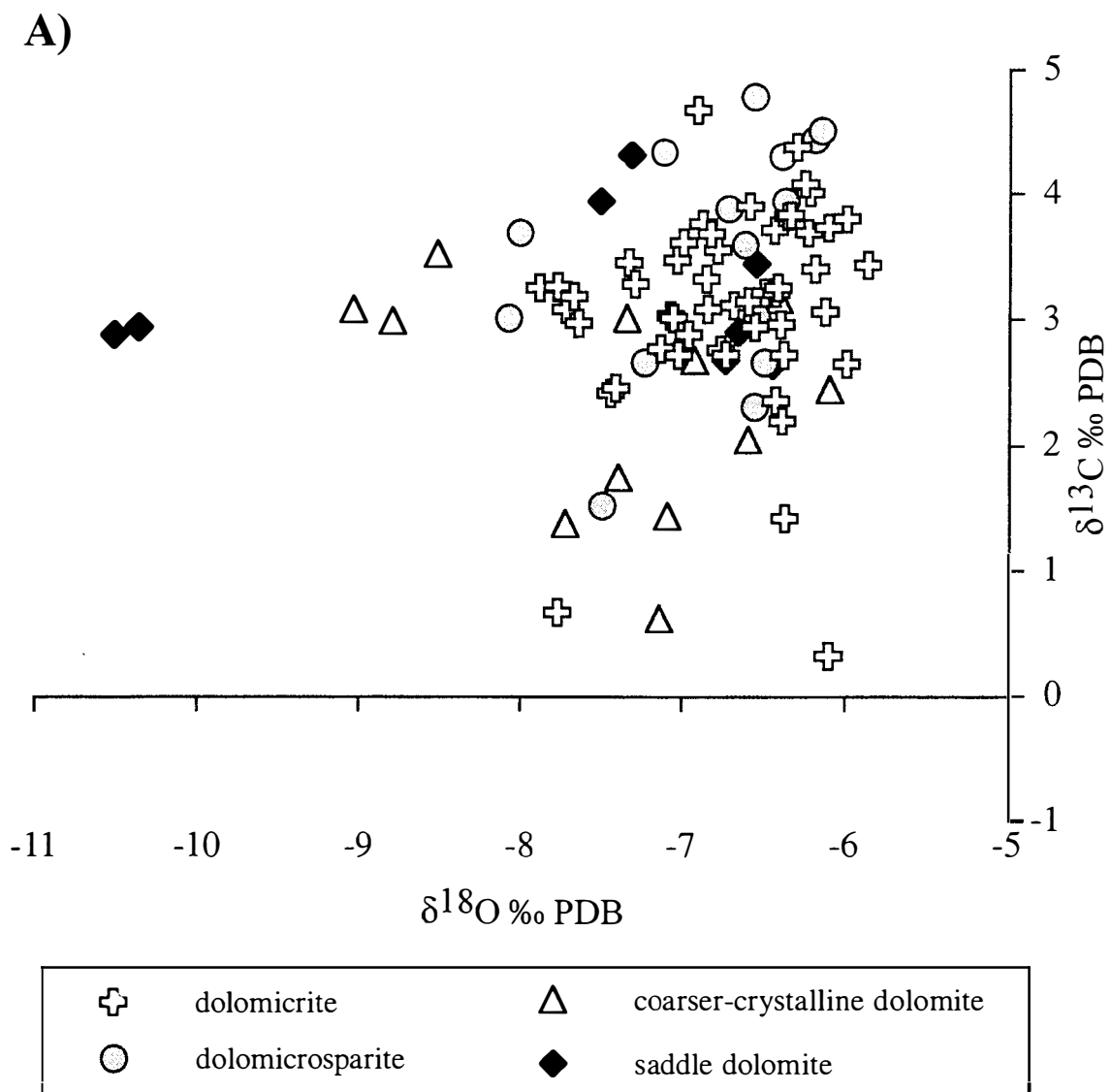
A)





+	fibrous/bladed calcite	▲	saddle dolomite cement
□	equant calcite	⊞	saddle dolomite replacement
●	ferroan equant calcite	⊕	equant calcite in fractures

Figure 4.7. Stable isotope composition of various carbonate components from the extensively dolomitized peritidal deposits. **A)** Replacement dolomite samples. **B)** Dolomite cement.



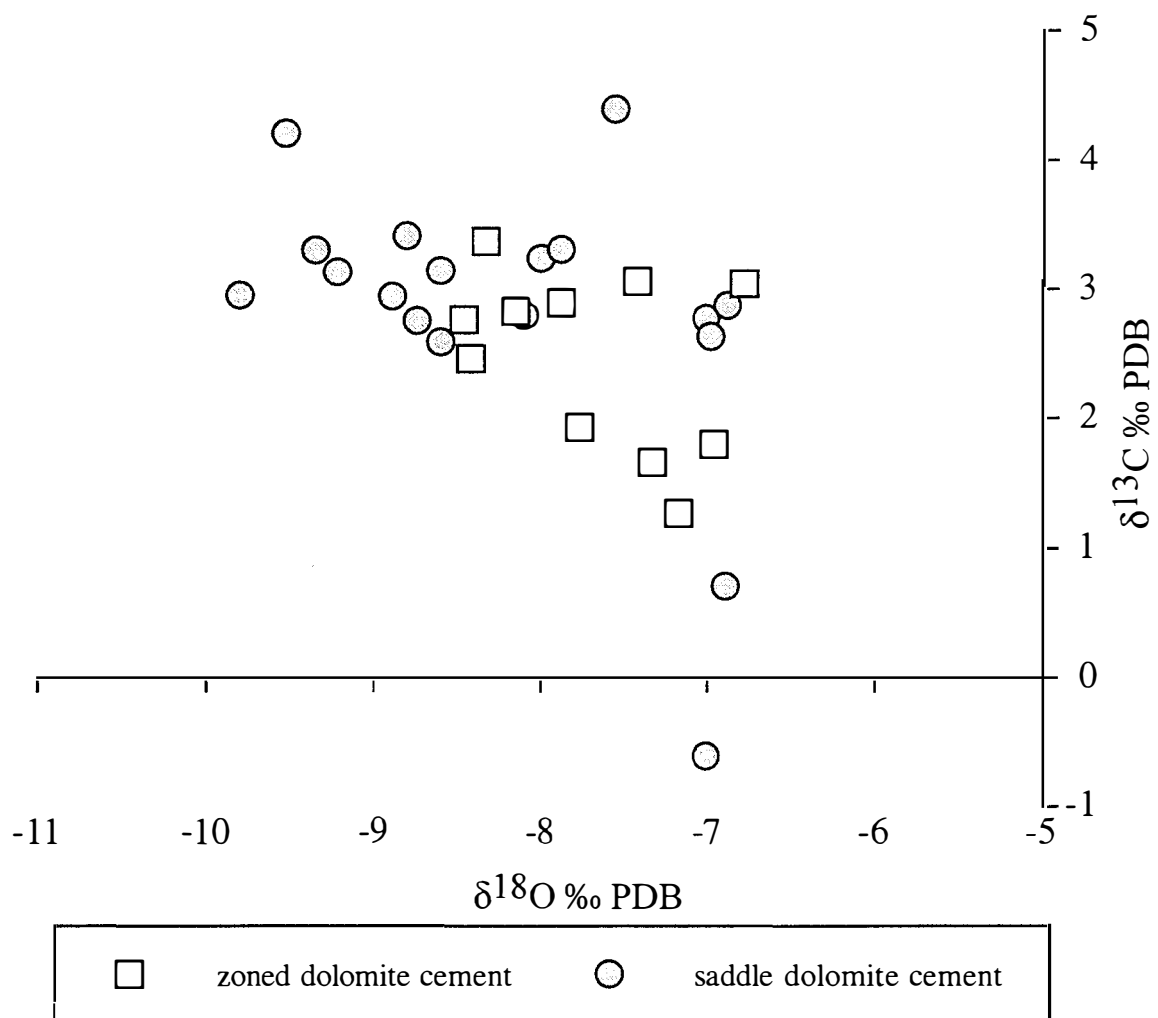


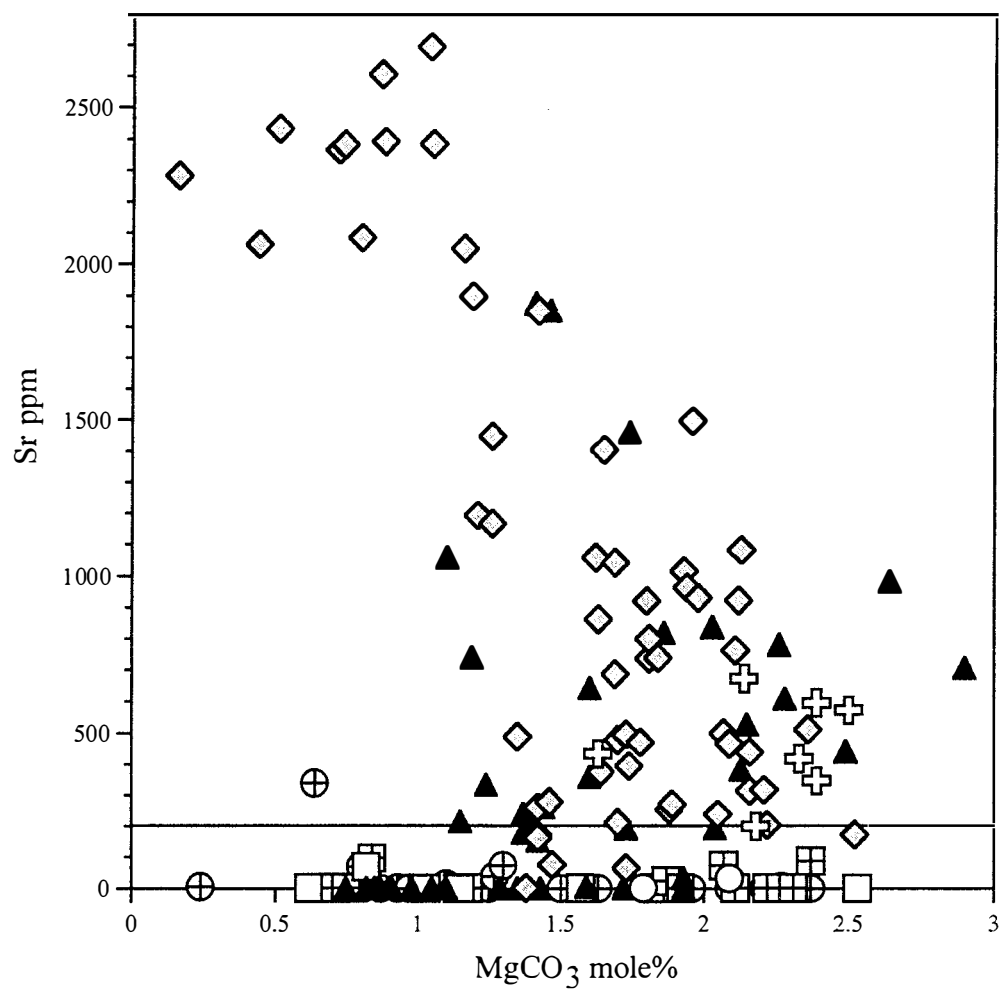
Figure 4.6 shows the stable isotope compositions for the subtidal depositional package of the Maynardville Formation. The compositions of different components overlap significantly. The $\delta^{18}\text{O}$ values generally range from -13.0 to -6.0 ‰ PDB, with dolomite from argillaceous layers being among the least depleted in ^{18}O . Conversely, the equant calcite cement from tectonic fractures has the most ^{18}O -depleted compositions (Fig. 4.6, Table 4.4). Figure 4.7 is a compilation of stable isotope data for the extensively dolomitized peritidal depositional package of the Maynardville Formation and the lower part of the Copper Ridge Dolomite. Oxygen isotope values for various replacement dolomite samples show substantial overlap (Fig. 4.7A), with average $\delta^{18}\text{O}$ values decreasing slightly from dolomicrite (replacement fabric 1) to saddle dolomite (replacement fabric 4; Table 4.5). Isotope values for the zoned and saddle dolomite cement of the peritidal package also overlap, but zoned dolomite is on average less depleted in ^{18}O than saddle dolomite (Figure 4.7B; Table 4.5). Because of sample size considerations and limited thickness, individual zones of dolomite cement were not sampled and analyzed separately for stable isotope compositions.

Major and Trace Element Compositions

The amount of magnesium in various depositional and diagenetic components composed of calcite ranges from 0.16 to 2.90 mole % MgCO_3 with significant intersample variations for most components (Fig. 4.8A; Table 4.4). Average MgCO_3 compositions range from 1.2 mole % in ferroan equant calcite, to 1.9 and 2.2 mole % in altered ooids and microcrystalline matrix, respectively (Table 4.4). Sr compositions range from below detection limit (< 200 ppm) to a maximum of 2695 ppm for some of the fibrous/bladed calcite cements (Fig. 4.8A; Table 4.4). Fe and Mn compositions of various components range from below detection limit (< 100 ppm) to a maximum of 3181 ppm and 531 ppm, respectively (Fig. 4.8B; Table 4.4).

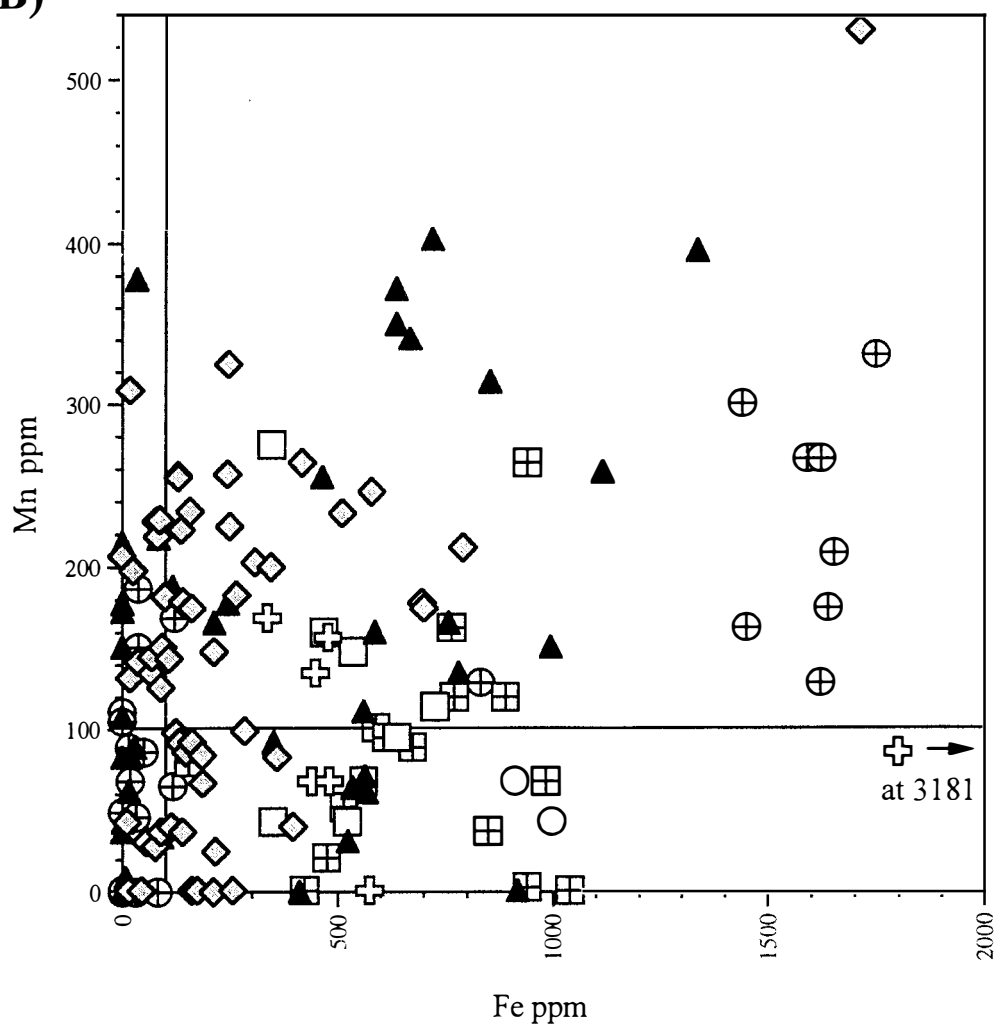
Figure 4.8. Elemental composition of various depositional and diagenetic components from the subtidal deposits, composed of calcite. **A)** MgCO_3 versus Sr composition. Detection limit for Sr is 200 ppm. Note the apparent negative correlation ($r^2 = 0.54$) between MgCO_3 and Sr compositions of fibrous/bladed calcite cement. **B)** Fe versus Mn composition. Detection limit for both elements is 100 ppm. Note: samples that plot below the detection limit for a certain element have indeterminate compositions less than the detection limit for that element.

A)



- ⊕ micrite
- ◇ fibrous/bladed calcite cement
- ooids (altered)
- ▲ equant calcite cement
- ferroan equant calcite cement
- ⊞ syntaxial calcite cement
- ⊕ equant calcite in fractures

B)



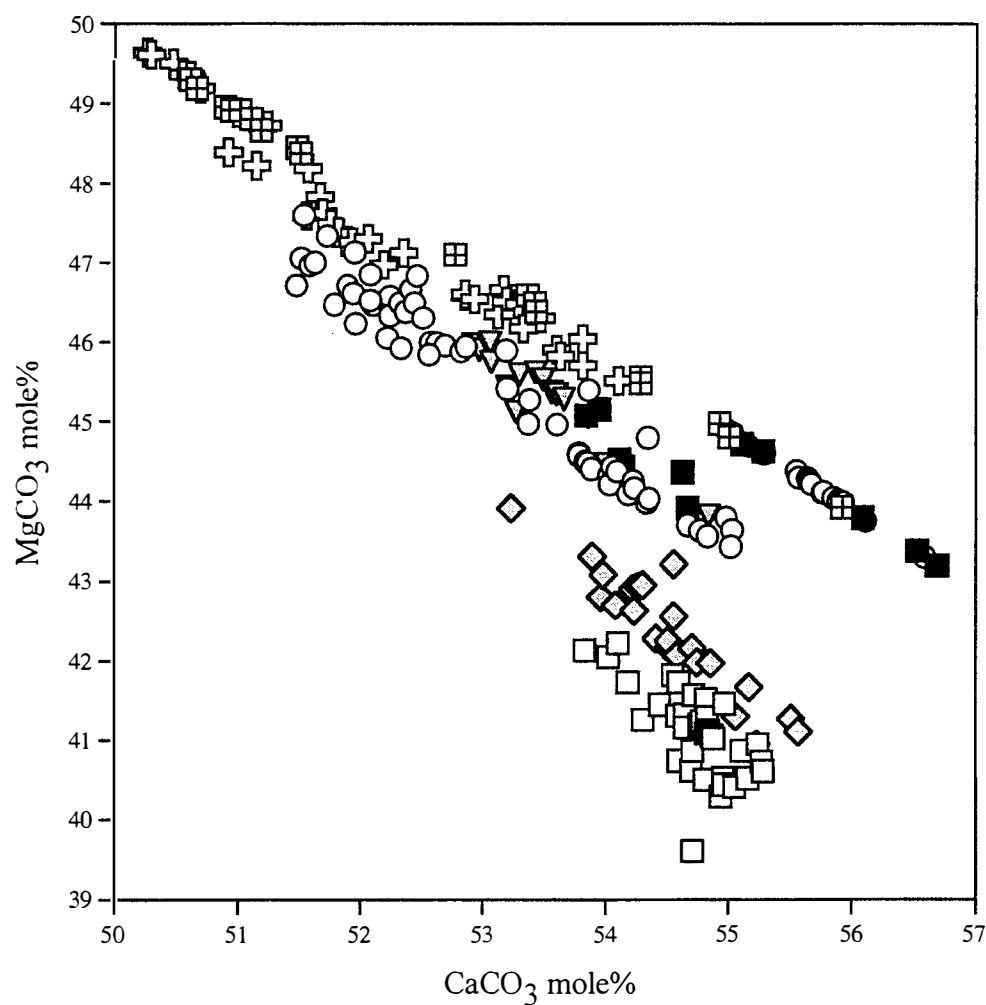
- ⊕ micrite
- ◇ fibrous/bladed calcite cement
- ooids (altered)
- ▲ equant calcite cement
- ferroan equant calcite cement
- ▣ syntaxial calcite cement
- ⊕ equant calcite in fractures

The elemental composition of fine-crystalline dolomite from argillaceous layers of the Maynardville was not determined because of the small size of individual crystals. Coarser-crystalline dolomite from the subtidal depositional package is non-stoichiometric or Ca-rich (Fig. 4.9A). The average MgCO_3 composition is the lowest (41.1 mole %) for the subtidal replacement dolomite, which is also characterized by an elevated Fe composition, averaging about 24000 ppm or 2.4 wt % (Fig. 4.9; Table 4.5). Saddle dolomite cement from the subtidal package has a somewhat higher MgCO_3 composition, and lower Fe concentration than subtidal replacement dolomite (Fig. 4.9). The peritidal replacement and cement dolomite have a stoichiometric to Ca-rich composition, and are on average enriched in MgCO_3 , and depleted in Fe and Mn relative to the subtidal saddle dolomite (Fig. 4.9).

The distribution of major and trace elements was examined along transects through pores filled with zoned peritidal dolomite cement (Fig. 4.10A), and from the rims to centers of pores occluded with saddle dolomite cement (Fig. 4.10B). The CaCO_3 compositions of zoned dolomite cement correlate well with the composition of dolomicrite in the host lithology, but do not show any systematic trends along the transects through the pore (Fig. 4.10A). Pore-rim saddle dolomite cement is least Ca-enriched (near stoichiometric; Fig. 4.10B). The amount of Ca in the saddle dolomite cement increases, in general, away from the pore rim, but fluctuates significantly. Pore-central saddle dolomite is characterized by a decrease in the amount of Ca (Fig. 4.10B). In both zoned and saddle dolomite cements, the Fe concentrations increase towards the pore centers (Fig. 4.10). The maximum Fe concentrations in the outer non-luminescent zones of the zoned dolomite cement are comparable to the lowermost Fe concentrations in the saddle dolomite cement measured along pore rims (Fig. 4.10).

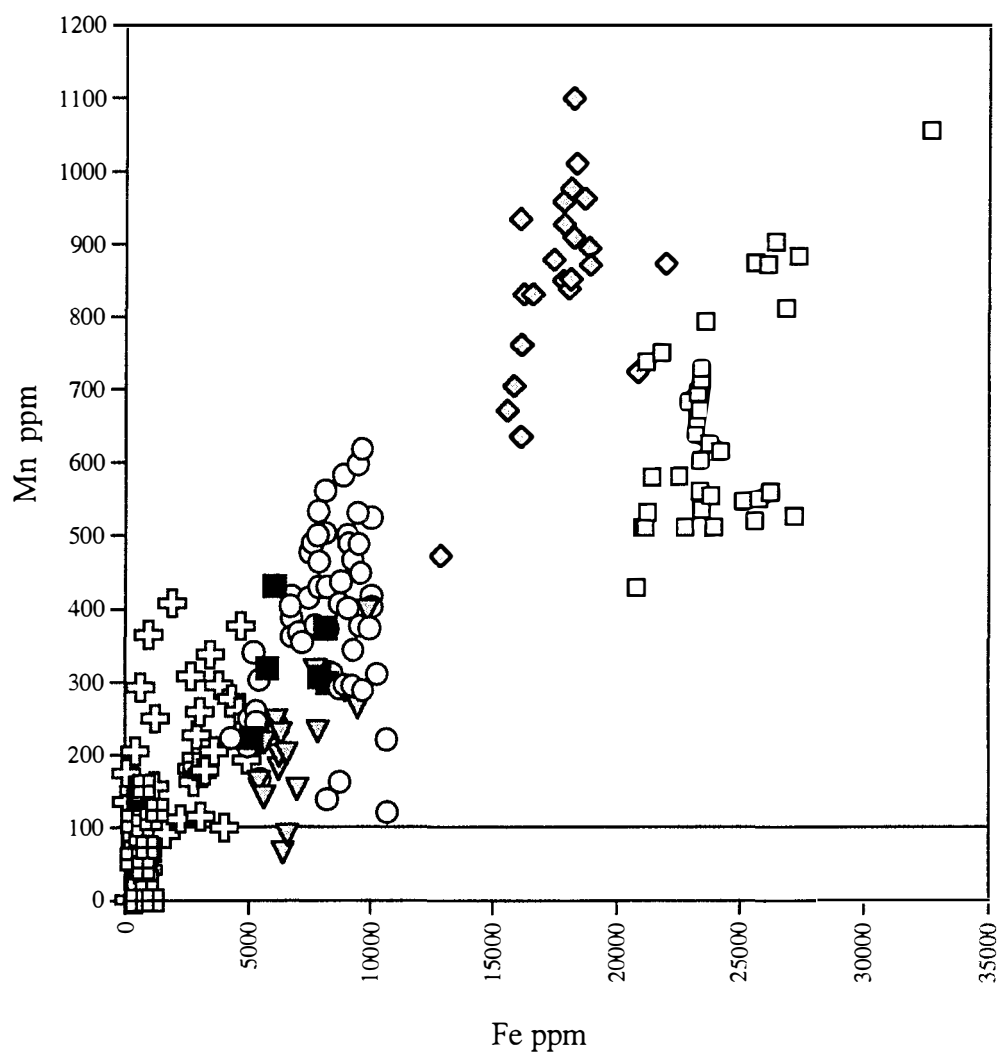
Figure 4.9. Comparison between elemental compositions of subtidal and peritidal dolomite phases. **A)** CaCO_3 versus MgCO_3 plot. **B)** Fe versus Mn plot. Detection limit for both Fe and Mn is 100 ppm. Note: samples that plot below the detection limit for a certain element have indeterminate compositions less than the detection limit for that element.

A)



Subtidal Dolomite			
□	replacement saddle dolomite	◇	saddle dolomite cement
Peritidal Replacement Dolomite		Peritidal Dolomite Cement	
⊞	dolomicrite	⊕	zoned dolomite
■	coarser-crystalline dolomite	○	saddle dolomite
▽	saddle dolomite		

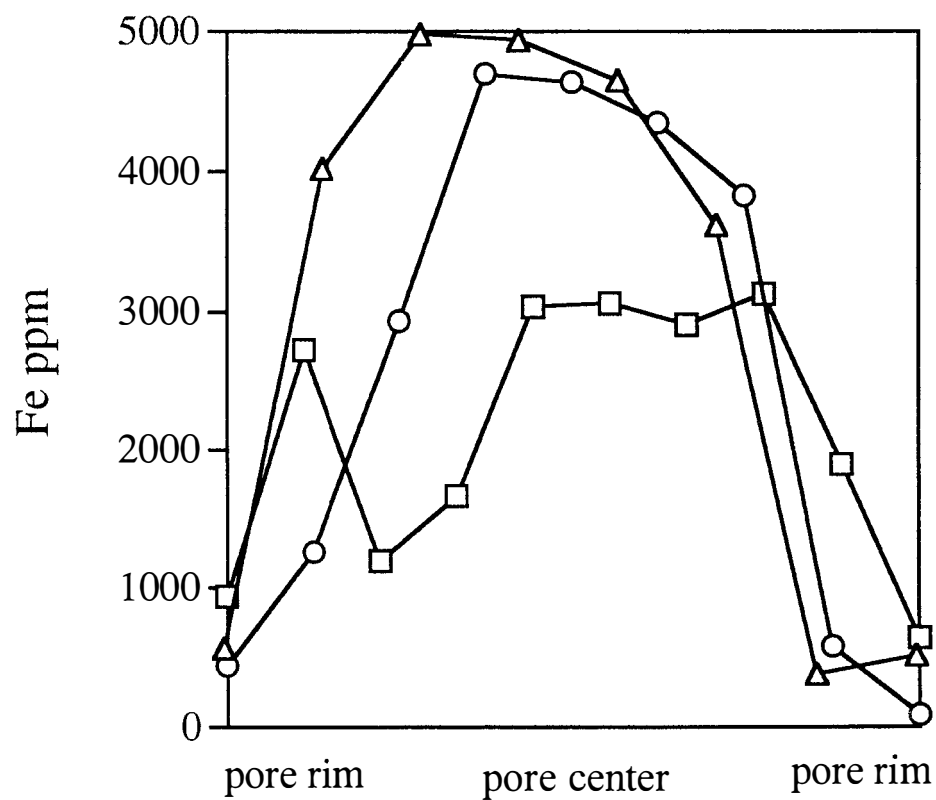
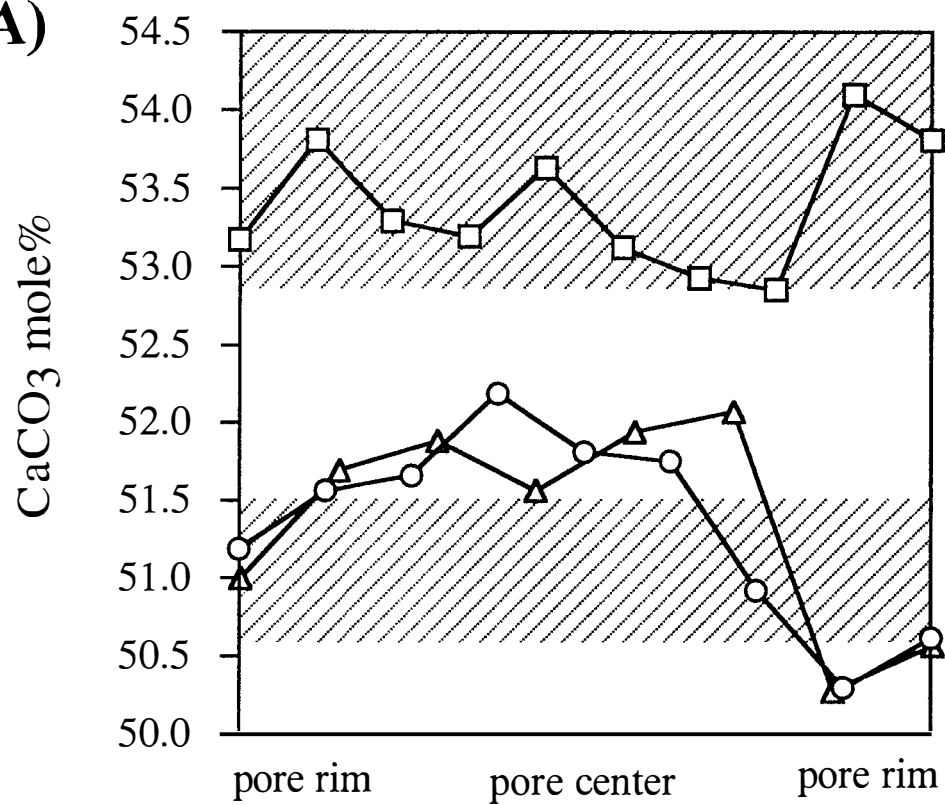
B)

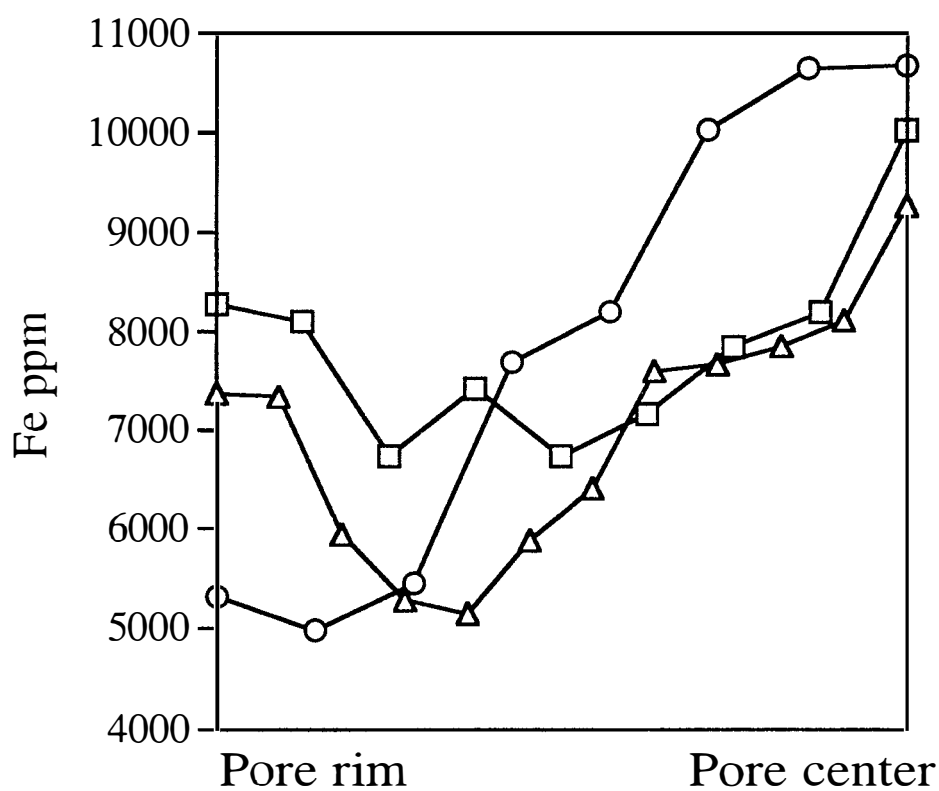
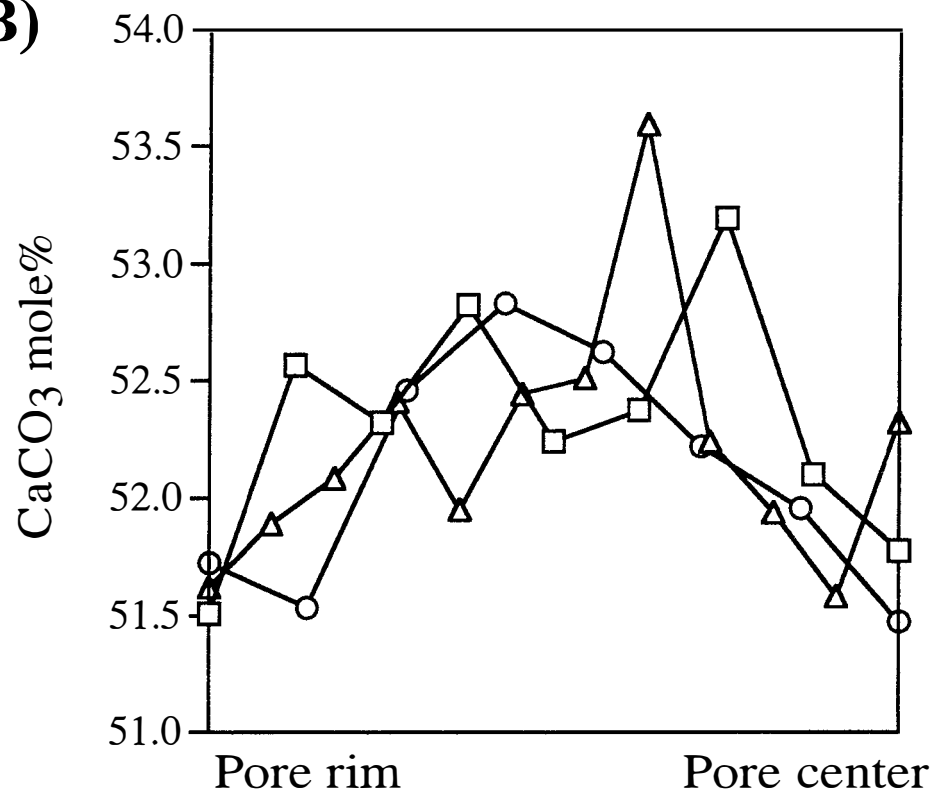


Subtidal Dolomite	
□ replacement saddle dolomite	◊ saddle dolomite cement
Peritidal Replacement Dolomite	
⊞ dolomicrite	⊕ zoned dolomite
■ coarser-crystalline dolomite	○ saddle dolomite
▽ saddle dolomite	

Figure 4.10. Compositional transects for peritidal dolomite cement. **A)** CaCO_3 and Fe compositional variations for zoned dolomite cement along transects through the pore. Circles and triangles denote transects (1.7 mm and 1.8 mm long, respectively) through fenestral and evaporite dissolutional voids of laminated microbial deposits (stratiform stromatolites). Squares mark a transect (2.7 mm long) through a desiccation void of “couplet” lithology. Hatched pattern denotes the CaCO_3 composition of the associated matrix dolomicrite. The maximum CaCO_3 concentration of dolomicrite from the “couplet” lithology (55.9 mole%) is not shown. **B)** CaCO_3 and Fe compositional variations for saddle dolomite cement along transects from pore rim to pore center. Transect lengths: 1.2 mm (circles), 0.9 mm (squares), and 1.6 mm (triangles).

A)



B)

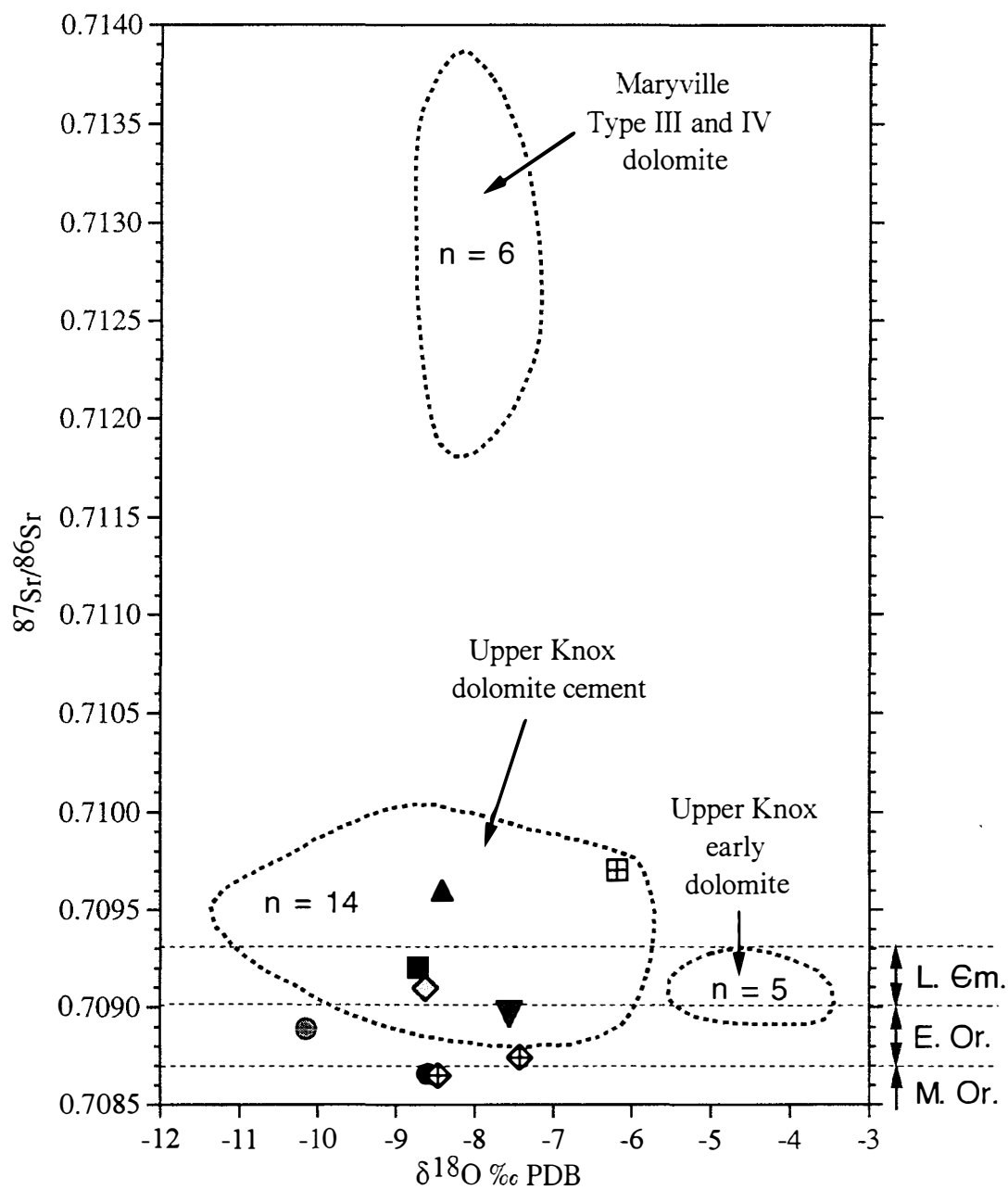
Strontium Isotope Ratios

Individual data points on Figure 4.11 illustrate the $^{87}\text{Sr}/^{86}\text{Sr}$ values for the samples from the Maynardville/lower Copper Ridge Dolomite carbonate succession. The Sr isotope ratio of the micritic matrix and the fibrous/bladed calcite cement from the subtidal deposits is within the predicted range for Late Cambrian seawater, whereas the subtidal saddle dolomite cement has a slightly higher $^{87}\text{Sr}/^{86}\text{Sr}$ value (Fig. 4.11). The Sr ratio for the dolomicrite sample from the peritidal succession (0.7097) is also enriched in ^{87}Sr relative to Late Cambrian seawater, but is comparable to some of the most radiogenic values reported for Upper Cambrian deposits (Burke et al. 1982; Keto and Jacobsen 1987). The $^{87}\text{Sr}/^{86}\text{Sr}$ compositions of all the other samples analyzed, including ferroan equant calcite cement and peritidal dolomite cements, are lower than that for the Late Cambrian, and are in fact similar in composition to Early to Middle Ordovician seawater (Fig. 4.11).

INTERPRETATION OF DIAGENETIC HISTORY

Paragenetic sequences were determined separately for the predominantly limestone and the extensively dolomitized peritidal lithofacies (Fig. 4.12), and are related to the constructed burial curve for the Maynardville Formation (Fig. 4.13). Limestone deposits comprise the subtidal to lowermost intertidal lithofacies including: 1) the entire subtidal diagenetic package of the Maynardville Formation; 2) the lower part of the microbially laminated (stratiform stromatolite) deposits which mark the transition into the peritidal package; and 3) the rare non-dolomitized deposits within the peritidal package. The dolomitized lithofacies represent the majority of the peritidal deposits of the upper Maynardville and the overlying Copper Ridge Dolomite.

Figure 4.11. Variations in Sr isotope composition. Individual data points show Sr isotope composition for various depositional and diagenetic components from the Upper Cambrian deposits. Compositional fields for the Lower Ordovician Upper Knox early dolomite and late diagenetic dolomite cement (from Montañez 1994), and the Middle Ordovician Maryville Limestone (Conasauga Group) burial dolomite (from Srinivasan et al. 1994) are shown for comparison. The Sr isotope composition for Ordovician and Late Cambrian seawater is also indicated in the right margin (from Burke et al. 1982).



Maynardville / lower Copper Ridge Dolomite			
■	subtidal micrite	▣	dolomicrite
◊	fibrous/bladed calcite	⊕	peritidal zoned dolomite cement
●	ferroan equant calcite	●	peritidal saddle dolomite cement
▲	subtidal saddle dolomite cement	▼	saddle dolomite in fracture, associated with sphalerite

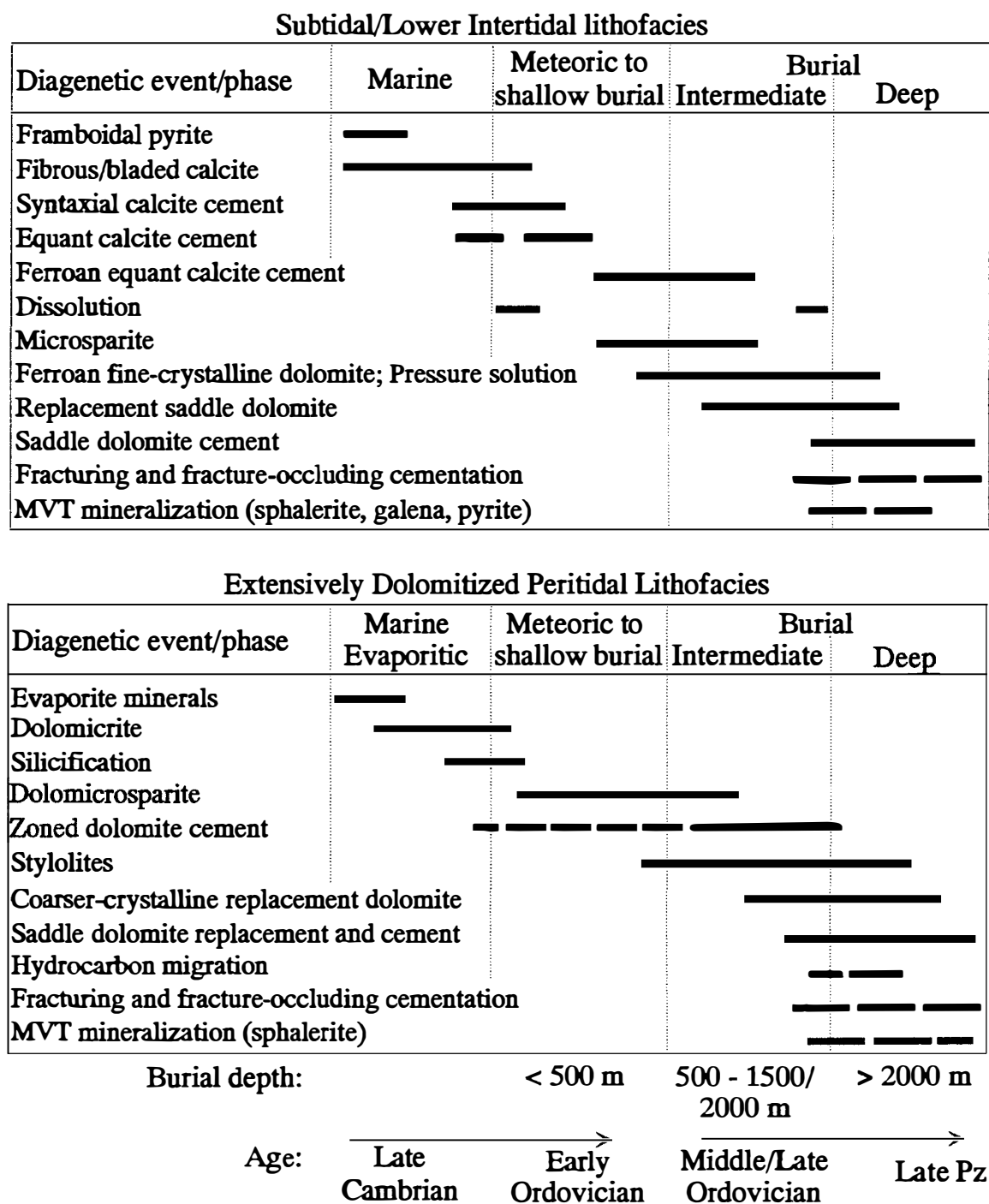


Figure 4.12. Paragenetic sequences for the Upper Cambrian deposits. Paragenesis is interpreted separately for the subtidal to lower intertidal deposits, which have not experienced substantial dolomitization and for the extensively dolomitized peritidal deposits. See Fig. 4.13 for illustration of the burial history of the Maynardville.

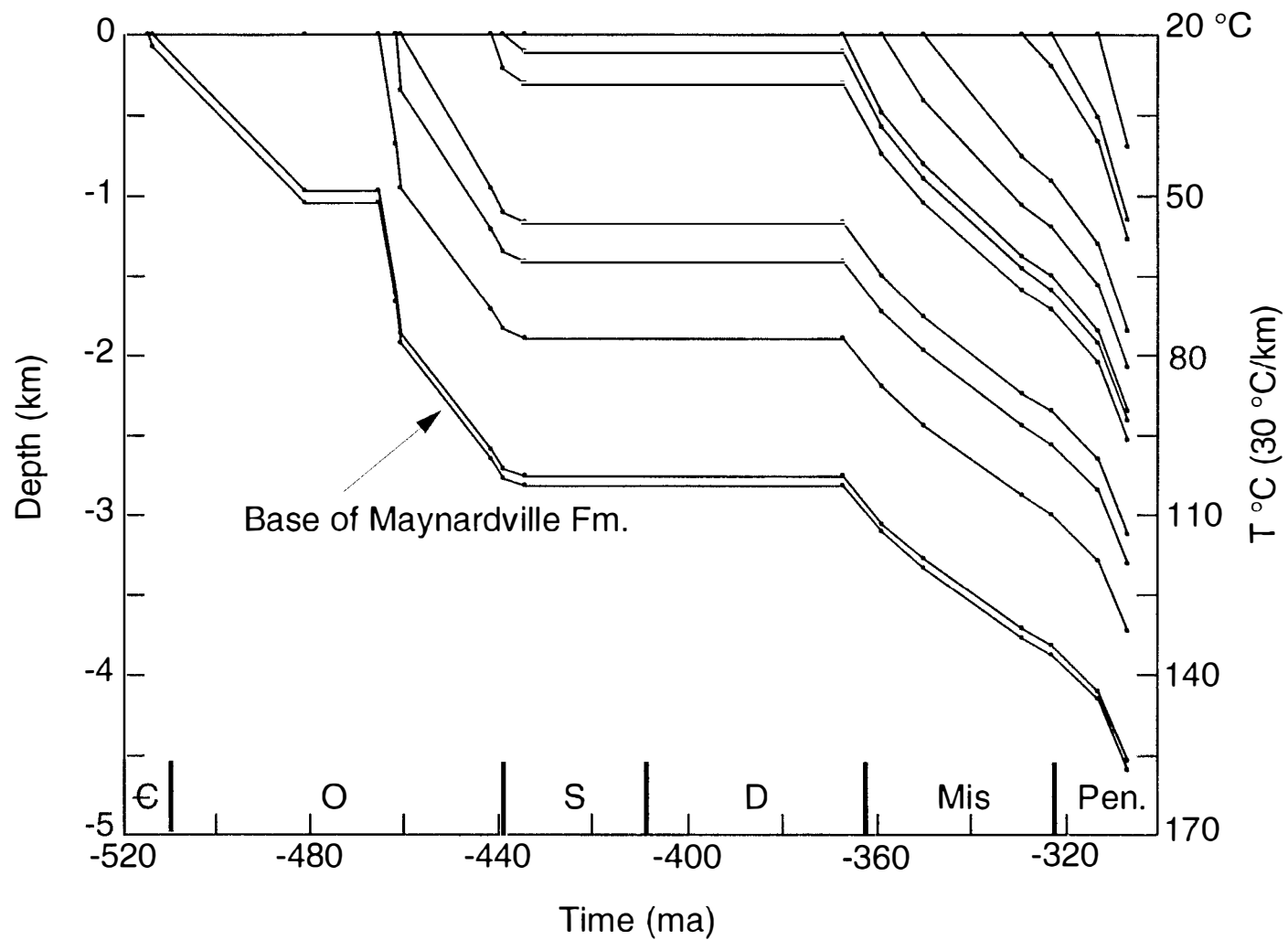


Figure 4.13. Burial curve for the Maynardville Formation.

Limestone Deposits

The lithification of carbonate mud was among the earliest syndepositional events in the diagenetic history of the deposits that did not experience substantial dolomitization. The formation of hardgrounds, intraclasts, and burrows with sharp walls occurred in carbonate sediment that was lithified to some degree. Calcification by cyanobacteria may have played an important role in the early lithification of thrombolite and digitate stromatolite deposits (see Chapter 6). The formation of framboidal pyrite started simultaneously with lithification of the carbonate mud. Early diagenetic framboidal pyrite forms in the sulfate reduction zone below the sediment/water interface, within the first several meters to tens of meters of burial (Berner 1984; Compton 1988b; Morse et al. 1992). Bacterially degrading organic matter and detrital clay minerals are important sources of Fe for the precipitation of framboidal pyrite (Compton 1988b). The subtidal sediments of the Maynardville were well suited for the formation of pyrite because of the presence of argillaceous layers, which were probably organic-rich when deposited. Additional evidence for the presence of organic matter in the subtidal deposits is bioturbation and the presence of skeletal fragments.

Fibrous/bladed calcite is the earliest pore-occluding cement phase (Figs. 4.1, 4.2; Table 4.1). The precipitation of this cement commenced syndepositionally from marine pore water. A marine origin for the fibrous/bladed calcite is supported by the morphological similarity to documented occurrences of modern and ancient marine cements (James et al. 1976; Longman 1980; Marshal and Davies 1981; James and Choquette 1983; Kendall 1985; Sandberg 1985; Freeman-Lynde et al. 1986; Saller 1986; Aissaoui 1988; Hird and Tucker 1988; Woo et al. 1993; among numerous others). The $^{87}\text{Sr}/^{86}\text{Sr}$ value of the fibrous/bladed calcite cement, is similar to that of depositional micrite, and is consistent with precipitation from Cambrian seawater (Fig. 4.11). The oxygen isotope compositions of the fibrous/bladed cement and micrite matrix samples,

however, are depleted in ^{18}O relative to Cambrian marine calcite (Fig. 4.6; Table 4.4). This, in conjunction with a wide range of CL patterns observed for the fibrous/bladed calcite cement (Fig. 4.2; Table 4.1), supports diagenetic modifications in the presence of isotopically light meteoric water or at elevated temperatures during burial (Dickson and Coleman 1980; Allan and Matthews 1982; James and Choquette 1984; Choquette and James 1987).

In the case of calcite cement with Mg and Sr derived from seawater, a covariant relationship between the concentrations of these elements indicates that a water-rock exchange through dissolution/precipitation reactions did not significantly influence calcite precipitation (Lohmann 1988; Banner and Hanson 1990; Carpenter et al. 1991; Saller and Moore 1991; Carpenter and Lohmann 1992; Frank and Lohmann 1996). The MgCO_3 composition of the analyzed fibrous/bladed calcite shows an apparent negative correlation with Sr abundances (Fig. 4.8A). This suggests that the precipitation of fibrous/bladed calcite, with an elevated Sr (close to and above 2000 ppm) and relatively low MgCO_3 (<1 to 1.5 mole %) content, may have been influenced by aragonite dissolution in a partially closed diagenetic system (Fig. 4.8A; Brand and Veizer 1980; Mazzullo 1980; James and Klappa 1983; Wiggins 1986; Budd 1988; Lohmann 1988; Budd and Land 1990; Saller and Moore 1991). In the absence of any unequivocal petrographic evidence for an aragonite precursor, an elevated Sr composition is the only indicator for the possible presence of aragonite in the subtidal deposits (see Lasemi and Sandberg 1984; Sandberg 1984; Moshier 1989). Fibrous/bladed calcite cement with elevated MgCO_3 (> 1.5 mole %) and lower Sr (< 1500 ppm) concentrations likely precipitated from marine pore water in a more open diagenetic system (Fig. 4.8A). The range of Sr concentration in this cement may reflect various degrees of diagenetic alteration, based on the similarity to the composition of modern marine calcite (900 to 1500 ppm Sr; Veizer 1983; Tucker and Wright 1990; Carpenter et al. 1991), and diagenetically stabilized calcite (tens or a few

hundred ppm Sr; Veizer 1983). The fibrous/bladed calcite and other marine components present (micrite and ooids) are now composed of low-Mg calcite (< 4 mole % MgCO_3 ; Fig. 4.8A; Table 4.4). The diagenetic stabilization of high-Mg calcite is commonly associated with the retention of “Mg-memory” or the preservation of up to several mole % of MgCO_3 in diagenetic low-Mg calcite (Lohmann and Meyers 1977; Marshal and Ashton 1980; Prezbindowski 1985). The presence of microdolomite, as an indicator for the diagenetic stabilization of high-Mg calcite (Lohmann and Meyers 1977), is only rarely observed within the fibrous/bladed calcite cement from the subtidal deposits. This may indicate an open system during diagenetic stabilization with an efficient removal of Mg, or a relatively low original MgCO_3 concentration, typical of a low- to intermediate-Mg calcite (< 12 mole % MgCO_3).

Calcite cement precipitated from modern oxic marine waters is expected to contain about 40 ppm Fe and 1 ppm Mn (Veizer 1983). The elevated Fe and Mn concentrations of fibrous/bladed calcite from the subtidal deposits indicate precipitation or diagenetic modifications under reducing conditions (Fig. 4.8B; Table 4.4). The stabilization of high-Mg calcite under reducing conditions can cause 500-1000 ppm Fe and 100-250 ppm Mn to be substituted into calcite with a subsequent loss of about 4-6 mole % MgCO_3 (Major et al. 1988; Meyers 1989). The amount of Fe and Mn in most of the fibrous/bladed calcite cement samples, as well as in the micritic matrix and ooids, may reflect a loss of up to about 4-6 mole % MgCO_3 (Fig. 4.8B; Table 4.4). This would additionally imply an original low- to intermediate-Mg calcite mineralogy for these marine depositional and diagenetic components, and could explain a well preserved radial structure in some of the Maynardville ooids (Fig. 4.1C). The CL zonation pattern observed in some of the fibrous/bladed calcite cement suggests that Fe and Mn could have also been added during precipitation of these cements (Fig. 4.2F; see also Tobin et al. 1996). Bladed and equant calcite crystals with elevated Fe and Mn concentrations, and which often show CL

zonation, have sometimes been interpreted as syndepositional marine precipitates from suboxic to anoxic pore waters (Pigott and Land 1986; Weiss and Wilkinson 1988; Sansone et al. 1990; Sun 1990; Major and Wilber 1991; Hendry 1993; Tribble 1993; Tobin et al. 1996). The preservation of CL zonation can be used as indicators for the absence of significant recrystallization, and thus an original low-Mg calcite mineralogy. It is possible, however, that the zoned calcite cements lost some Mg through fabric retentive recrystallization (Major et al. 1988; Rush and Chafetz 1990; Major and Wilber 1991; Budd and Hiatt 1993; Lavoie and Bourque 1993). Johnson and Goldstein (1993) interpreted bladed calcite cement in the Wilberns Formation from Texas with major and minor element and Sr isotope compositions comparable to those of the fibrous/bladed calcite from the Maynardville, but with more positive $\delta^{18}\text{O}$ values (-6.2 to -5.5 ‰ PDB), as a primary Late Cambrian low-Mg calcite that precipitated from oxic to suboxic marine pore waters, and has not undergone significant recrystallization. These observations are consistent with the hypothesis that, during the Late Cambrian, calcite with relatively low Mg content was preferred over aragonite and high-Mg calcite as the abiotic carbonate precipitate (Sandberg 1983).

The precipitation of calcite cement as syntaxial overgrowths on echinoderm fragments may have also started in the marine diagenetic environment (Table 4.1). This is suggested by the presence of compromise boundaries with marine fibrous/bladed calcite cement (Fig. 4.1D; Walker 1989; Walker et al. 1990). The turbid appearance of the initial overgrowth cement is indicative of precipitation from marine fluids, based on the similarity with the documented occurrences of inclusion-rich marine syntaxial cement (Fig. 4.1E; Meyers 1978; Hird and Tucker 1988; Walker 1989; Walker et al. 1990). Studies of intercrystalline isotopic variations within Mississippian syntaxial overgrowth cements, previously interpreted to be exclusively of meteoric origin, suggest that most of these cements formed during early diagenesis in marine phreatic and marine-meteoric mixing

environments (Frank and Lohmann 1995; Frank et al. 1995).

A marine origin for some of the equant calcite cement is suggested by the maximum MgCO_3 (2.9 mole %) and Sr (1874 ppm) compositions, which are similar to those of the interpreted marine depositional and diagenetic components (Fig. 4.8A; Table 4.4). The “anomalous occurrences” of marine equant calcite cement have been documented from both modern and ancient carbonate rocks (Schroeder 1972; Al-Hashimi 1977; James and Ginsburg 1979; Warme and Schneidermann 1983; Pierson and Shinn 1985; Wilkinson et al. 1982, 1985; Freeman-Lynde et al. 1986; Aissaoui 1988; Mayall and Cox 1988; Major and Wilber 1991). Equant calcite cement precipitates as a later phase in a succession of marine cement, or in smaller pores with substantially reduced fluid flow (Given and Wilkinson 1985; Harris et al. 1985; Gonzales et al. 1992). The composition of this cement is commonly identical to the associated marine calcite with an elongated crystal morphology, which precipitates in larger pores within carbonate reefs or other areas with active circulation (Gonzales et al. 1992). The type of substrate may also control the precipitation of elongated versus equant calcite cement from marine pore water (Major and Wilber 1991). The preferential precipitation of fibrous/bladed calcite on ooids and trilobite fragments, and equant calcite on micritic surfaces, observed within the subtidal deposits, may reflect such a substrate control on cement precipitation (Table 4.1).

During the precipitation of equant calcite cement in larger pores, pore-fluid chemistry fluctuated, as evidenced by the zonation observed in both plane light and under CL (Fig. 4.3A-B). The presence of an equant fabric, an increase in crystal size, and a decrease in the degree of turbidity are all consistent with a lower rate of precipitation from fluids of lower saturation (Fig. 4.3A). Inclusion-free equant and syntaxial overgrowth calcite cements are most commonly interpreted to represent precipitation from meteoric water (Longman 1980; James and Choquette 1984; Choquette and James 1988; Niemann and Read 1988). The paucity of aragonite, and the presence of calcite with relatively low

Mg content may have precluded extensive dissolution of the subtidal deposits in the presence of meteoric water.

The equant calcite is on average depleted in ^{18}O relative to the fibrous/bladed calcite (Fig. 4.6B; Table 4.4). This is consistent with the hypothesis of the involvement of meteoric diagenetic fluids in the precipitation of equant calcite cement. The overlap between the $\delta^{18}\text{O}$ values of the equant and fibrous/bladed calcite cement, on the other hand, suggests: 1) a similar composition of the fluids from which some of these cements precipitated; 2) stabilization of marine calcite in the presence of meteoric fluids; and 3) “contamination” of the samples. The first possibility is consistent with the interpretation that the precipitation of equant calcite cement started in the marine realm. It is also possible that the precipitation of fibrous/bladed calcite cement continued during the changes from marine to meteoric pore water. Occurrences of elongated, especially bladed or prismatic calcite cement, have been interpreted as a result of precipitation during mixed marine/meteoric, phreatic meteoric, and burial diagenesis (Longman 1980; James and Klappa 1983; Choquette and James 1987; Lavoie and Bourque 1993; Frank and Lohmann 1996). Similar interpretations are plausible for the bladed calcite crystals, which subsequently precipitated on calcite cement with the typical fibrous morphology of marine precipitates from the subtidal deposits (Table 4.1; Fig. 4.2F). A varying fluid chemistry is also suggested by the CL zonation observed in some of the bladed cement (Fig. 4.2F). The ^{18}O -depletion of both equant and fibrous/bladed calcite relative to predicted Cambrian marine calcite supports the involvement of meteoric fluids in the precipitation and/or diagenetic alteration of these cements (Fig. 4.6B). Finally, even though special care was taken to sample individual diagenetic phases, it was difficult to separate fibrous/bladed calcite from subsequently precipitated equant calcite, and some of the samples may contain a mixture of these cements (see Appendix B). Some of the calcite cements with equant crystal morphology, may in fact represent fibrous/bladed crystals cut

perpendicular to the c-axis along which the crystals are elongated.

Distinguishing between the results of meteoric phreatic and burial diagenesis is very difficult (Tucker and Wright 1990; Saller and Moore 1991). The precipitation of clear equant calcite as the first cement phase in dissolutional voids is likely a result of meteoric diagenesis, but the dissolution may also occur in the presence of marine pore fluid influenced by organic-matter degradation (Druckman and Moore 1985; Curtis 1987; Walter and Burton 1990; Hendry 1993). The low Sr concentrations of some of the equant calcite cement, and all analyzed ferroan equant and syntaxial calcite cements, coupled with elevated Fe and Mn concentrations, indicate precipitation from fluids with a low Sr/Ca ratio under reducing conditions, and may also reflect the effects of a low precipitation rate and increased temperature (Fig. 4.8; Table 4.4; Katz et al. 1972; Lorens 1981; Mucci and Morse 1983; Mucci 1988; Pingitore et al. 1988; Dromgoole and Walter 1990; Morse and Bender 1990; Machel and Burton 1991). All of this is consistent with precipitation in either meteoric phreatic and burial diagenetic environments. Formation during burial is also supported by the similarity in elemental composition with equant calcite cement from tectonic fractures (Fig. 4.8; Table 4.4). The ferroan equant calcite cement has the lowest determined average Mg concentration (1.25 mole % MgCO_3), followed by equant calcite cement from fractures (1.41 mole % MgCO_3). This is indicative of the precipitation from pore fluids with low Mg/Ca ratio, which is typical of meteoric water and many burial brines (Heydari and Moore 1993). The decrease in the amount of Mg incorporated in calcite may also be related to a locally elevated pCO_2 of pore waters due to organic-matter degradation (Burton and Walter 1991; Hendry 1993). The possible influence of organic matter on the diagenesis of the subtidal deposits is suggested by the association of ferroan calcite and microsparite with burrows, framboidal pyrite, fossiliferous lithofacies, and argillaceous layers. The ferroan microsparite represents the result of diagenetic neomorphism or recrystallization of micritic deposits that likely started under reducing

conditions in meteoric phreatic environment and continued during burial (Fig. 4.1A; Table 4.1). The anticipated decrease in the amount of Mg in meteoric and burial cements relative to marine cements can be counteracted by an increase in the Mg/Ca ratio of pore water with progressive calcite precipitation in a closed diagenetic system, and by temperature increase (Katz 1973; Mucci 1987; Mucci et al. 1989; Burton and Walter 1987, 1991). These processes could have influenced the Mg content of some of the pore central equant calcite and syntaxial overgrowth calcite cement (Table 4.4; Fig. 4.8A). The overlap of $\delta^{18}\text{O}$ values of non-ferroan and ferroan equant calcite cements suggests a similar isotope composition for the diagenetic fluids and/or comparable temperatures during precipitation. The slightly more negative average $\delta^{18}\text{O}$ value for the ferroan calcite, and the substantially ^{18}O -depleted compositions of equant calcite cement from fractures can be attributed to the higher temperatures associated with precipitation during progressive burial (Fig. 4.6B; Table 4.4).

The presence of tectonic fractures and MVT minerals indicates the migration of hot burial fluids through the subtidal deposits of the Maynardville. The occurrence of MVT minerals within the intraclastic deposits suggests the preferential migration of burial fluids through the coarse-grained porous lithofacies. The larger framework pores and burrows within the thrombolitic deposits, that have not been completely occluded during early marine diagenesis, also provided pathways for the preferential migration of both meteoric fluids during earlier diagenesis and burial fluids later on. This is evidenced by the dissolution enlargement of pores and their occlusion with non-ferroan and ferroan equant calcite, and pore-central saddle dolomite cement. The negative $\delta^{18}\text{O}$ values observed for the micrite samples comprising the microbial deposits can be related to diagenetic alteration by meteoric, and especially burial fluids at elevated temperature (Fig. 4.6A).

Dolomite

Dolomite is not an abundant diagenetic phase of the subtidal package and therefore an extensive external source of Mg is not required. Any postulated interpretations for the occurrence of fine-crystalline dolomite within the ribbon rocks should account for: 1) the stratigraphic distribution of dolomite within the centimeter-scale argillaceous layers; 2) the ferroan composition (revealed by staining); and 3) the negative $\delta^{18}\text{O}$ composition, but on average enrichment in ^{18}O relative to other subtidal carbonate components.

The occurrences of dolomite within subtidal argillaceous deposits have been interpreted as: 1) eolian transport of dolomite; 2) early diagenetic formation of organogenic dolomite or syndimentary dolomitization from normal seawater; and 3) burial dolomitization related to pressure solution, compaction and clay-mineral diagenesis. Deeper water sediments in the Persian Gulf contain up to 10 % windborn detrital dolomite (Narkiewicz 1983). Even though the eolian transport of clay minerals and silt-size siliciclastic detritus played an important role in the deposition of the argillaceous layers of the Maynardville Formation, it is unlikely that the associated dolomite represents a detrital phase. The expected degree of abrasion and weathering characteristic of detrital dolomite (Price and McHargue 1983), was not observed (Fig. 4.1B). Additionally, the ferroan composition of the dolomite is inconsistent with the syndepositional dolomitization of sediment on the contemporaneous tidal flat of the Maynardville/Elbrook carbonate platform to the east, which was the most probable source of detrital dolomite (Figs. 1.1, 1.3).

The mechanisms for the early diagenetic formation of dolomite, including organogenic and normal-marine dolomitization models, have been invoked for the occurrences of ferroan, fine-crystalline dolomite in subtidal, centimeter-thick, clay-rich layers (Behrens and Land 1972; Baker and Kastner 1981; Saller 1984; Land 1985; Mullins et al. 1985; Carballo et al. 1987; Mazzullo et al. 1987; Mitchell et al. 1987; Cander et al.

1988; Compton 1988a, 1988b; Ruppel and Cander 1988; Middelburg et al. 1990).

The source of Mg for dolomitization is a diffusive flux from the overlying seawater of normal salinity (Baker and Burns 1985). Additional Ca and carbonate ions are supplied from the dissolution of precursor carbonate (Compton 1988a). Precipitation of early diagenetic dolomite is promoted by: 1) an increase of the Mg/Ca ratio in interstitial marine pore-water due to the high smectite/calcium carbonate ratio in the siliciclastic-rich carbonate sediment, coupled with a decrease in the sedimentation rate, which promotes an interaction between seawater and sediment (Ruppel and Cander 1988); and 2) the degradation of organic matter by sulfate-reducing bacteria which increases the carbonate alkalinity and pH of the pore water, and decreases the sulfate ion concentration (Baker and Kastner 1981; Slaughter and Hill 1991). The ferroan composition of dolomite reflects a high clay mineral/organic-matter ratio, coprecipitation of dolomite and pyrite in the sulfate reduction zone, or a low precipitation rate (Compton 1988b; Ruppel and Cander 1988). The source of iron is from the reduction of Fe oxides and hydroxides during bacterial degradation of organic matter (Ruppel and Cander 1988). Additionally, the degradation of marine organic matter provides mechanisms for remobilizing Fe from siliciclastic phases and for the releasing of Fe bound with organic matter (Holail et al. 1988; Tucker and Wright 1990). The involvement of organic matter is reflected by the large variations in the carbon isotope composition of dolomite (-15 to +20 ‰ PDB; Irwin 1980, Kushnir and Kastner 1984). An early diagenetic formation, at or near normal sedimentary temperature, results in relatively positive $\delta^{18}\text{O}$ values for precipitated dolomite (Irwin 1980; Taylor and Sibley 1986; Gregg 1988).

The estimated $\delta^{18}\text{O}$ composition of dolomite precipitated in equilibrium with Cambrian seawater of normal salinity ranges between -3 and -1 ‰ PDB, or may even reach +1 ‰ PDB for Upper Cambrian dolomite. This range was estimated from the isotope compositions for Cambrian marine calcite reported in Lohmann and Walker

(1989), and Gao and Land (1991b), and by considering an equilibrium fractionation factor of 3 ± 1 ‰ between coprecipitated calcite and dolomite (Land 1980). The validity of this fractionation factor is supported by the observation that the CO_2 derived by dissolving dolomite in phosphoric acid has a $\delta^{18}\text{O}$ value of about 3.2 ‰ (McKenzie 1981) or 3.8 ‰ (Land 1985) more positive than the CO_2 derived from calcite that coprecipitated in equilibrium with dolomite. The $\delta^{18}\text{O}$ compositions of the dolomite from the argillaceous layers of the Maynardville (-8.2 to -6.1 ‰ PDB), is substantially lower than the estimated Cambrian seawater dolomite. This would imply a substantial diagenetic modification of syndepositional or early diagenetic dolomite. Thus, burial dolomitization models provide the most plausible explanation for the formation of dolomite which occur in the subtidal deposits.

The argillaceous layers contain pressure-solution features which indicate that the associated fine-crystalline dolomite may be of stylolite or stylolite origin (Fig. 4.1A). Pressure solution of Mg-calcite during burial serves as a source of Mg for the precipitation of dolomite as a stylolite mineral (Wanless 1979). The evidence for the stylolite origin of dolomite, which can be observed in the Maynardville, includes: 1) truncation of microstylolites by dolomite rhombs; 2) preferential concentration of dolomite along clay seams; and 3) a sharp drop in the amount of dolomite in the adjacent limestone layers (Logan and Semeniuk 1976; Wanless 1979; Zenger and Dunham 1988). Some of the dolomite from the argillaceous layers may also represent stylolite or a concentration of dolomite as a less soluble residue. The dolomite crystals disseminated in the interbedded limestone layers, however, are commonly coarser than dolomite crystals within the argillaceous seams. This, coupled with the paucity of disseminated dolomite in the limestone layers, indicates that pressure solution alone could not have produced all the dolomite as residue. Pre-burial stabilization of high-Mg calcite and the deep-burial origin for stylolites are possible drawbacks of the pressure-solution dolomitization model

(Morrow 1982). In the absence of substantial meteoric modifications, however, metastable carbonate phases may persist through shallow to intermediate burial (Tucker and Wright 1990). Additionally, pressure solution can start within the first few hundred meters of burial (Choquette and James 1987).

The burial compaction model of dolomitization involves the expulsion of pore water from argillaceous sediment during compaction. The source of Mg is trapped seawater and ions adsorbed on clay mineral surfaces. Additional Mg and Fe ions are supplied by the expulsion of structural water from clay minerals during diagenetic changes such as the transformation of montmorillonitic clay (smectite) to illite (Mattes and Mountjoy 1980; McHargue and Price 1982). This transformation occurs at temperatures between 50 and 125°C (Boles and Franks 1979; Lahann 1980), and produces substantial amounts of Mg^{2+} , Fe^{2+} , Ca^{2+} , Si^{4+} , and Na^+ (Mattes and Mountjoy 1980; McHargue and Price 1982). The released ions contribute to the formation of burial dolomite, which is commonly enriched in Ca and Fe, and is accompanied by ferroan calcite (Irwin 1980; Taylor and Sibley 1986; Gregg 1988). Burial compaction dolomitization has been proposed for the formation of the fine-crystalline ferroan dolomite disseminated in the argillaceous lime mudstone or in selectively replaced allochems, and as dolomite cement within voids in argillaceous carbonates and in carbonates adjacent to marine shales (McHargue and Price 1982; Gregg 1988).

A burial origin, from fluids derived locally by compaction of interbedded shale, carbonate dissolution, and diagenetic alteration of clay minerals, can account for the observed characteristics of the dolomite from argillaceous subtidal deposits. The relatively ^{13}C -enriched composition of dolomite may reflect organic matter degradation reactions including bacterial fermentation and methanogenesis (Fig. 4.6A; Irwin et al. 1977; Irwin 1980). The unusually high $\delta^{13}\text{C}$ values of the Maynardville carbonate components, however, are considered to reflect a secular increase in the carbon isotope ratio of Late

Cambrian seawater (see Chapter 5). Superimposed on the secular trend are variations due to diagenetic modifications in the presence of degrading organic matter.

Processes similar to that for the formation of dolomite within argillaceous layers can account for the formation of ferroan replacement calcite, disseminated replacement dolomite in limestone layers of ribbon rocks, and more coarse-crystalline replacement and cement saddle dolomite. Pyrite-coated hardgrounds provided an additional source of Fe for saddle dolomite replacement. A non-stoichiometric (Ca-rich) composition, elevated Fe and Mn concentrations, and negative $\delta^{18}\text{O}$ values support the burial origin for saddle dolomite (Figs. 4.6B, 4.9; Table 4.4). The coarse-crystalline, non-planar texture of the saddle dolomite is also consistent with precipitation at elevated temperatures (Fig. 4.3; Table 4.2; see Gregg and Sibley 1984). The paucity of saddle dolomite cement confirms that the precipitation from locally derived fluids can account for the formation of all of this cement. On the other hand, the presence of MVT minerals (sphalerite, pyrite, galena), are evidence for the migration of externally derived fluids through the Maynardville platform carbonates. The formation of saddle dolomite, associated with the MVT minerals, is interpreted as burial dolomitization involving the migration of basinal brines (Mattes and Mountjoy 1980; Kesson et al. 1981; Sverjensky 1981; Gregg 1985; Moore 1985; Scholle and Halley 1985; Banner et al. 1988). A dissolution episode prior to the precipitation of saddle dolomite in the Maynardville is indicative of the presence of chemically aggressive waters rich in organic acid or CO_2 , which is a common characteristic of subsurface brines, including MVT mineralizing fluids (Fig. 4.3A-B; Kharaka et al. 1983; Meshri 1986; Choquette and James 1987; Spirakis and Heyl 1988; Stueber and Walter 1991; Barnaby and Read 1992; Kharaka and Thordsen 1992; Gregg et al. 1993; Montañez 1994). Precipitation from basinal brines that underwent interaction with siliciclastic deposits at increased temperature commonly produces an elevated $^{87}\text{Sr}/^{86}\text{Sr}$ composition for burial cements (Kesson et al. 1981; Stueber et al. 1984, 1987; Chaudhuri et al. 1987; Morton

and Land 1987; Cander et al. 1988; Chaudhuri and Clauer 1992; Banner 1995). The Sr isotope composition of the analyzed subtidal saddle dolomite cement is elevated (0.7096) relative to Cambrian seawater (Fig. 4.11). This is consistent with precipitation from MVT basinal brines, as well as from locally derived dolomitizing fluids whose $^{87}\text{Sr}/^{86}\text{Sr}$ ratio was influenced by interaction with siliciclastic minerals from the argillaceous layers in the subtidal deposits.

Extensively Dolomitized Peritidal Deposits

Replacement Dolomite

The peritidal deposits of the Maynardville Formation have been substantially dolomitized. The formation of aphanocrystalline to very finely-crystalline replacement dolomite (Fig. 4.4A-B; Table 4.3) occurred penecontemporaneously with, or soon after, deposition of fine-grained carbonate sediment. Conditions during formation of the Maynardville dolomicrite may have been similar to the present-day formation of sabkha dolomites in the Persian Gulf, and other Holocene peritidal environments (McKenzie et al. 1980; McKenzie 1981; Patterson and Kinsman 1982; Illing and Taylor 1993). The sabkha model of dolomitization involves seepage reflux and the evaporative pumping of seawater. Seepage reflux refers to infiltration of dense marine water with elevated salinity through the underlying sediment. Marine water is constantly replenished by tidal action and storm flooding (Morrow 1982). Evaporative pumping involves a flow of seawater landward through sediment to replace water lost by evaporation near the sabkha surface (McKenzie et al. 1980; Morrow 1982). Under sabkha conditions the kinetic problems associated with dolomite precipitation are overcome by an increase in temperature, and by gypsum and anhydrite precipitation that elevates the Mg/Ca and CO_3/Ca ratios, and decreases sulfate concentrations (Machel and Mountjoy 1986). Dolomitization can be also promoted in the presence of mixed marine-meteoric waters during the exposure of tidal flat sediments.

Mixed brines are potential dolomitizing fluids due to their high Mg and HCO_3^- concentration, and the dilution effect (Morrow 1982; Hardie 1987; Tucker and Wright 1990). Evaporative conditions and periodic subaerial exposure are conducive to early silicification of tidal-flat carbonate sediments (Milliken 1979; Williams and Crerar 1985; Parnell 1986; Holail et al. 1988; Tribble et al. 1995). The early diagenetic silicification of the Upper Cambrian peritidal deposits under such conditions is suggested by the association of chert with exposure surfaces and evaporite pseudomorphs. Silicification predated significant mechanical compaction and stylolitization as evidenced by the presence of uncompacted silicified ooids adjacent to extensively compacted dolomitized ooids.

Dolomicrite from the peritidal package formed as an early diagenetic replacement of fine-grained carbonate sediment on a semi-arid tidal flat from fluids derived from modified seawater representing hypersaline brines, or seawater mixed with hypersaline or meteoric water. Evidence for the early diagenetic replacement origin of dolomicrite includes: 1) small crystal size; 2) retention of the depositional fabric; 3) association with indicators of intertidal to supratidal deposition such as evaporites, fenestrae, microbial laminae, desiccation features, and intraclasts; 4) paucity of fossils indicating a restricted hypersaline setting in which early dolomitization is favored; and 5) the presence of dolomitic intraclasts in rare coarser-grained intraclastic layers that have not been completely dolomitized, suggesting that dolomitization of the fine-grained carbonate sediment took place prior to formation and redeposition of intraclasts. Additionally, pervasive dolomitization of carbonate sediment requires an abundant supply of Mg, which can be provided by active circulation of seawater-derived fluids through the sediment during early diagenesis, prior to significant lithification and porosity occlusion (Land 1985; Hardie 1987).

Examples from the Holocene indicate that early diagenetic dolomite is commonly

non-stoichiometric (Ca-rich), and poorly ordered (Land 1980, 1985; McKenzie 1981; Carballo et al. 1987; Mitchell et al. 1987; Lasemi et al. 1989; Sibley 1990; Tucker and Wright 1990; Gregg et al. 1992; Mazzullo et al. 1987; Mazzullo 1992). These characteristics, in addition to very small crystal size, make early diagenetic dolomite susceptible to neomorphism and recrystallization during subsequent diagenesis. The criteria for the recognition of recrystallized early dolomite include: 1) stoichiometry and a high degree of ordering; 2) a coarse-crystalline mosaic; 3) non-planar crystal boundaries; 4) homogenized CL zonation; 5) low ^{18}O and Sr concentrations; 6) enrichment in Fe and Mn; and 7) a Sr isotope composition different than that predicted for marine deposits of the same age (Gao and Land 1991b; Mazzullo 1992; Kupecz et al. 1993).

The composition of the Maynardville dolomicrite ranges from stoichiometric to Ca-rich (Fig. 4.9A; Table 4.5). Such a wide range of compositions can be related to varying degrees of diagenetic alteration, but may also be a function of the conditions within the depositional and early diagenetic environment. Dolomite associated with hypersaline conditions commonly has a more stoichiometric composition than dolomite not associated with evaporites (Lumsden and Chimahusky 1980; Morrow 1982; Shatkay and Magaritz 1987). Additionally, Sass and Bein (1988) observed that dolomite associated with gypsum has a stoichiometric to Ca-rich (57 mole %) composition, whereas dolomite that accompanies halite is commonly stoichiometric.

A crystal size comparison of the Maynardville dolomicrite ($< 10\text{-}15\ \mu\text{m}$) and dolomicrosparite ($15\text{-}60\ \mu\text{m}$), with dolomite crystals ($1\text{-}5\ \mu\text{m}$) from the modern sabkhas (Paterson and Kinsman 1982), provides additional evidence for diagenetic recrystallization or neomorphism. Diagenetic alterations are also supported by the uniform to patchy distribution of luminescence, and the absence of CL zonation in the Maynardville replacement dolomite (Table 4.3).

The most negative $\delta^{18}\text{O}$ value for dolomite that precipitated in equilibrium with

normal salinity Cambrian seawater is estimated to be about -3 ‰ PDB. Dolomite that forms from hypersaline fluids is enriched in ^{18}O due to the evaporation effect. Thus, dolomite associated with gypsum has $\delta^{18}\text{O}$ values about 3 ‰ higher than marine non-evaporative dolomite (Sass and Bein 1988). Consequently, the $\delta^{18}\text{O}$ values of Cenozoic evaporative dolomite range from +0.5 to +7.5 ‰ PDB (McKenzie 1981; Botz and von der Borch 1984; Pierre et al. 1984; Carballo et al. 1987; Mitchell et al. 1987; Gregg et al. 1992). The $\delta^{18}\text{O}$ composition of the Maynardville peritidal dolomicrite is not typical of hypersaline fluids, and suggests diagenetic modifications in the presence of ^{18}O -depleted fluids or at elevated temperatures during burial (Fig. 4.7A; Table 4.5).

Most of the Tertiary and Holocene marine dolomites studied have between 60 and 1000 ppm Sr (Land 1980; Morrow 1982; Veizer 1983; Vahrenkamp and Swart 1990), with many containing > 600 ppm Sr (Mattes and Mountjoy 1980; Carballo et al. 1987; Dawans and Swart 1988; Banner 1995). The elevated Sr composition in dolomites may reflect the influence of precursor aragonite, or the rapid precipitation of dolomite from supersaturated fluids during early diagenesis (Land 1980; Lorens 1981; Morrow 1982; Bein and Land 1983; Spötl and Burns 1991; Banner 1995). Dolomitization of a marine calcite precursor produces dolomite with a maximum of several hundred ppm Sr (Tucker and Wright 1990). Dolomite with low Sr concentrations (60 ppm) may form from seawater due to a very low distribution coefficient for Sr in stoichiometric dolomite (Vahrenkamp and Swart 1990). The Sr content in non-stoichiometric dolomite is commonly reduced to < 200 ppm during diagenetic recrystallization (Land 1980; Mattes and Mountjoy 1980; Bein and Land 1983; Banner 1995). The low Sr content of the Maynardville replacement dolomite is consistent with diagenetic modifications (Table 4.5).

The measured $^{87}\text{Sr}/^{86}\text{Sr}$ ratio for dolomicrite, which is higher than that of Late Cambrian seawater, suggests diagenetic modifications in the presence of radiogenic pore fluids (Fig. 4.11). The analyzed dolomicrite sample is from the sequence boundary zone at

the Maynardville/Copper Ridge transition, which is characterized by common detrital quartz and some K-feldspar grains (Fig. 2.7). The diagenesis of K-feldspar may have provided the radiogenic component during recrystallization of the early dolomite. The elevated Sr isotope composition may also reflect a possible Late Cambrian $^{87}\text{Sr}/^{86}\text{Sr}$ seawater increase related to the increased erosion of the craton during the continent-wide Dresbachian/Franconian unconformity.

The succession of dolomite replacement fabric from: 1) dolomicrite; 2) dolomicrosparite; 3) coarser-crystalline dolomite; to 4) saddle dolomite, is accompanied with: 1) an increase in crystal size; 2) an increase in the number of non-planar crystal boundaries; 3) an increase in fabric obliteration; 4) the slight decrease in average $\delta^{18}\text{O}$ values; and 5) with the exception of dolomicrosparite, which was not analyzed for the trace element composition, an increase in the average Fe concentration and the maximum Mn concentration (Figs. 4.4, 4.7A, 4.9B; Table 4.5). All of these trends are consistent with progressive recrystallization during later diagenesis.

Recrystallization of sabkha-related dolomite starts during early diagenesis in the presence of marine water modified by mixing with meteoric water, and continues with subsequent burial (Kupecz and Land 1991, 1994; Gregg et al. 1992; Montañez and Read 1992b; Chafetz and Rush 1994). Dolomicrosparite and coarser-crystalline replacement dolomite are commonly interpreted to be the result of mixed marine/meteoric dolomitization (Magaritz et al. 1980; Simms 1984; Choquette and Steinen 1980; Randazzo and Cook 1987; Humprey 1988; Shukla 1988; Humphrey and Quinn 1989; Cander 1994). Less turbid outer parts of some of the coarser-crystalline replacement dolomite from the Maynardville may represent later diagenetic overgrowths on the early diagenetic turbid cores (Table 4.3). Such clear outer parts can form from dilute subsurface solutions of mixed marine-meteoric or meteoric origin (Morrow 1982; Moore et al. 1988; Montañez and Read 1992b).

Recrystallization of early dolomite during burial is an attractive interpretation for the formation of the coarse-crystalline replacement dolomite because no additional source of Mg is required (Banner et al. 1988; Wallace 1990; Mazzullo 1992; Montañez and Read 1992b; Gao et al. 1992; Gregg and Shelton 1990; Gregg et al. 1992). A xenotopic texture of the coarser-crystalline replacement dolomite from the Maynardville and the Copper Ridge Dolomite suggests formation at temperatures above 50°C (Fig. 4.4D; Table 4.3; Gregg and Sibley 1984; Sibley and Gregg 1987). The coarse-crystalline dolomite with a xenotopic fabric, ^{18}O -depleted compositions, and elevated trace element (Fe, Mn) contents is commonly interpreted to reflect the influence of hot, deep subsurface fluids (Zenger 1983; Zenger and Dunham 1988; Gregg 1985; Buelter and Guillemette 1988; Gregg and Shelton 1990).

A fabric-obliterate mosaic of coarse-crystalline dolomite can form as a result of multiple recrystallization events of fine-crystalline dolomite, or may be controlled by the coarse-grained texture of deposits being replaced (Kupecz and Land 1991; Kupecz et al. 1993). Similar coarse-crystalline dolomite fabrics can also form by the dolomitization of precursor limestone during burial (Machel and Anderson 1989; Qing and Mountjoy 1989; Mountjoy and Amthor 1994). Limestone layers, and grain-supported lithofacies in general, may have represented zones with higher porosity and permeability that served as pathways for preferential migration of dolomitizing fluids during burial (Lee and Friedman 1987; Sibley and Gregg 1987; Amthor and Friedman 1991; Gao and Land 1991a; Montañez and Read 1992b; Kupecz et al. 1993; Mountjoy and Amthor 1994). The presence of allochem ghosts in the mosaic of the coarser-crystalline dolomite in the upper Maynardville and the Copper Ridge Dolomite indicates replacement of the coarser-grained deposits (Fig. 4.4D). Evidence for the burial dolomitization of limestone is denoted by the patchy distribution of coarser-crystalline replacement dolomite within the rare limestone deposits in the peritidal depositional package (Table 4.3).

Based on the association with hydrocarbons and sulfide mineralization, saddle dolomite is most commonly interpreted to form by thermochemical sulfate reduction processes from fluids provided by pressure solution and basinal brine migration during burial at temperatures between 60 and 150°C (Radke and Mathis 1980; Machel 1987; Qing and Mountjoy 1992). The occurrence of saddle dolomite within a bituminous matrix in the peritidal deposits suggests dolomite formation associated with hydrocarbon migration and accumulation (Fig. 4.4E). Potential sources for hydrocarbons are the organic-rich shales of the Cambrian Conasauga basin or the Ordovician Sevier basin. The burial compaction of the basinal mudrocks, in response to sediment and tectonic loading, provides a mechanism for the migration of hydrocarbons and mineralizing brines into adjacent platform carbonates (Cathles and Smith 1983; Bethke 1985; Oliver 1986; Qing and Mountjoy 1989; Bethke and Marshak 1990; Audet and Fowler 1992; Cartwright 1994; Srinivasan et al. 1994). Most formational waters have low Mg/Ca ratios (Hanor 1983, 1987; Cander et al. 1988; Moore 1989), which can account for the Ca-rich composition of the late diagenetic replacement dolomite (Fig. 4.9A). The involvement of burial fluids can also account for the decrease in $\delta^{18}\text{O}$ values, and elevated Fe and Mn compositions of the coarser-crystalline and saddle dolomite relative to the fine-crystalline early diagenetic dolomite (Figs. 4.7A; 4.9B; Table 4.5).

Dolomite Cement

The dull luminescent cores of the zoned dolomite cement could have started precipitating under conditions similar to those for the formation of the early diagenetic dolomite. This is suggested by the occurrence of zoned dolomite as the first cement phase in the voids of synsedimentary origin such as fenestral voids and desiccation voids, as well as in evaporite-dissolution voids. The low Fe content of the pore-rim zoned dolomite is consistent with precipitation from oxygenated pore fluids (Fig. 4.10A). Additionally, the

pore-rim zoned dolomite cement is compositionally similar to the fine-crystalline replacement dolomite (Fig. 4.9; Table 4.5). The relationship between the CaCO_3 composition of the zoned dolomite cement and the associated dolomicrite matrix suggests formation from fluids similar in composition, or possibly the buffering of dolomitizing fluid to the host-rock composition (Fig. 4.10A)

The precipitation of dolomite cement could have been promoted by the introduction of meteoric water into the peritidal deposits during periods of subaerial exposure. The rhombohedral zoned dolomite crystals on walls of dissolution-enlarged voids may represent precipitation of dolomite under the influence of meteoric water (Fig. 4.5B-C; Table 4.3). This pore-rim dolomite cement is succeeded by equant calcite cement of meteoric phreatic/shallow burial origin, and pore-central non-luminescent, coarse-crystalline saddle dolomite cement. Similar occurrences of rhombohedral dolomite crystals (1 to 100 μm), lining cavities, which are occasionally zoned and postdated by meteoric calcite cements, have been interpreted as a result of mixing-zone dolomitization (Folk and Land 1975; Kaldi and Gidman 1982; Ward and Halley 1985; Humphrey and Quinn 1989; Humphrey and Radjef 1991; Gill et al. 1995).

Pressure-solution along numerous stylolites within the peritidal deposits could have provided a source for the continuing precipitation of dolomite cement into the burial environment. During burial, dolomitizing fluids could have also been provided by externally derived basinal brines. Both of these processes can account for the precipitation of dolomite cement with complex zones that can not be correlated between pores (Fig. 4.5D-E; Fisher 1988; Amthor and Friedman 1992). Cement zones may represent pulses of dolomitizing fluids that evolved along the fluid migration pathway and precipitated cement of various composition in different parts of the carbonate succession. With progressive burial and pore occlusion, precipitation under reducing conditions resulted in the increased incorporation of Fe in the outer non-luminescent parts of the zoned dolomite cement (Fig.

4.10A). The $\delta^{18}\text{O}$ composition of the zoned dolomite substantiates the involvement of dolomitizing fluids of meteoric origin and the precipitation from burial fluids at elevated temperature (Fig. 4.7B).

The microstratigraphic relationship between the pore-rim zoned dolomite cement and the pore-center saddle dolomite cement, the distribution in pores of various origin (syndimentary versus dissolutional or tectonic), and the differences in geochemical composition (Figs. 4.7B, 4.9, 4.10; Tables 4.3, 4.5), indicate a predominance of shallow to intermediate burial environments for the formation of zoned dolomite cement, and later burial diagenesis for the saddle dolomite cement. The isotope compositions of the zoned dolomite cement overlap with the fine-crystalline replacement dolomite of early diagenetic origin (Fig. 4.7B). The more stoichiometric composition, and lower Fe and Mn concentrations of the zoned dolomite cement are also comparable to those of dolomicrite (Fig. 4.9). The saddle dolomite cement, on the other hand, is compositionally similar to late diagenetic replacement dolomite, which may suggest their simultaneous formation (Fig. 4.9). The more negative average $\delta^{18}\text{O}$ composition of the saddle dolomite cement relative to the zoned dolomite cement is consistent with precipitation at a higher burial temperature (Fig. 4.7B). The substantial overlap between the $\delta^{18}\text{O}$ compositions of these dolomite cement types, however, indicates precipitation from fluids of similar isotopic composition. This overlap may also suggest that the outer non-luminescent parts of the zoned dolomite cement and the saddle dolomite cement may have precipitated under similar conditions.

The late burial origin for the saddle dolomite cement is substantiated by its presence in tectonic fractures and the association with MVT mineralization (sphalerite in fractures and dissolutional pores). The latter also indicates that during late burial, in addition to dolomitizing fluids provided locally by pressure solution, extraformational brines served as a source for the precipitation of dolomite cement. The near

stoichiometric composition of the pore-rim saddle dolomite cement may result from initial buffering of the dolomitizing fluid to the host rock composition (Fig. 4.10B). The generally increasing, but overall fluctuating amount of Ca in the subsequently precipitated saddle dolomite reflects the composition of the dolomitizing fluids, which is consistent with basinal brines with a low Mg/Ca ratio. The reduced amount of Ca in the pore-central saddle dolomite cement may represent slow precipitation under elevated temperatures (Fig. 4.10B). The same process can account for the concurrent increase in the incorporation of Fe (Fig. 4.10B).

The temperature range for saddle dolomite formation can be estimated from measured $\delta^{18}\text{O}$ values and the assumed $\delta^{18}\text{O}$ compositions of burial fluids. A commonly observed range of $\delta^{18}\text{O}$ compositions for formation waters in sedimentary basins of 0 to 8 ‰ SMOW (Kharaka and Thordsen 1992), yields a temperature range for saddle dolomite precipitation from 80°C to greater than the maximum burial temperature of 200°C (equations after Land 1985). The temperature at the onset of saddle dolomite cement precipitation was reached by the Middle to Late Ordovician when the Maynardville was buried to a depth of about 2 km (Fig. 4.13). Migration of hot brines from deeper parts of the sedimentary basin into shallow carbonate platform strata can account for the temperatures of mineral formation in excess of the maximum burial temperature (Coniglio et al. 1994; Montañez 1994; Mountjoy and Amthor 1994). Mechanisms for brine migration are sedimentary and tectonic compaction due to thrusting and tectonic compression as well as topography-driven recharge related to tectonic uplift (Garven and Freeze 1984; Oliver 1986; Leach and Rowan 1986; Bethke and Marshak 1990; Deming 1992; Kaufman 1994). The assumed range of burial fluid isotope composition yields a temperature of about 90 to 160°C for the precipitation of calcite cement in tectonic fractures (equations from Craig 1965, and Friedman and O'Neil 1977), suggesting the simultaneous precipitation of the fracture-occluding calcite and saddle dolomite cements.

The coprecipitation of these cements is also supported by the difference in their average $\delta^{18}\text{O}$ compositions of about 3 ‰ (Tables 4.4, 4.5).

The Sr isotope composition of the dolomite cement from the peritidal deposits (0.70865 to 0.70896) indicates the predominance of a dolomitizing fluid source different than: 1) Late Cambrian seawater; 2) dissolution of Upper Cambrian carbonates; or 3) highly radiogenic basinal brines (Fig. 4.11). The presence of non-radiogenic cements in the Upper Cambrian carbonate succession can be related to the precipitation from: 1) younger seawater; 2) marine pore-water expelled from younger shale successions during early diagenetic compaction; or 3) meteoric water that interacted with younger carbonate rocks (see also Gao 1990; Gao and Land 1991a, 1991b). The Sr isotope composition of the dolomite cement from the peritidal deposits is comparable to Early to Middle Ordovician seawater (Fig. 4.11). Thus, based on the burial history of the Maynardville carbonate platform succession (Fig. 4.13), the plausible explanations for the observed $^{87}\text{Sr}/^{86}\text{Sr}$ composition of dolomite are precipitation from: 1) marine fluids, which circulated downward into the Upper Cambrian platform carbonate deposits during the Early and Middle Ordovician; 2) marine pore-water expelled from the Middle Ordovician Sevier shale basin; and 3) burial fluids that interacted with the Ordovician carbonate rocks. Even though density-driven flow, including thermal convection, and eustatic-driven flow (see Kaufman 1994) could have provided the mechanism for circulation of the marine water overlying the Ordovician carbonate platform through the underlying Cambrian deposits, these mechanisms cannot account for the range of temperatures inferred for the precipitation of dolomite cement. The hypothesis of pore-water expulsion from the Sevier basin faces the same problem because mechanical dewatering and the release of marine pore-water from shale successions occur within the first 1 to 2 km of burial (Garven and Freeze 1984; Jones and Addis 1985; Machel and Mountjoy 1986; Bethke and Marshak 1990; Amthor and Friedman 1992). Thus, circulation of warm burial fluids that interacted

with Ordovician carbonate rocks may provide an explanation for both strontium and oxygen isotope compositions of dolomite cement from the Upper Cambrian carbonate succession.

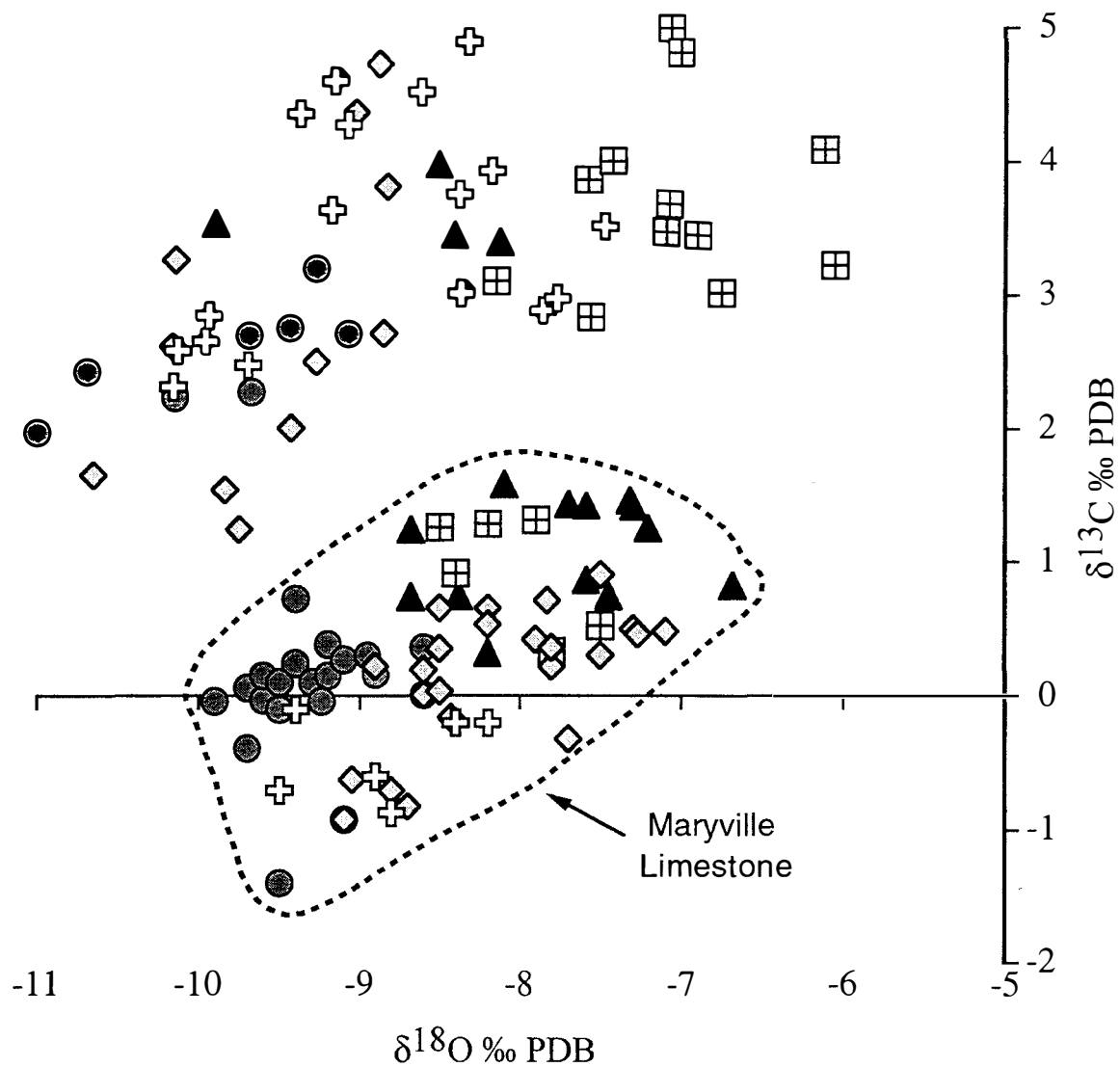
COMPARISON WITH THE UNDERLYING AND THE OVERLYING STRATA

In order to evaluate the effects of the cessation of Grand Cycle deposition on the diagenetic history of the Maynardville Formation, a comparison was made with the underlying and overlying strata. The diagenetic history of the Maryville Limestone (Middle Cambrian) was described in Srinivasan (1993) and Srinivasan et al. (1994). The diagenesis of the Nolichucky Shale (Upper Cambrian) was studied by Foreman (1991). No detailed diagenetic study has yet been conducted on the Upper Cambrian rocks of the overlying Knox Group. Therefore, comparison of the Maynardville was made with the diagenesis of the Lower Ordovician Upper Knox Group as reported in Montañez and Read (1992a and b) and Montañez (1994).

Maryville Limestone

The marine diagenetic phases within the subtidal deposits of the Middle Cambrian Maryville Limestone include: turbid fibrous calcite, syntaxial overgrowth calcite cements, and framboidal pyrite (Srinivasan 1993; Srinivasan et al. 1994). The average $\delta^{18}\text{O}$ value for the Maryville fibrous calcite (-8.8 ‰ PDB), is similar to the average value for the Maynardville fibrous/bladed calcite (-8.9 ‰ PDB), suggesting a similar diagenetic history (Fig. 4.14). The diagenesis of the Maryville was influenced by the establishment of a meteoric diagenetic environment that resulted in carbonate dissolution followed by precipitation of 'blocky' clear calcite spar, and its turbid equivalent during early and intermediate burial. These diagenetic phases are petrographically similar to the equant calcite from the Maynardville.

Figure 4.14. Comparison of stable isotope compositions between carbonate components from the subtidal Maynardville deposits and the Middle Cambrian Maryville Limestone. Data for the Maryville Limestone are from Srinivasan (1993), and Srinivasan et al. (1994).



Maynardville Formation:		Maryville Limestone:	
+	fibrous/bladed calcite	+	fibrous calcite
◊	equant calcite	◊	blocky calcite
●	ferroan equant calcite	●	ferroan blocky calcite
▣	dolomite from clay-seams	▣	Type III dolomite
▲	subtidal saddle dolomite	▲	Type IV dolomite

Four types of dolomite formed during the late diagenesis of the Maryville Limestone: I) small, irregular disseminations of dolomite crystals (2 μm to a few tens of μm) within mud-rich facies; II) planar rhombohedral dolomite (5-300 μm) inclusions in clear 'blocky' ferroan meteoric calcite; III) subhedral to anhedral crystals (10-150 μm) in thin seams and a few millimeter-thick bands associated with stylolites; and IV) saddle dolomite crystals (0.1 to 1.5 mm) occurring as void filling and rarely as a replacement of matrix (Srinivasan et al. 1994).

Type I and II dolomite formed during shallow to intermediate burial diagenesis. Scattered dolomite crystals replacing micritic matrix and allochems in the subtidal deposits of the Maynardville are similar to the type I Maryville dolomite, whereas the pore-rim, rhombohedral-zoned dolomite crystals, succeeded by the coarse-crystalline equant ferroan calcite (Fig. 4.5B-C), bears resemblance to the type II Maryville dolomite. The Maynardville rhombohedral dolomite, however, is interpreted as a cement phase, unlike the replacement type II Maryville dolomite.

The type III and IV Maryville dolomite formed from basinal brines during intermediate and deep burial. This is supported by their elevated Fe (1.2 to 4.5 wt %) and Mn (0.1 to 0.3 wt %) compositions, and highly radiogenic Sr isotope composition (0.7111 to 0.7139; Fig. 4.11). Based on the trace element geographic gradients, Srinivasan et al. (1994) inferred that the dolomitizing fluids originated in the adjacent Cambrian Conasauga shale basin and migrated to the east into the platform carbonates.

The type III Maryville dolomite is petrographically similar to the dolomite associated with pressure solution features in the subtidal Maynardville deposits. The $\delta^{18}\text{O}$ compositions of type III Maryville dolomite are slightly more negative than that of the Maynardville dolomite from the argillaceous layers (Fig. 4.14). This difference may be a function of the greater burial depth and higher temperatures of formation for the Maryville dolomite. Externally derived hot basinal fluids, proposed for the formation of type III

Maryville dolomite, could have been warmer and more ^{18}O -depleted than pressure-solution derived fluids that were responsible for the formation of the Maynardville dolomite.

The type IV Maryville dolomite resembles the cement and replacement saddle dolomite from the Maynardville subtidal deposits. The paucity of saddle dolomite cement in the Maynardville precluded the determination of any basin-to-platform compositional variations. The Maynardville saddle dolomite is on average more depleted in ^{18}O relative to the Maryville Type IV saddle dolomite (Fig. 4.14). Coupled with a difference in the Sr isotope composition (Fig. 4.11), and the presence of MVT minerals in the Maynardville, a different source is suggested for the fluids that precipitated saddle dolomite in the Maynardville versus the Maryville carbonate succession.

There are many common characteristics in the early diagenetic histories of the Maryville Limestone and the Maynardville subtidal deposits. On the other hand, the late burial diagenesis of the Maryville was influenced by the fluids expelled from the laterally adjacent Conasauga basin shale deposits, whereas burial diagenetic phases of the Maynardville formed from locally derived fluids and in association with MVT mineralizing fluids.

Nolichucky Shale

The diagenetic study of the carbonate deposits in the Upper Cambrian Nolichucky Shale by Foreman (1991) focused primarily on the diagenesis of oolitic lithologies and calcite vein formation. Foreman (1991) interpreted the Nolichucky ooids to represent stabilized high-Mg calcite based on: 1) a relict radial fibrous fabric; 2) the presence of microdolomite; 3) the elevated MgCO_3 (1.5-2.5 mole %), Fe (> 1000 ppm), and Mn (> 500 ppm) compositions; and 4) the low Sr content (below detection limit of 450 ppm). The diagenetic alteration of ooids occurred in the presence of pore water that underwent a

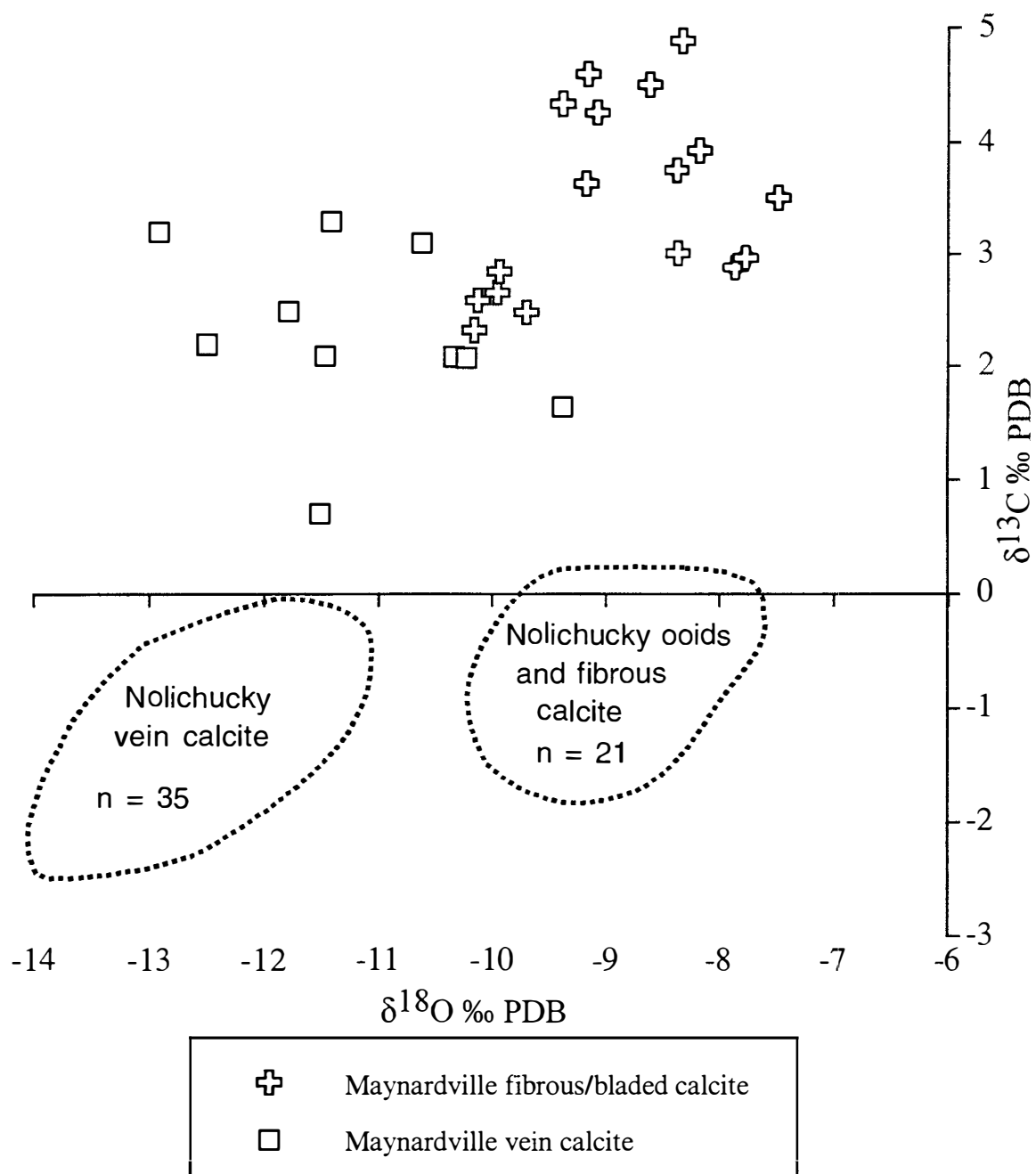
substantial interaction with clay minerals from the interbedded shale (Foreman 1991).

The difference in the present-day composition of the Nolichucky and the Maynardville ooids may be due to the difference in their original composition, and/or the difference in the style and degree of diagenetic modification (Table 4.4). The presence of abundant shale within the Nolichucky may have provided an important source of Fe and Mn that was of lesser influence in the diagenesis of the Maynardville subtidal deposits. Stable isotope analyses of the Maynardville ooids were not performed because of a sample size limitation, sample contamination concerns, and various degrees of alteration. The $\delta^{18}\text{O}$ composition of the Nolichucky ooids and fibrous calcite is similar to that of the Maynardville marine fibrous/bladed calcite cement, suggesting similar diagenetic modifications (Fig. 4.15).

Foreman (1991) described veins from the Nolichucky Shale within the Whiteoak Mountain thrust sheet in central eastern Tennessee. Fluid inclusion data indicate that bed-normal vein calcite precipitated at temperatures between 80 and 110°C (2.4 to 3.6 km burial) from highly saline brines, whereas bed-parallel vein calcite formed during maximum burial at 110°C, or at about 3.6 km. Based on these observations, the bed-normal veins are interpreted to have formed between the late Mississippian and early Pennsylvanian during the onset of the Alleghenian orogeny, but prior to the emplacement of the thrust sheet. The bed-parallel slickensided veins formed contemporaneously with thrusting (Foreman 1991). The temperatures determined for the precipitation of a single bed-oblique vein calcite (>200°C) exceed the maximum burial temperature for the Nolichucky. This indicates precipitation from warm external fluids that could have been expelled from more deeply buried (4 to 5 km) sedimentary successions of the underlying Conasauga Group and the Rome Formation, or the Ordovician Sevier Shale deposits that were buried to sufficient depths before the end of the Devonian (Foreman 1991).

A more detailed study of the Maynardville veins is needed to determine their

Figure 4.15. Stable isotope compositions of the comparable carbonate components from the Maynardville Formation and the underlying Upper Cambrian Nolichucky Shale. Data for the Nolichucky Shale are from Foreman (1991).



relative timing and the relationship to the vein sets in the Nolichucky Shale. Based on their orientation, it is plausible that some of the bed-parallel veins observed in the Maynardville are related to the Alleghenian thrusting, whereas bed-perpendicular, oblique and irregular veins formed prior to thrusting. Comparison of oxygen isotope compositions reveals that, even though a significant overlap exists, the Maynardville vein calcite cements have on average more positive $\delta^{18}\text{O}$ values than the Nolichucky vein calcite (Fig. 4.15). This suggests fluids of different compositions, and/or the effects of lower temperature in the precipitation of some of the Maynardville vein calcite. Foreman (1991), interpreted the carbon isotope values for the Nolichucky vein cements to reflect buffering to the host carbonate values, based on the similarity in the $\delta^{13}\text{C}$ of vein calcite and the surrounding matrix. Similarly, the $\delta^{13}\text{C}$ compositions of the Maynardville equant calcite cement from tectonic fractures indicate buffering to the elevated $\delta^{13}\text{C}$ compositions of the Maynardville host carbonate deposits (Fig. 4.6 B; see also Chapter 6).

Knox Group

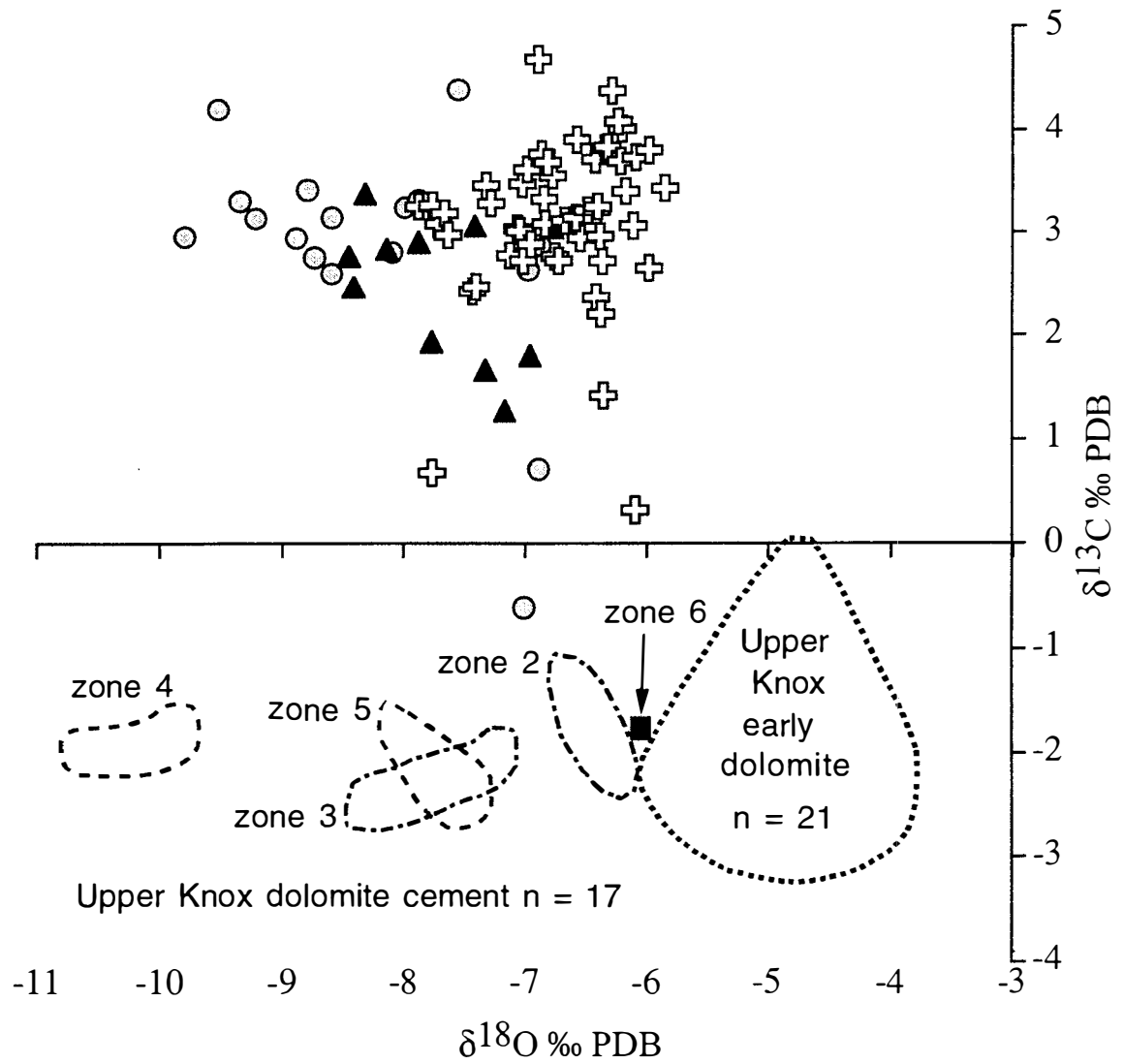
The Chepultepec, Kingsport and Mascot Formations of the Lower Ordovician Upper Knox Group consist of stacked meter-scale peritidal cycles composed of extensively dolomitized carbonate deposits (Montañez and Read 1992a). A sabkha model of dolomitization from modified sea water during tidal-flat progradation within high-frequency cycles (10^4 - 10^5 yr) was proposed for the formation of early diagenetic (syndimentary) dolomite. The early dolomite records a history of progressive diagenetic modification. The stabilization started syndepositionally in modified seawater, continued in fresh or mixed water, and was completed during deep burial by brines at elevated temperatures (Montañez and Read 1992b). The early dolomite from the Upper Cambrian peritidal deposits of the Maynardville and the lower Copper Ridge Dolomite underwent a similar diagenetic history. The Upper Cambrian dolomicrite is depleted in ^{18}O relative to

the Lower Ordovician early dolomite (Fig. 4.16). This is consistent with diagenetic alteration at a higher temperature during deeper burial of the Cambrian deposits, but may also indicate a difference in the composition of the precursor carbonate and dolomitizing fluids.

The Upper Knox late diagenetic dolomite formed as a result of the recrystallization of early dolomite, direct replacement of limestone at elevated temperature, and as cement in fractures and solution voids. This cement postdates non-ferroan meteoric and ferroan calcite cements, mechanical compaction and much stylolitization (Montañez and Read 1992b). The late diagenetic dolomitization of the Knox carbonates is associated with secondary porosity development, hydrocarbon migration, and local MVT mineralization (Montañez 1994). Many of these interpretations are similar to those for the late diagenetic replacement and cement dolomite from the Upper Cambrian peritidal deposits.

On the basis of CL zonation patterns, Montañez (1994) recognized five generations of late dolomite cements in the Knox. The nonluminescent, relict cores of early dolomite comprise zone 1 dolomite. The complexly zoned (zones 2 to 6) dolomite cement contains: 2) a dull brown luminescent zone; 3) a bright orange luminescent zone with alternating nonluminescent and dull luminescent cement subzones; 4) a dull brown luminescent zone, which corresponds to the transition from turbid to less turbid dolomite; 5) a very dark brown to dark red luminescent zone representing the transition from moderately turbid to inclusion-free dolomite; and 6) a thin (10-100 μm) series of alternating nonluminescent and very bright luminescent subzones corresponding to alternating turbid and inclusion-free zones. Zone 2 and 3 Knox dolomite cement in eastern Tennessee predates main MVT ore-stage sphalerite, and their minimum age is constrained based on the Devonian to Mississippian age for the MVT mineralization (Montañez 1994). Zone 4 to 6 dolomite cement fills the tectonic fractures interpreted to have formed during the Late Paleozoic Alleghenian orogeny (Hatcher et al. 1989;

Figure 4.16. Stable isotope compositions of the comparable carbonate components from the peritidal deposits of the upper Maynardville/lower Copper Ridge Dolomite and the Lower Ordovician Upper Knox Group from the Copper Creek thrust sheet in eastern Tennessee. Data for the Knox Group are from Montañez (1994). Isotope values of dolomite cement from the Knox Group are shown as compositional fields for zones 2 to 6 dolomite.



Montañez 1994). Bitumen observed within the Upper Knox deposits is synchronous with, or postdates the zone 4 dolomite cement, which in turn postdates all main ore-stage sphalerites. Cement zone 5 is synchronous with, or postdates sphalerite in eastern Tennessee (Montañez 1994).

The zoned dolomite cement from the Upper Cambrian peritidal deposits is petrographically similar to zones 2 and 3 of the Knox dolomite. The zoned dolomite, however, primarily occludes syndepositional and evaporite dissolution voids in the Cambrian deposits, whereas the Knox dolomite occurs in tectonic fractures and carbonate dissolution voids. The CaCO_3 composition of early dolomite from the Knox (mean: 51.1 mole %) is comparable to that of the first Knox dolomite cement generation (zone 2 mean: 50.8 mole %). A similar relationship has been observed between the comparable dolomite phases in the Upper Cambrian deposits (Fig. 4.10A). The Fe composition of the zoned dolomite from the Cambrian strata is similar to that of zones 2 and 3 Knox dolomite (109 to 5115 ppm), with the amount of Mn slightly higher in the Knox dolomite (30 to 1069 ppm; Table 4.5). On the other hand, zone 4 and 5 Knox dolomite petrographically resembles the saddle dolomite cement that occludes pore centers, tectonic fractures and dissolutional voids in the Upper Cambrian succession. Both Fe (2076 to 8452 ppm) and Mn (63 to 647 ppm) concentrations of zones 4 and 5 Knox dolomite are comparable with those of the Cambrian saddle dolomite cement (Table 4.5). The relationship between the $\delta^{18}\text{O}$ compositions of zoned (less ^{18}O -depleted) versus saddle dolomite (more ^{18}O -depleted) cement in the Upper Cambrian deposits is similar to the relationship observed between the combined $\delta^{18}\text{O}$ values of zones 2 and 3 Knox dolomite, in comparison to the zones 4 and 5 dolomite (Fig. 4.16). The dolomite cement equivalent to zone 6 Knox dolomite has not been observed in the Upper Cambrian peritidal deposits. The least ^{18}O -depleted saddle dolomite from the Upper Cambrian deposits has $\delta^{18}\text{O}$ compositions between those of zones 5 and 6 Knox dolomite (Fig. 4.16), which are interpreted to have

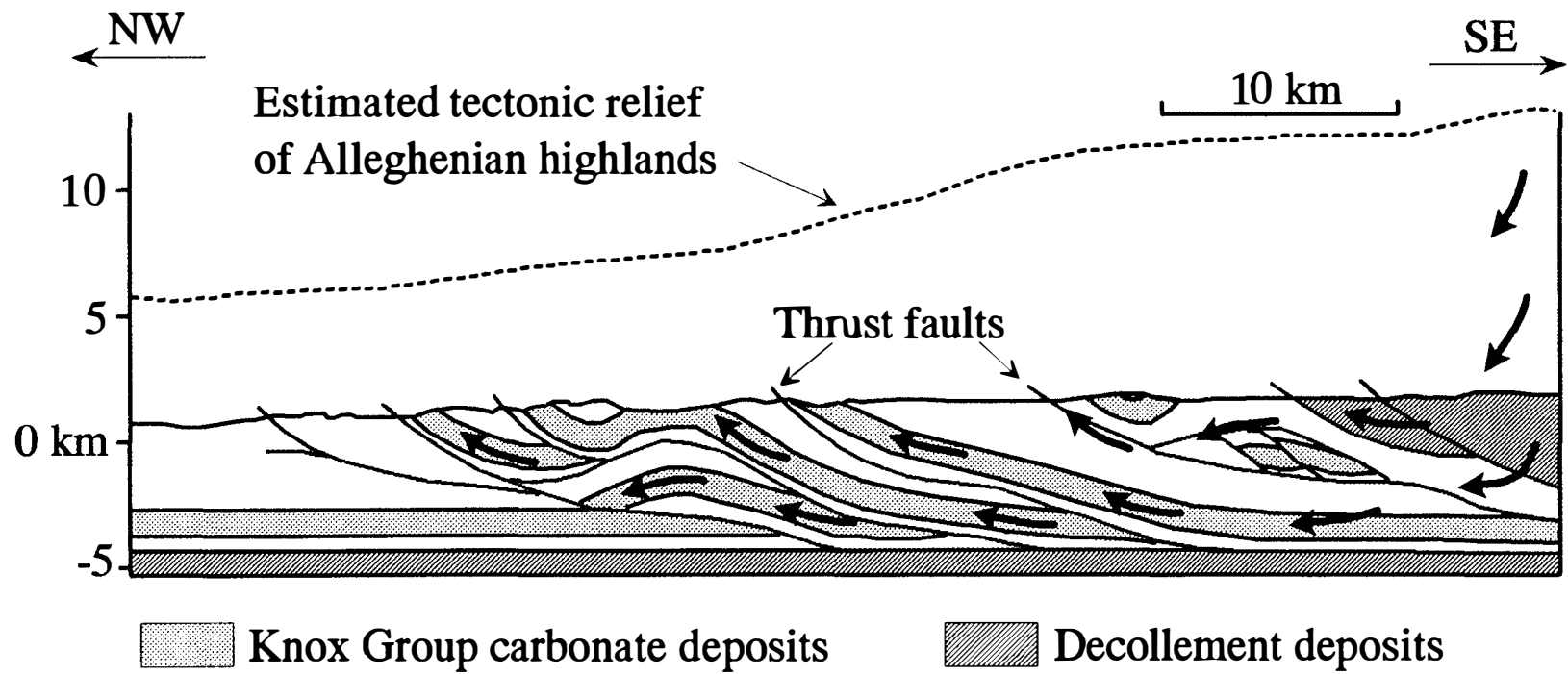
formed during progressively decreasing diagenetic temperatures related to denudation of tectonically uplifted terranes (Montañez 1994). The temperature determined for the formation of late diagenetic Knox dolomite (80°C to > 165°C) is identical to that estimated for the Upper Cambrian saddle dolomite. The observed similarities suggest similar processes of dolomitization from fluids of comparable composition and temperature, but do not imply simultaneous precipitation within the Upper Cambrian and Lower Ordovician carbonate successions from aurally extensive homogenous diagenetic fluids.

The Upper Knox late diagenetic dolomite cement is interpreted to represent precipitation from hot, saline basinal brines that underwent extensive fluid-rock interaction with siliciclastic deposits (Fig. 4.11; Montañez 1994). Dolomitizing fluids that migrated through the Knox carbonates at intermediate burial depths (1.5 - 2.5 km) originated from burial-compaction dewatering of the shale-rich Sevier basin. Most late diagenetic dolomite formed from a deep subsurface (2 to > 5 km) fluid migration in response to late Paleozoic Alleghenian tectonism (Fig. 4.17; Montañez 1994).

DIAGENETIC HISTORY IN THE CONTEXT OF GRAND CYCLE CESSATION

This study documents significant differences between the early diagenesis of the subtidal and the peritidal deposits of the examined Upper Cambrian sedimentary succession. The early diagenetic history of the Maynardville Formation subtidal deposits is comparable to that of the underlying Grand Cycle carbonate deposits of the Conasauga Group. The peritidal carbonate deposits of the upper Maynardville and the overlying Copper Ridge Dolomite experienced early diagenesis similar to the Upper Knox Group deposits. These observations indicate that the prominent change in the style of passive margin deposition, that resulted in the cessation of Cambrian Grand Cycle sedimentation in the southern Appalachians, triggered substantial changes in the diagenesis of associated

Figure 4.17. Schematic illustration of the topography-driven fluid flow (arrows) through the sedimentary succession of southwestern Virginia during the late Paleozoic Alleghenian orogeny (Figure 18 from Montañez 1994).



carbonate deposits.

The model developed for the deposition of the Maynardville Formation provides a means for the interpretation of the distribution and character of early diagenetic phases (Fig. 2.5). Diagenesis in the presence of normal seawater took place within the subtidal deposits of the Maynardville, as evidenced by the presence of various marine calcite cements. Pore water of marine origin was modified by the introduction of meteoric water into the subtidal package during an episode of sea-level fall that exposed areas along the slightly elevated platform rim at the Tazewell locality, and converted on-platform lagoonal settings into extensive tidal flats covered by microbial mats (Fig. 2.5). Meteoric water could have also been introduced in the subtidal deposits during repeated periods of subaerial exposure of the overlying peritidal package. The absence of substantial dissolution of the subtidal deposits may reflect the relatively short duration and magnitude of sea-level fall, coupled with arid to semi-arid climate. The transition into peritidal deposition resulted in the pervasive, penecontemporaneous dolomitization of the carbonate deposits by modified seawater under sabkha-like conditions.

Differences in the depositional regime and early diagenesis influenced the late diagenesis of the terminal Grand Cycle carbonate deposits. The establishment of widespread peritidal deposition was related to the infilling of the Conasauga intrashelf basin and carbonate platform progradation (Fig. 3.3). The associated decrease in the abundance of siliciclastic deposits resulted in a decrease in the amount of ferroan diagenetic phases within the peritidal deposits relative to the subtidal depositional package of the Maynardville. In the subtidal deposits, the presence of common argillaceous layers and the development of hardgrounds influenced the formation of ferroan dolomite during burial diagenesis. The late diagenetic dolomitization of the peritidal deposits, on the other hand, was controlled by recrystallization and pressure solution of early dolomite, and the dolomitization of limestone deposits by burial fluids.

The presence of MVT minerals confirms that the late diagenesis of the Maynardville Formation was influenced by the migration of externally derived burial fluids. The most probable source for the MVT basinal brines in eastern Tennessee is the Middle Ordovician Sevier shale basin (Kesler et al. 1988, 1989; Haynes and Kesler 1989; Haynes et al. 1989; Bethke and Marshak 1990). The low Sr isotope ratio of the dolomite cement from the peritidal deposits may reflect the shallow to intermediate burial expulsion of Middle Ordovician marine pore-water with an original $^{87}\text{Sr}/^{86}\text{Sr}$ ratio between 0.7080 and 0.7087 (Burke et al. 1982; Keto and Jacobsen 1987) from the Sevier shale basin, prior to substantial interaction with siliciclastic deposits (Fig. 4.18). The Sevier shale was deposited within a subsiding foreland basin, developed in response to conversion of the region into a convergent-margin setting (Fig. 4.18; Shanmugam and Walker 1980). In eastern Tennessee the Sevier shale deposits reach a thickness of more than 2000 m, and therefore the dewatering of these deposits could have started as early as the Middle Ordovician (Fig. 4.18). This interpretation is in agreement with a proposed Middle Ordovician to Middle Devonian age for the migration of MVT mineralizing fluids in the southern Appalachians (Kesler and Van Der Pluijm 1990), and with early MVT brines representing connate waters expelled from the Sevier shale basin (Kesler et al. 1989). The expelled pore-water moved laterally into the Upper Knox carbonate deposits, which had experienced extensive karstification, including brecciation, during subaerial exposure related to the formation of the Knox unconformity (Fig. 4.18). The most extensive MVT mineralization and evidence for hydrocarbon migration is associated with these highly porous carbonate deposits (Haynes and Kesler 1989; Montañez 1994). The basinal fluids could have migrated into the underlying Maynardville deposits along fracture systems that might have developed concomitantly with foreland basin formation. As noted earlier, the expulsion of connate waters from the Sevier Shale during shallow to intermediate burial, however, does not account for the wide range of temperatures proposed for the

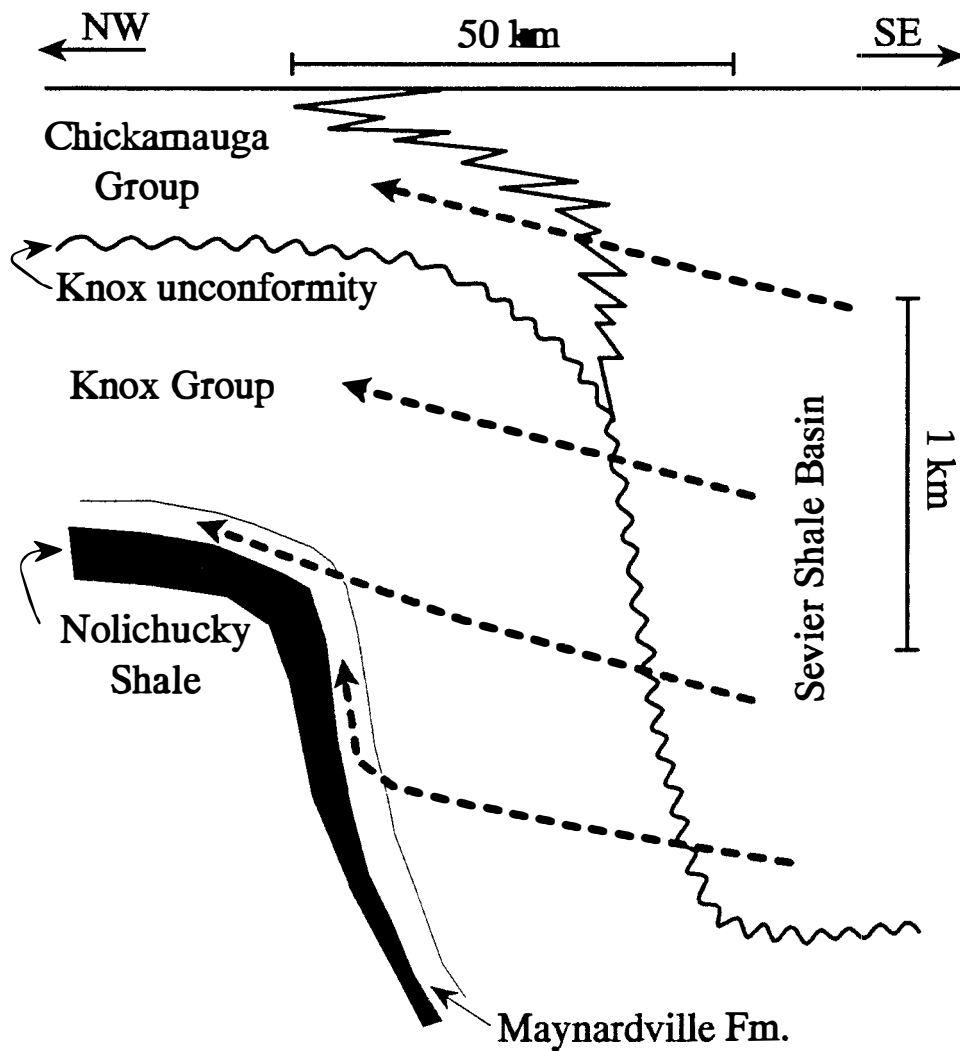


Figure 4.18. Schematic illustration of the compaction-driven fluid flow (dotted arrows) from the Sevier shale basin into the adjacent carbonate platform successions in eastern Tennessee. Stratigraphy from Walker (1980).

precipitation of the burial dolomite cement in the Upper Cambrian peritidal deposits.

Burial fluids may inherit their Sr isotope compositions from the carbonate successions they interact with along the fluid migration pathway (Müller et al. 1991; Banner et al. 1994; Banner 1995). In diagenetic systems characterized by high rates of recrystallization, involving dissolution and reprecipitation reactions, the Sr isotopic composition of the precursor carbonate is commonly inherited in the successor diagenetic carbonate phase (Veizer 1992). Non-radiogenic composition of warm basinal brines is, therefore, commonly interpreted to represent buffering of Sr isotope composition to carbonate host composition (Barnaby and Read 1992; Farr 1992). The late diagenetic dolomitization of the Lower Ordovician Upper Knox carbonate succession was associated with widespread dissolution and the development of secondary porosity. As a result, much of the Sr in burial diagenetic fluids was derived from the Knox host carbonate (Montañez and Read 1992b).

The relatively low Sr isotope composition of the dolomite cement from the Upper Cambrian peritidal deposits may therefore indicate precipitation from burial fluids that interacted with younger carbonate strata. The mechanism for the migration of fluids through deeply buried sedimentary successions is topography-driven recharge triggered by tectonic uplift (Fig. 4.17). This mechanism, in conjunction with tectonic compaction, has been proposed for the migration of later-stage MVT dolomitizing fluids, which were meteoric fluids that underwent interaction with the Sevier shale deposits (Kesler et al. 1989). The relationship between tectonic events and burial fluid migration provides a link between the Acadian and Alleghenian tectonism, and the two distinct ages determined for the MVT mineralization in southeastern North America, which are: 1) the Devonian (Grant et al. 1984; Stein and Kish 1985; Hay et al. 1988; Nakai et al. 1990, 1993); and 2) the Pennsylvanian/Early Permian (Hearn and Sutter 1985; Hearn et al. 1987; Elliot and Aronson 1987; Hay et al. 1988). The topography-driven migration of brines through the

Upper Knox carbonate succession during late burial (Montañez 1994; Fig. 4.17) may have influenced the underlying Upper Cambrian carbonates. This was possible because of the conformable transition between the Maynardville and the Knox Group peritidal carbonate deposits.

Differences in the Sr isotope compositions of burial cements can be attributed to the different source regions for the siliciclastic material with which the burial fluids interact. The highly radiogenic Sr isotope composition of the late diagenetic dolomite from the Maryville Limestone (Conasauga Group, Middle Cambrian) reflects the composition of fluids derived from the Cambrian Conasauga shale basin to the west (Fig. 4.11). Siliciclastic sediments from the Conasauga basin were derived by the weathering of cratonic crystalline basement rocks. The resulting siliciclastic deposits, rich in K-feldspars and mica, produce highly radiogenic formation waters (Stueber et al. 1987; McNutt et al. 1990; Banner 1995). On the other hand, interaction with plagioclase feldspar may result in relatively low Sr isotopic ratios of basinal brines (Franklyn et al. 1991). Srinivasan et al. (1995) reported a mean Sr isotope ratio for burial diagenetic phases of the Middle Ordovician Chickamauga Group of 0.7095. This value is interpreted to be the result of precipitation from basinal fluids expelled from the Sevier shale (Fig. 4.18). The Sevier basin deposits represent K-feldspar-poor volcanic detritus, which was derived from an evolved volcanic-arc source to the east (Srinivasan et al. 1995). The Sr isotope composition of the Middle Ordovician burial cement is comparable to that of the Upper Knox dolomite cement, suggesting a similar fluid source (Fig. 4.11). The same fluid source is suggested for the saddle dolomite cement, associated with sphalerite in tectonic fractures from the peritidal Maynardville, on the basis of its Sr isotope composition, which overlaps with the compositional field for the Upper Knox dolomite cement (Fig. 4.11). Other dolomite cement samples from the Upper Cambrian peritidal deposits are slightly less radiogenic than the Knox late dolomite (Fig. 4.11). The slight difference in Sr isotope

compositions may represent evolution of dolomitizing basinal fluids due to the interaction with Upper Knox carbonate deposits as they migrated from the Sevier basin to the Maynardville deposits (Fig. 4.18). On the other hand, the difference may suggest that while most pores in the Upper Cambrian deposits were occluded during shallow to intermediate burial, the substantial amount of porosity in the Upper Knox deposits remained available for the migration of fluids that interacted with the siliciclastics at higher temperatures during later burial diagenesis.

The pronounced difference in the Sr isotope compositions of burial dolomite cements indicate that the burial fluids that migrated through the Upper Cambrian/Lower Ordovician carbonate succession of the southern Appalachians did not significantly influence the underlying carbonate deposits of the Middle Cambrian Conasauga Group (Fig. 4.11). The Upper Cambrian Nolichucky Shale, which separates these two sedimentary successions, may have served as an aquitard to cross-formational fluid migration (Fig. 4.18). For the same reason the Maynardville deposits have not been significantly influenced by the migration of burial fluids from the Conasauga basin shale. A possible upward and lateral migration of these fluids may have had only a minor influence on the diagenesis of the lower part of the Maynardville subtidal deposits. This illustrates the consequences of the prominent change in the regional facies distribution, associated with the end of Grand Cycle deposition in the southern Appalachians, on the burial diagenetic patterns. The complex diagenetic history of the Maynardville Formation was influenced by processes related to passive-margin evolution, and later burial history in response to the conversion to a convergent margin.

CONCLUSIONS

The Maynardville Formation, as a terminal Grand Cycle carbonate succession in the southern Appalachians, marks a prominent change in the diagenetic patterns between

the Middle to Upper Cambrian Conasauga Group and the overlying Upper Cambrian to Lower Ordovician Knox Group carbonate deposits. The early diagenesis of the Maynardville has been significantly influenced by the change from subtidal into peritidal depositional regime. The subtidal deposits contain a variety of calcite cements representing marine, meteoric and burial diagenetic phases. The majority of dolomite in the subtidal package formed during burial from fluids provided locally by the diagenesis of clay minerals, compaction, and pressure solution.

The fine-crystalline replacement dolomite of the peritidal package formed under sabkha-like evaporitic conditions on a semi-arid tidal flat, and was subjected to modifications later in its diagenetic history. The coarser-crystalline replacement dolomite formed during burial from the recrystallization of early dolomite and dolomitization of limestone in the presence of warm basinal brines. The zoned dolomite cement in the peritidal package precipitated from fluids of varying composition such as modified marine fluids, mixed marine/meteoric, and deeper burial basinal brines. The saddle dolomite cement precipitated during later burial from fluids generated by the pressure-solution of matrix dolomite and from basinal brines related to MVT mineralization and hydrocarbon migration.

Burial fluids represent marine pore water expelled from the Middle Ordovician Sevier basin shale succession, and/or waters of meteoric origin that interacted with Ordovician carbonate rocks. This scenario is in contrast to the migration of basinal brines from the Conasauga shale into the adjacent Middle Cambrian carbonate platform succession. The differences in burial diagenesis between the underlying Conasauga Group and the overlying Maynardville/Knox carbonate deposits were influenced by changes in the regional facies distribution associated with the cessation of Grand Cycle deposition, coupled with the complex burial history of the passive margin sedimentary succession.

CHAPTER 5

A LATE CAMBRIAN CARBON-ISOTOPE EXCURSION: RELATION TO BIOSTRATIGRAPHY AND SEQUENCE STRATIGRAPHY, AND IMPLICATIONS FOR INTERPRETING DIAGENETIC HISTORY

INTRODUCTION

Carbon-isotope stratigraphy is a promising tool for a higher resolution stratigraphy that can greatly facilitate correlation of successions lacking prominent biostratigraphic markers. This type of stratigraphic correlation has been applied to numerous Proterozoic and Neoproterozoic successions (Kaufman et al. 1991, 1993; Wickham and Peters 1993; Narbonne et al. 1994; Kaufman and Knoll 1995; Knoll et al. 1986, 1995; Pelechaty et al. 1996; among others). In biostratigraphically better characterized parts of the Phanerozoic sedimentary successions, especially the Mesozoic and Cenozoic, carbon-isotope stratigraphy has been used for basin-to-platform and regional correlation of strata beyond the current level of biostratigraphic resolution (Magaritz 1991; Fölmli et al. 1994; Vahrenkamp 1996).

Of special interest in carbon-isotope studies are deviations from usual or expected isotopic values, referred to as positive or negative carbon-isotope excursions. Such excursions provide indicators of tectonic, climatic, paleoceanographic and evolutionary changes that influence carbon cycling. Carbon-isotope excursions associated with changes in organic productivity and extinction events commonly occur at major boundaries throughout the stratigraphic record (Marshall and Middleton 1990; Magaritz 1991).

Most studies of carbon-isotope variations deal with marine carbonate rocks and their constituents, including skeletal allochems, abiotically precipitated cement, or homogeneous micrites. Because of relatively small equilibrium carbon-isotope

fractionation effects and temperature effects, variations in carbon-isotope compositions of carbonate minerals most commonly reflect changes in the $^{13}\text{C}/^{12}\text{C}$ ratio of the solution from which they precipitated (Anderson and Arthur 1983). Therefore, changes in carbon-isotope values of marine carbonate components are considered useful indicators of changes in the marine bicarbonate reservoir composition. Temporal fluctuations in $\delta^{13}\text{C}$ of marine carbonate constituents are accordingly interpreted to represent secular trends of oceanic $\delta^{13}\text{C}$ variations related primarily to the changing rate of organic matter burial and/or primary organic productivity (Kump 1989; Marshall 1992).

Stable isotope analysis, for the purpose of deciphering the diagenetic history of the Upper Cambrian Maynardville Formation, reveals rather unusual carbon-isotope values. Measured $\delta^{13}\text{C}$ values of various individual diagenetic and depositional components are highly variable, but are in general more positive or more enriched in ^{13}C when compared to the underlying and the overlying strata (Figs. 4.14-16). Studies of time-equivalent successions elsewhere indicate that recorded carbon-isotope compositions may reflect a large, positive global excursion (Brasier 1993; Saltzman et al. 1995a; Saltzman 1996). The occurrence of positive carbon-isotope excursions are the result of: 1) increased primary organic productivity and the associated increase in the fraction of carbon buried as organic matter during explosive evolutionary events; 2) increased rates of sedimentation within the oceans and the associated increase in the rate of deposition of organic matter; and 3) enhanced preservation of organic material in the sediment caused by an expanded oxygen-minimum zone or marine anoxia (Weissert 1989; Derry et al. 1992; Brasier 1992; Brasier et al. 1994; among others). Table 5.1 is a compilation of documented Phanerozoic positive carbon-isotope excursions that appear to be global in scope and had a duration that exceeds the residence time of carbon in the modern ocean. The enhanced burial and preservation of organic matter associated with the positive carbon shifts at several important stratigraphic horizons in Mesozoic strata resulted in the deposition of 'black

Table 5.1. Phanerozoic positive carbon-isotope excursions with durations greater than the residence time of carbon in the modern ocean ($\sim 2 \times 10^5$ yrs; modified from Schidlowski and Aharon 1992).

$\delta^{13}\text{C}$ shift (‰)	age	duration ($\times 10^6$ yrs)	reference
1	Miocene	3-4	Vincent and Berger 1985; Berger and Vincent 1986
2	Late Paleocene	5.5	Shackleton 1987
2	Santonian/Campanian	5.7	Arthur et al. 1985
2-4	Cenomanian/Turonian	1-3	Scholle and Arthur 1980; Arthur et al. 1985, 1987, 1988; Schlanger et al. 1987; Pratt et al. 1991; Gale et al. 1993
2-3	Aptian/Albian	9.7	Arthur et al. 1985; Weissert 1989
1.5	Valanginian/Hauterivian	1-2	Lini et al. 1992; Föllmi et al. 1994
3	Toarcian	0.5	Jenkyns and Clayton 1986; Jenkyns 1988
3.5	Late Permian	1	Gruszczynski et al. 1989
3	Mid-Carboniferous	?	Popp et al. 1986
2	Devonian/Carboniferous	7-15	Lohmann and Walker 1989
2.5-3.5	Frasnian/Famennian	~ 1	Wang et al. 1996
4-5	Latest Ordovician	?	Marshall and Middleton 1990; Long 1993; Wang et al. 1993
4-5	Late Cambrian (Steptoean)	2-4	Brasier 1993; Saltzman et al. 1995, this study
1-3	Early Cambrian (multiple excursions)	~ 1	Brasier et al. 1994; Derry et al. 1994

shales' (Scholle and Arthur 1980; Jenkyns and Clayton 1986; Arthur et al. 1987; Schlanger et al. 1987; Weissert 1989; Marshall 1992). The association of a positive excursion with a glacial event during the Miocene suggests a possible correlation between the changes in carbon cycling, atmospheric $p\text{CO}_2$, eustatic sea-level changes and global climatic cooling (Vincent and Berger 1985; Berger and Vincent 1986). Similar relationships have been proposed for a positive carbon-isotope excursion at the end of the Ordovician, which is associated with extinction episodes and the glaciation of Gondwana (Marshall and Middleton 1990). Positive carbon-isotope shifts, however, do not necessarily represent secular trends in carbon cycling. Instead, they may be a result of regional variations related to basin evolution (Beauchamp et al. 1987). Therefore, any study of secular carbon-isotope variations should be concerned with recognizing possible variations caused by local-to-regional environmental factors and postdepositional diagenetic alterations.

This Chapter presents the results of a more detailed study of the carbon-isotope variations within the Upper Cambrian sedimentary succession of the southern Appalachians that includes the upper part of the Nolichucky Shale, the Maynardville Formation, and the lower part of the overlying Copper Ridge Dolomite. The study was designed to meet the following objectives: 1) to document the variations in the stable isotopes of carbon, with special emphasis on deciphering the anatomy of the positive carbon-isotope excursion which is recorded within this sedimentary succession. This was accomplished by selecting an outcrop with the most complete exposure of the stratigraphic interval in question, and by applying extensive sampling; 2) to apply carbon-isotope stratigraphy to this Upper Cambrian sedimentary succession by using the information available on time-equivalent, highly fossiliferous successions elsewhere. The purpose of this objective was to provide a more detailed chronostratigraphic framework for the deposition of this stratigraphic interval; and 3) to evaluate the effects of

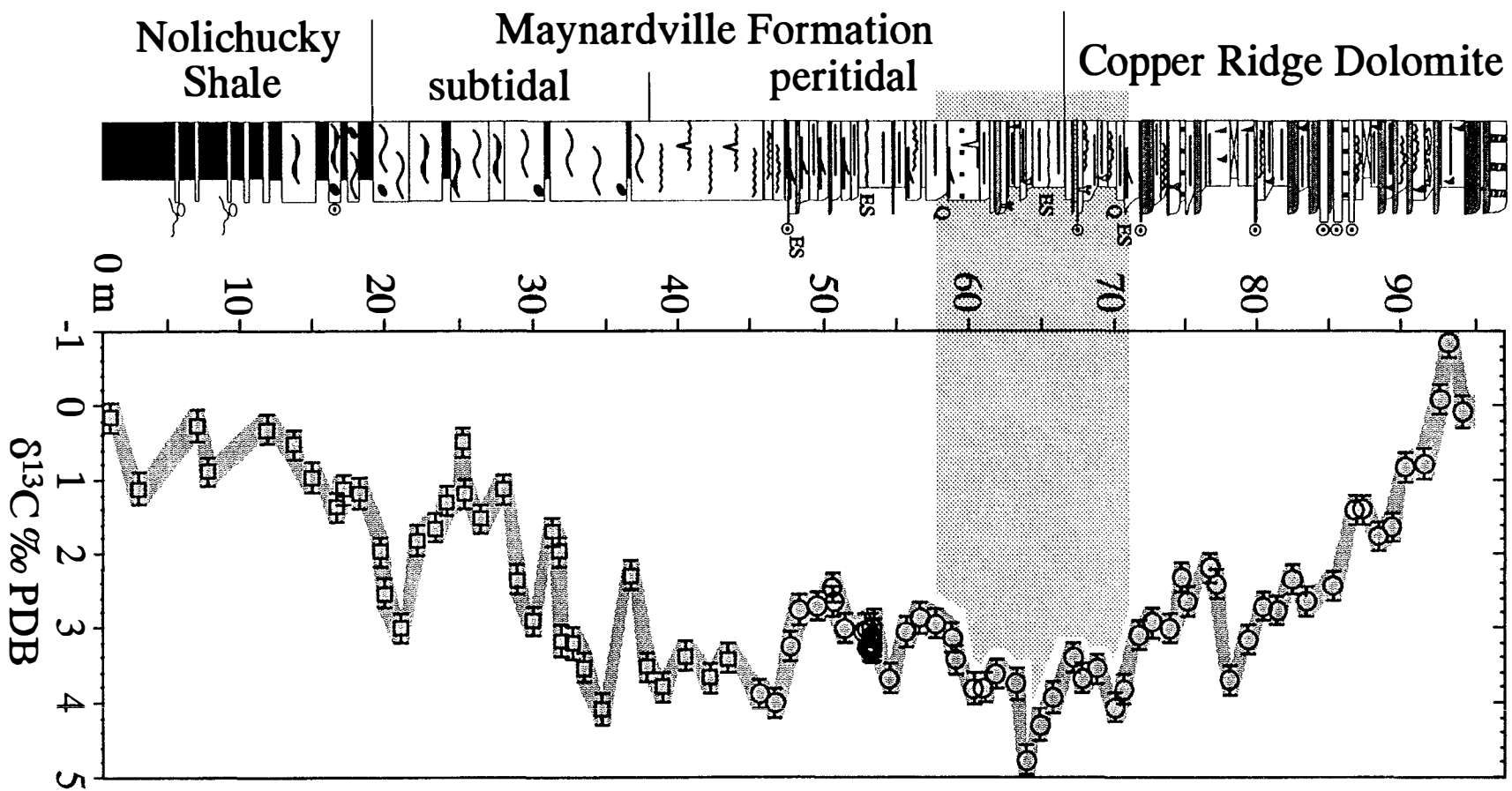
depositional environments and diagenesis on the carbon-isotope signature. To meet this objective, carbon-isotope compositions for samples from various lithofacies were compared and related to paleoenvironmental interpretations. In addition, $\delta^{18}\text{O}$ compositions of various individual depositional and diagenetic components were used to constrain the diagenetic environments and the extent of diagenetic modifications.

INVESTIGATIVE METHODS AND SAMPLING STRATEGY

Carbon-isotope stratigraphy was determined for the most complete of the five outcrops examined—the Thorn Hill section (Figs. 1.4, 2.1, 5.1, see also Appendix A). The samples for stable isotope analysis were collected at approximately 1 meter intervals, depending on the availability of suitable carbonate phases. Powdered samples were collected from polished and stained slabs and thin-section billets by using a microscope-mounted microdrill assembly after careful petrographic examination. An attempt was made to collect samples representing homogenous individual depositional and diagenetic components. Care was taken to prevent contamination from the surrounding phases. The mineral composition of the collected material was checked by the use of standard X-ray diffraction methods.

The majority of the samples are fine-grained carbonate matrix composed of calcite or dolomite, referred to as micrite and dolomicrite, respectively. Samples from the Nolichucky Shale and the subtidal package of the Maynardville are primarily composed of calcite, and were collected from the micritic or mudstone layers of the ribbon rocks. Some of the samples came from centimeter-scale micritic intraclasts comprising flat-pebble conglomerate layers, from micritic lenses encased within grainstone layers or from intergranular areas of micrite-supported lithofacies (see Appendix D for description of individual samples). The transition between the subtidal and the peritidal package is represented by micrite samples from microbial laminates or stratiform stromatolites. The

Figure 5.1. Stratigraphic column of the Thorn Hill section. For the explanation of lithologic symbols see Tables 2.1 and 2.2, and Appendix A. To the right of the stratigraphic column is a carbon-isotope variation curve constructed on the basis of measured $\delta^{13}\text{C}$ values for the samples representing micrite (open squares) and dolomicrite (open circles). See Appendix D for an individual sample description. The curve is constructed by plotting the measured $\delta^{13}\text{C}$ values with a $\pm 0.2\text{‰}$ analytical precision considered. The sequence boundary zone, defined on the basis of lithologic criteria (see Chapter 2), within which the Maynardville/Copper Ridge Dolomite transition is contained, is indicated with a shaded pattern.



mineralogy of these samples reflects the trend in the declining amount of calcite up-section and the predominance of dolomite in the peritidal deposits. Samples from the peritidal package of the Maynardville and the Copper Ridge Dolomite primarily consist of dolomicrite from mudstones, mechanical laminates or "couplets", and microbial deposits. Several samples represent dolomicrosparite, and rare coarser-crystalline replacement dolomite (see Appendix D). Individual cement phases were also collected where available. These include fibrous to bladed calcite, equant calcite and saddle dolomite cement. Rare calcite cement samples from the Copper Ridge Dolomite come from mostly undolomitized shallow subtidal lithofacies associated with microbial deposits. Calcite and dolomite samples were analyzed for the stable isotopes of carbon and oxygen following the procedure outlined previously in Chapter 4.

RESULTS OF STABLE ISOTOPE ANALYSIS

Stratigraphic variation in carbon-isotope composition of the micrite and dolomicrite samples is shown in Figure 5.1. The $\delta^{13}\text{C}$ values of subtidal micrite fluctuate greatly but in general show an increase from the upper Nolichucky into the subtidal depositional package of the Maynardville. Dolomicrite samples from the peritidal package of the Maynardville and the overlying Copper Ridge Dolomite form a smoother carbon-variation curve. Some of the most positive $\delta^{13}\text{C}$ values correspond to the samples collected from the sequence boundary zone within which the Maynardville/Copper Ridge transition is contained (Fig. 5.1). The $\delta^{13}\text{C}$ values decline in the lower part of the Copper Ridge Dolomite.

Figure 5.2 illustrates the stratigraphic variations in both carbon and oxygen isotope values. Overall, there is a poor correlation or covariation between the $\delta^{13}\text{C}$ and $\delta^{18}\text{O}$ values (Figs. 5.2, 5.3). In general, micrite samples from the Nolichucky Shale and the lower part of the Maynardville are more depleted in ^{18}O ($\delta^{18}\text{O} = -9.3$ to -7.2 ‰ PDB)

Figure 5.2. Variations in $\delta^{13}\text{C}$ and $\delta^{18}\text{O}$ values as a function of stratigraphic position of the micrite (open squares) and dolomicrite (open circles) samples. All error bars represent ± 0.2 ‰ analytical precision. The shaded area on the vertical axis indicates the sequence boundary zone. Note poor correlation or covariation between $\delta^{13}\text{C}$ and $\delta^{18}\text{O}$ values, and the difference between $\delta^{18}\text{O}$ values for micrite versus dolomicrite.

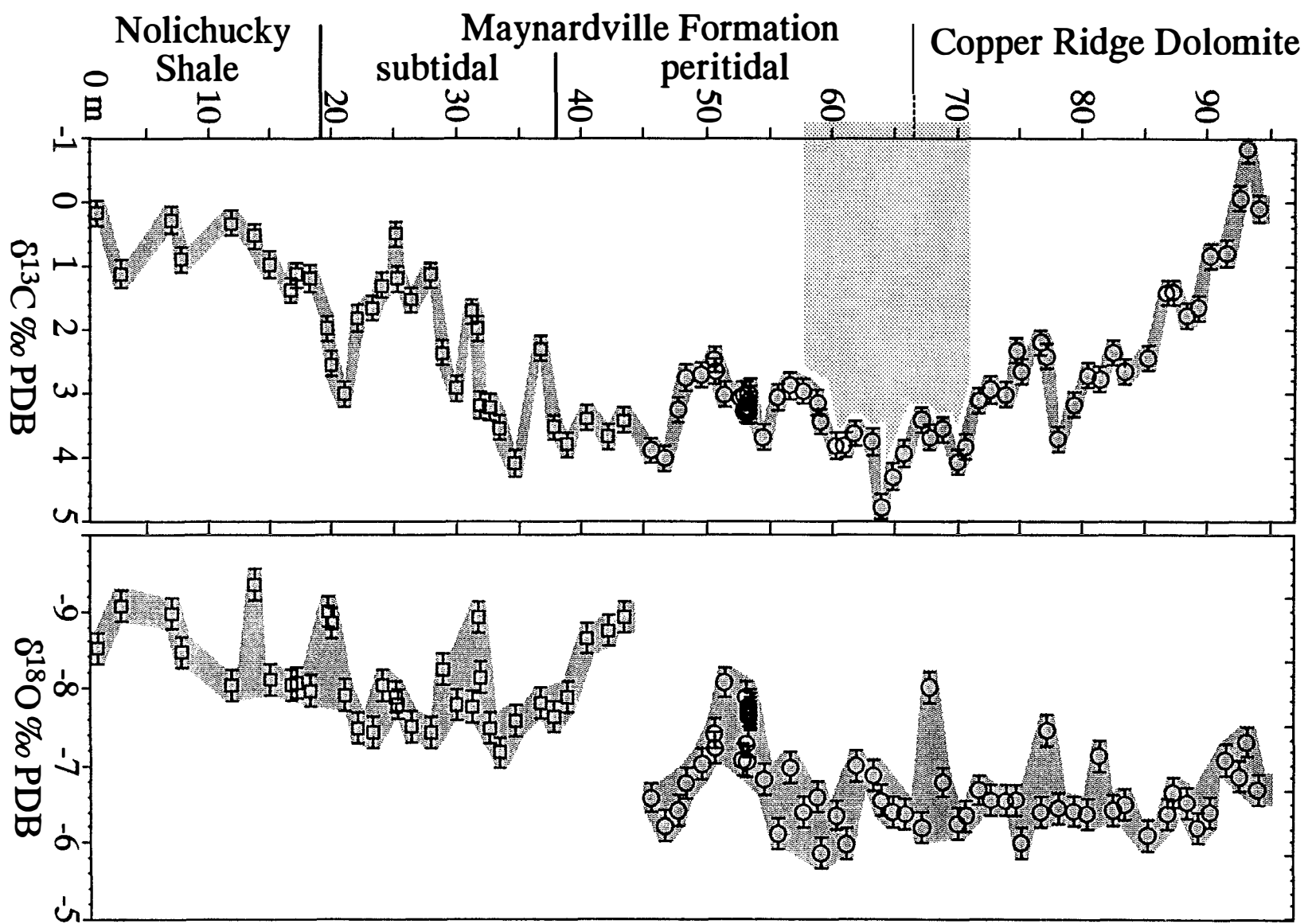
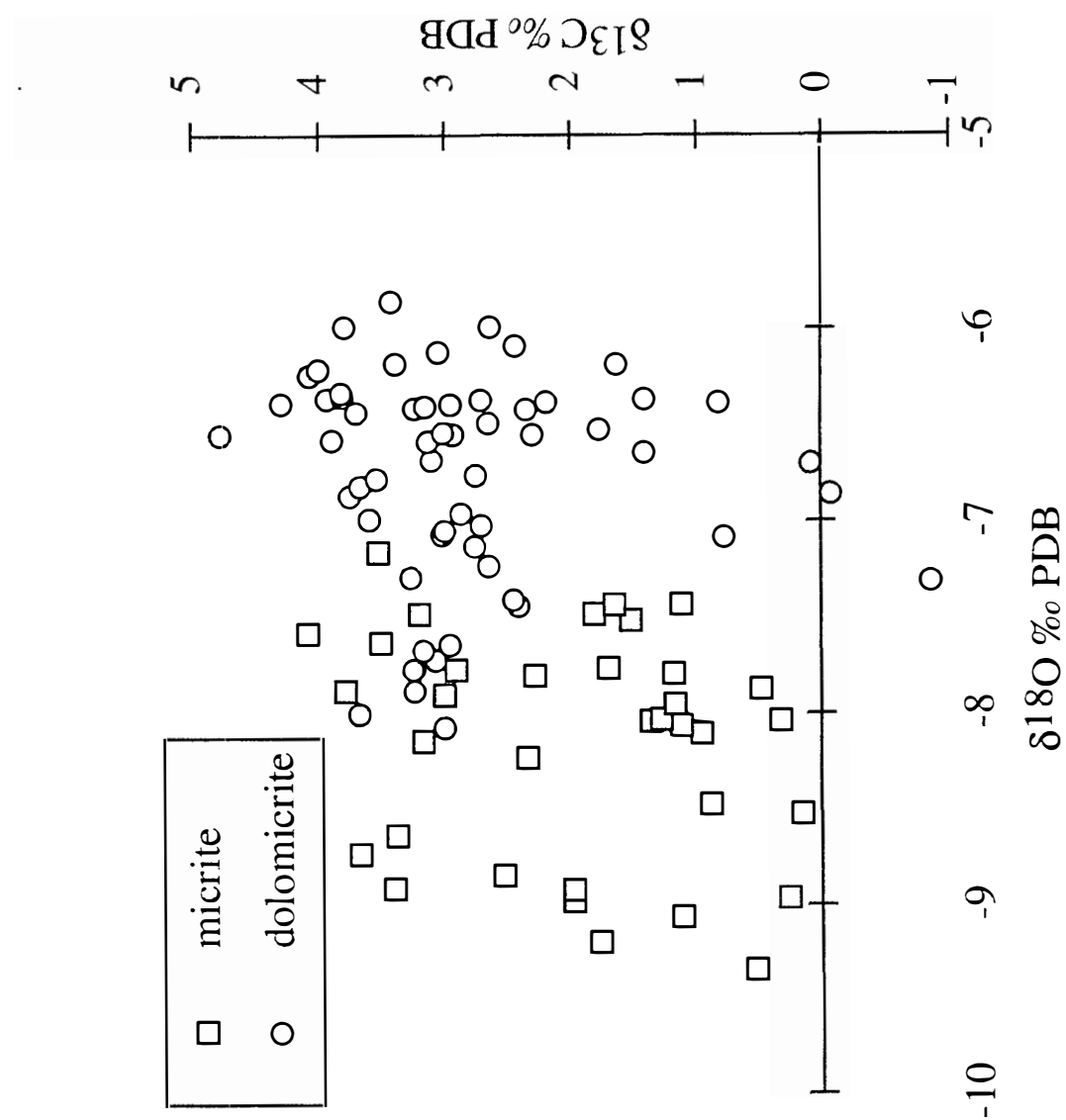


Figure 5.3. Crossplot illustrating poor correlation or covariation between $\delta^{13}\text{C}$ and $\delta^{18}\text{O}$ values for the micrite ($r^2 = 0.045$) and dolomicrite ($r^2 = 0.004$) samples.



relative to dolomicrite samples ($\delta^{18}\text{O} = -8.1$ to -5.9 ‰ PDB).

In Figure 5.4 the data points representing the individual diagenetic phases are superimposed on the $\delta^{13}\text{C}$ and $\delta^{18}\text{O}$ stratigraphic variation trends. Data points for the fibrous/bladed calcite cement from the subtidal depositional package of the Maynardville plot within the $\delta^{13}\text{C}$ and $\delta^{18}\text{O}$ variation curve. Rare fibrous/bladed calcite from the Copper Ridge Dolomite has the most negative $\delta^{18}\text{O}$ value (-10 ‰ PDB), and is significantly depleted in ^{18}O relative to the associated dolomicrite. Equant calcite cement is depleted in both ^{13}C and ^{18}O in comparison to the associated micrite samples. The $\delta^{13}\text{C}$ values of saddle dolomite show a rather good correlation with the dolomicrite $\delta^{13}\text{C}$ variation curve, with some values being only slightly depleted in ^{13}C relative to the dolomicrite. On the other hand, the saddle dolomite samples have similar $\delta^{18}\text{O}$ values or are depleted in ^{18}O in comparison to the associated dolomicrite (Fig. 5.4).

RELATIONSHIP OF CARBON-ISOTOPE STRATIGRAPHY TO BIOSTRATIGRAPHY AND SEQUENCE STRATIGRAPHY

Chronostratigraphic correlation of Cambrian strata by means of biostratigraphy is often limited due to the restricted geographic distribution of many skeletal fossil taxa whose occurrence and preservation are strongly influenced by various ecological and taphonomic factors (Brasier 1993). Carbon-isotope stratigraphy, developed for large Cambrian carbonate platform successions with a well-constrained biostratigraphic and sequence stratigraphic framework, has great potential to be used as a stratigraphic tool (Brasier 1993). Thus, the Late Cambrian carbon-isotope variations reported for several biostratigraphically well-characterized successions (Fig. 5.5; Brasier 1993; Saltzman et al. 1995a, Saltzman 1996) can be compared with the $\delta^{13}\text{C}$ variations documented for the coeval sedimentary succession of the southern Appalachians in this study (Fig. 5.1).

Figure 5.4. Comparison of carbon and oxygen isotope compositions of matrix samples and individual diagenetic phases. Variations in isotope composition as a function of stratigraphic position of matrix samples are denoted by the shaded curves. Superimposed data points represent the isotope compositions of the individual diagenetic phases including: fibrous to bladed calcite cement (solid triangles), equant calcite cement (open triangles) and saddle dolomite cement and replacement (open diamonds).

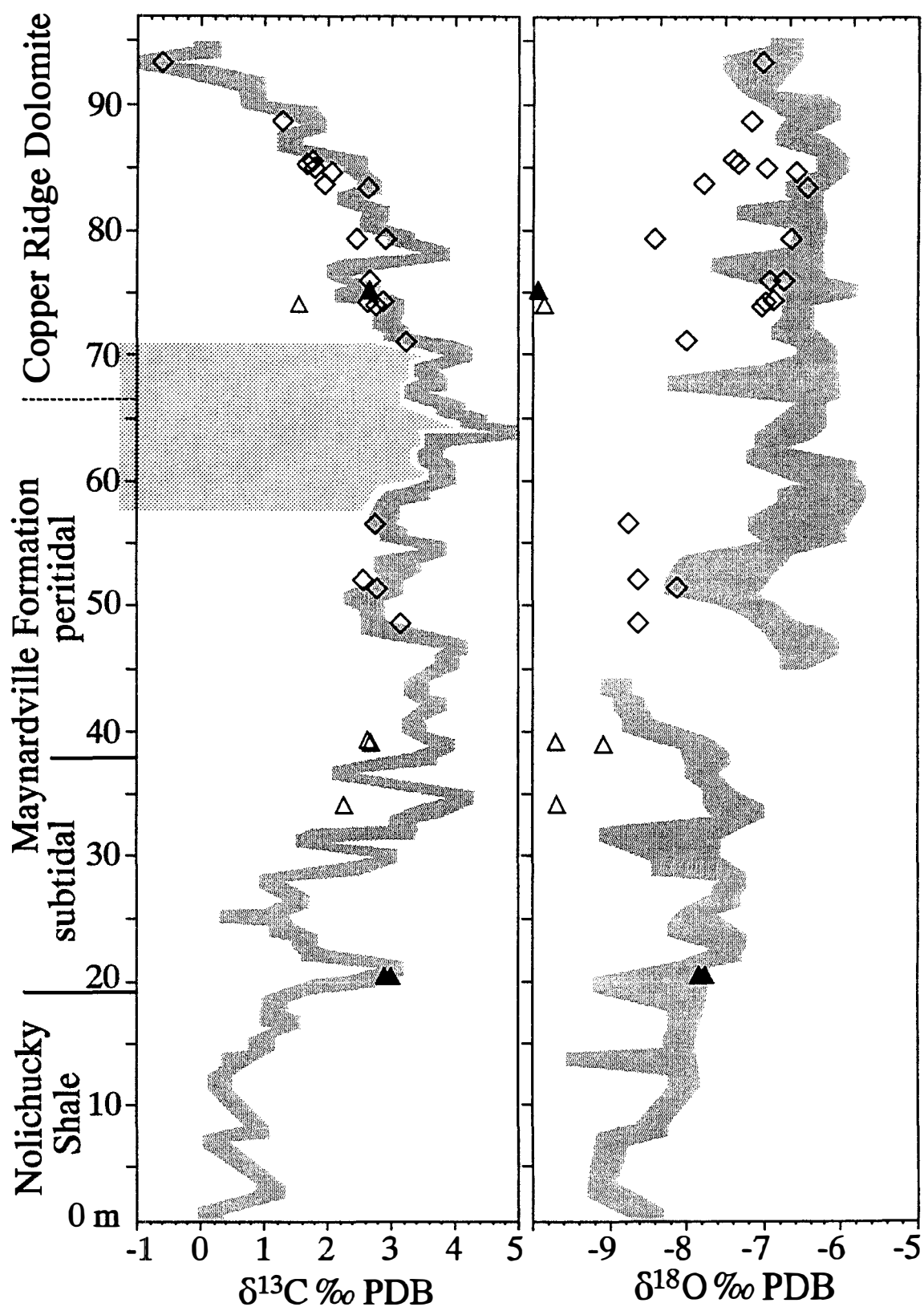
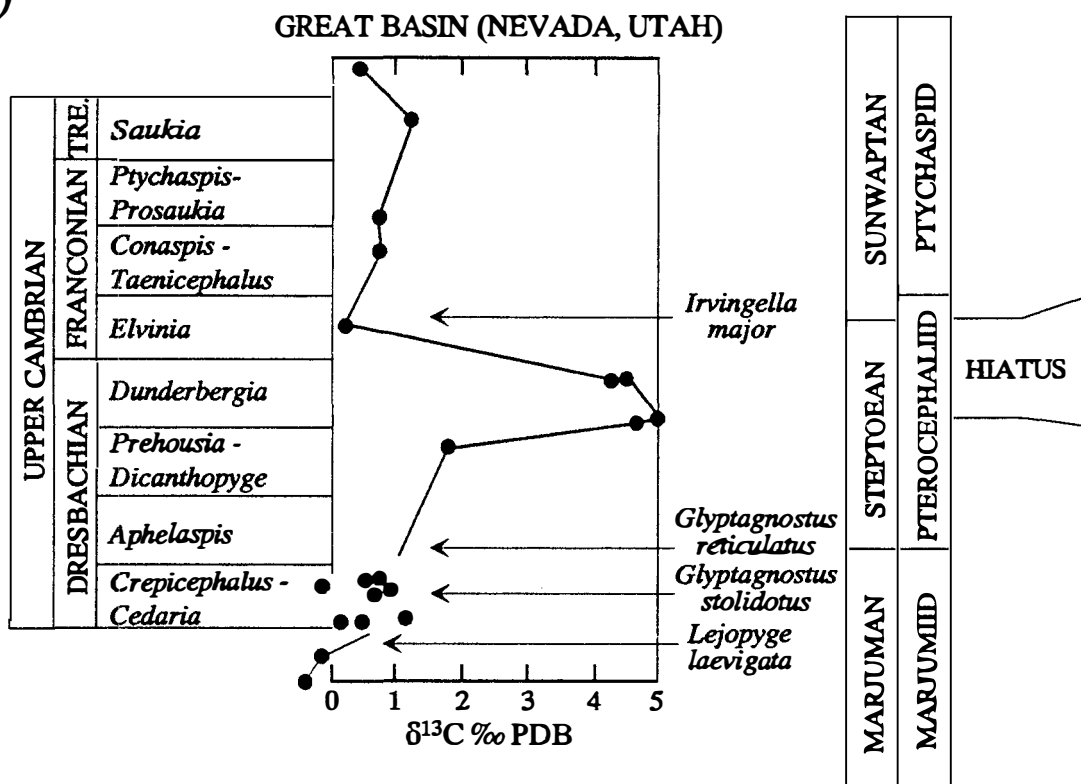
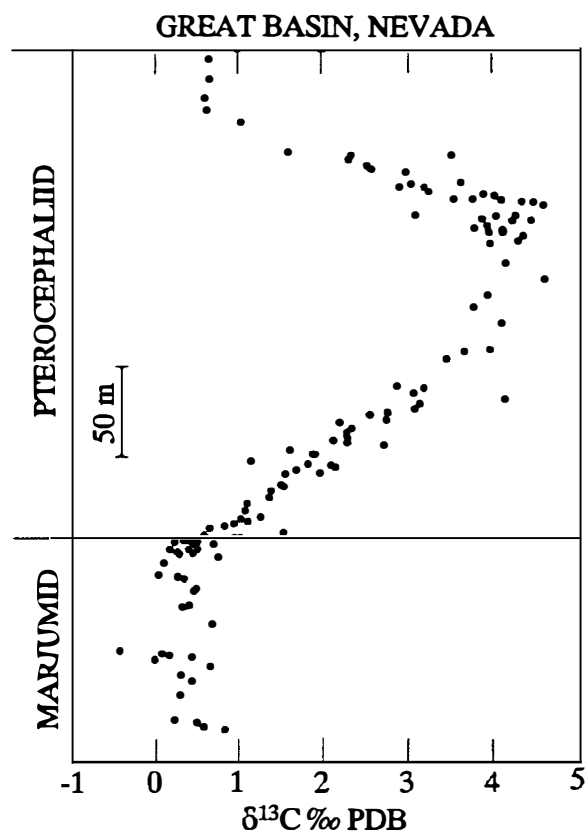


Figure 5.5. Positive carbon-isotope excursions documented for several time-equivalent Upper Cambrian sedimentary successions. **A)** the Great Basin of Nevada and Utah (from Brasier 1993); **B)** the Great Basin of Nevada (from Saltzman 1996); **C)** Kazakhstan and China (from Saltzman 1996).

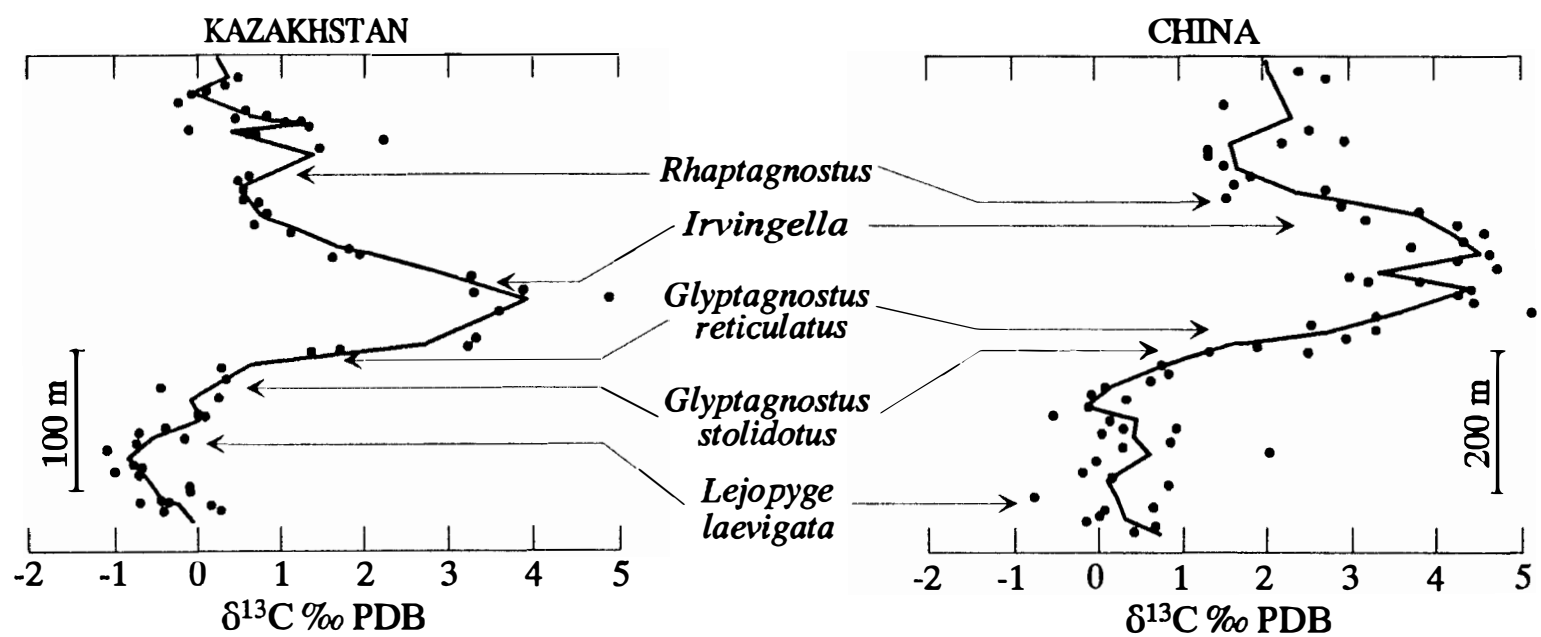
A)



B)



C)



The Upper Cambrian succession of the southern Appalachians lacks prominent biomarkers, especially in the upper part of the Maynardville Formation and the overlying Copper Ridge Dolomite. Consequently, the biostratigraphy of this stratigraphic interval is poorly constrained. On the other hand, a detailed sedimentologic and sequence stratigraphic framework, with an emphasis on the Maynardville Formation, has been developed and is reported in Chapters 2 and 3.

Figure 5.6 relates the stratigraphy of the southern Appalachians in northeastern Tennessee to established Upper Cambrian biostratigraphy. The presence of the *Cedaria* and *Crepicephalus* faunal zones has been reported in the highly fossiliferous Nolichucky Shale of northeastern Tennessee (Fig. 5.6; Bridge 1956; Derby 1965; Rasetti 1965). Bridge (1956) also reported that the elements of the *Crepicephalus* zone are sometimes present in the lower part of the Maynardville Formation. At the time these observations were made, the Maynardville was considered a member of the Nolichucky Shale. Derby (1965) argued that the base of the Maynardville is at or above the lower boundary of the *Aphelaspis* zone, and that the *Crepicephalus* fauna is absent in the Maynardville Formation (Fig. 5.6). In this study the base of the Maynardville is placed at the base of first thick-bedded limestone unit above the Nolichucky Shale, and as such it represents a facies boundary that may be at different time-stratigraphic horizons at different localities (Bridge 1956; Derby 1965). The presence of the *Aphelaspis* zone fauna in the lower part of the Maynardville Formation (the subtidal depositional package) constrains its age to the Dresbachian or Steptoean (Fig. 5.6). The upper part of the Maynardville, comprising the peritidal depositional package, is extensively dolomitized and is poorly fossiliferous. The Maynardville conformably grades upward into similar peritidal deposits of the overlying Copper Ridge Dolomite (Knox Group). Based on lithologic evidence, the conformable transitional interval between these two formations is correlative with the Dresbachian/Franconian unconformity (Fig. 5.6; Osleger and Read 1993; see also Chapter 2).

Figure 5.6. The Upper Cambrian stratigraphy of the southern Appalachians of northeastern Tennessee in relation to established Cambrian stratigraphy and biostratigraphy.

	Stages (Howell et al. 1944)	"New" Stages (Ludvigsen and Westrop 1985)	Biomeres (Palmer 1965)	Trilobite Zones	NE Tennessee Stratigraphy
UPPER CAMBRIAN	Trempealeauan	Sunwaptan	Ptychaspid	<i>Saukia</i>	Knox Group Copper Ridge Dolomite
	Franconian			<i>Saratogia</i> <i>Taenicephalus</i>	
	Dresbachian	Upper Steptoean	Pterocephaliid	<i>Irvingella major</i> <i>Elvinia</i>	Conasauga Group Maynardville Formation
				<i>Dunderbergia</i> <i>Prehousia</i> <i>Dicanthopyge</i> <i>Aphelaspis</i> (<i>Glyptagnostus reticulatus</i>)	
		Lower Marjuman	Marjumiid	<i>Crepicephalus</i> <i>Cedaria</i>	Nolichucky Shale

A major unconformity is absent in the southern Appalachians because the rate of passive-margin thermal subsidence exceeded the rate of sea-level fall (Bond et al. 1989; Osleger and Read 1993). It is possible that the stratigraphic interval deposited on the passive margin during the time period of continent-wide regression also represents a condensed interval. The presence of similar intervals was reported from the northern Appalachians of western Newfoundland by James and Stevens (1986), based on the occurrence of the upper four Dresbachian trilobite zones (*Aphelaspis*, *Dicanthopyge*, *Prehousia*, and *Dunderbergia*) in less than 20 m of strata associated with thin layers of quartz sand. Unfortunately, biostratigraphic control is insufficient to precisely determine the time period represented by the conformable succession in the southern Appalachians. As was the case for the uppermost highly dolomitized part of the Maynardville Formation, preserved skeletal fauna is very rare in the overlying Copper Ridge Dolomite. The presence of a Trempealeauan fauna has been documented from the upper part of the Copper Ridge Dolomite (Bridge 1956; Derby 1965), but to date, no fossil of Franconian age has been identified in the southern Appalachians. Therefore, the Copper Ridge Dolomite is considered to represent most of the Franconian and Trempealeauan stages (*Elvinia* to *Saukia* zones) of the Late Cambrian (Fig. 5.6; Bridge 1956; Rasetti 1965; Derby 1965; Osleger and Read 1993).

Palmer (1965b) described the late Dresbachian fauna of the Great Basin, including the *Aphelaspis*, *Dicanthopyge*, *Prehousia*, and *Dunderbergia* trilobite zones and the lower Franconian *Elvinia* zone, as the Pterocephaliid biomere (Fig. 5.6). A biomere is a regional biostratigraphic unit of stage magnitude defined by levels of trilobite mass extinction (Palmer 1965a). Ludvigsen and Westrop (1985) proposed that the Pterocephaliid biomere can be replaced by the Steptoean stage (Fig. 5.6). The Steptoean extends from the base of the *Aphelaspis* zone to the base of the *Irvingella major* subzone of the *Elvinia* zone (Ludvigsen and Westrop 1985; Fig. 5.6).

Brasier (1993), Saltzman et al. (1995a), and Saltzman (1996) reported a positive carbon-isotope excursion for the Upper Cambrian successions in the Great Basin, China, Kazakhstan and Australia, suggesting a likely global phenomenon (Fig. 5.5). The beginning of the $\delta^{13}\text{C}$ excursion is marked by an increase in $\delta^{13}\text{C}$ values of marine carbonate phases above the background values ranging between -1 and +1 ‰ PDB (Fig. 5.5). This increase is coincident with the first occurrence of the trilobite *Glyptagnostus reticulatus* which also corresponds to the base of the Pterocephaliid biomere, the Steptoean stage, and the *Aphelaspis* zone (Figs. 5.5 and 5.6). This stratigraphic horizon represents a marine extinction horizon at the Marjumiid-Pterocephaliid biomere boundary and can be correlated world-wide (Ludvigsen and Westrop 1985). Maximum $\delta^{13}\text{C}$ values (between 4 and 5 ‰ PDB) correspond to the late Steptoean time of a craton-wide hiatus separating the Sauk II and Sauk III sequences (Fig. 5.5A). This time of maximum excursion also coincides with the time of maximum faunal diversity within the Pterocephaliid biomere, which spans the late *Dunderbergia* to early *Elvinia* trilobite biozones (Palmer 1965b, Rowell and Brady 1976; Saltzman et al. 1995a; Saltzman 1996). The end of the excursion occurred prior to the end of the Pterocephaliid Biomere (Fig. 5.5A, B; Saltzman 1996).

The beginning of the positive carbon-isotope excursion in the stratigraphic succession of the southern Appalachians occurred during the deposition of the upper part of the Nolichucky Shale (Fig. 5.1). The analogy with the Great Basin localities relates the start of the excursion with the base of the *Aphelaspis* zone or the base of the Pterocephaliid biomere marked by the first occurrence of *Glyptagnostus reticulatus* (Fig. 5.6). Thus, carbon-isotope stratigraphy can potentially be used to make interpretations about the approximate position of the biozone and biomere boundaries in a stratigraphic succession for which detailed biostratigraphic determinations have not been previously made. Such interpretations are possible on the basis of the documented consistent

relationships between carbon-isotope excursions and biostratigraphic markers on different continents (Gale et al. 1993), but should be made with a great degree of caution. Saltzman (1996), for example, noted that the Steptoean excursion started slightly earlier in China than in the Great Basin. Such differences should also be anticipated between the Great Basin and the southern Appalachians.

The period of maximum carbon-isotope excursion at the Thorn Hill locality correlates with the sequence boundary zone within which the Maynardville/Copper Ridge transition is contained (Fig. 5.1). The sequence boundary zone is characterized by the presence of common sand-size quartz and feldspar detritus. The relationship between the time of maximum carbon-isotope excursion and sea-level low stand in western North America supports the interpretation that the sequence boundary zone is coeval with the time of continent-wide regression resulting in the Dresbachian/Franconian unconformity or Sauk II/Sauk III hiatus. In the southern Appalachians this stratigraphic interval is highly dolomitized and poorly fossiliferous. If the deposition of this interval corresponds to the time of maximum faunal diversity within the Pterocephaliid biomere it should be approximately correlative with the *Dunderbergia* (late Dresbachian) and *Elvinia* (early Franconian) faunal zones (Fig. 5.6). This is consistent with the correlation between the maximum carbon-isotope excursion and the widespread influx of siliciclastics during the *Dunderbergia* and/or early *Elvinia* zones of the Great Basin (Saltzman 1996).

The geometry of carbon variation curves can be used as indicators of sediment accumulation rates and the distribution of discontinuities in the geological record (Magaritz 1991; Pelechaty et al. 1996). The thickness of the stratigraphic interval which records the Steptoean positive carbon-isotope excursion in the Great Basin of Nevada is in excess of 200 m (Fig. 5.5B; Saltzman 1996). In comparison, the sedimentary succession at the Thorn Hill locality that contains the carbon-isotope excursion is about 80 m thick (Fig. 5.1). This implies a rather low sediment accumulation rate and thus indicates that the

stratigraphic interval deposited on the passive margin of the southern Appalachians during the time period of continent-wide regression represents a condensed interval.

The return to background $\delta^{13}\text{C}$ values occurred during the deposition of the lower Copper Ridge Dolomite (Fig. 5.1). Elsewhere, the end of the excursion occurred prior to the end of Pterocephaliid biomere and during the *Elvinia* zone, which supports an early Franconian or late Steptoean age for the lowermost Knox Group deposits in the southern Appalachians (Fig. 5.6).

RELATION TO ENVIRONMENTS OF DEPOSITION AND DIAGENESIS

Variations in $\delta^{13}\text{C}$ values of carbonate minerals are considered to represent changes in the composition of the solutions from which they precipitated. This can be attributed to the small fractionation of carbon during precipitation of carbonate minerals and to the relative insensitivity to temperature changes. Thus, $\delta^{13}\text{C}$ variations of unaltered marine carbonate components are expected to reflect changes in seawater $\delta^{13}\text{C}$ composition. The synchronous occurrence of the Steptoean carbon-isotope excursion in several geographically distinct areas suggests the global scope of this event. In order to fully constrain the anatomy of any secular oceanic carbon-isotope fluctuations, it is necessary to evaluate all possible effects of the depositional environment and post-depositional diagenetic changes upon the carbon-isotope signature.

Environmental Influence

The relatively short residence time of carbon in the oceans contributes to their isotopic heterogeneity, including geographic and depth-related, inter- and intrabasinal variations (Holser et al. 1986; Kaufman et al. 1993; Kaufman and Knoll 1995). This is supported by the carbon-isotope composition of modern oceans, which ranges between about -0.5 and +2.0 ‰ PDB (Kroopnick 1985). Therefore, 1 to 2 ‰ variations in ancient

contemporaneous carbonates from different basins may not necessarily be related to secular changes. Excursions of such magnitude are difficult to apply for interbasinal correlation in the absence of sufficient biostratigraphic control (Kaufman and Knoll 1995). The magnitude of the Steptoean excursion (4 to 5 ‰) is large enough to be attributed to the perturbation in carbon cycling on the global scale rather than the expected natural variation in oceanic carbon-isotope composition.

Variations controlled by environments of deposition were documented by Patterson and Walter (1994), who observed that the seawater of modern carbonate platforms (Bahama Banks and Florida) are depleted in ^{13}C by as much as 4 ‰ relative to open-ocean water. This is related to oxidation of marine and terrestrial organic matter, and changes in water chemistry caused by evaporation, freshwater discharge, and CaCO_3 withdrawal. Restricted tidal flat or lagoonal carbonates have a lower potential of recording $\delta^{13}\text{C}$ of global surface seawater than shelf margin lithofacies such as oolites and organic build-ups (Joachimski 1994; Patterson and Walter 1994). On the other hand, Gonzales and Lohman (1985) observed $\delta^{13}\text{C}$ variations within individual samples of Holocene reefal carbonates of up to 6 ‰. Despite these facts, the documented carbon-isotope variations for the entire Phanerozoic of up to about 11 ‰ is too large to be entirely a function of the depositional environment.

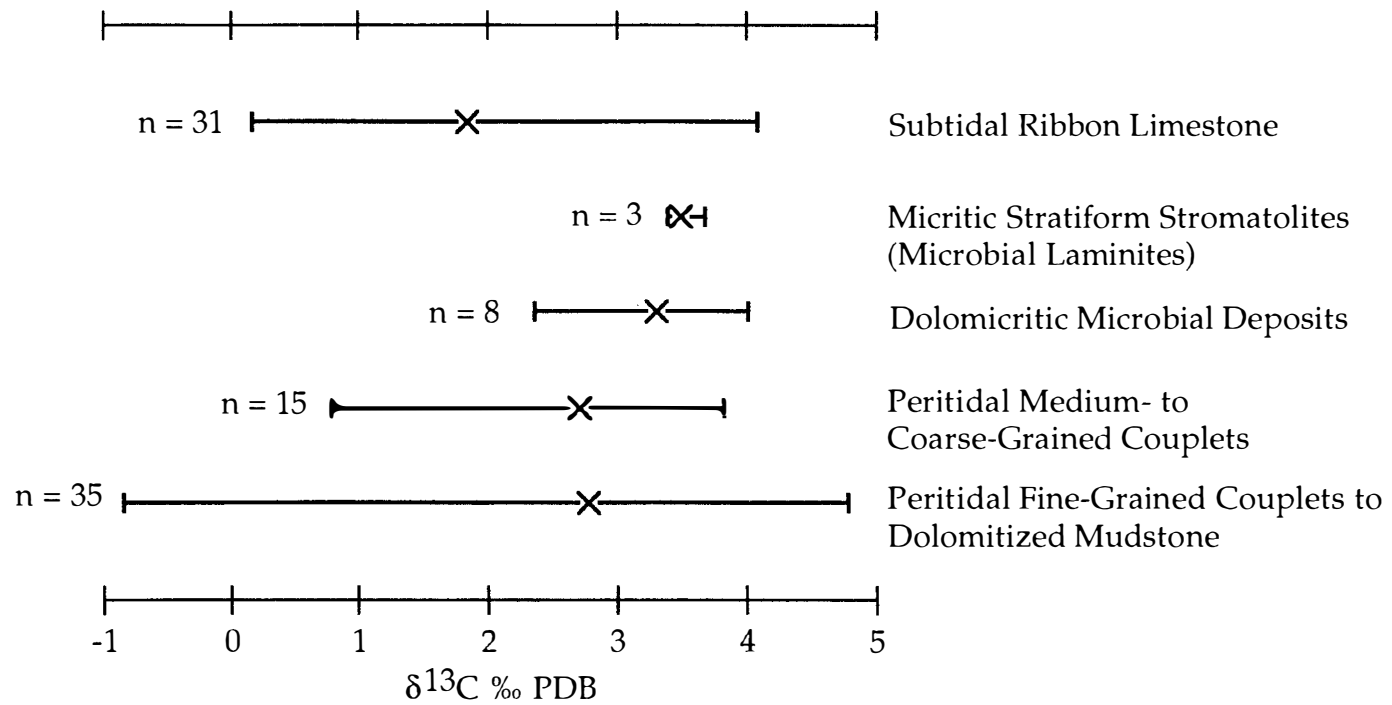
The examined Upper Cambrian succession represents depositional environments that range from less restricted (shallow ramp) to more restricted, shallow subtidal to supratidal (lagoonal to semi-arid tidal flat) settings. These environments existed on an isolated carbonate platform separated from the exposed craton by an intrashelf basin during the deposition of the Nolichucky Shale and the subtidal depositional package of the Maynardville Formation. The aggradation and progradation of this carbonate platform towards the craton, across a completely infilled intrashelf basin, resulted in the formation of a wide tidal flat during the deposition of the uppermost Maynardville and the Copper

Ridge Dolomite. Rare oolites and microbial bioherms were deposited on localized shoals and microbial patch reefs. Thus, the typical shelf-margin deposits needed for the comparison with more restricted tidal flat and lagoonal deposits are not present.

Carbon-isotope stratigraphy is not applicable if isotope compositions correlate strongly with facies (Kaufman and Knoll 1995). Figure 5.7 illustrates that there is no systematic variation between lithofacies and carbon-isotope values. The range of values for individual lithofacies is proportional to the number of samples analyzed (Fig. 5.7). The scatter of data for the peritidal fine-grained couplets and dolomitized mudstone deposits suggests that depositional environments alone cannot account for such a large (> 5.5 ‰) range of $\delta^{13}\text{C}$ values (Fig. 5.1). Mean $\delta^{13}\text{C}$ values for all peritidal lithofacies (microbial deposits and mechanical couplets) are similar (< 1 ‰ difference between four mean values; Fig. 5.7). These mean values are slightly higher than the mean value for the subtidal lithofacies (Fig. 5.7). Bonferroni T tests were performed to evaluate the nature of the mean differences among lithofacies (Lehmann 1975). A significant difference in mean $\delta^{13}\text{C}$ values was found only between subtidal ribbon limestone and stratiform stromatolite lithofacies ($df = 87$; $\alpha = 0.01$). The difference between the mean values for the subtidal and peritidal lithofacies can be attributed to the larger number of samples representing the period prior to the start of the excursion than the period following the end of the excursion (Fig. 5.1). Possible depth-related variations in $\delta^{13}\text{C}$, however, could have produced a similar trend.

The $\delta^{13}\text{C}$ composition of surface waters of modern oceans is highly variable, but is in general enriched in ^{13}C relative to deep ocean waters (by about 2 ‰), due to biological and air-sea exchange processes (Kroopnick 1985; Charles et al. 1993). Such depth-related variations do not apply to the Upper Cambrian deposits because they were deposited in shallow water. The carbonate deposits of the Nolichucky Shale are allochthonous deposits remobilized from shallower parts of the platform. This further

Figure 5.7. A range of $\delta^{13}\text{C}$ values for various lithofacies studied. The number of samples (n) and mean values (X) are indicated for each lithofacies.



excludes the possibility for pronounced depth-related variations in isotope composition. Depth-related variations are also improbable based on the studies of Cambrian carbonate strata from the Great Basin in which similar carbon-isotope values between contemporaneous deep and shallow water carbonates have been observed (Brasier 1993). Global carbon-isotope changes affected the deep- and shallow-marine carbonate sediments of the Early Cretaceous strata in the Arabian Gulf in a similar way and at a comparable time resolution (Vahrenkamp 1996).

Wide variations in carbon-isotope composition have been observed in modern marine hypersaline brines, ranging from a 12 ‰ decrease to a 20 ‰ increase in $\delta^{13}\text{C}$ values of total inorganic carbon relative to normal-marine water (Stiller et al. 1985; DesMarais et al. 1989; Lazar et al. 1989; Lazar and Erez 1992). These variations are caused by evaporation, precipitation of CaCO_3 , organic matter decomposition, atmospheric CO_2 invasion, and biogenic effects of microbial mat communities. Recognition of these effects are very important for the interpretation of isotopic compositions of ancient carbonates associated with evaporites and stromatolites. Stiller et al. (1985) suggested that the carbon-isotope compositions of carbonates formed in association with evaporating brines should be enriched in ^{13}C as a result of non-equilibrium gas-transfer isotope fractionation caused by the loss of CO_2 from the brines. Such processes could have influenced the ^{13}C -enrichment of the peritidal carbonate deposits of the Maynardville and the Copper Ridge Dolomite relative to the subtidal deposits. The least negative $\delta^{13}\text{C}$ values of dolomicrite samples from the sequence boundary zone are associated with the sea-level fall that could have resulted in enhanced evaporation (Fig. 5.1). Evaporite pseudomorphs and dissolution voids are fairly common in this part of the stratigraphic succession, but they are also present within the peritidal carbonates characterized with significantly lower $\delta^{13}\text{C}$ values. If extensive evaporation was the primary cause for the ^{13}C enrichment, then an associated enrichment in ^{18}O can

also be expected. Figure 5.2 illustrates that maximum $\delta^{13}\text{C}$ values are not paired with an increase in $\delta^{18}\text{O}$ values, and that the decrease in $\delta^{13}\text{C}$ values in the Copper Ridge Dolomite is not accompanied by a decrease in $\delta^{18}\text{O}$ values. The lack of correlation between $\delta^{13}\text{C}$ and $\delta^{18}\text{O}$ values provides evidence against the link between evaporitic conditions and increased $\delta^{13}\text{C}$ values.

In addition to evaporative effects, there is also a question of possible vital influence on the carbon-isotope composition for the analyzed Upper Cambrian microbial deposits or stromatolites (Fig. 5.7). The photosynthetic fractionation of carbon by cyanobacteria is dependent on CO_2 availability, growth rate, cell size and population density (Calder and Parker 1973; Pardue et al. 1976; Goericke et al. 1994). These factors control the variations in the $\delta^{13}\text{C}$ composition of the organic material produced. The $\delta^{13}\text{C}$ values of dolomicrites from the Upper Cambrian microbial deposits are comparable to that of inorganic micrites from the peritidal package, suggesting the absence of any significant vital influence (Fig. 5.7). This relationship can be predicted by the mode of formation for agglutinated stromatolites. These stromatolites form by the trapping of micritic particles which are basically the same constituents of inorganic micrites. The predicted and observed relationship is also in accordance with the lack of measurable carbon vital effects associated with Proterozoic stromatolites as determined from comparison of stromatolitic micrites and marine cements (Fairchild et al. 1990). Fine-grained stromatolite deposits are considered to be suitable for the studies of secular $\delta^{13}\text{C}$ changes (Fairchild et al. 1990; Marshall 1992; Knoll et al. 1995).

In general, there is a lack of correlation between conditions within environments of deposition and the observed $\delta^{13}\text{C}$ trend. It is unlikely that local variations in environmental conditions could have caused the large Steptoean positive carbon-isotope excursion. Minor variations in $\delta^{13}\text{C}$, superimposed on the general trend, may in part be related to varying environmental factors.

Diagenetic Influence

The carbon-isotope composition of ambient waters can best be reconstructed from $\delta^{13}\text{C}$ values of carbonate minerals precipitated under equilibrium conditions, and in the absence of substantial postdepositional modifications (Weissert 1989). Ideal samples for determining paleo-oceanic isotope compositions are unaltered abiotic marine cements precipitated as low-Mg calcite under oxic conditions and in isotopic equilibrium with their depositional environment (Lohmann and Walker 1989; Carpenter et al. 1991; Marshall 1992). Turner (1982) warned that a varying precipitation rate, temperature, and the mineralogy of the carbonate phase can cause variations in $\delta^{13}\text{C}$ values of CaCO_3 between 0.55 and 4.0 ‰. A temperature effect can cause an increase in $\delta^{13}\text{C}$ of calcite by about 1 ‰ for every 27°C increase in temperature (Emrich et al. 1970). Romanek et al. (1992), however, determined that fractionation in calcite shows no significant effects of temperature or precipitation rate, and that the discrepancies between observed and predicted carbon-isotope values are a function of non-equilibrium precipitation related to vital effects and the presence of diagenetic microenvironments.

Marine cements are not common in the Upper Cambrian succession examined, and the study of stratigraphic carbon-isotope variations relied primarily on the use of depositional micrites. As discussed previously, stromatolitic micrites have the potential for recording the original marine $\delta^{13}\text{C}$ values. Similarly, Magaritz et al. (1991) and Brasier et al. (1993) documented the potential of using shallow-water micrite and microspar with rare skeletal fragments for carbon stratigraphic studies. Brasier et al. (1994) observed that the Lower Cambrian micrite and microspar have $\delta^{13}\text{C}$ values very similar to associated early diagenetic marine fibrous cements, which do not show evidence for extensive diagenetic alteration based on trace element and $\delta^{18}\text{O}$ values. Marshall (1992) noted that in most cases non-luminescent micrite or microspar retain their original carbon-isotope ratios. Schidlowski and Aharon (1992) determined that diagenetically

stabilized sedimentary micrites preserve the isotope composition of the original carbonate muds within 1 ‰ of the original value inherited from a bicarbonate precursor with a shift of about +1 ‰ due to equilibrium fractionation. All of these observations suggest that micritic deposits can represent a fairly reliable indicator of oceanic carbon-isotope evolution.

Dolomicritic samples were also extensively utilized in this study. Based on the study of coexisting metamorphic calcite and dolomite and extrapolation from high temperatures, Sheppard and Schwartz (1970) determined that dolomite is enriched in ^{13}C by 2 to 3 ‰ relative to coprecipitated calcite. Even though fine-grained carbonate sediment has the potential to be isotopically altered during dolomitization, it has been demonstrated that fine-crystalline dolomites normally retain their carbon-isotope composition from the precursor CaCO_3 for the following reasons: 1) the dominant source of carbon in the dolomite is the precursor carbonate mineral phase; 2) the formation of fine-crystalline dolomite is most commonly a synsedimentary or very early diagenetic process occurring in the presence of fluids with similar isotope composition to seawater; and 3) pore space occlusion during penecontemporaneous cementation isolates dolostones from later diagenetic fluids (Narbonne et al. 1994; Kaufman and Knoll 1995). Because of these reasons, carefully selected dolomite samples can be used in the reconstruction of seawater carbon-isotope evolution (Kaufman et al. 1993).

Any interpretation of stratigraphic variations of carbon-isotope composition requires the recognition and understanding of the diagenetic processes capable of causing postdepositional changes (Schidlowski and Aharon 1992). Such processes include neomorphism and recrystallization, reequilibration with fluids of differing isotope composition, and precipitation of isotopically different diagenetic carbonate phases (Veizer 1983; Fairchild et al. 1990; Derry et al. 1992; Kaufman et al. 1992; Marshall 1992; Kaufman and Knoll 1995). The carbon-isotope composition of carbonate mineral phases

can be significantly influenced by the incorporation of organogenic carbon during precipitation from diagenetic fluids, which are affected by the presence and degradation of organic material. Meteoric diagenetic phases, for example, are commonly characterized by negative $\delta^{13}\text{C}$ values resulting from soil-derived CO_2 (Allen and Matthews 1982; Lohmann 1982, 1988; Beeunas and Knauth 1985). Such a trend is absent in carbonate successions subjected to meteoric diagenesis prior to the advent of land plants.

The carbon-isotope value of marine organic matter is about 25 ‰ more negative than inorganic bicarbonate (Marshall 1992). Thus, the degradation of organic matter has the potential to significantly change the carbon-isotope composition of marine carbonate sediment. The incorporation of organogenic carbon in diagenetic carbonate phases preferentially occurs in restricted environments such as in an oxygen-depleted burial diagenetic setting. Microbially mediated reactions of organic matter degradation include: 1) iron, manganese, sulphate and nitrate reduction in suboxic conditions; and 2) methanogenesis in anoxic conditions. With increasing temperature during burial, abiogenic degradation of organic matter or thermal carboxylation processes take place (Claypool and Kaplan 1974; Irwin et al. 1977; Coleman and Raiswell 1981; Marshall 1992; Winter and Knauth 1992). Most of the thermal and microbial reactions of organic matter degradation release organogenic carbon, which decreases the $\delta^{13}\text{C}$ value of dissolved bicarbonate and the resulting carbonate burial cements. The exception is CO_2 that forms during the degradation of organic matter by methanogenic bacteria with $\delta^{13}\text{C}$ values of up to +15 ‰, due to kinetic fractionation between methane and CO_2 (Irwin et al. 1977). Positive $\delta^{13}\text{C}$ values of diagenetic carbonate minerals may therefore represent precipitation during methanogenesis. The products of different reactions of organic matter degradation are commonly mixed with each other and with dissolved marine bicarbonate, thereby producing a wide range of carbon-isotope composition of diagenetic pore fluids and the resulting carbonate mineral phases (Gautier and Claypool 1984;

Marshall 1992; Iyer et al. 1995).

The massive alteration or resetting of $\delta^{13}\text{C}$ values in existing carbonate phases during diagenesis is hindered by small concentrations of carbon in diagenetic fluids (Banner and Hanson 1990). The carbon-isotope composition of porewater is commonly controlled by the composition of the dissolving carbonate phase (Marshall 1992). For example, the $\delta^{13}\text{C}$ composition of deep burial cements usually reflects the composition of the bicarbonate derived from pressure dissolution of the host carbonate. This effective buffering is promoted by low rates and short transport distances of fluid flow in the burial diagenetic environment (Marshall 1992). Carbonate $\delta^{13}\text{C}$ values can be modified only in very open systems (high fluid-rock ratio) and/or in the presence of brines with elevated total dissolved carbon compositions (Banner and Hanson 1990).

The majority of samples used in this study represent homogenous micrites and dolomicrites, without visible cements and skeletal fragments. The samples predominantly have non-luminescent to dark, dully luminescent CL patterns, but in some cases exhibit a patchy distribution of non- to more bright luminescence, suggesting possible diagenetic modifications. Examples of diagenetic alteration of these deposits include neomorphism and recrystallization of micrite to microsparite, and dolomitization of fine-grained carbonate deposit to dolomicrosparite and coarser-crystalline replacement dolomite. Diagenetic modifications are substantiated by the oxygen-isotope compositions which are more negative than the predicted Cambrian marine calcite value of about -5.0‰ PDB (Fig. 5.2; Lohmann and Walker 1989). The Upper Cambrian micritic carbonate deposits lack petrographic evidence for original aragonitic mineralogy, such as: 1) the abundance of coarser-crystalline or microspar texture; 2) crystal-mosaic fabric with inclusions of original aragonite or needle relicts; and 3) elevated strontium content (see also Chapter 4; Fig. 4.8; Lasemi and Sandberg 1984; Sandberg 1984; Moshier 1989). This is in accordance with Sandberg's (1983) notation of Late Cambrian 'calcite seas'. Calcite-dominated precursor

micrites have a potential for retaining their original or close to the original carbon-isotope value.

Superimposed on the general trend, which shows an increase of $\delta^{13}\text{C}$ values for subtidal micrite samples, is a wide scatter of $\delta^{13}\text{C}$ values (Fig. 5.1). Diagenesis in the presence of degrading organic matter can explain the scatter of data for the carbonate deposits of the Nolichucky Shale, and the limestone layers alternating with shaly and argillaceous dolomicritic layers in the Maynardville Formation (Fig. 5.1). This interpretation is substantiated by the association of subtidal deposits with framboidal pyrite, ferroan diagenetic phases, skeletal fragments, evidence for bioturbation, and interbedded shales that may have been organic-rich when deposited. Kaufman et al. (1992) noted the correlation between a wide range of $\delta^{13}\text{C}$ values and a high initial organic carbon content in carbonate deposits. Similarly, Ripperdan (pers. com. 1996) observed substantial intersample $\delta^{13}\text{C}$ variations for carbonate deposits interbedded with shales. Incorporation of organogenic carbon into precipitating carbonate phases may start in oxygen-deficient shallow-burial marine environments. Such environments are common in deeper-water organic-rich mudrocks and sandstones, but may also exist in shallow argillaceous lagoonal limestones, where anoxic conditions are promoted by the presence of clay material (Marshall 1992). The increase in $\delta^{13}\text{C}$ values within the Nolichucky Shale is accompanied by a decrease in the amount of shale (Fig. 5.1), but is not associated with any apparent changes in the diagenetic pattern that could have caused a shift in the carbon-isotope signature. The recorded $\delta^{13}\text{C}$ shift is consistent with a secular trend in marine $^{13}\text{C}/^{12}\text{C}$ increase.

Smaller intersample variation in a part of the stratigraphic carbon curve related to the peritidal dolomicrite is also consistent with a regional to global perturbation in carbon cycling, rather than local variations due to organic matter degradation. The less-scattered $\delta^{13}\text{C}$ values of the peritidal dolomicrites correspond to less evidence for the presence and

degradation of organic matter, and to the paucity of ferroan carbonate phases. Brasier (1993) cited the absence of ferroan carbonate phases and pyrite as a lack of evidence for methanogenic or sulphate-reducing diagenesis. The decline in $\delta^{13}\text{C}$ values within the Copper Ridge Dolomite is not associated with changes in the diagenetic pattern, nor with lithologic changes, and thus indicates a secular trend.

The comparison between stable isotopes of carbon and oxygen is used to evaluate the extent and type of diagenetic modification, as well as the influence of diagenesis upon the potential for the preservation of carbon-isotope signatures. The lack of systematic covariance between $\delta^{13}\text{C}$ and $\delta^{18}\text{O}$ values is commonly used as evidence that the carbon-isotope signal is not controlled by diagenetic alterations (Figs. 5.1, 5.2; Hudson and Anderson 1989; Derry et al. 1992; Brasier et al. 1994). The ^{18}O -depletion of analyzed samples relative to the predicted Upper Cambrian marine calcite value is consistent with alteration in the presence of meteoric waters and/or diagenetic modification during burial at elevated temperature (see Chapter 4).

Oxygen-isotope values of the peritidal dolomicrites are, in general, more enriched in ^{18}O relative to subtidal micrite samples (Figs. 5.1, 5.2). This trend can be explained by: 1) an equilibrium fractionation effect that predicts a 3 ± 1 ‰ enrichment of dolomite relative to coprecipitating calcite (Friedman and O'Neil 1977; Land 1980); 2) evaporative enrichment in ^{18}O of penecontemporaneous dolomite formed under sabkha-type conditions (McKenzie 1981; Carballo et al. 1987; Gregg et al. 1992); and 3) a lesser degree of later diagenetic alteration of dolomite relative to calcite, which is related to higher solubility and therefore higher reactivity of calcite (Knoll et al. 1995). The ^{18}O -depletion relative to estimated normal-marine Cambrian dolomite suggests that the analyzed dolomicrite samples have been diagenetically altered (see Chapter 4). The observed difference between the $\delta^{18}\text{O}$ values of micrite and dolomicrite samples is therefore most likely a function of the difference in precursor carbonate composition

coupled with different styles of diagenetic modification.

The comparison of isotopic compositions of carbonate matrix and associated cements provides insights into the diagenetic environments and the extent of diagenetic modifications (Fig. 5.4). The similarity of $\delta^{13}\text{C}$ and $\delta^{18}\text{O}$ values for the fibrous/bladed calcite cement from the subtidal lithofacies and the associated micrite suggests formation from marine water and similar diagenetic modification (Fig. 5.4). Depletion of ^{18}O in the fibrous/bladed calcite cement relative to the peritidal dolomicrite may be the result of meteoric modification during periods of subaerial exposure, or may reflect later burial alteration. During diagenetic modification, the $\delta^{13}\text{C}$ value for fibrous/bladed calcite was buffered to the host-rock composition (Fig. 5.4). Involvement of meteoric water may have been responsible for the ^{18}O - and ^{13}C -depletion observed in the equant calcite cement relative to the associated matrix samples (Fig. 5.4). Equant calcite cement from the Maynardville Formation is ferroan in composition, and is associated with burrows. This suggests the possible incorporation of ^{13}C -depleted organogenic carbon into the equant calcite cement under reducing conditions in deeper meteoric-phreatic or shallow-burial environments. The $\delta^{18}\text{O}$ values of saddle dolomite are comparable with, or are depleted in ^{18}O relative to associated dolomicrite (Fig. 5.4). This is coupled with similar $\delta^{13}\text{C}$ compositions for saddle dolomite and dolomicrite. These observations are consistent with saddle dolomite formation during burial at elevated temperatures in a rock-dominated system.

DISCUSSION

Fluctuations in $\delta^{13}\text{C}$ composition of marine carbonates through time are most commonly interpreted to represent secular trends of changing carbon-isotope values in the oceans. Positive carbon-isotope excursions are related to an increase in the rate of carbon buried as organic matter resulting from increased rates of sedimentation, increased primary

productivity, and/or marine anoxia (Derry et al. 1992; Brasier 1992; Brasier et al. 1994; Calvert et al. 1996; among numerous others). Removal of 1% of the oceanic organic carbon causes a positive isotopic shift in marine water of about 0.2 ‰ (Berger and Vincent 1986). This suggests that a 4 to 5 ‰ shift recorded in marine carbonates can be related to a dramatic local or global change involving the removal of 20 to 25% of the organic carbon from ocean water (Marshall and Middleton 1990). The Late Cambrian or Steptoean positive carbon-isotope excursion is apparently global in scope, because it has been documented in contemporaneous stratigraphic successions at several localities worldwide (Brasier 1993; Saltzman et al. 1995a; Saltzman 1996; this study). The following discussion focuses on the relative importance of organic productivity, sedimentation rate and marine anoxia as possible causes for the excursion, and on the consequences of this pronounced perturbation in global carbon cycling. Possible changes in ocean circulation patterns, temperature and salinity gradients, and global climate, are also included in the discussion as a part of the complex dynamics pertaining to the atmosphere-hydrosphere-biosphere system, which controls cycling of carbon on time scales $\leq 10^7$ years (Veizer 1985).

The early Paleozoic was characterized by the accumulation of organic-rich sediments in greater thickness, over larger area, and for longer periods of time than at any other time interval in the Phanerozoic (Leggett 1980; Thickpenney and Leggett 1987). The Middle to Late Cambrian time period was one of the three main episodes of 'black shale' deposition during the early Paleozoic (Leggett 1980; Thickpenney and Leggett 1987). The Alum shale of Scandinavia is one example of organic-rich sediments deposited on the continental shelf during that period of time (Thickpenney and Leggett 1987). The Conasauga Group shales were also deposited during the Middle to early Late Cambrian. These organic-rich deposits were a potential hydrocarbon source (Montañez 1994).

Following episodic glaciation in the Late Proterozoic, the Cambrian was a time

period with a relatively warm global climate (Wilde and Berry 1984). Long non-glacial intervals are characterized by sluggish, global ocean-current circulation, favoring ocean stratification and the formation of less-oxygenated deeper waters (Wilde and Berry 1984; Weissert 1989). Warmer waters contain less dissolved oxygen, which additionally promotes anoxic conditions. The sea-level was at one of its maxima on the Laurentian craton during the early Late Cambrian, spanning the *Cedaria* through *Aphelaspis* faunal zones (Fig. 5.6; Bond et al. 1988). A high sea-level contributes to salinity stratification and decreased terrestrial runoff, which cause nutrient depletion and reduced primary organic productivity (Brasier 1992). Such conditions probably resulted in the presence of nutrient-starved waters over deeper anoxic ocean waters during the Early through the Late Cambrian along the margins of Laurentia (Brasier 1992). The elevated Fe and Mn composition of the Upper Cambrian carbonates was interpreted by Gao and Land (1991b) as a possible consequence of the expansion of an oxygen-minimum zone in the oceans.

The sea-level maximum was followed by a regressive event and a wide-spread Dresbachian/Franconian (Sauk II/Sauk III) hiatus (Lohman-Balk 1971; Palmer 1971, 1981; Bond et al. 1988; Osleger and Read 1993). Increased terrestrial run-off during sea-level fall increases the amount of nutrients in surface waters, thus resulting in greater organic productivity and ^{12}C -depletion of surface waters (Brasier 1992). This scenario can explain the relationship between the sea-level fall and the maximum Steptoean $\delta^{13}\text{C}$ excursion (Brasier 1993; Saltzman et al. 1995a; Saltzman 1996). A similar explanation has been proposed for the positive carbon-isotope excursions near the Precambrian/Cambrian boundary (Magaritz et al 1986; Brasier 1990).

Trilobite and brachiopod diversity was at a maximum during the late *Dunderbergia* zone (Rowell and Brady 1976), but this does not necessarily imply increased organic productivity. Studies regarding the amount of organic matter stored in modern and more recent deposits suggest that high organic productivity may not be the best explanation for

the deposition of organic-rich 'black shales' during the early Paleozoic (Thickpenny and Leggett 1987). In the absence of a direct evidence for a significant increase in organic productivity, the maximum positive carbon-isotope excursion during the Steptoean can be explained by the increased rates of organic carbon removal due to increased rates of siliciclastic sediment deposition, caused by the onset of regression and the accompanied increase in the erosion rate. The presence of silt- and sand-size quartz and feldspar particles in the carbonate rocks from the sequence boundary zone at the Maynardville/Copper Ridge transition is a reflection of sea-level lowering and an increase in the input of cratonically derived detritus. The hypothesis of increased erosion as a possible cause of positive carbon-isotope excursions can be tested by comparing the stratigraphic variations of $\delta^{13}\text{C}$ with that of $^{87}\text{Sr}/^{86}\text{Sr}$ through the intervals in question (Kaufman et al. 1993; Saltzman et al. 1995b). A coupled increase in $\delta^{13}\text{C}$ and $^{87}\text{Sr}/^{86}\text{Sr}$ suggests that enhanced erosion rates could have caused elevated $\delta^{13}\text{C}$ values (Derry et al. 1994). A detailed study of $^{87}\text{Sr}/^{86}\text{Sr}$ variations has not yet been performed on the Upper Cambrian succession in the southern Appalachians. A compilation of Sr isotopic data (Burke et al. 1982; Kaufman et al. 1993) shows a significant scatter (0.7090 to 0.7097) for the Late Cambrian. This scatter may be related to a possible change in the erosion rate. Also, one of the dolomicrite samples from the sequence boundary zone has a $^{87}\text{Sr}/^{86}\text{Sr}$ ratio of 0.7097, which is among the highest values for Phanerozoic marine carbonates recorded by Burke et al. (1982). This value may reflect the high erosion rate related to the Dresbachian/Franconian unconformity.

Many early Paleozoic organic-rich deposits are characterized by extremely low sedimentation rates (Thickpenny and Leggett 1987). Under these conditions, organic carbon removal could have been favored by enhanced organic-matter preservation in the presence of stratified oceans with deep anoxic waters (Thickpenny and Leggett 1987). During the early Paleozoic such conditions were promoted by a high sea-level, a warm

climate and a low atmosphere and hydrosphere oxygen content (Thickpenny and Leggett 1987). These conditions may have triggered the positive carbon-isotope excursion in the Steptoean. Similarly, the Miocene positive carbon-isotope excursion started during high sea-level and warm climate conditions that contributed to poor aeration of ocean waters and to enhanced organic matter deposition (Vincent and Berger 1985; Berger and Vincent 1986).

A consequence of an increase in the removal of carbon from the ocean surface layer is the decline in atmospheric $p\text{CO}_2$ and the subsequent global climatic cooling that can cause glaciation and sea-level fall. Such a scenario was first proposed as the 'Monterey Hypothesis' by Vincent and Berger (1985) for the Miocene positive carbon-isotope excursion. The major cooling episode in the Miocene occurred about 15 Ma, in the middle of the carbon-isotope excursion, which lasted between 17 and 13 Ma (Berger and Vincent 1986). This suggests that the removal of organic carbon caused the cooling, rather than vice versa. A similar scenario has been proposed for the cooling episodes and the onset of glacial activity in the Late Proterozoic (Knoll et al. 1986) and the Late Ordovician (Marshall and Middleton 1990). Saltzman et al. (1995a) and Saltzman (1996) offered the 'Monterey Hypothesis' as a possible explanation for the linkage between the Steptoean carbon-isotope excursion and the maximum sea-level fall at the Sauk II/Sauk III boundary. The cause of this eustatic sea-level fall is unclear, especially because the Cambrian has been hypothesized as a time period with little or no continental glaciation (Hambrey and Harland 1981; Scotese and McKerrow 1990). A possible cause for eustatic sea-level variations of up to 10-50 m amplitude during the non-glacial Cambrian climate may have been small-scale continental or alpine glaciations (Read 1989; Osleger and Read 1993). Saltzman (1996) also suggested some alternative climate-controlled mechanisms for sea-level fall such as the storage of water in continental basins and subcontinental sediment-pore reservoirs (Hay and Leslie 1990; Jacobs and Sahagian 1993).

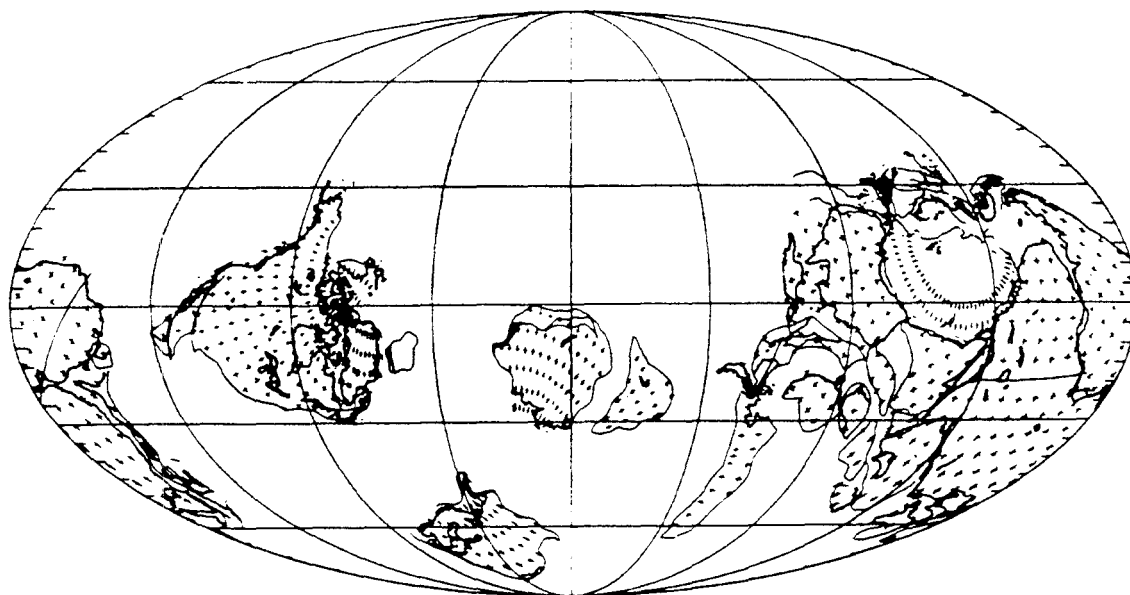
The lack of evidence for glaciation does not imply the absence of possible global climatic cooling during the Steptoean, related to the positive carbon-isotope excursion. The cooling event may not have caused glaciation because of the absence of continental land masses in polar regions during the Late Cambrian (Fig. 5.8). Global climatic cooling can, however, cause major paleoceanographic changes. During cooling events a destabilization in the oceanic density structure or ocean overturn occurs when high-latitude waters, forming at about 5°C, become denser than the middle-latitude waters with higher salinity (Wilde and Berry 1984, 1986). The ocean circulation models proposed by Weissert (1989) seem applicable for the Late Cambrian. The time period prior to, and during the onset of the carbon-isotope excursion was characterized by warm and equable climate, with high-latitude ocean water temperatures above 5°C. This was followed by a period with a cooler climate and cold polar areas without ice formation during the maximum excursion.

A climate-induced ocean overturn may cause major changes in the cycling of organic matter or nutrients, and can trigger pronounced changes in the carbon cycle (Arthur et al. 1987; Saltzman 1996). The end of the Steptoean carbon-isotope excursion may have been associated with these events. The return of $\delta^{13}\text{C}$ compositions back to normal values following a positive excursion is generally attributed to the following: 1) a decrease in the productivity of the upper ocean-water mass; 2) mixing of the oceans that brings deep, ^{13}C -depleted water to the surface; and 3) oxidation of organic carbon on land and on exposed continental shelves due to a sea-level fall (Berger and Vincent 1986; Holser and Magaritz 1987; Magaritz 1989; Kump 1991). With a lack of firm criteria to evaluate the change in the organic productivity, the end of the Steptoean carbon-isotope excursion can be sufficiently explained by climate-induced ocean mixing, coupled with the oxidation of organic matter enhanced by a sea-level fall.

The interpretations put forward here for the Steptoean excursion are similar to

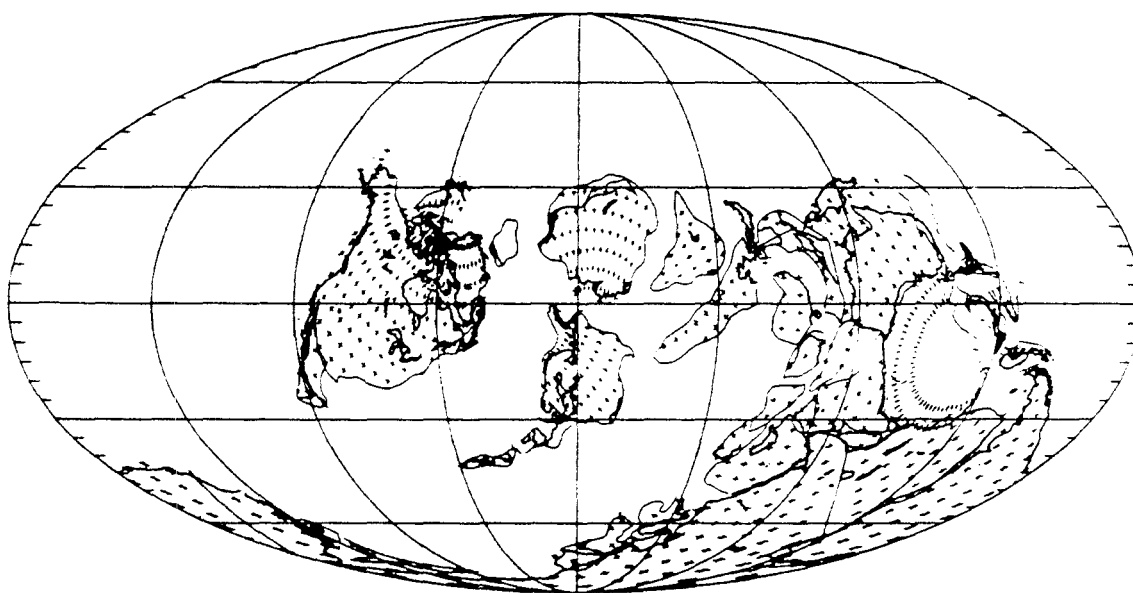
Figure 5.8. Paleogeographic reconstruction for the: **A)** Late Cambrian; and **B)** the Latest Ordovician (from Scotese and McKerrow 1990).

A)



Late Cambrian

B)



Latest Ordovician (Ashgill)

those for the Late Proterozoic (Knoll et al. 1986; Kaufman et al. 1991) and Late Ordovician positive isotope shifts (Marshall and Middleton 1990). High rates of organic burial, in the Late Proterozoic stratified ocean, resulted in ^{13}C -enrichment of preglacial carbonate deposits (Kaufman et al. 1991). The onset of Late Proterozoic glaciation caused upwelling and overturn of a stagnant water column bringing ^{13}C -depleted deep waters onto shallow shelves (Derry et al. 1992). The Late Ordovician excursion was accompanied by a eustatic regression related to the glaciation of Gondwana. The positive shift in $\delta^{13}\text{C}$ of up to 5 ‰ was accompanied by a positive $\delta^{18}\text{O}$ shift of 2 ‰, reflecting both a temperature decrease and an ice-volume effect (Marshall and Middleton 1990). The glaciation was favored by the presence of a land mass in the polar area during the Late Ordovician (Fig. 5.8). The end of Ordovician is also associated with faunal extinctions that may have been caused by the major oceanic overturn and the influx of deep, nutrient-rich, toxic waters onto the continental shelves (Wilde and Berry 1984). Some of the Mesozoic extinction events have been interpreted in the same way (Arthur et al. 1987, 1988; Schlanger et al. 1987). The Steptoean excursion ended prior to the end of the Pterocephaliid biomere (Saltzman 1996), and it is unclear whether a similar relationship existed between the proposed ocean overturn, and the extinctions at the Pterocephaliid/Ptychaspid biomere boundary.

Many aspects of the Late Proterozoic and the early Paleozoic carbon-isotope excursions are comparable to the Mesozoic and younger excursions. One of the prominent differences is that some of the Mesozoic positive carbon shifts, such as that at the Cretaceous Cenomanian/Turonian boundary, coincide with sea-level maxima (Berger and Vincent 1986; Arthur et al. 1987, 1988; Schlanger et al. 1987; Jenkyns 1996). The association of high sea-level and ^{13}C -enrichment in the oceans has been attributed to the storage of organic carbon in sediments on aerally extensive shelf seas at an above-normal rate during transgression (Berger and Vincent 1986; Jenkyns 1996). Föllmi et al. (1994),

based on the study of the pelagic carbon-isotope record of the Early Cretaceous, suggested that a sea-level rise due to climate warming accelerates the water cycle and intensifies weathering, causing nutrient mobilization and an increase in primary organic productivity, which leads to increased carbon burial and the occurrence of positive carbon-isotope excursions. Veizer (1985) however, warned that the models for carbon cycling based on the last 100 Ma, and especially on the Cretaceous isotope record, may not be appropriate for the whole Phanerozoic, and that the Cretaceous appears to represent an exception rather than a norm. Brasier (1992) suggested that the trend of increased nutrient availability in surface waters, and the associated increase in productivity and lowering of the $^{13}\text{C}/^{12}\text{C}$ ratio in the surface waters, occurs during *falling* sea-level and increased terrestrial run-off. These various interpretations suggest that prominent changes in carbon cycling are likely to occur during changes in relative sea-level, and that similar signals in the carbon-isotope record of marine carbonates could have resulted from rather different controlling factors.

Consequently, there is no unique explanation for the changes in carbon cycling throughout the geologic record. The difficulty in interpreting carbon-isotope excursions increases with increasing age of the rock successions in which the excursions are recorded. It is often difficult to determine the amount of time represented by an excursion (Magaritz 1991). Additionally, the timing and causal relationship between excursions and changes in sea-level, faunal composition, climate and oceanography remain uncertain in many cases (Marshall and Middleton 1990). Despite these problems and uncertainties, studies of carbon-isotope variations, in conjunction with other geologic and geochemical evidence, have great potential as a valuable stratigraphic tool and as important indicators of the dynamics of global environmental changes.

CONCLUSIONS

- 1) The recorded increase in the $\delta^{13}\text{C}$ values within the Upper Cambrian Nolichucky Shale, Maynardville Formation, and the Copper Ridge Dolomite of the southern Appalachians reflects the secular trend of the increased $^{13}\text{C}/^{12}\text{C}$ ratio in sea water, as a consequence of a major perturbation in the global cycling of carbon.
- 2) Comparison with coeval carbon-isotope excursions documented in biostratigraphically well-characterized successions elsewhere provides a means for improving the biostratigraphic resolution of this Upper Cambrian interval.
- 3) Superimposed on the secular trend are minor variations in $\delta^{13}\text{C}$ values related to varying conditions during deposition and postdepositional diagenetic modifications.
- 4) The comparison of the $\delta^{13}\text{C}$ and $\delta^{18}\text{O}$ values between depositional and diagenetic phases provided unique insights into the type and extent of diagenetic modifications.
- 5) The carbon-isotope excursion is related to the changes in the rate of organic carbon burial, which can be linked to the changes in ocean stratification, climate, sea-level, and possible paleoproductivity rate.
- 6) If carefully applied, studies of carbon-isotope variations provide a useful stratigraphic tool and serve as an indicator of the dynamics of global environmental changes.

CHAPTER 6

SELECTIVE DOLOMITIZATION OF CAMBRIAN MICROBIAL CARBONATE DEPOSITS: A KEY TO MECHANISMS AND ENVIRONMENTS OF ORIGIN

INTRODUCTION

The origin of ancient microbial deposits is often difficult to discern, especially in the case of poor preservation and absence of adequate modern analogs. Microbial deposit formation has been explained by analogy with modern microbial mats, but the relative importance of various processes in the formation of ancient microbial deposits is still controversial (Ginsburg 1991; Riding 1991c). Stromatolites, as a type of benthic microbial carbonate deposits characterized by a laminated fabric and produced primarily by the activities of cyanobacteria, bacteria, and algae, are good environmental indicators for shallow-marine carbonate deposits. The criteria commonly used for deducing paleoenvironments are stromatolite morphology and the characteristics of the associated deposits (Logan et al. 1964; Aitken 1967; Hoffinan 1967; Chafetz 1973; Monty 1977; Horodyski 1985; Beukes and Lowe 1989; and others).

This study focuses on the microbial carbonate deposits of the Upper Cambrian Maynardville Formation (Conasauga Group) and the lower part of the Copper Ridge Dolomite (Knox Group) in eastern Tennessee. The objective was to examine the diagenetic history of microbial deposits, with special emphasis on early diagenesis and selective dolomitization, in order to make inferences regarding the formation of these deposits. The selected stratigraphic succession is well suited for this study because it contains a variety of microbial carbonate deposit types, which presumably formed by different mechanisms and/or under different environmental conditions. Partial dolomitization of the succession preserved features that allow inference of diagenetic

events preceding dolomitization. Selective dolomitization of microbial deposits provides a useful indicator of the mechanisms and environments of their origin.

UPPER CAMBRIAN MICROBIAL CARBONATE DEPOSITS

Microbial carbonates are organosedimentary deposits produced by benthic microbial communities, and are therefore synonymous to the microbialites and microbolites of Burne and Moore (1987) and Riding (1991c), respectively. The term stromatolite is usually used for microbial deposits which have a laminated fabric (Burne and Moore 1987; Riding 1991c). A universally accepted classification of microbial deposits does not exist. The classification used in this study represents a combination of several classification schemes, such as Logan et al. (1964), Aitken (1967), and Riding (1991c).

The following types of microbial carbonate deposits have been observed within the Upper Cambrian Maynardville Formation and the lower part of the Copper Ridge Dolomite: 1) stratiform stromatolites (microbial or cryptalgal laminates); 2) laterally linked hemispheroidal (LLH) stromatolites; 3) vertically stacked hemispheroidal (SH) stromatolites; 4) columnar stromatolites; 5) digitate stromatolites; and 6) thrombolites (Fig. 2.1). These microbial deposits are described in Table 6.1 and illustrated in Figures 6.1 and 6.2.

FORMATION OF MICROBIAL DEPOSITS: AN OVERVIEW

Formation of microbial carbonate deposits is a result of a complex interplay between biologic, environmental, and diagenetic processes (Burne and Moore 1987). Though still controversial (see Ginsburg 1991), the formation of microbial deposits is believed to be the result of trapping of sediment particles and calcification of cyanobacteria (Fig. 6.3; Pentecost and Riding 1986; Riding 1991c). The presence of

Table 6.1. Description of microbial deposits. Symbols correspond to those on Figure 2.1.


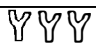

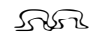


Deposits	Description	Occurrence	Present Mineralogy	Environment
 Thrombolites	clotted fabric; composed of patches (mesoclots) of dark, dense micrite embedded in fossiliferous-peloidal wackestone to grainstone; well preserved <i>Renalcis</i> , <i>Epiphyton</i> and <i>Girvanella</i> in subtidal package; <i>Renalcis</i> (?) present in peritidal package; common burrows.	bioherms; in subtidal package overlie ooid grainstone or flat-pebble conglomerate, and underlie shales and ribbon rocks; in peritidal package embedded in coarse- to medium-grained "couplets", overlain by LLH and stratiform stromatolites or grade into digitate and columnar stromatolites.	mesoclots composed of microcrystalline calcite; surrounding material calcitic or partially dolomitized.	Agitated shallow subtidal to lower intertidal; microbial patch reefs
 Digitate stromatolites (Dendrolites)	branching columns of low relief surrounded with ooid-peloidal packstone/grainstone; crudely laminated micritic pelleted (clotted) fabric; burrows and small desiccation cracks present.	bioherms and biostromes interbedded with thrombolites, coarse- to medium-grained "couplets" and calcareous siltstone.	microcrystalline calcite in columns; surrounding material extensively dolomitized.	
 Columnar stromatolites	laminated, non-linked, vertically stacked columns of cylindrical or clubbed shape, with a maximum diameter of 2-3 cm; intercolumnar space filled with ooids, peloids, and micrite arranged in "couplets"; small desiccation cracks and fenestrae.	present only in the Copper Ridge Dolomite; underlain by thrombolites and overlain by stratiform stromatolites.	mosaic of medium to coarse crystalline dolomite; partially silicified; saddle dolomite in fenestrae and desiccation voids.	Agitated to protected intertidal
 SH stromatolites	individual hemispheroids (maximum height = 20 cm; maximum diameter = 30 cm) composed of wavy laminated micrite; quartz silt, peloids and ooids in surrounding material; small desiccation cracks and fenestrae.	interbedded with fine- to coarse-grained couplets, LLH and stratiform stromatolites.	entirely dolomitized and occasionally partially silicified; saddle dolomite in fenestrae and desiccation voids.	
 LLH stromatolites	low relief (up to 1 cm) linked hemispheroids; wavy crinkly micritic laminae; common desiccation cracks and small fenestrae; some incorporated pellets/peloids and ooids; burrows present.	interbedded with stratiform and SH stromatolites, and fine- to medium-grained couplets; overlie digitate stromatolites and thrombolites.	entirely dolomitized; saddle dolomite in fenestrae and desiccation voids.	Restricted upper intertidal and supratidal
 Stratiform stromatolites (Cryptalgal laminates)	flat, planar crinkly micritic laminae (maximum 3-5 mm thick); common desiccation features, fenestrae, and evaporite molds; lenses with pellets, peloids, ooids, and quartz silt grains; some burrows; rare teepee structures.	from several mm (individual laminae) and several cm ("crusts") to 8 m thick units; interbedded with couplets and other microbial deposits.	laminae composed of microcrystalline calcite, dolomicrite and dolomicroparite; saddle dolomite in fenestrae.	

Figure 6.1. Photographs and photomicrographs illustrating different microbial deposits. Scale bar = 1 cm on all photographs of hand specimens, and 1 mm on all photomicrographs. **A)** Polished slab of stratiform stromatolite showing characteristic lamination and a subvertical desiccation crack. **B)** Photomicrograph of stratiform stromatolite. Lamina with common fenestrae is calcitic, the other laminae are dolomitic. **C)** Polished slab of LLH stromatolite showing wavy lamination. **D)** Photomicrograph of an entirely dolomitized LLH stromatolite. Note peloidal grains interbedded with micritic microbial laminae. **E)** Lower part of the photograph is a plan view of half an individual SH stromatolite specimen. Upper part of the photograph is a cross-section through the same specimen. **F)** Photomicrograph of SH stromatolite composed of laminated micritic deposit. The surrounding coarser-grained deposit contains peloids and quartz silt grains. The entire sample is dolomitized. **G)** Columnar stromatolite specimen. **H)** Photomicrograph of columnar stromatolite composed of a mosaic of medium-crystalline dolomite, and partially silicified. Intercolumnar space is filled with peloids and ooids.

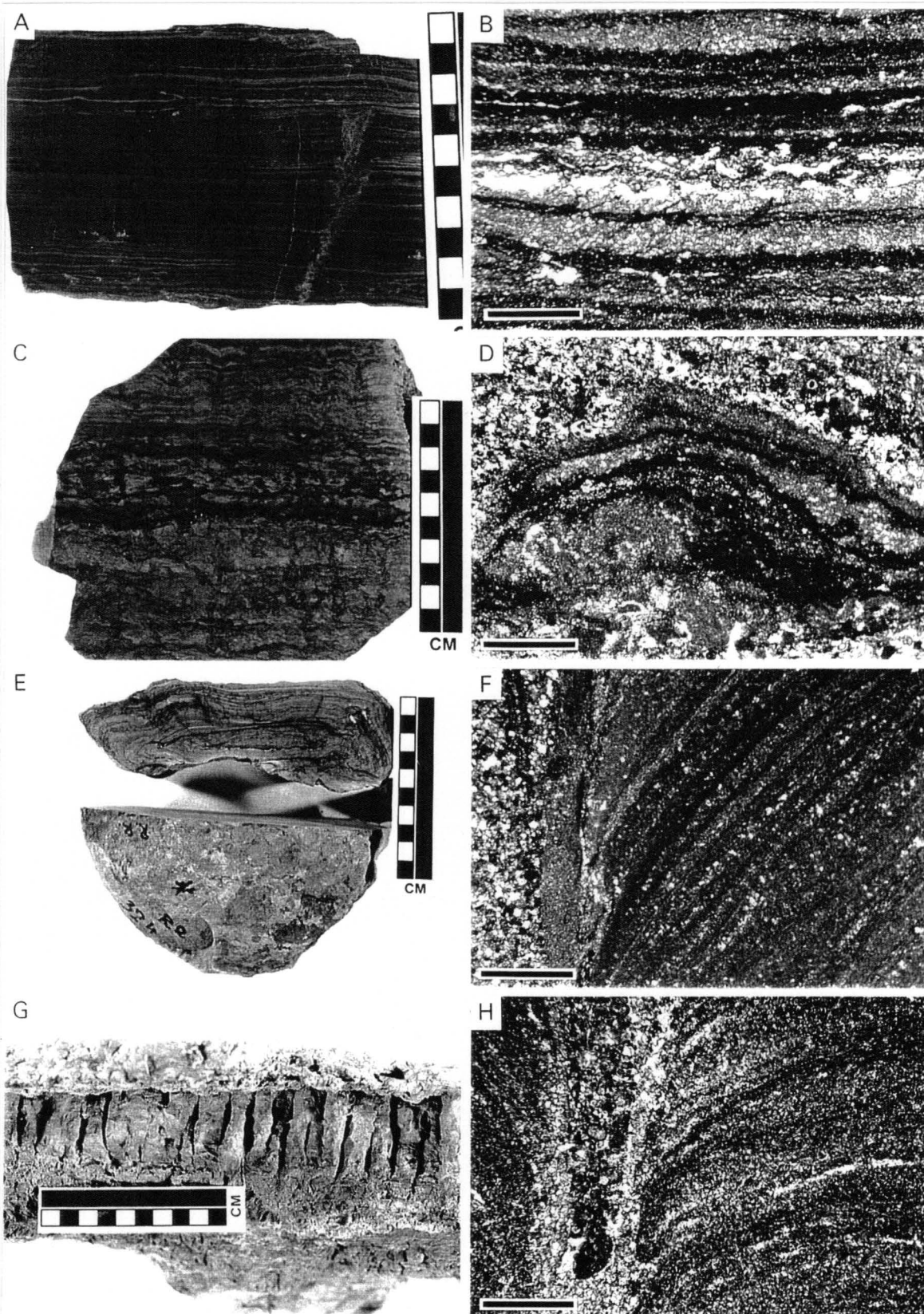


Figure 6.2. Photographs and photomicrographs illustrating different microbial deposits. **A)** Outcrop photograph of digitate stromatolite bioherm. Photo scale is 16.5 cm long. **B)** Photomicrograph of a part of an individual "digit" comprising digitate stromatolite. Note characteristic crudely laminated fabric composed primarily of microcrystalline calcite. The surrounding ooid-peloidal packstone/grainstone has been extensively dolomitized. Scale bar = 1 mm. **C)** Polished thrombolite slab showing characteristic clotted fabric. **D)** Photomicrograph of a predominantly calcitic thrombolite specimen from the subtidal package showing *Girvanella* filaments in the matrix surrounding darker micritic *Renalcis* grains. Scale bar = 0.25 mm. **E)** Photomicrograph of a thrombolite specimen from the subtidal package containing abundant *Epiphyton* grains. Scale bar = 1 mm. **F)** Photomicrograph of a thrombolite specimen from the peritidal package showing a micritic patch (mesoclot) composed primarily of calcite and embedded in a partially dolomitized fossiliferous-peloidal wackestone/packstone. Scale bar = 1 mm.

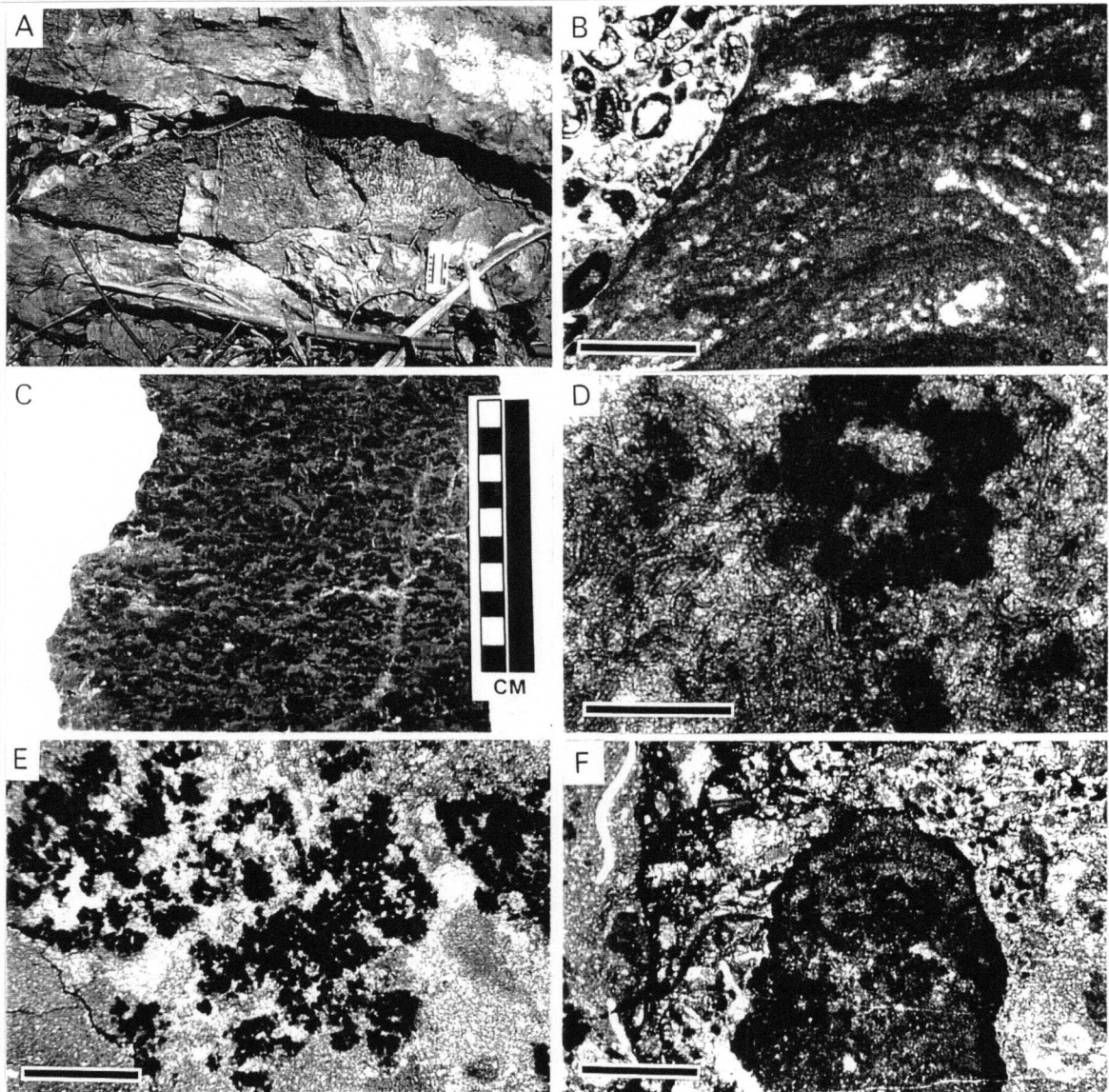
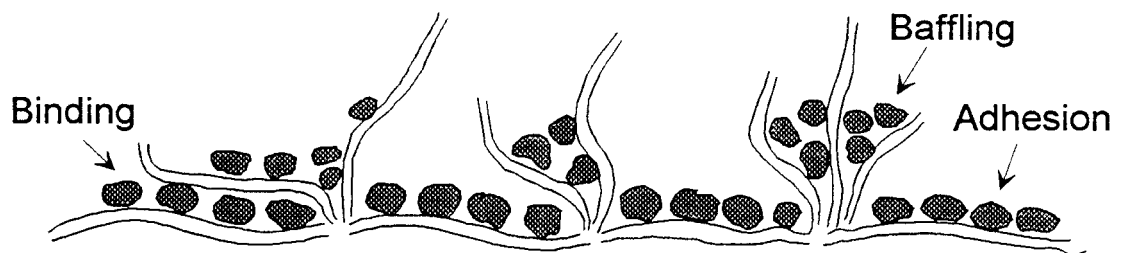


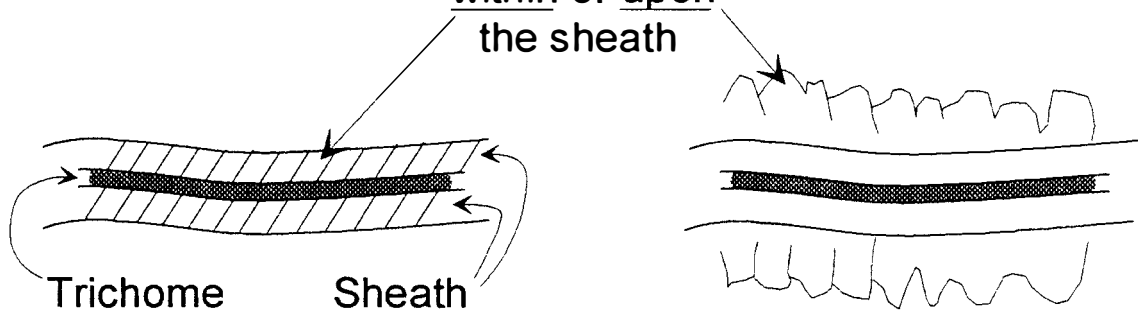
Figure 6.3. Schematic illustration of mechanisms responsible for the formation of microbial deposits using filamentous cyanobacteria as an example. **A)** Trapping of sediment particles. **B)** Calcification of cyanobacteria (modified after Riding 1991c).

A) TRAPPING OF SEDIMENT PARTICLES



B) CALCIFICATION OF CYANOBACTERIA

Nucleation of calcite crystals
within or upon
the sheath



suitable organisms and an adequate supply of detrital particles favor the trapping process in the formation of microbial deposits. The most common sediment trapping agent today is the network of interwoven mucilaginous sheaths of filamentous cyanobacteria which forms a sticky mat substrate (Golubić 1973, 1976). Trapping includes retention of sediment particles on such substrates by the processes of adhesion, baffling, and binding (Fig. 6.3A; Riding 1991c). Calcification, on the other hand, involves nucleation of calcite crystals within and upon the extracellular sheaths of cyanobacteria as a result of physicochemical and/or biotically induced precipitation (Fig. 6.3B; Lowenstam 1981; Riding 1991c). Biotically induced calcification involves calcite precipitation during the life of the organism and implies substantial biological control over carbonate mineral precipitation. In the case of cyanobacteria, it is believed that calcification is only partially controlled by the organism, and that it occurs only under suitable environmental conditions favoring physicochemical precipitation of calcium carbonate minerals (Pentecost and Riding 1986; Riding 1991a). The presence of dead cyanobacterial sheaths as nucleation sites, or changing water chemistry due to photosynthesis, may induce precipitation of calcium carbonate (Merz 1992; Défarge et al. 1994). Calcification of cyanobacteria can also be promoted by the metabolic processes of heterotrophic or sulfate reducing bacteria (Krumbein and Cohen 1977; Krumbein et al. 1977; Krumbein 1979; Lyons et al. 1984; Chafetz and Buczynski 1992). It should be noted that cyanobacterial biocalcification and physicochemical precipitation can proceed simultaneously, resulting in a complex microbial fabric (Riding 1991c; Défarge et al. 1994).

In the study of ancient microbial deposits it is often difficult to access the importance of the different processes which have influenced their formation. Processes involved may be highly variable, both spatially and temporally, calling for caution in applying modern analogs. A predominant mechanism in the formation of modern marine microbial deposits is the trapping of sediment particles, coupled with cementation

involving physicochemical precipitation of Mg-calcite and aragonite (Logan 1961; Gebelein 1969; Neumann et al. 1970; Logan et al. 1974; Playford and Cockbain 1976; Dravis 1983; Dill et al. 1986). Neoproterozoic and Cambrian time periods, on the other hand, were characterized by a decline in the abundance of agglutinated stromatolites and the expansion of calcified stromatolites (Riding 1982, 1991c; Riding and Veronova 1984; Pentecost and Riding 1986). This expansion is attributed to possible changes in ocean water chemistry (Riding 1982, 1991a; Pentecost and Riding 1986), evolutionary changes in cyanobacteria (Riding 1991b), and the evolution of skeletal organisms (Knoll et al. 1993). The development of marine calcareous plankton and the associated changes in seawater saturation levels caused the virtual disappearance of calcified marine cyanobacteria in the Cenozoic (Gebelein 1976; Kempe and Kazmierczak 1988). Calcified cyanobacteria exist today in fresh water, some alkaline lakes, and rare hypersaline coastal embayments (Horodyski and Vonder Haar 1975; Golubić and Campbell 1981; Gerdes and Krumbein 1987; Kempe and Kazmierczak 1988; Braithwaite et al. 1989; Riding 1991a; Chafetz and Buczynski 1992; Défarge et al. 1994). It is often assumed, based on modern analogs, that calcification of marine cyanobacteria in the past took place during early diagenesis, and was most likely influenced by bacterially induced calcium carbonate precipitation (Pratt 1984; Pentecost and Reading 1986; Chafetz and Buczynski 1992; Knoll et al. 1993).

SELECTIVE DOLOMITIZATION OF MICROBIAL DEPOSITS

Petrographic analysis reveals that different types of Upper Cambrian microbial deposits experienced different diagenetic modifications (Table 6.1). Stratiform stromatolites are commonly dolomitized, with only some calcitic laminae preserved (Fig. 6.1A, B). LLH, SH, and columnar stromatolites are completely dolomitized (Fig. 6.1C-H). This is in contrast to digitate stromatolites and thrombolites, which are most

commonly calcitic, even though they are commonly embedded within dolomitized deposits (Fig. 6.2).

Mechanisms of Microbial Deposit Origin

Different mechanisms of formation may account for the different styles of diagenesis for the microbial deposits examined. The relative importance of calcification versus trapping of sedimentary particles in the formation of these deposits can be evaluated on the basis of the observed patterns of selective dolomitization. Early lithification promoted by calcification of cyanobacteria may have significantly influenced the preservation potential of microbial deposits by making them less susceptible to dolomitization. This assertion is supported by the presence of microbial micritic structures that contain only scattered dolomite crystals, and are commonly embedded in completely dolomitized non-microbial deposits (Fig. 6.2B). Digitate stromatolites and thrombolites are therefore interpreted to be the result of the calcification of cyanobacteria. This interpretation is supported by the absence of coarser-grained agglutinated particles within the individual micritic microbial "digits" (Fig. 6.2B) and thrombotic mesoclots (Fig. 6.2D, F). Peloidal grains, ooids and skeletal fragments are present only in the deposits surrounding microbial micritic structures (Fig. 6.2B, F). The presence of *Renalcis*, *Epiphyton*, and *Girvanella* further supports the calcification of cyanobacteria as a mechanism for formation of thrombolites from this study (Fig. 6.2D, E). Coccoid cyanobacteria *Renalcis* and *Epiphyton* have been interpreted to represent products of bacterially induced calcification (Pratt 1984; Kennard and James 1986; Pentecost and Riding 1986; Thompson and Ferris 1990; Chafetz and Buczynski 1992). *Girvanella* filaments represent calcification of cyanobacterial sheaths as a result of both biotically and environmentally controlled processes (Riding 1975). Early lithification of thrombolites and digitate stromatolites is also substantiated by the presence of well preserved burrow

walls and the abundance of fibrous and bladed calcite cement representing marine diagenetic phases.

Entirely dolomitized microbial deposits formed primarily by sediment trapping. LLH, SH, and columnar stromatolites represent examples of such microbial deposits (Fig. 6.1C-H). This interpretation is supported by the absence of preserved calcified cyanobacterial forms, and the similarity with modern agglutinated stromatolites in terms of sediment size, nature of lamination, and disturbances in lamination (fenestrae and desiccation cracks). In the absence of processes that promote calcification, micritic sediment that was trapped on sticky microbial substrates could have been susceptible to dolomitization. Dolomitization would have been exceptionally pervasive if the dolomitizing fluids affected these deposits very early in the process of diagenesis.

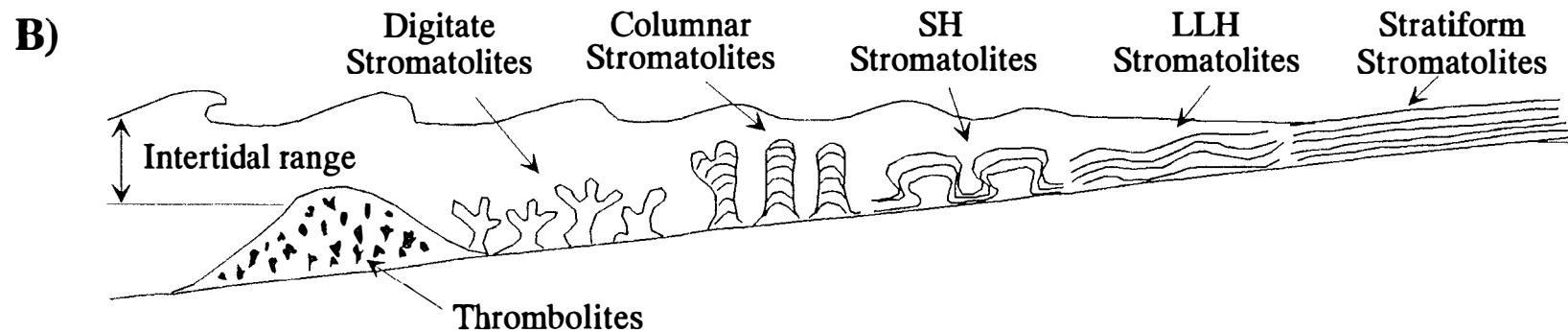
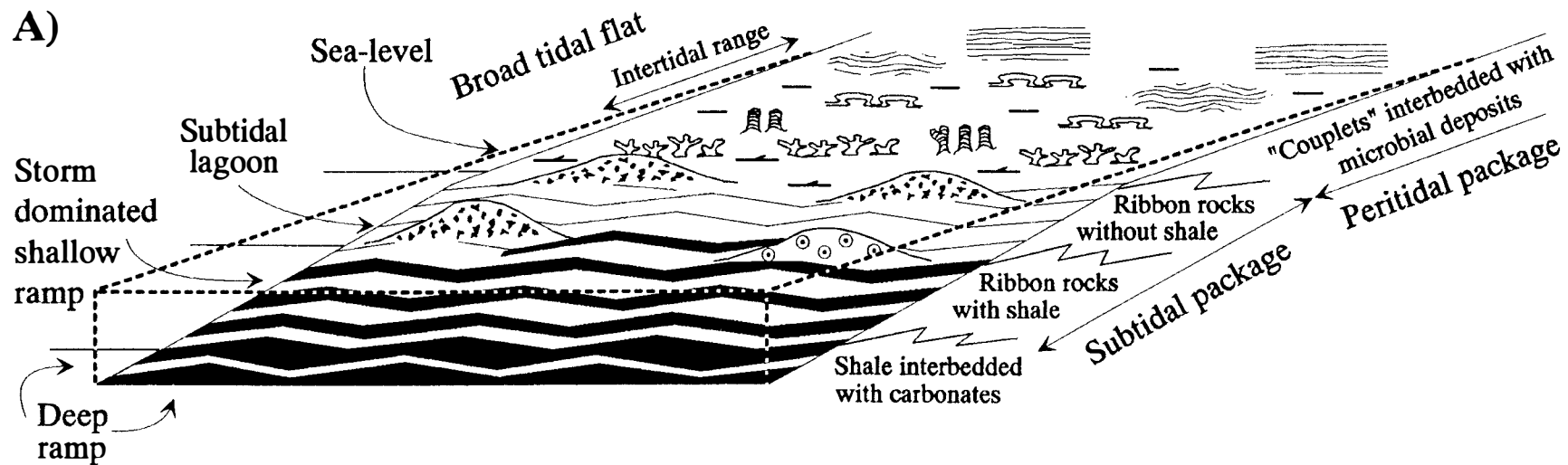
Stratiform stromatolites (cryptalgal laminates) contain both calcitic and dolomitic laminae (Fig. 6.1A, B). Preserved calcified cyanobacterial forms have not been observed within these deposits. The presence of calcitic laminae indicates that some of the laminae could have been firmly calcified fairly early in their diagenetic history, and were impermeable to dolomitizing fluids. Stratiform stromatolites are thus interpreted to be the result of both sediment trapping and early calcification.

Environments of Deposition and Early Diagenetic History

The environments of microbial deposition can be constrained based on the observed patterns of dolomitization because the calcification of cyanobacteria takes place only under favorable environmental conditions. The interpreted environments of deposition for the different types of microbial structures are shown schematically in Figure 6.4. The study of microbial deposits also helped to constrain the earliest events in a complex diagenetic history of the carbonate deposits.

Entirely dolomitized stromatolites formed in supratidal and upper intertidal

Figure 6.4. Interpretation of the environments of deposition. **A)** Generalized illustration of depositional environments for the most common lithofacies present within the succession examined (not to scale). **B)** Schematic representation of the relationship between environments of deposition for different types of microbial deposit on a tidal flat. The succession from left to right represents decreasing water agitation and shallowing from subtidal into supratidal environment (not to scale).



environments (Fig. 6.4). These environments were the primary sites for dolomitization on the Upper Cambrian arid to semi-arid tidal flat. Calcification of cyanobacteria was not prominent during formation of these microbial deposits. This was likely due to periodic emergence and increased salinity, as evidenced by the presence of numerous desiccation cracks, and evaporite-mineral pseudomorphs. Under these conditions dolomitization of microbial deposits may have even preceded substantial lithification. Dolomitization of these deposits occurred during the very early diagenetic history as penecontemporaneous or syngenetic dolomitization operating under a sabkha-like tidal flat regime.

Digitate stromatolites and thrombolites formed in a lower intertidal and upper subtidal environment where they comprised broad, low relief microbial patch reefs (Figs. 6.2A, 6.4). This environmental interpretation is supported by the presence of common bioturbation, the absence or scarcity of exposure indicators, and the association with coarser-grained deposits containing skeletal fragments, ooids, peloids, and intraclasts (Fig. 6.2B, F). These deposits represent deposition under less restricted and more agitated shallow water conditions. Deposits formed within the lower intertidal and subtidal environments were subjected to less extensive early dolomitization. Under these conditions calcification of cyanobacteria was an important process in the formation of microbial deposits. Due to the calcification, microbial deposits became less susceptible to dolomitization. This interpretation is substantiated by the presence of microbial deposits composed of microcrystalline calcite surrounded by non-microbial deposits, which are commonly extensively dolomitized (Fig. 6.2B). Additionally, thrombolites and digitate stromatolites are commonly the only lithofacies from the peritidal package of the Maynardville Formation that have escaped extensive dolomitization, even though the peritidal package contains other lithologies deposited in a shallow subtidal setting (Fig. 2.1; Table 2.2). Such selective dolomitization would not have been possible if environmental conditions were solely controlling the dolomitization patterns. Therefore,

preferential calcification of microbial deposits was likely biotically influenced and is responsible for the preservation of calcified microbial deposits.

DISCUSSION

The response of stromatolites to diagenesis and the resulting selective dolomitization was used to distinguish between stromatolites formed by calcification of cyanobacteria and those formed by simple agglutination of sediment. The different mechanisms of formation and the presence of different microbial assemblages are supported by the microfabric difference among the microbial deposits studied. The clotted fabric of thrombolites and the crudely laminated to clotted fabric of digitate stromatolites (Fig. 6.2) differ from the laminated fabric of stratiform, LLH, SH, and columnar stromatolites (Fig. 6.1). The clotted fabric may form as a result of *in situ* calcification of coccoid-dominated microbial communities (Hofmann 1973; Kennard and James 1986). In contrast to the clotted fabric, stromatolitic laminae represent the results of sediment trapping and lithification of microbial mats containing primarily filamentous cyanobacteria (Gebelein 1974, 1976; Awramik 1984; Kennard and James 1986). Stratiform, LLH, SH, and columnar stromatolites all have similar laminated microfabric (Fig. 6.1). This suggests that similar processes and a similar assemblage of mat-forming organisms were responsible for the formation of these stromatolite types. The difference in the macrostructure of these stromatolites was likely controlled by conditions within the environments of formation, such as water agitation (Gebelein 1974; Hoffman 1976; Semikhatov et al. 1979; Knoll and Awramik 1983).

A unique aspect in the study of Cambrian microbial deposits is determining the importance of calcification by cyanobacteria. Despite the decline in diversity and abundance following the Proterozoic, stromatolites were still widespread during the Cambrian (Howe 1966; Aitken 1967; Ahr 1971; Chafetz 1973; Edhorn and Anderson

1977; Demicco et al. 1982; Geldsetzer et al. 1989; Kennard 1988; and others). The Cambrian and Early Ordovician are characterized by the abundance of thrombolites, which has been related to the appearance of calcification in marine cyanobacteria near the Proterozoic-Cambrian boundary and to the evolution of calcareous microbes *Renalcis*, *Epiphyton*, and *Girvanella* (Riding 1982, 1991a; Riding and Veronova 1984; Kennard and James 1986; Pentecost and Riding 1986). Several authors related the occurrence of thrombolites to the evolution of metazoa, and interpreted them as a result of bioturbation causing disruption of the original laminated fabric (Chafetz 1973; Hofmann 1973; Monty 1976; Walter 1977; Walter and Heys 1985). Bioturbation is common within the Cambrian thrombolites examined and has caused a significant modification of the original fabric. Parts of the thrombolites, however, that were not bioturbated do not contain remnant laminae. We, therefore, interpret the thrombolitic fabric to be the primary result of calcification of microbes, rather than bioturbation.

Knoll et al. (1993) proposed a hypothesis for the expansion of calcified microbes near the Proterozoic-Cambrian boundary. Due to the evolution of skeletal organisms both the saturation level of seawater with respect to carbonate mineral precipitates and the significance of non-skeletal precipitation decreased. In the absence of competing carbonate crystals cyanobacterial sheaths served as important sites for carbonate nucleation (Knoll et al. 1993). The Upper Cambrian agglutinated stromatolites contain abundant trapped micrite-size carbonate particles, which may have served as competing sites for carbonate precipitation (Fig. 6.1). Under these conditions, syndepositional calcification of cyanobacteria was not an important process and even in the presence of fabric retentive dolomitization the preservation of sheaths is unlikely. Ancient calcified microbes commonly occur surrounded by sparry cement (Kennard and James 1986; Riding 1991b; Knoll et al. 1993). The thrombolites and digitate stromatolites from this study occur in association with coarser-grained wackestone/packstone and grainstone lithologies

(Figs. 2.1, 6.2B, F; Table 2.1). Even though micrite was present within the environment of deposition, the lesser amount of micritic particles in the more agitated lower intertidal to subtidal environments may have influenced the preferential calcification of thrombolites and digitate stromatolites relative to other microbial deposit types. Stratiform stromatolites, however, contain micritic laminae composed of both calcite and dolomite (Fig. 6.1B). Calcified laminae may represent mats with a more dense cyanobacterial population within which trapped micrite was less abundant (Fig. 6.1B). The calcification of these laminae may have occurred as an early diagenetic process in the presence of a suitable organic substrate. The cyanobacterial filaments were destroyed by taphonomic and/or diagenetic processes.

The studies of modern unlithified intertidal microbial mats composed of filamentous cyanobacteria show that these stromatolite precursors form primarily by the trapping of fine-grained sediment (Fig. 6.3A; Gebelein 1969; Davies 1970; Monty 1976; Bauld 1984). The alternation of calcitic and dolomitic laminae in Holocene stromatolites has been attributed to the compositional variations within the sediment (Gebelein and Hoffman 1973; Monty 1976). Similarly, alternation of organic-rich and organic-poor laminae may have been responsible for the presence of calcitic and dolomitic laminae within Cambrian stratiform stromatolites (Fig. 6.1B). The preferential calcification of some of the laminae may have also been environmentally controlled. Slight changes in water salinity, for example, may influence calcification of microbial mats (Défarge et al. 1994). Monty (1976) noted that on modern arid intertidal and supratidal flats microbial organisms generally form uncalcified mats, as opposed to tropical supratidal flats characterized by seasonal freshwater flooding, where calcification of cyanobacterial filaments is likely to occur during growth. The analogy with these modern examples supports an arid to semi-arid intertidal and supratidal settings for the entirely dolomitized Cambrian stromatolites.

Early lithification is one of the main prerequisites for the preservation of microbial deposits (Park 1977; Gerdes et al. 1991). Once preserved, microbial deposits are subject to later diagenetic alterations. The complex paragenetic diagrams constructed for the succession examined (Fig. 4.12) has led to questions about the extent of diagenetic overprinting. Even though calcified microbial deposits may be considered to have a greater potential for preserving syndepositional and/or early diagenetic features, the oxygen-isotope composition of these deposits is indicative of diagenetic modifications in the presence of meteoric water or at elevated temperature during later burial (Fig. 4.6A). The presence of partially silicified columnar and SH stromatolites, and the mosaic of medium- to coarse-crystalline dolomite comprising some of the columnar stromatolites, suggest diagenetic alteration of these deposits beyond penecontemporaneous dolomitization (Fig. 6.1H; see also Chapter 4).

It is likely that similar trends in selective dolomitization as those observed in this study could be present in other partially dolomitized carbonate successions containing a variety of microbial deposits. The approach used in this study should serve as a preliminary assessment of the origin of microbial deposits. The relative importance of processes influencing the formation of microbial deposits is expected to vary greatly, both spatially and temporally as a result of numerous factors, including evolutionary trends, and differing physical and geochemical characteristics of sedimentary settings. All available environmental indicators, such as morphologic characteristics, sedimentary structures and sediment composition, should be used in conjunction with diagenetic information to infer the mechanisms responsible for the formation and *preservation* of microbial deposits. A diagenetic study may reveal subtle details about the origin of microbial deposits that may not be available otherwise.

CONCLUSIONS

Detailed petrographic analysis of microbial carbonate deposits that have undergone differential degrees of dolomitization allows a better understanding of the mechanisms and environments of microbial deposit formation. The Upper Cambrian Maynardville Formation and Copper Ridge Dolomite of the southern Appalachians contain several different types of microbial carbonate deposits. Entirely dolomitized laminae within stratiform, LLH, SH, and columnar stromatolites formed primarily by the trapping of sediment in intertidal and supratidal environments. These arid to semi-arid tidal flat environments were primary sites for very early dolomitization. Digitate stromatolites and thrombolites, composed primarily of microcrystalline calcite, formed in an upper subtidal and lower intertidal environment by calcification of cyanobacteria. This early calcification reduced their susceptibility to dolomitization. Stratiform stromatolites, composed of both calcitic and dolomitic laminae, formed by the combination of sediment trapping and early calcification. The presence of a variety of microbial structures with differing modes of formation was primarily controlled by the conditions within the environment of deposition, but was also biotically influenced to a certain degree.

CHAPTER 7

CONCLUSIONS

1. Deposition of the Upper Cambrian Maynardville Formation of the southern Appalachians marks a prominent change in the pattern of Lower Paleozoic passive-margin sedimentation. This change is reflected in the cessation of the Middle to Upper Cambrian, predominantly subtidal, mixed siliciclastic/carbonate Grand Cycles of the Conasauga Group, and the establishment of peritidal carbonate deposition of the Upper Cambrian to Lower Ordovician Knox Group.
2. The Maynardville consists of a lower subtidal depositional package underlain by the Nolichucky Shale, and an upper peritidal package overlain by the Copper Ridge Dolomite. The upper Nolichucky represents mixed carbonate and siliciclastic deposition in a deep-ramp setting. The subtidal Maynardville was deposited in a gently sloping, shallow-subtidal ramp and lagoonal environment, which was protected by locally developed microbial patch reefs and ooid shoals. To the east, the ramp was linked to a broad, semi-arid carbonate tidal flat characterized by a variety of peritidal environments within which the upper Maynardville and the Copper Ridge Dolomite were deposited.
3. The Nolichucky Shale represents a retrogradational depositional package characteristic of transgressive system tracts, which formed in response to deepening caused by an increase in the rate of relative sea-level rise. The Nolichucky/Maynardville transition corresponds to a maximum flooding of the carbonate platform during the early Late Cambrian. The shallowing-upward trend (subtidal-to-peritidal carbonate deposition) of the Maynardville Formation reflects an aggradational-to-progradational stacking pattern characteristic of highstand system tracts, which form during decreasing rates of relative sea-level rise, a sea-level stillstand, and during an initial relative sea-level fall.

4. The Maynardville Formation and the underlying Upper Shale Member of the Nolichucky Formation comprise a third-order sequence, which represents a terminal Upper Cambrian Grand Cycle in the southern Appalachians. Unlike the Middle Cambrian Grand Cycles of the Conasauga Group, the deposition of the Maynardville was not terminated by carbonate platform exposure followed by drowning and basinal shale onlap. The transition into the overlying Copper Ridge Dolomite of the Knox Group is marked by a conformable interval, which is characterized by the occurrences of common siliciclastic sand. This interval is interpreted as a sequence boundary zone correlative with the Dresbachian/Franconian unconformity.

5. The changing style of passive-margin deposition during the Cambrian was a consequence of passive-margin evolution. The Middle Cambrian Grand Cycles of the Conasauga Group were deposited during an immature stage of passive-margin development. This time period was characterized by short-term, episodic, non-thermal tectonic subsidence, which was enhanced by loading, coupled with possible eustatic sea-level changes, and superimposed on thermal subsidence. Deposition of the Maynardville marked the transition into a mature or stabilized passive margin, as reflected by the cessation of tectonic activity, a decreased rate of thermal subsidence, infilling of the Conasauga basin, and carbonate platform progradation. Deposition of the thick peritidal carbonates of the overlying Knox Group represents the final stabilization of the passive margin with the sedimentation controlled primarily by thermal subsidence and possible eustatic sea-level changes.

6. The stacking patterns of the Maynardville lithofacies were influenced by numerous processes operating on various scales. Besides mechanisms related to passive-margin evolution, other local- to regional-scale processes that controlled the deposition of the Maynardville were related to: A) the properties intrinsic to the carbonate depositional system, including variable sedimentation rates, facies migration, and lag time; and B) the

extrinsic factors controlling the rate of sediment input, dispersal, and the infilling of the adjacent siliciclastic basin. The transition from the subtidal to peritidal depositional regime, subaerial exposure surfaces, and some meter-scale shallowing-upward successions within the Maynardville, may reflect short-term eustatic sea-level changes. Alternatively, they may represent the effects of platform aggradation and tidal flat migration.

7. The Maynardville Formation contains a record of a prominent change in diagenetic patterns. A transition from subtidal, mixed carbonate and siliciclastic deposits into extensively dolomitized peritidal deposits influenced early diagenesis of the Maynardville. Burial diagenesis of the Maynardville was affected by the regional facies distribution related to the cessation of Grand Cycle deposition, coupled with the infilling of the Conasauga basin and carbonate platform progradation, and burial history of the passive-margin sedimentary succession.

8. A variety of calcite cements (fibrous/bladed, syntaxial overgrowth, equant and ferroan equant calcite) within the subtidal deposits of the Maynardville represent marine, meteoric and burial diagenetic phases. These cements fill in intergranular voids, burrows, framework voids of thrombotic deposits, and less-common dissolution voids. Dolomite is not abundant within subtidal deposits. Ferroan dolomite occurs as a fine-crystalline phase associated with argillaceous layers, and coarser-crystalline replacement and saddle dolomite cement. The majority of the dolomite formed during burial from fluids provided locally by the diagenesis of clay minerals, compaction, and pressure solution. The association of saddle dolomite cement with MVT minerals suggests the involvement of externally-derived diagenetic fluids.

9. Peritidal deposits of the Maynardville are extensively dolomitized. Fine-crystalline, fabric-retentive replacement dolomite formed penecontemporaneously with, or soon after deposition on a semi-arid tidal flat. Fabric-destructive coarser-crystalline replacement dolomite formed during burial by the recrystallization of early dolomite and dolomitization

of limestone. Dolomite cement, commonly complexly zoned, fills in fenestrae, desiccation and evaporite dissolution voids, and sparse intergranular voids within the peritidal deposits. This zoned dolomite precipitated from modified marine fluids, mixed marine/meteoric, and deeper burial basinal brines. The saddle dolomite cement occluding pore-centers, tectonic fractures and dissolutional voids precipitated during later burial from fluids generated by the pressure-solution of matrix dolomite and from basinal brines related to MVT mineralization and hydrocarbon migration.

10. The combination of radiogenic strontium and stable oxygen isotope compositions provides insights into the source of fluids responsible for the precipitation of burial dolomite cement within the Upper Cambrian peritidal deposits. Strontium isotope compositions of dolomite cement are less radiogenic than Cambrian seawater, and are similar to Early to Middle Ordovician seawater. This suggests that a source of fluids may have been: A) Ordovician marine fluids that circulated downward into the Cambrian deposits; or B) marine pore fluids expelled from the Middle Ordovician Sevier basin shale succession during shallow to intermediate burial. Oxygen isotopic compositions of dolomite cement, on the other hand, indicate elevated burial temperatures ($> 80^{\circ}\text{C}$), and suggest the involvement of deep-burial fluids, which may represent waters of meteoric origin that interacted with Ordovician carbonate rocks.

11. The Maynardville Formation contains a record of a secular increase in the $^{13}\text{C}/^{12}\text{C}$ ratio in Late Cambrian sea water. The study of this carbon-isotope excursion provides a means for improving the biostratigraphic resolution of the poorly fossiliferous and extensively dolomitized Upper Cambrian interval in the southern Appalachians. Comparison with coeval carbon-isotope excursions documented in biostratigraphically well-characterized successions elsewhere indicates that the carbon-isotope excursion started near the base of the Pterocephaliid Biome, the Steptoean stage, and the *Aphelaspis* trilobite zone of the Late Cambrian (Dresbachian). The maximum excursion is

associated with the Sauk II/Sauk III unconformity. The excursion ended prior to the end of the Pterocephaliid Biomere. In the southern Appalachians the excursion started during the deposition of the upper Nolichucky Shale. The maximum $\delta^{13}\text{C}$ values of about 4 to 5‰ PDB are recorded within the sequence boundary zone containing the Maynardville/Copper Ridge Dolomite transition. The excursion ended during the deposition of the lower Copper Ridge Dolomite. The carbon-isotope stratigraphy supports the correlation between the Sauk II/Sauk III or Dresbachian/Franconian sea-level fall and the sequence boundary at the end of Grand Cycle deposition in the southern Appalachians.

12. The study of carbon isotope variations provides insights into the dynamics of the global cycling of carbon, including the changes in the rate of organic-carbon burial related to the changes in ocean stratification, climate, sea-level, and paleoproductivity rate. The positive carbon-isotope excursion reflects the enhanced burial of organic carbon promoted by ocean stratification, a warm, non-glacial climate, and a sea-level maximum during the early Late Cambrian. The onset of regression contributed to the maximum carbon-isotope excursion by increasing erosion and siliciclastic accumulation rates. Organic productivity could have been enhanced by the increase in nutrient availability. The removal of carbon from the ocean surface caused a decrease in pCO_2 of the atmosphere. The resulting cooling episode may have caused an oceanic overturn bringing bottom ^{12}C -enriched waters to the surface to end the carbon-isotope excursion. The regression also caused oxidation of ^{12}C -enriched organic matter previously stored in marginal sediments.

13. The comparison of $\delta^{13}\text{C}$ and $\delta^{18}\text{O}$ values of matrix samples and the associated cement phases provides insights into diagenetic environments and the extent of diagenetic modifications. The $\delta^{13}\text{C}$ values of peritidal dolomicrite plotted against stratigraphic position define a rather smooth curve, whereas the values for subtidal micrite have a significant scatter resulting from organic matter involvement in diagenesis. Fibrous/bladed calcite cement from the subtidal deposits has $\delta^{13}\text{C}$ and $\delta^{18}\text{O}$ values comparable to those

of the associated micrite, suggesting precipitation from marine water and similar diagenetic modifications. The involvement of meteoric water may be responsible for the ^{13}C - and ^{18}O -depletion in equant calcite cement relative to the associated micrite. The depletion of ^{18}O in saddle dolomite cement, and $\delta^{13}\text{C}$ values similar to those for the peritidal dolomicrite, are consistent with formation during burial at elevated temperatures in a rock-dominated system.

14. An array of selectively dolomitized Upper Cambrian microbial deposits represent different mechanisms of formation and styles of diagenetic preservation, which were controlled by the conditions within the environment of deposition, and were also biotically influenced. Entirely dolomitized laminae of stratiform, LLH, SH, and columnar stromatolites formed by the trapping of sediment in intertidal and supratidal environments on a semi-arid tidal flat. These environments were the loci of penecontemporaneous dolomitization of carbonate deposits. The susceptibility to dolomitization of digitate stromatolites and thrombolites was reduced by calcification of cyanobacteria in upper subtidal and lower intertidal environments.

REFERENCES CITED

- Ahr, W.M., 1971, Paleoenvironment, algal structures, and fossil algae in the Upper Cambrian of central Texas: *Journal of Sedimentary Petrology*, v. 41, p. 205-216.
- Aissaoui, D.M., 1988, Magnesian calcite cements and their diagenesis: dissolution and dolomitization, Mururoa Atoll: *Sedimentology*, v. 35, p. 821-841.
- Aitken, J.D., 1966, Middle Cambrian to Middle Ordovician cyclic sedimentation, southern Rocky Mountains of Alberta: *Canadian Petroleum Geology Bulletin*, v. 14, p. 405-441.
- Aitken, J.D., 1967, Classification and environmental significance of cryptalgal limestones and dolomites, with illustrations from the Cambrian and Ordovician of southwestern Alberta: *Journal of Sedimentary Petrology*, v. 37, p. 1163-1178.
- Aitken, J.D., 1978, Revised models for depositional grand cycles, Cambrian of the southern Rocky Mountains, Canada: *Canadian Petroleum Geology Bulletin*, v. 26, p. 515-542.
- Aitken, J.D., 1981, Generalizations about Grand Cycles, *in* Taylor, M.E., ed., *Short Papers for the Second International Symposium on the Cambrian System*: United States Geological Survey Open File Report 81-743, p. 8-14.
- Al-Hashimi, W.S., 1977, Recent carbonate cementation from seawater in some weathered dolostones, Northumberland, England: *Journal of Sedimentary Petrology*, v. 47, p. 1375-1391.
- Allan, J.R., and Matthews, R.K., 1982, Isotope signatures associated with early meteoric diagenesis: *Sedimentology*, v. 29, p. 797-817.
- Amthor, J.E., and Friedman, G.M., 1991, Dolomite-rock textures and porosity development in Ellenburger Group carbonates (Lower Ordovician), Western Texas and Southeastern New Mexico: *Sedimentology*, v. 38, p. 343-362.
- Amthor, J.E., and Friedman, G.M., 1992, Early- to late-diagenetic dolomitization of platform carbonates: Lower Ordovician Ellenburger Group, Permian Basin, West Texas: *Journal of Sedimentary Petrology*, v. 62, p. 131-144.
- Anderson, T.F., and Arthur, M.A., 1983, Stable isotopes of oxygen and carbon and their application to sedimentologic and paleoenvironmental problems, *in* Arthur, M.A., Anderson, T.F., Kaplan, I.R., Veizer, J., and Land, L.S., eds., *Stable Isotopes in Sedimentary Geology*, SEPM Short Course 10, p. 1-1 - 1-151.
- Angevine, C.L., 1989, Relationship of eustatic oscillations to regressions and transgressions on passive continental margins, *in* Price, R.A., ed., *The Origin and Evolution of Sedimentary Basins and their Energy and Mineral Resources*: American Geophysical Union, Geophysical Monograph Series 48, p. 29-35.
- Arthur, M.A., Dean, W.E., and Pratt, L.M., 1988, Geochemical and climatic effects of increased marine carbon burial at the Cenomanian/Turonian boundary: *Nature*, v. 335, p. 714-717.
- Arthur, M.A., Dean, W.E., and Schlanger, S.O., 1985, Variations in the global carbon cycle during the Cretaceous related to climate, volcanism, and changes in atmospheric CO₂: *Geophysical Monograph* 32, p. 504-529.
- Arthur, M.A., Schlanger, S.O., and Jenkyns, H.C., 1987, The Cenomanian-Turonian oceanic anoxic event, II. Palaeoceanographic controls on organic-matter

- production and preservation, in Brooks, J., and Fleet, A.J., eds., *Marine Petroleum Source Rocks: Geological Society Special Publication 26*, p. 401-420.
- Aubry, M.P., 1991, Sequence stratigraphy: Eustasy or tectonic imprint: *Journal of Geophysical Research*, v. 96, p. 6641-6679.
- Audet, D.M., and Fowler, A.C., 1992, A mathematical model for compaction in sedimentary basins: *Geophysical Journal International*, v. 110, p. 577-590.
- Awramik, S.M., 1984, Ancient stromatolites and microbial mats, *in* COHEN, Y., Castenholtz, R.W., and Halvorsen, H.O., eds., *Microbial Mats: Stromatolites: MBL Lectures in Biology*, Alan R. Liss, New York, p. 1-22.
- Baker, P.A., and Kastner, M., 1981, Constraints on the formation of sedimentary dolomite: *Science*, v. 213, p. 214-216.
- Baker, P.A., and Burns, S.J., 1985, Occurrence and formation of dolomite in organic-rich continental margin sediments: *American Association of Petroleum Geologists Bulletin*, v. 40, p. 721-730.
- Bally, A.W., 1982, Musings over sedimentary basin evolution: *Philosophical Transactions of the Royal Society of London*, v. 305, p. 325-338.
- Banner, J.L., 1995, Application of the trace element and isotope geochemistry of strontium to studies of carbonate diagenesis: *Sedimentology*, v. 42, p. 805-824.
- Banner, J.L., and Hanson, G.N., 1990, Calculation of simultaneous isotopic and trace element variations during water-rock interaction with applications to carbonate diagenesis: *Geochimica and Cosmochimica Acta*, v. 54, p. 3123-3127.
- Banner, J.L., Hanson, G.N., and Meyers, W.J., 1988, Water-rock interaction history of regionally extensive dolomites of the Burlington-Keokuk Formation (Mississippian): Isotopic evidence, *in* Shukla, V., and Baker, P.B., eds., *Sedimentology and Geochemistry of Dolostones: SEPM Special Publication 43*, p. 97-113.
- Banner, J.L., Musgrove, M., and Capo, R., 1994, Tracing ground-water evolution in a limestone aquifer using Sr isotopes: effects of multiple sources of dissolved ions and mineral-solution reactions: *Geology*, v. 22, p. 687-690.
- Barnaby, R.J., and Read, J.F., 1990, Carbonate ramp to rimmed shelf evolution: Lower to Middle Cambrian continental margin, Virginia Appalachians: *Geological Society of America Bulletin*, v. 102, p. 391-404.
- Barnaby, R.J., and Read, J.F., 1992, Dolomitization of a carbonate platform during late burial: Lower to Middle Cambrian Shady Dolomite, Virginia Appalachians: *Journal of Sedimentary Petrology*, v. 62, p. 1023-1043.
- Bathurst, R.G.C., 1987, Diagenetically enhanced bedding in argillaceous platform limestones: stratified cementation and selective compaction: *Sedimentology*, v. 34, p. 749-778.
- Bauld, J., 1984, Microbial mats in marginal marine environments: Spencer Gulf, South Australia, and Shark Bay, Western Australia, *in* Cohen, Y., Castenholtz, R.W., and Halvorsen, H.O., eds., *Microbial Mats: Stromatolites: MBL Lectures in Biology*, Alan R. Liss, New York, p. 39-58.
- Beauchamp, B., Oldershaw, A.E., and Krouse, H.R., 1987, Upper Carboniferous to Upper Permian ^{13}C -enriched primary carbonates in the Sverdrup Basin, Canadian Arctic:

- Comparison to coeval western North American ocean margins: *Chemical Geology, Isotope Geoscience Section*, v. 65, p. 391-413.
- Beaumont, C., Keen, C.E., and Boutilier, R., 1982, Evolution of rifted continental margins: Comparison of models and observations for the Nova Scotian margin: *Royal Astronomical Society Geophysical Journal*, v. 70, p. 667-715.
- Beeunas, M.A., and Knauth, L.P., 1985, Preserved stable isotope signatures of subaerial diagenesis in the 1.2 Ga Mescal Limestone, central Arizona: Implications for the timing and development of a terrestrial plant cover: *Geological Society of America Bulletin*, v. 96, p. 737-745.
- Behrens, E.W., and Land, L.S., 1972, Subtidal Holocene dolomite, Baffin Bay, Texas: *Journal of Sedimentary Petrology*, v. 42, p. 155-161.
- Bein, A., and Land, L.S., 1983, Carbonate sedimentation and diagenesis associated with Mg-Ca-chloride brines: the Permian San Andres Formation in the Texas Panhandle: *Journal of Sedimentary Petrology*, v. 53, p. 243-260.
- Benedict, G.L., and Walker, K.R., 1978, Paleobathymetric analysis in Paleozoic sequences and its geodynamic significance: *American Journal of Science*, v. 278, p. 579-607.
- Berger, W.H., and Vincent, E., 1986, Deep-sea carbonates: Reading the carbon-isotope signal: *Geologische Rundschau*, v. 75, p. 249-269.
- Berner, R.A., 1984, Sedimentary pyrite formation: An update: *Geochimica et Cosmochimica Acta*, v. 48, p. 605-615.
- Bethke, C.M., 1985, A numerical model of compaction-driven groundwater flow and heat transfer and its application to the paleohydrology of intracratonic sedimentary basins: *Journal of Geophysical Research*, v. 90, p. 6817-6828.
- Bethke, C.M., and Marshak, S., 1990, Brine migrations across North America—the plate tectonics of groundwater: *Annual Review of Earth and Planetary Sciences*, v. 18, p. 287-315.
- Beukes, N.J., and Lowe, D.R., 1989, Environmental control on diverse stromatolite morphologies in the 3000 Myr Pongola Supergroup, South Africa: *Sedimentology*, v. 36, p. 383-397.
- Bird, J.M., and Dewey, J.F., 1970, Lithosphere plate-continental margin tectonics and the evolution of the Appalachian Orogen: *Geological Society of America Bulletin*, v. 81, p. 1031-1060.
- Boggs, S., Jr., 1987, *Principles of Sedimentology and Stratigraphy*: Merril Publishing Company, Columbus, Ohio, 784 p.
- Boles, J.R., and Franks, S.G., 1979, Clay diagenesis in Wilcox sandstones of Southwest Texas: implications of smectite diagenesis on sandstone cementation: *Journal of Sedimentary Petrology*, v. 49, p. 55-70.
- Bond, G.C., and Kominz, M.A., 1984, Construction of tectonic subsidence curves for the early Paleozoic miogeocline, southern Canadian Rocky Mountains: Implications for subsidence mechanisms, age of breakup and crustal thinning: *Geological Society of America Bulletin*, v. 95, p. 155-173.
- Bond, G.C., Kominz, M.A., and Beavan, J., 1991, Evidence for orbital forcing of Middle Cambrian peritidal cycles—Wah Wah range, south central Utah, *in* Franseen, E.K., Watney, W.L., Kendall, C.G.St.C., and Ross, W., eds, *Sedimentary Modeling—*

- Computer Simulations and Methods for Improved Parameter Definition: Kansas Geological Survey Bulletin 233, p. 239-318.
- Bond, G.C., Nickeson, P.A., and Kominz, M.A., 1984, Breakup of a supercontinent between 625 Ma and 555 Ma: New evidence and implications for continental histories: *Earth and Planetary Science Letters*, v. 70, p. 325-345.
- Bond, G.C., Kominz, G.C., and Grotzinger, J.P., 1988, Cambro-Ordovician eustasy: evidence from geophysical modeling of subsidence in Cordilleran and Appalachian passive margins, *in* Kleinspehn, K.L., ed., *New Perspectives in Basin Analysis*: Springer-Verlag, New York, p. 125-160.
- Bond, G.C., Kominz, M.A., Steckler, M.S., and Grotzinger, J.P., 1989, Role of thermal subsidence, flexure, and eustasy in the evolution of early Paleozoic passive-margin carbonate platforms, *in* Crevello, P., Wilson, J.L., Sarg, J.F., and Read, J.F., eds., *Controls on Carbonate Platform and Basin Development: SEPM Special Publication 44*, p. 39-61.
- Bott, M.H.P., 1992, Passive margins and their subsidence: *Journal of the Geological Society*, London, v. 149, p. 805-812.
- Botz, R.W., and von der Borch, C.C., 1984, Stable isotope study of carbonate sediments from the Coorong area, South Australia: *Sedimentology*, v. 31, p. 837-849.
- Braithwaite, C.J.R., Casanova, J., Frevert, T., and Whitton, B.A., 1989, Recent stromatolites in landlocked pools on Aldabra, western Indian Ocean: *Palaeogeography, Palaeoclimatology, and Palaeoecology*, v. 69, p. 145-165.
- Brand, U., and Veizer, J., 1980, Chemical diagenesis of a multicomponent carbonate system - 1: Trace elements: *Journal of Sedimentary Petrology*, v. 50, p. 1219-1236.
- Brasier, M.D., 1990, Nutrients in the early Cambrian. *Nature*, v. 347, p. 521-522.
- Brasier, M.D., 1992, Nutrient-enriched waters and the early skeletal fossil record: *Journal of the Geological Society of London*, v. 149, p. 621-629.
- Brasier, M.D., 1993, Towards a carbon isotope stratigraphy of the Cambrian system: potential of the Great Basin succession, *in* Hailwood, E.A., and Kidd, R.B., eds., *High Resolution Stratigraphy: Geological Society Special Publication 70*, p. 341-359.
- Brasier, M.D., Anderson, M.M., and Corfield, R.M., 1992, Oxygen and carbon isotope stratigraphy of early Cambrian carbonates in southeastern Newfoundland and England: *Geological Magazine*, v. 3, p. 265-279.
- Brasier, M.D., Corfield, R.M., Derry, L.A., Rozanov, A.Yu., and Zhuravlev, A.Yu., 1994, Multiple $\delta^{13}\text{C}$ excursions spanning the Cambrian explosion to the Botomian crisis in Siberia: *Geology*, v. 22, p. 455-458.
- Brasier, M.D., Khomentovsky, V.V., and Corfield, R.M., 1993, Stable isotopic calibration of the earliest skeletal fossil assemblages in eastern Siberia (Precambrian-Cambrian boundary: *Terra Nova*, v. 5, p. 225-232.
- Bridge, J., 1956, Stratigraphy of the Mascot-Jefferson City Zinc District, Tennessee: U.S. Geological Survey Professional Paper 277, 74 p.

- Budd, D.A., 1988, Aragonite-to-calcite transformation during freshwater diagenesis of carbonates: insights from pore-water chemistry: *Geological Society of America Bulletin*, v. 100, p. 1260-1270.
- Budd, D.A., and Harris, P.M., eds., 1990, Carbonate-Siliciclastic Mixtures: SEPM Reprint Series 14, 272 p.
- Budd, D.A., and Hiatt, E.E., 1993, Mineralogical stabilization of high-magnesium calcite: geochemical evidence for intracrystal recrystallization within Holocene porcellaneous foraminifera: *Journal of Sedimentary Petrology*, v. 63, p. 261-274.
- Budd, D.A., and Land, L.S., 1990, Geochemical imprint of meteoric diagenesis in Holocene ooid sands, Schooner Cays, Bahamas: correlation of calcite cement geochemistry with extant groundwaters: *Journal of Sedimentary Petrology*, v. 60, p. 361-378.
- Buelter, D.P., and Guillemette, R.N., 1988, Geochemistry of epigenetic dolomite associated with lead-zinc mineralization of the Viburnum Trend, southeast Missouri: A reconnaissance study, *in* Shukla, V., and Baker, P.B., eds., *Sedimentology and Geochemistry of Dolostones*: SEPM Special Publication 43, p. 85-93.
- Burke, W.H., Denison, R.E., Hetherington, E.A., Koepnick, R.B., Nelson, H.F., and Otto, J.B., 1982, Variation of seawater $^{87}\text{Sr}/^{86}\text{Sr}$ throughout Phanerozoic time: *Geology*, v. 10, p. 516-519.
- Burne, R.V., and Moore, L.S., 1987, Microbialites: organosedimentary deposits of benthic microbial communities: *PALAIOS*, v. 2, p. 241-254.
- Burton, E.A., and Walter, L.M., 1987, Relative precipitation rates of aragonite and Mg calcite from seawater: Temperature or carbonate ion control: *Geology*, v. 15, p. 111-114.
- Burton, E.A., and Walter, L.M., 1991, The effects of P_{CO_2} and temperature on magnesium incorporation in calcite in seawater and $\text{MgCl}_2\text{-CaCl}_2$ solutions: *Geochimica et Cosmochimica Acta*, v. 55, p. 777-785.
- Cander, H.S., 1994, An example of mixing-zone dolomite, Middle Eocene Avon Park Formation, Floridan Aquifer System: *Journal of Sedimentary Research*, v. A64, p. 615-629.
- Cander, H.D., Kaufman, J., Daniels, L.D., and Meyers, W.J., 1988, Regional dolomitization of shelf carbonates in the Burlington-Keokuk Formation (Mississippian), Illinois and Missouri: Constraints from cathodoluminescent zonal stratigraphy, *in* Shukla, V., and Baker, P.B., eds., *Sedimentology and Geochemistry of Dolostones*: SEPM Special Publication 43, p. 129-144.
- Calder, J.A., and Parker, P.L., 1973, Geochemical implications of induced changes in C^{13} fractionation by blue-green algae: *Geochimica et Cosmochimica Acta*, v. 37, p. 133-140.
- Calvert, S.E., Bustin, R.P., and Ingall, E.D., 1996, Influence of water column anoxia and sediment supply on the burial and preservation of organic carbon in marine shales: *Geochimica et Cosmochimica Acta*, v. 60, p. 1577-1593.

- Carballo, J.D., Land, L.S., and Miser, D.E., 1987, Holocene dolomitization of supratidal sediments by active tidal pumping, Sugarloaf Key, Florida: *Journal of Sedimentary Petrology*, v. 57, p. 153-165.
- Carpenter, S.J., and Lohmann, K.C., 1992, Sr/Mg ratios of modern marine calcite: empirical indicators of ocean chemistry and precipitation rate: *Geochimica et Cosmochimica Acta*, v. 56, p. 1837-1849.
- Carpenter, S.J., Lohmann, K.C., Holden, P., Walter, L.M., Huston, T.J., and Halliday, A.N., 1991, $\delta^{18}\text{O}$ values, $^{87}\text{Sr}/^{86}\text{Sr}$ and Sr/Mg ratios of Late Devonian abiotic marine calcite: Implications for the composition of ancient seawater: *Geochimica et Cosmochimica Acta*, v. 55, p. 1991-2010.
- Cartwright, J.A., 1994, Episodic basin-wide fluid expulsion from geopressed shale sequences in the North Sea basin: *Geology*, v. 22, p. 447-450.
- Cathles, L.M., and Smith, A.T., 1983, Thermal constraints on the formation of Mississippi Valley-type lead-zinc deposits and their implications for episodic basin dewatering and deposit genesis: *Economic Geology*, v. 78, p. 983-1002.
- Chafetz, H.S., 1973, Morphological evolution of Cambrian algal mounds in response to a change in depositional environment: *Journal of Sedimentary Petrology*, v. 43, p. 435-446.
- Chafetz, H.S., and Buczynski, C., 1992, Bacterially induced lithification of microbial mats: *PALAIOS*, v. 7, p. 277-293.
- Chafetz, H.S., and Rush, P.F., 1994, Diagenetically altered sabkha-type Pleistocene dolomite from the Arabian Gulf: *Sedimentology*, v. 41, p. 409-421.
- Charles, C.D., Wright, J.D., and Faribanks, R.G., 1993, Thermodynamic influences on the marine carbon isotope record: *Paleoceanography*, v. 8, p. 691-697.
- Chaudhuri, S., Broedel, V., and Clauer, N., 1987, Strontium isotopic evolution of oil-field waters from carbonate reservoir rocks in Bindley field, central Kansas, USA: *Geochimica et Cosmochimica Acta*, v. 51, p. 45-53.
- Chaudhuri, S., and Clauer, N., 1992, Signatures of radiogenic isotopes in deep subsurface waters in continents, *in* Clauer, N., and Chaudhuri, S., eds., *Isotopic Signatures and Sedimentary Records*: Springer-Verlag, New York, p. 497-529.
- Choquette, P.W., and James, N.P., 1987, Diagenesis in limestones - 3. The deep burial environment: *Geoscience Canada*, v. 14, p. 3-35.
- Choquette, P.W., and Steinen, R.P., 1980, Mississippian non-supratidal dolomite, Ste. Genevieve limestone, Illinois basin: evidence for mixed-water dolomitization, *in* Zenger, D.H., Dunham, J.B., and Ethington, R.L., eds., *Concepts and Models of Dolomitization*: SEPM Special Publication, 28, p. 163-196.
- Chow, N., and James, N.P., 1987, Cambrian Grand Cycles: A northern Appalachian perspective: *Geological Society of America Bulletin*, v. 98, p. 418-429.
- Chow, N., and James, N.P., 1992, Synsedimentary diagenesis of Cambrian peritidal carbonates: evidence from hardgrounds and surface paleokarst in the Port au Port Group, western Newfoundland: *Bulletin of Canadian Petroleum Geology*, v. 40, p. 115-127.
- Christie-Blick, N., and Driscoll, N.W., 1995, Sequence stratigraphy: *Annual Reviews in Earth and Planetary Science*, v. 23, p. 451-478.

- Claypool, G.E., and Kaplan, I.R., 1974, The origin and distribution of methane in marine sediments, in Kaplan, I.R., ed., *Natural Gases in Marine Sediments*: New York, Plenum Press, p. 99-140.
- Cloetingh, S., 1986, Intraplate stresses: A new tectonic mechanism for fluctuations of relative sea level: *Geology*, v. 14, p. 617-621.
- Cloetingh, S., 1988, Intraplate stresses: A tectonic cause for third-order cycles in apparent sea level, in Wilgus, C.K., Hastings, B.S., Kendall, C.G.St.C., Posamentier, H.W., Ross, C.A., and Van Wagoner, J.C., eds., *Sea-Level Changes: An Integrated Approach*: SEPM Special Publication 42, p. 19-29.
- Cloetingh, S., 1991, Tectonics and sea-level changes: a controversy?, in Mueller, D.W., McKenzie, J.A., and Weissert, H., eds., *Controversies in Modern Geology*: Academic Press, p. 249-277.
- Cloetingh, S., McQueen, H., and Lambeck, K., 1985, On a tectonic mechanism for regional sealevel variations: *Earth and Planetary Sciences Letters*, v. 75, p. 157-166.
- Coleman, M.L., and Raiswell, R., 1981, Carbon, oxygen and sulphur isotope variations in concretions from the Upper Lias of N.E. England: *Geochimica et Cosmochimica Acta*, v. 45, p. 329-340.
- Compton, J.S., 1988a, Degree of supersaturation and precipitation of organogenic dolomite: *Geology*, v. 16, p. 318-321.
- Compton, J.S., 1988b, Sediment composition and precipitation of dolomite and pyrite in the Neogene Monterey and Sisquoc Formations, Santa Maria Basin area, California, in Shukla, V., and Baker, P.B., eds., *Sedimentology and Geochemistry of Dolostones*: SEPM Special Publication 43, p. 53-64.
- Coniglio, M., Sherlock, R., Williams-Jones, A.E., Middleton, K., and Frape, S.K., 1994, Burial and hydrothermal diagenesis of Ordovician carbonates from the Michigan Basin, Ontario, Canada, in Purser, B., Tucker, M., and Zenger, D., eds., *Dolomites: A Volume in Honour of Dolomieu*: International Association of Sedimentologists, Special Publication 21, p. 231-254.
- Cowan, C.A., and James, N.P., 1993, The interactions of sea-level change, terrigenous-sediment influx, and carbonate productivity as controls on Upper Cambrian Grand Cycles of western Newfoundland, Canada: *Geological Society of America Bulletin*, v. 105, p. 1576-1590.
- Craig, H., 1965, The measurements of oxygen isotope paleotemperatures, in Tongiorgi, E., ed., *Stable Isotopes in Oceanographic Studies and Paleotemperatures*: Consiglio Nazionale delle Ricerche, Laboratorio di Geologia Nucleare, Pisa, p. 1-24.
- Curtis, C.D., 1987, Mineralogical consequences of organic matter degradation in sediments: inorganic/organic diagenesis, in Legget, J.K., and Zuffa, G.G., eds., *Marine Clastic Sedimentology*: Graham and Trotman, London, p. 108-123.
- Dalrymple, R.W., Narbonne, G.M., and Smith, L., 1985, Eolian action and the distribution of shales in North America: *Geology*, v. 13, p. 607-610.
- Davies, G.R., 1970, Algal laminated sediments, Gladstone Embayment, Shark Bay, Western Australia, in Logan, B.W., ed., *Carbonate Sediments and Environments*,

- Shark Bay, Western Australia: American Association of Petroleum Geologists Memoir 13, p.169-205.
- Dawans, J.M., and Swart P.K., 1988, Textural and geochemical alteration in late Cenozoic Bahamian dolomites: *Sedimentology*, v. 35, p. 385-403.
- Défarge, C., Trichet, J., and Couté, A., 1994, On the appearance of cyanobacterial calcification in modern stromatolites: *Sedimentary Geology*, v. 94, p. 11-19.
- Demicco, R.V., 1983, Wavy and lenticular-bedded carbonate ribbon rocks of the Upper Cambrian Conococheague Limestone, central Appalachians: *Journal of Sedimentary Petrology*, v. 53, p. 1121-1132.
- Demicco, R.V., 1985, Platform and off-platform carbonates of the Upper Cambrian of western Maryland, U.S.A.: *Sedimentology*, v. 32, p. 1-22.
- Demicco, R.V., Hardie, L.A., and Haley, J.S., 1982, Algal mounds of Upper Cambrian carbonates of Appalachians, western Maryland: Examples of early patch and marginal reefs: American Association of Petroleum Geologists Bulletin Abstracts, v. 66, p. 563.
- Deming, D., 1992, Catastrophic release of heat and fluid flow in the continental crust: *Geology*, v. 20, p. 83-86.
- Derby, J.R., 1965, Paleontology and stratigraphy of the Nolichucky Formation in southeast Virginia and northeast Tennessee [unpublished Ph.D. thesis]: Virginia Polytechnic Institute and State University, Blacksburg, 465 p.
- Derry, L.A., Brasier, M.D., Corfield, R.M., Rozanov, A. Yu., and Zhuravlev, A. Yu., 1994, Sr and C isotopes in Lower Cambrian carbonates from the Siberian craton: A peleoenviromental record during the 'Cambrian explosion': *Earth and Planetary Science Letters*, v. 128, p. 671-681.
- Derry, L.A., Kaufman, A.J., and Jacobsen, S.B., 1992, Sedimentary cycling and environmental change in the Late Proterozoic: Evidence from stable and radiogenic isotopes: *Geochimica et Cosmochimica Acta*, v. 56, p. 1317-1329.
- DesMarais, D.J., Cohen, Y., Nguyen, H., Cheatham, T., and Munoz, E., 1989, Carbon isotopic trends in the hypersaline ponds and microbial mats at Guerrero Negro, Baja California Sur, Mexico: Implications for Precambrian stromatolites, *in* Cohen, Y., and Rosenberg, E., eds., *Microbial Mats, Physiological Ecology of Benthic Microbial Communities*: American Society for Microbiology, p. 191-203.
- Dever, G.R., 1986, Mississippian reactivation along the Irvine-Paint Creek fault system in the Rome trough, east-central Kentucky: *Southeastern Geology*, v. 27, p. 95-105.
- Dickson, J.A.D., 1965, A modified staining technique for carbonates in thin section: *Nature*, v. 205, p. 587.
- Dickson, J.A.D., 1966, Carbonate identification and genesis as revealed by staining: *Journal of Sedimentary Petrology*, v. 36, p. 491-505.
- Dickson, J.A.D., and Coleman, M.L., 1980, Changes in carbon and oxygen isotope composition during limestone diagenesis: *Sedimentology*, v. 27, p. 107-118.
- Dill, R.F., Shinn, E.A., Jones, A.T., Kelly, K., and Steinen, R.P., 1986, Giant subtidal stromatolites forming in normal salinity waters: *Nature*, v. 324, p. 55-58.
- Doyle, L.J., and Roberts, H.H., eds., 1988, *Carbonate-Clastic Transitions: Developments in Sedimentology* 42, Elsevier, Amsterdam, 304 p.

- Dravis, J.J., 1983, Hardened subtidal stromatolites, Bahamas: *Science*, v. 219, p. 385-386.
- Dromgoole, E.L., and Walter, L.W., 1990, Iron and Manganese incorporation into calcite: Effects of growth kinetics, temperature and solution chemistry: *Chemical Geology*, v. 81, p. 311-336.
- Druckman, Y., and Moore, C.H., 1985, Late subsurface secondary porosity in a Jurassic grainstone reservoir, Smackover Formation, Mt. Vernon field, southern Arkansas: *in* Roehl, P.O., and Choquette, P.W., eds., *Carbonate petroleum reservoirs*: Springer Verlag, New York, p. 369-384.
- Drummond, C.N., and Wilkinson, B.H., 1993, Aperiodic accumulation of cyclic peritidal carbonate: *Geology*, v. 21, p. 1023-1026.
- Edhorn, A.S., and Anderson, M.M., 1977, Algal remains in the Lower Cambrian Bonavista Formation, Conception Bay, Southeastern Newfoundland, *in* Flügel, E., ed., *Fossil Algae - recent Results and Development*: Springer-Verlag, Berlin, p. 113-123.
- Edwards, J.D., and Santogross, P.A., eds., 1990, *Divergent/Passive Margin Basins*: American Association of Petroleum Geologists Memoir 48, 252 p.
- Elliot, W.C., and Aronson, J.L., 1987, Alleghenian episode of K-bentonite illitization in the southern Appalachian basin: *Geology*, v. 15, p. 735-739.
- Embry, A.F., 1989, A tectonic origin for third-order depositional sequences in extensional basins - Implications for basin modeling, *in* Cross, T.A., ed., *Quantitative Dynamic Stratigraphy*: Prentice Hall, New York, p. 491-501.
- Emrich, K., Ehhalt, D.H., and Vogel, J.C., 1970, Carbon isotope fractionation during the precipitation of calcium carbonate: *Earth and Planetary Science Letters*, v. 8, p. 363-371.
- Epstein, S., Graf, D.L., and Degens, E.T., 1963, Oxygen isotope studies on the origin of dolomites, *in* Craig, H., Miller, S.L., and Wasserburg, G.J., eds., *Isotopic and Cosmic Chemistry*: North-Holland Publishing Company, Amsterdam, p. 169-180.
- Fairchild, I.J., Marshall, J.D., and Bertrand-Sarfati, J., 1990, Stratigraphic shifts in carbon isotopes from Proterozoic stromatolitic carbonates (Mauritania): Influences of primary mineralogy and diagenesis: *American Journal of Science*, v. 290-A, p. 46-79.
- Farr, M.R., 1992, Geochemical variation of dolomite cement within the Cambrian Bonnetterre Formation, Missouri: evidence for fluid mixing: *Journal of Sedimentary Petrology*, v. 62, p. 636-651.
- Ferrill, B.A., 1989, Middle Cambrian to Lower Mississippian synsedimentary structures in the Appalachian fold-thrust belt in Alabama and Georgia [unpublished Ph.D. thesis]: The University of Alabama, Tuscaloosa, 268 p.
- Finlayson, C.P., Vest, W.C., Henderson, A.R., and McReynolds, J.L., Jr., 1965, Geologic map of the Powder Springs quadrangle, Tennessee: Tennessee Division of Geology, Geologic Map GM-154-SW.
- Fischer, A.G., 1964, The Lofer cyclothems of the Alpine Triassic, *in* Merriam, D.F., ed., *Symposium on Cyclic Sedimentation*: State Geological Survey of Kansas, Bulletin 169, p. 107-149.

- Fisher, H.J., 1988, Dolomite diagenesis in the Metaline Formation, northeastern Washington State, *in* Shukla, V., and Baker, P.B., eds., *Sedimentology and Geochemistry of Dolostones: SEPM Special Publication 43*, p. 209-219.
- Folk, R.L., and Land, L.S., 1975, Mg/Ca ratio and salinity, two controls over crystallization of dolomite: *American Association of Petroleum Geologists Bulletin*, v. 59, p. 60-68.
- Föllmi, K.B., Weissert, H., Bispin, M., and Funk, H., 1994, Phosphogenesis, carbon-isotope stratigraphy, and carbonate-platform evolution along the Lower Cretaceous northern Tethyan margin: *Geological Society of America Bulletin*, v. 106, p. 729-746.
- Foreman, J.L., 1991, Petrologic and geochemical evidence for water-rock interaction in the mixed carbonate-siliciclastic Nolichucky Shale (Upper Cambrian) in east Tennessee [unpublished Ph.D. thesis]: The University of Tennessee, Knoxville, 228 p.
- Foreman, J.L., Walker, K.R., Weber, L.J., Driese, S.G., and Dreier, R.B., 1991, Slope and basinal carbonate deposition on the Nolichucky Shale (Upper Cambrian), east Tennessee: Effect of carbonate suppression by siliciclastic deposition on basin-margin morphology, *in* Lomando, A.J., and Harris, P.M., eds., *Mixed Carbonate-Siliciclastic Sequences: SEPM Core Workshop 15*, p. 511-539.
- Frank, T.D., and Lohmann, K.C., 1995, Early cementation during marine-meteoric fluid mixing: Mississippian Lake Valley Formation, New Mexico: *Journal of Sedimentary Research*, v. A65, p. 263-273.
- Frank, T.D., and Lohmann, K.C., 1996, Diagenesis of fibrous magnesian calcite marine cement: Implications for the interpretation of $\delta^{18}\text{O}$ and $\delta^{13}\text{C}$ values of ancient equivalents: *Geochimica et Cosmochimica Acta*, v. 60, p. 2427-2436.
- Frank, T.D., Lohmann, K.C., and Meyers, W.J., 1995, Chronostratigraphic significance of cathodoluminescence zoning in syntaxial cement: Mississippian Lake Valley Formation, New Mexico: *Sedimentary Geology*, v. 105, p. 29-50.
- Franklyn, M.T., McNutt, R.H., Kamineni, D.C., Gascoyne, M., and Frape, S.K., 1991, Groundwater $^{87}\text{Sr}/^{86}\text{Sr}$ values in the Eye-Dashwa Lakes Pluton: evidence for plagioclase-water reaction: *Chemical Geology, Isotope Geoscience Section*, v. 86, p. 111-122.
- Freeman-Lynde, R.P., Whitley, K.F., and Lohmann, K.C., 1986, Deep marine origin of equant spar cements in Bahama escarpment limestones: *Journal of Sedimentary Petrology*, v. 56, p. 799-811.
- Friedman, I., and O'Neil, J.R., 1977, Compilation of stable isotope fractionation factors of geochemical interest: United States Geological Survey Professional Paper 440-KK, p. 1-12.
- Frostick, L.E., and Steel, R.J., 1993a, Sedimentation in divergent plate-margin basins, *in* Frostick, L.E., and Steel, R.J., eds., *Tectonic Controls in Sedimentary Successions: International Association of Sedimentologists Special Publication 20*, p. 111-128.
- Frostick, L.E., and Steel, R.J., 1993b, Tectonic signatures in sedimentary basin fills: an overview, *in* Frostick, L.E., and Steel, R.J., eds., *Tectonic Controls in Sedimentary*

- Successions: International Association of Sedimentologists Special Publication 20, p. 1-9.
- Gale, A.S., Jenkyns, H.C., Kennedy, W.J., and Corfield, R.M., 1993, Chemostratigraphy versus biostratigraphy: data from around the Cenomanian-Turonian boundary: *Journal of the Geological Society, London*, v. 150, p. 29-32.
- Gao, G., 1990, Geochemical and isotopic constraints on the diagenetic history of a massive stratal, late Cambrian (Royer) dolomite, Lower Arbuckle Group, Slick Hills, SW Oklahoma, U.S.A.: *Geochimica and Cosmochimica Acta*, v. 54, p. 1979-1989.
- Gao, G., and Land, L.S., 1991a, Early Ordovician Cool Creek Dolomite, Middle Arbuckle Group, Slick Hills, SW Oklahoma, USA: Origin and modification: *Journal of Sedimentary Petrology*, v. 61, p. 161-173.
- Gao, G., and Land, L.S., 1991b, Geochemistry of Cambro-Ordovician Arbuckle limestone, Oklahoma: Implications for diagenetic $\delta^{18}\text{O}$ alteration and secular $\delta^{13}\text{C}$ and $^{87}\text{Sr}/^{86}\text{Sr}$ variation: *Geochimica et Cosmochimica Acta*, v. 55, p. 2911-2920.
- Gao, G., Land, L.S., and Folk, R.L., 1992, Meteoric modification of early dolomite and late dolomitization by basinal fluids, Upper Arbuckle Group, Slick Hills, southwestern Oklahoma: *American Association of Petroleum Geologists Bulletin*, v. 76, p. 1649-1664.
- Garven, G., and Freeze, R.A., 1984, Theoretical analysis of the role of groundwater flow in the genesis of stratabound ore deposits: 1. Mathematical and numerical model: *American Journal of Science*, v. 284, p. 1085-1124.
- Gautier, D.L., and Claypool, G.E., 1984, Interpretation of methanogenic diagenesis in ancient sediments by analogy with processes in modern diagenetic environments, *in* McDonald, D.A., and Surdam, R.C., eds., *Clastic Diagenesis*: American Association of Petroleum Geologists Memoir 37, p. 111-123.
- Gebelein, C.D., 1969, Distribution, morphology, and accretion rate of Recent subtidal algal stromatolites, Bermuda: *Journal of Sedimentary Petrology*, v. 39, p. 49-69.
- Gebelein, C.D., 1974, Biologic control of stromatolite microstructure: implications for Precambrian time stratigraphy: *American Journal of Science*, v. 274, p. 575-598.
- Gebelein, C.D., 1976, The effects of physical, chemical, and biological evolution of the earth, *in* Walter, M.R., ed., *Stromatolites: Developments in Sedimentology*, Elsevier, v. 20, p. 499-515.
- Gebelein, C.D., and Hoffman, P., 1973, Algal origin of dolomite laminations in stromatolitic limestone: *Journal of Sedimentary Petrology*, v. 43, p. 603-613.
- Geldsetzer, H.H.J., James, N.P., and Tebbutt, G.E., 1989, Reefs, Canada and Adjacent Areas: Canadian Society of Petroleum Geologists Memoir No. 13, 775 p.
- Gerdes, G., and Krumbein, W.E., 1987, Biolaminated Deposits: Lecture Notes in Earth Sciences 9, Springer-Verlag, Berlin, 183 p.
- Gerdes, G., Krumbein, W.E., and Reineck, H.E., 1991, Biolaminations - ecological versus depositional dynamics, *in* Einsele, G., Ricken, W., and Seilacher, A., eds., *Cycles and Events in Stratigraphy*: Springer-Verlag, Berlin, p. 592-607.
- Gill, I.P., Moore, C.H. Jr., and Aharon, P., 1995, Evaporitic mixed-water dolomitization on St. Croix, U.S.V.I.: *Journal of Sedimentary Research*, v. A65, p. 591-604.

- Ginsburg, R.N., 1971, Landward movement of carbonate mud: new model for regressive cycles in carbonates (abstract): American Association of Petroleum Geologists Bulletin, v. 55, p. 340.
- Ginsburg, R.N., 1991, Controversies about stromatolites: vices and virtues, *in* Mueller, D.W., McKenzie, J.A., and Weissert, H, eds., Controversies in Modern Geology: Academic Press, London, p. 25-36.
- Given, R.K., and Wilkinson, B.H., 1985, Kinetic control of morphology, composition, and mineralogy of abiotic sedimentary carbonates: Journal of Sedimentary Petrology, v. 55, p. 109-119.
- Goericke, R., Montoya, J.P., and Fry, B., 1994, Physiology of isotopic fractionation in algae and cyanobacteria, *in* Lajtha, K., and Michener, R.H., eds., Stable Isotopes in Ecology and Environmental Science: Blackwell Scientific Publications, p. 187-221.
- Goldhammer, R.K., Dunn, P.A., and Hardie, L.A., 1987, High frequency glacio-eustatic sea-level oscillations with Milankovitch characteristics recorded in Middle Triassic platform carbonates in northern Italy: American Journal of Science, v. 287, p. 853-892.
- Golubić, S., 1973, The relationship between blue-green algae and carbonate deposits, *in* Carr, N.G., and Whitton, B.A., eds., The Biology of Blue-Green Algae: Blackwell, Oxford, p. 434-472.
- Golubić, S., 1976, Biology of stromatolites: Organisms that build stromatolites, *in* Walter, M.R., ed., Stromatolites: Developments in Sedimentology, Elsevier, v. 20, p. 113-126.
- Golubić, S., and Campbell, S.E., 1981, Biogenically formed aragonite concretions in marine Rivularia, *in* Monty, C.L.V., ed., Phanerozoic Stromatolites: Springer-Verlag, Berlin, p. 209-229.
- González, L.A., and Lohmann, K.C., 1985, Carbon and oxygen isotopic composition of Holocene reefal carbonates: Geology, v. 13, p. 811-814.
- Gonzales, L.A., Carpenter, S.J., and Lohmann, K.C., 1992, Inorganic calcite morphology: Roles of fluid chemistry and fluid flow: Journal of Sedimentary Petrology, v. 62, p. 382-399.
- Goodwin, P.W., and Anderson, E.J., 1985, Punctuated aggradational cycles: A general hypothesis of episodic stratigraphic accumulation: Journal of Geology, v. 93, p. 515-533.
- Grant, N.K., Laskowski, T.E., and Foland, K.A., 1984, Rb-Sr and K-Ar ages of Paleozoic glauconites from Ohio-Indiana and Missouri, U.S.A., Isotope Geoscience, v. 2, p. 217-239.
- Gregg, J.M., 1985, Regional epigenetic dolomitization in the Bonneterre Dolomite (Cambrian), southeastern Missouri: Geology, v. 13, p. 503-506.
- Gregg, J.M., 1988, Origins of dolomite in the offshore facies of the Bonneterre Formation (Cambrian), southeast Missouri, *in* Shukla, V., and Baker, P.B., eds., Sedimentology and Geochemistry of Dolostones: SEPM Special Publication 43, p. 67-83.

- Gregg, J.M., and Shelton, K.L., 1990, Dolomitization and dolomite neomorphism in the back reef facies of the Bonnetterre and Davies formations (Cambrian), southeastern Missouri: *Journal of Sedimentary Petrology*, v. 60, p. 549-562.
- Gregg, J.M., and Sibley, D.F., 1984, Epigenetic dolomitization and the origin of xenotopic dolomite texture: *Journal of Sedimentary Petrology*, v. 54, p. 908-931.
- Gregg, J.M., Howard, S.A., and Mazzullo, S.J., 1992, Early diagenetic recrystallization of Holocene (<3000 years old) peritidal dolomites, Ambergris Bay, Belize: *Sedimentology*, v. 39, p. 143-160.
- Gregg, J.M., Laudon, P.R., Woody, R.E., and Shelton, K.L., 1993, Porosity evolution of the Cambrian Bonnetterre Dolomite, south-eastern Missouri, USA: *Sedimentology*, v. 40, p. 1153-1169.
- Gruszczynski, M., Halas, S., Hoffman, A., and Malkowski, K., 1989, A brachiopod calcite record of the oceanic carbon and oxygen isotope shifts at the Permian/Triassic transition: *Nature*, v. 337, p. 64-68.
- Hall, G.M., and Amick, H.C., 1934, The section on the west side of Clinch Mountain, Tennessee: *Tennessee Academy of Science Journal*, v. 9, no. 2, p. 157-168; no. 3, p. 195-200.
- Hallam, A., 1984, Pre-Quaternary sea-level changes: *Annual Reviews in Earth and Planetary Science*, v. 12, p. 204-243.
- Hambrey, M.J., and Harland, W.B., eds., 1981, *Earth's Pre-Pleistocene Glacial Record*: Cambridge University Press, New York, 1004 p.
- Handford, C.R., and Loucks, R.G., 1993, Carbonate depositional sequences and system tracts—Responses of carbonate platforms to relative sea-level changes, *in* Loucks, R.G., and Sarg, J.F., eds., *Carbonate Sequence Stratigraphy: Recent Developments and Applications*: American Association of Petroleum Geologists Memoir 57, p. 3-41.
- Hanor, J.S., 1983, Fifty years of development of thought on the origin and evolution of subsurface sedimentary brines, *in* Boardman, S.J., ed., *Revolution in the earth sciences: Advances in the past half-century*: Kendall/Hunt, Dubuque, p. 99-111.
- Hanor, J.S., 1987, Origin and migration of subsurface sedimentary brines: *SEPM Short Course 21*, 247 p.
- Haq, B.U., ed., 1995, *Sequence Stratigraphy and Depositional Response to Eustatic, Tectonic and Climatic Forcing*: Kluwer Academic, Amsterdam.
- Haq, B.U., Hardenbol, J., and Vail, P.R., 1987, Chronology of fluctuating sea-levels since the Triassic: *Science*, v. 235, p. 1156-1167.
- Haq, B.U., Hardenbol, J., and Vail, P.R., 1988, Mesozoic and Cenozoic chronostratigraphy and cycles in sea level change, *in* Wilgus, C.K., Hastings, B.S., Kendall, C.G.St.C., Posamentier, H.W., Ross, C.A., and Van Wagoner, J.C., eds., *Sea-Level Changes: An Integrated Approach*: SEPM Special Publication 42, p. 71-108.
- Hardie, L.A., 1987, Dolomitization: a critical view of some current views: *Journal of Sedimentary Petrology*, v. 57, p. 166-183.
- Hardie, L.A., and Ginsburg, R.N., 1977, Layering: the origin and environmental significance of lamination and thin bedding, *in* Hardie, L.A., ed., *Sedimentation on*

- the Modern Carbonate Tidal Flats of Northwest Andros Island, Bahamas: The Johns Hopkins University Studies in Geology 22, p. 50-123.
- Hardie, L.A., Dunn, P.A., and Goldhammer, R.K., 1991, Field and modelling studies of Cambrian carbonate cycles, Virginia Appalachians - Discussion: *Journal of Sedimentary Petrology*, v. 61, p. 636-646.
- Harland, W.B., Armstrong, R.L., Cox, A.V., Smith, A.G., and Smith, D.G., 1989, A geologic time scale: Cambridge University Press, New York, 263 p.
- Harris, L.D., 1964, Facies relations of exposed Rome Formation and Conasauga Group of northeastern Tennessee with equivalent rocks in the subsurface of Kentucky and Virginia: U.S. Geological Survey Professional Paper 501-B, p. B25-B29.
- Harris, L.D., 1965, Geologic map of the Tazewell, Clairborne County, Tennessee: U.S. Geological Survey Geological Quadrangle Map GQ-465.
- Harris, L.D., and Mixon, R.B., 1970, Geologic map of the Howard Quarter quadrangle, northeastern Tennessee: U.S. Geological Survey Geological Quadrangle Map GQ-842.
- Harris, P.M., Kendall, C.G.St.C., and Lerche, I., 1985, Carbonate cementation—A brief review, *in* Schneidermann, N., and Harris, P.M., eds., *Carbonate Cements: SEPM Special Publication 36*, p. 79-95.
- Hasson, K.O., and Haase, S.C., 1988, Lithofacies and paleogeography of the Conasauga Group, (Middle and Late Cambrian) in the Valley and Ridge province of east Tennessee: *Geological Society of America Bulletin*, v. 100, p. 234-246.
- Hatcher, R.D., Jr., 1987, Tectonics of the southern and central Appalachian Internides: *Annual Reviews in Earth and Planetary Science*, v. 15, p. 337-362.
- Hatcher, R.D., Jr., 1989, Tectonic synthesis of the U.S. Appalachians, *in* Hatcher, R.D., Jr., Thomas, W.A., and Viele, G.W., eds., *The Appalachian-Ouachita Orogen in the United States: Geological Society of America, The Geology of North America*, v. F-2, p. 511-535.
- Hatcher, R.D.Jr., Thomas, W.A., Geiser, P.A., Snoke, A.W., Mosher, S., and Wiltschko, D.V., 1989, Alleghenian orogen, *in* Hatcher, R.D.Jr., Thomas, W.A., and Viele, G.W., eds., *The Appalachian-Ouachita Orogen in the United States: The Geology of North America: Geological Society of America*, v. F-2, p. 233-318.
- Hay, R.L., Lee, M., Kolata, D.R., Matthews, J.C., and Morton, J.P., 1988, Episodic potassic diagenesis of Ordovician tuffs in the Mississippi Valley area: *Geology*, v. 16, p. 743-747.
- Hay, W.M., and Leslie, M.A., 1990, Could possible changes in global groundwater reservoir cause eustatic sea-level fluctuations, *in* *Sea-level Change: National Academy Press, Washington, D.C.*, p. 161-170.
- Haynes, F.M., Beane, R.E., and Kesler, S.E., 1989, Simultaneous transport of metal and reduced sulfur, Mascot-Jefferson City zinc district, east Tennessee: evidence from fluid inclusions: *American Journal of Science*, v. 289, p. 994-1038.
- Haynes, F.M., and Kesler, S.E., 1989, Pre-Alleghenian (Pennsylvanian-Permian) hydrocarbon emplacement along Ordovician Knox unconformity, eastern Tennessee: *American Association of Petroleum Geologists Bulletin*, v. 73, p. 289-297.

- Hearn, P.P. Jr., and Sutter, J.F., 1985, Authigenic potassium feldspar in Cambrian carbonates: evidence of Alleghenian brine migration: *Science*, v. 228, p. 1529-1531.
- Hearn, P.P. Jr., Sutter, J.F., and Belkin, H.E., 1987, Evidence for late-Paleozoic brine migration in Cambrian carbonate rocks of the central and southern Appalachians: implications for Mississippi Valley-type sulfide mineralization: *Geochimica et Cosmochimica Acta*, v. 51, p. 1323-1334.
- Heller, P.L., Wentworth, C.M., and Poag, C.W., 1982, Episodic post-rift subsidence of the United States Atlantic continental margin: *Geological Society of America Bulletin*, v. 93, p. 379-390.
- Helton, W.L., 1967, Lithostratigraphy of the Conasauga Group between Rogersville and Kingsport, Tennessee: unpublished Ph.D. Dissertation, University of Tennessee, Knoxville, 96 p.
- Hendry, J.P., 1993, Calcite cementation during bacterial manganese, iron, and sulphate reduction in Jurassic shallow marine carbonates: *Sedimentology*, v. 40, p. 87-106.
- Heydari, E., and Moore, C.H., 1993, Zonation and geochemical patterns of burial calcite cements: Upper Smackover Formation, Clarke County, Mississippi: *Journal of Sedimentary Petrology*, v. 63, p. 44-60.
- Hird, K., and Tucker, M.E., 1988, Contrasting diagenesis of two carboniferous oolites from South Wales: a tale of climatic influence: *Sedimentology*, v. 35, p. 587-602.
- Hoffman, P., 1967, Algal stromatolites: use in stratigraphic correlation and paleocurrent determination: *Science*, v. 157, p. 1043-1045.
- Hoffman, P., 1976, A stromatolite morphogenesis in Shark Bay, Western Australia, *in* Walter, M.R., ed., *Stromatolites: Developments in Sedimentology*, Elsevier, Amsterdam, v. 20, p. 261-273.
- Hofmann, H.J., 1973, Stromatolites: characteristics and utility: *Earth Science Reviews*, v. 9, p. 339-373.
- Holail, H., Lohmann, K.C., and Sanderson, I., 1988, Dolomitization and dedolomitization of Upper Cretaceous carbonates: Bahariya Oasis, Egypt, *in* Shukla, V., and Baker, P.B., eds., *Sedimentology and Geochemistry of Dolostones: SEPM Special Publication 43*, p. 191-207.
- Holser, W.T., and Magaritz, M., 1987, Events near the Permian-Triassic boundary: *Modern Geology*, v. 11, p. 155-180.
- Holser, W.T., Magaritz, M., and Wright, J., 1986, Chemical and isotopic variations in the world ocean during Phanerozoic time. *in* Walliser, O.H., ed., *Global Bio-Events: Lecture Notes in Earth Sciences*, v. 8., p. 63-74.
- Horodyski, R.J., 1985, Stromatolites of the Middle Proterozoic Belt Supergroup, Glacier National Park, Montana: a summary and a comment on the relationship between their morphology and paleoenvironment, *in* Toomey, D.F., and Nitecki, M.H., *Paleoalgology: Contemporary Research and Applications*: Springer-Verlag, New York, p. 34-39.
- Horodyski, R.J., and Vonder Haar, S.P., 1975, Recent calcareous stromatolites from Laguna Mormona (Baja California) Mexico: *Journal of Sedimentary Petrology*, v. 45, p. 894-906.

- Howe, W.B., 1966, Digitate algal stromatolite structures from the Cambrian and Ordovician of Missouri: *Journal of Paleontology*, v. 40, p. 64-77.
- Howell, B.F., Bridge, J., Deiss, C.F., Edwards, I., Lochman, C., Raasch, G.O., and Resser, C.E., 1944, Correlation of the Cambrian formations of North America: *Geological Society of America Bulletin*, v. 55, p. 993-1003.
- Hubbard, R.J., 1988, Age and significance of sequence boundaries on Jurassic and Early Cretaceous rifted continental margins: *American Association of Petroleum Geologists Bulletin*, v. 72, p. 49-72.
- Hudson, J.D., and Anderson, T.F., 1989, Ocean temperatures and isotopic compositions through time: *Transactions of the Royal Society of Edinburgh: Earth Sciences*, v. 80, p. 183-192.
- Humphrey, J.D., 1988, Late Pleistocene mixing zone dolomitization, southeastern Barbados, West Indies: *Sedimentology*, v. 35, p. 327-348.
- Humphrey, J.D., and Quinn, T.M., 1989, Coastal mixing zone dolomite, forward modeling, and massive dolomitization of platform-margin carbonates: *Journal of Sedimentary Petrology*, v. 59, p. 438-454.
- Humphrey, J.D., and Radjef, E.M., 1991, Dolomite stoichiometric variability resulting from changing aquifer conditions, Barbados, West Indies: *Sedimentary Geology*, v. 71, 129-136.
- Illing, L.V., and Taylor, J.C.M., 1993, Penecontemporaneous dolomitization in sabkha Faishakh, Qatar: Evidence from changes in the chemistry of the interstitial brines: *Journal of Sedimentary Petrology*, v. 63, p. 1042-1048.
- Irwin, H., Curtis, C., and Coleman, M., 1977, Isotopic evidence for source of diagenetic carbonates formed during burial of organic sediments: *Nature*, v. 269, p. 209-213.
- Irwin, H., 1980, Early diagenetic carbonate precipitation and pore fluid migration in the Kimmeridge Clay of Dorset, England: *Sedimentology*, v. 27, p. 577-591.
- Iyer, S.S., Babinski, M., Krouse, H.R., and Chamele, F., 1995, Highly ^{13}C -enriched carbonate and organic matter in the Neoproterozoic sediments of the Bambui Group Brasil, in Knoll, A.H., and Walter, M., eds., *Neoproterozoic Stratigraphy and Earth History: Precambrian Research*, v. 73, p. 271-282.
- Jacobs, D.K., and Sahagian, D.L., 1993, Climate-induced fluctuations in sea level during non-glacial times: *Nature*, v. 361, p. 710-712.
- James, N.P., and Choquette, P.W., 1983, Diagenesis 6. Limestones - The sea floor diagenetic environment: *Geoscience Canada*, v. 10, p. 162-179.
- James, N.P., and Choquette, P.W., 1984, Diagenesis 9. Limestones - The meteoric diagenetic environment: *Geoscience Canada*, v. 11, p. 161-194.
- James, N.P., and Ginsburg, R.N., 1979, The seaward margin of Belize barrier and atoll reefs: *International Association of Sedimentologists Special Publication 3*, 191 p.
- James, N.P., and Klappa, C.F., 1983, Petrogenesis of Early Cambrian reef limestones, Labrador, Canada: *Journal of Sedimentary Petrology*, v. 53, p. 1051-1096.
- James, N.P., Ginsburg, R.N., Marszalek, D.S., and Choquette, P.W., 1976, Facies and fabric specificity of early subsea cements in shallow Belize (British Honduras) reefs: *Journal of Sedimentary Petrology*, v. 46, p. 523-544.

- James, N.P., and Stevens, R.K., 1986, Stratigraphy and correlation of the Cambro-Ordovician Cow Head Group, western Newfoundland: Geological Society of Canada Bulletin, v. 366, 143 p.
- James, N.P., Stevens, R.K., Barnes, C.R., and Knight, I., 1989, Evolution of a Lower Paleozoic continental-margin carbonate platform, northern Canadian Appalachians, *in* Crevello, P., Wilson, J.L., Sarg, J.F., and Read, J.F., eds., Controls on Carbonate Platform and Basin Development: SEPM Special Publication 44, p. 123-146.
- Jenkyns, H.C., 1988, The early Toarcian (Jurassic) anoxic event: stratigraphic, sedimentary, and geochemical evidence: American Journal of Science, v. 288, p. 101-151.
- Jenkyns, H.C., 1996, Relative sea-level change and carbon isotopes: data from the Upper Jurassic (Oxfordian) of central and Southern Europe: Terra Nova, v. 8, p. 75-85.
- Jenkyns, H.C., and Clayton, C.J., 1986, Black shales and carbon isotopes in pelagic sediments from the Tethyan Lower Jurassic: Sedimentology, v. 33, p. 87-106.
- Joachimski, M.M., 1994, Subaerial exposure and deposition of shallowing upward sequences: evidence from stable isotopes of Purbeckian peritidal carbonates (basal Cretaceous), Swiss and French Jura Mountains: Sedimentology, v. 41, p. 805-824.
- Johnson, W.J., and Goldstein, R.H., 1993, Cambrian sea water preserved as inclusions in marine low-magnesium calcite cement: Nature, v. 362, p. 335-337.
- Jones, B., and Desrochers, A., 1992, Shallow platform carbonates, *in* Walker, R.G., and James, N.P., eds., Facies Models: Response to Sea level Change: Geological Association of Canada, p. 277-301.
- Jones, M.A., and Addis, M.A., 1985, Burial of argillaceous sediments: Marine and Petroleum Geology, v. 2, p. 247-253.
- Kaldi, J., and Gidman, J., 1982, Early diagenetic dolomite cements: examples from the Permian Lower Magnesian Limestone of England and the Pleistocene carbonates of the Bahamas: Journal of Sedimentary Petrology, v. 52, p. 1073-1085.
- Katz, A., 1973, The interaction of magnesium with calcite during crystal growth at 25° - 90° C and one atmosphere: Geochimica et Cosmochimica Acta, v. 37, p. 1563-1586.
- Katz, A., Sass, E., Starinsky, A., and Holland, H.D., 1972, Strontium behavior in the aragonite-calcite transformation: an experimental study at 40-908°C: Geochimica et Cosmochimica Acta, v. 36, p. 481-496.
- Kaufman, A.J., Hayes, J.M., Knoll, A.H., and Germs, G.J.B., 1991, Isotopic compositions of carbonates and organic carbon from upper Proterozoic successions in Namibia: stratigraphic variation and the effects of diagenesis and metamorphism: Precambrian Research, v. 49, p. 301-327.
- Kaufman, A.J., Jacobsen, S.B., and Knoll, A.H., 1993, The Vendian record of Sr and C isotopic variations in seawater: Implications for tectonics and paleoclimate: Earth and Planetary Science Letters, v. 120, p. 409-430.
- Kaufman, A.J., and Knoll, A.H., 1995, Neoproterozoic variations in the C-isotopic composition of seawater: stratigraphic and biogeochemical implications: Precambrian Research, v. 73, p. 27-49.

- Kaufman, J., 1994, Numerical models of fluid flow in carbonate platforms: implications for dolomitization: *Journal of Sedimentary Research*, v. A64, p. 128-139.
- Kempe, S., and Kazmierczak, J., 1988, Calcium carbonate supersaturation and the formation of in situ calcified stromatolites, *in* Ittekkot, V., Kempe, S., Michaelis, W., and Spitz, A., eds., *Facets of Modern Biogeochemistry*: Springer-Verlag, p. 255-278.
- Kendall, A.C., 1985, Radial fibrous calcite: a reappraisal, *in* Schneidermann, N., and Harris, P.M., eds., *Carbonate Cements: SEPM Special Publication 36*, p. 59-77.
- Kennard, J.M., 1988, The structure and origin of Cambro-Ordovician thrombolites, western Newfoundland [Ph.D. dissertation]: St. John's Memorial University, 600 p.
- Kennard, J.M., and James, N.P., 1986, Thrombolites and stromatolites: two distinct types of microbial structures: *PALAIOS*, v. 1, p. 492-503.
- Kesler, S.E., Jones, L.M., and Ruiz, J., 1988, Strontium isotopic geochemistry of Mississippian Valley-type deposits, east Tennessee: implications for age and source of mineralizing brines: *Geological Society of America Bulletin*, v. 100, p. 1300-1307.
- Kesler, S.E., Gasink, J.A., and Haynes, F.M., 1989, Evolution of mineralizing brines in the east Tennessee Mississippian Valley-type ore field: *Geology*, v. 17, p. 466-469.
- Kesler, S.E., and van der Pluijm, B.A., 1990, Timing of Mississippian Valley-type mineralization: Relation to Appalachian orogenic events: *Geology*, v. 18, p. 1115-1118.
- Kesson, K.M., Woddruff, M.S., and Grant, N.K., 1981, Gangue mineral $^{87}\text{Sr}/^{86}\text{Sr}$ ratios and the origin of Mississippian Valley-type mineralization: *Economic Geology*, v. 76, p. 913-920.
- Keto, L.S., and Jacobsen, S.B., 1987, Nd and Sr isotopic variations of Early Paleozoic oceans: *Earth and Planetary Science Letters*, v. 84, p. 27-41.
- Kharaka, Y.K., Carothers, W.W., and Rosenbauer, R.J., 1983, Thermal decarboxylation of acetic acid: implications for origin of natural gas: *Geochimica et Cosmochimica Acta*, v. 47, p. 397-402.
- Kharaka, Y.K., and Thordsen, J.J., 1992, Stable isotope geochemistry and origin of waters in sedimentary basins, *in* Clauer, N., and Chaudhuri, S., eds., *Isotopic Signatures and Sedimentary Records*: Springer-Verlag, New York, p. 411-466.
- King, P.B., and Ferguson, H.W., 1960, Geology of northeastern-most Tennessee: U.S. Geological Survey Professional Paper 311.
- Knoll, A.H., and Awramik, S.M., 1983, Ancient microbial ecosystems, *in* Krumbein, W.E., ed., *Microbial Geochemistry*: Blackwell, Oxford, p. 287-315.
- Knoll, A.H., Fairchild, I.J., and Swett, K., 1993, Calcified microbes in Neoproterozoic carbonates: Implications for our understanding of the Proterozoic/Cambrian transition: *PALAIOS*, v. 8, p. 512-525.
- Knoll, A.H., Grotzinger, J.P., Kaufman, A.J., and Kolosov, P., 1995, Integrated approaches to terminal Proterozoic stratigraphy: An example from the Olenek Uplift, northeastern Siberia: *Precambrian Research*, v. 73, p. 251-270.

- Knoll, A.H., Hayes, J.M., Kaufman, A.J., Swett, K., and Lambert, I.B., 1986, Secular variations in carbon isotope ratios from upper Proterozoic successions of Svalbard and East Greenland: *Nature*, v. 321, p. 832-838.
- Knoll, A.H., Kaufman, A.J., and Semikhatov, M.A., 1995, The carbon-isotopic composition of Proterozoic carbonates: Riphean successions from Northwestern Siberia (Anabar massif, Turukhansk uplift): *American Journal of Science*, v. 295, p. 823-850.
- Koerschner, W.F., III, and Read, J.F., 1989, Field and modeling studies of Cambrian carbonate cycles, Virginia Appalachians: *Journal of Sedimentary Petrology*, v. 59, p. 654-687.
- Kozar, M.G., Weber, L.J., and Walker, K.R., 1990, Field and modelling studies of Cambrian carbonate cycles, Virginia Appalachians - Discussion: *Journal of Sedimentary Petrology*, v. 60, p. 790-794.
- Kriesa, R.D., 1981, Storm-generated sedimentary structures in subtidal marine facies with examples from the Middle and Upper Ordovician of southwest Virginia: *Journal of Sedimentary Petrology*, v. 51, p. 823-848.
- Kroopnick, P.M., 1985, The distribution of ^{13}C of ΣCO_2 in the world oceans: *Deep-Sea Research*, v. 32, p. 57-84.
- Krumbein, W.E., 1979, Calcification by bacteria and algae, *in* Trudinger, P.A., and Swaine, D.J. eds., *Biogeochemical Cycling of Mineral-Forming Elements*: Elsevier, Amsterdam, p. 47-68.
- Krumbein, W.E., and Cohen, Y., 1977, Primary production, mat formation and lithification: contribution of oxygenic and facultative anoxygenic cyanobacteria, *in* Flügel, E., ed., *Fossil Algae - recent Results and Development*: Springer-Verlag, Berlin, p. 37-56.
- Krumbein, W.E., Cohen, Y., and Shilo, M., 1977, Solar Lake (Sinai). 4. Stromatolitic cyanobacterial mats: *Limnology and Oceanography*, v. 22, p. 635-656.
- Kump, L.R., 1989, Alternative modeling approaches to the geochemical cycles of carbon, sulfur, and strontium isotopes: *American Journal of Science*, v. 289, p. 390-410.
- Kump, L.R., 1991, Interpreting carbon-isotope excursions: Strangelove oceans: *Geology*, v. 19, p. 299-302.
- Kupecz, J.A., and Land, L.S., 1991, Late-stage dolomitization of the Lower Ordovician Ellenburger Group, west Texas: *Journal of Sedimentary Petrology*, v. 61, p. 551-574.
- Kupecz, J.A., and Land, L.S., 1994, Progressive recrystallization and stabilization of early-stage dolomite, *in* Purser, B., Tucker, M., and Zenger, D., eds., *Dolomites: A Volume in Honour of Dolomieu*: International Association of Sedimentologists, Special Publication 21, p. 255-279.
- Kupecz, J.A., Montañez, I.P., and Gao, G., 1993, Recrystallization of dolomite with time, *in* Rezak, R., and Lavoie, D.L., *Carbonate Microfabrics: Frontiers in Sedimentary Geology*, Springer-Verlag, New York, p. 187-194.
- Kushnir, J., and Kastner, M., 1984, Two forms of dolomite occurrences in the Monterey Formation, California: Concretions and layers—A comparative mineralogical, geochemical and isotopic study, *in* Garrison, R.E., Kastner, M., and Zenger, D.H.,

- eds., Dolomites of the Monterey Formation and other organic-rich units: SEPM Special Publication 41, p. 171-184.
- Lahann, R.W., 1980, Smectite diagenesis and sandstone cement: the effect of reaction temperature: *Journal of Sedimentary Petrology*, v. 50, p. 755-760.
- Lambeck, K.S., Cloeting, S., and McQueen, H., 1987, Intraplate stresses and apparent changes in sea level: The basins of northwestern Europe, *in* Beaumont, C., and Tankard, A., eds, *Sedimentary Basins and Basin Forming Mechanisms*: Canadian Society of Petroleum Geologists Memoir 12, p. 259-268.
- Land, L.S., 1980, The isotopic and trace element geochemistry of dolomite: the state of art, *in* Zenger, D.H., Dunham, J.B., and Ethington, R.L., eds., *Concepts and Models of Dolomitization*: SEPM Special Publication, 28, p. 87-110.
- Land, L.S., 1985, The origin of massive dolomites: *Journal of Geological Education*, v. 33, p. 112-125.
- Lasemi, Z., and Sandberg, P.A., 1984, Transformation of aragonite-dominated lime muds to microcrystalline limestone: *Geology*, v. 12, p. 420-423.
- Lasemi, Z., Boardman, M.R., and Sandberg, P.A., 1989, Cement origin of supratidal dolomite, Andros Island, Bahamas: *Journal of Sedimentary Petrology*, v. 59, p. 249-257.
- Lavoie, D., and Bourque, P.A., 1993, Marine, burial, and meteoric diagenesis of early Silurian carbonate ramps, Quebec Appalachians, Canada: *Journal of Sedimentary Petrology*, v. 63, p. 233-247.
- Lazar, B., and Erez, J., 1992, Carbon geochemistry of marine-derived brines: I. ^{13}C depletion due to intense photosynthesis: *Geochimica et Cosmochimica Acta*, v. 56, p. 335-345.
- Lazar, B., Javor, B., and Erez, L., 1989, Total alkalinity in marine-derived brines and pore waters associated with microbial mats, *in* Cohen, Y., and Rosenberg, E., eds., *Microbial Mats, Physiological Ecology of Benthic Microbial Communities*: American Society for Microbiology, p. 84-93.
- Leach, D.L., and Rowan, E.L., 1986, Genetic link between Ouachita foldbelt tectonism and the Mississippi Valley-type lead-zinc deposits of the Ozarks: *Geology*, v. 14, p. 931-935.
- Lee, Y.I., and Friedman, G.M., 1987, Deep-burial dolomitization in the Lower Ordovician Ellenburger Group carbonates in west Texas and southeastern New Mexico: *Journal of Sedimentary Petrology*, v. 57, p. 544-557.
- Leggett, J.K., 1980, British Lower Paleozoic black shales and their palaeo-oceanographic significance: *Journal of Geological Society of London*, v. 137, p. 139-156.
- Lehmann, E.L., 1975, *Nonparametrics: Statistical Methods Based on Ranks*: McGraw-Hill, New York, 457 p.
- Lini, A., Weissert, H., and Erba, E., 1992, The Valanginian carbon isotope event: A first episode of greenhouse climate conditions during the Cretaceous: *Terra Nova*, v. 4, p. 374-384.
- Lochman-Balk, C., 1971, Cambrian of the craton, *in* Holland, E.R., ed., *Cambrian of the New World, Lower Paleozoic Rocks of the World (Volume 1)*: Wiley Interscience, New York, p. 79-167.

- Lohmann, K.C., 1982, Inverted J carbon and oxygen isotopic trends—criteria for shallow meteoric phreatic diagenesis: Geological Society of America Annual Meeting, Abstracts with Program, p. 548.
- Lohmann, K.C., 1988, Geochemical patterns of meteoric diagenetic systems and their application to studies of paleokarst, *in* James, N.P., and Choquette, P.W., ed., *Paleokarst*: Springer-Verlag, New York, p. 58-80.
- Lohmann, K.C., and Meyers, W.J., 1977, Microdolomite inclusions in cloudy prismatic calcites: A proposed criterion for former high magnesium calcites: *Journal of Sedimentary Petrology*, v. 47, p. 1078-1088.
- Lohmann, K.C., and Walker, J.C.G., 1989, the $\delta^{18}\text{O}$ record of Phanerozoic abiotic marine calcite cements: *Geophysical Research Letters*, v. 16, p. 319-322.
- Logan, B.W., 1961, Cryptozoan and associated stromatolites from the Recent, Shark Bay, Western Australia: *Journal of Geology*, v. 69, p. 517-533.
- Logan, B.W., and Semeniuk, V., 1976, Dynamic metamorphism: processes and products in Devonian carbonate rocks, Canning Basin, Western Australia: Geological Society of Australia, Special Publication 6, 138 p.
- Logan, B.W., Hoffman, P., and Gebelein, C.D., 1974, Algal mats, cryptalgal fabrics and structures, Hamelin Pool, Western Australia: *American Association of Petroleum Geologists Memoir* 22, p. 140-194.
- Logan, B.W., Rezak, R., and Ginsburg, R.N., 1964, Classification and environmental significance of algal stromatolites: *Journal of Geology*, v. 72, p. 68-83.
- Lomando, A.J., and Harris, P.M., eds., 1991, Mixed Carbonate-Siliciclastic Sequences: SEPM Core Workshop 15, 569 p.
- Long, D.G.F., 1993, Oxygen and carbon isotopes and event stratigraphy near the Ordovician-Silurian boundary, Anticosti Island, Quebec: *Palaeogeography, Palaeoclimatology, Palaeoecology*, v. 104.
- Longman, M.W., 1980, Carbonate diagenetic textures from near-surface diagenetic environments: *American Association of Petroleum Geologists*, v. 64, p. 461-487.
- Lorens, R.B., 1981, Sr, Cd, Mn, and Co distribution coefficients in calcite as a function of calcite precipitation rate: *Geochimica et Cosmochimica Acta*, v. 45, p. 553-561.
- Loucks, R.G., and Sarg, J.F., eds., 1993, Carbonate Sequence Stratigraphy: Recent Developments and Applications: *American Association of Petroleum Geologists Memoir* 57, 545 p.
- Lowenstam, H.A., 1981, Minerals formed by organisms: *Science*, v. 211, p. 1126-1231.
- Ludvigsen, R., and Westrop, S.R., 1985, Three new Upper Cambrian stages for North America: *Geology*, v. 13, p. 139-143.
- Lumsden, D.N., and Chimahusky, J.S., 1980, Relationship between dolomite nonstoichiometry and carbonate facies parameters, *in* Zenger, D.H., Dunham, J.B., and Ethington, R.L., eds., *Concepts and Models of Dolomitization*: SEPM Special Publication, 28, p. 123-137.
- Lyons, W.B., Long, D.T., Hines, M.E., Gaudette, H.E., and Armstrong, P.B., 1984, Calcification of cyanobacterial mats in Solar lake, Sinai: *Geology*, v. 12, p. 623-626.

- Machel, H.G., 1987, Saddle dolomite as a by-product of chemical compaction and thermochemical sulfate reduction: *Geology*, v. 15, p. 936-940.
- Machel, H.G., and Anderson, J.H., 1989, Pervasive subsurface dolomitization of the Nisku Formation in Central Alberta: *Journal of Sedimentary Petrology*, v. 59, p. 891-911.
- Machel, H.G., and Burton, E.A., 1991, Factors governing cathodoluminescence in calcite and dolomite, and their implications for studies of carbonate diagenesis, *in* Barker, C.E., and Kopp, O.C., eds., *Luminescence Microscopy and Spectroscopy: Qualitative and Quantitative Applications: SEPM Short Course 25*, p. 37-57.
- Machel, H.G., and Mountjoy, E.W., 1986, Chemistry and environments of dolomitization - a reappraisal: *Earth Science Reviews*, v. 23, p. 175-222.
- Magaritz, M., 1989, ^{13}C minima follow extinction events: A clue to faunal radiation: *Geology*, v. 17, p. 337-340.
- Magaritz, M., 1991, Carbon isotopes, time boundaries and evolution: *Terra Nova*, v. 3, p. 251-256.
- Magaritz, M., and Stemmerik, L., 1989, Oscillation of carbon and oxygen isotope compositions of carbonate rocks between evaporative and open marine environments, Upper Permian of East Greenland: *Earth and Planetary Science Letters*, v. 93, p. 233-240.
- Magaritz, M., Goldenberg, L., Kafri, U., and Arad, A., 1980, Dolomite formation in seawater-freshwater interface: *Nature*, v. 287, p. 622-624.
- Magaritz, M., Holser, W.T., and Kirschvink, J.L., 1986, Carbon-isotope events across the Precambrian-Cambrian boundary on the Siberian Platform: *Nature*, v. 320, p. 258-259.
- Magaritz, M., Kirschvink, J.L., Latham, A.J., Zhuravlev, A.Yu., and Rozanov, A.Yu., 1991, Precambrian/Cambrian boundary problem: Carbon isotope correlations for Vendian and Tommotian time between Siberia and Morocco: *Geology*, v. 19, p. 847-850.
- Major, R.P., Halley, R.B., and Lukas, K.J., 1988, Cathodoluminescent bimineralic ooids from the Pleistocene of the Florida continental shelf: *Sedimentology*, v. 35, p. 843-855.
- Major, R.P., and Wilber, R.J., 1991, Crystal habit, geochemistry, and cathodoluminescence of magnesian calcite marine cements from the lower slope of Little Bahama Bank: *Geological Society of America Bulletin*, v. 103, p. 461-471.
- Manspeizer, W., ed., 1988, Triassic-Jurassic Rifting: Continental Breakup and the Origin of the Atlantic Ocean and Passive Margins: *Developments in Geotectonics 22*, Elsevier, New York.
- Markello, J.R., and Read, J.F., 1981, Carbonate ramp-to-deeper-shale shelf transitions of an Upper Cambrian intrashelf basin, Nolichucky Formation, southwest Virginia Appalachians: *Sedimentology*, v.28, p. 573-597.
- Markello, J.R., and Read, J.F., 1982, Upper Cambrian intrashelf basin, Nolichucky Formation, southwest Virginia Appalachians: *American Association of Petroleum Geologists Bulletin*, v. 66, p. 860-878.

- Marshall, J.D., 1992, Climatic and oceanographic isotopic signals from the carbonate rock record and their preservation: *Geological Magazine*, v. 2, p. 143-160.
- Marshall, J.D., and Middleton, P.D., 1990, Changes in marine isotopic composition and the late Ordovician glaciation: *Journal of the Geological Society of London*, v. 147, p. 1-4.
- Marshall, J.D., and Ashton, M., 1980, Isotopic and trace element evidence for submarine lithification of hardgrounds in the Jurassic of England: *Sedimentology*, v. 27, p. 271-289.
- Marshall, J.F., and Davies, P.J., 1981, Submarine lithification on windward reef slopes: Capricorn-Bunker Group, southern Great Barrier Reef: *Journal of Sedimentary Petrology*, v. 51, p. 953-960.
- Mattes, B.W., and Mountjoy, E.W., 1980, Burial dolomitization of the Upper Devonian Miette Buildup, Jasper National Park, Alberta, *in* Zenger, D.H., Dunham, J.B., and Ethington, R.L., eds., *Concepts and Models of Dolomitization*: SEPM Special Publication 28, p. 259-297.
- Mayall, M.J., and Cox, M., 1988, Deposition and diagenesis of Miocene limestones, Senkang Basin, Sulawesi, Indonesia: *Sedimentary Geology*, v. 59, p. 77-92.
- Mazzullo, S.J., 1980, Calcite pseudospar replacive of marine acicular aragonite, and implications for aragonite cement diagenesis: *Journal of Sedimentary Petrology*, v. 49, p. 409-422.
- Mazzullo, S.J., 1992, Geochemical and neomorphic alteration of dolomite: a review: *Carbonates and Evaporites*, v. 7, p. 21-37.
- Mazzullo, S.J., Reid, A.M., and Gregg, J.M., 1987, Dolomitization of Holocene Mg-calcite supratidal deposits, Ambergris Cay, Belize: *Geological Society of America Bulletin*, v. 98, p. 224-231.
- McConnell, R.L., 1967, Lithostratigraphy and petrography of the Upper Cambrian Maynardville Formation within the Copper Creek fault belt of east Tennessee [unpublished M.S. thesis]: The University of Tennessee, Knoxville, 92 p.
- McHargue, T.R., and Price, R.C., 1982, Dolomite from clay in argillaceous or shale-associated marine carbonates: *Journal of Sedimentary Petrology*, v. 52, p. 873-886.
- McKenzie, J.A., 1981, Holocene dolomitization of calcium carbonate sediments from the coastal sabkhas of Abu Dhabi, U.A.E.: a stable isotope study: *Journal of Geology*, v. 89, p. 185-198.
- McKenzie, J.A., Hsu, K.J., and Schneider, J.F., 1980, Movement of subsurface waters under the sabkha, Abu Dhabi, U.A.E., and its relationship to evaporative dolomite genesis, *in* Zenger, D.H., Dunham, J.B., and Ethington, R.L., eds., *Concepts and Models of Dolomitization*: SEPM Special Publication 28, p. 11-30.
- McLean, D.J., and Mountjoy, E.W., 1994, Allocyclic control on Late Devonian buildup development, Southern Canadian Rocky Mountains: *Journal of Sedimentary Research*, v. B64, p. 326-340.
- McNutt, R.H., Frape, S.K., Fritz, P., Jones, M.G., and MacDonald, I.M., 1990, The $^{87}\text{Sr}/^{86}\text{Sr}$ values of Canadian Shield brines and fracture minerals with applications

- to groundwater mixing, fracture history, and geochronology: *Geochimica et Cosmochimica Acta*, v. 54, p. 205-215.
- Merz, M.U.E., 1992, The biology of carbonate precipitation by cyanobacteria: *Facies*, v. 26, p. 81-102.
- Meshri, I.D., 1986, On the reactivity of carbonic and organic acids and generation of secondary porosity, *in* Gautier, D.L., ed., *Roles of Organic Matter in Sediment Diagenesis*: SEPM Special Publication 38, p. 123-128.
- Meyer, A., Davis, T., and Wise, S.W., Jr., eds., 1991, *Evolution of Continental Margins: Marine Geology Special Issue*, v. 102.
- Meyers, W.J., 1978, Carbonate cements: their regional distribution and interpretation in Mississippian limestones of southwestern New Mexico: *Sedimentology*, v. 25, p. 371-400.
- Meyers, W.J., 1989, Trace element and isotope geochemistry of zoned calcite cements, Lake Valley Formation (Mississippian, New Mexico): insights from water-rock interaction modelling: *Sedimentary Geology*, v. 63, p. 355-370.
- Miall, A.D., 1986, Eustatic sea level changes interpreted from seismic stratigraphy: a critique of the methodology with particular reference to the North Sea Jurassic record: *American Association of Petroleum Geologists Bulletin*, v. 70, p. 131-137.
- Miall, A.D., 1992, Exxon global cycle chart: An event for every occasion?: *Geology*, v. 20, p. 787-790.
- Middelburg, J.J., de Lange, G.J., and Kreulen, R., 1990, Dolomite formation in anoxic sediments of Kau Bay, Indonesia: *Geology*, v. 18, p. 399-402.
- Milici, R.C., 1973, The stratigraphy of Knox County, Tennessee: *Tennessee Division of Geology Bulletin* 70, p. 9-24.
- Milici, R.C., Brent, W.B., and Walker, K.R., 1973, Depositional environments in upper Conasauga lagoon-fill sequences along I-75 at Copper Ridge, Knox County, Tennessee: *Tennessee Division of Geology Bulletin*, 70, p. 138-143.
- Miller, R.L., and Fuller, J.O., 1954, Geology and oil resources of the Rose Hill District - the Fenster area of the Cumberland overthrust block - Lee County, Virginia: *Virginia Geological Survey Bulletin*, 71, 383 p.
- Milliken, K.L., 1979, The silicified evaporite syndrome—two aspects of silicification history of former evaporite nodules from southern Kentucky and northern Tennessee: *Journal of Sedimentary Petrology*, v. 49, p. 245-256.
- Mitchell, J.T., Land, L.S., and Miser, D.N., 1987, Modern marine dolomite cement in a north Jamaican fringing reef: *Geology*, v. 15, p. 557-560.
- Montañez, I.P., 1994, Late diagenetic dolomitization of Lower Ordovician, Upper Knox carbonates: A record of the hydrodynamic evolution of the southern Appalachian Basin: *American Association of Petroleum Geologists Bulletin*, v. 78, p. 1210-1239.
- Montañez, I.P., and Osleger, D.A., 1993, Parasequence stacking patterns, third order accommodation events, and sequence stratigraphy of Middle to Upper Cambrian platform carbonates, Bonanza King Formation, southern Great Basin, *in* Loucks, R.G., and Sarg, J.F., eds., *Carbonate Sequence Stratigraphy: Recent*

- Developments and Applications: American Association of Petroleum Geologists Memoir 57, p. 305-325.
- Montañez, I.P., and Read, J.F., 1992a, Eustatic control on early dolomitization of cyclic peritidal carbonates: Evidence from the Early Ordovician Upper Knox Group, Appalachians: Geological Society of America Bulletin, v. 104, p. 872-886.
- Montañez, I.P., and Read, J.F., 1992b, Fluid-rock interaction history during stabilization of early dolomites, Upper Knox Group (Lower Ordovician), U.S. Appalachians: Journal of Sedimentary Petrology, v. 62, p. 753-778.
- Monty, C.L.V., 1976, The origin and development of cryptalgal fabrics, *in* Walter, M.R., ed., Stromatolites: Developments in Sedimentology, Elsevier, Amsterdam, v. 20, p. 193-249.
- Monty, C.L.V., 1977, Evolving concepts on the nature and the geological significance of stromatolites, *in* Flügel, E., ed., Fossil Algae - recent Results and Development: Springer-Verlag, Berlin, p. 15-35.
- Moore, C.H., 1985, Upper Jurassic subsurface cements: A case history, *in* Schneidermann, N., and Harris, P.M., eds., Carbonate Cements: SEPM Special Publication 36, p. 291-308.
- Moore, C.H., 1989, Carbonate Diagenesis and Porosity: Elsevier, New York, 338 p.
- Moore, C.H., Chowdhury, A., and Chan, L., 1988, Upper Jurassic platform dolomitization, northwestern Gulf of Mexico: A tale of two waters, *in* Shukla, V., and Baker, P.B., eds., Sedimentology and Geochemistry of Dolostones: SEPM Special Publication 43, p. 175-189.
- Morrow, D.W., 1982, Diagenesis 2. Dolomite - Part 2: Dolomitization models and ancient dolostones: Geoscience Canada, v. 9, p. 95-107.
- Morse, J.W., and Bender, M.L., 1990, Partition coefficients in calcite: examination of factors influencing the validity of experimental results and their applications to natural systems: Chemical Geology, v. 82, p. 265-277.
- Morse, J.W., Cornwell, J.C., Arakaki, T., Lin, S., and Huerta-Diaz, M., 1992, Iron sulfide and carbonate mineral diagenesis in Baffin Bay, Texas: Journal of Sedimentary Petrology, v. 62, p. 671-680.
- Morton, R.A., and Land, L.S., 1987, Regional variations in formation water chemistry, Frio Formation (Oligocene), Texas Gulf Coast: American Association of Petroleum Geologists Bulletin, v. 71, p. 191-206.
- Moshier, S.O., 1989, Lime-mud diagenesis and microcrystalline cements, *in* Walker, K.R., ed., The Fabric of Cements in Paleozoic Limestones: The University of Tennessee, Studies in Geology 20, p. 78-90.
- Mount, J.F., and Rowland, S.M., 1981, Grand Cycle A (Lower Cambrian) of the southern Great Basin: A Product of differential rates of relative sea-level rise, *in* Taylor, M.E., ed., Short Papers for the Second International Symposium on the Cambrian System: United States Geological Survey Open-File Report 81-743, p. 143-146.
- Mountjoy, E.W., and Amthor, J.E., 1994, Has burial dolomitization come of age? Some Answers from the western Canada Sedimentary Basin, *in* Purser, B., Tucker, M., and Zenger, D., eds., Dolomites: A Volume in Honour of Dolomieu: International Association of Sedimentologists, Special Publication 21, p. 203-229.

- Mucci, A., 1987, Influence of temperature on the composition of magnesian calcite overgrowths precipitated from seawater: *Geochimica et Cosmochimica Acta*, v. 51, p. 1977-1984.
- Mucci, A., 1988, Manganese uptake during calcite precipitation from seawater: conditions leading to the formation of pseudokutnahorite: *Geochimica et Cosmochimica Acta*, v. 52, p. 1859-1868.
- Mucci, A., Canuel, R., and Zhong, S., 1989, The solubility of calcite and aragonite in sulfate-free seawater and the seeded growth kinetics and composition of the precipitates at 25°C: *Chemical Geology*, v. 74, p. 309-320.
- Mucci, A., and Morse, J.W., 1983, The incorporation of Mg^{2+} and Sr^{2+} into calcite overgrowths: influences of growth rate and solution composition: *Geochimica et Cosmochimica Acta*, v. 47, p. 217-233.
- Müller, D.W., McKenzie, J.A., and Mueller, P.A., 1991, Abu Dhabi Sabkha, Persian Gulf, revisited: Application of strontium isotopes to test an early dolomitization model: *Geology*, v. 18, p. 618-621.
- Mullins, H.T., Wise, S.W., Land, L.S., Siegel, D.I., Masters, P.M., Hinchey, E.J., and Price, K.R., 1985, Authigenic dolomite in Bahamian periplatform slope sediment: *Geology*, v. 13, p. 292-295.
- Mussman, W.J., and Read, J.F., 1986, Sedimentology and development of a passive- to convergent-margin unconformity: Middle Ordovician Knox unconformity, Virginia Appalachians: *Geological Society of America Bulletin*, v. 97, p. 282-295.
- Nakai, S., Halliday, A.N., Kesler, S.E., and Jones, H.D., 1990, Rb-Sr dating of sphalerites from Tennessee and the genesis of Mississippi Valley type ore deposits: *Nature*, v. 346, p. 354-357.
- Nakai, S., Halliday, A.N., Kesler, S.E., Jones, H.D., Kyle, J.R., and Lane, T.E., 1993, Rb-Sr dating of sphalerites from Mississippi Valley-type (MVT) ore deposits: *Geochimica et Cosmochimica Acta*, v. 57, p. 417-427.
- Narbonne, G.M., Kaufman, A.J., and Knoll, A.H., 1994, Integrated chemostratigraphy and biostartigraphy of the upper Windermere Supergroup (Neoproterozoic), Mackenzie Mountains, northwestern Canada: *Geological Society of America Bulletin*, v. 106, p. 1281-1291.
- Narkiewicz, M., 1983, Dolomite from clay in argillaceous or shale-associated marine carbonates—Discussion: *Journal of Sedimentary Petrology*, v. 53, p. 1353-1354.
- Neumann, A.C., Gebelein, C.D., and Scoffin, T.P., 1970, The composition, structure and erodability of subtidal mats, Abaco, Bahamas: *Journal of Sedimentary Petrology*, v. 40, p. 274-297.
- Niemann, J.C., and Read, J.F., 1988, Regional cementation from unconformity-recharged aquifer and burial fluids, Mississippian Newman Limestone, Kentucky: *Journal of Sedimentary Petrology*, v. 58, p. 688-705.
- Oder, C.R.L., 1934, Preliminary subdivision of the Knox dolomite in East Tennessee: *Journal of Geology*, v. 42, p. 469-497.
- Oder, C.R.L., and Bumgarner, J.G., 1961, Stromatolitic bioherms in the Maynardville (Upper Cambrian) Limestone, Tennessee: *Geological Society of America Bulletin*, v. 72, p. 1021-1028.

- Oder, C.R.L., and Milici, R.C., 1965, Geologic map of the Morristown quadrangle, Tennessee: Tennessee Division of Geology Geologic Map GM-163-NE.
- Oliver, J., 1986, Fluids expelled tectonically from orogenic belts: their role in hydrocarbon migration and other geologic phenomena: *Geology*, v. 14, p. 99-102.
- Osleger, D.A., 1990, Cyclostratigraphy of Late Cambrian cyclic carbonates: an interbasinal field and modeling study, U.S.A. [unpublished Ph.D. thesis]: Virginia Polytechnic Institute and State University, Blacksburg, 303 p.
- Osleger, D.A., and Read, J.F., 1991, Relation of eustasy to stacking patterns of meter-scale carbonate cycles, Late Cambrian, U.S.A.: *Journal of Sedimentary Petrology*, v. 61, p. 1225-1252.
- Osleger, D.A., and Read, J.F., 1993, Comparative analysis of methods used to define eustatic variations in outcrop: Late Cambrian interbasinal sequence development: *American Journal of Science*, v. 293, p. 157-216.
- Palmer, A.R., 1965a, Biomere - A new kind of biostratigraphic unit: *Journal of Paleontology*, v. 39, p. 149-153.
- Palmer, A.R., 1965b, Trilobites of the Late Cambrian Pterocephaliid Biomere in the Great Basin, United States: U.S. Geological Survey Professional Paper 493, 103 p.
- Palmer, A.R., 1971, The Cambrian of the Appalachian and eastern New England regions, eastern United States, *in* Holland, C.H., ed., *Lower Paleozoic Rocks of the World: Cambrian of the New World (Volume 1)*: Wiley Interscience, New York, p. 169-217.
- Palmer, A.R., 1981a, On the correlatability of Grand Cycle tops, *in* Taylor, M.E., ed., *Short papers for the Second International Symposium on the Cambrian system*: United States Geological Survey Open File Report 81-743, p. 156-159.
- Palmer, A.R., 1981b, Subdivision of the Sauk sequence, *in* Taylor, M.E., ed., *Short papers for the Second International Symposium on the Cambrian system*: United States Geological Survey Open File Report 81-743, p. 160-163.
- Palmer, A.R., and Halley, R.B., 1979, Physical stratigraphy and trilobite biostratigraphy of the Carrara Formation (Lower and Middle Cambrian) in the southern Great Basin: U.S. Geological Survey Professional Paper 1047, 131 p.
- Pardue, J.W., Scalan, R.S., Van Baalen, C., and Parker, P., 1976, Maximum carbon isotope fractionation in photosynthesis by blue-green algae and green alga: *Geochimica et Cosmochimica Acta*, v. 40, p. 309-312.
- Park, R.K., 1977, The preservation potential of some recent stromatolites: *Sedimentology*, v. 24, p. 485-506.
- Parnell, J., 1986, Devonian Magadi-type cherts in the Orcadian basin, Scotland: *Journal of Sedimentary Petrology*, v. 56, p. 495-500.
- Patchen, D.G., Avary, K.L., and Erwin, R.B., 1985, Southern Appalachian Region, Correlation of Stratigraphic Units of North America (COSUNA) Project: American Association of Petroleum Geologists.
- Patterson, R.J., and Kinsman, D.J.J., 1982, Formation of diagenetic dolomite in coastal sabkha along Arabian (Persian) Gulf: *American Association of Petroleum Geologists Bulletin*, v. 66, p. 28-43.

- Patterson, W.P., and Walter, L.M., 1994, Depletion of ^{13}C in seawater ΣCO_2 on modern carbonate platforms: Significance for the carbon isotopic record of carbonates: *Geology*, v. 22, p. 885-888.
- Pelechaty, S.M., Kaufman, A.J., and Grotzinger, J.P., 1996, Evaluation of $\delta^{13}\text{C}$ chemostratigraphy for intrabasinal correlation: Vendian strata of northeast Siberia: *Geological Society of America Bulletin*, v. 108, p. 992-1003.
- Pentecost, A., and Riding, R., 1986, Calcification in cyanobacteria, *in* Leadbeater, B.S.C., and Riding, R., eds., *Biomining in Lower Plants and Animals: The Systematics Association, Special Volume 30*, Claredon, Oxford, p. 73-90.
- Pfeil, R.W., and Read, J.F., 1980, Cambrian carbonate platform margin facies, Shady Dolomite, southwestern Virginia, U.S.A.: *Journal of Sedimentary Petrology*, v. 50, p. 91-116.
- Pierre, C., Ortlieb, L., and Person, A., 1984, Supratidal evaporitic dolomite at Ojo de Liebre Lagoon: Mineralogy and isotopic arguments for primary crystallization: *Journal of Sedimentary Petrology*, v. 54, p. 1049-1061.
- Pierson, B.J., and Shinn, E.A., 1985, Cement distribution and carbonate mineral stabilization in Pleistocene limestones of Hogsty Reef, Bahamas, *in* Schneidermann, N., and Harris, P.M., eds., *Carbonate Cements: SEPM Special Publication 36*, p. 153-168.
- Pigott, J.D., and Land, L.S., 1986, Interstitial water chemistry of Jamaican Reef sediment Sulfate reduction and submarine cementation: *Marine Chemistry*, v. 19, p. 355-378.
- Pingitore, N.E., Eastman, M.P., Sandidge, M., Oden, K., and Freiha, B., 1988, The coprecipitation of manganese (II) with calcite: an experimental study: *Marine Chemistry*, v. 25, p. 107-120.
- Pitman, W.C., III, 1978, The relationship between eustacy and stratigraphic sequences of passive margins: *Geological Society of America Bulletin*, v. 89, p. 1389-1403.
- Pitman, W.C., III, and Golovchenko, X., 1988, Sea level changes and their effect on the stratigraphy of Atlantic-type margins, *in* Sheridan, R.E., and Grow, J.A., eds., *The Atlantic Continental Margin: U.S.: Geological Society of America, The Geology of North America*, v. I-2, p. 429-436.
- Playford, P.E., and Cockbain, A.E., 1976, Modern algal stromatolites at Hamelin Pool, a hypersaline barred basin in Shark Bay, Western Australia, *in* Walter, M.R., ed., *Stromatolites: Developments in Sedimentology*, Elsevier, Amsterdam, v. 20, p. 389-412.
- Popp, B.N., Anderson, T.F., and Sandberg, P.A., 1986, Brachiopods as indicators of original isotopic compositions in some Paleozoic limestones: *Geological Society of America Bulletin*, v. 97, p. 1262-1269.
- Posamentier, H.W., Summerhayes, C.P., Haq, B.U., and Allen, G.P., eds., 1993, *Sequence Stratigraphy and Facies Associations: International Association of Sedimentologists Special Publication 18*, 644 p.
- Pratt, B.R., 1984, Epiphyton and Renalcis - diagenetic microfossils from calcification of coccoid blue-green algae: *Journal of Sedimentary Petrology*, v. 54, p. 948-971.

- Pratt, L.M., Force, E.R., and Pomeroy, B., 1991, Coupled manganese and carbon-isotopic events in marine carbonates at the Cenomanian-Turonian boundary: *Journal of Sedimentary Petrology*, v. 61, p. 370-383.
- Prezbindowski, D.R., 1985, Burial cementation - is it important? A case study, Stuart City trend, south-central Texas, *in* Schneidermann, N., and Harris, P.M., eds., *Carbonate Cements: SEPM Special Publication 36*, p. 241-264.
- Price, R.C., and McHargue, T.R., 1983, Dolomite from clay in argillaceous or shale-associated marine carbonates—Reply: *Journal of Sedimentary Petrology*, v. 53, p. 1355.
- Qing, H., and Mountjoy, E.W., 1989, Multistage dolomitization in Rainbow buildups, Middle Devonian Keg River Formation, Alberta, Canada: *Journal of Sedimentary Petrology*, v. 59, p. 114-126.
- Qing, H., and Mountjoy, E.W., 1992, Large-scale fluid flow in the Middle Devonian Presqu'ile barrier, Western Canada sedimentary basin: *Geology*, v. 20, p. 903-906.
- Railsback, L.B., 1993, Lithologic controls on morphology of pressure-dissolution surfaces (stylolites and dissolution seams) in Paleozoic carbonate rocks from the mideastern United States: *Journal of Sedimentary Petrology*, v. 63, p. 513-522.
- Radke, B.M., and Mathis, R.L., 1980, On the formation and occurrence of saddle dolomite: *Journal of Sedimentary Petrology*, v. 50, p. 1149-1168.
- Randazzo, A.F., and Cook, D.J., 1987, Characterization of dolomitic rocks from the coastal mixing zone of the Floridan aquifer, U.S.A.: *Sedimentary Geology*, v. 43, p. 219-239.
- Rankey, E.C., 1993, Carbonate platform response to tectonism and eustasy: The Middle Cambrian carbonates of the Lower and Middle Conasauga Group, East Tennessee [unpublished M.S. thesis]: The University of Tennessee, Knoxville, 191 p.
- Rankey, E.C., Walker, K.R., and Srinivasan, K., 1994, Gradual establishment of Iapetan "passive" margin sedimentation: stratigraphic consequences of Cambrian episodic tectonism and eustasy, southern Appalachians: *Journal of Sedimentary Research*, v. B64, p. 298-310.
- Rankin, D.W., Drake, A.A., Jr., Glover, L., III, Goldsmith, R., Hall, L.M., Murray, D.P., Ratcliffe, N.M., Read, J.F., Secor, D.T., Jr., and Stanley, R.S., 1989, Pre-orogenic terranes, *in* Hatcher, R.D., Jr., Thomas, W.A., and Viele, G.W., *The Appalachian-Ouachita Orogen in the United States*: Boulder, Colorado, Geological Society of America, *The Geology of North America*, v. F-2, p. 7-99.
- Rasetti, F., 1965, Upper Cambrian trilobite faunas of northeastern Tennessee: *Smithsonian Miscellaneous Collection*, v. 148, 140 p.
- Rast, N., and Kohles, K.M., 1986, The origin of the Ocoee Supergroup: *American Journal of Science*, v. 286, p. 593-616.
- Raymond, R.H., 1959, Paleontology of a portion of the Nolichucky Shale and Maynardville Limestone (Cambrian) of the Powell quadrangle, Tennessee [unpublished M.S. thesis]: The University of Tennessee, Knoxville, 58 p.
- Read, J.F. 1980, Carbonate ramp to basin transitions and foreland basin evolution, Middle Ordovician sequence, Virginia: *American Association of Petroleum Geologists Bulletin*, v. 64, p. 1575-1612.

- Read, J.F., 1982, Carbonate platforms of passive (extensional) continental margins: types, characteristics and evolution: *Tectonophysics*, v. 81, p. 195-212.
- Read, J.F., 1989, Controls on evolution of Cambro-Ordovician passive margin, U.S. Appalachians, *in* Crevello, P., Wilson, J.L., Sarg, J.F., and Read, J.F., eds., *Controls on Carbonate Platform and Basin Development: SEPM Special Publication 44*, p. 147-165.
- Read, J.F., Grotzinger, J.P., Bova, J.A., and Koerschner, W.F., 1986, Models for generation of carbonate cycles: *Geology*, v. 14, p. 107-110.
- Resser, C.E., 1938, Cambrian system (restricted) of the southern Appalachians: *Geological Society of America Special Paper 15*, 140 p.
- Reynolds, D.J., Steckler, M.S., and Coakley, B.J., 1991, The role of sediment load in sequence stratigraphy: The influence of flexural isostasy and compaction: *Journal of Geophysical Research*, v. 96, p. 6931-6949.
- Riding, R., 1975, Girvanella and other algae as depth indicators: *Lethaia*, v. 8, p. 173-179.
- Riding, R., 1982, Cyanophyte calcification and changes in ocean chemistry: *Nature*, v. 299, p. 814-815.
- Riding, R., 1991a, Calcified cyanobacteria, *in* Riding, R., ed., *Calcareous Algae and Stromatolites: Springer-Verlag*, p. 55-87.
- Riding, R., 1991b, Cambrian calcareous cyanobacteria and algae, *in* Riding, R., ed., *Calcareous Algae and Stromatolites: Springer-Verlag*, p. 305-334.
- Riding, R., 1991c, Classification of microbial carbonates, *in* Riding, R., ed., *Calcareous Algae and Stromatolites: Springer-Verlag*, p. 21-51.
- Riding, R., and Veronova, L., 1984, Assemblages of calcareous algae near the Precambrian-Cambrian boundary in Siberia and Mongolia: *Geological Magazine*, v. 121, p. 205-210.
- Rodgers, J., 1953, Geologic map of east Tennessee with explanatory text: *Tennessee Division of Geology Bulletin 58, Part II*, 168 p.
- Rodgers, J., 1968, The eastern edge of the North American continent during the Cambrian and early Ordovician, *in* Zen, E.-A., and others, eds., *Studies of Appalachian geology: Northern and Maritime: Wiley, New York*, p. 141-150.
- Rodgers, J., and Kent, D.F., 1948, Stratigraphic section at Lee Valley, Hawkins County, Tennessee: *Tennessee Division of Geology Bulletin 55*.
- Roeder, D., and Witherspoon, W.D., 1978, Palinspastic map of east Tennessee: *American Journal of Science*, v. 278, p. 543-550.
- Romanek, C.S., Grossman, E.L., and Morse, J.W., 1992, Carbon isotopic fractionation in synthetic aragonite and calcite: Effects of temperature and precipitation rate: *Geochimica et Cosmochimica Acta*, v. 56, p. 419-430.
- Rowell, A.J., and Brady, M.J., 1976, Brachiopods and Biomeres: *Brigham Young University Geology Studies 23*, p. 165-180.
- Ruppel, S.C., and Cander, H.S., 1988, Dolomitization of shallow-water platform carbonates by sea water and seawater-derived brines: San Andres Formation (Guadalupian), west Texas, *in* Shukla, V., and Baker, P.B., eds., *Sedimentology and Geochemistry of Dolostones: SEPM Special Publication 43*, p. 245-262.

- Rush, P.F., and Chafetz, H.S., 1990, Fabric-retentive, non-luminescent brachiopods as indicators of original $\delta^{13}\text{C}$ and $\delta^{18}\text{O}$: a test: *Journal of Sedimentary Petrology*, v. 60, p. 968-981.
- Saller, A.H., 1984, Petrologic and geochemical constraints on the origin of subsurface dolomite, Enewetak Atoll: An example of dolomitization by normal seawater: *Geology*, v. 12, p. 217-220.
- Saller, A.H., 1986, Radial calcite in Lower Miocene strata, subsurface Enewetak Atoll: *Journal of Sedimentary Petrology*, v. 56, p. 743-762.
- Saller, A.H., and Moore, C.H., 1991, Geochemistry of meteoric calcite cements in some Pleistocene limestones: *Sedimentology*, v. 38, p. 601-621.
- Saltzman, M.R., 1996, Extinction and Environmental Change, Late Cambrian, Wyoming and Utah [Ph.D. Dissertation]: The University of California, Los Angeles, 169 p.
- Saltzman, M.R., Brasier, M.D., Ripperdan, R.L., Lohmann, K.C., and Runnegar, B., 1995a, A large and global positive carbon isotope excursion during the Late Cambrian: correlation with marine extinctions and sea-level fluctuations: *Geological Society of America Annual Meeting Abstracts with Programs*, v. 27, p. 331.
- Saltzman, M.R., Davidson, J.P., Holden, P., Runnegar, B., and Lohmann, K.C., 1995b, Sea-level-driven changes in ocean chemistry at an Upper Cambrian extinction horizon: *Geology*, v. 23, p. 893-896.
- Sandberg, P.A., 1983, An oscillating trend in Phanerozoic non-skeletal carbonate mineralogy: *Nature*, v. 305, p. 19-22.
- Sandberg, P.A., 1984, Recognition criteria for calcitized skeletal and non-skeletal aragonites: *Palaeontographica Americana*, v. 54, p. 272-281.
- Sandberg, P.A., 1985, Aragonite cements and their occurrence in ancient limestones, *in* Schneidermann, N., and Harris, P.M., eds., *Carbonate Cements: SEPM Special Publication 36*, p. 33-57.
- Sansone, F.J., Tribble, G.W., Andrews, C.C., and Chanton, J.P., 1990, Anaerobic diagenesis within Recent, Pleistocene, and Eocene marine carbonate frameworks: *Sedimentology*, v. 37, p. 997-1009.
- Sass, E., and Bein, A., 1988, Dolomites and salinity: A comparative geochemical study, *in* Shukla, V., and Baker, P.B., eds., *Sedimentology and Geochemistry of Dolostones: SEPM Special Publication 43*, p. 223-233.
- Schidlowski, M., and Aharon, P., 1992, Carbon cycle and carbon isotope record: Geochemical impact of life over 3.8 Ga of Earth history: *in* Schidlowski, M., et al. eds., *Early Organic Evolution: Implications for Mineral and Energy Resources: Springer-Verlag*, p. 147-175.
- Schlanger, S.O., Arthur, M.A., Jenkyns, H.C., and Scholle, P.A., 1987, The Cenomanian-Turonian oceanic anoxic event, I. Stratigraphy and distribution of organic carbon-rich beds and the marine $\delta^{13}\text{C}$ excursion, *in* Brooks, J., and Fleet, A.J., eds., *Marine Petroleum Source Rocks: Geological Society Special Publication 26*, p. 371-399.
- Schlager, W., 1981, The paradox of drowned reefs and carbonate platforms: *Geological Society of America Bulletin*, v. 92, p. 197-211.

- Schlager, W., 1991, Depositional bias and environmental change - important factors in sequence stratigraphy, *in* Biddle, K.T., and Schlager, W., eds., *The Record of Sea-Level Fluctuations: Sedimentary Geology*, v. 70, p. 109-130.
- Schlager, W., 1992, Sedimentology and sequence stratigraphy of reefs and carbonate platforms: American Association of Petroleum Geologists, Short Course 34, 71 p.
- Schlager, W., Reijmer, J.J.G., and Droxler, A., 1994, Highstand shedding of carbonate platforms: *Journal of Sedimentary Research*, v. B64, p. 270-281.
- Scholle, P.A., and Arthur, M.A., 1980, Carbon isotope fluctuations in Cretaceous pelagic limestones: potential stratigraphic and petroleum exploration tool: *American Association of Petroleum Geologists Bulletin*, v. 64, p. 67-87.
- Scholle, P.A., and Halley, R.B., 1985, Burial diagenesis: out of sight, out of mind!, *in* Schneidermann, N., and Harris, P.M., eds., *Carbonate Cements: SEPM Special Publication 36*, p. 309-334.
- Schroeder, J.H., 1972, Fabrics and sequences of submarine carbonate cements in Holocene Bermuda cup reefs: *Geologische Rundschau*, v. 61, p. 708-730.
- Scotese, C.R., and McKerrow, W.S., 1990, Revised world maps and introduction: *in* McKerrow, W.S., and Scotese, C.R., eds., *Palaeozoic Palaeogeography and Biogeography: Geological Society of London Memoir 12*, p. 1-24.
- Scruton, R.A., 1982a, Passive continental margins: A review of observations and mechanisms, *in* Scruton, R.A., ed., *Dynamics of Passive Margins: American Geophysical Union, Geodynamics Series*, v. 6, p. 5-11.
- Scruton, R.A., ed., 1982b, *Dynamics of Passive Margins: American Geophysical Union, Geodynamics Series*, v. 6.
- Semikhatov, M.A., Gebelein, C.D., Cloud, P., Awramik, S.M., and Benmore, W.C., 1979, Stromatolite morphogenesis: progress and problems: *Canadian Journal of Earth Science*, v. 16, p. 992-1014.
- Sepkoski, J.J., Jr., 1982, Flat-pebble conglomerates, storm deposits and the Cambrian bottom fauna, *in* Einsele, G., and Seilacher, A., eds., *Cyclic and Event Stratification: Springer-Verlag, New York*, p. 371-385.
- Shackleton, N.J., 1987, The carbon isotope record of the Cenozoic: history of organic carbon burial and of oxygen in the ocean and atmosphere, *in* Brooks, J., and Fleet, A.J., eds., *Marine Petroleum Source Rocks: Geological Society Special Publication 26*, p. 423-434.
- Shanmugam, G., and Walker, K.R., 1978, Tectonic significance of distal turbidites in the Middle Ordovician Blockhouse and lower Sevier formations in east Tennessee: *American Journal of Science*, v. 278, p. 551-578.
- Shanmugam, G., and Walker, K.R., 1980, Sedimentation, subsidence, and evolution of a foredeep basin in the Middle Ordovician, southern Appalachians: *American Journal of Science*, v. 280, p. 479-496.
- Shatkay, M., and Magaritz, M., 1987, Dolomitization and sulfate reduction in the mixing zone between brine and meteoric water in the newly exposed shores of the Dead Sea: *Geochimica et Cosmochimica Acta*, v. 51, p. 1135-1141.

- Sheppard, S.M.F., and Schwarcz, H.P., 1970, Fractionation of carbon and oxygen isotopes and magnesium between coexisting metamorphic calcite and dolomite: *Contributions to Mineralogy and Petrology*, v. 26, p.161-198.
- Sheridan, R.E., and Grow, J.A., eds., 1988, *The Atlantic Continental Margin: U.S.: Geological Society of America, The Geology of North America*, v. I-2, 610 p.
- Shukla, V., 1988, Sedimentology and geochemistry of a regional dolostone: correlation of trace elements with dolomite fabrics, *in* Shukla, V., and Baker, P.B., eds., *Sedimentology and Geochemistry of Dolostones: SEPM Special Publication 43*, p. 145-157.
- Sibley, D.F., 1990, Unstable to stable transformation during dolomitization: *Journal of Geology*, v. 98, p. 739-748.
- Sibley, D.F., and Gregg, J.M., 1987, Classification of dolomite rock textures: *Journal of Sedimentary Petrology*, v. 57, p. 967-975.
- Simmons, W.A., 1984, Stratigraphy and depositional environments of the Middle Cambrian Maryville Limestone (Conasauga Group) near Thorn Hill Tennessee [unpublished M.S. thesis]: The University of Tennessee, 275 p.
- Simms, M., 1984, Dolomitization by groundwater-flow systems in carbonate platforms: *Gulf Coast Association of Geological Societies Transactions*, v. 34, p. 411-420.
- Simpson, E.L., and Eriksson, K.A., 1989, Sedimentology of the Unicoi Formation in southern and central Virginia: Evidence for late Proterozoic to Early Cambrian rift-to-passive margin transition: *Geological Society of America Bulletin*, v. 101, p. 42-54.
- Simpson, J., 1985, Stylolite-controlled layering in an homogeneous limestone: pseudo-bedding produced by burial diagenesis: *Sedimentology*, v. 32, p. 495-505.
- Slaughter, M., and Hill, R.J., 1991, The influence of organic matter in organogenic dolomitization: *Journal of Sedimentary Petrology*, v. 61, p. 296-303.
- Sloss, L.L., 1991, The tectonic factor in sea level change: a countervailing view: *Journal of Geophysical Research*, v. 96, p. 6609-6617.
- Spirakis, C.S., and Heyl, A.V., 1988, Possible effects of thermal degradation of organic matter on carbonate paragenesis and fluorite precipitation in Mississippi Valley-type deposits: *Geology*, v. 16, p. 1117-1120.
- Spötl, C., and Burns, S.J., 1991, Formation of ^{18}O -depleted dolomite within a marine evaporitic sequence, Triassic Reichenhall Formation, Austria: *Sedimentology*, v. 38, p. 1041-1057.
- Srinivasan, K., 1993, Depositional history, sequence stratigraphy and diagenesis of Maryville Limestone (Middle Cambrian), southern Appalachians [unpublished Ph.D. thesis]: The University of Tennessee, Knoxville, 166 p.
- Srinivasan, K., and Walker, K.R., 1993, Sequence stratigraphy of an intrashelf basin carbonate ramp to rimmed platform transition: Maryville Limestone (Middle Cambrian), southern Appalachians: *Geological Society of America Bulletin*, v. 105, p. 883-896.
- Srinivasan, K., Walker, K.R., and Goldberg, S.A., 1994, Determining fluid source and possible pathways during burial dolomitization of Maryville Limestone (Cambrian), Southern Appalachians, USA: *Sedimentology*, v. 41, p. 293-308.

- Srinivasan, K., Walker, K.R., Steinhaff, D.M., Goldberg, S.A., and Riciputi, L.R., 1995, Radiogenic Sr isotopes and rare earth elements as indicators of burial fluid sources in platform carbonates: Revisited: Geological Society of America Annual Meeting, Abstracts with Programs, p. 273-274.
- Steckler, M.S., and Watts, A.B., 1982, Subsidence history and tectonic evolution of Atlantic-type continental margins, *in* Scrutton, R.A., ed., Dynamics of Passive Margins: American Geophysical Union, Geodynamics Series, v. 6, p. 184-196.
- Steckler, M.S., Reynolds, D.J., Coakley, B.J., Swift, B.A., and Jarrard, R., 1993, Modelling passive margin sequence stratigraphy, *in* Posamentier, H.W., Summerhayes, C.P., Haq, B.U., and Allen, G.P., eds., Sequence Stratigraphy and Facies Associations: International Associations of Sedimentologists Special Publication 18, p. 19-41.
- Stein, H.J., and Kish, S.A., 1985, The timing of ore formation in southeast Missouri: Rb-Sr glauconite dating at the Magmont Mine, Viburnum Trend: Economic Geology, v. 80, p. 739-753.
- Stephenson, R.A., 1989, Beyond first-order thermal subsidence models for sedimentary basins?, *in* Cross, T.A., ed., Quantitative Dynamic Stratigraphy: Prentice Hall, p. 113-125.
- Stiller, M., Rounick, J.S., and Shasha, S., 1985, Extreme carbon-isotope enrichments in evaporating brines: Nature, v. 316, p. 434-435.
- Stueber, A.M., Pushkar, P., and Hetherington, E.A., 1984, A strontium isotopic study of Smackover brines and associated solids, southern Arkansas: Geochimica et Cosmochimica Acta, v. 48, p. 1637-1649.
- Stueber, A.M., Pushkar, P., and Hetherington, E.A., 1987, A strontium isotopic study of formation waters from the Illinois Basin, U.S.A.: Applied Geochemistry, v. 2, p. 477-494.
- Stueber, A.M., and Walter, L.M., 1991, Origin and chemical evolution of formation waters from Silurian-Devonian strata in the Illinois basin, U.S.A.: Geochimica et Cosmochimica Acta, v. 55, p. 309-325.
- Summerhayes, C.P., 1986, Sea level curves based on seismic stratigraphy: their chronostratigraphic significance: Palaeogeography, Palaeoclimatology, Palaeoecology, v. 57, p. 27-42.
- Sun, S.Q., 1990, Facies-related diagenesis in a cyclic shallow marine sequence: The Corallian Group (Upper Jurassic) of the Dorset coast, southern England: Journal of Sedimentary Petrology: v. 60, p. 42-52.
- Sverjensky, D.A., 1981, The origin of a Mississippi Valley-type deposit in the Viburnum Trend, southeast Missouri: Economic Geology, v. 76, p. 1848-1872.
- Tankard, A.J., and Balkwill, H.R., eds., 1989, Extensional Tectonics and Stratigraphy of the North Atlantic Margins: American Association of Petroleum Geologists Memoir 49, 641 p.
- Tarkoy, P.J., 1967, Lithostratigraphy and petrography of the Upper Cambrian Maynardville Formation within the Hunter Valley fault belt of East Tennessee [unpublished M.S. thesis]: The University of Tennessee, Knoxville, 99 p.

- Tarkoy, P.J., 1970, Upper Cambrian Maynardville Formation within the Clinchport fault belt of east Tennessee: *Transactions of the Illinois State Academy of Science*, v. 63, p. 305-318.
- Taylor, T.R., and Sibley, D.F., 1986, Petrographic and geochemical characteristics of dolomite types and the origin of ferroan dolomite in the Trenton Formation, Ordovician, Michigan Basin: *Sedimentology*, v. 33, p. 61-86.
- Thickpenny, A., and Leggett, J.K., 1987, Stratigraphic distribution and palaeo-oceanographic significance of European early Palaeozoic organic-rich sediments, in Brooks, J., and Fleet, A.J., eds., *Marine Petroleum Source Rocks: Geological Society Special Publication 26* p. 231-247.
- Thomas, W.A., 1977, Evolution of Appalachian-Ouachita salients and recesses from reentrants and promontories in the continental margin: *American Journal of Science*, v. 277, p. 1233-1278.
- Thomas, W.A., 1983, Continental margins, orogenic belts, and intracratonic structures: *Geology*, v. 11, p. 270-272.
- Thomas, W.A., 1986, A Paleozoic synsedimentary structure in the Appalachian fold-thrust belt in Alabama, in McDowell, R.C., and Glover, L., III, eds., *The Lowry Volume: Studies in Appalachian Geology: Virginia Tech Department of Geological Sciences Memoir 3*, p. 1-12.
- Thomas, W.A., 1991, The Appalachian-Ouachita rifted margin of southeastern North America: *Geological Society of America Bulletin*, v. 103, p. 415-431.
- Thomas, W.A., 1993, Low-angle detachment geometry of the late Precambrian-Cambrian Appalachian-Ouachita rifted margin of southeastern North America: *Geology*, v. 21, p. 921-924.
- Thompson, J.B., and Ferris, F.G., 1990, Cyanobacterial precipitation of gypsum, calcite, and magnesite from natural alkaline lake water: *Geology*, v. 18, p. 995-998.
- Tobin, K.J., Walker, K.R., Srinivasan, K., and Steinhauß, D.M., 1996, Suboxic to anoxic diagenesis of platform-marginal ooids and bladed-to-fibrous calcite from the Middle Ordovician Ottosee Formation (east Tennessee): *Geological Society of America Bulletin*, v. 108, p. 155-167.
- Tribble, G.W., 1993, Organic matter oxidation and aragonite diagenesis in a coral reef: *Journal of Sedimentary Petrology*, v. 63, p. 523-527.
- Tribble, J.S., Arvidson, R.S., Lane, M., III, and Mackenzie, F.T., 1995, Crystal chemistry, and thermodynamic and kinetic properties of calcite, dolomite, apatite, and biogenic silica: applications to petrologic problems: *Sedimentary Geology*, v. 95, p. 11-37.
- Tucker, M.E., and Wright, V.P., 1990, *Carbonate Sedimentology*: Blackwell Scientific, Boston, 482 p.
- Turcotte, D.L., 1982, The state of stress at passive continental margins, in Scrutton, R.A., ed., *Dynamics of Passive Margins: American Geophysical Union, Geodynamics Series*, v. 6, p. 141-146.
- Turner, J.V., 1982, Kinetic fractionation of carbon-13 during calcium carbonate precipitation: *Geochimica et Cosmochimica Acta*, v. 46, p. 1183-1191.

- Ulrich, E.O., 1911, Revision of the Paleozoic systems: Geological Society of America Bulletin, v. 22. p.281-680.
- Vahrenkamp, V.C., 1996, Carbon isotope stratigraphy of the Upper Kharaib and Shuaiba Formations: Implications for the Early Cretaceous evolution of the Arabian Gulf Region: American Association of Petroleum Geologists, v. 80, p. 647-662.
- Vahrenkamp, V.C., and Swart, P.K., 1990, New distribution coefficient for the incorporation of strontium into dolomite and its implications for the formation of ancient dolomites: *Geology*, v. 18, p. 387-391.
- Vail, P.R., Mitchum, R.M., Jr., and Thompson, S., III, 1977, Seismic stratigraphy and global changes of sea level, Part 4: Global cycles of relative changes of sea level, *in* Payton, C.E., ed., *Seismic Stratigraphy - Applications to Hydrocarbon Exploration*: American Association of Petroleum Geologists Memoir 26, p. 83-97.
- Vail, P.R., Van Wagoner, J.C., Mitchum, R.M., Jr., and Posamentier, H.W., 1987, Seismic stratigraphy interpretation using sequence stratigraphy, *in* Bally, A.W., ed., *Atlas of Seismic Stratigraphy*, v. 1: American Association of Petroleum Geologists, *Studies in Geology* 27, p. 1-14.
- VanArsdall, D.E., 1974, Lithostratigraphy of the Conasauga Group within the Hunter Valley and Copper Creek strike belts, northeastern Tennessee [unpublished M.S. thesis]: Eastern Kentucky University, Richmond, Kentucky.
- Van Wagoner, J.C., Posamentier, H.W., Mitchum, R.M., Vail, P.R., Sarg, J.F., Loutit, T.S., and Hardenbol, J., 1988, An overview of the fundamentals of sequence stratigraphy and key definitions, *in* Wilgus, C.K., Hastings, B.S., Kendall, C.G.St.C., Posamentier, H.W., Ross, C.A., and Van Wagoner, J.C., eds., *Sea-Level Changes: An Integrated Approach*: SEPM Special Publication 42, p. 39-45.
- Veizer, J., 1983, Trace elements and isotopes in sedimentary carbonates, *in* Reeder, R.J., ed., *Carbonates: Mineralogy and Chemistry: Reviews in Mineralogy*, v. 11, p. 265-299.
- Veizer, J., 1985, Carbonates and ancient oceans: Isotopic and chemical record on time scales of 10^7 - 10^9 years, *in* Sundquist, E.T., and Broecker, W.S., eds., *The Carbon Cycle and Atmospheric CO₂*: American Geophysical Union Monograph 32, p. 595-601.
- Veizer, J., 1992, Depositional and diagenetic history of limestones: stable and radiogenic isotopes, *in* Clauer, N., and Chaudhuri, S., eds., *Isotopic Signatures and Sedimentary Records*: Springer-Verlag, New York, p. 13-48.
- Vincent, E., and Berger, W.H., 1985, Carbon dioxide and polar cooling in the Miocene: the Monterey hypothesis, *in* Sundquist, E.T., and Broecker, W.S., eds., *The Carbon Cycle and Atmospheric CO₂*: American Geophysical Union Monograph 32, p. 455-468.
- Wada, H., and Suzuki, K., 1983, Carbon isotopic thermometry calibrated by dolomite-calcite solvus temperatures: *Geochimica et Cosmochimica Acta*, v. 47, p. 697-706.
- Wallace, M.W., 1990, Origin of dolomitization in the Devonian carbonates on the Barrow Terrace, Canning basin, Western Australia: *Sedimentology*, v. 37, p. 105-122.

- Walker, K.R., 1980, Introduction to the stratigraphy and paleoenvironments of the Middle Ordovician of Tennessee (southern Appalachians, U.S.A.), *in* Walker, K.R., Broadhead, T.W., and Keller, F.B., eds., Middle Ordovician carbonate shelf to deep water basin deposition in the southern Appalachians: The University of Tennessee, Studies in Geology 4, p. 4-12.
- Walker, K.R., ed., 1985, The geologic history of the Thorn Hill Paleozoic section (Cambrian - Mississippian), eastern Tennessee: The University of Tennessee, Studies in Geology 10, 128 p.
- Walker, K.R., 1989, Petrographic criteria for interpreting the origin of pore-fillings, *in* Walker, K.R., ed., The Fabric of Cements in Paleozoic Limestones: The University of Tennessee, Studies in Geology 20, p. 4-10.
- Walker, K.R., Foreman, J.L., and Srinivasan, K., 1990, The Cambrian Conasauga Group of Eastern Tennessee: A preliminary general stratigraphic model with a more detailed test for the Nolichucky Formation: Appalachian Basin Industrial Associates, v. 17, p. 184-189.
- Walker, K.R., Jernigan, D.G., and Weber, L.J., 1990, Petrographic criteria for the recognition of marine, syntaxial overgrowths and their distribution in geologic time: Carbonates and Evaporites, v. 5, p. 141-152.
- Walker, K.R., Shanmugam, G., and Ruppel, S.C., 1983, A model for carbonate to terrigenous clastic sequences: Geological Society of America, Bulletin, v. 94, p. 700-712.
- Walter, L.M., and Burton, E.A., 1990, Dissolution of recent platform carbonate sediments in marine pore fluids: American Journal of Science, v. 290, p. 601-643.
- Walter, M.R., 1977, Interpreting stromatolites: American Scientist, v. 65, p. 563-571.
- Walter, M.R., and Heys, G.R., 1985, Links between the rise of the Metazoa and the decline of stromatolites: Precambrian Research, v. 29, p. 149-174.
- Walters, L.J., Claypool, G.E., and Choquette, P.W., 1972, Reaction rates and δO^{18} variation for the carbonate-phosphoric acid preparation method: Geochimica et Cosmochimica Acta, v. 36, p. 129-140.
- Wang, K., Geldsetzer, H.H.J., Goodfellow, W.D., and Krouse, H.R., 1996, Carbon and sulfur isotope anomalies across the Frasnian-Famenian extinction boundary, Alberta, Canada: Geology, v. 24, p. 187-191.
- Wang, K., Orth, C.J., Strep, M., Jr., Chatterton, B.D.E., Wang, X., and Li, J., 1993, The great latest Ordovician extinction on the South China Plate: Chemostratigraphic studies of the Ordovician-Silurian boundary interval on the Yangtze Platform: Palaeogeography, Palaeoclimatology, Palaeoecology, v. 104, p. 61-79.
- Wanless, H.R., 1979, Limestone response to stress: pressure solution and dolomitization: Journal of Sedimentary Petrology, v. 49, p. 437-462.
- Ward, W.C., and Halley, R.B., 1985, Dolomitization in a mixing zone of near-seawater composition, Late Pleistocene, northeastern Yucatan Peninsula: Journal of Sedimentary Petrology, v. 55, p. 407-420.
- Warne, J.E., and Schneidermann, N., 1983, Patch-reef cementation: Holocene of Enewetak Atoll and Jurassic of Morocco (abstract): American Association of Petroleum Geologists Bulletin, v. 67, p. 566.

- Watts, A.B., 1981, The U.S. Atlantic continental margin: Subsidence history, crustal structure, and thermal evolution, *in* *Geology of Passive Continental Margins: History, Structure, and Sedimentologic Record (with Special Emphasis on the Atlantic Margin)*: American Association of Petroleum Geologists, Education Course Note Series 19, 75 p.
- Watts, A.B., 1982, Tectonic subsidence, flexure, and global changes in sealevel: *Nature*, v. 297, p. 469-474.
- Watts, A.B., and Thorne, J., 1984, Tectonics, global changes in sea level and their relationship to stratigraphical sequences at the US Atlantic continental margin: *Marine and Petroleum Geology*, v. 1., 319-339.
- Webb, E.J., 1980, Cambrian sedimentation and structural evolution of the Rome trough in Kentucky [unpublished Ph.D. thesis]: The University of Cincinnati, Ohio, 98 p.
- Weber, L.J., 1988, Paleoenvironmental analysis and test of stratigraphic cyclicity in the Nolichucky Shale and Maynardville Limestone (Upper Cambrian) in central East Tennessee [unpublished Ph.D. thesis]: The University of Tennessee, Knoxville, 389 p.
- Weiss, C.P., and Wilkinson, B.H., 1988, Holocene cementation along the central Texas coast: *Journal of Sedimentary Petrology*, v. 58, p. 468-478.
- Weissert, H., 1989, C-isotope stratigraphy, a monitor of paleoenvironmental change: A case study from the early Cretaceous: *Surveys in Geophysics*, v. 10, p. 1-61.
- Wickham, S.M., and Peters, M.T., 1993, High $\delta^{13}\text{C}$ Neoproterozoic carbonate rocks in western North America: *Geology*, v. 21, p. 165-168.
- Wiggins, W.D., 1986, Geochemical signatures in carbonate matrix and their relation to deposition and diagenesis, Pennsylvanian Marble Falls Limestone, Central Texas: *Journal of Sedimentary Petrology*, v. 56, p. 771-783.
- Wilde, P., and Berry, W.B.N., 1984, Destabilization of the oceanic density structure and its significance to marine "extinction" events: *Palaeogeography, Palaeoclimatology, Palaeocology*, v. 48, p. 143-162.
- Wilde, P., and Berry, W.B.N., 1986, The role of oceanographic factors in the generation of global bio-events, *in* Walliser, O.H., ed., *Global Bio-Events: Lecture Notes in Earth Sciences*, v. 8., p. 75-91.
- Wilkerson, M.S., and Hsui, A.T., 1989, Application of sediment backstripping corrections for basin analysis using microcomputers: *Journal of Geological Education*, v. 37, p. 337-340.
- Wilkinson, B.H., Diedrich, N.W., and Drummond, C.N., 1996, Facies successions in peritidal carbonate sequences: *Journal of Sedimentary Research*, v. 66, p. 1065-1078.
- Wilkinson, B.H., Janecke, S.U., and Brett, C.E., 1982, Low-magnesian calcite marine cement in Middle Ordovician hardgrounds from Kirkfield, Ontario: *Journal of Sedimentary Petrology*, v. 52, p. 47-57.
- Wilkinson, B.H., Owen, R.M., and Carroll, A.R., 1985, Submarine hydrothermal weathering, global eustacy, and carbonate polymorphism in Phanerozoic marine oolites: *Journal of Sedimentary Petrology*, v. 55, p. 171-183.

- Williams, H., and Hiscott, R.N., 1987, Definition of the Iapetus rift-drift transition in western Newfoundland: *Geology*, v. 15, p. 1044-1047.
- Williams, L.A., and Crerar, D.A., 1985, Silica diagenesis, II. General mechanisms: *Journal of Sedimentary Petrology*, v. 55, p. 312-321.
- Winter, B.L., and Knauth, L.P., 1992, Stable isotope geochemistry of carbonate fracture fills in the Monterey Formation, California: *Journal of Sedimentary Petrology*, v. 62, p. 208-219.
- Woo, K.S., Anderson, T.F., and Sandberg, P.A., 1993, Diagenesis of skeletal and nonskeletal components of Mid-Cretaceous limestones: *Journal of Sedimentary Petrology*, v. 63, p. 18-32.
- Yang, W., Harmsen, F., and Kominz, M.A., 1995, Quantitative analysis of a cyclic peritidal sequence, the Middle and Upper Devonian Lost Burro Formation, Death Valley, California—a possible record of Milankovitch climatic cycles: *Journal of Sedimentary Research*, v. B65, p. 306-322.
- Zenger, D.H., 1983, Burial dolomitization in the Lost Burro Formation (Devonian), east-central California, and the significance of late diagenetic dolomitization: *Geology*, v. 11, p. 519-522.
- Zenger, D.H., and Dunham, J.B., 1988, Dolomitization of Siluro-Devonian limestones in a deep core (5,350 m), southeastern New Mexico, *in* Shukla, V., and Baker, P.B., eds., *Sedimentology and Geochemistry of Dolostones*: SEPM Special Publication 43, p. 161-173.

APPENDICES

APPENDIX A

DESCRIPTION OF STRATIGRAPHIC SECTIONS

This appendix contains detailed descriptions of measured stratigraphic intervals (Figs. 1.4, 2.1). All measured intervals or units, and collected samples are shown on detailed stratigraphic columns. Each stratigraphic column is accompanied by a description of individual units containing:

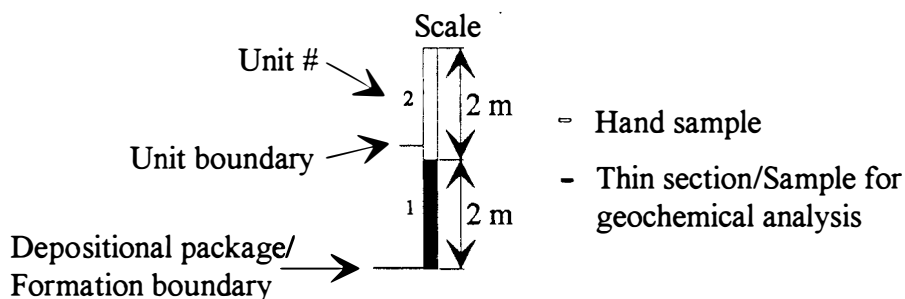
Unit # - corresponds to the division of a measured stratigraphic succession into units as indicated on each stratigraphic column.

T (m) - thickness of individual unit in meters.

C.T. (m) - cumulative thickness of measured stratigraphic succession.

Description - contains the lithologic content, layer thickness, characteristics of the layer boundaries, color, sedimentary structure, weathering pattern, and/or any other characteristic feature. Samples collected are listed in ascending stratigraphic order within each unit. Samples in bold denote samples for which petrographic thin sections were made. Geochemical data also exist for some of these samples (see Appendices B and C). The exact stratigraphic position of each sample is indicated on the stratigraphic columns.

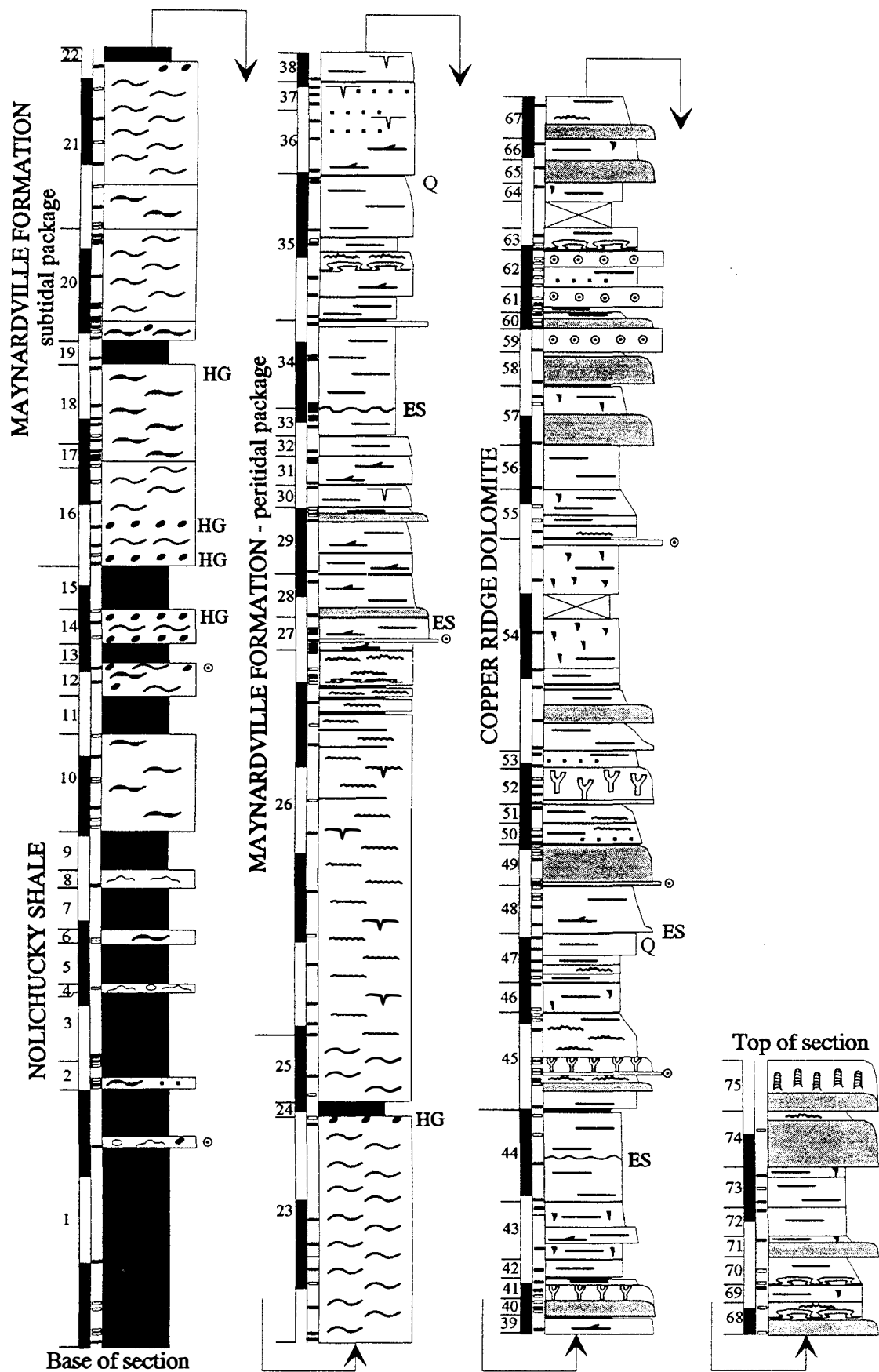
Explanation for Stratigraphic Columns



	Shale
	Ribbon rock without shale
	Ribbon rock with shale
	Fossiliferous-peloidal packstone/grainstone
	Oolite
	Dolomitized mudstone/Fine-grained couplets
	Medium-grained couplets
	Coarse-grained couplets
	Calcareous siltstone
	Thrombolite
	Digitate stromatolite
	Columnar stromatolite
	Stacked hemispheroidal (SH) stromatolite
	Laterally linked hemispheroidal (LLH) stromatolite
	Microbial laminate (Stratiform stromatolite)
	Covered interval
	Intraclasts (Flat pebbles)
	Ooids
	Bioturbation (Burrows)
	Desiccation cracks (Mudcracks)
ES	Exposure surface
HG	Hardground
Q	Quartz sand grains

For additional explanations see descriptions of individual units, and Tables 2.1 and 2.2.

Figure A.1. Stratigraphic column measured at the Thorn Hill outcrop.



The Thorn Hill Outcrop (TH)

The Thorn Hill outcrop is located along U.S. Highway 25E, in Grainger County, approximately 4 miles northwest of the Clinch Mountain Outlook. The exposure dips 45° to the southeast and is a part of the Thorn Hill stratigraphic section contained within the Copper Creek thrust block. The Thorn Hill section represents one of the most complete and best exposed Paleozoic sedimentary successions in the southern Appalachians, ranging from the Lower Cambrian Rome Formation to the Lower Mississippian Grainger Formation (Walker 1985). As first noted by Hall and Amick in 1934, the Thorn Hill locality probably contains the best exposure of both the Maynardville Formation and the Knox Group in this part of the southern Appalachians. The measured stratigraphic interval includes the uppermost 18.4 m of the underlying Nolichucky Shale, the complete Maynardville Formation (47.55 m), and the lowermost 30.5 m of the overlying Copper Ridge Dolomite of the Knox Group.

Unit	T (m)	C.T. (m)	Description
			Nolichucky Shale
1	6.0	6.0	Started measuring at the first better exposed shale interval of the Nolichucky Shale. Paper-laminated, light gray, calcareous shale with occasionally interbedded laterally extensive, moderately to extensively weathered, individual skeletal (trilobite and brachiopod) wackestone to grainstone layers. These layers have wavy lower and upper bedding planes and they range in thickness from 1 to 4 cm. In the upper part of the unit, there is a 30 cm thick packstone/grainstone layer with common skeletal fragments, micritic intraclasts (flat-pebbles) and ooids. Interbedded with shale are also laterally discontinuous argillaceous mudstone nodules variably weathered. Samples: N0.4(-18.85) (skeletal packstone/wackestone), N0.6 and N0.7 (skeletal packstone/grainstone), N1.2 (very weathered coarse-grained skeletal limestone), N1.4 (carbonate nodule), N2.3(-16.95) (skeletal packstone/grainstone with some intraclasts), N4.9(-14.35) .
2	0.6	6.6	Lowermost part of the unit is composed of 4-5 cm thick, weathered carbonate layers separated by thin argillaceous siltstone layers and overlain by thicker shale. Wavy layer planes give a characteristic ribbon appearance to this basal part. The carbonate layers are represented by skeletal (trilobite) wackestone/grainstone with occasional flat-pebbles (up to 5-6 cm long). The uppermost 5 cm of the unit consist of a weathered carbonaceous siltstone layer overlain by nodular mudstone. Samples: N6.3A, N6.3B(-12.95) , N6.3C, N6.3D, N6.85A, N6.85B.

- | | | | |
|----|------|-------|--|
| 3 | 1.7 | 8.3 | The base of the unit is a very weathered carbonaceous siltstone layer, 2-3 cm thick. Rare nodular mudstone with incorporated pockets of skeletal packstone/wackestone and scattered pyrite occurs in the lower part of the unit. The rest is composed of calcareous, light gray shale. Samples: N6.9 (carbonaceous siltstone), N7.1(-12.15) (nodule). |
| 4 | 0.2 | 8.5 | Skeletal (trilobite) packstone/grainstone layer. Sample: N-10.55. |
| 5 | 1.0 | 9.5 | Calcareous shale. |
| 6 | 0.3 | 9.8 | Ribbon limestone composed of fine-grained horizontally laminated, weathered packstone/grainstone interbedded with a more coarse-grained skeletal (trilobites and some phosphatic brachiopods) packstone/grainstone and dark gray argillaceous layers. Samples: N-9.45A, N-9.45B. |
| 7 | 1.0 | 10.8 | Calcareous shale. |
| 8 | 0.35 | 11.15 | The unit consists of two skeletal (trilobite) packstone/grainstone layers. Sample: N-8.15. |
| 9 | 0.9 | 12.05 | Calcareous shale. |
| 10 | 2.5 | 14.55 | Ribbon limestone composed of carbonate layers interbedded with common shale. Layer thickness: 2-5 cm. Carbonate layers include skeletal and peloidal wackestone/grainstone and less common mudstone layers and lenses. Skeletal fragments include trilobites and phosphatic brachiopods. Common clay seams and horizontally laminated argillaceous dolomitic layers. Scattered framboidal pyrite present. Samples: N-6.75, N-6.55, N-6.25, N-5.6, N-5.5, N-5.0, N-4.5. |
| 11 | 0.9 | 15.45 | Calcareous shale. |
| 12 | 0.8 | 16.1 | Ribbon limestone with common interbedded shale in the lower part. Carbonate layers are composed of medium to dark gray mudstone and flat-pebble conglomerate layers interbedded with skeletal wackestone/grainstone layers. Uppermost 15 cm composed of one layer with coarse flat-pebbles (up to 7 - 8 cm long) in the lower part grading upward into ooid-skeletal packstone/grainstone. Common framboidal pyrite. Samples: N-3.3, N-2.8. |
| 13 | 0.45 | 16.55 | Calcareous shale. |

- | | | | |
|-------------------------------|------|-------|--|
| 14 | 0.85 | 17.4 | Ribbon limestone with very little shale incorporated. Carbonate layers include mudstone layers with truncated tops, and peloidal-skeletal wackestone/grainstone. Mudstone layers have nodular appearance in places. Many layers are bioturbated. Scattered framboidal pyrite present. Base of the unit is composed of 15 cm thick flat-pebble conglomerate layer. A similar layer marks the top of the unit. Hardground development is evidenced by the presence of pyrite/Fe-oxide coated pebbles (micritic intraclasts). Inverse grading suggests debris flow. Samples: N-2.1, N-1.75 , N-1.5. |
| 15 | 1.0 | 18.4 | Calcareous shale at the top of the Nolichucky Shale. |
| Maynardville Formation | | | |
| 16 | 2.3 | 20.7 | Base of the Maynardville defined as the first thicker carbonate unit above the Nolichucky Shale. Ribbon rock composed of cm-size medium to dark gray limestone layers interbedded with light gray to brownish argillaceous dolostone. Carbonate layers are both laterally discontinuous (nodular) and continuous, and are composed of burrow mottled mudstone, and skeletal (trilobite, inarticulate and articulate brachiopods) wackestone/packstone. Carbonate layers have wavy, undulatory, truncational boundaries. Individual, up to 10 cm thick, intraclastic packstone/grainstone (flat-pebble conglomerate with pebbles up to 5 cm in diameter) layers present. Hardground development on these layers is indicated by pyrite coating on intraclasts. Pyrite is common in the basal 5-10 cm of the unit. Upper boundary at the first thin shale layer. Samples: TH-0.4 , TH-0.2, TH0.0 , TH0.55 , TH1.1 , TH1.5. |
| 17 | 0.65 | 21.35 | Very weathered and poorly exposed. Lower part consists of shale-free ribbon rocks (similar to Unit 16) that grade upward into ribbon rocks comprised of carbonate layers interbedded with calcareous shale. Amount of shale increases upward. Carbonate layers composed of burrow-mottled mudstone and skeletal wackestone/grainstone. Horizontal and cross- lamination visible. Samples: TH1.8, TH2.15 , TH2.20 , TH2.35 . |
| 18 | 1.9 | 23.25 | Ribbon rock composed of carbonate layers interbedded with calcareous shale and siltstone. Carbonate layers are dominated by skeletal packstone/grainstone that occasionally grade upward into laminated and burrowed mudstone with common truncational upper boundaries. Micritic intraclasts are incorporated in the bases of some of the layers. Upper boundary of the unit is marked by a pyrite crust. Samples: TH 2.15 , TH2.2 , TH2.35 , TH2.55 , TH2.65 , TH2.85 , TH.3.0 , TH3.35 , TH4.2 . |

- | | | | |
|----|------|-------|---|
| 19 | 0.5 | 23.75 | Dark gray shale with one 5-6 cm thick carbonate layer interbedded in the lower part. The layer consists of skeletal packstone/ grainstone and is characterized by a wavy lower and a planar upper boundary. Sample: TH4.45 . |
| 20 | 2.65 | 26.4 | Lower part composed of carbonate layers interbedded with silty shale. The amount of shale decreases upward. Upper part consists of horizontally and cross-laminated calcareous siltstone layers interbedded with argillaceous dolostone, mudstone and skeletal packstone/grainstone layers. Upper boundary marked by 5 cm thick shale layer. Poorly exposed part of the outcrop. Samples: TH4.9 , TH5.05 , TH5.2 , TH5.3 , TH5.35 , TH5.4 , TH5.65 , TH5.7 , TH6.4 , TH7.2 , TH7.3 , TH7.35 . |
| 21 | 3.9 | 30.3 | Lower 80 cm composed of laminated silty carbonate layers and calcareous siltstone interbedded with shale. Upper part lacks shale and consists of skeletal wackestone/packstone interbedded with horizontally and cross- laminated calcareous siltstone and argillaceous dolostone. Scattered pyrite present. Uppermost part of the unit is very poorly exposed. Samples: TH7.5 , TH7.55 , TH8.0 , TH8.5 , TH9.0 , TH9.5 , TH10.05 , TH10.7 , TH11.3 . |
| 22 | 0.35 | 30.65 | Light gray calcareous shale. Two carbonate layers with a maximum thickness of 2.5 cm incorporated within the shale. Carbonate layers are characterized with skeletal lag bases and laminated muddy upper parts. |
| 23 | 5.2 | 35.85 | Ribbon rocks composed of medium to dark gray limestone layers interbedded with light brownish argillaceous dolostone. Limestone layers include some skeletal wackestone/packstone layers in the lower part of the unit. Upper part of the unit is dominated by mudstone layers with some bioturbation and horizontal lamination visible. Scattered pyrite present. Top of the unit is marked by a intraclastic lag deposit with pyrite/Fe-oxide coated intraclasts. Samples: TH11.75 , TH11.9 , TH12.6 , TH13.25 , TH13.45 , TH14.0 , TH14.65 , TH16.75 , TH16.9 . |
| 24 | 0.3 | 36.15 | Shale with some incorporated isolated lenses/nodules composed of carbonate mudstone. |
| 25 | 1.5 | 37.65 | Ribbon rocks with gradational transition upward into microbially laminated deposits (microbial laminates or stratiform stromatolites). Limestone layers of ribbon rocks are primarily mudstone layers, |

some of which are horizontally laminated. Less commonly skeletal and intraclastic wackestone/packstone lag deposits are present in the bases of limestone layers. Samples: TH17.45, **TH17.85**.

- | | | | |
|----|------|-------|--|
| 26 | 9.0 | 46.65 | Microbially laminated deposits. Prominent horizontal wavy, crinkly lamination. Mud-cracks and small fenestrae filled with sparite present. The abundance of dolomicritic laminae increases upward. Thin (3-7 cm) shale layers present in the upper part. The uppermost part of the unit composed of SH and LLH stromatolites. Top is sharp, planar, and marked by a 2 cm thick shale. Samples: TH18.8, TH19.1, TH19.6, TH20.5, TH21.2, TH22.2, TH23.45, TH24.35, TH25.55, TH26.0, TH26.6, TH27.0, TH27.1, TH27.2, TH27.4, TH27.7. |
| 27 | 0.85 | 47.5 | Coarse-grained mechanical laminates or couplets. Individual couplets are up to 20 cm thick and are composed of coarse, basal intraclastic deposits grading upward into mudstone. Couplet tops are commonly truncated. Horizontal and cross-lamination visible. Light gray, entirely dolomitized. A single silicified oolitic layer (6-7 cm thick) is present in the lower part. Common stylolites. Upper contact is a sharp, wavy surface with 10-15 cm of erosional relief and a 2-3 cm thick shale. Samples: TH27.8, TH27.9, TH28.0, TH28.2, TH28.35. |
| 28 | 1.0 | 48.5 | Thrombolite in the lower 30 cm. Dark gray, massive appearance. Some voids with sparite present. Top of the thrombolitic layer is sharp and wavy. Upper part of the unit is composed of medium gray, dolomitized, medium-grained couplets with some horizontal and cross-lamination visible. Common stylolites. Upper contact is sharp, slightly wavy, and marked by 2-3 cm thick shale. Samples: TH28.6, TH29.3. |
| 29 | 1.4 | 49.9 | Medium-grained couplets. Light to medium gray, dolomitized. Horizontal lamination visible. Planar to slightly wavy couplet contacts with minor evidence for scouring and truncation. A thin (2 cm) shale layer present at 40 cm above the base of the unit. Laterally discontinuous, maximum 10-15 cm thick thrombolitic layer is present near the unit top. Upper unit contact is sharp, wavy, and marked by a 4 cm thick carbonaceous siltstone and shale. Samples: TH29.6, TH30.7, TH30.85, TH30.9, TH30.95. |
| 30 | 0.5 | 50.4 | Medium to fine-grained couplets. Medium to dark gray, dolomitized. No prominent lamination visible. Voids occluded with sparite and some stylolites present. Unit top is a weathered, |

wavy surface with a 3 cm thick shale. Sample: **TH31.4**.

- | | | | |
|----|------|-------|---|
| 31 | 0.7 | 51.1 | Medium to fine-grained couplets. Medium to dark gray. Parts have common vugs partially filled with sparite. Common stylolites. Faint horizontal and cross-lamination visible. Upper unit contact is sharp, planar, with very thin (< 1 cm) weathered shale. Samples: TH31.5, TH32.05, TH32.1 . |
| 32 | 0.5 | 51.6 | Medium to fine-grained couplets. Medium gray. Individual couplets are not laterally continuous. Common stylolites. Layer thickness: 2-3 cm, with a maximum of 10 cm. Upper unit contact is sharp, planar, and marked by 2 cm thick shale. Samples: TH32.3 . |
| 33 | 0.75 | 52.35 | Fine-grained couplets. Light to medium gray. Common stylolites. Some horizontal lamination visible. Upper unit contact is a very prominent, sharp surface with up to 20 cm of erosional relief and about 3-4 cm of shaly interval on topographic highs with some associated sphalerite. Vuggy porosity, with voids partially filled with calcite cement, present immediately below the erosional surface. Samples: TH32.9, TH33.1B, TH33.1T, TH33.55 . |
| 34 | 2.1 | 54.45 | Fine-grained couplets to dolomitized mudstone. Light to medium gray. Common stylolites. Base contains deformed (brecciated and fractured) dark gray grainstone deposits infilling topographic lows of the underlying erosional surface. These deposits contain dolomitized angular micritic clasts, some chert fragments and silica cement. Uppermost part of the unit contains coarse-grained couplets with intraclastic bases. Upper unit contact is sharp, planar, with about a 5 cm thick shale interval interbedded with up to 1.5 cm thick carbonaceous siltstone layers. Samples: TH33.4, TH33.45, TH34.6, TH34.65, TH35.4 . |
| 35 | 3.45 | 57.9 | Fine-grained couplets to dolomitized mudstone with occasional medium-grained couplets, SH and LLH stromatolites in the lower part. Upper part composed of fine- to medium-grained couplets with some quartz sand grains incorporated near the top of the unit. Several thin calcareous shale layers present throughout the unit. Vuggy porosity related to evaporite dissolution common in parts of the unit. Some horizontal lamination and mud-cracks visible, as well as cross-lamination in the bases of medium-grained couplets. Upper unit contact is a prominent wavy surface marked by 1 cm thick shale. Samples: TH35.6, TH36.15, TH36.55, TH37.35, TH37.4, TH37.6, TH38.7, TH38.85 . |

- 36 1.4 59.3 Medium-grained couplets grading upward into calcareous siltstone. Prominent horizontal lamination, including less common microbial laminae. Some cross-lamination visible. Bioturbation and mud-cracks present as well as small voids (fenestrae and burrows) filled with sparite. Upper unit contact is gradational. Samples: **TH39.05**, **TH39.75**, **TH40.25**.
- 37 0.75 60.05 Calcareous siltstone. Light gray. Horizontally and cross-laminated. Trace-fossils (horizontal burrows) visible along bedding planes. Mud-cracks present. Some sandy (calcarenite) layers present near the unit base. Upper unit contact is sharp, planar and marked with thin shale. Samples: **TH40.65**, **TH40.75**, **TH40.95**.
- 38 0.75 60.8 Medium-grained couplets with light gray basal parts and darker gray micritic upper parts. Couplet thickness ranges from 1 cm to maximum 10 cm, and it decreases upward with concomitant increase in the thickness of basal grainy portions. Couplet bases are sharp, planar to slightly wavy, truncational. Horizontal and cross-lamination as well as bioturbation visible. Mud-cracks present along upper bedding planes in the uppermost part of the unit. Upper unit contact is sharp, marked by 3 cm thick calcareous shale and siltstone. Sample: **TH41.15**.
- 39 0.4 61.2 Medium- to coarse-grained couplets. Cross-laminated couplet bases overlain by horizontally laminated upper micritic parts. Basal portions of couplets are up to 10 cm thick and have sharp planar to slightly wavy, truncational bases. Micritic portions are much thinner, laterally discontinuous and in places truncated. Light to medium gray. Upper unit contact is sharp, planar and marked by a very thin (<1 cm) highly weathered shale. Sample: **TH41.9**.
- 40 0.4 61.6 Thrombolite. Dark gray. Massive appearance. Common vuggy porosity in the lower third of the unit. Upper unit contact is sharp and wavy, with wavelengths of about 1 m and amplitude of 10-15 cm, and is also marked by about 2 cm thick shale. Some stylolites present. Samples: **TH42.3**, **TH42.45**, **TH42.6**.
- 41 0.4 62.0 Digitate stromatolites. Dark gray. Weathered parts are reddish, buff in color and characterized by large vugs. Massive to mottled appearance. Top of digitate stromatolite is very irregular and is likely stylolite-related with a thin (about 1 cm), weathered argillaceous accumulation. Uppermost 10-15 cm of the unit is composed of medium-grained couplets with visible lamination. Upper unit contact is sharp, planar and marked by a highly

weathered, maximum 7 cm thick shale. Samples: TH42.7, TH42.8, TH43.0.

- | | | | |
|------------------------------|------|-------|--|
| 42 | 0.45 | 62.45 | Fine-grained couplets to dolomitized mudstone. Medium gray. Stylolites present. Some lamination visible on weathered surfaces. Upper unit contact is weathered with stylolites and a thin (<1 cm) shale present. Sample: TH43.3. |
| 43 | 1.35 | 63.8 | Fine-grained couplets to dolomitized mudstone, with some medium-grained couplets in the middle part of the unit. Light to medium gray. Common stylolites. Burrow-mottling expressed as reddish oxidized patches throughout. Some horizontal lamination visible. Layer thickness ranges from 5 cm to maximum 15-20 cm. Layer boundaries are sharp, planar. Upper unit contact is prominent, sharp, slightly wavy, and marked with 1-3 cm thick shale. Samples: TH43.8, TH44.75. |
| 44 | 2.15 | 65.95 | Fine-grained couplets to dolomitized mudstone. Light to medium gray. Layer thickness ranges from 40 cm in the lower part to 5 cm in the upper part. Layer boundaries are slightly wavy with very thin interbedded calcareous shale. Rare stylolites and vuggy porosity present. Horizontal lamination visible. An erosional surface characterized by up to 10 cm of relief and a thin (about 1 cm) shale is present in the middle part of the unit. Top of unit marked by a 10 cm thick, light gray, silty, calcareous shale with rare, thin (up to 1 cm) carbonate to calcareous siltstone layers. This uppermost shaly part of the unit has a slightly wavy base and a rather planar top marking the upper boundary of the Maynardville Formation. Samples: TH44.95, TH45.7, TH46.45, TH46.85. |
| Copper Ridge Dolomite | | | |
| 45 | 2.35 | 68.3 | Base of the Copper Ridge Dolomite placed at the base of the first thicker unit with massive appearance. Medium- to fine-grained couplets, exhibiting some horizontal and cross-lamination, and with rare, thin (<1 cm), wavy shale layers, present in the lowermost and the uppermost parts of the unit. Central part of the unit has more massive appearance, common stylolites, and some vuggy porosity. Close examination of samples reveals the presence of a thrombolitic layer overlying the basal couplets, which is in turn overlain by LLH stromatolites and a silicified oolite layer with a maximum thickness of about 10 cm. Overlying the oolite are digitate and LLH stromatolites. Medium to dark gray in color. Upper unit boundary is planar to slightly wavy and is marked by a 2 cm thick shale. Samples: TH47.1, TH47.65, TH47.7, TH47.8, TH47.85, TH48.1, |

TH48.15, **TH48.9**, TH49.25, TH49.35.

- | | | | |
|----|------|-------|--|
| 46 | 0.7 | 69.0 | Fine-grained couplets to dolomitized mudstone. Medium to dark gray. Some horizontal lamination and mottling related to bioturbation visible. Common stylolites and vuggy porosity partially filled with spar cement. Upper unit boundary is slightly wavy and marked by a thin (about 1 cm) shale. Samples: TH49.4, TH50.0 . |
| 47 | 1.1 | 70.1 | Fine-grained couplets interbedded with LLH stromatolites in the lower part. Horizontal lamination visible. Layer boundaries are wavy, irregular, and the layers are separated by thin shale. Upper part of the unit is composed of medium- to fine-grained couplets with common quartz sand grains. Stylolites and vuggy porosity are common in this part of the unit. Upper unit boundary is a prominent surface characterized by irregular erosional topography and the deposition of a maximum 5 cm thick shale. Samples: TH50.15, TH50.35 , TH50.5 , TH50.7 , TH51.0 . |
| 48 | 1.1 | 71.2 | Medium- to fine-grained couplets with some thin (3-5 mm) oolites as couplet bases. Minimum layer thickness is 20-40 cm. Horizontal- and cross-laminations visible. Common stylolites and vuggy porosity. Upper unit boundary is sharp, slightly wavy, and characterized by a thin shaly interval. Samples: TH51.2 , TH51.75 , TH51.9, TH51.95, TH52.25. |
| 49 | 0.8 | 72.0 | Thrombolite overlain by a silicified oolite layer. Medium to dark gray. Massive appearance. Common vuggy porosity. Extensively weathered. Some stylolites with argillaceous stylocumulate present. Upper unit boundary is a very prominent, slightly wavy surface, marked with 2-3 cm thick shale. Samples: TH52.3 , TH52.35, TH52.75 , TH52.9, TH52.95, TH53.05. |
| 50 | 0.45 | 72.45 | Calcareous siltstone interbedded with medium- to fine-grained couplets and microbially laminated deposits (stratiform stromatolites). Horizontal lamination prominent throughout. Medium gray. Upper boundary is sharp, planar, and marked by 2-3 cm thick shale. Samples: TH53.1 , TH53.25 , TH53.35. |
| 51 | 0.45 | 72.9 | Medium- to fine-grained couplets interbedded with some microbial laminae (stratiform stromatolites). Medium to darker gray. Upper contact planar. Sample: TH53.9 . |
| 52 | 0.9 | 73.8 | Digitate stromatolite originated on medium to coarse-grained |

- couplets with intraclastic lag deposits in couplet bases. Massive appearance. Dark gray. Common stylolites and vugs partially filled with sparite. Upper contact characterized by a sharp surface with broad wavy, synoptic relief producing mound-like, biohermal appearance. Samples: **TH54.0, TH54.2, TH54.4, TH54.6.**
- 53 0.45 74.25 Carbonaceous siltstone interbedded with medium- to coarse-grained couplets. Medium to dark gray. Some weathered carbonaceous shale present in the lower part. A maximum layer thickness is 10 cm. Stylolites visible in the upper part. Upper contact planar. Sample: **TH54.8, TH55.25.**
- 54 4.8 79.05 Coarse- to medium-grained couplets in the lower part, overlain by a thrombotic deposit. The remainder of the unit composed primarily of dolomitized mudstone and fine-grained couplets with less common medium-grained couplets. Layer thickness ranges from 15-20 cm to more massive appearance. Horizontal lamination and some burrow(?) mottling visible. Stylolites common in the upper part. Occasional thin calcareous shale interbeds. Vuggy porosity common in parts of the unit which are also commonly weathered to chalky material, white to reddish-buff in color. The most extensively weathered part of the unit, with large (>50 cm) dissolutional voids, is indicated as covered interval on the stratigraphic column. The uppermost part of the unit contains an individual ooid grainstone layer. Upper unit contact is weathered, irregular, wavy surface marked with about 5 cm thick shale. Samples: **TH55.4, TH56.05, TH56.8, TH57.25, TH58.15, TH59.35, TH60.05.**
- 55 1.2 80.25 Microbial laminates overlain by medium- to fine-grained couplets. Calcareous shale and siltstone interbeds (3-7 cm thick) present in the central part of the unit. Prominent horizontal lamination, both microbial, crinkly in the lower part, and physical, planar in the upper part of the unit. Layer thickness ranges from 1 to 20 cm and it increases upward. Upper unit contact is sharp, planar, and marked by 2-3 cm thick shale. Samples: **TH60.4, TH60.6, TH60.95.**
- 56 1.05 81.3 Fine-grained couplets to dolomitized mudstone. Light gray to darker gray in the upper part. Horizontal lamination present. Rare carbonaceous silty shale interbedded in the lower part. Layer thickness ranges from 2-3 cm to maximum 10-15 cm. Upper unit contact is marked by a prominent irregular, wavy stylolite and 2-3 cm thick shale. Sample: **TH61.4.**

- 57 1.3 82.6 Thrombolite overlain with medium- to fine-grained couplets. Highly weathered. Light to medium gray. Thrombolite is characterized by massive appearance, vuggy porosity, and common stylolites. Top of the thrombolite layer is a prominent wavy, irregular surface, along which extensive weathering and dissolution occurred as evidenced by the presence of large dissolutional voids. Upper part of the unit contains laterally discontinuous couplets and common stylolites along which weathering is the most prominent. Some mottling likely due to bioturbation visible. Uppermost 10 cm consists of thin bedded silty carbonate layers interbedded with calcareous shale. Upper unit contact is planar to slightly wavy. Samples: **TH62.45**, TH63.35, **TH63.5**.
- 58 0.9 83.5 Thrombolite capped by medium- to fine-grained couplets. Vuggy porosity present within the thrombolitic deposit whose top is a wavy surface with mound-like, biohermal shape. Overlying lithology is thin-bedded with layers averaging 1-2 cm in thickness. Upper unit contact is sharp, wavy. Sample: **TH63.7**.
- 59 0.5 84.0 Ooid grainstone comprising 2-3 layers ranging in thickness from 5 to 25 cm. Layer boundaries are wavy and layer thickness varies laterally. Dark gray individual ooids, composite ooids, and cm-size angular clasts composed of ooid grainstone are surrounded with white dolomitic sparite. Upper unit contact is sharp, wavy. Sample: **TH64.6**.
- 60 0.25 84.25 Thrombolite overlain by fine- to medium-grained couplets. Thrombolite is dark gray to brown in color, and contains many vugs both partially and completely infilled with sparite. Top of the thrombolite is an irregular contact, represented in places by a stylolite and marked by some reddening of the underlying deposits. Overlying couplets are darker gray. Upper unit contact is sharp, planar. Samples: **TH65.0**, TH65.1, TH65.15, **TH65.3**.
- 61 0.7 84.95 Fine-grained couplets overlain by ooid grainstone. Layer thickness 15 to 20 cm. Layer boundaries sharp, planar to slightly wavy. Horizontal lamination and stylolites are visible in the basal layer composed of couplets. The contact between couplets and oolite is sharp, planar and marked by 1 cm thick shale. Oolitic lithofacies contains common vugs partially or completely filled with cement. In part more thinly bedded with maximum layer thickness reaching about 6 cm. Layers have very irregular, wavy contacts and they pinch and swell laterally. Upper unit contact is sharp, planar. Samples: TH65.35, TH65.45, **TH65.55**, TH65.7.

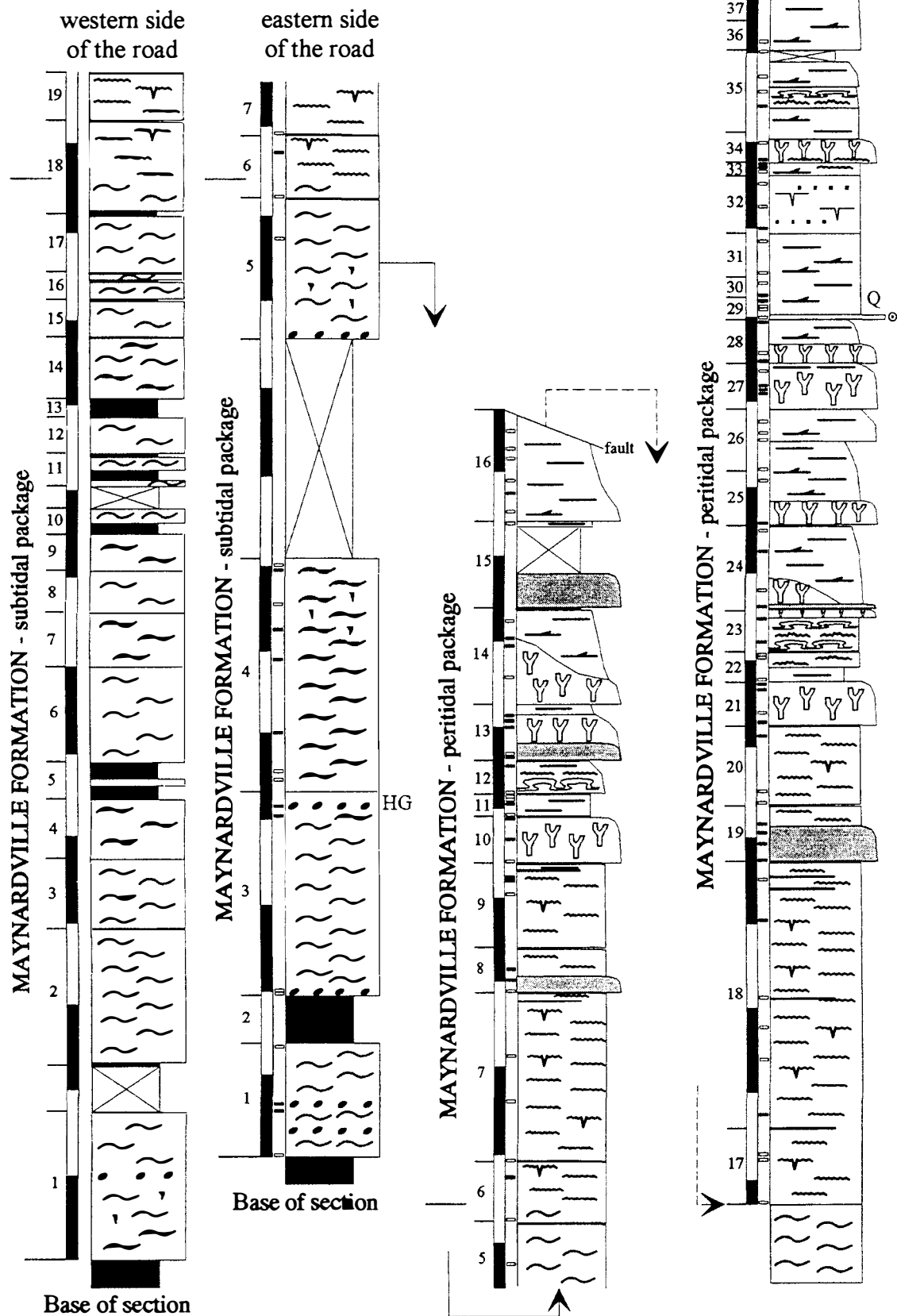
- 62 0.85 85.8 Carbonaceous siltstone overlain by medium-grained couplets and ooid grainstone. The lowermost part is thinly bedded (maximum layer thickness 2 cm). Layer boundaries are very irregular, wavy and marked with common trace fossils (horizontal burrows). This silty deposit gradually grades upward into 10-13 cm thick layers composed of couplets, which in turn grade upward into oolitic deposits. The uppermost part of the unit has reddish, buff coloration due to weathering. Layer thickness reaches a maximum of 5 cm, and layer boundaries are irregular, wavy, with some thin shale interbedded. Cross-lamination is visible. Unit top is wavy, marked by a thin shaly interval. Samples: TH66.1, TH66.25, TH66.4, TH66.6, TH66.7.
- 63 0.5 86.3 Medium- to fine-grained couplets with occasional SH stromatolites in the base. Thick bedded to massive appearance. Couplets are light gray, whereas stromatolite heads are darker gray. Couplets have truncational bases and cross-laminated basal deposits. Upper parts of couplets exhibit horizontal lamination with planar to slightly wavy laminae. Unit top is not exposed. Samples: **TH66.9**, TH67.0, TH67.25.
- 0.6 86.9 Covered interval.
- 64 0.4 87.3 Burrowed dolomitized mudstone to fine-grained couplets. Mottled, light to medium gray in color. Faint horizontal lamination visible. Unit top planar. Sample: **TH68.35**.
- 65 0.5 87.8 Thrombolite. Massive appearance. Mottled, light to dark gray in color. Common vuggy porosity. Dolomitized and partially silicified. Unit top is sharp, slightly undulatory. Sample: **TH68.75**.
- 66 0.55 88.35 Medium- to fine-grained couplets. Massive, burrow-mottled appearance. Some horizontal lamination visible. Certain layers have common vuggy porosity related to evaporite dissolution voids. Unit top is sharp, slightly wavy. Sample: **TH69.3**.
- 67 0.95 89.3 Thrombolite overlain by silicified LLH stromatolites and medium- to fine-grained couplets. Thrombolite has characteristic massive, mottled appearance. Top of the thrombolitic layer is marked by laminated crust representing silicified stromatolites. The uppermost part of the unit contains common evaporite molds and exhibits some planar to wavy horizontal lamination. Maximum layer thickness 15 cm. Top is poorly exposed. Sample: **TH70.2**.

- 68 0.7 90.0 Thrombolite overlain with stromatolites. Thrombolite is dark gray in color and has characteristic mottled appearance. It is extensively dolomitized, with dolomite cement filled voids, and is partially silicified. Upper part of the unit is medium to dark gray and is composed primarily of LLH stromatolites with occasional SH to columnar stromatolite head with low relief. Unit top is poorly exposed but the unit overall has a biohermal shape. Samples: TH70.4, TH71.0.
- 69 0.45 90.45 Medium-grained couplets comprising an individual, medium to dark gray layer with rare vuggy porosity partially or completely filled with dolomite cement. Burrow-mottled appearance. Iron-oxides coated clasts present in some of the couplet bases. Unit top is poorly exposed. Sample: **TH71.45**.
- 70 0.65 91.1 SH stromatolites overlain by fine- to medium grained couplets. Dark to medium gray microbial deposits from the base of the unit have biohermal shape and pinch out laterally. Couplets from the upper part are up to 3 cm thick and comprise layers of maximum thickness of 20 cm. Unit top is poorly exposed. Samples: TH71.55, TH71.8.
- 71 0.5 91.6 Thrombolite overlain by fine- to medium-grained couplets. Poorly exposed. Thrombolite has a characteristic massive, mottled appearance, and some vuggy porosity. Overlying couplets have truncated, slightly burrow-mottled tops. Iron-oxide staining visible along couplet contacts. Couplet bases are partially silicified. Sample: **TH72.55**.
- 72 0.7 92.3 Dolomitized mudstone to fine-grained couplets. Poorly exposed. Rare horizontal lamination and burrow-mottling. Layer thickness 5-20 cm. Light to medium gray. Unit top, containing cm-scale carbonate layers with thin interbedded shale is extensively weathered. Sample: **TH73.25**.
- 73 0.95 93.25 Dolomitized mudstone to fine-grained couplets. Dark gray base, lighter gray upper part. Patches of Fe-oxide present. Faint horizontal lamination visible. A thin silicified crust, without visible lamination, separates the uppermost layer which contains couplets with rather wavy, disturbed lamination as a result of bioturbation, compaction, and stylolitization. Samples: **TH73.4**, TH73.8, **TH74.15**.
- 74 1.3 94.55 Thrombolite overlain with LLH stromatolites. Thrombolitic body is

dark gray in color, and is composed of undulatory layers ranging in thickness from 5 cm to maximum 20-30 cm. Common vuggy porosity. The overlying stromatolites comprise a single layer with prominent wavy lamination. Sample: TH75.1.

75	1.9	96.45	Thrombolite in the lower part. Massive appearance. Partially silicified columnar stromatolites in the upper part. The rest of the Copper Ridge Dolomite was not measured.
----	-----	-------	---

Figure A.2. Stratigraphic column measured at the River Ridge outcrop.



The River Ridge Outcrop (RR)

The River Ridge locality is within the Clinchport thrust sheet in Clairborne County, approximately 3 miles northwest of the Thorn Hill locality along U.S. Highway 25E. At this locality parts of the Maynardville Formation are exposed on both sides of the highway. Exposures along the eastern side of the road are described in greater detail and were sampled. The lower part of the Maynardville comprising the subtidal depositional package, however, is better exposed on the western side of the road. This part of the succession was also measured and only briefly described. For the purpose of comparison, the two measured stratigraphic columns of the subtidal package are illustrated one next to another on Figure A.2. The columns are hung at the contact with the overlying peritidal depositional package marked by the first occurrence of microbially laminated deposits. Part of the peritidal depositional package of the Maynardville is repeated due to faulting. The fault is not exposed. The repeated parts of the stratigraphic successions are reconstructed and compared on Figure A.2. Figure 2.1 contains a composite stratigraphic section comprised of the subtidal depositional package measured at the western side of the road, and the uppermost part of the succession that contains the more completely exposed part of the Maynardville Formation overlying the fault zone. The lower part of the Copper Ridge Dolomite is not exposed at this locality (see Figure 2.1).

Unit	T (m)	C.T. (m)	Description
			Eastern side of the road: Maynardville Formation
1	2.8	2.8	Base of the Maynardville is placed at the base of the first exposed carbonate unit overlying a poorly exposed interval representing the shale deposits of the uppermost Nolichucky Shale. This basal unit consists of ribbon laminated limestone. Medium gray with brownish argillaceous dolomitic portions. Skeletal (trilobites) lag deposits are present in basal parts of carbonate interlayers. Upper muddy parts of limestone layers are occasionally burrow-mottled. Flat pebbles are present within several layers (maximum 10 cm thick). These flat pebble conglomerate layers show normal grading. Pyrite is present. Upper unit boundary is a sharp, slightly wavy layer boundary overlain by shale. Samples: RR0.0, RR1.2 , RR1.4 , RR2.7 .
2	1.1	3.9	Shale. Light gray. Poorly exposed. No interbedded carbonate layers were observed.
3	4.8	8.7	Ribbon limestone. Unit base is a sharp, slightly wavy surface. Pyrite is common near the base of the unit. Carbonate layers containing coarse-grained, intraclastic basal lag deposits, grading upward into mudstone, present in the lower part of the unit. Limestone layers in the remaining part of the unit are dominated by

mudstone interbedded with some fossiliferous (trilobite) wackestone to grainstone. Ribbon rocks from the uppermost part of the unit contain some thin interbedded shale as well as some intraclastic lag deposits with intraclasts, reaching a maximum length of 3 cm, and skeletal fragments. Weathered pyrite coatings and crusts, typical of marine hardgrounds, are present in this part of the succession. Samples: RR3.9, RR4.0, **RR8.1, RR8.4**.

- | | | | |
|---|------|-------|---|
| 4 | 5.4 | 14.1 | <p>Poorly exposed ribbon rocks interbedded with shaly intervals. Carbonate layers pinch and swell laterally, reaching a maximum thickness of about 5 cm, and giving this unit a nodular appearance in places. Common fossiliferous (trilobite) packstone/grainstone layers, with some incorporated intraclasts (up to 1 cm in diameter), grading upward into mudstone layers. Cross-stratification present in the basal grainy deposits, whereas horizontal lamination is visible in the upper muddy deposits of some of the carbonate layers. Extensive bioturbation observed in parts of the unit. Scattered pyrite present. Some trace fossils and trilobite fragments can be observed along bedding planes of argillaceous layers. Samples: RR8.9, RR9.1, RR10.0, RR11.8, RR12.5, RR13.2, RR13.9, RR14.0.</p> |
| | 5.0 | 19.1 | <p>Covered interval due to a road leading to a nearby house. It is impossible to precisely determine the thickness of this covered interval. Some ribbon limestone is present at the unpaved road surface as well as in a ditch on a southern side of the road.</p> |
| 5 | 3.35 | 22.45 | <p>Ribbon limestone. Some intraclasts present near the base of the unit. Limestone layers dominated by fine-grained wackestone/packstone and mudstone layers. Bioturbation common in places. Some cross-stratification and horizontal lamination present. Unit top marked by a thin shale interval. Sample: RR21.6.</p> |
| 6 | 1.4 | 23.85 | <p>Transition from ribbon limestone into microbial (cryptalgal) laminates (see Fig. 2.2C). Ribbon rocks from the lower part of the unit are composed primarily of fine-grained, micritic carbonate layers (up to 2-3 cm thick) interbedded with argillaceous layers (maximum 1.5-2 cm thick). Some bioturbation present. Wavy, crinkly microbial lamination and desiccation cracks apparent in the upper part of the unit. Small fenestrae and/or burrows filled with sparite observed within transitional and microbial deposits. Pyrite present. Unit top is a sharp, slightly wavy surface, marked by a thin shaly interval. Samples: RR22.45, RR23.45.</p> |

- 7 3.9 27.75 Microbial (cryptalgal) laminates. Light to medium gray. Characteristic horizontal crinkly, wavy microbial lamination visible throughout the unit. Common prominent vertical desiccation cracks (see Fig. 2.2D). Unit top is sharp, planar and marked by a thin shale. Samples: RR23.9, RR25.3, RR26.35.
- 8 1.15 28.9 Thrombolitic bioherm with planar base and synoptic relief. Medium to dark gray/brownish. Very porous and weathered. Upper boundary of the bioherm is gradual or is represented by a sharp, wavy surface, marked with a thin shale. Light gray microbial (cryptalgal) laminates overlie thrombolite. Characteristic microbial lamination visible. Unit top is sharp, planar, and marked with a thin shale. Samples: RR27.75, **RR28.05**, **RR28.35**.
- 9 1.9 30.8 Microbial (cryptalgal) laminates. Light to medium gray/brownish. Prominent horizontal, crinkly lamination and some mudcracks. Some laminae contain incorporated intraclasts. The uppermost part of the unit contains some mechanical laminates or couplets separated from the underlying microbial deposits by a thin shale layer. Unit top is sharp, planar and marked with a thin shale. Samples: RR30.1, **RR30.55**, **RR30.6**.
- 10 1.0 31.8 Digitate stromatolite bioherm. Medium to dark gray. Base is very weathered and may contain some thrombolites. Unit top is poorly exposed, characterized by synoptic relief, and a maximum of 5 cm thick shale interval. Samples: RR30.8, **RR31.4**, **RR31.75**.
- 11 0.6 32.4 Fine-grained dolomitized couplets. Light gray. Bed thickness: 15-25 cm. Planar, horizontal lamination and stylolites present. Some crinkly microbial laminae are also visible. Unit top is a sharp, undulatory surface, marked with 2-3 cm thick shale. Samples: RR31.8, **RR32.2**, RR32.3, RR32.35.
- 12 0.7 33.1 Stromatolitic hemispheroids (SH stromatolites) overlain by stratiform stromatolites (microbial laminates) and some fine-grained couplets. Stromatolitic hemispheroids reach 20-30 cm in diameter and about 15 cm in height (see Fig. 6.1E). Characteristic microbial, crinkly lamination visible. Pyrite present. Upper unit boundary is sharp and marked by 3-4 cm thick shale. Samples: RR32.4, **RR33.0**.
- 13 1.45 34.55 Thrombolite and digitate stromatolite bioherms overlain by fine-grained couplets to dolomitized mudstone. Medium gray. Basal thrombolite is extensively weathered. Common vuggy porosity and

some stylolites. The thickness of microbial bioherms varies laterally. Upper part of the unit is also weathered and not well exposed. Samples: **RR33.15**, RR33.2, **RR34.0**, **RR34.15**, **RR34.3**,

- | | | | |
|----|------|-------|--|
| 14 | 2.15 | 36.7 | Similar to previous unit. Microbial (predominantly digitate stromatolite, and some thrombolite) bioherms of variable lateral thickness, overlain by medium- to fine-grained couplets. Microbial deposits have mottled appearance, whereas some planar, horizontal lamination is associated with couplets. Structural deformation (fracturing) present. Samples: RR35.3, RR35.9 , RR36.1 , RR36.5. |
| 15 | 2.2 | 38.9 | Poorly exposed (partially covered) interval. Lower part consists of microbial (thrombolitic) deposit. Medium gray. Massive, mottled appearance. Middle part of the unit is covered. The uppermost part of the unit consists of highly fractured, light gray, dolomitized, fine-grained couplets. Sample: RR38.85. |
| 16 | 2.45 | 41.35 | Poorly exposed and structurally deformed interval composed primarily of dolomitized medium-grained couplets and with some coarse-grained couplets at the unit base. Medium to light gray. Intraclasts, and some ooids present in basal parts of coarse-grained couplets. Rare vuggy porosity present. Sharp, planar (some truncational) bases, cross-stratification, and planar, horizontal lamination, typical of mechanical laminates (couplets), can be observed. Unit top is highly weathered. The uppermost part is not exposed. Observed structural deformation is related to faulting, and this poorly exposed interval represents a fault zone above which the stratigraphic succession is partially repeated. Samples: RR39.05, RR39.6 , RR39.75, RR40.35, RR40.55, RR40.95. |
| 17 | 1.8 | 43.15 | Microbial (cryptalgal) laminates. Substantial structural deformation complicates the stratigraphy. This unit seemed to represent the first exposed interval overlying the poorly exposed/covered fault zone interval. However, in one part of the outcrop, the unit is underlain by a maximum of 1.5 to 1.7 m of ribbon limestone which was then used to reconstruct the repetition of stratigraphic section due to faulting (see Fig. A.2). Structural deformation (folding and faulting) of microbially laminated deposits is obvious in this part of the succession. Some pyrite present. Unit top is marked by a thin shale. Samples: RR41.4, RR42.55, RR42.65. |
| 18 | 6.35 | 49.5 | Microbial (cryptalgal) laminates. Light to medium gray/brown. |

Characteristic crinkly lamination, some mudcracks, incorporated micritic intraclasts and small fenestrae are visible. Lower part of the unit is deformed (fractures, small-scale faults and folds are present). Layer thickness ranges from several mm to about 50 cm. Unit top is sharp, marked by 2 cm thick shale. Samples: **RR43.5**, **RR44.85**, **RR45.65**, **RR46.35**, **RR48.1**, **RR49.0**.

- | | | | |
|----|------|-------|---|
| 19 | 1.2 | 50.7 | Thrombolite overlain by microbial laminates. Thrombolite is characterized by mottled fabric and common vuggy porosity. In places it grades upward and possibly laterally into digitate stromatolite. Characteristic fabric is not readily observed and distinction between the two is difficult in the field. Transition into overlying laminated deposits is gradual. Horizontal microbial lamination visible in the upper part of the unit. Layer thickness ranges from several mm to 10-15 cm. Medium gray. Upper unit contact is highly weathered. Samples: RR49.5 , RR49.85 , RR50.1 , RR50.35 . |
| 20 | 1.85 | 52.55 | Microbial (cryptalgal) laminates. Medium gray. Horizontal, crinkly, microbial lamination is readily observable. Minor incorporated intraclasts and desiccation cracks are present. Layer boundaries are sharp, planar. Unit top is marked by about 5 cm thick, weathered shaly interval. Samples: RR50.7 , RR50.0 , RR52.3 . |
| 21 | 1.05 | 53.6 | Digitate stromatolite bioherm. Massive, mottled appearance (some mottling may be related to bioturbation). Rare vuggy porosity. Stromatolite digits are darker gray; interdigitate deposits are lighter gray in color. Parts of the unit, without prominent microbial digits, resemble thrombolite. Unit top is a sharp, undulatory surface. Samples: RR52.65 , RR52.85 , RR53.3 , RR53.5 . |
| 22 | 0.6 | 54.2 | Consists of two layers that vary laterally in thickness from 20-40 cm each. The lower layer is composed predominantly of fine- and some medium-grained couplets. Planar, horizontal lamination and some cross-lamination present. The upper layer contains wavy microbial lamination characteristic of LLH stromatolites. Unit top is a wavy surface characterized by about 5 cm thick weathered shale. Samples: RR53.6 , RR54.1 , RR54.15 . |
| 23 | 0.9 | 55.1 | Alternation of SH, LLH and some stratiform (microbial laminate) stromatolites. Characteristic microbial lamination is prominent. Stromatolite hemispheroids reach a maximum height of about 5 cm. Small fenestrae and desiccation cracks visible. Small (maximum 20 |

cm high) digitate stromatolite bioherm in the uppermost part of the unit. Unit top is a sharp, undulatory surface. Samples: **RR54.4, RR54.95.**

- | | | | |
|----|-----|------|---|
| 24 | 2.0 | 57.1 | Microbial deposits overlain by mechanical laminates. Thrombolite to digitate stromatolite bioherm present at the base of the unit. Mottled appearance. Thickness of these microbial deposits varies laterally. Some burrows present. The overlying mechanical laminates are dominated by medium-grained and rare coarse-grained couplets. Light to medium gray. Maximum couplet thickness: 5 cm. Couplet bases are commonly truncational. Couplet tops are occasionally burrowed. Several prominent stylolites present. Unit top is sharp, slightly undulatory, and marked by a thin shale. Samples: RR55.1, RR55.6, RR56.6, RR57.0. |
| 25 | 1.3 | 58.4 | Similar to underlying unit: digitate stromatolite at the base, overlain by medium-grained couplets. Stromatolitic bioherm varies laterally in thickness from 15 to 50 cm. Some horizontal to wavy lamination visible in the upper part of the unit, as well as common vuggy pores related to evaporite molds and nodules (up to 2 cm in diameter). Unit top is sharp, irregular, wavy, associated with a large stylolite. Samples: RR57.1, RR58.2. |
| 26 | 1.4 | 59.8 | Medium- to coarse-grained couplets. Medium gray. Burrow-mottled in places. Similar to underlying unit, but contains less common evidence for evaporites. Massive layering; laterally splits into 3-4 layers with planar to undulatory boundaries. Cross-stratification and horizontal lamination visible. These sedimentary structures are more prominent in the upper part of the unit which also contains common coarse-grained intraclastic (lag) deposits comprising couplet bases. Intraclasts are most commonly 3-5 mm in diameter; the largest are about 2 cm long. Some stylolites present. Unit top is poorly exposed. Samples: RR58.4, RR59.1, RR59.3, RR59.6. |
| 27 | 1.1 | 60.9 | Microbial deposits overlain by mechanical laminates. Basal part is very weathered. The lower 80 cm of the unit consists primarily of a digitate stromatolite bioherm with some thrombolite present. Microbial deposits are characterized by mottled fabric and vuggy porosity. The remaining part of the unit is composed of medium- to coarse-grained couplets, characterized by cross-laminated basal parts and horizontally laminated upper parts which are commonly truncated by the basal deposits of the overlying couplets. Some of |

the coarse-grained basal couplet deposits are partially silicified, and contain intraclasts up to 5-7 cm long. Thin calcareous shale intervals are present in the uppermost part of the unit. Unit top is poorly exposed. Samples: **RR60.2**, **RR60.25**, **RR60.3**, **RR60.75**.

- | | | | |
|----|------|-------|---|
| 28 | 1.05 | 61.95 | Microbial deposit overlain by mechanical laminates. Microbial deposits comprise the lower, highly weathered and porous 40 cm of the unit, and consists of digitate stromatolite and some thrombolite. Upper boundary of the microbial deposit is a sharp, slightly undulatory surface, that may have been marked by thin shale but is now completely weathered. The upper unit part consists of medium- to coarse-grained couplets. Cross-stratification and horizontal lamination present. Intraclasts are present in the bases of some couplets, and reach up to 2-6 cm in length. Several thin (up to 2 mm) calcareous shale interbedded with couplets in the upper part of the unit. Unit top is a sharp, undulatory surface. Samples: RR61.05 , RR61.2 , RR61.9 . |
| 29 | 0.55 | 62.5 | Oolite overlain by medium-grained couplets. The basal oolite is composed of several 3-4 cm thick, undulatory, dark gray ooid grainstone layers which also contains some micritic intraclasts (up to 6 mm in diameter). It grades upward into light gray to brownish dolomitized couplet deposits characterized by common vuggy porosity related to evaporite molds and nodules. Couplet bases contain ooids and some quartz sand grains. Some stylolite, horizontal lamination and rare cross-lamination visible. Uppermost part of the unit contains thin (maximum layer thickness: 2 cm), undulatory, silty to arenaceous carbonate layers. Unit top is not exposed. Samples: RR61.95 , RR62.2 , RR62.25 , RR62.35 . |
| 30 | 0.4 | 62.9 | Predominantly medium-grained couplets with some fine-grained couplets in the upper part. Light to medium gray. Very poorly exposed. Lower part is similar to silty to arenaceous couplets of the uppermost part of the underlying unit. Couplet bases contain ooids, small intraclasts, and quartz sand grains. Planar horizontal laminations visible in the upper part of the unit together with some vugs (evaporite nodules). Couplet thickness: several mm to about 1 cm. Upper unit contact is a sharp, planar layer surface. Samples: RR62.55 , RR62.85 . |
| 31 | 1.0 | 63.9 | Medium-grained dolomitized couplets. Grainy couplet bases are darker gray, occasionally cross-laminated, and contain ooids and quartz grains. Muddy couplet tops are lighter gray. Couplet boundaries are sharp, planar, truncational surfaces. Couplet |

thickness ranges from several mm to 2-3 cm. Layer thickness: 10-30 cm. Unit top is a sharp, planar surface. Samples: RR63.0, RR63.7.

- | | | | |
|----|------|-------|---|
| 32 | 1.4 | 65.3 | <p>Calcareous siltstone, sandstone and shale. Light gray to brownish. Very weathered. Undulatory layers range in thickness from several mm to 7-8 cm. Trace fossils and desiccation cracks visible along bedding planes. Small vugs (fenestrae, burrows?) present. Horizontal and cross-lamination visible. Some micritic, angular intraclast present at the base of the unit. Unit top is weathered, slightly undulatory. Samples: RR64.05, RR64.5, RR65.05.</p> |
| 33 | 0.35 | 65.65 | <p>Medium-grained dolomitized couplets overlain by microbial deposits. Light to medium gray/brownish. Horizontal and cross-lamination visible in the lower part. Small micritic intraclasts present in couplet bases. Couplet tops contain microbially laminated deposits which are occasionally silicified and make 2-3 mm thick silicified crusts. Chert also occurs in small nodules. Fabric of microbial deposits in the upper part is obscured by extensive dolomitization. Microbial lamination is well preserved in partially silicified deposits. Unit top is an undulatory, weathered surface. Samples: RR65.45, RR65.5, RR65.6.</p> |
| 34 | 0.65 | 66.3 | <p>Microbial bioherm overlain by medium-grained couplets. Microbial deposits are dark gray, very porous, extensively weathered, and consist of digitate stromatolite and some thrombolite. The overlying couplets are light to medium gray/brownish, have truncational bases, and exhibit common planar, horizontal lamination and rare cross-stratification. Couplet thickness ranges from several mm to about 2 cm. Some stylolites present. Unit top is a sharp, slightly undulatory surface. Samples: RR65.7, RR66.0.</p> |
| 35 | 1.85 | 68.15 | <p>Medium to fine-grained dolomitized couplets interbedded with microbial deposits in the middle part of the unit. Poorly exposed. Medium to dark gray. Characteristic lamination and truncational bases visible in the couplet deposits from the lower part of the unit. Microbial deposits consist of dolomitized and partially silicified SH, LLH and some stratiform (microbial laminate) stromatolites. Characteristic microbial lamination, small fenestrae and mudcracks visible. Couplets in the upper part of the unit are in part burrow(?) mottled, contain common vugs representing evaporite molds and nodules, and some stylolites. Most of the upper part of the unit is covered. The uppermost 10 cm is poorly exposed and highly weathered. It consists of burrow(?) mottled dolomitized mudstone.</p> |

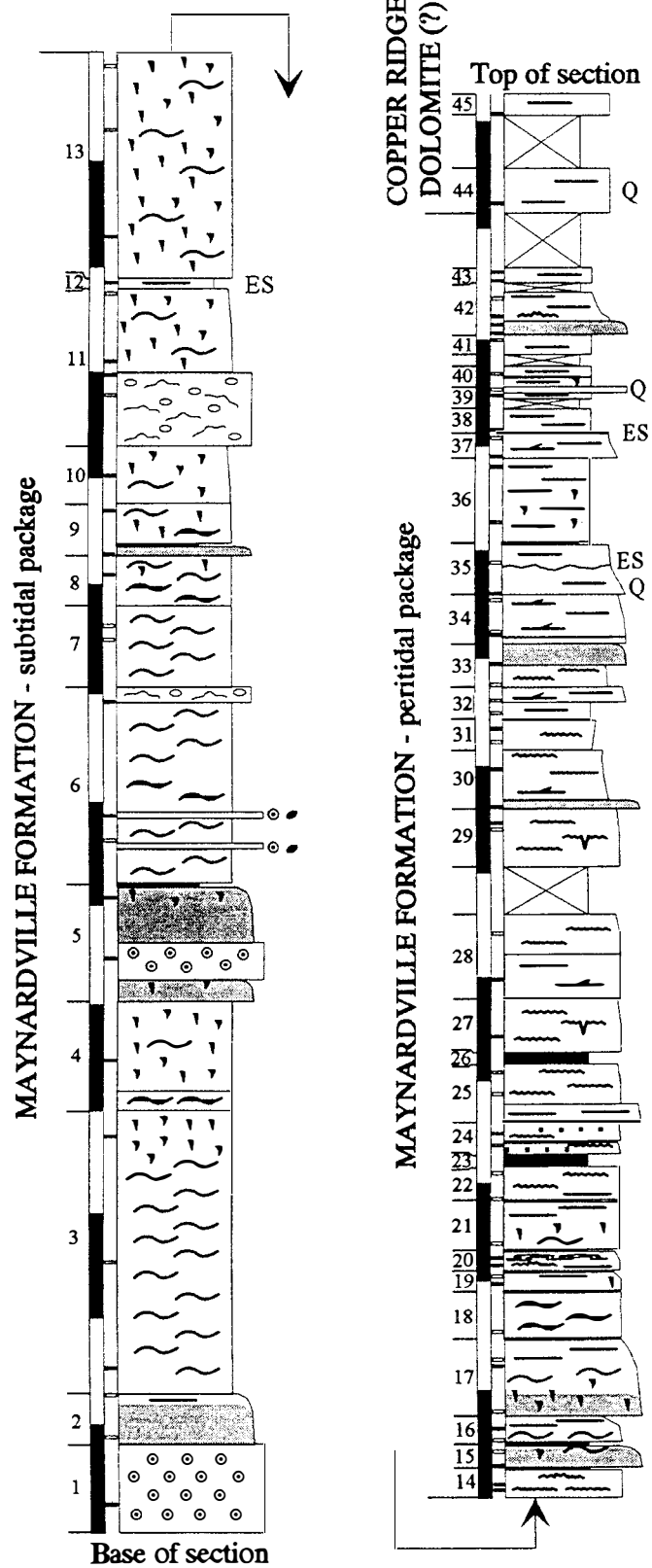
Unit top is weathered and slightly undulatory. Samples: **RR66.8**, RR67.15, RR67.55, RR68.05.

- 36 0.7 68.85 Dolomitized medium- to fine-grained couplets. Medium gray. Massive, in places have a mottled appearance. Some planar, horizontal lamination and stylolites are present. Common vuggs (evaporite nodules?), up to 3 cm in diameter. Unit top is poorly exposed and slightly undulatory. Sample: RR68.35.
- 37 0.55 69.4 Dolomitized medium- to fine-grained couplets comprise two layers (20 and 35 cm thick). Medium to dark gray. Poorly exposed. Some planar, horizontal lamination visible. Unit top is not exposed. The rest of the succession is covered.

Unit	T (m)	C.T. (m)	Description
<hr/>			
1	3.6	3.6	Western side of the road: Maynardville Formation Ribbon limestone overlying a covered to poorly exposed shale interval of the uppermost Nolichucky Shale. Lower 60 cm of the unit contains interbedded shale interlayers and is substantially weathered. Evidence for bioturbation present in the lower half of the unit. One 10 cm-thick flat-pebble conglomerate layer, overlain and underlain by thin shaly/silty layers, present in the central part of the unit. Ribbon limestone with very thin argillaceous portions comprises the upper part of the unit. Carbonate layers are predominantly micritic, with some grainy layers present. Horizontal lamination and some burrows visible. Rare vuggy porosity present.
	1.1	4.7	Covered interval with minor exposure of paper laminated shale interbedded with rare, very thin carbonate layers.
2	3.1	7.8	Ribbon rocks without interbedded shale. Unit base is a sharp, planar surface overlying paper laminated shale. Unit top is marked by 2-3 cm thick shale interval.
3	1.7	9.5	Similar to underlying ribbon rocks without interbedded shale interlayers.
4	1.5	11.0	Ribbon limestone interbedded with shale interlayers.
5	0.8	11.8	Paper laminated shale. Ribbon limestone comprises a 15 cm thick carbonate layer in the central part of the unit.

6	2.2	14.0	Ribbon limestone without shale interlayers. In places, appears nodular.
7	1.4	15.4	Ribbon limestone containing interbedded shale interlayers. Poorly exposed lower part.
8	0.9	16.3	Ribbon limestone without interbedded shale.
9	0.8	17.1	Ribbon limestone with common shaly interlayers.
10	0.55	17.65	Calcareous shale overlain by shale-free ribbon limestone.
	0.6	18.25	Covered interval.
11	0.65	18.9	Alternating layers of carbonaceous shale and shale-free ribbon limestone.
12	0.9	19.8	Weathered ribbon limestone without prominent interbedded shale.
13	0.5	20.3	Shale.
14	1.3	21.6	Weathered ribbon limestone containing shale interbeds in the lower and upper part. Unit top is a sharp surface marked by 2-3 cm thick shale.
15	0.85	22.45	Ribbon limestone without shale interbeds. Unit top is marked by 5 cm thick shale interval.
16	0.75	23.2	Ribbon limestone without obvious shale interlayers. Shale occurs only as a 5 cm thick interval in the upper part of the unit as well as a thin (1-2 cm) interval marking the unit top.
17	1.25	24.45	Shale-free ribbon limestone bound on top with a 10 cm thick interval of calcareous shale.
18	1.9	26.35	Gradual transition from ribbon rocks into microbial (cryptalgal) laminates. Mudcracks present in the upper part of the unit. Unit top is marked by a shale about 1 cm thick.
19	1.05	27.4	Microbial laminates. Horizontal laminations and mudcracks present. Unit top marked by 5-6 cm thick calcareous shale.

Figure A.3. Stratigraphic column measured at the Tazewell outcrop.



The Tazewell Outcrop (TZ)

The Tazewell locality is 1.5 miles southeast of the town of Tazewell, within the Wallen Valley thrust block (Fig. 1.4). At this locality, the Maynardville, overlain by the Copper Ridge Dolomite, is exposed in a quarry on the northeastern side of the U.S. 25E. Here, the base of the Maynardville is thrust over the Hurricane Bridge Limestone (lower Middle Ordovician) by the Wallen Valley fault. The Nolichucky Shale and the lowermost Maynardville are absent due to the faulting. Poorly exposed parts of the outcrop preclude the determination of the Maynardville/Copper Ridge transition. The uppermost part of the stratigraphic succession is tentatively placed within the Copper Ridge Dolomite based on the similarity with deposits that belong to the lower Knox Group at other outcrops.

Unit	T (m)	C.T. (m)	Description
Maynardville Formation			
1	1.7	1.7	Ooid grainstone. Dark gray. Abundant centimeter-spaced stylolites. Common vuggy porosity. Cross-stratification was not observed. Some micritic intraclasts present. Base not exposed. Upper contact is sharp and slightly undulatory. Sample: TZ0.5 .
2	1.0	2.7	Thrombolite. Dark gray. Mottled appearance. Some vuggy porosity present. The uppermost 30 cm consists of intraclastic-fossiliferous grainstone. Micritic intraclasts reach a maximum of 3-4 mm in diameter. Skeletal fragments include common trilobites and some echinoderm fragments. The transition between thrombolite and grainstone deposits appears to be gradual. Samples: TZ1.8, TZ2.6.
3	5.3	8.0	Ribbon limestone. Centimeter-scale, medium gray limestone interlayers are interbedded with light brownish argillaceous dolomicritic interlayers. Ribbon rocks are massive to thick bedded (bed thickness ranges from 20 cm to over 2 m). Limestone interlayers are primarily composed of intraclastic and fossiliferous (predominantly trilobite) packstone/grainstone deposits. Scattered pyrite present. Argillaceous deposits display horizontal lamination. Uppermost 1 meter of the unit consists of burrow-mottled ribbon rocks. Samples: TZ3.1 , TZ5.1, TZ7.6 .
4	2.1	10.1	Lower 40 cm consists of poorly exposed ribbon rock interbedded with shale. Burrow-mottled ribbon rock comprises the remaining portion of the unit. Limestone layers are composed predominantly of fossiliferous (trilobite) and intraclastic packstone/grainstone. Micritic intraclasts are angular and irregular in shape, and reach a maximum size of 1 cm in diameter. Sample: TZ9.0 .

- 5 2.45 12.55 A thrombolite layer with mottled appearance comprises the lower 45 cm of the unit. The basal thrombolite is overlain by a light to medium gray ooid grainstone layer which also contains some intraclasts. The oolite does not exhibit cross-stratification, but horizontal lamination and stylolites are visible. The uppermost 1 m of the unit consists of an another thrombolitic layer. Burrow-mottling present. Upper unit contact is a sharp, slightly undulatory surface, and is marked by 3-4 cm of reddish soil that might represent weathered shale. Samples: **TZ10.9, TZ12.3.**
- 6 3.5 16.05 Ribbon limestone containing thin (< 5 mm), brownish, argillaceous dolomicritic portions interbedded with medium gray limestone portions reaching a maximum thickness of about 3 cm. Limestone layers are occasionally burrowed and horizontally laminated. Framboidal pyrite is present. Some shale interbeds (2 to 5 cm in thickness) are present in the middle part of the unit. Several 10 cm-thick intraclastic-ooid grainstone layers observed within the unit. The uppermost 25 cm of the unit consists of fossiliferous (trilobite, echinoderms)-intraclastic packstone grainstone. Cross-stratification is visible. Unit top is slightly undulatory. Samples: **TZ13.4, TZ13.85, TZ15.85.**
- 7 1.5 17.55 Ribbon rocks. Medium to dark gray in color. Limestone units are primarily composed of fine-grained fossiliferous-intraclastic packstone/grainstone layers. Some burrows are present. Argillaceous portions reach a maximum thickness of about 1 cm. Some stylolites visible. Layer thickness ranges from 20 to 70 cm. Samples: **TZ16.9, TZ17.25.**
- 8 1.05 18.6 Ribbon rocks interbedded with thin shale interlayers comprise the lower 60 cm of the unit. Upper part is composed primarily of laminated mudstone interbedded with thin, wavy argillaceous laminae. Medium gray in color. Common burrows with some associated pyrite. Unit top is sharp and undulatory. Sample: **TZ18.25.**
- 9 0.95 19.55 Thrombolitic layer, overlain by a thin shale, comprises the lower 25 cm of the unit. The rest of the unit is composed of medium gray, burrowed ribbon rocks interbedded with thin laminated argillaceous portions. Boundaries between layers are wavy, undulatory. Carbonate layers are composed primarily of fine-grained fossiliferous-intraclastic packstone/grainstone. Unit top is a prominent sharp, planar surface. Samples: **TZ18.7, TZ19.45.**

- 10 1.2 20.75 Similar to the underlying lithology. Sedimentary structures are not readily observable due to a rather fresh exposure. Some stylolites are visible. Limestone layers are composed of packstone/grainstone deposits containing micritic intraclasts and some skeletal fragments. Burrow-mottled appearance. Some parts of the unit appear to have mottled thrombolitic fabric. Upper unit boundary is a prominent, sharp, planar surface. Sample: **TZ20.05**.
- 11 2.9 23.65 The lower half of the unit consists of ooid-fossiliferous-intraclastic grainstone. Skeletal fragments include trilobite and some echinoderm fragments. Some stylolites present. The upper part of the unit consists of burrowed ribbon limestone with patchy, irregular distribution of argillaceous dolomicritic partings. Vuggy porosity and voids filled with dolomite cement and rare sphalerite present. The unit has a massive appearance. Fresh exposures in the quarry preclude observation of sedimentary structures. Parts of the unit resemble mottled thrombolitic fabric. Dark gray to reddish weathering coloration. Unit top is a sharp, prominent exposure surface characterized with a maximum of 15 cm of erosional relief. Samples: TZ21.65, **TZ21.95**, TZ23.55.
- 12 0.2 23.85 Laminated dolomicrite of variable lateral thickness (20 to 50 cm). Light to reddish brown. Unit top is a very prominent, sharp surface, characterized with wavy, undulatory relief. Sample: **23.75**.
- 13 4.15 28.0 Light to dark gray burrow-mottled ribbon limestone. Common fossiliferous-intraclastic packstone/grainstone deposits. Stylolites present. Massive to thick bedded appearance. Parts may be thrombolitic. Sedimentary structures are difficult to observe due to a fresh exposure. Unit top is wavy, irregular and may represent a dissolution surface. Samples: **TZ24.65**, TZ26.65, TZ27.75.
- 14 0.65 28.65 Dolomitized microbial (cryptalgal) laminate or stratiform stromatolite characterized with horizontal, slightly crinkly lamination. Some laterally linked hemispheroidal (LLH) stromatolite, containing wavy, crinkly lamination, is present in the upper part of the unit. Small fenestrae and desiccation cracks filled with dolomite cement are visible. Some small incorporated intraclasts. Light gray to brownish. Unit top is a prominent, sharp, slightly wavy to planar surface marked by a thin (1-2 cm) shale. Samples: **TZ28.15**, **TZ28.25**.
- 15 0.3 28.95 Dark, reddish gray thrombolite layer with characteristic mottled fabric overlain by weathered ribbon limestone with argillaceous

portions reaching 2-3 cm in thickness. Stylolites present. Unit top is weathered and marked with about 5 cm thick shale. Samples: **TZ28.65**, TZ28.8.

- | | | | |
|----|------|-------|--|
| 16 | 0.55 | 29.5 | Ribbon rocks containing undulose, 1-3 cm thick, weathered limestone layers interbedded with argillaceous layers in the lower part. Small intraclasts (2-3 mm) and some skeletal (trilobite) fragments visible within the limestone layers. The upper part of the unit is composed of dolomitized, light to medium gray, medium- to fine grained couplets. These deposits comprise 15 and 25 cm thick layers, with visible horizontal physical lamination. Unit top is a planar, very subtle surface that separates the underlying couplets from the overlying mottled limestone. Samples: TZ29.0, TZ29.25 . |
| 17 | 1.5 | 31.0 | Thrombolitic deposit with massive to mottled appearance in the lower part of the unit. Gradational contact with the overlying ribbon limestone composed primarily of fossiliferous-intraclastic packstone/grainstone layers. Some burrow-mottling and stylolites present. The upper part of the unit composed of light to medium gray to brownish couplets containing intraclastic bases overlain by dolomicritic deposits. Couplet deposits are separated from the underlying ribbon rocks along a prominent stylolite. Upper boundary of the unit is a prominent, sharp, slightly wavy surface marked by a thin 1-2 cm shale. Samples: TZ29.65, TZ30.5 , TZ30.65. |
| 18 | 0.75 | 31.75 | Ribbon rocks composed of laterally continuous, undulatory limestone layers interbedded with thin shale. Top of the unit is a planar surface marked by 2-3 cm thick shale. Sample: TZ31.15. |
| 19 | 0.4 | 32.15 | Burrow-mottled ribbon limestone. Medium to dark gray. Some intraclasts, skeletal fragments and pyrite visible. The uppermost 10 cm of the unit composed of one layer of light gray to brownish, dolomitized, medium-grained couplets bounded by thin shale. Unit top is weathered and not well exposed. Sample: TZ31.95 , TZ32.05. |
| 20 | 0.4 | 32.55 | Dolomitized coarse- to medium-grained couplets in the basal 10 cm of the unit. Light to medium gray to brownish. Micritic intraclasts visible in couplet bases. Horizontal lamination, some likely of microbial origin present at couplet tops. The upper part of the unit consists of dolomitized microbial deposits: LLH stromatolites overlain by stacked hemispheroidal (SH) stromatolites. Wavy, crinkly microbial lamination and very small fenestrae visible. Some |

micritic intraclasts incorporated. Upper unit boundary is sharp, undulatory, and marked by 2-3 cm thick shale. Samples: **TZ32.2**, **TZ32.4**.

- | | | | |
|----|------|-------|---|
| 21 | 1.2 | 33.75 | Burrow-mottled ribbon rocks comprise the lower 80 cm of the unit. Medium to dark gray in color. May in part be thrombolitic. Small voids with sparite visible. Layer thickness: 10-15 cm, to massive appearance. Upper part is composed of primarily medium-grained couplets with small intraclasts in couplet bases, and horizontally laminated couplet tops. Unit top is sharp, slightly wavy, and marked by a very thin shale. Sample: TZ32.7. |
| 22 | 0.7 | 34.45 | Light gray, dolomitized medium- to coarse grained couplets in the basal part of the unit. The remaining part of the unit consists of microbial laminates (stratiform stromatolite) characterized by prominent crinkly horizontal laminations, and interbedded with several thin (< 1 cm) calcareous shale intervals. Unit top is weathered and not well exposed. Samples: TZ33.75, TZ34.35. |
| 23 | 0.25 | 34.7 | Light gray to brownish calcareous shale interbedded with thin microbial (cryptalgal) laminates and calcareous siltstone layers. Poorly exposed. |
| 24 | 0.65 | 35.35 | Light gray calcareous siltstone interbedded with microbial laminate and thin (2-3 cm) shale layers. Fissile to very-thinly bedded. Planar horizontal laminations visible. Layer thickness increases and the amount of shale decreases upward. Unit top is sharp, planar. Samples: TZ34.8, TZ35.05 . |
| 25 | 0.95 | 36.4 | Lower part of the unit consists of light gray to brownish coarse- and medium-grained couplets with intraclastic bases and microbial laminae in upper parts. Couplet thickness ranges from several mm to 2-3 cm. Microbial (cryptalgal) laminate dominates in the upper part of the unit. Prominent horizontal, crinkly to wavy lamination. Some incorporated intraclasts. Unit top is partially covered and not well exposed. Samples: TZ35.8, TZ36.25. |
| 26 | 0.2 | 36.6 | Medium gray carbonaceous shale interbedded with thin microbial (cryptalgal) laminate layers. Fissile to 1-2 cm thick layers. Unit top is slightly undulatory. |
| 27 | 1.05 | 37.65 | Light gray, microbially laminated deposits. In the lower part interbedded with thin calcareous shale to carbonaceous siltstone. Thin (< 1 cm) shaly intervals also present in the middle part of the |

unit. Prominent horizontal, crinkly to slightly wavy laminations. Desiccation features (mud cracks) and some incorporated intraclasts visible. Unit top is sharp and slightly wavy. Sample: **TZ36.85**.

- | | | | |
|----|------|-------|--|
| 28 | 1.5 | 39.15 | Medium-grained couplets in the lower part. Light to medium gray in color. Horizontal and cross-stratification, as well as truncational couplet bases visible. Stylolites present. Microbial (cryptalgal) laminates dominate in the upper part of the unit. Some interbedded mechanical couplets present. Horizontal lamination is visible, both wavy, crinkly microbial and planar, physical laminae. Common intraclasts (maximum 5 mm in diameter). Unit top is not exposed. Samples: TZ37.95 , TZ38.85 . |
| | 0.9 | 40.05 | Covered interval. |
| 29 | 1.1 | 41.15 | Dolomitized microbial (cryptalgal) laminates. Light to medium gray. In the lower part interbedded with thin shaly intervals. Common mudcracks. Layer thickness: from fissile to 20 cm. Pronounced horizontal crinkly, wavy lamination in the upper part of the unit. Unit top is not well exposed. Samples: TZ40.75 , TZ40.85 . |
| 30 | 1.1 | 42.25 | Thrombolitic bioherm (0 to 30 cm thick) in the base of the unit. Dark brownish-gray; massive to mottled appearance. Separated from the fine- to medium-grained dolomitized couplets in the upper part of the unit by a thin (about 1 cm) shale. Light gray. Cross-stratification visible in the deposits comprising couplet bases, and horizontal laminations are common in the upper parts of couplets. Some microbial laminae visible in the upper part of the unit. Unit top is sharp and marked by a prominent stylolite. Samples: TZ41.15 , TZ41.95 . |
| 31 | 0.65 | 42.9 | Dolomitized microbial (cryptalgal) laminates. Light to medium gray. Horizontal, planar to crinkly lamination and some stylolites present. Thin, calcareous shale intervals present in the middle, extremely weathered part of the unit. Layer thickness: from fissile to 20 cm. Some laminae contain common small intraclasts. Unit top is wavy and marked with thin (2 cm) shale. Samples: TZ42.45 , TZ42.7 . |
| 32 | 0.65 | 43.55 | Dolomitized mudstone to fine-grained couplets in the lower part of the unit. Abundant vuggy porosity related to evaporite molds and small (2-3 cm) nodules. Some mottling (burrows?) present. The |

upper part of the unit is dominated by coarse-grained couplets composed of intraclastic bases and horizontally laminated upper micritic parts. Medium gray. Unit top is sharp, planar to slightly wavy. Samples: TZ43.0, TZ43.15.

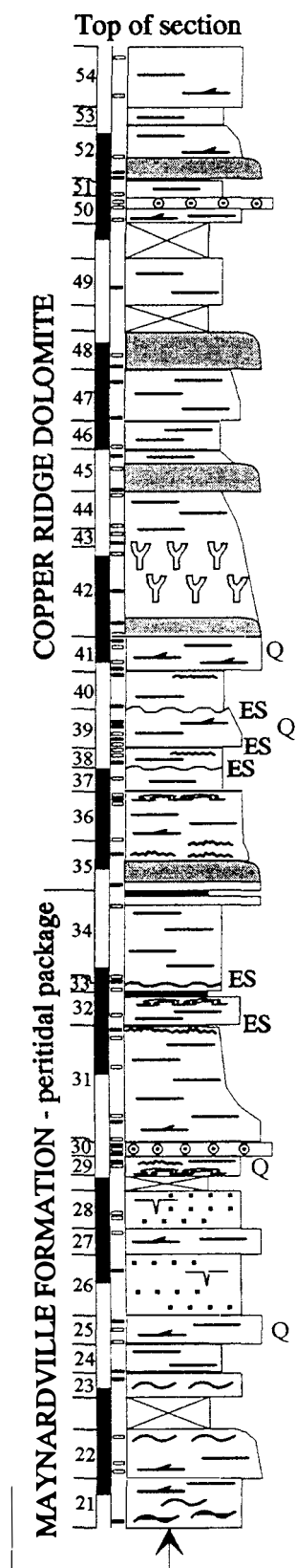
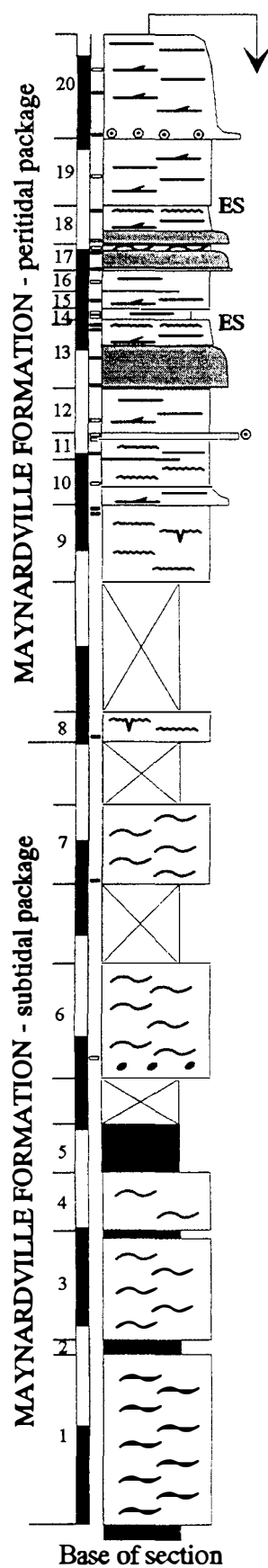
- | | | | |
|----|------|-------|--|
| 33 | 0.7 | 44.25 | Microbial (cryptalgal) laminates overlain by thrombotic deposits. Common horizontal, crinkly to wavy lamination in the lower part. The contact with the overlying thrombolite is marked by a stylolite or a sharp, wavy surface. The thickness of the thrombolite varies laterally from about 15 to 45 cm. Mottled appearance with some vuggy porosity present. Medium to dark gray. Unit top is a wavy surface marked by a 1-2 cm thick shale. Sample: TZ43.55, TZ44.0 . |
| 34 | 1.0 | 45.25 | Coarse- to medium-grained couplets. Light to medium gray. Prominent horizontal lamination and some cross-stratification is visible in the basal couplet parts. A silicified oolite layer (8-9 cm thick) occurs near the base of the unit. Ooids, and some large (1 cm) intraclasts present in the bases of coarse couplets. Upper part of the unit contains thinly bedded medium-grained couplets, interbedded with fissile shale intervals. Unit top is weathered and not well exposed. Samples: TZ44.35 , TZ44.45, TZ45.15. |
| 35 | 0.9 | 46.15 | Dolomitized medium-grained couplets. Some coarse-grained couplet deposits, containing intraclasts 3-5 cm long, are present at the unit base. Intraclastic couplet bases also contain some ooids and quartz sand grains, and are commonly silicified. Well developed medium-grained couplets in the remaining part of the unit are 1-3 cm thick and have up to 5 mm thick bases containing ooids and some quartz sand grains. An irregular erosional surface occurs in the middle part of the unit. The surface is marked by a thin shaly/silicified crust and likely represents an exposure surface. Stylolites are common in the upper part of the unit. Unit top is weathered and marked by 5-10 cm thick shale. Samples: TZ45.25 , TZ45.8. |
| 36 | 1.65 | 47.4 | Dolomitized mudstone to fine-grained couplets. Mottled fabric is indicative of bioturbation, but also resembles a thrombotic fabric. Medium to dark gray. Stylolites are abundant. They occur spaced at every 8-12 cm, and have a maximum amplitude of about 1.5 cm. Small vugs present. Some horizontal, slightly wavy laminations visible in the upper part of the unit. Unit top is sharp, planar. Samples: TZ46.55, TZ47.65 . |

- 37 0.45 48.25 Dolomitized coarse- to medium-grained couplets. Coarse-grained intraclastic bases are prominent in the basal, 15 cm thick layer, which is bound on top by a thin shale interval. Upper part of the unit consists primarily of medium grained couplets with ooids and small intraclasts in the bases. Some horizontal laminations visible in the upper parts of couplets. Thin shaly layers separate some of the couplets and give this unit a ribbon laminated appearance. Unit top is an irregular, wavy, erosional surface, marked by a thin shale and substantially weathered. Samples: **TZ47.85**, TZ48.15.
- 38 0.5 48.75 Fine-grained, dolomitized couplets. Planar, horizontal laminations visible. Medium gray. Unit top is not exposed. Sample: **TZ48.25**.
- 0.2 48.95 Covered interval.
- 39 0.25 49.2 Dolomitized mudstone truncated by coarse-grained intraclastic packstone deposit containing micritic intraclasts reaching a maximum length of 6-7 cm. The intraclastic lag deposit is overlain by several burrow(?) -mottled, undulatory, dolomitized mudstone layers (1-2 cm thick). Light to medium gray to brownish. Samples: **TZ48.95**, TZ49.1.
- 40 0.4 49.60 Dolomitized couplets to fine-grained couplets comprise two layers separated by 2-3 cm thick shale interval. Some horizontal laminations and stylolites are visible. Some mottling present. Unit top is not exposed. Sample: TZ49.45.
- 0.2 49.8 Covered interval.
- 41 0.35 50.15 Dolomitized mudstone to fine-grained couplets. Medium gray. Very poorly exposed. Some stylolites and horizontal lamination visible. Unit top is weathered and poorly exposed. Sample: TZ50.05.
- 42 0.9 51.05 Thrombolite overlain by microbial deposits and fine-grained couplets. Light to medium gray/brownish. Unit base is wavy and extensively weathered. Vuggy porosity is common within the thrombolitic deposit. The contact with the overlying microbial deposits is gradational. Microbial deposits show wavy, crinkly, discontinuous lamination typical of laterally linked hemispheroidal (LLH) stromatolites. Small fenestral voids, stylolites, and rare desiccation cracks are present. Upper part of the unit is poorly exposed. It consists of 5-25 cm thick layers composed of fine-

grained couplets. Stylolites and planar, horizontal lamination are visible. Unit top is covered. Samples: **TZ50.15**, **TZ50.25**, **TZ50.45**, TZ50.8.

- | | | | |
|----|------|-------|---|
| 43 | 0.3 | 51.35 | Dolomitized mudstone to fine-grained couplets. Light to medium gray to brownish. Mottled appearance. Some pyrite weathered to Fe-oxide present. Unit top is not exposed. Samples: TZ51.05 , TZ51.25 . |
| | 1.25 | 52.3 | Covered interval. |
| | | | Copper Ridge Dolomite (?) |
| 44 | 0.75 | 53.05 | Medium- to fine-grained couplets. Light to medium gray. Unit base is sharp, planar. Layer thickness: 10-25 cm. Layer boundaries are sharp, planar to slightly wavy. Average couplet thickness: about 1 cm. Some dark gray, small (maximum 2-3 mm) intraclasts visible in the bases of some couplets. Planar horizontal lamination present. Sample: TZ52.45 . |
| | 1.05 | 54.1 | Covered interval. |
| 45 | 0.4 | 54.5 | Medium- to fine-grained couplets. Very poorly exposed. Medium gray. Common vuggy porosity. Some horizontal lamination visible. Unit top is not exposed. Sample: TZ54.1 .
The rest of the section is not exposed. |

Figure A.4. Stratigraphic column measured at the Flat Gap outcrop.



The Flat Gap Outcrop (FG)

The Flat Gap outcrop is contained within the Copper Creek thrust sheet, 12.5 miles northeast from Thorn Hill. The exposure is located in Hancock County, 1.3 miles from state highway 131, along the northeastern side of the road from Flat Gap toward Sneedville. At this locality the upper part of the Nolichucky Shale is partially exposed. The contact with the overlying Maynardville Formation as well as the lowermost Maynardville are poorly exposed and extensively weathered. This part of the stratigraphic succession is described only briefly and was not sampled.

Unit	T (m)	C.T. (m)	Description
Maynardville Formation			
1	3.35	3.35	Very poorly exposed ribbon rocks overlying paper laminated silty shale of the Nolichucky Shale. Thin limestone layers, composed primarily of fossiliferous packstone occur interbedded with shale and laminated calcareous siltstone.
2	0.3	3.65	Carbonaceous shale interbedded with several thin argillaceous/silty carbonate layers.
3	2.3	5.95	Ribbon rocks without interbedded shale intervals. Limestone layers are composed primarily of mudstone, and some packstone/grainstone deposits which are more abundant in the lowermost part of the unit. Mudstone layers are occasionally laminated and burrow-mottled. Packstone/grainstone layers contain small intraclasts and trilobite fragments. Argillaceous dolomicrite portions are rather thick (up to 7 cm). Unit top is marked by 20 cm thick calcareous shale.
4	1.2	7.15	Similar to the underlying ribbon rocks composed of alternating limestone and argillaceous dolomicrite layers. Limestone layers are dominated by mudstone, in addition to several fossiliferous packstone/grainstone layers.
5	1.0	8.15	Poorly exposed and extensively weathered paper laminated calcareous shale interbedded with several thin (up to 1 cm) calcareous siltstone and argillaceous/silty carbonate layers.
	1.0	9.15	Covered interval. Most likely represents a shale interval.
6	2.4	11.55	Ribbon rocks without interbedded shale. Nodular appearance in places. Mudstone layers predominate. Some horizontal laminations and burrow-mottling visible. Lenses of flat-pebble conglomerate present in the lower part of the unit. Sample: FG0.6.

- 1.5 13.05 Covered interval. Some layers of ribbon rock (without interbedded shale) are exposed, but may not be in place.
- 7 1.65 14.7 Ribbon rocks composed of limestone layers interbedded with argillaceous dolomicritic layers. Only partially exposed. Light to medium gray. Limestone layers are primarily composed of mudstone. Horizontal lamination and burrow mottling present in some of the layers. Thickness of limestone layers decreases upward. Both lower and upper unit boundaries are not exposed. Sample: **FG5.1**.
- 1.5 16.2 Covered interval.
- 8 0.5 16.7 Microbial (cryptalgal) laminates. Medium gray. Composed of two layers of approximately the same thickness, separated by thin (2-5 mm) shale. Wavy, crinkly, horizontal microbial lamination, some mudcracks, and small fenestrae present. The unit may not be entirely in place. Unit boundaries are not exposed. Sample: **FG8.2**.
- 2.7 19.4 Covered interval.
- 9 1.7 21.1 Microbial (cryptalgal) laminates. Fissile to about 30 cm thick layers. Prominent wavy, crinkly horizontal microbial lamination, mudcracks, and some small fenestral voids. Thin shaly intervals present along upper layer plane. Unit top is sharp, wavy, and marked by 2-3 mm thick shale. Samples: **FG12.9**, **FG13.0**.
- 10 0.7 21.8 Dolomitized coarse- to medium-grained couplets overlain by microbial laminates. Couplet bases are truncational, and consists of lag deposits, up to 4 cm thick, containing common intraclasts (maximum 2-3 cm long), some ooids, and skeletal fragments (trilobites, echinoderms). Stylolites and some pyrite present. The upper part of the unit is not well exposed. It consists of microbial deposits that exhibit horizontal, crinkly lamination, and some mudcracks. Medium to dark gray. Unit top is planar and marked by up to 8 cm of shale. Sample: **FG13.45**.
- 11 0.65 22.45 Microbial (cryptalgal) laminates comprising two layers (20 and 25 cm thick). Medium gray/brownish. Characteristic microbial lamination present but no mudcracks nor fenestrae were observed. The boundary between the two layers is wavy and marked with a thin shale interval. One stylolite is present in the upper layer. Some lamination characteristic of mechanical laminates (couplets) present

at the top of the second layer which is capped by silicified medium to dark gray, intraclastic-oid grainstone that comprise truncational couplet bases. Unit top is a planar upper couplet boundary, and not a layer boundary. Samples: **FG14.0**, **FG14.35**, **FG14.4**.

- | | | | |
|----|------|-------|---|
| 12 | 0.75 | 23.2 | Medium-grained couplets. Light to medium gray. Prominent planar horizontal lamination. Couplet bases contain small intraclasts and ooids. Couplet thickness: several mm to about 5 cm. Stylolites and some chert present. Unit top is a sharp, planar to slightly wavy surface, marked by about 1 cm thick shale and a silicified crust. Sample: FG14.65 . |
| 13 | 1.35 | 24.55 | Thrombolite overlain by medium-grained couplets and capped by stromatolites. Thrombolitic deposit is dark gray, very porous, and has mottled appearance. Some burrows present. Coupled deposits are dolomitized, medium gray/brownish, and are composed of oolitic packstone in the basal part, overlain by laminated mudstone. Some burrows and/or desiccation cracks present in the upper, muddy parts of the couplets. Uppermost 20 cm of the unit consist predominantly of LLH stromatolites, interbedded with some burrow(?) -mottled and partially silicified thrombolite(?) deposits. The unit top is a prominent, irregular surface marked by about 10 cm of erosional relief and capped by a maximum of 5 cm silicified laminated crust. Samples: FG15.2 , FG15.8 , FG16.4 , FG16.45 . |
| 14 | 0.25 | 24.8 | Fine-grained dolomitized couplets. Medium gray to brownish. Planar horizontal lamination visible. Thin (1-2 mm) grainy (peloidal?) bases. Couplet thickness: several mm to 2 cm. The uppermost 5 cm of the unit contain thin muddy couplets capped by partially silicified microbial laminae, giving the unit top a wavy, cherty, laminated crust appearance. The unit is capped by a thin (< 5 mm) shaly interval. Samples: FG16.55 , FG16.75 . |
| 15 | 0.35 | 25.15 | Medium- to fine-grained, dolomitized, 1 to 5 cm thick couplets. Light to medium gray. Couplet boundaries are sharp, and range from planar to truncated and irregular. Some cross-lamination present in the basal couplet deposits. Unit top is marked by a laminated crust, and a 1-2 cm thick shale, similar to the top of the underlying unit. Sample: FG17.0 . |
| 16 | 0.45 | 25.6 | Medium- to fine-grained, dolomitized, couplets similar to the deposits from the underlying unit. Medium to dark gray. Couplets are slightly thinner (several mm to 2 cm), and the couplet bases are |

slightly more wavy. Some silicified lenses and nodules are present, as well as the lenses of a yellowish argillaceous deposit. Unit top is a prominent pressure dissolution (stylolite) zone, about 7 cm thick. Sample: FG17.3.

- | | | | |
|----|------|-------|---|
| 17 | 0.5 | 26.1 | Thrombolite deposit with an intraclastic lag deposit at the base and capped with a ribbon-laminated deposit. Planar horizontal lamination, typical of couplet deposits is present at the very base of the unit, and is truncated by intraclastic packstone/grainstone lenses. Micritic intraclasts are up to 2 cm long, and occur associated with some pyrite. The overlying thrombolite is medium to dark gray, and has mottled appearance. Burrows with geopetal fabric are common. The uppermost 10 cm of the unit consists of couplet-like deposits composed primarily of mudstone with very thin grainy (peloidal) lenses at the base. The couplets have a wavy to nodular appearance and are separated by thin argillaceous interlayers, which give these deposits a ribbon-laminated appearance. Unit top is wavy, and marked by 1-2 cm thick shale. Samples: FG17.6 , FG17.95 , FG18.0. |
| 18 | 0.8 | 26.9 | Thrombolite overlain by couplets capped by microbial deposits. The basal thrombolitic deposit (about 17 cm thick) is very porous, weathered, and has a mottled appearance. Burrows and evaporite molds are common. Some vugs (evaporite molds) are also present in the lowermost part of the overlying couplets. The couplets are medium- to fine-grained and exhibit planar, horizontal lamination. Some stylolites present. The unit top is marked by a medium to dark gray silicified crust, characterized by clotted to laminated microbial fabric. Vuggy porosity is associated with this interval. Samples: FG18.1, FG18.85 . |
| 19 | 1.4 | 28.3 | Medium- to fine-grained, up to 3-4 cm thick couplets. Dark gray. Horizontal lamination and rare cross-stratification present. Small intraclasts and ooids present at couplet bases. Stylolites present. Couplet tops are commonly capped by partially silicified laminated microbial crusts. Unit top is a planar surface marked with some evidence for pressure solution (stylolitization). Sample: FG19.5. |
| 20 | 2.25 | 30.55 | Dolomitized medium- to fine-grained couplets. The basal part consists of weathered, poorly exposed, dark gray, ooid grainstone deposit. The overlying couplets are 1-4 cm thick. The thickness of basal, grainy couplet deposits decreases upward. Common stylolites. Shaly intervals (up to 2 cm thick) interbedded with couplets in the upper part of the unit. The upper unit contact is |

sharp, planar. Samples: **FG20.4**, **FG21.25**, **FG21.75**.

- | | | | |
|----|------|-------|---|
| 21 | 0.7 | 31.25 | Ribbon to nodular limestone overlain by couplets. The lower part of the unit contains wavy, undulatory limestone layers interbedded with extensively weathered shaly intervals, and laminated, brownish argillaceous dolomicritic interlayers. Limestone layers are composed of skeletal (trilobite) packstone to mudstone deposits. Rare burrows present. The upper part of the unit lacks shale, and is composed of 3-4 cm thick couplets with planar, horizontal bases. Unit top is sharp, slightly wavy. Sample: FG22.65 . |
| 22 | 1.0 | 32.25 | Coarse- to medium-grained, up to 5-6 cm thick couplets. Light to medium gray/brownish. The basal, grainy parts of couplets are up to 2-3 cm thick, and contain common ooids and intraclasts (maximum 2 cm long). Common horizontal and cross-lamination. Stylolites present. The uppermost 15 cm of the unit resembled ribbon-laminated deposits from the lower part of the underlying unit. Limestone layers are wavy, undulatory, and are composed of dark to medium gray burrow(?) mottled mudstone. Unit top is not exposed. Samples: FG23.4 , FG23.6 , FG24.1 . |
| | 0.55 | 32.8 | Covered interval. |
| 23 | 0.45 | 33.25 | Similar to the upper part of unit 22. Ribbon rocks composed of wavy, undulatory, micritic limestone layers interbedded with argillaceous dolomicritic partings. Medium to dark gray. Unit top is planar to slightly wavy, and is marked by 5 cm thick shale interval interbedded with thin (1-2 mm) carbonate layers. Sample: FG25.15 . |
| 24 | 0.55 | 33.8 | Fine-grained couplets. Light to medium gray. Couplets are 1 to 10 cm thick, and have planar, horizontal boundaries. Couplet bases are composed of thin (up to 5 mm) lenses containing ooids. Vugs (most likely after evaporite nodules), up to 7 cm in diameter, are common in the uppermost part of the unit. Unit top is sharp and slightly undulatory. Sample: FG25.25 . |
| 25 | 0.65 | 34.45 | Coarse- to medium-grained couplets. The lowermost (about 5 cm thick) part of the unit is weathered out, which may suggest the presence of a shaly interval along the contact with the underlying unit. Couplet thickness: < 1 cm to > 10 cm. Couplets have wavy to irregular (truncational) contacts. Intraclasts from the bases of coarse-grained couplets are up to 3-4 cm long, and occur in association with common quartz sand grains. The basal, grainy |

couplet deposits are occasionally cross-stratified and partially silicified. Samples: FG25.85, FG26.1, **FG26.3**.

- | | | | |
|----|------|-------|---|
| 26 | 1.15 | 35.6 | Calcareous siltstone interbedded with silty carbonate layers and calcareous shale. Light to medium gray/brownish. Weathered and not well exposed. Fissile to 15 cm thick, undulatory layers. Horizontal lamination, some cross-stratification and vertical burrows visible. Several intraclastic lag deposits present. Some trace fossils and mudcracks visible along bedding planes. Unit top is sharp, planar. Sample: FG27.2 . |
| 27 | 0.45 | 36.05 | Coarse- to medium-grained couplets comprising three layers (20 cm, 15 cm, and 10 cm thick) with planar layer boundaries. Light to medium gray/brownish. Planar, horizontal lamination visible. Couplet bases contain common intraclasts (up to 2 cm long), some ooids and quartz sand grains. Vugs (up to 2 cm in diameter) are common in the uppermost layer. Unit top is sharp, planar. Sample: FG27.95. |
| 28 | 0.8 | 36.85 | Similar to unit 26. Calcareous siltstone interbedded with argillaceous/silty/arenaceous carbonate layers and carbonaceous shale. Light gray/brownish. Fissile to 3 cm thick layers. Horizontal lamination and some cross-stratification visible. Trace fossils and mudcracks visible along bedding planes. Unit top is not exposed. Samples: FG28.2, FG28.3. |
| | 0.2 | 37.05 | Covered interval. |
| 29 | 0.35 | 37.4 | Partially silicified microbial deposits. Light to medium gray. SH stromatolites (up to 5-7 cm high hemispheroids) in the lower part. Middle part of the unit consists of LLH to stratiform (microbial laminates) stromatolites. Medium- to coarse-grained couplets comprise the uppermost part of the unit. Intraclasts ranging in size from < 1 mm to 3 cm, occur associated with quartz sand grains. Micritic deposits comprising upper parts of couplets contain evaporite molds and have mottled fabric. Unit top is sharp, planar, marked by < 1 cm thick shale. Samples: FG29.25, FG29.3 . |
| 30 | 0.3 | 37.7 | Silicified oolite. Medium to dark gray. Thin-burrow mottled thrombolite at the base. Burrows with geopetal fabric common. Ooids and micritic intraclasts (up to 2-3 mm) present at burrow bottoms; upper parts of burrows contain sparite. Middle part of the unit dominated by silicified oolite without observable sedimentary structures. Weathered pyrite present. The uppermost part of the |

unit contains partially silicified microbial laminates. Brecciated fabric. Intraclasts and common quartz grains present. Unit top is wavy and marked by a 3 cm thick shaly interval. Samples: **FG29.4**, FG29.45, FG29.5.

- | | | | |
|----|------|-------|---|
| 31 | 2.1 | 39.8 | Dolomitized couplets. Intraclastic basal lags present in the coarse-grained couplets from the lower part of the unit. Intraclasts reach a maximum size of about 2 cm. Middle part of the unit dominated by medium-grained couplets. Some vuggy porosity present, primarily related to evaporite molds. The uppermost part of the unit dominated by light gray, fine-grained couplets and dolomitized mudstone. Mottled appearance in places. Common stylolites, and some horizontal lamination present throughout the unit. Unit top is a wavy surface, marked by an about 3 cm thick dark gray, laminated, silicified crust. Samples: FG29.7, FG30.15 , FG30.25, FG31.15, FG31.65, FG31.75 . |
| 32 | 0.75 | 40.55 | Medium-grained couplets overlain by microbial deposits. Medium gray. Planar, horizontal lamination and stylolites present in the lower part of the unit. Couplet thickness: from several mm to 5 cm. Microbial deposits are represented by SH stromatolites. Individual hemispheroids are up to 10 cm high. Unit top is marked by a 10 cm thick shale. Sample: FG32.05. |
| 33 | 0.15 | 40.7 | Fine- to medium-grained dolomitized couplets. Wavy, discontinuous lamination present. Unit top is a wavy surface characterized with up to 10 cm of erosional relief, and capped by a laminated, dark gray, 3-4 cm thick, shaly crust. Sample: FG32.6. |
| 34 | 1.95 | 42.65 | Similar to the underlying unit. Fine-grained couplets and dolomitized mudstone with mottled fabric. Light to medium gray. Horizontal lamination, evaporite molds, partially silicified evaporite nodules, and several stylolites present. Thin shale intervals occur between carbonate layers, which range in thickness between 5 cm and 30 cm. The uppermost layer consists of coarse-grained couplets with intraclastic lag deposits. Unit top is marked by a 10 cm thick shale. Samples: FG32.7 , FG33.85, FG34.4. |

Copper Ridge Dolomite

- | | | | |
|----|------|------|---|
| 35 | 0.95 | 43.6 | Thrombolite overlain by laminated microbial deposits. The lowermost part of the unit is composed of coarse-grained couplets. The contact with the overlying microbial deposits is marked by a stylolite. Thrombolite is dark gray in color, has mottled appearance and contain vuggy porosity. Parts have a digitate stromatolite |
|----|------|------|---|

fabric. The upper part of the unit exhibits prominent wavy lamination typical of LLH stromatolites. Medium to dark gray. Partially silicified. Unit top is slightly wavy, and resembles a stylolite. Samples: **FG34.7**, **FG35.35**.

- | | | | |
|----|------|-------|--|
| 36 | 1.0 | 44.6 | Medium-grained couplets overlain by SH stromatolites. Medium gray. Layer thickness: 5 cm to 30 cm. Lower part of the unit is weathered and poorly exposed. Stylolites present. Some microbial laminates occur interbedded with couplets in the lower part. Couplet thickness: several mm to 2 cm. Characteristic horizontal lamination, cross-stratification and truncational couplet bases visible in better exposed parts. The upper part of the unit contains microbial hemispheroids, over 5 cm high, composed of laminated micritic deposits. Deposits in between stromatolitic hemispheroids are coarser-grained and contain micritic intraclasts, peloids, ooids, and quartz grains. Small mudcracks present. Unit top is sharp, wavy, and marked by 2-3 cm thick shaly interval. Samples: FG35.6, FG36.4, FG36.45 , FG36.5. |
| 37 | 0.4 | 45.0 | Fine-grained dolomitized couplets. Light to medium gray/brownish. Vuggy pores, partially filled with sparite present. Mottled (burrowed?) appearance in place. Some planar, horizontal lamination present. Unit top is a prominent wavy to irregular surface characterized by 15-20 cm of erosional relief and capped by a 2-3 cm thick shaly crust. Sample: FG36.85. |
| 38 | 0.35 | 45.35 | Fine-grained dolomitized couplets overlain by microbial laminates. Light to medium gray/brownish. Horizontal, planar laminations in the lower part of the unit are replaced by wavy, crinkly microbial laminations in the upper part. Mudcracks and fenestrae occur associated with microbial deposits. Unit top is a wavy to irregular erosional surface capped by 1-3 cm thick, medium to dark gray, dolomitized crust associated with some stylolites. Samples: FG37.1 , FG37.25, FG37.32. |
| 39 | 0.75 | 46.1 | Medium- to fine-grained dolomitized couplets. Light to medium gray. Stylolites present. Common mottled fabric likely related to bioturbation which caused disruption of the original couplet fabric resulting in discontinuous lamination. Couplet bases are occasionally cross-laminated and are composed of common quartz sand grains, and some small micritic intraclasts. Quartz grains interbedded in dolomicritic matrix form 3-5 cm thick, cross-bedded layers. Vuggy porosity, primarily represented by evaporite molds, is common in some of the layers which are correspondingly very |

weathered. Upper part of the unit is very porous and partially silicified. Unit top is marked by an erosional surface with up to 10 cm of relief. Topographical lows are filled with ooids and micritic intraclasts; microbial laminae are present on topographical highs. Samples: FG37.35, **FG37.5**, FG37.55, **FG37.8**, **FG37.9**.

- | | | | |
|----|------|-------|--|
| 40 | 0.65 | 46.75 | Fine- to medium-grained dolomitized couplets overlain by some microbial laminates. Light gray. Horizontal and cross-lamination visible in the lower part of the unit. Vuggy pores representing evaporite molds and nodules (up to 2-2.5 cm in diameter) also occur associated with these deposits. Couplets in the uppermost part of the unit are capped by some wavy, crinkly microbial laminae. Upper unit contact is an irregular, wavy surface marked by a thin (< 1 cm) shale. Samples: FG38.1 , FG38.7 . |
| 41 | 0.8 | 47.55 | Coarse-grained couplets. Light to medium gray. Layer boundaries are planar to slightly wavy, and marked by thin shaly intervals. Couplet thickness reaches a maximum of about 5 cm. Coarse-grained couplet bases are up to 2.5-3 cm thick and contain common micritic intraclasts and quartz grains. Intraclasts are up to 1 cm long. Some pyrite and chert occurs within the grainy couplet bases. Stylolites present. Micritic parts of couplets are often burrow(?) mottled, and contain some vuggy pores (evaporite molds and nodules?) associated with some chert. The upper unit contact is marked by a prominent stylolite. Samples: FG38.75 , FG39.0, FG39.35, FG39.45 . |
| 42 | 1.6 | 49.15 | Thrombolite overlain by digitate stromatolite. Thrombolite is dark gray, and has massive, mottled appearance, and variable thickness laterally. Intraclastic lag deposit and common pyrite are present at the base of thrombolite. The upper part of the unit is composed of digitate stromatolites. The typical branching microbial fabric is visible only on weathered surfaces. Microbial digits have crudely laminated fabric and contain small fenestrae. Interdigitate area contains small intraclasts and ooids. Some stylolites present. Unit top is a planar bedding plane along which some dissolution (stylolitization) appeared. Samples: FG39.55, FG39.75 , FG40.4 , FG41.05. |
| 43 | 0.35 | 49.5 | Digitate stromatolite with a gradual transition upward into medium- to fine-grained couplets. Medium to dark gray. Stylolites present. Intraclasts (up to 4 mm in diameter) present in the base of some of the couplets. Micritic parts of couplets are commonly burrow-mottled. Unit top is marked by a low relief stylolite. |

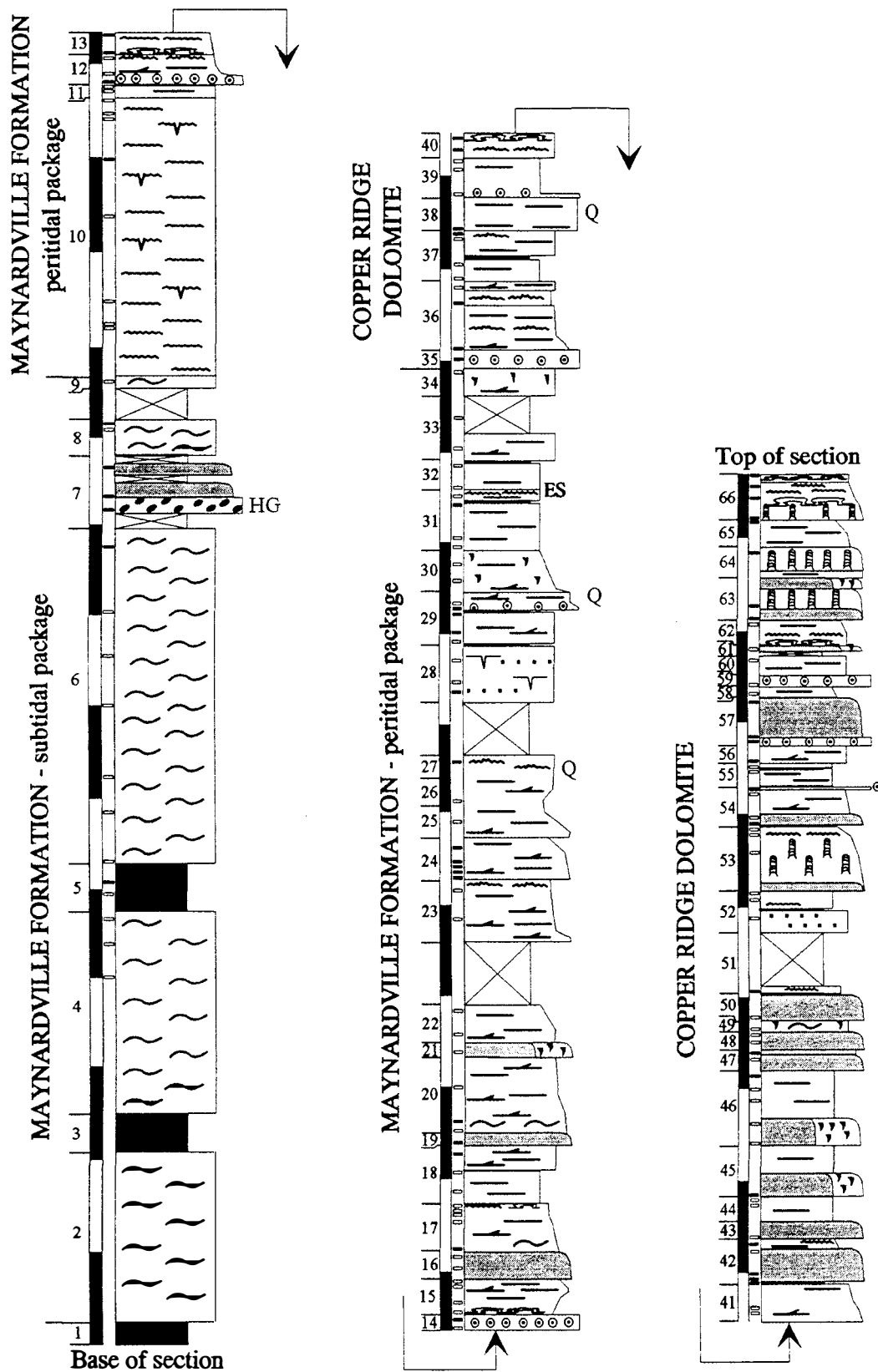
Samples: **FG41.15**, FG41.4.

- | | | | |
|----|------|-------|---|
| 44 | 0.8 | 50.3 | Similar to the uppermost part of the underlying unit. Medium- to fine-grained couplets. Medium to dark gray. Commonly bioturbated. Layer thickness: 20 cm, 10 cm, and 50 cm. Layer boundaries are planar to slightly wavy. Some horizontal planar lamination visible. Couplet thickness reaches a maximum of 2 cm. Unit top is irregular, weathered, and probably represents a stylolite. Samples: FG41.55, FG42.2. |
| 45 | 0.7 | 51.0 | Thrombolitic bioherm overlain by couplets. Thrombolite is characterized by mottled, clotted fabric. Dark gray. Many vuggy pores, likely related to evaporites, and some pockets with sparite present. The thrombolite has a biohermal shape with planar lower contact, and sharp, wavy upper boundary. The overlying couplets are fine- to medium-grained. Light to medium gray. Horizontal and cross-lamination visible. Evaporite voids, brecciation and some pyrite present. Mottled fabric in places. Unit top is sharp, slightly wavy, and marked by a 2-3 cm dark, black shaly interval. Samples: FG42.3 , FG42.5, FG42.9 . |
| 46 | 0.55 | 51.55 | Fine-grained dolomitized couplets. Light to medium gray. Layer thickness: 5-20 cm. Couplets range in thickness from several mm to 5 cm thick, and contain up to 5 mm thick grainy (peloidal) bases. Couplet contacts are planar, with only minor truncation present in some cases. Some horizontal lamination visible. Vuggy pores (maximum 2 mm in size) and stylolites present. Unit top is sharp, planar, and marked by thin (< 1 cm) shaly interval, reddish in color. Sample: FG43.05. |
| 47 | 1.05 | 52.6 | Medium- to fine-grained dolomitized couplets. Medium to light gray. Common vuggy porosity, likely related to evaporite dissolution. Couplet contacts are wavy, truncational in the lower part of the unit. The upper part exhibits horizontal lamination and some burrow-mottling. Stylolites present. Unit top is sharp, wavy, and marked by thin (< 1 cm) shale. Samples: FG43.6 , FG44.35 . |
| 48 | 0.7 | 53.3 | Thrombolite. Light to medium gray. Very weathered and poorly exposed. Mottled, clotted micritic fabric. Upper unit contact is not exposed. Samples: FG44.6 , FG44.85. |
| | 0.55 | 53.85 | Covered interval. |
| 49 | 0.85 | 54.7 | Fine-grained dolomitized couplets. Medium to dark gray. Layer |

thickness ranges from 2 cm to 7-8 cm. Stylolites present. Some wavy lamination visible. Parts of the unit are porous and very weathered. Unit top is not exposed. Sample: FG46.05.

- | | | | |
|----|------|-------|--|
| | 0.6 | 55.3 | Covered interval. |
| 50 | 0.55 | 55.85 | Medium-grained dolomitized couplets overlain by a silicified oolite. Very weathered and poorly exposed. Layer thickness: 7-8 cm. Horizontal lamination and some cross-lamination visible in the lower part of the unit. Upper part of the unit consists of poorly exposed, weathered, dark gray, silicified oolite layers. Some stylolites present. Unit top is poorly exposed. Samples: FG47.4, FG47.7, FG47.75. |
| 51 | 0.3 | 56.15 | Fine-grained couplets comprise one very porous, poorly exposed layer. Dark gray. Unit top is poorly exposed; appears planar and capped by thin (< 1 cm) dark, black, fissile shale. Sample: FG47.85. |
| 52 | 1.05 | 57.2 | Thrombolitic bioherm overlain by medium- to fine-grained couplets. The bioherm reaches a maximum thickness of 40 cm, and pinches out laterally. It consists of dark gray micritic deposit. Intraclastic lag deposit present at the bioherm base. Thin (about 2 cm) shale marks the top of the thrombolite. The overlying couplets are poorly exposed. Light to medium gray/brownish. Couplet thickness: several mm to 2 cm. Some planar, horizontal lamination and cross-lamination visible. Rare stylolites. Samples: FG48.15 , FG48.2 , FG48.45. |
| 53 | 0.4 | 57.6 | Fine-grained dolomitized couplets. Light to medium gray. Very weathered and poorly exposed. Layer thickness: 1 cm to 15 cm. Planar, horizontal lamination present. |
| 54 | 1.2 | 58.8 | Medium-grained dolomitized couplets. Medium gray. Layer thickness ranges from 5 to 25 cm, with a maximum of 60-70 cm. Couplet contacts are planar to wavy. Couplet thickness: from several mm to about 1 cm. Prominent horizontal and cross-lamination. Some chert nodules present in the lower part of the unit. Unit top is poorly exposed. Samples: FG49.85, FG50.6. Overlying 29 m of the succession is covered, followed by 16 m of exposed Copper Ridge Dolomite. |

Figure A.5. Stratigraphic column measured at the Lee Valley outcrop.



The Lee Valley Outcrop (LV)

The Lee Valley outcrop is located within the Copper Creek thrust sheet, 17.5 miles northeast from Thorn Hill. The Lee Valley section was first described and measured by Rodgers and Kent in 1948. This outcrop is located along state highway 66 in Hawkins County, approximately 1.1 miles northwest of the intersection between state highways 66 and 131. An almost complete exposure of the Maynardville Formation, and the lower Knox Group is present along the northeastern side of the road. The lowermost part of the Maynardville, and the underlying Nolichucky Shale are poorly exposed. This part of the stratigraphic succession was only briefly described and was not sampled.

Unit	T (m)	C.T. (m)	Description
Nolichucky Shale			
1	0.4	0.4	Poorly exposed paper laminated shale interbedded with several thin carbonate layers which are lithologically similar to limestone from the ribbon rocks in the lower part of the Maynardville.
2	3.8	4.2	Ribbon rocks composed of limestone layers interbedded with shale intervals. Weathered and partially covered.
3	0.8	5.0	Shale interbedded with several thin carbonate layers.
4	4.4	9.4	Ribbon rocks composed of limestone layers interbedded with shale intervals in the lower 50 cm of the unit. The remaining part of the unit consists of weathered, yellowish to brown, ribbon rocks without prominent interbedded shale. Less weathered parts reveal gray limestone layers, and brownish argillaceous dolomitic parts. Limestone layers are composed of fossiliferous (trilobite) packstone and laminated mudstone. Scattered pyrite present. Samples: LV0.0, LV0.7, LV1.35.
5	1.2	10.6	Carbonaceous shale and siltstone interbedded with several carbonate layers. Limestone layers exhibit some horizontal and cross-lamination, and are composed of mudstone, fossiliferous (trilobite) and peloidal wackestone/packstone. The uppermost part of the unit consists of nodular ribbon rock. Samples: LV1.9, LV2.2.
6	7.3	17.9	Thick bedded ribbon rock composed of limestone layers interbedded with thin argillaceous dolomicritic partings. Limestone layers are composed of skeletal (trilobite) and peloidal wackestone/grainstone, laminated mudstone and burrow-mottled mudstone. Samples: LV2.6, LV3.7, LV4.45, LV6.0, LV7.1,

LV8.1, LV9.5.

- | | | | |
|----|------|-------|---|
| 7 | 1.65 | 19.55 | <p>A 30 cm gap interval at the base of the unit may represent a weathered out shale. Overlying the gap is a weathered coarse-grained intraclastic packstone/grainstone deposit. Intraclasts are up to 3 cm long, and are commonly coated with pyrite/Fe-oxide, which is also common in intergranular pores, together with rare sphalerite and galena. Some skeletal (trilobite, echinoderm) fragments present. Thrombolite overlies this intraclastic deposit. Thrombolite deposit is very porous (burrowed?), medium to dark gray, with common weathered brownish patches. Some stylolites present. Some micritic intraclasts and skeletal fragments present in between micritic thrombolite mesoclots. Parts of the unit, including the uppermost part, are weathered out. Some remnant light gray calcareous shale present at the unit top. Samples: LV10.35, LV10.5, LV11.3.</p> |
| 8 | 0.95 | 20.5 | <p>Ribbon rock composed of limestone layers interbedded with argillaceous/silty dolomite layers and some shale intervals. The lower contacts of limestone layers are sharp; the upper contacts with the overlying argillaceous partings are gradational. Limestone layers are composed of mudstone and fine-grained fossiliferous wackestone/packstone. Rare layer-parallel veins filled with calcite cement present. Unit top is not exposed. Samples: LV12.2, LV12.3.</p> |
| | 0.65 | 21.15 | <p>Covered interval.</p> |
| 9 | 0.25 | 21.4 | <p>Ribbon rocks similar to the underlying unit, with slightly thinner limestone and dolomite partings. Planar, horizontal lamination visible in some of the limestone layers. Some crinkly, microbial lamination present in the upper part of the unit. Unit top is marked by a 5 cm thick gap. Sample: LV13.25.</p> |
| 10 | 5.9 | 27.3 | <p>Microbial (cryptalgal) laminate. The lower 20 cm is transitional between ribbon rocks and microbially laminated deposits. Prominent horizontal, wavy, crinkly lamination. Some burrows and mudcracks present. Some laminae are disturbed, broken, and deposits are reworked into elongated micritic intraclasts and peloids (maximum 1 mm thick, and 1 cm long). Rare small fenestrae visible. Layers range from fissile to about 30 cm thick. Light to medium gray/brownish. Parts of the unit are poorly exposed. Unit top is a sharp, planar layer boundary. Samples: LV14.4, LV14.5, LV14.95, LV16.75, LV17.95, LV18.9, LV18.95, LV19.2.</p> |

- | | | | |
|----|------|-------|--|
| 11 | 0.25 | 27.55 | Medium- to fine-grained couplets composed of peloidal bases and laminated micritic upper parts. Light gray. Couplet bases are planar to truncational. Lower part of the unit is highly weathered and partially covered. Unit top is wavy, and marked by 5 cm thick, medium to dark gray/brownish, calcareous shale to siltstone forming fissile to 1 cm thick, undulatory layers. Samples: LV19.45, LV19.5. |
| 12 | 0.65 | 28.2 | Medium- to fine-grained couplets underlain by intraclastic-oid packstone/grainstone deposit and capped by microbial deposits. Light to medium gray/brownish. Horizontal lamination and cross-stratification visible. Some of the couplets have burrow-mottled fabric. The uppermost part of the unit is composed primarily of LLH stromatolites and microbial laminates (stratiform stromatolites) with laminae commonly disrupted by desiccation cracks. Samples: LV19.55 , LV19.85, LV20.15. |
| 13 | 0.5 | 28.7 | SH stromatolites, interbedded with and overlain by stratiform stromatolites (microbial laminates). Medium gray/brownish. Characteristic wavy, crinkly microbial lamination and small fenestrae visible. Some laminae contain incorporated peloids. Rare sheet cracks present. Layer thickness: 5 cm to 30 cm. Samples: LV20.2 , LV20.6 . |
| 14 | 0.4 | 29.1 | Ooid wackestone/grainstone. Dark gray. Dolomitized and partially silicified. Chert and vuggy porosity is common in the lowermost part of the unit. Some micritic intraclasts (up to 2 cm long) present. The uppermost part of the unit is composed of couplets with oolitic bases. Layer thickness: 5-10 cm. Samples: LV20.7, LV21.0 . |
| 15 | 0.75 | 29.85 | SH stromatolites overlain by medium- to coarse-grained couplets. Light to medium gray. Microbial hemispheroids are up to 30 cm wide, and 10 cm high. Planar, horizontal lamination present in the upper part. Round, elongated intraclasts (up to 7-8 mm long), and ooids make up grainy couplet bases which are up to 2 cm thick and are occasionally silicified. Upper parts of couplets are composed of laminated mudstone deposits, some of which contain vuggy pores (after evaporite minerals). Upper couplet contacts are commonly truncated. Stylolites, with maximum amplitude of 5 cm, are present. Rare microbial lamination visible. Unit top is planar to slightly wavy. Samples: LV21.1, LV21.35, LV21.7, LV21.75. |
| 16 | 0.7 | 30.55 | Thrombolite. Very porous and weathered. Clotted, burrow- |

mottled fabric. Dark to light gray with weathered brownish patches. Samples: LV22.05, LV22.35.

- | | | | |
|----|------|-------|--|
| 17 | 0.9 | 31.45 | <p>Dolomitized coarse- to medium-grained couplets capped by microbial deposits. Medium to dark gray. Couplets exhibit common horizontal and cross-lamination. Muddy deposits comprising the upper parts of couplets contain shallow vertical burrows, and some evidence for soft sediment deformation and truncation. Couplets are not laterally continuous (pinch and swell), which coupled with argillaceous dolomicritic deposits present at some couplet tops, give this deposit a texture that resembles ribbon rocks. Oolitic and intraclastic packstone deposits, some partially silicified, form lenses, and bases of couplets. Micritic intraclasts are up to 1 cm long. The uppermost part of the unit is composed of silicified SH stromatolites. Wavy lamination and fenestral voids visible. Unit top is a sharp, wavy surface. Samples: LV22.55, LV23.0, LV23.15, LV23.2, LV23.4.</p> |
| 18 | 1.3 | 32.75 | <p>Fine-grained couplets in the lower part; medium-grained couplets in the upper part of the unit. Light to medium gray/brownish. Weathered stylolite surfaces with insoluble argillaceous residue present. Subtle horizontal lamination visible. Intraclastic (\pm ooids, peloids), truncational couplet bases present in the upper part of the unit. Rare chert (silicification of grainy couplet bases) present. Unit top is a planar, sharp surface. Samples: LV23.75, LV24.1, LV24.6.</p> |
| 19 | 0.25 | 33.0 | <p>Thrombolite. Dark gray. Clotted micritic fabric. Extensively burrowed. Burrows have geopetal fabric: infilled with internal sediment and occluded by sparite. Very porous and weathered. Rare intraclasts present at unit base. Upper unit contact is sharp, wavy. Sample: LV24.8.</p> |
| 20 | 1.7 | 34.7 | <p>Coarse- to medium-grained couplets. Undulatory, wavy layers in the lower part of the unit resemble a ribbon rock texture. Dark gray. Some sparite-filled burrows present. Common ooid-intraclastic grainstone layers. Horizontal lamination and stylolites common in the upper part of the unit which is dominated by medium-grained couplets. Medium to dark gray. Couplet have a maximum thickness of about 1.5 cm, with up to 5 mm thick grainy bases (small intraclasts, ooids, peloids), overlain by laminated mudstone. Couplet tops contain V shaped features (vertical burrows or mudcracks) filled with grainy deposits of the overlying couplets. Layer thickness reaches up to 15-25 cm. Layer</p> |

boundaries are planar. Layers are also commonly separated along stylolite surfaces. Samples: LV25.0, **LV25.25**, LV26.0.

- | | | | |
|----|------|-------|---|
| 21 | 0.3 | 35.0 | Thrombolite. Dark gray. Burrow-mottled with common vuggy pores. Rare evaporite molds present. Unit base is sharp, slightly irregular. Massive layering. Small amplitude stylolites and some clay seams present. Samples: LV26.8. |
| 22 | 0.7 | 35.7 | Medium- to fine-grained dolomitized couplets. Medium to light gray. Small intraclasts, some ooids and peloids comprise bases of well exposed, medium-grained couplets in the lower part of the unit. Upper parts of couplets are laminated, have truncated tops, and are occasionally disturbed by mudcracks. The upper part of unit is partially covered. Exposed layers represent fine-grained couplets composed of laminated dolomicrite and very thin bases. Couplet boundaries are planar. Some burrow-mottling visible. Unit top is not exposed. Samples: LV27.7, LV27.65. |
| | 1.45 | 37.15 | Covered interval. |
| 23 | 1.45 | 38.6 | Medium-grained couplets. The lowermost part of the unit contains coarse-grained couplets composed of ooid-intraclastic bases overlain by laminated dolomicrite. Horizontal lamination and stylolites are common in the remaining part of the unit together with less prominent cross-lamination. Some of the couplets have burrow-mottled fabric and vuggy porosity. Mudcracks present at upper couplet contacts. The uppermost 20 cm of the unit is comprised of LLH stromatolites with wavy, crinkly, commonly disrupted laminae. Common micritic peloids incorporated. Some vugs present (likely evaporite molds). Medium to light gray. Layer thickness: 10-30 cm. Unit top is sharp, irregular to wavy. Samples: LV29.75, LV30.3, LV30.45 . |
| 24 | 0.9 | 39.5 | Coarse- to medium-grained couplets. Light to medium gray. Couplet thickness: 2-3 cm. Layer thickness: 8-25 cm. Irregular, elongated, dolomicritic intraclasts and some ooids present in basal parts of couplets. Horizontal (planar to slightly wavy) and cross-lamination present. Couplet contacts are sharp, truncational. Burrow(?)mottling and vuggy porosity related to dissolution of evaporite minerals common in parts of the unit. Some small amplitude stylolites present. Samples: LV30.6 , LV30.8 , LV30.9 , LV31.35 . |
| 25 | 0.6 | 40.1 | Coarse- to medium-grained couplets. Medium to dark gray. Not |

- well exposed. Couplets reach a maximum thickness of about 5 cm. Planar, horizontal lamination and truncated couplet tops visible. Rare evidence for bioturbation (brownish patches), and some stylolites present. Parts of the unit are covered. Unit top is a wavy surface. Sample: LV31.75.
- 26 0.65 40.75 Fine- to medium-grained couplets comprising several layers with a maximum thickness of about 25 cm. Light to medium gray/brownish. Planar, horizontal lamination and some cross-lamination (especially in the upper part of the unit) visible. Couplets are not laterally continuous, and are thinner than in the underlying unit. Unit top is a gap marked by a spring (plastic tube). Sample: LV32.2.
- 27 0.55 41.3 Medium-grained couplets grading upward into microbial deposits. Planar horizontal lamination in the lower part is replaced by wavy crinkly lamination in the upper part of the unit. Microbial deposits are represented by LLH stromatolites. Some mudcracks and incorporated micritic intraclasts and quartz grains present. Unit top is sharp, slightly wavy, and not well exposed. Sample: LV33.15.
- 1.35 42.65 Covered interval.
- 28 1.15 43.8 Calcareous siltstone and shale interbedded with argillaceous/silty to arenaceous carbonate layers. Light gray to brownish. The deposits comprise undulatory layers that pinch and swell laterally. The layers are thin, fissile, to a maximum 10 cm thick. Shale is more common in the middle part of the unit which is poorly exposed. Carbonate layers become more abundant and thicker in the upper part of the unit. Carbonate layers are commonly normally graded (have a couplet texture), with some horizontal and cross-lamination visible. Prominent mudcracks and some trace fossils present along bedding planes. Small vugs (fenestrae?) and mottling (burrows?) visible. Unit top is marked by weathered, 5-7 cm thick shale interval. Samples: LV34.85, LV35.0, LV35.5.
- 29 1.1 44.9 Medium- to some fine-grained couplets in the lower part comprising several layers, with a maximum thickness of 25 cm, and separated by thin shale. Light to medium gray/brownish. Couplets near the base of the unit have upper parts disrupted by mudcracks and capped by microbial laminae. Horizontal (planar to wavy) and cross-lamination present. Couplets are several cm thick. Evaporite molds and some large vugs with *in situ* brecciation caused by dissolution of evaporites present. Middle part of the unit is poorly

exposed and reveals several dark gray to brown, 2-4 cm thick, undulatory ooid grainstone layers. The uppermost part of the unit consists of coarse-grained, light to medium gray, up to 5 cm thick couplets. Couplet bases contain common quartz grains and micritic intraclasts (up to 1.5 cm in diameter). Couplet contacts are sharp, truncational. Laminated mudstone comprises upper parts of couplets. Upper unit contact is sharp and slightly undulatory. Samples: LV35.8, **LV36.0**, **LV36.5**, **LV36.6**, LV36.7.

- | | | | |
|----|-----|------|---|
| 30 | 0.9 | 45.8 | <p>Burrow-mottled couplets and mudstone. Medium to dark gray. Massive layering; laterally splits into two layers. Lower part of the unit contains some coarse-grained couplets with intraclastic bases, and planar, horizontal laminations. The remaining part of the unit consists of burrowed mudstone to disturbed medium- to fine-grained couplets with wavy, discontinuous laminae. The laminae are commonly disrupted by evaporite molds, responsible for the vuggy porous appearance, and by rare mudcracks. Grainy deposits occur as discontinuous lenses and irregular pockets, rather than continuous basal couplet deposits. Some stylolites present. Samples: LV37.25, LV37.6.</p> |
| 31 | 1.4 | 47.2 | <p>Fine-grained couplets to dolomitized mudstone. Medium to light gray/brownish. Layer thickness: 7-20 cm. Burrow-mottling present. Small vugs (evaporite molds) and stylolites present. Faint planar, horizontal lamination and some truncated couplet tops present. Couplets reach a thickness of 2-3 cm, and are composed primarily of laminated mudstone, and very thin grainy (peloids, quartz silt) bases. Rare mudcracks and small amplitude stylolites present. Parts of the unit are poorly exposed and may represent intervals with interbedded shale. Near the unit top an erosional exposure surface is developed on dolomitized, faintly laminated mudstone. The surface is capped by dark colored, microbial (cryptalgal) laminae exhibiting antigravitational fabric (thicker on topographic highs). Samples: LV37.95, LV38.05, LV38.8, LV39.0.</p> |
| 32 | 0.7 | 47.9 | <p>Fine-grained couplets to laminated dolomicrite (dolomitized mudstone). Medium to light gray. Burrow(?) -mottled fabric. Common vuggy pores representing small evaporite nodules and euhedral molds. Faint horizontal (wavy to planar) lamination present. Unit top is sharp, planar, and marked by a thin shale. Samples: LV39.2, LV39.7.</p> |
| 33 | 1.4 | 49.3 | <p>Medium-grained dolomitized couplets exposed in the lower 50 cm</p> |

of the unit. Light to medium gray. Layer thickness: 10-20 cm. Horizontal lamination, rare cross-lamination, and common evaporite molds visible. Common light gray to pink, and reddish-brown chert lenses and nodules. The upper part of the unit is mostly covered with only several carbonate layers (10-15 cm thick), representing fine-grained couplets, are exposed. Some planar, horizontal lamination visible. Unit top is not exposed. Samples: LV40.1, LV40.75.

- 34 0.5 49.8 Burrowed, disturbed medium-grained dolomitized couplets. Dark to medium gray with brownish patches. Burrow-mottled appearance. Layer thickness: 10-20 cm. Horizontal and cross-lamination visible. Laminae are commonly disturbed by bioturbation and/or evaporite mineral growth. Grainy deposits form discontinuous lenses along couplet bases. Evaporite-related vugs and molds present in the lower part of the unit. Unit top is poorly exposed. Sample: LV41.7.

Copper Ridge Dolomite

- 35 0.4 50.2 Dolomitized oolitic packstone/grainstone. Dark to medium gray/brownish. Deposits comprise three layers, that average about 10 to 20 cm in thickness, and pinch and swell laterally. Small micritic intraclasts present. Rare stylolites, faint lamination, and pyrite visible. The deposits in the uppermost part of the unit are partially silicified. Unit top is sharp, wavy, and significantly weathered. Sample: LV42.05.
- 36 1.5 51.7 Medium-grained dolomitized couplets interbedded with microbial deposits. Light to medium gray. Some coarse-grained couplets present at the unit base. Couplets are up to 5 cm thick, and are composed primarily of intraclastic packstone/grainstone with very thin (or lacking) overlying micritic deposits. Horizontal lamination is more pronounced in the upper part of the unit, ranging from planar to wavy associated with couplets, and crinkly microbial lamination characteristic of LLH stromatolites. Small fenestrae occur associated with microbial deposits. Scattered evaporite molds. Abundant stylolites, up to 4-5 cm in amplitude. Some chert present in the upper part of the unit. The upper unit contact is sharp, slightly undulatory. Samples: LV42.2, LV43.25, LV43.6.
- 37 1.2 52.9 Fine-grained couplets to dolomitized mudstone in the lower part, separated from the overlying medium- to coarse-grained couplets by about a 10 cm thick calcareous shale/argillaceous carbonate. Light to medium gray. Layer thickness ranges from < 1 cm to 20

cm. Layer boundaries are planar to slightly undulatory. Unit base is weathered and not well exposed. Some fine-grained couplets, commonly < 1 cm and up to about 1.5 cm thick, are present in the lower part of the unit. Horizontal lamination, vuggy pores (evaporite molds), and burrow-mottling occur associated with these deposits. Medium-grained, normally graded, couplets in the upper part of the unit are up to 5 cm thick, and contain ooids, quartz grains and micritic intraclasts at the couplet bases. Intraclasts reach a maximum thickness of 3.5 cm. Couplet contacts are commonly truncational. Some horizontal and cross-lamination present. Unit top is sharp, wavy. Samples: LV43.7, LV44.1, LV44.7, **LV44.85**.

- | | | | |
|----|------|-------|--|
| 38 | 0.7 | 53.6 | Coarse- to medium-grained couplets. Medium gray/brownish. Coarse-grained bases contain intraclasts up to 1.5 cm in size, ooids and quartz sand grains. Some horizontal, planar to slightly wavy lamination and burrow-mottling present. Bioturbation of couplets resulted in a patchy distribution of mudstone and coarser-grained deposits. Common small vugs (evaporite molds) present. Rare stylolites. Unit top is sharp, wavy. Sample: LV44.9. |
| 39 | 0.85 | 54.45 | Fine-grained couplets to dolomitized mudstone. The unit base consists of several undulatory layers comprising a 8 cm thick, medium to dark gray, silicified oolite. The overlying deposits are light gray in color. Faint planar, horizontal lamination visible. Several stylolites present. Some large vugs (up to 5 cm in diameter), likely related to dissolution of evaporite nodules, present in the middle part of the unit. Upper unit contact is sharp, irregular to wavy, and marked by a 7-8 cm thick dark laminated shaly crust. Samples: LV45.6, LV46.1, LV46.3. |
| 40 | 0.5 | 54.95 | Dolomitized laminated microbial deposits comprising one layer of variable thickness laterally. Medium to dark gray/brownish. Wavy, crinkly lamination characteristic of LLH stromatolites comprise most of the unit. Laminae are discontinuous, disturbed. Many short mudcracks present. Incorporated peloids present. SH stromatolites are present in the uppermost part of the unit. Individual hemispheroids reach a maximum height of 5 cm. Upper unit contact is sharp, wavy. Samples: LV46.6, LV46.85 . |
| 41 | 0.8 | 55.75 | Coarse- to medium-grained dolomitized couplets comprising two layers (25 and 55 cm thick). Medium to dark gray. Intraclasts and some ooids present at the bases of coarse-grained couplets in the lower part of the unit. Couplet bases are planar. Micritic upper parts of couplets are laminated and in places burrow-mottled |

(brownish patches). Couplets in the remaining part of the unit are more substantially bioturbated. Laminae are discontinuous, whereas grainy deposits form pockets or patches. Unit top is not well exposed; appears sharp, planar. Samples: LV47.25, LV47.35.

- | | | | |
|----|------|-------|--|
| 42 | 1.0 | 56.75 | Unit base is composed of 10 cm thick interval consisting of dark gray to brown, shaly and laminated argillaceous carbonate layers, overlain by a thrombolite bioherm. Thrombolite deposit is medium to dark gray and has massive, mottled appearance. The upper part of the thrombolite is poorly exposed and partially covered. The exposed layers (up to 15 cm thick) are composed of faintly laminated, dolomitized mudstone with some microbially laminated deposits in the upper part. Light gray/brownish. Stratiform stromatolite predominates; some lamination characteristic of LLH and small relief SH stromatolites present. Some laminae are disrupted by desiccation cracks and vuggy porosity (evaporite dissolution voids). Unit top is a prominent, sharp, wavy surface. Samples: LV47.75, LV47.8, LV47.85, LV48.4, LV48.65. |
| 43 | 0.3 | 57.05 | Thrombolite. Medium to dark gray/brownish. Massive, burrow(?) - mottled appearance. Clotted micritic fabric with pockets of grainy (peloids, small intraclasts, ooids) deposit. Some vuggy pores, and small veins and voids with sparite present. Rare wavy lamination visible in the uppermost part. Unit top is sharp, planar. Sample: LV48.75. |
| 44 | 0.7 | 57.75 | Dolomitized mudstone to fine-grained couplets. Poorly exposed. Base is covered. Varies in color from light to dark gray/brownish. Burrow-mottled. Middle part consist of layers up to 15 cm thick with planar layer boundaries. Some faint planar, horizontal, and discontinuous wavy lamination visible. Upper part of the unit contain undulatory layers, up to 5 cm thick, interbedded with thin argillaceous carbonate intervals. Unit top is very weathered and not well exposed. Samples: LV49.4, LV49.65. |
| 45 | 1.05 | 58.8 | Thrombolite in the lowermost 50 cm of the unit comprises three layers that pinch and swell laterally. Thrombolitic deposits are very porous, weathered, and have mottled appearance. Dark gray, with some voids filled with cement. Top of the thrombolite is poorly exposed, but appears wavy. The upper part of the unit is only partially exposed. The exposed parts reveal planar horizontal lamination characteristic of fine grained couplets to laminated dolomitized mudstone. Unit top is not exposed. Sample: LV49.75. |

- 46 1.7 60.5 Thrombolite in the lower part of the unit. Several thin (2-3 cm), undulatory layers composed of medium gray/brownish burrowed mudstone with some discontinuous wavy lamination present at the unit base. Thrombolitic deposits comprise two layers (45 cm and 15 cm thick), with characteristic mottled (burrowed?) appearance. Medium to dark gray in color. Some discontinuous wavy lamination present in the uppermost part of the thrombolite. Upper contact of the thrombolite is poorly exposed. Upper part of the unit is partially covered. Several exposed, 10-15 cm thick, layers are composed of burrow-mottled (light gray with brownish and black patches), dolomitized mudstone to fine-grained couplets. Some horizontal lamination and rare cross-stratification visible. Unit top is not well exposed. Samples: LV50.8, LV51.3, LV51.8, LV52.0, **LV52.4**.
- 47 0.4 60.9 Thrombolitic bioherm. Light to medium gray/brownish. Mottled appearance. Very porous (evaporite molds), fractured, and weathered. Lenses of intraclastic-oolitic wackestone/packstone present. Rare stylolites present in the upper part. Unit top is poorly exposed, weathered and marked by 2-3 cm thick intraclastic layer with some shale on top. Samples: LV52.7, **LV52.85**.
- 48 0.4 61.3 Thrombolite bioherm. Several thin (2-3 cm), undulatory layers present at the unit base. Thrombolitic deposits comprise 7-8 cm thick layers with wavy, irregular layer boundaries. Medium to dark gray, with some brownish patches. Mottled, clotted appearance. Common small voids filled with sparite. Some wavy, discontinuous lamination present. Unit top is sharp, undulatory, and marked with thin shale. Samples: LV53.1, LV53.2.
- 49 0.2 61.5 Medium-grained, burrow-mottled, undulatory couplets, texturally reminiscent of ribbon-rock. Medium to dark gray. Some horizontal lamination and vuggy pores visible in the lower part. Burrow-mottling is more prominent in the upper part of the unit. Common voids with sparite. Upper unit contact is sharp, slightly wavy. Sample: LV53.35.
- 50 0.6 62.1 Thrombolite comprising several layers of variable lateral thickness ranging from 5 cm to 30 cm. Dark gray. Mottled appearance. Common vuggy pores and small voids filled with cement. Very weathered. Patches of grainy deposits, containing peloids, small ooids and intraclasts, present. Unit top is marked by a 2-3 cm thick, dark, wavy, shaly crust. Sample: LV53.55.

- 51 1.45 63.55 Only the lowermost part of the unit, comprising two layers (7 cm and 8 cm thick), is exposed. Medium- to fine grained couplets interbedded with microbially laminated deposit. Light gray. The rest of the unit is covered, with the exception of one layer (about 30 cm thick) containing planar, horizontal lamination typical of couplets, which occurs in the middle part of the interval. Unit top is poorly exposed; appears shaly. Sample: **LV54.1**.
- 52 0.85 64.4 Calcareous siltstone to silty carbonate overlain by microbial deposits. Unit base is a sharp, planar surface. Deposits comprising the lower part of the unit are light to medium gray, thin bedded (maximum layer thickness: 5 cm), with planar to slightly undulatory layer boundaries. Horizontal lamination and rare cross-stratification visible. Layers are normally graded and have a texture of fine-grained, less than 1 cm thick, couplets with thin lenticular, slightly coarser-grained basal deposits. The contact with the overlying dolomicritic microbial deposits is a poorly exposed, thin shaly interval. The deposits in the upper part of the unit are medium to dark gray/brownish, and comprise slightly thicker (up to 12 cm) undulatory layers. Some faint, discontinuous, wavy lamination, characteristic of stratiform to LLH stromatolites, is visible. Mottled (burrowed?) texture. Parts of the unit may represent a thrombolite. Small vugs (evaporite molds) present. Upper unit contact is sharp, wavy. Samples: LV55.8, LV56.15, LV56.35.
- 53 1.35 65.75 Microbial deposits. Medium to dark gray. Biohermal shape. Thrombolite in the lowermost part. Common small vugs (evaporite voids, burrows). Major part of the unit consists of columnar stromatolites. Massive appearance. Only rare laminated stromatolitic columns apparent in outcrop. Rare stylolites present. Columnar stromatolites are capped by LLH stromatolites. The uppermost part of the unit looks burrow-mottled. Unit top is sharp, wavy, weathered, and marked by < 5 cm shale interval. Samples: LV57.3, LV57.6, LV57.7.
- 54 0.9 66.65 Thrombolite overlain by medium- to fine-grained couplets. Medium to dark gray. Thrombolite is very porous and weathered. Biohermal shape. The overlying couplets exhibit some horizontal and cross-lamination, and contain common evaporite molds. The unit is capped by about 5 cm thick, undulatory, and very porous ooid grainstone layer. Unit top is sharp, wavy, and marked by thin shale. Samples: **LV57.75**, LV57.9, LV58.55, **LV58.6**.

- 55 0.45 67.1 Fine-grained couplets to dolomitized mudstone. Light to medium gray. The lowermost part of the unit is very fractured in the outcrop. Some horizontal planar lamination visible. A prominent, planar to wavy layer boundary with thin (2-3 cm) shaly crust occurs on top of this fractured interval (about 10 cm from the top of the unit). The uppermost part of the unit is represented by one layer with slightly undulatory boundaries, composed of several thin, fine-grained couplets exhibiting some horizontal lamination. Samples: LV58.9, LV59.0.
- 56 0.4 67.5 Medium- to coarse-grained dolomitized couplets. Light to medium gray. Prominent horizontal and cross-lamination present in the lower and upper parts of the unit. Couplet bases are composed of peloidal-intraclastic packstone, with some ooids. Middle part appears burrow-mottled, and contains common vuggy pores, some of which are related to dissolution of evaporites. Unit top is sharp, wavy. Sample: LV59.1.
- 57 1.15 68.65 Ooid grainstone overlain by thrombolite. Oolite in the lower part of the unit comprises several weathered, porous, dark gray, undulose layers. The lower part of the overlying thrombolite is extensively weathered; the upper part has a massive appearance. Medium to dark gray. Some vuggy pores, resembling evaporite nodules and molds, and voids filled with sparite present. Unit top is weathered; appears sharp, planar. Samples: LV59.6, LV59.7, LV60.5.
- 58 0.2 68.85 Fine-grained couplets to dolomitized mudstones. Light to medium gray. Planar, horizontal lamination visible. Thin bedded (maximum layer thickness: 4-5 cm). Layer boundaries are planar to slightly undulatory. Unit top is sharp, planar. Sample: LV60.7.
- 59 0.2 69.05 Oolite comprising several undulatory layers of a maximum thickness of about 8 cm. Partially silicified. Light to dark gray. Unit top is slightly undulatory and very weathered. Sample: LV60.85.
- 60 0.5 69.55 Medium- to fine-grained dolomitized couplets. Medium gray. Horizontal (planar to wavy, discontinuous) and cross-lamination visible. Some parts have mottled fabric (brownish patches). Upper unit contact is slightly wavy and weathered. Sample: LV61.45.
- 61 0.25 69.8 Lower part is covered (tree roots). Thrombolite comprises the upper exposed part of the unit. Medium gray. Biohermal shape with planar lower surface and wavy, undulatory upper surface.

Mottled appearance. Some wavy, discontinuous laminae visible. Several vuggy pores (up to 1 cm in diameter) and voids filled with cement present. Sample: LV61.7.

- | | | | |
|----|------|-------|---|
| 62 | 0.55 | 70.35 | Microbial deposits interbedded with couplets. Light to medium gray. Layers are 5-20 cm thick and have planar to slightly wavy boundaries. Lower part of the unit contain SH stromatolites overlain by wavy laminated stratiform stromatolites (microbial laminates) and some LLH stromatolites. The upper part of the unit is dominated by fine- to medium-grained couplets. Planar, horizontal and cross-lamination visible. Some vugs present. Upper unit contact is sharp, planar. Sample: LV62.2. |
| 63 | 0.85 | 71.2 | The unit consists of two microbial bioherms. Medium to dark gray. The lower bioherm is composed of basal thrombolite grading upward into columnar stromatolite. The upper part of the bioherm has well exposed laminated microbial columnar structures. Bioherm upper contact is wavy. The overlying bioherm is thrombotic, and had both upper and lower boundaries wavy. Thrombotic deposits are porous, weathered and have mottled appearance. Upper unit contact is also weathered. Samples: LV62.35, LV62.55. |
| 64 | 0.65 | 71.85 | Coarse-grained couplets with ooid-intraclastic bases present in the lowermost part of the unit. Light gray. Some planar horizontal lamination visible. The remaining part of the unit consists of columnar stromatolite. Dark gray. Biohermal shape. Massive appearance. Very porous and weathered. Some voids filled with sparite present. Laminated columnar microbial structures visible in the outcrop. Unit top is sharp, slightly wavy. Sample: LV63.75. |
| 65 | 0.65 | 72.5 | Predominantly medium-grained couplets interbedded with some coarse- and fine-grained dolomitized couplets. Light to medium gray. Ooid-intraclastic packstone deposits present at bases of coarser-grained couplets in the lower part of the unit. Vuggy porosity present. Middle part of the unit is weathered, and composed of thinly bedded (maximum layer thickness: 1 cm) layers with planar layer boundaries composed of coarse- to medium-grained couplets. Medium- to fine-grained couplets predominate in the upper part of the unit. Some horizontal lamination, and rare cross-lamination, vuggy pores, and patches of Fe-oxides visible. Sample: LV64.45. |
| 66 | 1.05 | 73.55 | Columnar stromatolites in the lower part comprise one layer with |

wavy upper layer boundary. Laminated columns with small fenestrae well exposed in the upper part of the layer. Intercolumnar space contains oolitic-peloidal packstone/grainstone. The overlying deposits contain substantially silicified microbial deposits. Some SH stromatolites visible, as well as stratiform to LLH stromatolites. Characteristic wavy, crinkly lamination and small fenestrae visible. Some grainy laminae and patches present. Rare vertical mudcracks and sheet cracks can be observed. In the uppermost part of the unit, stromatolitic hemispheroids are overlain by some fine-grained couplets to laminated dolomitized mudstone. Unit top is weathered, wavy. Samples: **LV64.5, LV64.9, LV65.2, LV65.55**. The remaining part of the Copper Ridge Dolomite is exposed, but was not measured.

APPENDIX B

STABLE ISOTOPE DATA

SUBTIDAL DEPOSITIONAL PACKAGE

MICRITIC MATRIX OF MICROBIAL DEPOSITS

Sample	Description	$\delta^{18}\text{O}$	$\delta^{13}\text{C}$
TZ 9.0t	micrite comprising a thrombotic mesoclot incorporated within ribbon limestone	-9.06	3.67
TZ 18.7	dark, dense micrite comprising thrombotic mesoclots	-8.71	3.47
RR 31.75	micrite comprising thrombolite/digitate stromatolite; minor disseminated replacement dolomite possible	-10.74	2.44
RR 35.9	micrite comprising digitate stromatolite; minor contamination from fenestrae with calcite cement and from disseminated replacement dolomite possible	-10.98	2.29
TH 20.5	micrite from microbial laminates; contains about 30% dolomicrite; time extraction used	-8.63	3.39
TH 22.2	micrite from microbial laminates; contains about 10% dolomicrite; time extraction used	-8.73	3.68
TH 23.45	micrite from microbial laminates; contains common dolomicrite; time extraction used	-8.91	3.41
TH 54.2C	micrite comprising digitate stromatolites from the peritidal package; minor contamination from small fenestrae and scattered dolomite possible	-9.52	1.53
FG 40.4	micrite comprising digitate stromatolite; contamination from small fenestrae possible	-10.39	2.58
FG 41.15	micrite from digitate stromatolite; minor contamination from small fenestrae possible	-9.74	2.48
Total (n): 10		Minimum:	-10.98 1.53
		Maximum:	-8.63 3.68
		Average:	-9.54 2.89

MICRITIC MATRIX OF NON-MICROBIAL DEPOSITS

Sample	Description	$\delta^{18}\text{O}$	$\delta^{13}\text{C}$
TH -0.4	micrite from intraclasts and irregular patches from fossiliferous-intraclastic packstone layer of ribbon limestone	-8.98	1.98
TH 0.0	micrite from a mudstone layer of ribbon limestone	-8.84	2.54
TH 1.1	micrite from burrow-mottled ribbon limestone	-7.90	3.01
TH 2.15	micrite from a laminated mudstone layer of ribbon limestone	-7.48	1.82
TH 3.35	micrite from a mudstone layer of ribbon limestone	-7.43	1.66
TH 4.2	micritic matrix in between trilobite fragments from a limestone layer of ribbon rocks	-8.03	1.29
TH 5.2	micrite from intraclasts (flat pebbles) imbedded within argillaceous dolomicritic layers of ribbon rocks	-7.87	0.49
TH 5.4	micrite from a lense interbedded within argillaceous dolomicrite of ribbon rocks	-7.79	1.19
TH 6.4	micrite from a mudstone to peloidal mudstone layer of ribbon limestone	-7.51	1.53
TH 8.0 b	micrite in between trilobite fragments in fossiliferous wackestone/packstone of ribbon limestone	-7.43	1.13
TH 10.05	micrite from a mudstone layer interbedded within argillaceous dolomicrite of ribbon rocks	-7.77	2.92
TH 11.3	micrite from a mudstone layer underlying flat pebble conglomerate of ribbon limestone	-7.76	1.71

TH	11.9	micrite from a mudstone/peloidal layer of ribbon limestone	-8.14	3.18
TH	12.6	micrite from a lense within ribbon limestone	-7.48	3.21
TH	13.45	micrite from a lense within ribbon limestone	-7.16	3.54
TH	14.65	micrite from a mudstone layer of ribbon limestone	-7.58	4.09
TH	16.75	micrite from a mudstone layer of ribbon limestone	-7.80	2.29
TH	17.85	micrite to peloidal packstone from lenses in ribbon limestone	-7.63	3.52
TH	18.8	micrite from burrowed lenses from transitional interval between ribbon limestone and microbially laminated deposits	-7.88	3.80
FG	0.6	micrite from a mudstone layer of ribbon limestone	-7.98	3.06
Total (n): 20			Minimum:	-8.98 0.49
			Maximum:	-7.16 4.09
			Average:	-7.82 2.40

FIBROUS/BLADED CALCITE CEMENT

Sample	Description	$\delta^{18}\text{O}$	$\delta^{13}\text{C}$
TZ 9.0	fibrous/bladed calcite cement from interparticle space within ribbon rocks: some pore central equant calcite cement possible	-8.62	4.51
TZ 9.0a	bladed calcite cement from interparticle space of grainstone layers within ribbon rocks	-8.33	4.89
TZ 24.65a	bladed calcite from intergranular space of a peloidal packstone/grainstone	-9.16	4.60
TZ 24.65b	bladed calcite from burrows in peloidal packstone/grainstone; some pore central equant calcite cement possible	-9.38	4.35
TZ 26.65	bladed calcite from intergranular space of a peloidal packstone/grainstone	-9.08	4.27
TZ 28.65a	pore-rim bladed calcite cement from a void (burrow likely) within peloidal packstone/grainstone with thrombolitic texture	-8.18	3.93
RR 28.05b	pore rim bladed calcite cement; some equant calcite possible	-8.37	3.01
RR 33.15	pore-rim bladed calcite cement from burrows within thrombolites; some pore-central equant calcite cement likely	-10.13	2.58
RR 34.0	pore-rim bladed calcite cement from burrows within thrombolites; some pore-central equant calcite cement likely	-9.94	2.84
RR 49.5	fibrous/bladed calcite cement from burrows within thrombolitic deposits	-9.18	3.63
RR 49.85	bladed calcite cement from burrows within thrombolitic deposits	-8.38	3.75
RR 52.65b	fibrous/bladed calcite cement from burrows in thrombolites; some pore central equant calcite cement possible	-9.70	2.47
TH 0.55 a	bladed calcite cement in between intraclasts of flat pebble conglomerate	-7.86	2.88
TH 0.55 c	bladed calcite cement in between intraclasts of flat pebble conglomerate	-7.77	2.97
TH 55.4	bladed calcite cement between micritic intraclasts of rare calcitic deposits within peritidal package: succeeded by equant calcite and pore-central saddle dolomite cement	-9.96	2.65
FG 20.4	bladed calcite cement from intergranular and shelter voids of a grainstone layer: rare equant calcite cement possible	-10.16	2.31
LV 10.35	bladed/fibrous calcite cement in between intraclasts and peloids	-7.48	3.51
Total (n): 17		Minimum:	-10.16 2.31
		Maximum:	-7.48 4.89
		Average:	-8.92 3.48

CALCITE FROM ARGILLACEOUS DOLOMICRITIC LAYERS

Sample	Description	$\delta^{18}\text{O}$	$\delta^{13}\text{C}$
TH 9.0	time-extracted calcite from argillaceous dolomicrite or calcareous siltstone	-8.23	2.35
TH 11.75	time-extracted calcite from argillaceous dolomicrite/calcareous siltstone	-8.92	1.98
		Average:	-8.57 2.17

FERROAN MICROSPARITE

Sample	Description	$\delta^{18}\text{O}$	$\delta^{13}\text{C}$
TH 2.15b	ferroan microsparite associated with burrows within mudstone layers of ribbon limestone	-8.01	3.03

EQUANT CALCITE CEMENT

Sample	Description	$\delta^{18}\text{O}$	$\delta^{13}\text{C}$
TZ 3.1b	pore-rim non-ferroan equant calcite cement from a grainstone layer of ribbon limestone	-10.16	2.61
TZ 9.0b	pore central equant calcite cement from interparticle pores of a grainstone layer within ribbon limestone	-8.88	4.72
TZ 18.25	turbid equant calcite cement from burrows in laminated micritic deposits	-8.83	3.80
TZ 24.65c	pore-central equant calcite cement in one large (dissolutional) void within peloidal packstone/grainstone	-9.03	4.36
TZ 28.65b	pore-central equant calcite cement from a void (burrow likely) within peloidal packstone/grainstone with thrombotic texture	-10.14	3.25
RR 55.1	pore-central equant calcite cement from burrows in thrombotic deposits; some pore-rim bladed calcite likely	-9.75	1.24
TH 54.0b	pore-central equant calcite cement in a layer-parallel void within micritic layer	-9.84	1.54
FG 5.1	equant calcite cement from vertical voids (burrows?, syneresis cracks?) in a micritic layer of ribbon rocks	-8.85	2.71
FG 17.6b	equant calcite from a burrow within a ribbon laminated layer interbedded with mechanical couplets	-10.65	1.65
FG 18.1	equant calcite cement from burrows in thrombotic deposits; some pore-rim bladed calcite cement possible	-9.28	2.50
LV 24.8	pore-central equant calcite from burrows within thrombotic deposits; some pore-rim bladed calcite possible	-9.43	2.00
Total (n): 11		Minimum:	-10.65 1.24
		Maximum:	-8.83 4.72
		Average:	-9.53 2.76

FERROAN EQUANT CALCITE CEMENT

Sample	Description	$\delta^{18}\text{O}$	$\delta^{13}\text{C}$
TZ 3.1a	pore-central (burrow?) ferroan equant calcite cement from a grainstone layer of ribbon limestone	-10.69	2.42
RR 23.45	ferroan equant calcite cement from burrows in microbial laminates	-9.28	3.19
RR 28.05a	equant calcite cement subsequently precipitated on bladed calcite and succeeded by saddle dolomite cement	-9.44	2.75
TH 14.0	ferroan equant calcite cement in voids (burrows?) within a micritic layer of ribbon rocks	-9.68	2.27
TH 18.8	ferroan equant calcite cement in voids (burrows likely) within ribbon limestone	-9.07	2.70
TH 19.1	ferroan equant calcite cement from burrows in microbially laminated deposits	-9.69	2.69
FG 17.6c	ferroan equant calcite cement from a burrow within a ribbon laminated layer interbedded with mechanical couplets	-11.00	1.97
FG 29.4	coarse-crystalline ferroan equant calcite cement from burrows within thrombotic deposits	-10.15	2.23
Total (n): 8		Minimum:	-11.00 1.97
		Maximum:	-9.07 3.19
		Average:	-9.87 2.53

DOLOMITE FROM ARGILLACEOUS LAYERS

Sample	Description	$\delta^{18}\text{O}$	$\delta^{13}\text{C}$
TZ 3.1c	argillaceous dolomicrite from ribbon limestone; minor scattered calcite possible	-7.08	3.67
TZ 7.6	argillaceous dolomicrite from ribbon limestone	-7.01	4.81
TZ 9.0	argillaceous dolomicrite from ribbon limestone; does not stain ferroan	-7.07	4.99
RR 1.2a	argillaceous, ferroan dolomicrite from ribbon limestone; minor calcite present	-7.10	3.46
RR 1.4	argillaceous, ferroan dolomicrite from ribbon limestone	-6.90	3.45
RR 13.9	argillaceous dolomicrite from ribbon limestone	-6.75	3.01
TH 0.0	argillaceous, ferroan dolomicrite from ribbon limestone	-8.15	3.10
TH 5.35	argillaceous dolomicrite from ribbon limestone	-7.56	2.83
TH 9.0	dolomicrite from argillaceous dolomicrite/calcareous siltstone; time extraction used	-6.05	3.22
FG 5.1	argillaceous dolomicrite from ribbon limestone; low carbonate content	-6.12	4.08
LV 10.35b	dolomicrite from argillaceous layers interbedded with intraclastic packstone of ribbon limestone	-7.43	4.00
LV 10.35c	argillaceous, ferroan dolomicrite from ribbon limestone	-7.58	3.86
Total (n): 12		Minimum:	-8.15 2.83
		Maximum:	-6.05 4.99
		Average:	-7.07 3.71

SUBTIDAL SADDLE DOLOMITE CEMENT

Sample	Description	$\delta^{18}\text{O}$	$\delta^{13}\text{C}$
TZ 12.3	ferroan saddle dolomite cement associated with burrows in borrowed mottled subtidal lithofacies	-8.51	3.97
RR 8.1a	ferroan, coarse-crystalline saddle dolomite cement from shelter voids beneath skeletal fragments in ribbon limestone	-8.41	3.44
LV 10.35	ferroan, pore-central saddle dolomite cement associated with MVT minerals (pyrite, galena, sphalerite)	-9.90	3.53
Total (n): 3		Minimum:	-9.90 3.44
		Maximum:	-8.41 3.97
		Average:	-8.94 3.65

SUBTIDAL SADDLE DOLOMITE REPLACEMENT

Sample	Description	$\delta^{18}\text{O}$	$\delta^{13}\text{C}$
RR 8.1b	ferroan saddle dolomite replacing internal deposits on the bottom of shelter voids in fossiliferous layers of ribbon limestone	-8.13	3.39

PERITIDAL DEPOSITIONAL PACKAGE

DOLOMICRITIC MATRIX OF NON-MICROBIAL DEPOSITS

Sample	Description	$\delta^{18}\text{O}$	$\delta^{13}\text{C}$
TZ 22.25d	dolomicrite with peloidal texture from a lens within calcitic peloidal packstone/grainstone with clay-seam dolomite and veins with saddle dolomite and sphalerite	-6.90	4.68
TZ 48.25	dolomicrite from fine-grained couplets	-6.73	2.72
TZ 48.95	dolomicrite from fine-grained couplets	-6.22	3.69
TH 27.8	dolomicrite from a layer overlying microbially laminated deposits	-6.41	3.25
TH 28.35	dolomicrite from upper parts of coarse-grained couplets	-6.76	2.76
TH 29.6	dolomicrite from fine-grained couplets	-7.02	2.72
TH 30.7 a	dolomicrite from fine-grained couplets	-7.41	2.46
TH 32.9	dolomicrite from upper parts of fine/medium-grained couplets	-7.07	3.03
TH 33.1 B	dolomicrite from fine-grained couplets	-7.05	3.01
TH 33.1 T	dolomicrite from dolomitized mudstone	-7.88	3.25
TH E2-33.35	dolomicrite from dolomitized mudstone; 5 cm below a prominent exposure surface	-7.29	3.28
TH 33.4a	dolomicrite from clasts in topographic lows immediately above the exposure surface	-7.77	3.25
TH 33.4b	dolomicrite from clasts in topographic lows immediately above the exposure surface	-7.67	3.18
TH D-33.45	dark argillaceous dolomicritic matrix from a condensed shaly interval deposited on the erosional exposure surface; associated with sphalerite	-7.77	3.26
TH 1-33.42	dolomicrite with a lamina interbedded with argillaceous laminae in the condensed shaly interval deposited on the exposure surface	-7.64	2.97
TH 2-33.43	laminated dolomicrite from fine-grained couplets with desiccation cracks; deposited about 5 cm above the exposure surface	-7.72	3.08
TH 34.6	dolomicrite from dolomitized mudstone	-6.82	3.68
TH 35.6	dolomicrite from dolomitized mudstone/fine-grained couplets	-6.12	3.06
TH 36.55 T	dolomicrite from upper parts of medium-grained couplets with common desiccation cracks	-6.96	2.88
TH 37.6	dolomicrite from fine/medium-grained couplets with desiccation cracks	-6.39	2.96
TH 38.7	dolomicrite from dolomitized mudstone	-6.59	3.14
TH 39.05	dolomicrite from upper parts of fine/medium-grained couplets	-5.86	3.43
TH 40.25	dolomicrite from upper parts of medium-grained couplets	-6.35	3.82
TH 41.15	dolomicrite from upper, burrowed parts of medium-grained couplets	-5.99	3.80
TH 41.9	dolomicrite from upper parts of medium-grained couplets	-6.99	3.61
TH 43.3	slightly laminated dolomicrite from dolomitized mudstone/very fine-grained couplets	-6.87	3.76
TH 47.1	dolomicrite from fine-grained couplets/dolomitized mudstone	-6.18	3.40
TH 50.0	dolomicrite from burrowed mudstone/fine-grained couplets	-6.24	4.08
TH 50.7	dolomicrite from dolomitized mudstone/fine-grained couplets associated with evaporites and abundant quartz sand grains	-6.33	3.83
TH 51.75	laminated dolomicrite from fine-grained couplets	-6.68	3.11
TH 55.25	dolomicrite from upper micritic part of coarse-grained couplets	-5.99	2.65
TH 56.8	dolomicrite from fine-grained couplets	-6.38	2.20
TH 57.25	dolomicrite from fine-grained couplets	-7.44	2.42
TH 58.15	dolomicrite from burrow-mottled mudstone/fine-grained couplets	-6.43	3.71
TH 61.4	dolomicrite from fine to medium-grained couplets	-7.13	2.77
TH 66.9	dolomicrite from fine-grained couplets overlying SH stromatolites	-6.36	1.42

TH	68.05	dolomicrite from disturbed (burrow mottled) fine-grained couplets with some microbial laminae possible	-6.10	0.32
FG	32.7	dolomicrite from dolomitized mudstone in the vicinity of an evaporite nodule with common silica cement	-7.33	3.45
FG	38.1a	dolomicrite from dolomitized mudstone; immediately underneath a karst surface	-6.42	3.21
FG	38.1b	dolomicrite from dolomitized mudstone; about 1 cm above the karst surface	-6.49	3.21
LV	44.85	dolomicrite from medium/coarse grained couplets associated with common quartz sand grains	-6.10	3.73
Total (n): 41			Minimum:	-7.88 0.32
			Maximum:	-5.86 4.68
			Average:	-6.78 3.13

DOLOMICRITIC MATRIX OF MICROBIAL DEPOSITS

Sample	Description	$\delta^{18}\text{O}$	$\delta^{13}\text{C}$
TZ 28.25	dolomicritic laminae from stratiform stromatolites	-6.29	4.38
TH 25.55	dolomicritic laminae from stratiform stromatolites	-6.58	3.90
TH 26.6	dolomicritic laminae from stratiform stromatolites	-6.21	4.01
TH 48.9	dolomicrite from LLH stromatolites; contamination from small fenestrae with saddle dolomite cement possible	-6.78	3.55
TH 52.75	laminated dolomicrite from microbial lumps imbedded within deposits with thrombolitic texture	-6.55	2.94
TH 60.4	dolomicrite from stratiform stromatolite laminae	-6.37	2.72
TH 62.45	dolomicrite from extensively dolomitized LLH or digitate stromatolites	-6.42	2.36
TH U46	dolomicrite from partially silicified SH stromatolites	-7.77	0.67
FG 14.0	dolomicritic laminae from stratiform stromatolites	-6.85	3.32
FG 36.45	dolomicrite from SH stromatolites; contamination from small fenestrae with saddle dolomite cement possible	-6.84	3.08
LV 20.2	dolomicritic laminae from stratiform stromatolites; contamination from small fenestrae with saddle dolomite cement possible	-7.03	3.47
Total (n): 11		Minimum:	-7.77 0.67
		Maximum:	-6.21 4.38
		Average:	-6.70 3.13

DOLOMICROSPARITE

Sample	Description	$\delta^{18}\text{O}$	$\delta^{13}\text{C}$
TZ 35.05	dolomicrosparite replacing mudstone to peloidal wackestone	-6.18	4.44
TZ 29.25	dolomicrosparite from medium-grained couplets	-6.14	4.51
TZ 47.85	dolomicrosparite from medium-grained couplets	-6.71	3.88
TH 30.7 b	dolomicrosparite from fine-grained couplets	-7.23	2.66
TH 31.4	dolomicrosparite from fine/medium-grained couplets	-8.07	3.01
TH 43.8	dolomicrosparite from extensively dolomitized, burrowed mudstone	-6.55	4.78
TH 44.75	dolomicrosparite from burrowed mudstone/fine-grained couplets	-6.38	4.30
TH 45.7	dolomicrosparite from extensively dolomitized, slightly burrowed mudstone/fine-grained couplets	-6.36	3.94
TH 47.7	dolomicrosparite from LLH stromatolites	-8.00	3.69
TH 53.9	dolomicrite to dolomicrosparite from burrowed fine-grained couplets	-6.54	3.02
TH 54.8	dolomicrite to dolomicrosparite from dolomitized mudstone	-6.55	2.31
TH 63.5	dolomicrosparite from extensively dolomitized bioturbated peloidal packstone/wackestone	-6.49	2.66
FG 43.6	dolomicrosparite replacing muddy parts of medium-grained couplets	-6.61	3.59

LV 36.5	dolomicrosparite replacing peloidal mudstone/wackestone of medium-grained couplets	-7.11	4.34
LV 65.55	dolomicrosparite from burrowed mudstone/fine-grained couplets	-7.49	1.52
Total (n): 15		Minimum:	-8.07 1.52
		Maximum:	-6.14 4.78
		Average:	-6.83 3.51

COARSER-CRYSTALLINE REPLACEMENT DOLOMITE

Sample	Description	$\delta^{18}\text{O}$	$\delta^{13}\text{C}$
RR 34.0b	medium-crystalline replacement dolomite from patches (burrows?) within thrombolite deposits	-8.51	3.52
RR 55.1	medium-crystalline replacement dolomite from patches (burrow-related) within bioturbated thrombolite	-9.04	3.08
TH 56.05	saddle dolomite cement between angular clasts from coarser-crystalline extensively dolomitized deposits	-6.92	2.68
TH 59.35	medium-crystalline replacement dolomite; originally the lithofacies might have been bioturbated couplets	-6.40	3.16
TH 64.6	replacing cement within a composite-oid grainstone	-6.59	2.05
TH 65.3	dolomicrosparite to medium-crystalline replacement dolomite from dolomitized mudstone overlying thrombolitic deposits	-6.09	2.45
TH 65.55	replacing cement between extensively dolomitized angular peloidal clasts	-7.39	1.75
FG 42.3c	fabric obliterating mosaic of medium- to coarse-crystalline replacement dolomite	-8.79	2.99
LV 49.75	fabric obliterating mosaic of medium-crystalline replacement dolomite; some remnant thrombolitic fabric visible	-7.34	3.01
LV 59.6	replacing cement within a composite-oid grainstone	-7.72	1.38
LV 63.75	medium-crystalline replacement dolomite from digitate to columnar stromatolites	-7.09	1.44
LV 64.5	medium- to coarse-crystalline dolomite replacing columnar stromatolites	-7.14	0.62
Total (n): 12		Minimum:	-9.04 0.62
		Maximum:	-6.09 3.52
		Average:	-7.42 2.34

SADDLE DOLOMITE (REPLACEMENT)

Sample	Description	$\delta^{18}\text{O}$	$\delta^{13}\text{C}$
TZ 22.25e	replacement saddle dolomite from burrows of peloidal packstone with thrombolitic fabric; associated with argillaceous matrix	-7.31	4.32
RR 65.6	coarse-crystalline replacement saddle dolomite from deposits with completely obliterated fabric; some associated argillaceous matrix	-7.50	3.94
TH 56.05a	saddle dolomite in argillaceous/bituminous matrix replacing patches of microbial thrombolitic deposits	-6.73	2.68
TH 59.35b	replacement saddle dolomite embedded in bituminous matrix; from patches in mudstone or couplets replaced by a mosaic of coarser-crystalline dolomite	-6.65	2.90
TH 63.5b	replacement saddle dolomite in argillaceous/bituminous matrix; associated with burrows in burrowed mudstone or fine-grained couplets	-6.44	2.64
FG 37.8	replacement saddle dolomite in burrows of dolomitized mudstone/fine-grained couplets; associated with argillaceous/bituminous matrix	-6.54	3.44

FG 42.3a	coarse-crystalline saddle dolomite in dark argillaceous/bituminous matrix	-10.51	2.88
FG 42.3b	coarse-crystalline saddle dolomite in dark argillaceous/bituminous matrix	-10.36	2.94
Total (n): 8		Minimum:	-10.51 2.64
		Maximum:	-6.44 4.32
		Average:	-7.75 3.22

PERITIDAL ZONED DOLOMITE CEMENT

Sample	Description	$\delta^{18}\text{O}$	$\delta^{13}\text{C}$
RR 33.15	zoned saddle dolomite cement from calcitic thrombolitic deposits;	-6.78	3.04
RR 34.15	zoned saddle dolomite cement from couplets with some microbial laminae	-8.33	3.37
TH 59.35a	complexly zoned saddle dolomite cement in voids (desiccation?, burrows?) within extensively dolomitized bioturbated couplets	-8.42	2.46
TH 63.7	complexly zoned saddle dolomite cement in voids in extensively dolomitized microbial (thrombolitic) deposits	-7.77	1.93
TH 65.0	zoned saddle dolomite cement in voids in extensively dolomitized microbial (thrombolitic) deposits	-6.96	1.80
TH 65.3b	complexly zoned saddle dolomite cement in layer-parallel voids in thrombolitic deposits	-7.33	1.66
TH 68.75	zoned saddle dolomite cement from voids in extensively dolomitized and partially silicified microbial (thrombolitic) deposits	-7.17	1.27
FG 42.9	zoned saddle dolomite cement from evaporite dissolution voids in medium-grained couplets	-7.88	2.90
FG 42.9b	pore-rim zoned dolomite cement from evaporite dissolution voids in medium-grained couplets	-8.15	2.83
LV 48.65a	zoned dolomite cement from evaporite dissolution and desiccation voids within stratiform to LLH stromatolites	-8.46	2.76
TZ 44.0	zoned dolomite cement from desiccation cracks in fine/medium grained couplets	-7.42	3.06
Total (n): 11		Minimum:	-8.46 1.27
		Maximum:	-6.78 3.37
		Average:	-7.70 2.46

PERITIDAL SADDLE DOLOMITE CEMENT

Sample	Description	$\delta^{18}\text{O}$	$\delta^{13}\text{C}$
RR 41.4b	saddle dolomite cement from layer-perpendicular and oblique veins within microbially laminated deposits; associated with equant calcite cement	-9.53	4.20
RR 52.65a	saddle dolomite cement from calcitic thrombolitic deposits	-9.22	3.13
TH 28.6	saddle dolomite cement from larger voids and fractures in deformed lithofacies with remnant thrombolitic fabric	-8.60	3.14
TH 31.5B	saddle dolomite cement in large dissolutional or dissolution enlarged void in couplets; similar to TH 32.05	-8.10	2.80
TH 32.05	coarse-crystalline saddle dolomite cement from voids in fine-grained couplets	-8.60	2.59
TH 36.55T	saddle dolomite cement in desiccation cracks in medium-grained couplets	-8.74	2.75
TH 51.2	saddle dolomite cement from tectonic veins	-8.00	3.24
TH 54.0a	saddle dolomite cement from voids (desiccation?) in between clasts in calcitic lithofacies	-7.01	2.77
TH 54.2	saddle dolomite cement from calcitic digitate stromatolites	-6.98	2.63
TH 54.4	saddle dolomite cement from calcitic microbial deposits (digitate stromatolites)	-6.88	2.87
TH 73.4	saddle dolomite cement from bed-perpendicular fractures in recrystallized couplets	-7.01	-0.61

FG	15.8	saddle dolomite cement from voids (desiccation cracks or fractures) in fine/medium-grained couplets	-8.80	3.41
FG	17.6	pore-central coarse-crystalline saddle dolomite cement from voids of uncertain origin (desiccation voids or burrows) in coarse/medium-grained couplets	-9.80	2.95
FG	32.7b	saddle dolomite cement associated with evaporite nodules in disturbed fine-grained couplets	-9.35	3.30
FG	42.3	coarse-crystalline turbid saddle dolomite cement from one large void in a fabric-obliterate mosaic of coarse crystalline replacement dolomite	-7.88	3.31
LV	64.5a	saddle dolomite cement in voids within extensively dolomitized columnar stromatolites	-6.89	0.71
TZ	22.25	saddle dolomite cement from veins; adjacent to sphalerite	-7.56	4.39
TZ	51.05	coarse-crystalline, turbid saddle dolomite cement in desiccation cracks in medium-grained couplets	-8.89	2.94
Total (n): 18			Minimum:	-9.80 -0.61
			Maximum:	-6.88 4.39
			Average:	-8.21 2.81

CALCITE CEMENT IN FRACTURES

Sample	Description	$\delta^{18}\text{O}$	$\delta^{13}\text{C}$
TZ 20.05A	coarse-crystalline ferroan equant calcite cement from a bed-perpendicular vein within thrombotic deposits	-12.92	3.20
RR 8.1	equant, turbid, ferroan calcite from large veins of irregular shape within fossiliferous layers of ribbon limestone	-11.79	2.48
RR 8.4	ferroan equant calcite in bed-parallel elongated void (fracture?) above hardground in a skeletal packstone/grainstone layer of ribbon limestone	-10.23	2.07
RR 12.5	coarse-crystalline ferroan equant calcite from bed-perpendicular fractures within ribbon limestone; associated with saddle dolomite cement	-11.47	2.09
RR 35.3	equant calcite cement (does not stain ferroan) from a bed-oblique fracture in fine-grained couplets/dolomitized mudstone	-10.34	2.08
RR 40.95	coarse-crystalline equant calcite cement from bed-oblique fractures of an extensively deformed layer	-11.51	0.70
RR 41.4a	equant calcite cement from layer-perpendicular and oblique veins within microbially laminated deposits; associated with saddle dolomite cement	-11.42	3.29
RR 43.5	ferroan equant calcite from tectonic veins in stratiform stromatolites	-10.62	3.10
FG 32.7a	ferroan equant calcite from a large void (associated with evaporite nodule) fed by a vertical fracture through dolomitized mudstone	-12.50	2.19
LV 12.3a	ferroan equant calcite from a bed-parallel vein in ribbon limestone	-9.38	1.64
Total (n): 10		Minimum:	-12.92 0.70
		Maximum:	-9.38 3.29
		Average:	-11.22 2.28

APPENDIX C

ELECTRON MICROPROBE DATA

Explanation of Data Tables

Electron microprobe (EMP) data are organized according to the diagenetic and depositional components analyzed. For each sample, individual data points are indicated as PT, followed by the analysis number. For some data points, it is also indicated whether they represent analyses along pore-rims or pore-centers. Data points comprising compositional transects are indicated as LINE, followed by the transect number. Start and end points of transects are labeled relative to their position within the pore (rim or center).

Analyses were performed on polished thin sections using a defocused beam (10-20 μm in diameter), 25 kV accelerating voltage, and 10 nA beam current. Detection limits were 0.1 mole % MgCO_3 for Mg (count time = 20 sec), 100 ppm for Mn and Fe, and 200 ppm for Sr (count time = 60 sec). Minimum, maximum, and average values for the analyses performed are calculated for individual components within each sample. For the components that were analyzed in more than one sample, a summary of data which contains minimum, maximum, and average values for all the analyses of that particular component, are also reported. The values from these data summaries are presented in Tables 4.4 and 4.5. Average values for the sets of data that contain analyses below detection limits are reported as two numbers separated by a slash (/). The first number represents the percentage of analyses below detection limit, and the second number represent the average value for the analyses above the detection limit.

CALCITE**MICRITIC MATRIX: non-microbial****Sample: RR 28.05**

Data points	CaCO ₃ mol%	MgCO ₃ mol%	Fe (ppm)	Mn (ppm)	Sr (ppm)
PT44	98.23	1.63	438	<100	434
PT45	97.70	2.18	335	169	200
minimum:	97.70	1.63	335	<100	200
maximum:	98.23	2.18	438	169	434
average:	97.97	1.91	387	50 / 169	317

Sample: LV 10.35

Data points	CaCO ₃ mol%	MgCO ₃ mol%	Fe (ppm)	Mn (ppm)	Sr (ppm)
PT64	97.44	2.39	574	<100	596
PT65	97.52	2.33	447	135	418
PT66	97.67	2.14	476	157	673
PT67	97.47	2.39	479	<100	347
PT68	96.85	2.50	3181	<100	573
minimum:	96.85	2.14	447	<100	347
maximum:	97.67	2.50	3181	157	673
average:	97.39	2.35	1031	60 / 146	521

Summary:

minimum:	96.85	1.63	335	<100	200
maximum:	98.23	2.50	3181	169	673
average:	97.55	2.22	847	57 / 154	463

FIBROUS/BLADED CALCITE CEMENT**Sample: RR 8.4**

Data points	CaCO ₃ mol%	MgCO ₃ mol%	Fe (ppm)	Mn (ppm)	Sr (ppm)
BC1-PT1	98.31	1.42	129	256	1851
BC1-PT2	98.51	1.42	<100	207	261
BC1-PT3	98.62	1.21	113	<100	1193
BC1-PT5	97.77	2.16	<100	142	314
BC1-PT6	98.55	1.16	<100	229	2050
BC1-PT7	97.77	2.09	244	257	466
BC1-PT8	98.13	1.69	246	325	688
BC1-PT9	98.02	1.81	265	183	738
BC1-PT10	99.28	0.44	184	<100	2064
BC1-PT11	98.54	1.26	283	<100	1167
BC1-PT12	98.59	1.04	212	148	2695
BC1-PT13	97.55	2.36	<100	198	511
BC1-PT14	98.13	1.65	<100	309	1404
BC1-PT17	97.67	2.22	249	225	205
BC1-PT18	98.20	1.63	136	223	862
minimum:	97.55	0.44	<100	<100	205
maximum:	99.28	2.36	283	325	2695
average:	98.24	1.57	33 / 206	20 / 225	1098

Sample: LV 10.35

Data points	CaCO ₃ mol%	MgCO ₃ mol%	Fe (ppm)	Mn (ppm)	Sr (ppm)
PT3	98.36	1.47	701	175	<200
PT4	97.83	1.96	147	<100	1496
PT16	97.38	2.52	395	<100	<200

PT17	98.22	1.62	211	<100	1059
PT18	98.19	1.74	<100	132	395
PT19	98.16	1.73	<100	182	496
PT20	98.02	1.84	<100	228	740
PT21	98.22	1.70	<100	219	213
PT22	97.68	2.13	156	234	1083
PT23	97.88	1.98	161	<100	930
PT24	97.74	2.11	140	179	763
PT26	98.09	1.80	<100	<100	921
PT31	98.52	1.26	161	175	1448
PT32	98.80	0.88	<100	145	2392
PT33	98.27	1.64	256	<100	376
PT34	98.50	1.35	308	203	489
PT39	97.86	2.07	<100	<100	500
PT40	98.54	1.19	186	<100	1898
PT44	97.88	2.05	124	<100	239
PT45	97.83	1.94	416	264	964
PT46	97.71	2.16	358	<100	440
PT48	97.99	1.88	345	200	254
PT49	98.40	1.42	697	178	<200
PT50	98.38	1.46	510	233	279
PT61	98.04	1.89	<100	135	272
PT62	98.68	1.05	<100	<100	2384
PT63	98.15	1.69	216	<100	1043
PT73	98.41	1.42	579	246	<200
PT72	98.93	0.80	161	<100	2085
PT71	98.08	1.73	792	212	<200
PT70	98.21	1.38	1712	531	<200
PT75	98.20	1.70	161	<100	478
PT86	98.10	1.78	129	255	471
PT87	98.96	0.74	139	<100	2383
PT88	98.82	0.87	<100	<100	2606
PT89	98.08	1.81	<100	<100	800
PT90	99.54	0.16	174	<100	2283
PT92	98.97	0.72	<100	126	2365
PT93	97.73	2.12	<100	151	922
PT94	97.91	1.93	108	144	1015
PT95	99.20	0.51	<100	<100	2432
PT96	97.71	2.21	132	<100	318
minimum:	97.38	0.16	<100	<100	<200
maximum:	99.54	2.52	1712	531	2606
average:	98.24	1.58	33 / 342	48 / 207	14 / 1090

Summary:

minimum:	97.38	0.16	<100	<100	<200
maximum:	99.54	2.52	1712	531	2695
average:	98.24	1.58	33 / 306	40 / 213	11 / 1092

OODS**Sample: TZ 13.85**

Data points	CaCO ₃ mol%	MgCO ₃ mol%	Fe (ppm)	Mn (ppm)	Sr (ppm)
PT12	98.03	1.79	910	<100	<200
PT13	97.72	2.09	998	<100	<200
average:	97.88	1.94	954		

EQUANT CALCITE CEMENT

Sample: RR 8.4

Data points	CaCO ₃ mol%	MgCO ₃ mol%	Fe (ppm)	Mn (ppm)	Sr (ppm)
BC1-PT4	97.38	2.49	<100	378	441
BC1-PT15	98.29	1.46	<100	173	1852
BC1-PT16	97.63	2.28	<100	108	610
minimum:	97.38	1.46		108	441
maximum:	98.29	2.49	<100	378	1852
average:	97.77	2.08		220	968

Sample: LV 10.35

Data points	CaCO ₃ mol%	MgCO ₃ mol%	Fe (ppm)	Mn (ppm)	Sr (ppm)
PT35	97.93	2.04	<100	<100	194
PT36	98.37	1.41	<100	<100	1874
PT37	97.75	2.13	245	178	382
PT38	98.61	1.15	854	314	216
PT41	98.40	1.37	995	151	240
PT43	98.39	1.42	637	350	<200
PT47	98.95	0.87	637	372	<200
PT51	98.34	1.35	1337	396	<200
PT74	98.23	1.59	669	341	<200
PT76	97.87	1.93	721	403	<200
PT77	98.15	1.72	463	255	<200
PT78	98.41	1.44	560	111	263
PT85	98.33	1.43	1116	258	<200
PT91	98.98	0.85	758	166	<200
minimum:	97.75	0.85	<100	<100	<200
maximum:	98.98	2.13	1337	403	1874
average:	98.34	1.48	14 / 749	14 / 275	57 / 528

Sample: RR 28.05

Data points	CaCO ₃ mol%	MgCO ₃ mol%	Fe (ppm)	Mn (ppm)	Sr (ppm)
PT1	96.98	2.90	<100	215	708
PT2	98.33	1.60	<100	178	359
PT3	97.24	2.64	<100	<100	983
PT4	97.77	2.15	<100	<100	527
PT5	97.85	2.03	<100	<100	837
PT6	98.67	1.19	<100	218	742
PT14	98.71	1.24	<100	<100	334
PT15	98.72	1.10	116	188	1059
PT16	98.30	1.60	<100	151	643
PT17	98.04	1.86	<100	<100	820
PT18	97.64	2.26	<100	<100	781
PT19	98.07	1.74	<100	<100	1461
PT20	98.23	1.73	<100	<100	<200
minimum:	96.98	1.10	<100	<100	<200
maximum:	98.72	2.90	116	218	1461
average:	98.04	1.85	92 / 116	62 / 190	8 / 771

Sample: TZ 13.85

Data points	CaCO ₃ mol%	MgCO ₃ mol%	Fe (ppm)	Mn (ppm)	Sr (ppm)
PT1	99.18	0.75	410	<100	<200
PT10	98.60	1.29	563	<100	<200
PT14	97.90	1.93	918	<100	<200

PT23	98.45	1.37	782	135	<200
PT24	98.79	1.10	568	<100	<200
PT25	98.99	0.91	523	<100	<200
PT26	98.94	0.98	350	<100	<200
PT27	98.85	1.05	534	<100	<200
PT28	99.07	0.86	213	166	<200
PT29	99.05	0.82	587	160	<200
<hr/>					
minimum:	97.90	0.75	213	<100	
maximum:	99.18	1.93	918	166	<200
average:	98.78	1.11	545	70 / 154	

Summary:

minimum:	96.98	0.75	<100	<100	<200
maximum:	99.18	2.90	1337	403	1874
average:	98.23	1.63	43 / 633	43 / 233	47 / 730

FERROAN EQUANT CALCITE**Sample: RR 28.05**

Data points	CaCO3 mol%	MgCO3 mol%	Fe (ppm)	Mn (ppm)	Sr (ppm)
PT7	98.30	1.57	638	<100	<200
PT8	99.31	0.62	348	<100	<200
PT12	98.74	1.15	345	275	<200
PT13	98.84	1.03	535	148	<200
PT21	97.31	2.53	727	114	<200
PT22	99.07	0.82	522	<100	<200
PT23	98.87	1.02	467	160	200
<hr/>					
minimum:	97.31	0.62	345	<100	
maximum:	99.31	2.53	727	275	<200
average:	98.63	1.25	512	43 / 174	

SYNTAXIAL OVERGROWTH CALCITE**Sample: TZ 13.85**

Data points	CaCO3 mol%	MgCO3mol%	Fe (ppm)	Mn (ppm)	Sr (ppm)
PT2	97.71	2.07	939	264	<200
PT3	97.46	2.37	940	<100	<200
PT4	98.03	1.83	674	<100	<200
PT5	97.50	2.31	984	<100	<200
PT6	97.70	2.11	1039	<100	<200
PT7	98.75	1.14	560	<100	<200
PT8	97.92	1.92	771	120	<200
PT9	99.12	0.75	589	101	<200
PT15	97.97	1.86	765	163	<200
PT16	97.60	2.22	889	120	<200
PT17	99.20	0.71	473	<100	<200
PT18	99.19	0.71	513	<100	<200
PT19	98.70	1.18	613	<100	<200
PT20	97.97	1.87	850	<100	<200
PT21	99.21	0.75	153	<100	<200
PT22	99.07	0.84	421	<100	<200
<hr/>					
minimum:	97.46	0.71	153	<100	
maximum:	99.21	2.37	1039	264	<200
average:	98.32	1.54	698	69 / 154	

CALCITE CEMENT IN FRACTURES

Sample: FG 17.0

Data points	CaCO₃ mol%	MgCO₃ mol%	Fe (ppm)	Mn (ppm)	Sr (ppm)
PT2	97.31	2.32	1748	331	<200
PT3	97.75	1.96	1453	163	<200
PT4	97.29	2.37	1654	209	<200
PT5	97.47	2.21	1640	175	<200
PT7	99.15	0.64	832	129	340
PT8	98.48	1.50	<100	<100	<200
PT9	99.11	0.83	121	169	<200
PT18	99.75	0.24	<100	<100	<200
PT19	97.36	2.32	1623	129	<200
PT23	97.41	2.25	1592	267	<200
PT24	97.56	2.09	1624	267	<200
PT25	97.41	2.27	1442	301	<200
PT33	98.89	1.10	<100	<100	<200
PT34	98.85	1.13	<100	111	<200
PT35	99.28	0.70	<100	<100	<200
PT36	99.11	0.87	<100	105	<200
PT37	99.05	0.93	<100	<100	<200
PT38	98.71	1.27	<100	<100	<200
PT40	99.16	0.81	116	<100	<200
PT41	99.15	0.80	<100	151	<200
PT43	98.74	1.25	<100	<100	<200
PT44	99.03	0.97	<100	<100	<200
PT45	98.69	1.30	<100	<100	<200
PT46	98.33	1.63	<100	187	<200
minimum:	97.29	0.24	<100	<100	<200
maximum:	99.75	2.37	1748	331	340
average:	98.46	1.41	54 / 1259	42 / 192	96 / 340

DOLOMITE

SUBTIDAL REPLACEMENT SADDLE DOLOMITE

Sample: RR 8.4

Data points	CaCO₃ mol%	MgCO₃ mol%	Fe (ppm)	Mn (ppm)	Sr (ppm)
LINE1	54.71	40.87	25734	550	<200
LINE1	55.24	40.95	21778	750	<200
PT1	54.02	42.05	22752	511	<200
PT2	55.11	40.87	23359	671	<200
PT3	54.72	41.57	21388	580	<200
PT4	54.84	41.13	23356	560	<200
PT5	54.82	41.52	21123	511	<200
PT6	54.18	41.73	23922	511	<200
PT7	54.60	41.73	21193	532	<200
PT8	53.83	42.13	23378	602	<200
PT9	54.65	41.32	23442	535	<200
PT10	55.27	40.73	23169	638	<200
PT11	54.71	39.59	32663	1057	<200
PT13	54.97	41.46	20752	429	<200
PT14	54.55	41.82	20992	511	<200
PT15	55.28	40.61	23740	625	<200
PT16	54.59	41.31	23792	554	<200
PT18	54.96	40.52	25591	876	<200

PT17	55.16	40.52	25118	548	<200
PT19	54.96	40.44	26109	873	<200
PT20	54.77	41.20	23239	660	<200
PT21	54.81	40.50	26839	813	<200
PT22	54.82	41.09	23413	729	<200
PT23	54.87	41.06	23251	659	<200
PT24	54.60	40.74	26419	904	<200
PT25	54.44	41.45	23410	713	<200
PT26	54.10	42.22	21162	738	<200
PT27	54.84	41.09	23284	695	<200
PT28	54.83	41.29	22495	581	<200
PT29	55.05	40.41	26199	559	<200
PT30	54.30	41.26	25577	520	<200
PT31	54.79	41.24	22898	683	<200
PT32	54.65	41.16	24178	614	<200
PT33	54.94	40.29	27317	885	<200
PT34	54.88	41.02	23615	793	<200
PT35	54.70	40.62	27175	526	<200
minimum:	53.83	39.59	20752	429	
maximum:	55.28	42.22	32663	1057	<200
average:	54.74	41.10	23995	653	

SUBTIDAL SADDLE DOLOMITE CEMENT

Sample: LV 10.35

Data points	CaCO ₃ mol%	MgCO ₃ mol%	Fe (ppm)	Mn (ppm)	Sr (ppm)
PT1	54.22	42.90	16071	935	<200
PT2	54.56	43.21	12821	472	<200
PT5	54.26	42.93	16109	635	<200
PT6	54.30	42.95	15573	671	<200
PT7	53.23	43.91	16137	761	<200
PT8	53.89	43.31	15833	705	<200
PT9	54.41	42.28	18319	1011	<200
PT10	54.71	42.16	17425	879	<200
PT11	53.98	43.08	16571	831	<200
PT12	53.96	42.80	18106	852	<200
PT13	54.08	42.70	18033	839	<200
PT14	54.56	42.56	16224	831	<200
PT15	54.51	42.17	18675	963	<200
PT42	55.06	41.30	20816	724	<200
PT56	55.51	41.27	18118	977	<200
PT57	54.23	42.63	17836	928	<200
PT58	55.57	41.11	18897	872	<200
PT59	55.23	40.95	21962	874	<200
PT79	54.86	41.97	17803	850	<200
PT80	55.17	41.67	17820	959	<200
PT81	54.75	41.98	18195	1100	<200
PT82	54.51	42.25	18225	910	<200
PT83	54.59	42.07	18868	895	<200
minimum:	53.23	40.95	12821	472	
maximum:	55.57	43.91	21962	1100	<200
average:	54.53	42.36	17584	847	

PERITIDAL DOLOMICRITIC MATRIX: non-microbial**Sample: TZ 44.0**

Data points	CaCO₃ mol%	MgCO₃mol%	Fe (ppm)	Mn (ppm)	Sr (ppm)
PT5	54.93	44.97	318	109	288
PT6	54.28	45.55	906	<100	<200
PT7	55.01	44.80	1062	112	<200
PT8	54.28	45.48	1315	124	<200
PT20	53.36	46.59	281	<100	<200
PT22	53.43	46.38	1137	<100	<200
PT23	52.77	47.10	742	<100	<200
PT24	53.42	46.49	487	<100	<200
PT35	55.92	43.92	722	103	219
minimum:	52.77	43.92	281	<100	<200
maximum:	55.92	47.10	1315	124	288
average:	54.16	45.70	774	56 / 112	78 / 254

PERITIDAL DOLOMICRITIC MATRIX: microbial**Sample: LV 48.65**

Data points	CaCO₃ mol%	MgCO₃mol%	Fe (ppm)	Mn (ppm)	Sr (ppm)
PT20	51.01	48.92	349	<100	<200
PT21	51.10	48.81	424	<100	<200
PT22	50.61	49.30	541	<100	<200
PT23	51.18	48.67	840	<100	<200
PT24	51.47	48.45	473	<100	<200
PT25	50.89	48.96	772	157	<200
PT26	50.94	48.92	691	151	<200
PT27	50.66	49.19	892	<100	<200
PT28	51.50	48.38	626	<100	<200
minimum:	50.61	48.38	349	<100	
maximum:	51.50	49.30	892	157	<200
average:	51.04	48.84	623	78 / 154	

PERITIDAL COARSER CRYSTALLINE REPLACEMENT DOLOMITE**Sample: FG 42.3**

Data points	CaCO₃ mol%	MgCO₃mol%	Fe (ppm)	Mn (ppm)	Sr (ppm)
PT22-near pore	54.14	44.43	8122	374	<200
PT44	56.69	43.19	554	139	<200
PT45	56.53	43.38	343	<100	<200
PT46	55.11	44.71	1027	<100	<200
PT47	55.28	44.62	515	<100	<200
PT48	56.09	43.79	655	103	<200
PT49	53.95	45.15	5126	223	<200
PT50	54.67	43.91	8214	299	<200
PT51	54.11	44.52	7893	307	<200
PT52	53.84	45.07	6051	431	<200
PT53	54.63	44.36	5779	319	<200
minimum:	53.84	43.19	343	<100	
maximum:	56.69	45.15	8214	431	<200
average:	55.00	44.29	4025	27 / 274	

PERITIDAL SADDLE DOLOMITE REPLACEMENT

Sample: FG 42.3

Data points	CaCO ₃ mol%	MgCO ₃ mol%	Fe (ppm)	Mn (ppm)	Sr (ppm)
PT23	53.56	45.37	6402	<100	<200
PT24	53.49	45.53	5634	142	<200
PT25	53.86	45.06	6235	181	<200
PT26	53.06	45.99	5458	214	<200
PT27	53.66	45.28	6249	199	<200
PT28	54.84	43.82	7733	316	<200
PT29	53.30	45.59	6326	229	<200
PT30	53.43	45.62	5426	163	<200
PT31	54.00	44.46	8914	289	<200
PT32	52.97	45.90	6556	202	<200
PT33	54.31	43.98	9867	397	<200
PT34	53.07	45.75	6991	153	<200
PT35	53.60	45.34	6147	247	<200
PT36	53.20	45.44	7830	232	<200
PT37	53.27	45.12	9459	265	<200
PT38	54.76	43.63	8975	488	<200
PT39	53.05	45.97	5664	217	<200
PT40	52.92	45.97	6581	<100	<200
minimum:	52.92	43.63	5426	<100	
maximum:	54.84	45.99	9867	488	<200
average:	53.58	45.21	7025	11 / 246	

PERITIDAL SADDLE DOLOMITE CEMENT

Sample: TH 32.05

Data points	CaCO ₃ mol%	MgCO ₃ mol%	Fe (ppm)	Mn (ppm)	Sr (ppm)
1 pore rim	51.51	47.05	8282	314	<200
LINE1	52.57	45.99	8103	561	<200
LINE1	52.32	46.49	6737	418	<200
LINE1	52.82	45.88	7429	415	<200
LINE1	52.24	46.57	6735	388	<200
LINE1	52.37	46.38	7167	355	<200
LINE1	53.20	45.41	7846	464	<200
LINE1	52.10	46.47	8197	373	<200
LINE1-center	51.78	46.47	10017	418	<200
LINE2 rim	51.72	47.34	5319	245	<200
LINE2	51.53	47.60	4977	212	<200
LINE2	52.46	46.83	5447	303	<200
LINE2	52.69	45.95	7690	378	<200
LINE2	52.62	45.98	8203	139	<200
LINE2	52.22	46.05	10026	403	<200
LINE2	51.96	46.23	10642	221	<200
LINE2 center	51.47	46.71	10670	121	<200
LINE3 center	52.33	45.92	10019	524	<200
LINE3	51.58	46.96	8701	163	<200
LINE3	51.94	46.61	8400	312	<200
LINE3	52.24	46.33	8195	430	<200
LINE3	53.60	44.96	8112	503	<200
LINE3	52.51	46.30	6752	363	<200
LINE3	52.44	46.49	6149	242	<200
LINE3	51.95	47.13	5310	260	<200
LINE3	52.41	46.66	5468	167	<200
LINE3	52.08	46.85	6216	236	<200

LINE3	51.89	46.71	7821	533	<200
LINE3 rim	51.62	47.00	7852	430	<200
minimum:	51.47	44.96	4977	121	
maximum:	53.60	47.60	10670	561	<200
average:	52.21	46.46	7672	341	

Sample: FG 42.3

Data points	CaCO ₃ mol%	MgCO ₃ mol%	Fe (ppm)	Mn (ppm)	Sr (ppm)
PT1	55.26	44.61	634	103	<200
PT2	55.64	44.28	499	<100	<200
PT3	55.76	44.10	702	124	<200
PT4	54.98	43.79	7022	368	<200
PT5	55.89	44.00	523	100	<200
PT6	55.93	43.98	458	106	<200
PT7	55.67	44.21	611	<100	<200
PT8	55.77	44.11	616	151	<200
PT9	53.19	45.89	5216	341	<200
PT10	53.38	45.27	7603	490	<200
PT11	54.34	44.79	5016	250	<200
PT12	55.29	44.59	647	<100	<200
PT13	55.03	44.85	595	127	<200
PT14	55.65	44.24	512	<100	261
PT15	55.16	44.69	767	100	<200
PT16	55.57	44.29	569	145	<200
PT17	56.59	43.30	548	<100	<200
PT18	55.89	43.99	556	130	<200
PT19	54.97	44.91	619	<100	<200
PT20	55.03	43.64	7492	477	<200
PT41	55.55	44.37	468	<100	<200
PT42	56.11	43.75	666	127	<200
PT43	55.85	44.04	629	<100	<200
minimum:	53.19	43.30	458	<100	<200
maximum:	56.59	45.89	7603	490	261
average:	55.33	44.33	1868	35 / 209	96 / 261

Sample: RR 28.05

Data points	CaCO ₃ mol%	MgCO ₃ mol%	Fe (ppm)	Mn (ppm)	Sr (ppm)
PT9	52.08	46.52	7796	500	<200
PT10	53.37	44.97	9670	289	<200
PT11	54.03	44.21	10253	311	<200
PT24	52.56	45.84	8827	582	<200
PT25	53.83	44.49	9449	531	<200
PT26	53.85	44.48	9566	449	<200
PT27	54.33	43.98	9449	597	<200
PT28	54.83	43.56	9061	489	<200
PT29	53.78	44.60	9227	295	<200
PT30	53.78	44.57	9486	488	<200
PT31	54.02	44.32	9502	377	<200
PT32	55.02	43.43	8912	296	<200
PT33	54.67	43.70	9246	344	<200
PT34	52.86	45.94	6679	404	<200
PT35	53.86	45.39	4290	223	<200
PT36	54.05	44.43	8681	292	<200
PT37	54.23	44.16	9023	500	<200
PT38	54.09	44.37	8747	437	<200
PT39	54.22	44.25	8684	407	<200

PT40	54.18	44.09	9612	618	<200
PT41	54.35	44.03	9236	467	<200
PT42	53.88	44.40	9939	374	<200
PT43	54.77	43.63	9034	401	<200
minimum:	52.08	43.43	4290	223	
maximum:	55.02	46.52	10253	618	<200
average:	53.94	44.49	8886	420	
Summary:					
minimum:	51.47	43.30	458	<100	<200
maximum:	56.59	47.60	10670	618	261
average:	53.70	45.21	6264	11 / 339	99 / 261

PERITIDAL ZONED DOLOMITE CEMENT

Sample: TZ 44.0

Data points	CaCO ₃ mol%	MgCO ₃ mol%	Fe (ppm)	Mn (ppm)	Sr (ppm)
PT2 - pore rim	53.26	46.35	2265	112	<200
PT1	52.85	46.58	3237	178	<200
PT9	52.35	47.12	2935	184	<200
PT10	53.33	46.17	2670	308	<200
PT11	53.60	45.90	2787	163	<200
PT12 - center	53.47	46.30	942	365	<200
PT25 -pore rim	53.17	46.66	939	<100	<200
PT26	53.81	45.70	2732	181	<200
PT27	53.29	46.48	1194	157	<200
PT28	53.19	46.51	1668	<100	<200
PT29 - center	53.63	45.82	3037	259	<200
PT30 - center	53.12	46.35	3063	115	<200
PT31	52.93	46.54	2912	227	<200
PT32	52.85	46.60	3128	175	<200
PT33	54.10	45.51	1897	408	<200
PT34 -pore rim	53.81	46.04	635	293	<200
minimum:	52.35	45.51	635	<100	
maximum:	54.10	47.12	3237	408	<200
average:	53.30	46.29	2253	13 / 223	

Sample: LV 48.65

Data points	CaCO ₃ mol%	MgCO ₃ mol%	Fe (ppm)	Mn (ppm)	Sr (ppm)
PT1 -pore rim	51.19	48.71	411	205	<200
PT2	51.56	48.19	1233	250	<200
PT3	51.66	47.83	2907	196	<200
PT4- center	52.19	46.97	4673	377	<200
PT5- center	51.81	47.39	4612	259	<200
PT6- center	51.75	47.49	4325	277	<200
PT7	50.92	48.39	3805	296	<200
PT8	50.29	49.61	549	<100	<200
PT9	50.61	49.35	<100	175	<200
PT10-pore rim	50.69	49.19	630	<100	<200
PT11-pore rim	50.99	48.89	567	112	<200
PT12	51.68	47.63	4019	100	<200
PT13	51.87	47.26	4982	250	<200
PT14	51.55	47.59	4939	193	<200
PT15	50.47	49.50	<100	136	<200
PT16	51.93	47.26	4650	229	<200
PT17	52.06	47.30	3618	205	<200

PT18	50.26	49.64	377	151	<200
PT19-pore rim	50.55	49.36	510	<100	<200
PT29-pore center	51.14	48.22	3466	338	<200
PT30-pore rim	51.23	48.73	187	<100	<200
<hr/>					
minimum:	50.26	46.97	<100	<100	
maximum:	52.19	49.64	4982	377	<200
average:	51.26	48.31	10 / 2656	19 / 221	
<hr/>					
Summary:					
minimum:	50.26	45.51	<100	<100	
maximum:	54.10	49.64	4982	408	<200
average:	52.28	47.30	5 / 2471	16 / 222	
<hr/>					

APPENDIX D

DATA FOR CARBON ISOTOPE STRATIGRAPHY

MICRITE

NOLICHUCKY SHALE

Sample	Description	$\delta^{18}\text{O}$	$\delta^{13}\text{C}$
N -18.85	micritic matrix in between trilobite and brachiopod fragments of a limestone layer interbedded with shale	-8.52	0.16
N -16.95	micritic matrix in between skeletal fragments and from small micritic lenses and patches of a packstone/grainstone layer interbedded with shale	-9.06	1.12
N -12.95	micrite from small patches and in between skeletal fragments of wackestone/grainstone layers interbedded with argillaceous layers	-8.96	0.27
N -12.15	micrite from a nodular layer interbedded with shale	-8.47	0.89
N -8.15	micrite from lenses and in between skeletal fragments of a packstone/grainstone layer	-8.03	0.33
N -6.25	micrite from a mudstone layer interbedded with argillaceous layers of ribbon laminated rocks	-9.34	0.53
N -5.0	micrite from a mudstone layer interbedded with argillaceous layers of ribbon laminated rocks	-8.10	0.97
N -3.3	micrite from mudstone layers and lenses interbedded with flat-pebble conglomerate and skeletal packstone/grainstone of ribbon rocks	-8.04	1.37
N -2.8	micrite from one small flat pebble incorporated within skeletal packstone/grainstone layer	-8.06	1.13
N -1.75	micrite from a mudstone layer with nodular appearance inbedded within ribbon rocks	-7.95	1.18

MAYNARDVILLE FORMATION

Sample	Description	$\delta^{18}\text{O}$	$\delta^{13}\text{C}$
TH -0.4	micrite from intraclasts and irregular patches from fossiliferous-intraclastic packstone layer of ribbon limestone	-8.98	1.98
TH 0.0	micrite from a mudstone layer of ribbon limestone	-8.84	2.54
TH 1.1	micrite from burrow-mottled ribbon limestone	-7.90	3.01
TH 2.15	micrite from a laminated mudstone layer of ribbon limestone	-7.48	1.82
TH 3.35	micrite from a mudstone layer of ribbon limestone	-7.43	1.66
TH 4.2	micritic matrix in between trilobite fragments from a limestone layer of ribbon rocks	-8.03	1.29
TH 5.2	micrite from intraclasts (flat pebbles) imbedded within argillaceous dolomicritic layers of ribbon rocks	-7.87	0.49
TH 5.4	micrite from a lense interbedded within argillaceous dolomicrite of ribbon rocks	-7.79	1.19
TH 6.4	micrite from a mudstone to peloidal mudstone layer of ribbon limestone	-7.51	1.53
TH 8.0b	micrite in between trilobite fragments in fossiliferous wackestone/packstone of ribbon limestone	-7.43	1.13
TH 9.0	time-extracted calcite from argillaceous dolomicrite or calcareous siltstone	-8.23	2.35
TH 10.05	micrite from a mudstone layer interbedded within argillaceous dolomicrite of ribbon rocks	-7.77	2.92
TH 11.3	micrite from a mudstone layer underlying flat pebble conglomerate of ribbon limestone	-7.76	1.71
TH 11.75	time-extracted calcite from argillaceous dolomicrite/calcareous siltstone	-8.92	1.98
TH 11.9	micrite from a mudstone/peloidal layer of ribbon limestone	-8.14	3.18

TH	12.6	micrite from a lense within ribbon limestone	-7.48	3.21
TH	13.45	micrite from a lense within ribbon limestone	-7.16	3.54
TH	14.65	micrite from a mudstone layer of ribbon limestone	-7.58	4.09
TH	16.75	micrite from a mudstone layer of ribbon limestone	-7.80	2.29
TH	17.85	micrite to peloidal packstone from lenses in ribbon limestone	-7.63	3.52
TH	18.8	micrite from burrowed lenses from transitional interval between ribbon limestone and microbially laminated deposits	-7.88	3.80
TH	20.5	micrite from microbial laminates; contains about 30% dolomicrite; time extraction used	-8.63	3.39
TH	22.2	micrite from microbial laminates; contains about 10% dolomicrite; time extraction used	-8.73	3.68
TH	23.45	micrite from microbial laminates; contains common dolomicrite; time extraction used	-8.91	3.41

DOLOMICRITE

MAYNARDVILLE FORMATION

Sample	Description	$\delta^{18}\text{O}$	$\delta^{13}\text{C}$
TH 25.55	dolomicritic laminae from stratiform stromatolites	-6.58	3.90
TH 26.6	dolomicritic laminae from stratiform stromatolites	-6.21	4.01
TH 27.8	dolomicrite from a layer overlying microbially laminated deposits	-6.41	3.25
TH 28.35	dolomicrite from upper parts of coarse-grained couplets	-6.76	2.76
TH 29.6	dolomicrite from fine-grained couplets	-7.02	2.72
TH 30.7a	dolomicrite from fine-grained couplets	-7.41	2.46
TH 30.7b	dolomicrosparite from fine-grained couplets	-7.23	2.66
TH 31.4	dolomicrosparite from fine/medium-grained couplets	-8.07	3.01
TH 32.9	dolomicrite from upper parts of fine/medium-grained couplets	-7.07	3.03
TH 33.1B	dolomicrite from fine-grained couplets	-7.05	3.01
TH 33.1T	dolomicrite from dolomitized mudstone	-7.88	3.25
TH E2-33.35	dolomicrite from dolomitized mudstone; 5 cm below a prominent exposure surface	-7.29	3.28
TH 33.4a	dolomicrite from clasts in topographic lows immediately above the exposure surface	-7.77	3.25
TH 33.4b	dolomicrite from clasts in topographic lows immediately above the exposure surface	-7.67	3.18
TH 1-33.42	dolomicrite with a lamina interbedded with argillaceous laminae in the condensed shaly interval deposited on the exposure surface	-7.64	2.97
TH 2-33.43	laminated dolomicrite from fine-grained couplets with desiccation cracks; deposited about 5 cm above the exposure surface	-7.72	3.08
TH D-33.45	dark argillaceous dolomicritic matrix from a condensed shaly interval deposited on the erosional exposure surface; associated with sphalerite	-7.77	3.26
TH 34.6	dolomicrite from dolomitized mudstone	-6.82	3.68
TH 35.6	dolomicrite from dolomitized mudstone/fine-grained couplets	-6.12	3.06
TH 36.55T	dolomicrite from upper parts of medium-grained couplets with common desiccation cracks	-6.96	2.88
TH 37.6	dolomicrite from fine/medium-grained couplets with desiccation cracks	-6.39	2.96

SEQUENCE BOUNDARY ZONE

Sample	Description	$\delta^{18}\text{O}$	$\delta^{13}\text{C}$
TH 38.7	dolomicrite from dolomitized mudstone	-6.59	3.14
TH 39.05	dolomicrite from upper parts of fine/medium-grained couplets	-5.86	3.43
TH 40.25	dolomicrite from upper parts of medium-grained couplets	-6.35	3.82
TH 41.15	dolomicrite from upper, burrowed parts of medium-grained couplets	-5.99	3.80
TH 41.9	dolomicrite from upper parts of medium-grained couplets	-6.99	3.61
TH 43.3	slightly laminated dolomicrite from dolomitized mudstone/very fine-grained couplets	-6.87	3.76
TH 43.8	dolomicrosparite from extensively dolomitized, burrowed mudstone	-6.55	4.78
TH 44.75	dolomicrosparite from burrowed mudstone/fine-grained couplets	-6.38	4.30
TH 45.7	dolomicrosparite from extensively dolomitized, slightly burrowed mudstone/fine-grained couplets	-6.36	3.94
TH 47.1	dolomicrite from fine-grained couplets/dolomitized mudstone	-6.18	3.40
TH 47.7	dolomicrosparite from LLH stromatolites	-8.00	3.69
TH 48.9	dolomicrite from LLH stromatolites; contamination from small fenestrae with saddle dolomite cement possible	-6.78	3.55
TH 50.0	dolomicrite from burrowed mudstone/fine-grained couplets	-6.24	4.08
TH 50.7	dolomicrite from dolomitized mudstone/fine-grained couplets associated with evaporites and abundant quartz sand grains	-6.33	3.83
TH 51.75	laminated dolomicrite from fine-grained couplets	-6.68	3.11

COPPER RIDGE DOLOMITE

Sample	Description	$\delta^{18}\text{O}$	$\delta^{13}\text{C}$
TH 52.75	laminated dolomicrite from microbial lumps imbedded within deposits with thrombolitic texture	-6.55	2.94
TH 53.9	dolomicrite to dolomicrosparite from burrowed fine-grained couplets	-6.54	3.02
TH 54.8	dolomicrite to dolomicrosparite from dolomitized mudstone	-6.55	2.31
TH 55.25	dolomicrite from upper micritic part of coarse-grained couplets	-5.99	2.65
TH 56.8	dolomicrite from fine-grained couplets	-6.38	2.20
TH 57.25	dolomicrite from fine-grained couplets	-7.44	2.42
TH 58.15	dolomicrite from burrow-mottled mudstone/fine-grained couplets	-6.43	3.71
TH 59.35	medium crystalline replacement dolomite; originally the lithofacies might have been bioturbated couplets	-6.40	3.16
TH 60.4	dolomicrite from stratiform stromatolite laminae	-6.37	2.72
TH 61.4	dolomicrite from fine to medium-grained couplets	-7.13	2.77
TH 62.45	dolomicrite from extensively dolomitized LLH or digitate stromatolites	-6.42	2.36
TH 63.5	dolomicrosparite from extensively dolomitized bioturbated peloidal packstone/wackestone	-6.49	2.66
TH 65.3	dolomicrosparite to medium crystalline replacement dolomite from dolomitized mudstone overlying thrombolitic deposits	-6.09	2.45
TH 66.9	dolomicrite from fine-grained couplets overlying SH stromatolites	-6.36	1.42
TH 67.25	dolomicrite from fine-grained couplets	-6.64	1.42
TH 68.35	dolomicrosparite from mottled (burrowed) dolomitized mudstone	-6.52	1.78
TH 69.3	dolomicrite from non-burrowed parts of extensively mottled medium-grained couplets	-6.18	1.64
TH 70.2	dolomicrite from upper part of medium-grained couplets	-6.38	0.83
TH 71.45	dolomicrite from relatively undisturbed parts of extensively mottled fine/medium-grained couplets	-7.08	0.79
TH 72.55	dolomicrite from relatively undisturbed parts of mottled dolomitized mudstone	-6.86	-0.07

TH 73.25	dolomicrite from dolomitized mudstone	-7.31	-0.85
TH 74.15	dolomicrite from dolomitized mudstone	-6.70	0.09

OTHER DIAGENETIC AND DEPOSITIONAL COMPONENTS

Sample	Description	$\delta^{18}\text{O}$	$\delta^{13}\text{C}$
TH 0.55a	bladed calcite cement in between intraclasts of flat pebble conglomerate	-7.86	2.88
TH 0.55c	bladed calcite cement in between intraclasts of flat pebble conglomerate	-7.80	2.97
TH 0.0	argillaceous, ferroan dolomicrite from ribbon limestone	-8.15	3.10
TH 2.15b	ferroan microsparite associated with burrows within mudstone layers of ribbon limestone	-8.01	3.03
TH 5.35	argillaceous dolomicrite from ribbon limestone	-7.56	2.83
TH 9.0	dolomicrite from argillaceous dolomicrite/calcareous siltstone; time extraction used	-6.05	3.22
TH 14.0	ferroan equant calcite cement in voids (burrows?) within a micritic layer of ribbon rocks	-9.68	2.27
TH 18.8	ferroan equant calcite cement in voids (burrows likely) within ribbon limestone	-9.07	2.70
TH 19.1	ferroan equant calcite cement from burrows in microbially laminated deposits	-9.69	2.69
TH 28.6	saddle dolomite cement from larger voids and fractures in deformed lithofacies with remnant thrombotic fabric	-8.60	3.14
TH 31.5B	saddle dolomite cement in large dissolutional or dissolution enlarged void in couplets; similar to TH 32.05	-8.10	2.80
TH 32.05	coarse crystalline saddle dolomite cement from voids in fine-grained couplets	-8.60	2.59
TH 36.55T	saddle dolomite cement in desiccation cracks in medium-grained couplets	-8.74	2.75
TH 51.2	saddle dolomite cement from tectonic veins	-8.00	3.24
TH 54.0b	pore-central equant calcite cement in a layer-parallel void within micritic layer	-9.84	1.54
TH 54.0a	saddle dolomite cement from voids (desiccation?) in between clasts in calcitic lithofacies	-7.01	2.77
TH 54.2	saddle dolomite cement from calcitic digitate stromatolites	-6.98	2.63
TH 54.2C	micrite comprising digitate stromatolites from the peritidal package; minor contamination from small fenestrae and scattered dolomite possible	-9.52	1.53
TH 54.4	saddle dolomite cement from calcitic microbial deposits (digitate stromatolites)	-6.88	2.87
TH 55.4	bladed calcite cement between micritic intraclasts of rare calcitic deposits within peritidal package; succeeded by equant calcite and pore-central saddle dolomite cement	-9.96	2.65
TH 56.05	saddle dolomite cement between angular clasts from coarser crystalline extensively dolomitized deposits	-6.92	2.68
TH 56.05a	saddle dolomite in argillaceous/bituminous matrix replacing patches of microbial thrombotic deposits	-6.73	2.68
TH 59.35a	saddle dolomite cement in voids (desiccation?, burrows?) within extensively dolomitized bioturbated couplets	-8.42	2.46
TH 59.35b	replacement saddle dolomite embedded in bituminous matrix; from patches in mudstone or couplets replaced by a mosaic of coarser-crystalline dolomite	-6.65	2.90
TH 63.5b	replacement saddle dolomite in argillaceous/bituminous matrix; associated with burrows in burrowed mudstone or fine-grained couplets	-6.44	2.64
TH 63.7	saddle dolomite cement in voids in extensively dolomitized microbial (thrombotic) deposits	-7.77	1.93
TH 64.6	replacing cement within a composite-oid grainstone	-6.59	2.05

TH	65.0	saddle dolomite cement in voids in extensively dolomitized microbial (thrombolitic) deposits	-6.96	1.80
TH	65.3b	saddle dolomite cement in layer-parallel voids in thrombolitic deposits	-7.33	1.66
TH	65.55	replacing cement between extensively dolomitized angular peloidal clasts	-7.39	1.75
TH	68.75	saddle dolomite cement from voids in extensively dolomitized and partially silicified microbial (thrombolitic) deposits	-7.17	1.27
TH	73.4	saddle dolomite cement from bed-perpendicular fractures in recrystallized couplets	-7.01	-0.61

VITA

Bosiljka Glumac was born in Raša, Croatia on June 12, 1967. She attended elementary school in the picturesque village of Čepić on the Istrian peninsula of Croatia. In 1985, Bosiljka graduated from high school in Labin—a small town near the Adriatic coast of eastern Istria. Beautiful rocky beaches and the coal-mining tradition of the area sparked Bosiljka's interest in earth science. In the Fall of 1985, Bosiljka became an undergraduate student in geology at the University of Zagreb, Croatia. In 1988, Bosiljka was selected one of the best students at the University of Zagreb, and in 1989 she graduated from the School of Mining, Geology, and Petroleum Engineering with the highest grade average. Traveling was always one of Bosiljka's passions. She enjoyed meeting people and sightseeing while spending her summers working as a fruit-picker in Great Britain, or participating in international student exchange programs in Poland and Israel. This experience made Bosiljka interested in studying abroad. Bosiljka's first trip to the United States was to start her graduate studies at the University of Tennessee, Knoxville in the Fall of 1991. Among the hills of the southern Appalachians, Bosiljka found rocks of the same type (carbonates), but much, much older, than those that make up the beaches of Istria. These rocks became the focus of her dissertation research. In the Spring of 1997, Bosiljka Glumac received her doctorate degree from the Department of Geological Sciences at the University of Tennessee.